MECHANICAL PROPERTIES OF HEAVILY OVERCONSOLIDATED CLAYS

(Laboratory Investigation of the Compressibility of Lower Lias Clay)

a thesis presented by

COLIN PAUL THOMAS

for the degree of Doctor of Philosophy

Department of Civil Engineering
The University of Aston in Birmingham

December 19

The research work described in this thesis was carried out in the Department of Civil Engineering at the University of Aston in Birmingham during the four year period from October 1968. For the first two years, the author held a Science Research Council research studentship, and for the following two year period was employed by the University as a lecturer in the same Department. Much of this thesis was written in the period subsequent to October 1972 while the author was an employee of Ove Arup and Partners.

SYNOPSIS

A laboratory investigation was carried out to study the compressibility characteristic of heavily over-consolidated clays, and in particular the Lower Lias Clay from a site at Blockley, Gloucestershire.

It has been estimated that the sampling site has been subjected to an overburden in excess of 520m. This is tentitively confirmed by high pressure oedometer tests on undisturbed and remoulded samples.

The in-situ value of the coefficient of earth pressure at rest, K_o, is determined by measurement of the pore suction in undisturbed samples in both triaxial and oedometer apparatus; a value of 1.0 is obtained.

The deformation of cylindrical undistrubed samples are studied under various axi-symmetric stress paths in the triaxial apparatus and under one-dimensional strain conditions in the oedometer.

A new triaxial cell is developed in which axial and radial stresses are applied independently, in order that samples can be returned to in-situ stress state (i.e. $\sigma'_r > \sigma'_a$) and loaded under stress or strain controlled conditions.

Results obtained from the series of triaxial tests demonstrates that the Lias clay exhibits a high degree of anisotropy. It is found that under drained conditions the strain ratio ($\varepsilon_v/\varepsilon_a$)- incremental effective stress ratio ($\bar{K}$) relationship can be predicted by an orthotropic elastic theory.

The vertical 'Young's' modulus, E'_v, is found to be reasonably linear at low stress range, although dependent on the incremental stress ratio $\bar{K}$.

Results from block, core and tube samples demonstrate that mechanical disturbance has little effect on the Young's modulus but significantly reduces the volumetric strains.

ACKNOWLEDGEMENTS

I wish to acknowledge the help and encouragement given by my supervisor, K. Starzewski, B.Sc., Ph.D., C.Eng., M.I.C.E., during the course of my research studies and the interest shown by Professor M. Holmes, D.Sc., Ph.D., C.Eng., F.I.C.E., F.I. Struct.E., F.I. Mun. E., and D.H. Bennett,B.Sc.,(Eng.), C.Eng., F.I.C.E., A.M.I.E.(Aust.), F.G.S.

The author is indebted to M.J. Lyons (Senior Technician) for the valuable assistance provided throughout the course of the experimental work and particularly for his help during the ardeous task of obtaining the block samples. My thanks also go to M. Coulthard, B.Sc., for his assistance during the block sampling and also his advice on the Geological aspects of this thesis.

Much of the apparatus used for the experimental work was manufactured in the Departmental Workshop, and I am grateful to W.C. Parsons (Chief Technician) and his staff for their cooperation.

Much of this thesis has been written since the author has been an employee of Ove Arup and Partners. I must therefore also thank F.G.E. Irwin B.A., B.A.I., M.Sc., M.I.C.E., M.I.Struct.E. for his consideration and constant encouragement over the past 12 months.

Finally particular thanks go to my wife for typing the manuscript and also tracing many of the figures. I am also thankful for her understanding and constant encouragement particularly during the latter stages of this work.

NOMENCLATURE

A	Pore pressure parameter
A_s	Pore pressure parameter relevant to sampling
A_f	Pore pressure parameter at failure
a	Radius of footing
B	width of footing
C'	Apparent cohesion
C_r	Coefficient of radial consolidation
C_u	Undrained cohesion
C_v, C_{v1}	Coefficient of one dimensional consolidation
C_{v3}	Coefficient of three dimensional consolidation
E	Young's (elastic) Modulus
E'_v	Effective stress Young's Modulus in vertical direction
E'_h	Effective stress Young's Modulus in horizontal direction
e	Voids ratio
e_o	Initial voids ratio
G	Shear modulus
G_{hh}	Orthotropic shear modulus in plane of isotropy
G_{hv}	Orthotropic shear modulus perpendicular to plane of isotropy
H,h	Height
i	Hydraulic gradient
K	Stress ratio - ratio of radial to axial effective stresses
$\overline{K}$	Incremental stress ratio
K_o	Coefficient of earth pressure at rest
K_p	Coefficient of passive earth pressure
M	Deformation modulus (tangent)
M_a	Axial deformation modulus
M_v	Volumetric deformation modulus

m	Modulus number
m_v	Coefficient of volume compressibility
n	Modulus ratio (Young's)
Q	Point load
q	Load intensity
S	Degree of saturation
t	Time
T	Time factor
u	Pore water pressure
w	Water content
Z	Depth

γ	Unit weight of soil
γ_w	Unit weight of water
ε_a	Axial strain
ε_r	Radial strain
ε_v	Volumetric strain
ν	Poissons ratio (isotropic)
ν_{hh}	Poissons ratio for effect of horizontal strain on the horizontal strain in the orthogonal direction
ν_{hv}	Poissons ratio for the effect of vertical strains on horizontal strains
ν_{vh}	Possons ratio for the effect of horizontal strains on vertical strains
ρ	Settlement
ρ_i	Immediate settlement
ρ_{con}	Consolidation settlement
σ	Total stress
$\sigma_{1,2,3}$	Principal stresses
σ'_a	Effective axial stress
σ'_c	Preconsolidation stress
σ_c	Cell stress

σ'_h	In-situ horizontal effective stress
σ'_k	Equilibrium stress
σ'_r	Effective radial stress
σ_t	tangential stress
σ_v	Total vertical stress
σ'_v	Effective vertical stress
τ	Shear stress
ϕ'	Angle of internal shearing resistance

CHAPTER 1

INTRODUCTION

One of the most common problems enountered by a foundation engineer is the prediction of stresses and displacements resulting from the loads transferred to a soil mass from a structure. With the present trends of higher and heavier structures the necessity for economic foundation designs is increasing. To enable the engineer to produce an economic and safe design, he must have a clear understanding of the deformational behaviour of the foundation soil.

In the past research studies of clays have generally been heavily biased towards the determination of their shear strength. However, for overconsolidated clays in particular, the criterion for foundation design is usually one of settlement and not bearing capacity failure, i.e. the shear strength.

London clay has been studied and tested far more intensively than any other overconsolidated clay, both in the laboratory and in-situ. However it is only in relatively recent years that the pre-failure deformation characteristics, both drained and undrained, have received close attention.

To study the deformational characteristics of a given soil it is necessary to carry out in-situ tests and/or a series of laboratory tests on undisturbed samples. However, because of the relative cost of these two forms of testing the laboratories studies are far more extensively used for both research and design purposes. In order to start to obtain an overall understanding of the behaviour of even one particular soil it is necessary to carry out a wide range of extensive tests on that soil.

The aim of this research programme was to begin a laboratory study of the deformational behaviour of the heavily overconsolidated Lower Lias Clay from the Gloucester area. It is noted that all the test

results reported in this thesis are from a single site at Northcot Brickworks, Blockley, Gloucestershire.

As the investigation was carried out on undisturbed samples it was necessary to consider the effects of sample disturbance. Therefore the effects of the change of stress on an element due to sampling and the effects of mechanical disturbance on the mechanical properties of soils are reviewed in Chapter 2.

The methods of determining the stresses induced below loaded foundations and the available methods of predicting the magnitude of settlement are discussed in Chapter 3. The methods of determining the deformation characteristics are also reviewed in that chapter.

The geological history of the sampling site and the methods of sampling, storage and in-situ measurements are presented in Chapter 4 together with the determined physical properties of the material.

The testing programme carried out to study the deformational behaviour of Lower Lias clay in both the oedometer and the triaxial apparatus under various loading conditions (stress paths) and to investigate the effects of sampling method (disturbance) is presented in Chapter 5. The testing apparatus including a new independent stress triaxial cell is also described in this chapter.

The results of the oedometer and triaxial tests are presented respectively in chapters 6 and 7. A comparison of these results is made in Chapter 8. The final summary and conclusions of the project together with further suggestions for future research arising from this thesis are presented in the ninth and final chapter.

The general layout of the thesis takes the form of the text of each chapter followed immediately by the relevant Tables, Figures and Plates respectively. Certain appendices referred to in the text are collected together at the end of this thesis.

CHAPTER 2

IN-SITU STRESS, SAMPLING AND SAMPLE DISTURBANCE

2.1 IN-SITU STRESSES

It is not possible to directly measure the in-situ stresses in a natural deposit of soil, as the installation of measuring devices necessitates disturbance of the ground, and hence induces stress changes. The stresses are, therefore, computed from parameters that can be measured from soil samples. In homogeneous soils the total in-situ vertical stress (σ_v) is generally accepted as being equal to the product of the depth (Z) and the unit weight of the overlying soil (γ), fig. 2.1:

$$\sigma_v = \gamma.Z \qquad (2.1)$$

If the free water surface is present at a depth H, below ground level, then the effective vertical stress (σ'_v), below the free water surface and in the capillary zone above, is given by:

$$\sigma'_v = \gamma.Z - (Z-H)\,\gamma_w \qquad (2.1a)$$

However, the horizontal stress (σ'_h) is not so readily computed, as it is dependent on the processes of the geological evolution of the soil, in which the continuously changing stress conditions play a prominent role. Natural sedimentary soils are generally deposited, at a very slow rate, in almost horizontal layers of considerable lateral extent, thus the consolidation which takes place, due to the weight of the succeeding overburden, is virtually one-dimensional, i.e. with zero lateral strain. The ratio of horizontal and vertical effective stresses in this condition is termed the 'coefficient of earth pressure at rest' (or 'the coefficient of lateral stress at rest') K_o, where

$$K_o = \sigma'_h/\sigma'_v \qquad (2.2)$$

and is virtually constant during the virgin loading. Many researchers

have attempted to measure K_o in the laboratory, predominantly for remoulded soils. The first documented attempt was made by Donath 1891, although at this time the principle of effective stress was not appreciated. Terzaghi (1920) obtained a value of 0.42 for coarse sand using a friction tape method and later in 1925 reported values of 0.70 for two clays using a modified version of the same equipment. Work by Jaky (1944) led him to suggest a relationship between K_o and the angle of internal shearing resistance, ϕ' (in terms of effective stress) such that $K_o = 1-\sin \phi'$. Published results of Bishop (1958), Simons (1958), Sowa (1963), Brooker and Ireland (1965) and, Henkel and Wade (1966), using much more sophisticated equipment, showed that this relationship gives good agreement for normally consolidated clays, fig. 2.2, although Brooker and Ireland showed preference to the expression $K_o = 0.95 - \sin \phi'$.

Many deposits have in their geological history had much of their overburden eroded. Thus the vertical effective stress was reduced, swelling took place in the vertical direction, under zero lateral strain conditions and hence changes in the lateral stress resulted. Although no direct measurements of the horizontal stresses have been recorded in-situ, Langer (1936) for example, observed that in a clay mine in Provins, east of Paris, horizontal timber struts were crushed after a period of three months, at a depth of approximately 40 m. He estimated the horizontal stress to be in the order of 2500 kN/m^2 (25ton/ft^2), far exceeding the in-situ vertical stress, which was estimated to be in the order of 800 kN/m^2. Similar incidents were reported by Bjerrum (1967) in the upper crust of the Norwegian marine clay. Smith and Redlinger (1957) reported that saw cuts 80 mm wide by 2 m deep, made at a depth of 25 m in the Fort Union clay shales closed in 24 hours, indicating a rapid relief of high horizontal

stresses. Observations were made in Canada on the Bearspaw shales (essentially the same material as the Fort Union clay shales in the USA) by Peterson (1959), in a pilot heading at 20 m depth. The heading was braced right round, and vertical and horizontal pressures were measured with load gauges from the moment the heading was made. Observations made over four years, gave the total vertical stress as 340 kN/m^2 (3.4ton/ft^2) the pore pressure as 60 kN/m^2 (0.6 ton/ft^2) and the total horizontal stress of 500 kN/m^2 (5 ton/ft^2) thus giving K_o = 1.57. This was probably low as some relief of the horizontal stresses must have taken place during construction.

Large horizontal stresses in overconsolidated soils have been demonstrated in the laboratroy, as early as 1936, by Kjellmann. Using a triaxial apparatus he obtained K_o values for a sand of 0.5 during loading with values approaching 1.5 during unloading. Brooker and Ireland (1965) published results of oedometer tests, with horizontal stress measurements, on five remoulded clays, consolidated to a vertical stress of 15000 kN/m^2 before unloading, fig. 2.3 shows their plot of σ'_h against σ'_v for a sample of remoulded London Clay. Bjerrum (1967) pointed out that the slope of the rebound curve (Fig. 2.4a) depended on the amount and strength of diagenetic bonds formed between the solid particles during its geological history. For tests on a remoulded soil the diagenetic bonds will be minimal because the period under high stress is very small compared to that which the original soil experienced during the process of its formation. Therefore the tendency to swell during unloading of such a soil is greater than in-situ fig. 2.4(a), and thus, for any given overconsolidation ratio, higher horizontal stresses would be expected in the laboratory than in the field fig. 2.4 (b). This precludes the use of the above type of test as a method of prediction of the in-situ horizontal stresses in overconsolidated soils. Skempton (1961) suggested a method of determination

of the in-situ horizontal stress based on the measurement (in the laboratory) of the effective stress existing in an undisturbed specimen and the consideration of the stress changes during sampling, this is considered in the following two sections.

2.2 CHANGES IN STRESSES DUE TO SAMPLING

When a specimen of soil is removed from the ground it undergoes significant stress changes. Both vertical and horizontal total stresses are released and hence the sample will tend to expand. If sampling is a quick (undrained) operation expansion is arrested by the creation of negative pore pressure, (due to capillary pressure). Before considering the stress changes in detail it is necessary to make the following assumptions:

a) that there is no mechanical disturbance due to the sampling and handling,

b) that the absorption of free water is negligible during sampling (undrained), thus there is no change in water content and

c) that the suction induced in the pore water by the release of the total stresses does not produce cavitation.

The change in pore pressure induced by the change in total stresses, under undrained conditions for a saturated clay, was expressed by Skempton (1960), and revised by Henkel and Wade (1966), as

$$\Delta u = \frac{1}{3}(\Delta\sigma_1 + \Delta\sigma_2 + \Delta\sigma_3) + \alpha \Delta\sqrt{(\sigma_1 - \sigma_2)^2 + (\sigma_2 - \sigma_3)^2 + (\sigma_3 - \sigma_1)^2} \quad (2.3)$$

where σ_1, σ_2 and σ_3 are the three principal stresses, and $\alpha = -D/C$, where D and C are coefficients of dilatancy and compressibility respectively. However, for the axially symetric case where $\sigma_2 = \sigma_3 = \sigma_r$, (the radial stress) and $\sigma_1 = \sigma_a$, (the axial stress)

the equation reduces to,

$$\Delta u = \tfrac{1}{3}(\Delta\sigma_a + 2\Delta\sigma_r) + \alpha\sqrt{2}\,\Delta|\sigma_a - \sigma_r| \qquad (2.4)$$

Since that part of the pore pressure change associated only with the change of shear stress cannot be dependent on the sign of the shear stress, the positive root must be used in equation (2.3) or the module of the deviator in equation (2.4). The term $\alpha\sqrt{2}$ is numerically equal to the more familiar term $(A-\frac{1}{3})$ (Skempton 1954), where A is the pore pressure coefficient associated with the change in deviatoric stress. Equation (2.4) then becomes

$$\Delta u = \tfrac{1}{3}(\Delta\sigma_a + 2\Delta\sigma_r) + (A - \tfrac{1}{3})\,\Delta|\sigma_a - \sigma_r| \qquad (2.5)$$

The stresses acting on an element of saturated clay under in-situ conditions and after "perfect" sampling are summarised in Table 2.1.

Table 2.1

		IN-SITU	SAMPLED
Total Stress	Vertical	σ_v	0
	Horizontal	σ_h	0
Pore Pressure		u_o	u_k
Effective Stress	Vertical	$\sigma'_v = \sigma_v - u_o$	$\sigma'_a = 0 - u_k$
	Horizontal	$\sigma'_h = K_o\,\sigma'_v$	$\sigma'_r = 0 - u_k$

Note: sufficies 'v' and 'h' are used for in-situ stress, corresponding to the vertical and horizontal directions, while sufficies 'a' and 'r' are used for labortory specimens corresponding to axial and radial directions.

A perfect sampled specimen, thus, experiences a change in the total axial stress, $\Delta\sigma_a = 0-\sigma_v$, and a change in the total radial stress, $\Delta\sigma_r = 0-\sigma_h$, which induces a change in pore pressure of $\Delta u = u_k - u_o$.

If these stress changes are substituted into equation (2.5) it becomes

$$u_k - u_o = \tfrac{1}{3}\,(-\sigma_v - 2\sigma_h) + (A_s - \tfrac{1}{3})\,|-\sigma_v + \sigma_h| \qquad (2.6a)$$

where A_s is the pore pressure coefficient, A, relevant to sampling. In terms of effective stresses and pore pressures, equation (2.6a) becomes (Skempton and Sowa, 1963)

$$u_k - u_o = -\tfrac{1}{3}\,\sigma'_v\,(1+2K_o) - u_o + \sigma'_v\,(A_s - \tfrac{1}{3})\,|K_o - 1| \qquad (2.6b)$$

and hence

$$u_k = -\sigma'_v\left[(1 + 2\,K_o)\,/3 - (A_s - \tfrac{1}{3})\,|K_o - 1|\right] \qquad (2.6c)$$

For normally consolidated and lightly overconsolidated clays, where $K_o < 1$, equation (2.6c) becomes:

$$u_k = -\sigma'_v\left[(1 + 2\,K_o)\,/3 - (A_s - \tfrac{1}{3})\,(1 - K_o)\right] \qquad (2.7a)$$

For heavily overconsolidated clays, where $K_o < 1$, equation (2.6c) becomes:

$$u_k = -\sigma'_v\left[K_o - A_s\,(K_o - 1)\right] \qquad (2.7b)$$

Hence the isotropic effective stress, σ'_k (often called the capillary or equilibrium stress) existing on the sampled specimens would be, for normally consolidated and overconsolidated samples, respectively

$$\sigma'_k = \sigma'_v \left[(1 + 2 K_o) /3 - (A_s - \tfrac{1}{3}) (1 - K_o) \right] \qquad (2.8a)$$

and

$$\sigma'_k = \sigma'_v \left[K_o - A_s (K_o - 1) \right] \qquad (2.8b)$$

It is perhaps unfortunate that equation (2.5) is better known in the form

$$\Delta u = \Delta\sigma_3 + A(\Delta\sigma_1 - \Delta\sigma_3) \qquad (2.5a)$$

(Skempton 1954) which is only valid for the case when σ_a and σ_r are the major and minor principal stresses (σ_1 and σ_3), respectively and the changes of total stress are positive. The use of this form of equation (2.5) has led to several publications, (e.g. Noorany (1963)) and Noorany and Seed (1965)), concerning stress changes due to sampling, to develop incorrect relationships between the equilibrium stress, σ'_k, and the in-situ stresses.

2.3 INDIRECT METHOD FOR THE DETERMINATION OF K_o (SKEMPTON)

Skempton (1961) proposed a method for the determination of the in-situ value of K_o from the equations (2.8) developed in the previous section and laboratory tests on 'undisturbed' samples to determine the pore suction u_k and the pore pressure coefficient A relevant to sampling, A_s. Skempton suggested four methods by which u_k could be determined, one employing the standard oedometer apparatus, and the others using the triaxial apparatus.

2.3.1 Measurement of Equilibrium Stress

(a) Oedometer test - load found which just prevents change of height (volume change) when the oedometer specimen is brought into

contact with free water. In the oedometer, when no swelling or consolidation is permitted the change in pore pressure is equal to the change in axial stress, therefore the resulting stress, $(\sigma_a)_o$, is taken as being numerically equal to the original suction in the specimen, u_k.

(b) Isotropic consolidation/swelling in the triaxial apparatus - at various isotropic stress levels volume changes are measured; under low stresses the sample swells, whereas under higher stresses it consolidates. By interpolation the 'swelling pressure' corresponding to zero volume change can be readily found, and is taken as equal to the original suction.

(c) Measurement of pore pressure under isotropic stresses in the triaxial apparatus - a cell pressure is applied under undrained conditions and the pore pressure recorded. The original suction in the sample is taken as equal to the cell pressure less the recorded pore pressure providing the sample and system are saturated.

(d) Conventional undrained strength test in the triaxial apparatus - For a saturated clay the undrained cohesion intercept $c_u = \frac{1}{2}(\sigma_a - \sigma_r)_f = \frac{1}{2}(\sigma'_a - \sigma'_r)_f$ therefore it can be shown that:

$$c_u = c' \frac{\text{Cos } \phi'}{1-\text{Sin}\phi'} + (\sigma'_r)_f \frac{\text{Sin } \phi'}{1-\text{Sin } \phi'} \qquad (2.9)$$

where c' and ϕ' are the drained shear strength parameters and $(\sigma'_r)_f$ is the minor principal effective stress at failure. The effective minor principal stress at failure is equal to

$$(\sigma'_r)_f = \sigma'_k - \Delta u_f \qquad (2.10)$$

where σ'_k is the equilibrium stress and Δu_f is the change in pore pressure during shearing. Also, since during shearing

$$\Delta\sigma_r = 0$$

then

$$\Delta u_f = A_f \left|\Delta\sigma_a - \Delta\sigma_r\right|_f$$

$$= A_f (2c_u)$$

therefore

$$\sigma'_r = (\sigma'_r - 2A_f c_u) \qquad (2.11)$$

Hence with the value of c_u from the quick undrained test and if A_f, c' and ϕ' are known from other test results, σ_k can be obtained by substituting equation (2.11) into equation (2.9) thus

$$c_u = c' \frac{\text{Cos } \phi'}{\text{Sin } \phi'} + (\sigma'_k - A_f c_u) \frac{\text{Sin } \phi'}{1-\text{Sin } \phi'}$$

2.3.2 Determination of Pore Pressure coefficient, A_s

The pore pressure parameter A_s relevant to sampling is in general not equal to the parameter at failure, A_f. It is therefore necessary to determine A_s under stress changes that represent the in-situ condition. Skempton (1961) proposed that a special triaxial test be performed where a sample is reconsolidated to the expected in-situ effective stresses, using a triaxial cell with a plunger and sample of the same diameter. The specimen is 'sampled' by reducing the stresses to a hydrostatic value in an undrained manner. The change in pore pressure is recorded and the pore pressure parameter, A_s, determined from equation (2.5). However Skempton did not report results from such tests. In this thesis A_s is measured by such methods and reported in Chapter 7.

2.3.3 Summary

Table 2.2 (below) gives a summary of the results obtained by Skempton using the four methods. Som (1968) used methods (a) and (c) to determine σ'_k, but, as Skempton, did not favour the oedometer method.

Som showed that despite no apparent swelling of the sample there was an increase in the water content, and in general low values of σ'_k were obtained. The results of similar tests are described in chapters 6 and 7 of this thesis.

Table 2.2

Depth m	σ'_v KN/m^2	EQUILIBRIUM STRESS, σ'_k by method a	b	c	d	Av	$\frac{\sigma'_k}{\sigma'_v}$
3.35	35	67 100	81	-	91	86	2.4
6.10	63	-	110	124	120	120	1.9
7.01	68	-	120	-	144	132	1.9

Skempton (1961) used results from the quick undrained test to determine the variation of K_o with depth for London clay at Bradwell, Essex. As shown in Fig.2.5 he obtained values ranging from 1.46 to 2.80, also shown on this figure are values of the coefficient of passive earth pressure, K_p, as obtained from the expression

$$K_p = \frac{c'}{\sigma'_v} \quad \frac{2\cos\phi'}{1-\sin\phi'} + \frac{1+\sin\phi'}{1-\sin\phi'}$$

It can be seen that $K_o \simeq K_p$ over the depth range of 8m to 13m, i.e. within that range the soil seems to be in the state of limiting equilibrium induced by reduction of the vertical in-situ stress. If this is the case then any further reduction in σ'_v would not increase the value of K_o which remains approximately equal to K_p.

2.4 METHODS OF SAMPLING

It is not intended here to make a comprehensive review of sampling methods, this may be found elsewhere, e.g. Hvorslev (1949), but only to indicate the general methods used for obtaining 'undisturbed' samples of heavily overconsolidated clays.

The most common method of sampling cohesive soils is by the open-tube sampler. The sampler is either hammered or, preferably, jacked into the ground. The quality of the sample obtained depends not only on the method by which the sampler is introduced but also on its geometry and inside and outside friction. The geometry of a sampler is usually defined by the following three parameters

(a) Area ratio (A_r) - represents the volume of soil displaced by the sampler in proportion to the volume of the sample and is defined as:

$$A_r = \frac{D_w^2 - D_c^2}{D_c^2} \times 100$$

where D_w is the maximum outside diameter of the cutting shoe

and D_c is the inside diameter of the cutting shoe

(b) Inside clearance, C_I

$$C_I = \frac{D_s - D_c}{D_s} \times 100$$

where D_c is as defined above and

D_s is the inside diameter of the sample tube.

C.P. 2001 (1957) recommends that the inside clearance should be in the order of 1 to 3%

(c) Outside clearance

$$C_o = \frac{D_w - D_T}{D_T} \times 100$$

where D_W is as defined in (a) and

D_T is the outside diameter of the sample tube.

C.P. 2001 (1957) recommends that $C_O \nmid C_I$

A_r should be kept as low as possible, C.P. 2001 (1957) recommended that for routine work it should not exceed 25%.

The internal friction of the tube can be reduced by a suitable inside clearance, a smooth finish to the sample tube and lubrication, this reduces disturbance to the sample as it enters the tube. Ward et al (1959) recommended that, for a stiff fissured clay, it was preferable not to have an inside clearance, as this increased the possibilities of the samples breaking up.

The other principle method of 'undisturbed' sampling of over-consolidated clays is by rotary drilling. Samples are obtained in this method by rotating the core barrel and bit to grind away an annulus of soil, which is flushed out by circulating water, air or drilling mud, the core sample then enters the core barrel and is finally retrieved. The simplest core barrel is the single tube core barrel, which is not really suitable for 'undisturbed' samples as the ciruclating fluid is in direct contact with the sample. It is thus normal to use the double tube core barrel which carries a stationary inner tube, to protect the core from the circulating water and from rotation of the outer tube and bit. Therefore the torsion transmitted to the core, and attendant danger of breaking it, are reduced.

Hand cut block samples are sometimes taken, but normally only for special jobs and research because of the expense involved. These can only be taken from excavations, shafts and tunnels where blocks can be excavated and trimmed with the minimum of mechanical disturbance.

2.5 EFFECTS OF SAMPLING

The process of soil sampling for laboratory testing produces 'sample disturbance', thus the soil parameters obtained in the laboratory may not be representative of the in-situ soil mass. The cause of this disturbance can, basically, be divided into two catagories:

(a) change of stress state and

(b) mechanical disturbance

2.5.1 Perfect Sampling

The changes in the stress state of an element of soil due to 'perfect' sampling was considered in Section 2.2. The effect of these stress changes can only be investigated in the laboratory, with laboratory produced 'field' specimens in the triaxial apparatus. Specimens can then be tested directly from 'field' condition without sampling, or be subjected to 'perfect' sampling followed by axi-symmetric loading.

The effects of stress relief, due to perfect sampling has been considered and reported, notably by Skempton and Sowa (1963), Noorany and Seed (1965), Ladd and Varallyay (1965), and, Davis and Poulos (1967), on various normally consolidated clays. It is seen from these results that such sampling only produces a small reduction (<20%) of the undrained shear strength on normally consolidated soils (Fig. 2.6 and 2.7). However Davis and Poulos (1967) showed that this error could be reduced by reconsolidating under 'K_o' conditions to the 'field' overburden stress (Fig. 2.7). Skempton and Sowa's (1963) results for a laboratory overconsolidated sample (K_o = 1.35) indicated that 'perfect' sampling has a negligible effect on the undrained strength (Fig. 2.6), this may not be true for higher values of K_o.

The stress paths (Fig. 2.6 and 2.7) clearly indicate the effect of 'perfect' sampling on the pore pressure parameter A. It was generally shown that A was reduced by 50%, however Davis and Poulos's (1967) results indicated that reconsolidation to field overburden stress under 'K_o' conditions reduces this error. The over consolidated samples (Skempton and Sowa) appear to be less sensitive to perfect sampling as seen by the closely matching stress paths (Fig. 2.6).

The undrained stress-strain relationship (Fig. 2.8) presented by Davis and Poulos (1967) for normally consolidated Kaolin demonstrates the trends suggested by Skempton and Sowa's and by Ladd's (1964) tests, that the initial tangent modulus for the 'field' element is greater than for the unconfined 'perfect' specimen. Davis and Poulos's results also show that reconsolidation under K_o conditions to the 'field' stress level produces an initial tangent modulus approaching the 'field' value. However it was found that when hydrostatically reconsolidated to the 'field' mean stress the undrained tangent modulus was well in excess of the field value.

The effect of perfect sampling on drained parameters was also observed by Davis and Poulos on normally consolidated Kaolin. They observed, for the case of one dimensional strain conditions, that the void ratio-effective stress curves of a 'perfect' sample lies below the 'field' curve (Fig. 2.9), thus indicating that the change in stress environment causes some structural disturbance. In the case of a stiffer soil this disturbance is likely to be less. The coefficient of consolidation appeared to be little affected by 'perfect' sampling.

The results of a series of triaxial tests, by Davis and Poulos are shown in Table 2.4 (below) where a single increment of axial and radial stress was applied, with a factor of safety against undrained

failure of at least 3.

TABLE 2.4

(after Davis and Poulos (1967))

Type of Specimen	Stress state prior to testing		E_u	E'	ν'	C_{v3}
	σ'_a kN/m^2	σ'_r kN/m^2	kN/m^2	kN/m^2		m^2/year
Field element	207	97	11,885	3485	0.395	20.78
K_o reconsolidated, 'Perfect specimen	207	104	10,100	3655	0.390	19.23
K_o reconsolidated, undisturbed	207	104	10,880	3740	0.380	16.34
K_o reconsolidated, remoulded	207	104	12,940	4856	0.354	13.90
'Perfect' hydrostatically reconsolidated	138	138	49,390	20625	0.075	11.43

It is seen from these results that the drained 'elastic' constants are not seriously affected (<8% error) by stress relieve, providing the sample is reconsolidated under K_o condition. The undrained modulus however is reduced by approximately 20%. Reconsolidation under the 'field' mean stress resulted in substantial errors in all reported parameters. However, it is considered that hydrastatic reconsolidation of very stiff clays would not have such serious repercussions.

2.5.2 Mechanical disturbance

Skempton and Sowa (1963) showed that mechanical disturbance further reduced the undrained strength of the 'laboratory' samples. The effect on overconsolidated clays is best illustrated by the results of various types of 'undisturbed' samples. Ward, Samuels and Butler (1959) tested block samples, which are generally recognised as being

the least disturbed 'undisturbed' sample, and driven, 38mm diameter, tube samples of London clay from the same venue. The results showed (Fig. 2.10) the tube samples to have undrained strengths 20 to 50% lower than the block samples, and undrained modulus reduced by a factor of 2 to 5 on first loading and up to 2 on second loading. Similar results were also reported by Seychuk and Adam (1971) for a heavily dessicated glacio-lacustrine clay. Ward et al reported that tube samplers with inside clearance are not suitable for sampling stiff fissured overconsolidated clays, as sample breaking occurred due to the opening of fissures. Samples of London clay recovered by hydraulically pushed tube samplers have been found (Butler and Hooper 1966) to give strengths up to 20% higher than those from driven tube samplers. Further low undrained strength values for tube samples in London clay were reported by Ward, Marsland and Samuels (1965), however it was found that rotary cored samples gave strength values comparable to the upper limits of the block samples, showing that this method of sampling can offer minimal mechanical disturbance in heavily overconsolidated clay deposits.

The effect of mechanical disturbance on the drained parameters of clays has received less attention. Several early researchers considered the effects of mechanical disturbance on oedometer results. Rutledge (1944) compared results of oedometer tests on undisturbed (hand cut samples from 12" blocks), partially disturbed and fully remoulded specimens of normally and lightly overconsolidated clays. He concluded that sampling disturbance (a) decreases the voids ratio at any given vertical stress, (b) displaces the compression curve downward from that for the undisturbed specimen and decreases the measured compression index.

Van Zeist (1948) demonstrated that laboratory preparation of oedometer samples could be a major source of disturbance, mainly from planing the end faces. Van Zeist defined the disturbance factor (m) as the ratio of disturbed to total volume of soil (V), i.e. the volume of the undisturbed soil is (1-m) V and disturbed (remoulded) soil is mV. Considering the e-log σ' plot, Fig. 2.11 one can relate the disturbance factor to the changes in voids ratio:

$$\Delta e_x = (1 - m)\,\Delta e_1 + m\,\Delta e_2$$

or

$$m = \frac{(\Delta e_x - \Delta e_1)}{\Delta e_2 - \Delta e_1}$$

If the disturbances due to trimming are represented by a thickness, x on a horizontal plane, then x = m. H. From tests on Crookston clay with specimens of various thickness, Van Zeist demonstrated that the disturbed thickness is independent of the sample thickness, hence the disturbance factor increases with decrease in sample thickness, Fig. 2.12. These results indicate that a standard 20mm sample cut from a block would have a degree of disturbance of the order of 25%.

Schmertmann (1955) suggested a method of correcting laboratory data, from the oedometer test, to estimate the true field relationship between voids ratio and effective stress. The method was based on the assumption that the virgin consolidation lines obtained from samples of various degrees of disturbance intersect at 0.42 e_o, where e_o is the field voids ratio of the sample. After establishing the laboratory e - σ'_v curve for an undisturbed sample, the field curve can be constructed using the in-situ stress and voids ratio, the preconsolidation stress and the point of intersection (0.42 e_o) on the virgin consolidation line. However this method is not likely to be successful with heavily overconsolidated soils. Davis and Poulos

confirmed the results of Rutledge, Schmertmann etc., that disturbance reduces the void ratio (Fig. 2.9) at any effective stress. The 'field' void ratio effective stress relationship is plotted according to the Schmertmann correction (Fig. 2.9), it is seen to coincide fairly well with the actual 'field' behaviour.

It is seen from Table 2.4 that increased mechanical disturbance causes the drained modulus to increase and the drained Poisson ratio to decrease. This is attributed to the decrease of void ratio due to the mechanical disturbance and is in accordance with the results of Rutledge (1944), Schmertmann (1953) and others.

These results clearly indicated that disturbed samples, even when reconsolidated to the insitu stress conditions, give erroneous values of deformation modulus. In particular hydrostatic reconsolidation to the mean effective stress can result in large errors in the deformation properties.

A further aspect of sampling, which should not go unmentioned here, is that of sample size. It has been demonstrated by many researchers (e.g. Rowe 1972) that unless the sample is sufficiently large to represent the 'fabric' of the soil then the results of laboratory tests on those samples will not be representative of the soil mass. The effect of sample size on overconsolidated clays, generally in the London clay, has received considerable attention (e.g Skempton and Henkel (1957), Bishop (1966), Bishop and Little (1967), Marsland and Butler (1967), Agarwall (1967) and Marsland (1971a)) mainly in connection with the measurement of undrained shear strength. It is seen (Fig. 2.13) that specimens with diameter less than one third the fissure spacing result in greatly overestimated values of strength.

Marsland (1971b) presented results from tests on London clay which demonstrated the effect of sample size on undrained modulus. Marsland's results indicated that the undrained modulus decreased with increase of specimen diameter (Fig. 2.14) for specimens trimmed from block samples. A further aspect brought out by these tests (Fig. 2.14) was the effect of time lapse between sampling and testing. The undrained modulus was seen to decrease with time, while the origin correction increased. Marsland reported the same effect on the modulus obtained from plate tests, where the decrease was observed to be very rapid within the first few hours after excavation. The 'time effect' has been attributed to the opening of fissures within the laboratory samples or below the test plate in the case of the in-situ tests. It is thus seen that disturbance of samples, including in-situ, is, to some extent, time dependent for heavily fissured clays.

2.6 Summary

It has been seen, for heavily overconsolidated clays, that the in-situ effective horizontal stress can be considerably greater than the effective vertical stress, with values of K_o, reported up to three or more. However, the only present method of determining the in-situ value of K_o is from laboratory tests on 'undisturbed' samples, and a consideration of the changes of total stresses and pore pressures due to its removal from the ground.

However sampling, by whatever means, causes disturbance due to changes in stress state and mechanical disturbance. The study of the effect that changes of stress have on the mechanical properties can only be carried out on laboratory prepared 'field' samples. A true 'field' element of heavily overconsolidated clay cannot be produced in the laboratory because the combined action of great loads, time and various other chemical and physical

agents cannot be reproduced (Bjerrum (1967)). Therefore the effect of stress release can only by hypothesised from the result on remoulded samples, which essentially lack stress history, and therefore must be expected to behave in a different manner.

The effect of mechanical disturbance on heavily overconsolidated clays has been reported by several authors. Most of this work has been directed towards the undrained deformation and strength, where tube sample results have been compared against hand carved block samples. In general it appears that the undrained modulus of tube samples is only 25-50% of that obtained from blocks in first loading cycles and 50% on second loading cycles. It appears from tests on 'laboratory' samples that the drained modulus is less effected by sample disturbance. Sample size has been shown to have a very significant effect on the deformation properties of material such as overconsolidated clays where the large scale 'fabric' can play an important role. Comparison with deformation moduli obtained from plate tests and also observed field deformations (Ward 1971) indicate laboratory results are generally low.

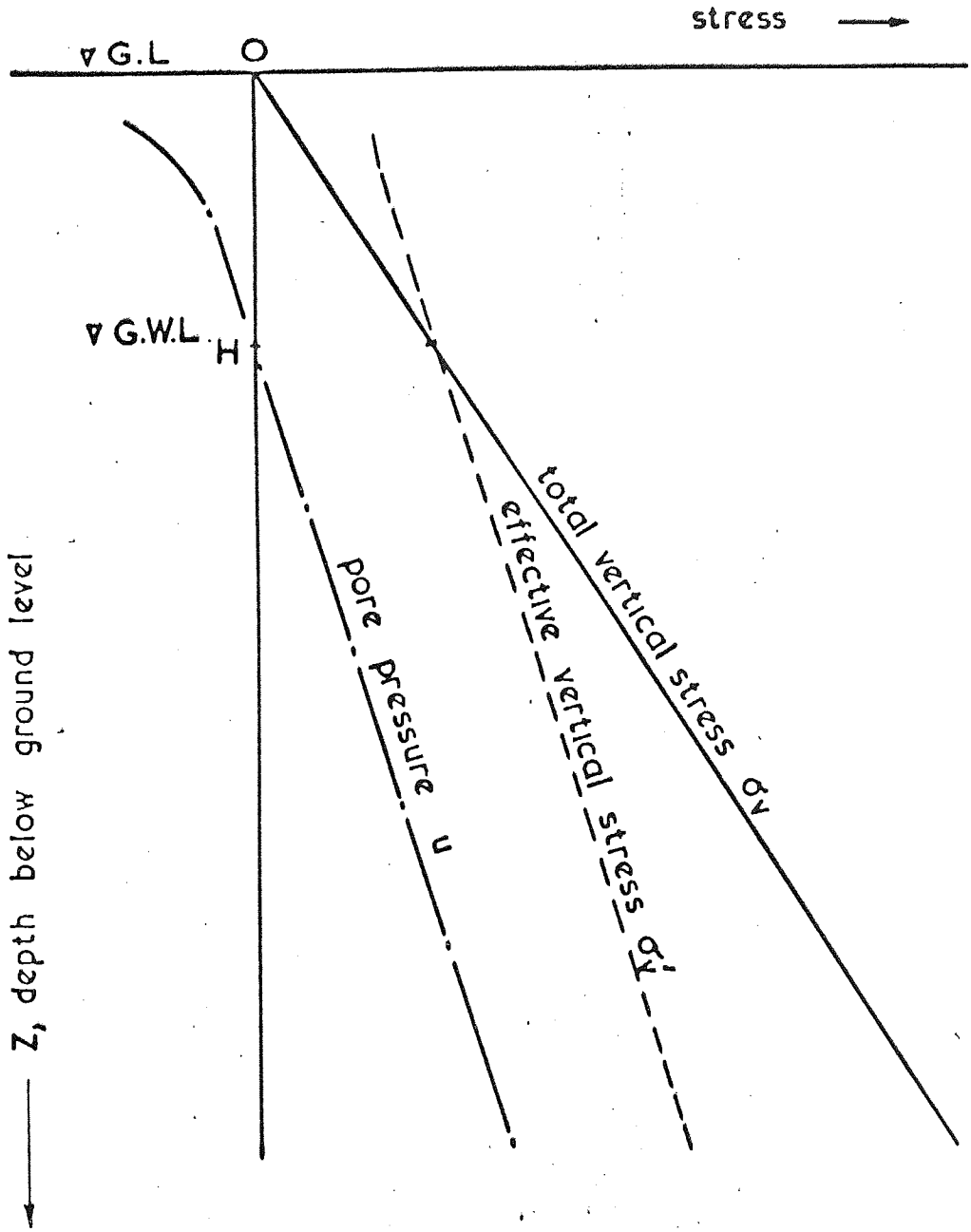

Fig. 2.1 Insitu Stresses

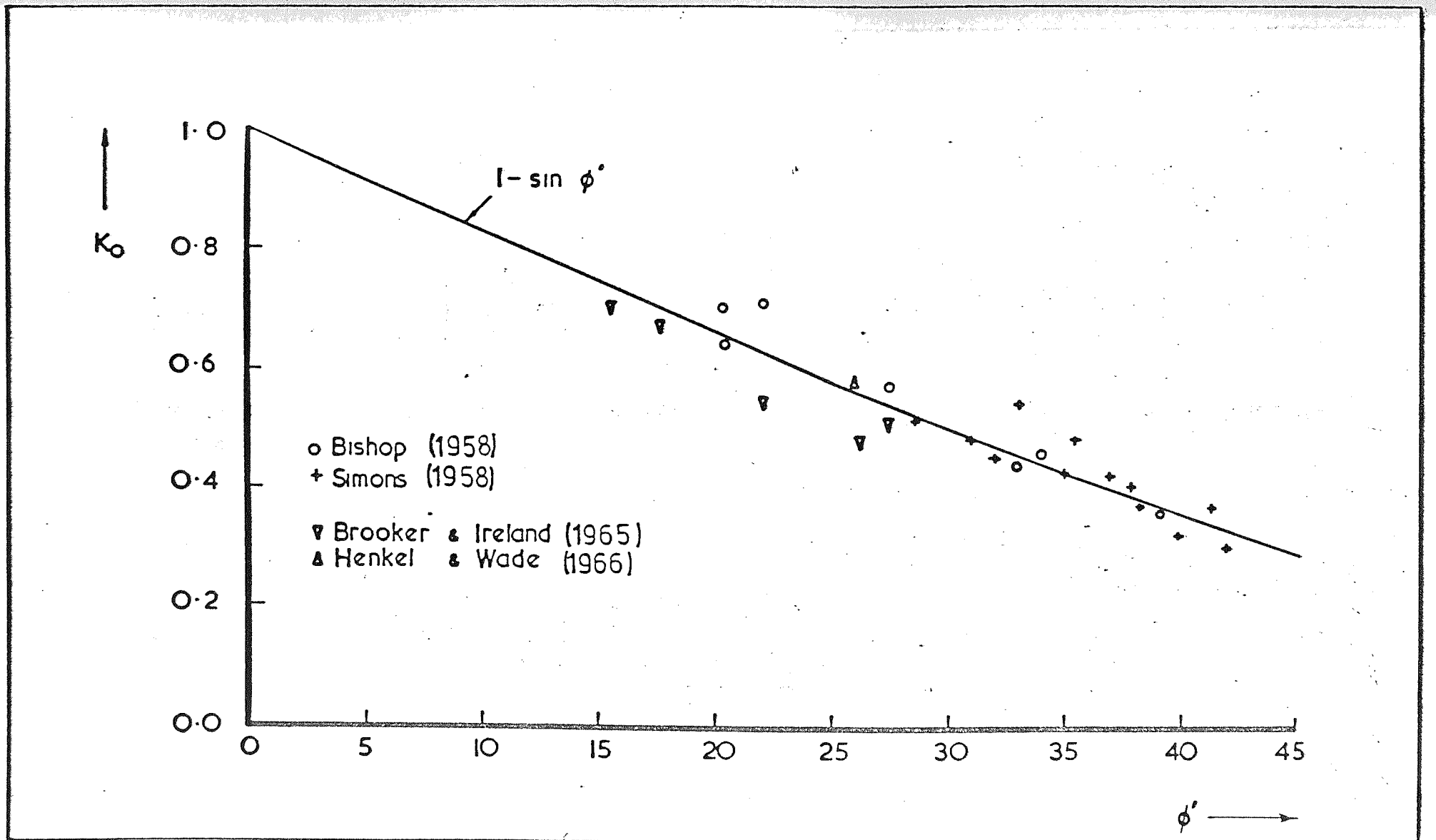

FIG. 2.2 Relationship between K_o and ϕ' for normally consolidated clays

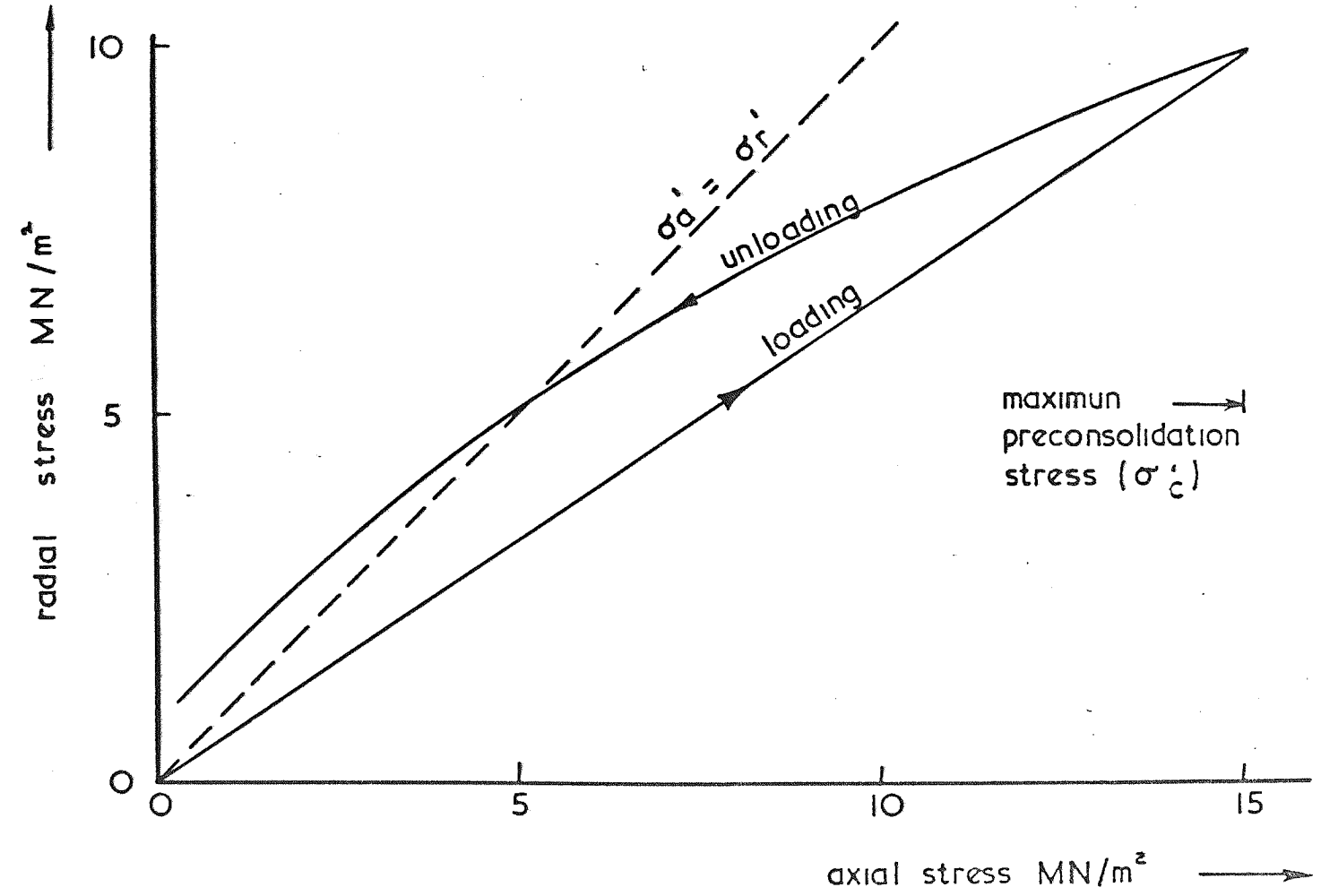

Fig 2.3 Stresses during oedometer tests on remoulded London clay (Brooker and Ireland 1965)

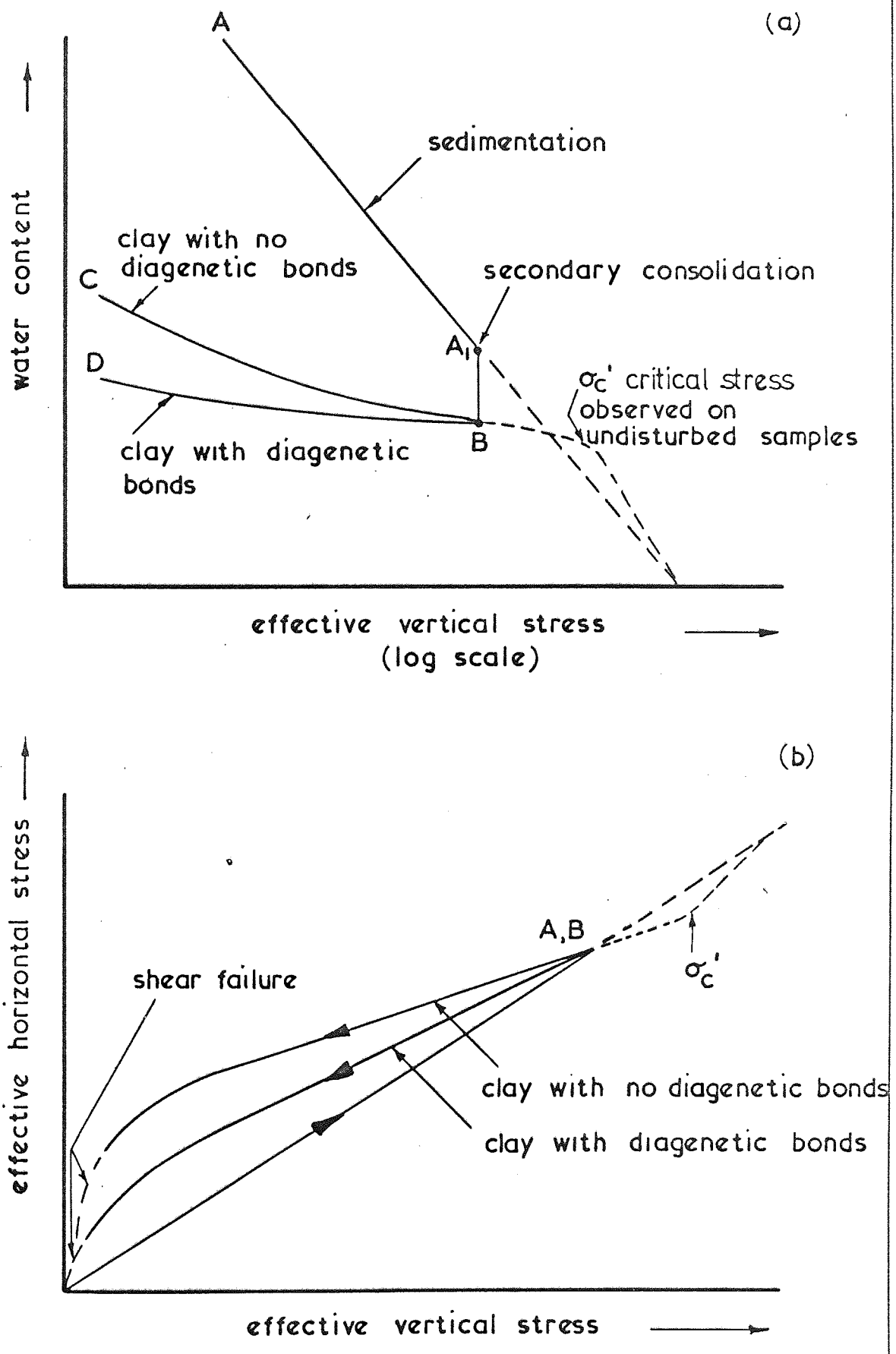

Fig. 2.4 Geological history of overconsolidated clay — Bjerrum 1967.

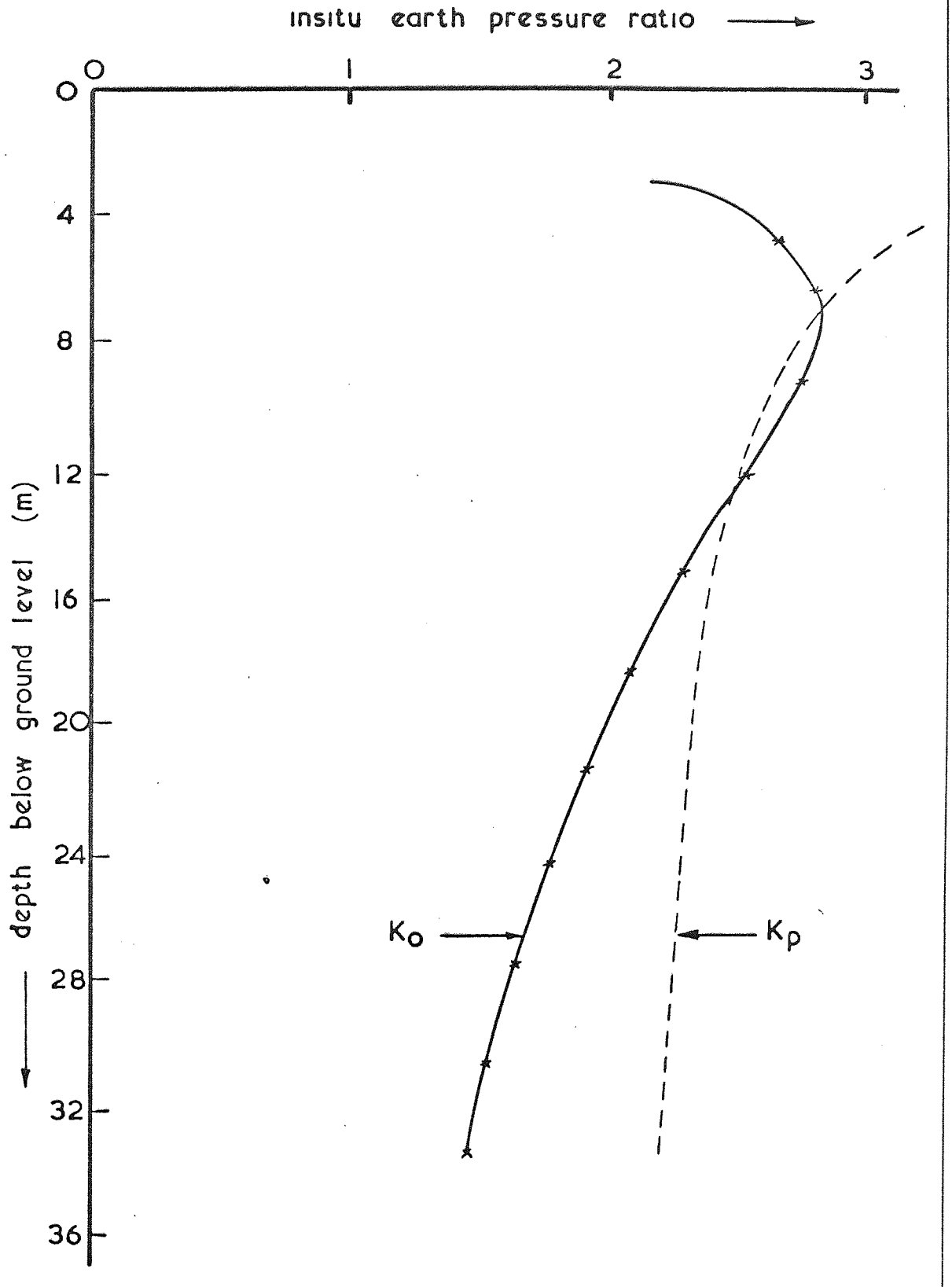

Fig. 2.5 Variations of insitu stress ratio, K_o, with depth, at Bradwell - (Skempton 1961)

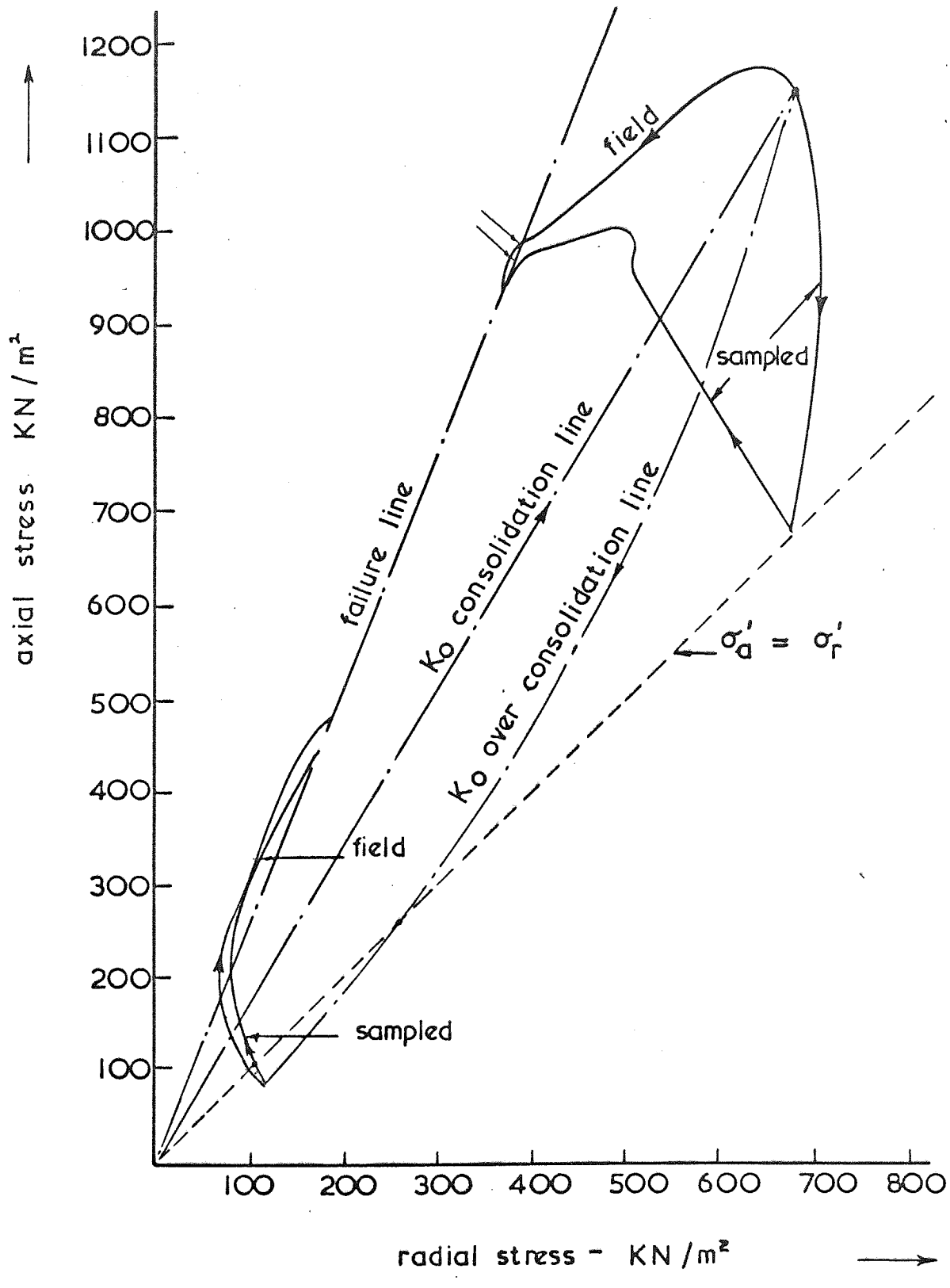

Fig. 2.6 Stress path for 'field' and 'sampled' weald clay under undrained shear. (Skempton and Sowa 1963)

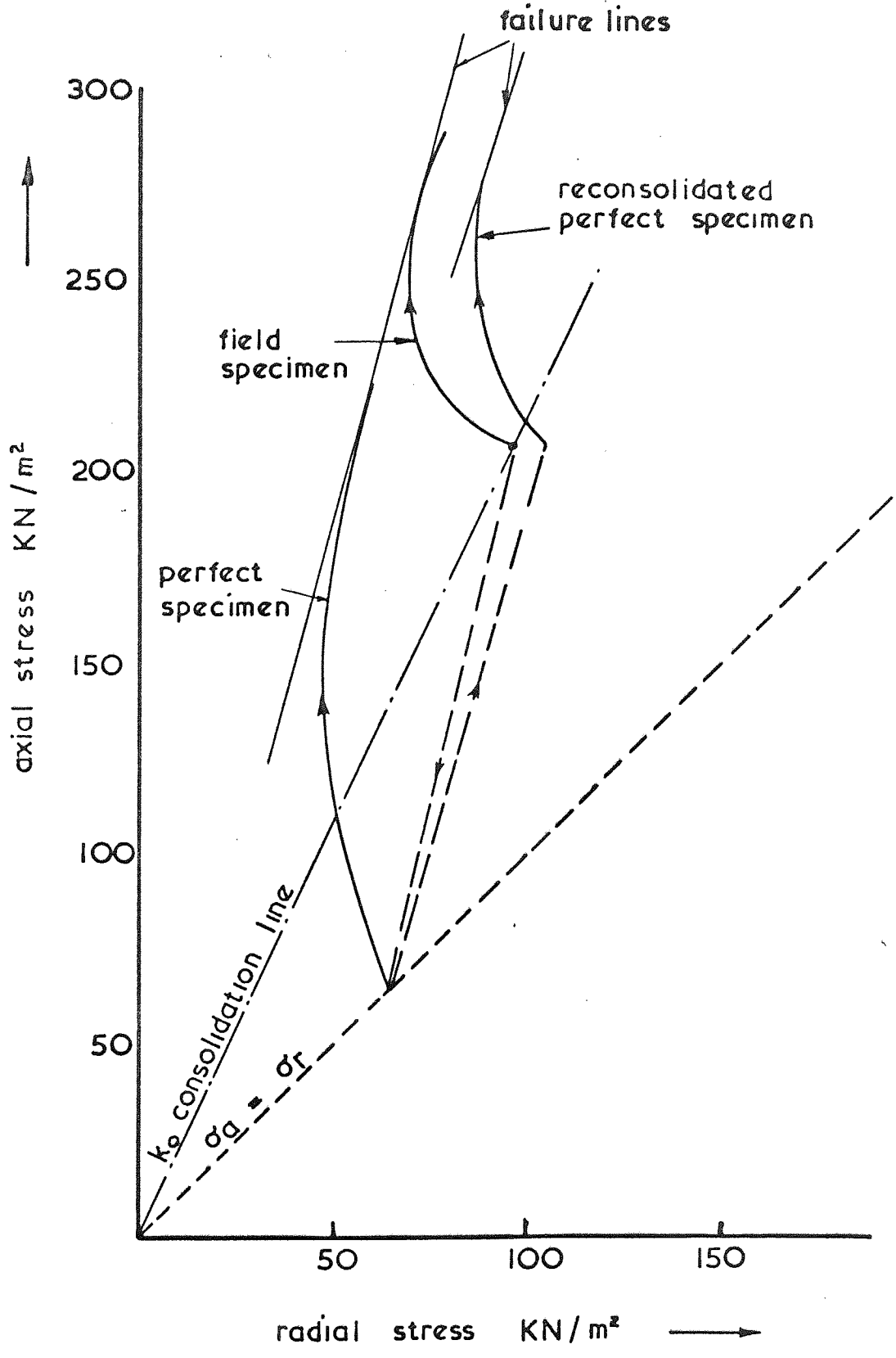

Fig 2.7 Stress path for 'field' and 'sampled' kaolin under undrained shear. (Davis and Poulos 1967)

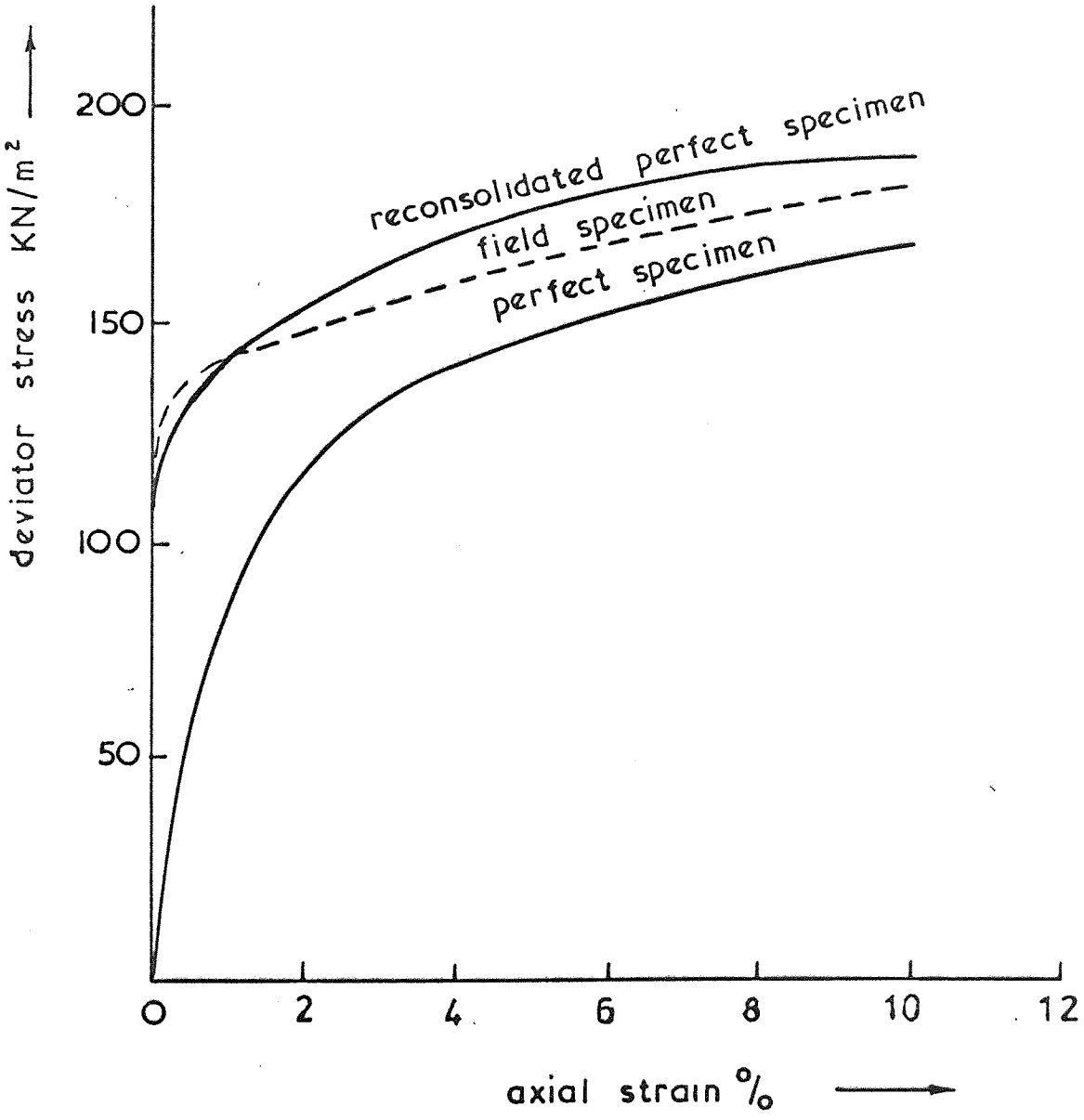

Fig 2.8 Stress - Strain curves from undrained tests on kaolin - (Davis and Poulos 1967)

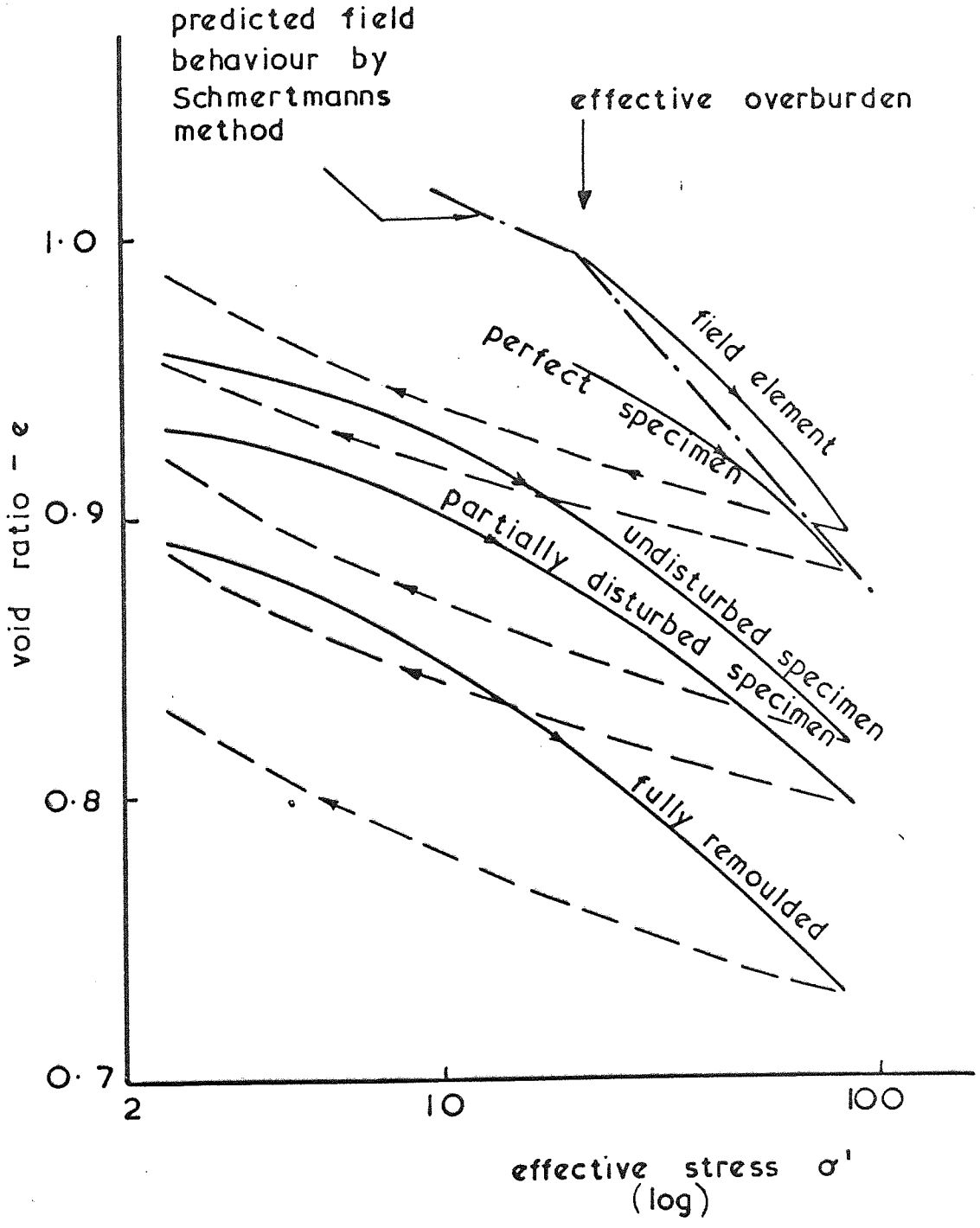

Fig. 2.9 Effective stress - void ratio plot from one - dimensional tests.
(Davis and Poulos 1967)

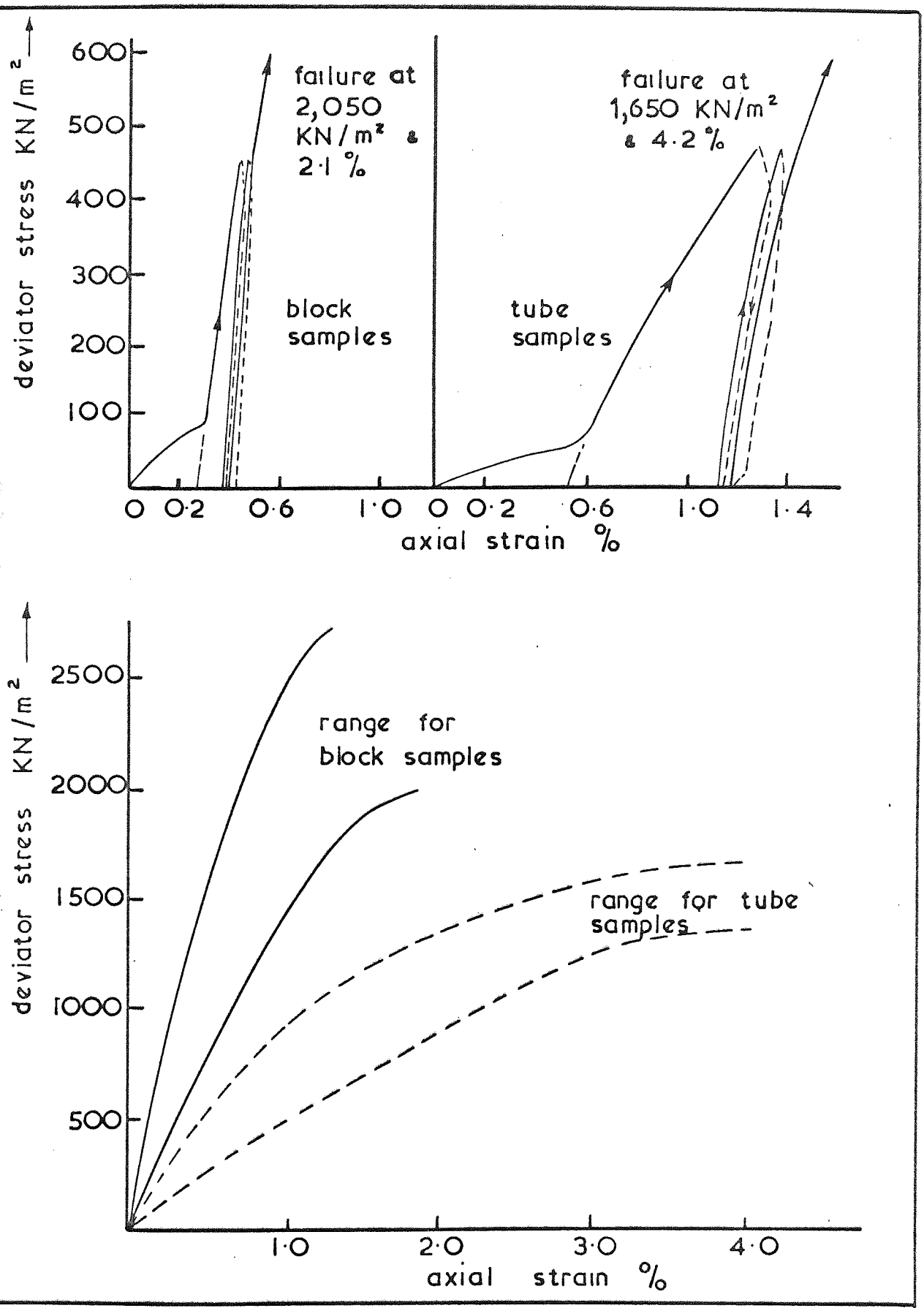

Fig 2.10 Stress - Strain plot for undrained test on London clay - (Ward et al 1959)

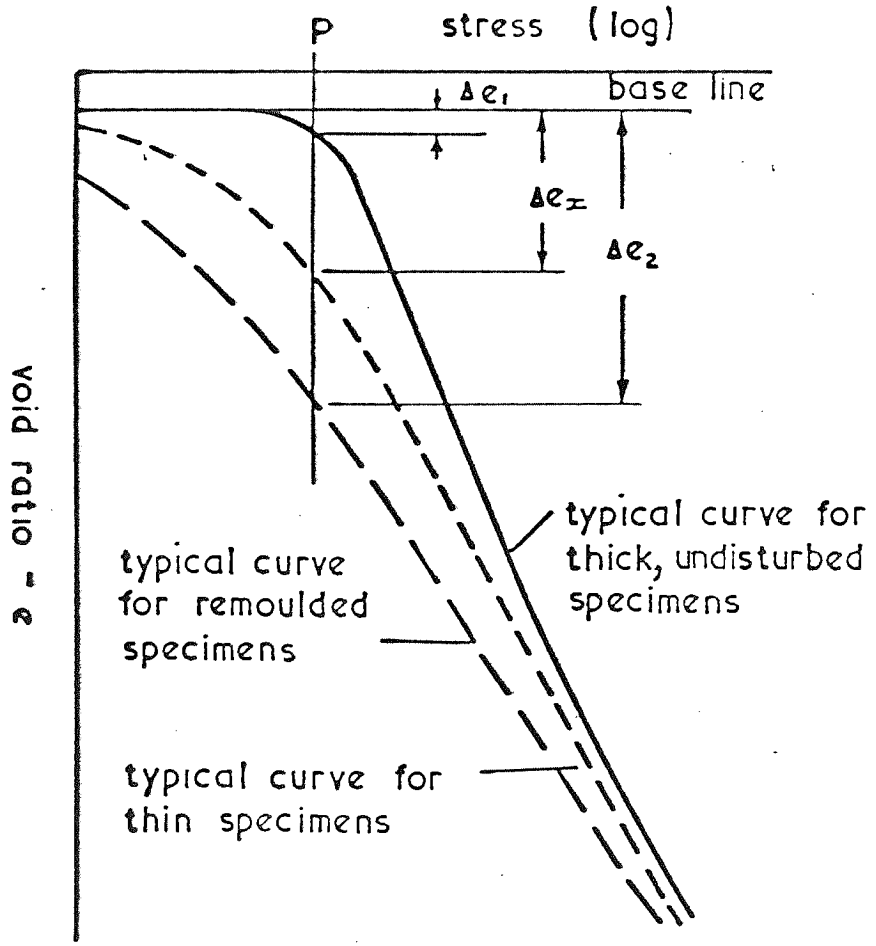

Fig. 2.11 Determination of disturbance factor - (Van Zeist 1948)

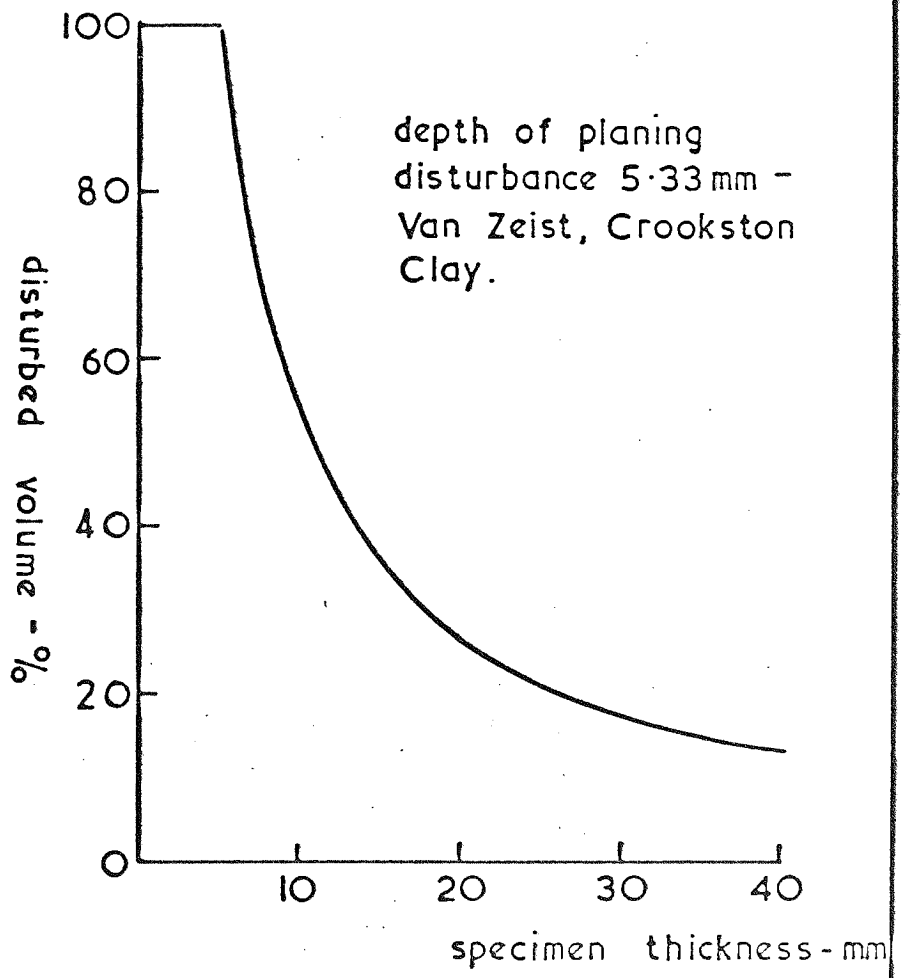

Fig. 2.12 Volume disturbance due to oedometer preparation

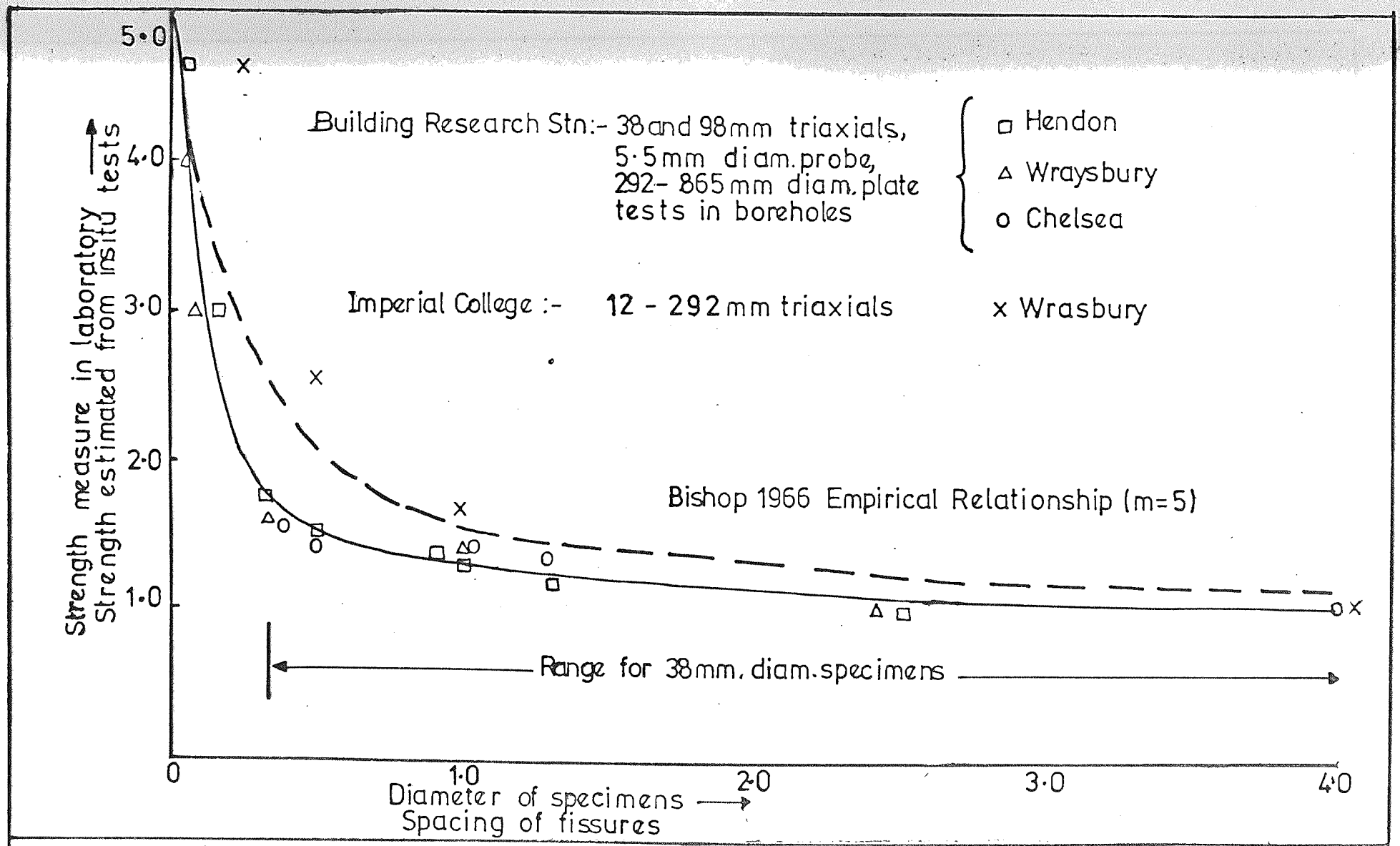

Fig. 2.13 Influence of the ratio of sample size to the fissure spacing on the strengths measured in laboratory tests

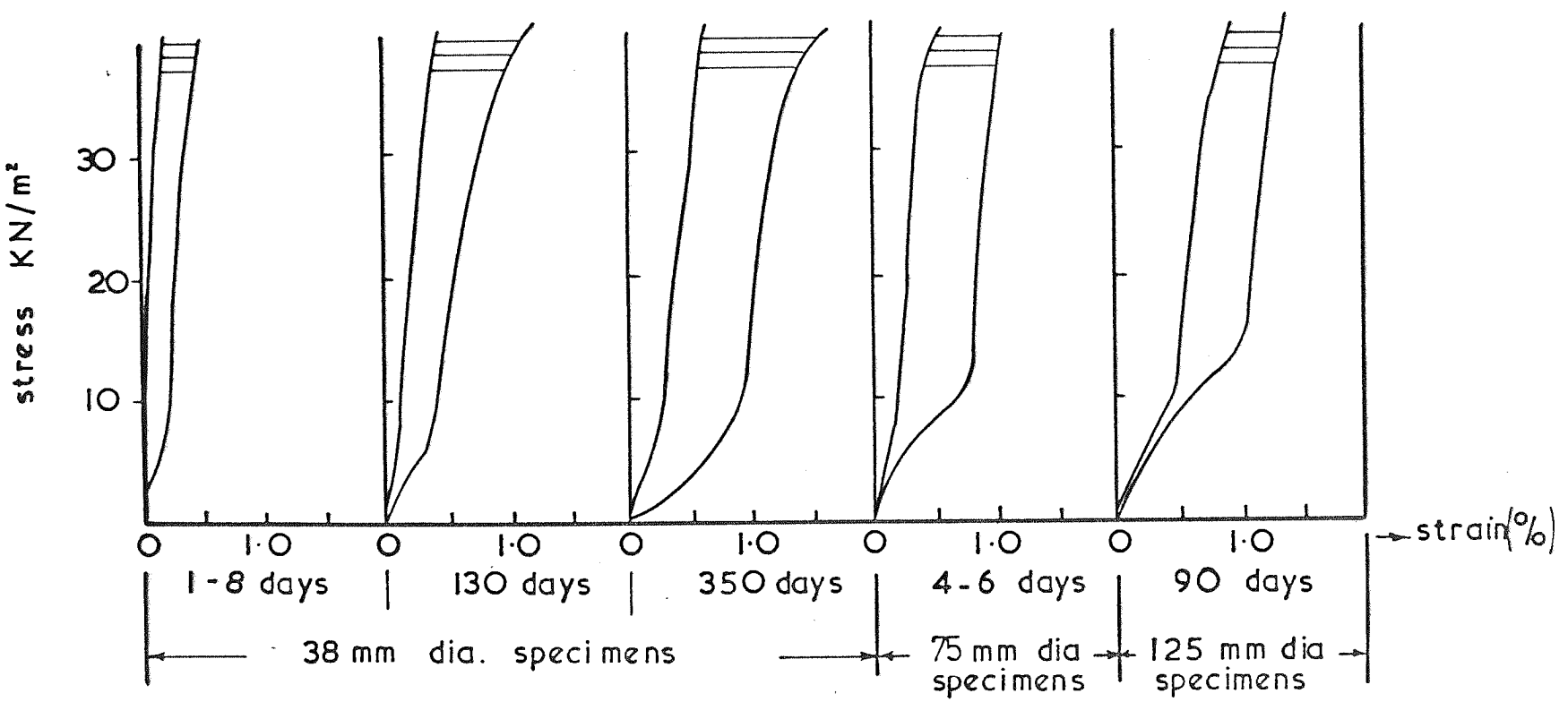

Fig. 2.14 Effect of specimen size and time from sampling on undrained stress - strain relationships for London clay. (Marsland 1971)

CHAPTER 3

SETTLEMENT ANALYSIS

3.1 INTRODUCTION

The application of surface, or subsurface, loads to the ground causes a change in the stress state within the underlying soil. The stress changes will cause the soil to deform, the resultant vertical displacement reflected at the founding level is known as the 'settlement'. In order to predict the settlement of the foundations of a structure it is necessary to determine the subsoil profile, the magnitude and distribution of stresses induced in the soil and the deformation characteristics of the soils within the significantly stressed zone.

It is intended in this chapter to review the methods available for the determination of induced stress and the subsequent settlement analyses. The available methods for the determination of the deformation parameters of soils and results of settlement observations are considered at the end of the chapter. The subject of the determination of the subsoil profile does not form part of this thesis.

3.2 STRESSES INDUCED BY FOUNDATIONS

3.2.1 Semi-infinite Homogeneous Elastic Medium

In order to analyse the stresses induced in a soil medium by the application of external loads it is necessary to make certain simplifying assumptions regarding its properties. The simplest case is to assume the soil mass to be a semi-infinite, homogeneous, isotropic and linearly elastic medium. Using these assumptions Boussinesq (1885) presented his well known expressions

$$\sigma_z = \frac{Q}{2\pi z^2} (3 \cos^5\theta) \qquad (3.1a)$$

$$\sigma_z = \frac{Q}{2\pi z^2} \left(3 \sin^2\theta . \cos^3\theta - (1-2\nu) \frac{\cos^2\theta}{1 + \cos\theta}\right) \qquad (3.1b)$$

$$\sigma_t = -\frac{Q}{2\pi z^2}(1-2\nu).\left(\cos^3\theta - \frac{\cos^2\theta}{1+\cos\theta}\right) \qquad (3.1c)$$

$$\tau_{rz} = \frac{Q}{2\pi z^2}(3\sin\theta.\cos^4\theta) \qquad (3.1d)$$

for the increments of stress within the medium due to a point load, Q, acting on the upper boundary (Fig. 3.1a). Using the principle of super position Boussinesq's equations were soon developed to cover line loads (Flamant 1892, Mitchell 1900) and distributed loads. Carothers (1920), Jurgenson (1934) and others presented solutions for symetrically loaded infinite strips; for the special case of a uniformly loaded strip of intensity, q, (Fig. 3.1b) the following expressions were obtained:-

$$\sigma_z = \frac{q}{\pi}\left[\psi - \frac{2az(x^2-z^2-a^2)}{(x^2+z^2-a^2)^2+4a^2z^2}\right] \qquad (3.2a)$$

$$\sigma_x = \frac{q}{\pi}\left[\psi - \frac{2az(x^2-z^2-a^2)}{(x^2+z^2-a^2)^2+4a^2z^2}\right] \qquad (3.2b)$$

$$\sigma_y = \nu(\sigma_z + \sigma_x) = \frac{\nu q}{\pi} 2\psi \qquad (3.2c)$$

$$\tau_{xz} = \frac{q}{\pi}\left[\frac{4ax\,z^2}{(x^2+z^2-a^2)^2+(4a^2z^2)}\right] \qquad (3.2d)$$

which on the axis of the foundation (i.e. for x = 0) reduces to

$$\sigma_z = \frac{q}{\pi}[\psi + \sin\psi] \qquad (3.3a)$$

$$\sigma_x = \frac{q}{\pi}[\psi - \sin\psi] \qquad (3.3b)$$

$$\tau_{xz} = 0 \qquad (3.3c)$$

The distribution of the induced stresses with depth along the axis

of symmetry of a strip foundation is shown in figure 3.2a. Similar expressions were obtained by Love (1928) for stresses induced below a circular footing, which on the axis of symmetry may be written (fig. 3.1c) as:-

$$\sigma_z = q\left[1-\cos^3\theta\right] \qquad (3.4a)$$

$$\sigma_r = \frac{q}{2}\left[1+2\nu - 2(1+\nu)\cos\theta + \cos^3\theta\right] \qquad (3.4b)$$

$$\tau_{rz} = 0 \qquad (3.4c)$$

and are shown graphically in figure (3.2b).
Ahlvin and Ulery (1962) presented a set of tables based on Love's equations for rapid computation of the complete pattern of stresses and strains below a circular footing.

Following the early solutions of the plane strain and axi-symmetric cases, Steinbrenner (1936) presented his numerical solutions for the determination of stresses below the corner of a rectangular uniformly loaded area. A few years later Newmark (1942) developed his 'Influence Charts' which permitted the determination of stresses below any irregular shaped uniformly loaded area.

From all these results it was evident that the vertical stresses induced in a semi-infinite, homogeneous, isotropic, linearly elastic medium are a function of the foundation dimension and are independent of the deformation modulus, E, and Poisson ratio, ν, of the soil. The induced horizontal stresses are also independent of the deformation modulus, but are dependent on the Poissons ratio, ν, except in the plane strain case where σ_x is independent of both E and ν.

However the idealised assumptions used to obtain the above solutions do not give a realistic representation of a natural soil deposit. The variation from the 'ideal' case can manifest itself in many ways and are considered in the following sections.

3.2.2 Finite Non-homogeneous elastic medium

The non-homogeneity of a soil deposit can be considered under two basic categories. The more obvious one being the layered nature of the underlying deposit either due to completely differing geological strata or differing degree of weathering of a particular geological stratum, where the the deformation properties change abruptly from one layer to the next. It is the special case of the layered system, where the underlying layer is rock, that is used to demonstrate the effect of a finite thickness of a soil deposit on the induced stresses.

The less obvious source of the non-homogeneity arises from the variation of the soil deformation modulus with depth due to the increase of the overburden stresses. In this case the variation is considered to be a continuous function of depth, thus differentiating it from the discontinuous layered system

3.2.2.1 Layered System

The problem of multi-layered systems has attracted considerable attention, primarily from Highway Engineers for pavement design. Burmister (1958) evaluated the variation of the vertical stresses, under a vertical load, in a two layered system (Fig. 3.3). It can be seen that the presence of the stiffer upper layer has a considerable influence on the distribution of the induced vertical stresses, and reduces them considerably below those obtained for a homogeneous soil. Although Burmister did not publish the stress distribution for the deformation modulii ratio (E_1/E_2) of less than unity it can be deduced

that the stresses would be in excess of those obtained for the homogeneous soil. Results published for three-layer systems by Jones (1962), Peattie (1962) and Kirk (1966) show similar trends to those of the two layer system.

A particular case of the two layer system is with a completely rigid lower layer i.e. with a rigid boundary (e.g. rock). Poulos (1967) extended Burmister's work and published graphical influence coefficients for line, strip and sector loading on an elastic layer underlain by a rough rigid base. His results (Fig. 3.4) indicate that if the rigid base is below the depth equal to 8 times the radius of the loaded area ($z = 8a$) then the homogeneous semi-infinite solution only slightly under estimates the stresses. In general, the rough rigid base produces a concentration of stress at the base of the layer near the axis, of the loading while away from the axis the stresses die away more rapidly than in the Boussinesq solution. In conclusion, if the depth of a layer is in excess of eight times the radius (or half width) of the loaded area then the layer may be considered as a semi-fimite mass.

3.2.2.2 Deformation Modulus as function of depth

The case of the deformation modulus varying continuously with depth ($E = f(z)$) has received scant attention compared to the layered systems. In fact it was normal to consider this case as a layered system using the mean value of E for each layer. However Gibson (1967 and 1968) considered the problem involving elastic non-homogeneity, in the case of an incompressible medium with a shear modulus G, ($G = E/2(1 + \nu)$), increasing with depth according to the law (Fig. 3.5)

$$G(z) = G(o) + mz \qquad (3.5)$$

Gibson demonstrated that when $\beta = 0$, i.e. $G(o) = 0$, (Fig. 3.5) the

stress distribution obtained is the same as in the homogeneous elastic case, i.e. $\beta = \infty$ Using Gibsons results Som (1968) demonstrated that for an incompressible material the stress components corresponding to finite values of β do not vary appreciably from the homogeneous value (Fig. 3.6).

Gibson and Sills (1971) analysing a strip foundation for the case of $\beta = 0$ found that both vertical and horizontal stresses, on the axis of symmetry, are dependent on the value of Poissons ratio, ν (Fig. 3.7). This is in contrast with the corresponding homogeneous case where Poisson's ratio is only significant to the intermediate stress. A reduction on the numerical value of Poisson's ratio causes the vertical stress to concentrate at the axis.

3.2.3 Anisotropy

As most soils were deposited by sedimentation followed by approximately one dimensional consolidation, it can be expected that the soil properties in the horizontal and vertical directions are significantly different, (i.e. anisotropic). However there will, in general, be no preferred direction in the horizontal planes and therefore the elastic properties of the soil may be assumed to be symmetrical about the vertical axis (i.e. the horizontal plane is a plane of isotropy). The soil is therefore said to exhibit a cross or transverse anisotropy. It has been shown (Love 1892) that a cross anisotropic elastic material has five independent elastic parameters:-

E_v - deformation (Youngs) modulus in the vertical direction

E_h - deformation modulus in the horizontal direction

ν_{vh} - Poissons ratio for strain in the vertical direction due to a horizontal direct stress

ν_{hh} - Poisson's ratio for strain in the horizontal direction due to a horizontal direct stress at right angles

and

G_{hv} - modulus of shear deformation in a vertical plane

The remaining parameters were shown not to be independent. Thus the Poisson's ratio for strain in the horizontal direction due to a vertical direct stress, ν_{hv}, and the modulus of shear deformation in a horizontal plane, G_{hh} can be expressed in terms of the above five parameters.

$$\nu_{hv} = \nu_{vh} \frac{E_v}{E_h} = \frac{\nu_{vh}}{n} \qquad \text{where } n = E_h/E_v$$

and $G_{hh} = E_h / 2(1 + \nu_{hh})$

Because of the difficulty involved in the determination of the five parameters Barden (1963) attempted to express G_{hv} in terms of the other four independent parameters and showed, for a particular case, that:-

$$G_{hv} = nE_v / (1 + n + 2n\,\nu_{vh})$$

he then assumed this to approximate to a general solution. The limitations of Bardens assumption has been discussed by Dooley (1964) and others. However, accepting this limitation, Barden's results, for a point load, show that the vertical stress is dependent on the ratio of the deformation moduli and to a lesser extent on the values of the Poissons ratio. For a heavily overconsolidated clay, where $n > 1$, the soil shows a greater spreading capacity than suggested by the isotropic analysis, Gerrard (1968) demonstrated similar results for a strip and circular loadings on a finite single layer and a two layer system.

3.2.4 Non-Elastic Medium

The cases considered above have all assumed that the soil is a linear elastic material, however the stress-strain relationship is often non-linear. Several studies have been made for various non-linear stress strain relationships (Hoeg, Christian and Whitman 1968; Huang 1968; Phukan 1968) which have demonstrated that the vertical stress distribution below a foundation vary only slightly from the Boussinesq distribution. The horizontal stresses have shown greater variation particularly when failure stresses were approached.

3.2.5 Summary

From the above review of the distribution of stresses in a soil medium, due to the application of surface loading, the following conclusions are drawn:

1. For a deep layer of saturated clay (i.e. with a depth greater than eight times the foundation radius or half width), any deviation from the classical Bouessinesq problem, in terms of non-homogeneity and non-linearity of the stress-strain relationship has only marginal effects on the distribution of stresses in the undrained (immediate) conditions.

2. Poisson's ratio has a significant influence on the stress distribution on a deposit with the deformation modulus increasing with depth. Thus the whole stress distribution changes during consolidation.

3. Stress distribution due to surface load on a layered system is not represented well by the Boussinesq solution. One of the methods referred to in 3.2.2.1 should thus be used.

4. The presence of a rigid base at relatively shallow depths (depths less than eight times the foundation radius or half width) is a

special case of a layered system. As with the layered system the Boussinesq solution does not give a good representation of the distribution of stresses and thus it should be treated accordingly, (e.g. Poulos 1967).

5. The effect of cross anisotropy is difficult to assess because of the problem of the determination of the five independent elastic parameters. However it appears that for values of the ratio of the horizontal to vertical deformation modulus (E_h/E_v) greater than unity the soil has a greater spreading capacity than for the Boussinesq case.

3.3 STRESS PATHS BELOW FOUNDATION

A stress path is essentially a locus of the stresses at a point during the transition from one stress state to another. The stress path can be plotted in several manners. In order to study the deformation below a loaded area it is convenient to use a plot of vertical stress against horizontal stress.

The in-situ stresses existing before the soil is loaded has been considered in Chapter Two where it is seen that in heavily overconsolidated clays the effective horizontal stress (σ'_h) is greater than the effective vertical stress (σ'_v). The in-situ effective stresses, at a point, defines the start of the effective stress path at that point and are represented by the point S in figure 3.8(c) (the suffices 0.5, 1, 2 etc., indicate the depths below founding level in terms of the circle radius).

The application of a surface load, q, will cause an increase of total stresses, $\Delta\sigma_v$ and $\Delta\sigma_h$, as defined by the Boussinesq equation (Fig. 3.2). If this load is applied quickly, without drainage, there will be a corresponding increase of pore water pressure Δu, where

according to Skempton (1954) for a saturated clay,

$$\Delta u = \Delta\sigma_h + A\,(\Delta\sigma_v - \Delta\sigma_h)$$

Now, for most heavily overconsolidated clays, the value of A will be positive and less than unity within the stress range normally encountered below foundation, therefore there will be an increase in the effective vertical stress, $(\Delta\sigma'_v)_i$, and a decrease in the effective horizontal stress, $(\Delta\sigma'_h)_i$, (Fig. 3.8(a)). Therefore considering the stress path, the stress point moves from S to I (Fig. 3.8(c)) during undrained loading. The soil then begins to drain and the pore pressure dissipate during the process of consolidation. However as consolidation takes place the Poisson's ratio decreases to its fully drained value, thus decreasing the total horizontal stress (Fig. 3.2) while the total vertical stress remains unchanged, (providing the soil is homogeneous). Thus the change in the effective horizontal stress during consolidation is less than the change in the effective vertical stress (Fig. 3.8(a)). Thus considering the stress path during the consolidation process the stress point moves along I to C (Fig. 3.8 (c)) completing the stress path. It will be observed that below one radius depth there is no resultant increase in a horizontal stress, hence the increase in horizontal stress during consolidation is all recompression. Above this level a resultant increase of horizontal stress is observed although much of this is recompression during the consolidation stage.

It is thus seen that the stress paths below a foundation are a function of depth.

3.4 DETERMINATION OF THE MAGNITUDE OF SETTLEMENT

3.4.1 Simple (or Conventional) Analysis

A review of settlement analyses must essentially begin with the Terzaghi's classical consolidation theory. Almost half a century ago Terzaghi (1925) presented his theory of consolidation which has since formed the basis of most settlement analyses on clay soils.

Terzaghi's theory was developed specifically to deal with the compression of clays under one dimensional strain conditions. Under these conditions the settlement, ρ, of a clay layer, (thickness H) subjected to an increase of vertical stress, $\Delta\sigma_v$, can be simply expressed as

$$\rho = H\Delta\sigma_v.m_v \qquad (3.6)$$

where m_v, the coefficient of volume compressibility, is determined from the stress-strain (or voids ratio)relationship obtained from the standard oedometer test. The condition of zero lateral strain is approximately true in the field where the thickness of the compressible layer under consideration is small compared to the width of the loaded area. Regardless of this, the use of Terzaghi's one dimensional analysis was extended to deeper layers of clay and the principle of integration (or summation) was used to determine the settlement of a point within the loaded area as though the soil below it was deforming under one dimensional strain conditions:

$$\rho = \int_0^H m_v.\Delta\sigma_v \, dz \qquad (3.7)$$

The increase in vertical stress was obtained from the Boussinesq's analysis discussed earlier.

It was recognised at an early stage (Terzaghi 1936) that for the

thicker deposits there would be some immediate undrained deformation due to significant shear deformation which could occur at a constant volume. This could not be analysed using the oedometer tests as, in this test, the undrained deformation of the soil is prevented by the lateral restraint imposed on it by the apparatus. The immediate settlement, ρ_i, was therefore obtained from the elastic theory using an undrained deformation modulus, Eu, obtained from a quick triaxial test and assuming Poisson's ratio equal to half:

$$\rho_i = q \frac{B(1 - \nu^2)}{Eu} . Ip = 0.75 \frac{qBIp}{Eu} \qquad (3.8)$$

Ip is an influence factor which depends on the shape of the loaded area (foundation) its stiffness and also on the position of the point under consideration (Steinbreiher, 1934). However, for many years controversy existed as to whether the total settlement was equal to the oedometric settlement or the sum of the oedometric settlement and the immediate settlement.

A study by Skempton et al (1955) of the recorded settlements of five structures on normally consolidated clays and five on overconsolidated clays led to the conclusion that the total final settlement was best predicted by the oedometric settlement alone. However, for the purpose of predicting the settlement-time relationship the actual consolidation settlement was given by the difference between computed consolidation settlement and the immediate settlement.

3.4.2 Skempton and Bjerrum Method

With a better understanding of the induced pore pressures beneath a loaded area Skempton and Bjerrum (1957) proposed a modified method of settlement analysis. As consolidation is a direct result of dissipation of pore pressures, the magnitude of the consolidation settlement will be proportional to the induced pore pressures rather

than the induced vertical stress. Skempton (1954) showed that for a saturated clay the pore pressure increment, Δu, induced by axi-symmetric undrained loading increments, $\Delta\sigma_1$ and $\Delta\sigma_3$, is given by the following expression

$$\Delta u = \left[\Delta\sigma_3 + A(\Delta\sigma_1 - \Delta\sigma_3)\right] \qquad (3.9)$$

Skempton and Bjerrum have than suggested that because during the consolidation stage of an element the lateral strains will be small, the vertical compression during consolidation will be given by

$$\delta\rho_c = m_v . \Delta u . \delta z$$

and since $\Delta u = \Delta\sigma_1\left[A + \frac{\Delta\sigma_3}{\Delta\sigma_1}.(1-A)\right]$ then for a layer of saturated clay of thickness H the consolidation settlement would be

$$\rho_c = \int_o^H m_v \Delta\sigma_1\left[A + \frac{\Delta\sigma_3}{\Delta\sigma_1}.(1-A)\right] dz \qquad (3.10)$$

Rewriting this equation in a simpler form one obtains:

$$\rho_c = \mu\rho_{oed}$$

where ρ_{oed} is the consolidation settlement computed direct from the results of the oedometer tests, and

$$\mu = \frac{\int_o^H m_v \Delta\sigma_1\left[A + \frac{\Delta\sigma_3}{\Delta\sigma_1}.(1-A)\right] dz}{\int_o^H m_v \Delta\sigma_1 \, dz}$$

By assuming that m_v and A are constant with depth, the above expression simplifies to

$$\mu = A + \alpha (1-A) \quad \text{where} \quad \alpha = \frac{\int \Delta\sigma_3 \, dz}{\int \Delta\sigma_1 \, dz}$$

The relationship between μ and A for various shape foundations was presented by Skempton and Bjerrum and is shown in Fig. 3.9.
The total settlement, ρ, is now written as the sum of the immediate undrained settlement, ρ_i , and the consolidation settlement ρ_c.

$$\rho = \rho_i + \rho_c \qquad (3.11)$$

where ρ_i is obtained from equation (3.8).

Results presented by Skempton and Bjerrum demonstrated this method to give good correlation with observed settlements for both normally and over consolidated clays; the mean ratio of calculated to observed values being 0.99 for both. Using the conventional method ($\rho = \rho_{oed}$) the settlement was, on average, over estimated by 25% for the overconsolidated clays and under-estimated by 20% for the normally consolidated clays. Where the total settlement is taken as the sum of the immediate and oedometric settlements, the calculated results overestimated the settlement by 60%, on average, for the overconsolidated and by 10% for the normally consolidated clays. Thus the Skempton and Bjerrum method appears to offer a much improved method of settlement analysis.

3.4.3 Three Dimensional Elastic Analysis

Elastic analysis has been used extensively and is generally acceptable in the computation of the stresses induced by loaded foundations (Section 3.2). Initial settlement has also been computed by the elastic theory. Davis and Poulos (1963) recommended that three dimensional elastic analysis should also be used to determine total

settlement, either from the elastic deformation theory, in the form of

$$\rho = \frac{qB(1-\nu'^2)}{E'} I_\rho \qquad (3.12)$$

where q, B and I_ρ are as described for Equation 3.8 and E' and ν' are the drained deformation modulus and Poisson ratio respectively or alternatively in the form of the elastic stress distribution theory, from the equation

$$\rho = \Sigma \frac{1}{E} (\sigma_z - \nu\sigma_x - \nu\sigma_y)\, \delta z \qquad (3.13)$$

where σ_x, σ_z and σ_y are obtained from the Boussinesq analysis. The initial and total final settlements being obtained by using the undrained parameters (E_u, ν_u) and the drained parameters (E', ν') respectively in these equations.

The values of the 'elastic' constants can only be obtained from triaxial testing, and as the soil may not be truely elastic, the parameters should be obtained from a specimen returned to its in-situ effective stress condition and subjected to increments of stress appropriate to the in-situ increments. In other words the triaxial specimen should be tested under a stress path similar to that experienced by the in-situ element of soil

3.4.4 Stress Path Method

Stress paths below loaded foundations have been considered earlier (Section 3.3). Lambe (1964, 1968) proposed a method of settlement analysis which took into consideration the change of stress path with depth. Samples from selected depths below the foundations are reconsolidated to the relevant in-situ effective stresses. The subsequent strains produced, when the sample is subjected to the relevant stress path loading, is recorded at each depth. The

settlement of the foundation then being computed by integration of the experimental strain-depth curve.

The standard triaxial apparatus can only simulate axi-symmetric stress paths. For the case of a long strip footing a plane strain apparatus would be required. Although several such apparatuses have been developed, (see for example Dyson (1970)) they are not commercially available.

The plane strain case and also the rectangular loaded area have been considered by Kerisel and Quatre(1968). Based on the results of Shibata and Karube (1965), on an alluvial clay, it is suggested that the axial deformation caused by the tensor $\Delta\sigma_1$, $\Delta\sigma_2$ and $\Delta\sigma_3$ may be adequately represented by the axi-symmetric tensor $\Delta(\sigma_1-(\sigma_2-\sigma_3)/5), \Delta\sigma_3$ which can be applied in the normal triaxial apparatus.

3.4.5 Summary

The major developments concerning the determination of the magnitude of settlement has been presented above. It is seen that the Terzaghi theory of one dimensional consolidation has played a major role in the settlement analysis of clay soils. With the aid of the Skempton and Bjerrum modification the Terzaghi theory is still a very useful method of settlement prediction.

Despite the development of the stress path techniques the oedometer methods of settlement are still the most commonly used. The relatively complex laboratory testing required for the stress path methods, as compared to the oedometer methods, results in this method only being used for special cases. With the use of numerical methods, finite difference or finite element, the three dimensional, elastic analysis need not be restricted to a homogeneous, isotropic,

linearly elastic material providing the necessary stress-strain parameters can be determined.

3.5 RATE OF SETTLEMENT

It has been shown in the previous section that settlements of foundations on clay consists basically of two components, 'immediate' and 'consolidation' settlement. A complete settlement analysis comprises the determination of immediate settlement, final settlement and the rate of settlement. At any time (t) after a foundation has been loaded the settlement (ρ_t) will be given by the equation

$$\rho_t = \rho_i + U_t \rho_{con} \qquad (3.14)$$

where ρ_i and ρ_{con} are as defined in the previous section, and U_t is the degree of consolidation after time (t). To obtain the rate of settlement it is therefore necessary to establish the relationship between U_t and t.

The Terzaghi one-dimensional consolidation theory has been used extensively to determine the rate of settlement of structures founded on clays. However it is clear that the soil often has a horizontal component of drainage as well as vertical. In this instance the rate of settlement should be analysed by a three-dimensional consolidation theory.

3.5.1 One-dimensional consolidation

The rate of consolidation settlement on clay is usually predicted on the assumption of the Terzaghi theory of one dimensional consolidation where the pore water drainage is in the vertical direction only. The Terzaghi theory gives a relationship between pore pressure distribution, u, and the time, t.

$$C_{v1} \cdot \frac{\partial^2 u}{\partial Z^2} = \frac{\partial u}{\partial t} \qquad (3.15a)$$

where C_{v1} is the one dimensional coefficient of consolidation and Z is the length of drainage path

The degree of consolidation U is given by

$$U = 1 - \frac{\int_{U_t} dz}{\int_{U_o} \partial z} = \frac{\rho_{con(t)}}{\rho_{con}} \qquad (3.15b)$$

Numerical solutions to the above equations have been presented by Terzaghi and Frohlich (1936) in terms of the degree of consolidation, U, and a time factor, $T = \frac{C_{v1} \cdot t}{h^2}$ (Fig. 3.10)

3.5.2 Three-dimensional Consolidation

The general theory of three dimensional consolidation for an isotropic elastic medium was developed by Biot (1941). The use of three dimensional analysis has been hindered by the mathematical complexity of the rigorous analytical solutions. Consequently several numerical approximations have been proposed, and it is results of these approximate solutions that are considered below. Gibson and Lumb (1953) rewrote Biot's general consolidation equation into a form similar to the Terzaghi equation, thus

$$C_{v3} \nabla^2 u = \frac{\partial u}{\partial t} - \frac{1}{3} \frac{\partial \theta}{\partial t} \qquad (3.16)$$

where $\theta = \sigma_x + \sigma_y + \sigma_z$

$$\nabla^2 u = \frac{\partial^2 u}{\partial x^2} + \frac{\partial^2 u}{\partial y^2} + \frac{\partial^2 u}{\partial z^2}$$

and C_{v3} is the three-dimensional coefficient of consolidation. With the assumption that the sum of the total stresses remains constant during consolidation, which is often approximately true

(Section 3.2), then $\partial\theta/\partial t = 0$, and equation (3.16) reduces to a simple diffusion equation:

$$\frac{\partial u}{\partial t} = C_{v3}\nabla^2 u \qquad (3.17)$$

Gibson and Lumb solved equation (3.17) by a finite difference method for various drainage conditions. They demonstrated the validity of this approach by comparison with one dimensional and radial consolidation where exact solutions were available. Davis and Poulos (1972) with the same technique demonstrated the effect of three dimensional drainage of finite layers over a range of depth to 'width' ratios for both strip and circular footings. Their results for circular and strip footings are shown in figure (3.11) for the case of a permeable upper surface and impermeable base. It can be seen from the figure that the rate of consolidation increases considerably with increase in depth of the consolidating layer particularly in the case of the circular loading. The one dimensional analysis would give the degree of consolidation within a factor of two for a depth to radius ratio and depth to full width ratio 1 for the circle and strip loadings respectively.

It is thus obvious that a three dimensional consideration of the rate of settlement would be worth while, for a depth to radius (or width) ratio in excess of unity, where an accurate prediction of the rate of consolidation is required, providing the parameter C_v can be determined with confidence.

3.8 DETERMINATION OF DEFORMATION PARAMETERS

The deformation parameters of soils are usually determined in the laboratory on 'undisturbed' samples of the soils to be loaded. The effects of sampling on the measured parameters were discussed in the previous chapter. Alternatively the deformation parameters

can be determined by in-situ measurement although this is generally very expensive and is therefore usually limited to major projects for which such expense can be justified.

The oedometer has, formany years, been the basic instrument for assessing the compressibility of clay soils. Terzaghi and Peck (1948) noted that settlements of overconsolidated clays were over-estimated by factors of 2 to 5 when using the oedometer results. Similar errors were subsequently reported by many authors. However Burminster (1952) Tschabotarioff (1952), Hansen (1957) and others reported that satisfactory predictions were obtained when the reloading curves were used from the oedometer tests. It is considered that the first loading cycle obliterates much of the disturbance in the sample. Nevertheless the apparatus should be calibrated for 'machine error' as this can be significant for very stiff soils. It is concluded that for overconsolidated soils the reloading modulus of volume compressibility, m_v, should be used in equation 3.6 to estimate the consolidation settlement.

In order to determine the immediate settlement, undrained triaxial tests are required to determine the undrained deformation modulus, Eu. It is important that the sample is initially reconsolidated, either to the in-situ mean effective stress or preferably to the in-situ effective vertical and horizontal stresses. However, it was observed by Ward et al (1959) that reconsolidation under hydrostatic stress has little effect in reducing the origin correction. It has also been observed (Chapter 2) that the undrained modulus is seriously effected by sample disturbance. If the Skempton and Bjerrum approach is to be used, then in addition it is necessary to determine the pore pressure coefficient A, therefore the pore water pressure should be recorded during the consolidated undrained test over the appropriate stress range. Alternatively the coefficient, A, can

be estimated from the clay consistency together with published values although it should be noted that the values of A for the stress ranges appropriate to foundation loading will generally be significantly different from the values at failure, A_f.

The Davis and Poulos and the Lambe methods require the use of a triaxial apparatus that can reapply the in-situ effective stresses and subsequently allows the undrained and drained deformation parameter to be determined from one test representing the stress path that the sample would experience below the loaded foundation. Davis and Poulos (1963) describe such an apparatus and procedure suitable for testing of 38mm diameter samples of normally consolidated clays. For heavily over consolidated clays it is necessary to return the sample to insitu effective stresses where $\sigma_r > \sigma_a$ and subsequently apply increments of $\Delta\sigma_r$ and $\Delta\sigma_a$ such that $\Delta\sigma_a > \Delta\sigma_r$. The apparatuses described by Bishop and Henkel (1962) for extension tests are not very suitable for the above testing. As there was no suitable commercial apparatus available for this type of test a triaxial apparatus was developed as part of this project and is described in Chapter 5.

In-situ measurement of the deformation modulus may be determined by plate loading tests. Plate tests, because of their limited size, only determine the deformation modulus of the soil within the vicinity of the test, it is therefore necessary to carry out tests at various depths within the influence of the proposed foundation. Results of plate tests in London clay, reported by Marsland (1971), indicate the necessity of hand preparation of the test area, otherwise low modulus values were obtained. As indicated earlier it is essential that tests are carried out as early as possible after excavation to reduce the effect of deterioration due to stress relieve. However Marslands plate results produced undrained modulus values up to five

times greater than those obtained by triaxial testing.

3.7 FIELD OBSERVATIONS

Som (1968) (see also Simons and Som 1970) collected together published settlement data for 12 structures on overconsolidated (o.c.) clays and nine on normally consolidated (n.c.) clays. For each case the initial, primary, and secondary settlements were tabulated as a percentage of the extrapolated 50 year settlement. This showed, on average, that the immediate consolidation and secondary settlements for an o.c. clay represented 57.5, 33.7 and 8.8% of the total settlement respectively, while for a n.c. clay the contributions were 15.6, 62.8 and 21.6% respectively. This is simply explained by considering the changes in effective stress during loading. For the same applied load the final increase in effective stresses will be approximately equal for both the o.c. and the n.c. clay. The increase of effective stresses in the undrained case will be less for the n.c. clay than for the o.c. clay because the pore pressure coefficient A is generally greater in the former case, and thus the increase in pore pressure is greater. The subsequent change in effective stress due to consolidation must, therefore, be greater for the n.c. clay than the o.c. clay. It would therefore be expected that the immediate settlement would be a greater proportion of the total settlement for the o.c. clay than for the n.c. clay, as the above results show. The possibility of the existence of a hydraulic gradient threshold value (i_o), which must be exceeded before any appreciable volume change can occur, has been suggested by Terzaghi (1941). Terzaghi produced a case record showing that the settlement under a given point some depth beneath the Charity Hospital, New Orleans was zero despite the fact that increase of vertical stress existed under that point. Som (1968) suggested from laboratory tests that the

threshold value for London clay was of the order of 10 per cent.

The work on the Middle Chalk at Munford presented a unique chance to carry out field (including a full scale loading test) and laboratory studies to a research standard. It should be realised that the results of the Munford work may not be directly applicable to overconsolidated clays as chalk is in the soft rock category with the stiffness modulus (E) one or two orders of magnetude higher than for heavily overconsolidated clays. Also Chalk does not offer a consolidation problem but consists of immediate settlement plus creep. However, some of the major points which may be of significance to the problem of overconsolidated clays are considered below.

Details of the site and project were presented by Ward, Burland and Gallois (1968) together with results of the tank tests and some plate loading tests. Further comparison of tank tests and plate tests together with some laboratory tests results were presented by Burland and Lord (1969). Observations of deflection at various levels directly below and outside the loaded area during the short term loading proved to be elastic.

The deflected shape at ground level was localised around the loaded area compared with the simple elastic case. This was predicted by Gibson (1967) for the case of an elastic material whose stiffness increases with depth. On unloading the strains were found to be recoverable within 3% except for the grade V chalk where 25% of strain was irrecoverable. Using the recorded strains, an isotropic elastic stress distribution and a poissons ratio of 0.1 it was demonstrated that E increased with depth. To obtain more accurate values of E, the stress distribution for E increasing with depth should be used. The determined values of E would be greater as this type of elastic profile concentrates the stress around the axis of the loaded area. Results of plate tests also indicated this trend. Good agreement between

plate and tank tests were obtained within the grades III - V chalk (Fig. 3.12). Agreement between tank tests and plate tests for the grade II chalk was not so good, the plate E's falling to 0.5 - 0.7 of the tank values. This was suspected to be the result of the effect of stress reduction disturbance on the grade II chalk. Laboratory tests were only carried out on grade II, the poorer grades could not be sampled satisfactorily. The E values obtained from this method showed fairly good agreement, approximately 20-30% greater than from the tank tests (Fig. 3.12). Long term creep was also monitored during the Munford investigations, however this is not considered here.

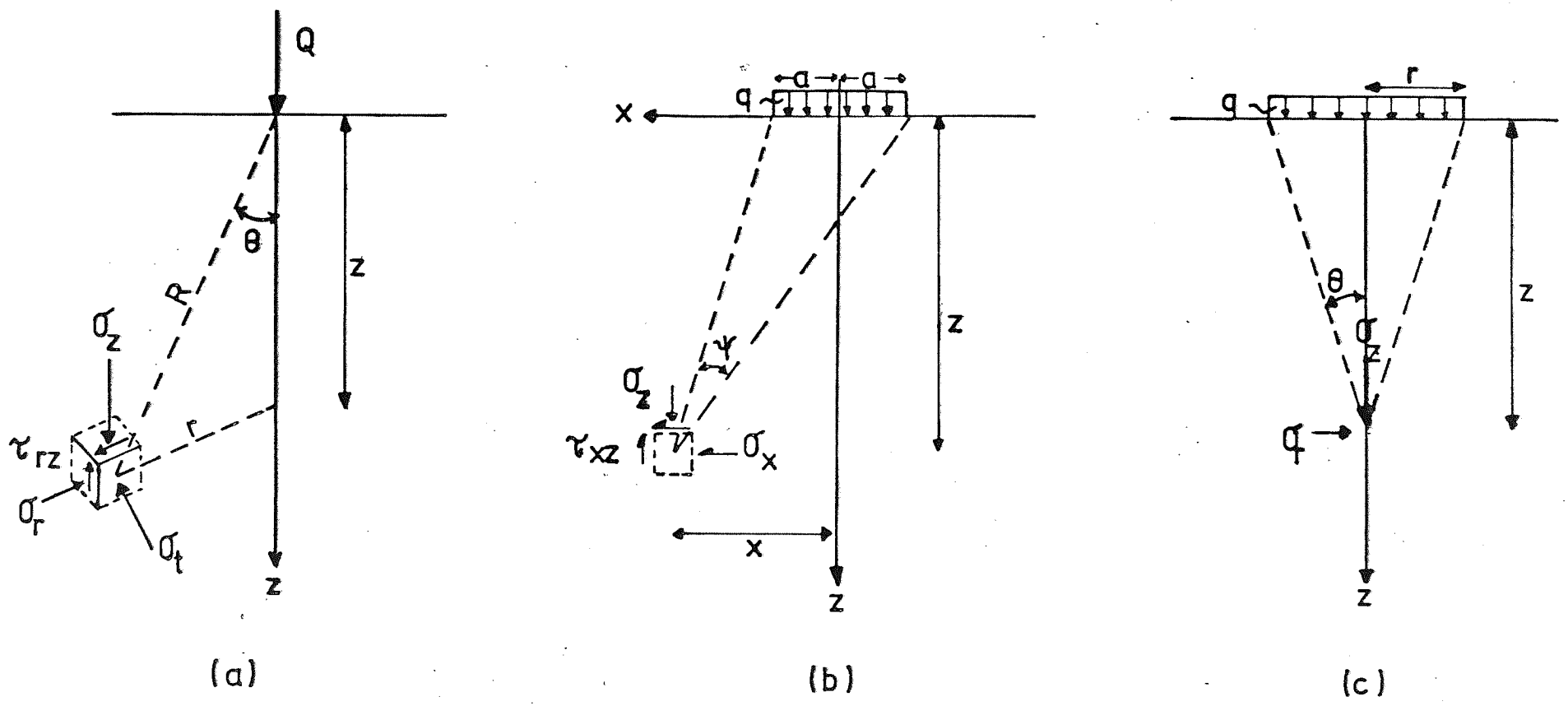

FIG. 3.1 Stresses at a point in a semi-infinite mass due to surface loading (a) point load; (b) strip load; (c) circular load.

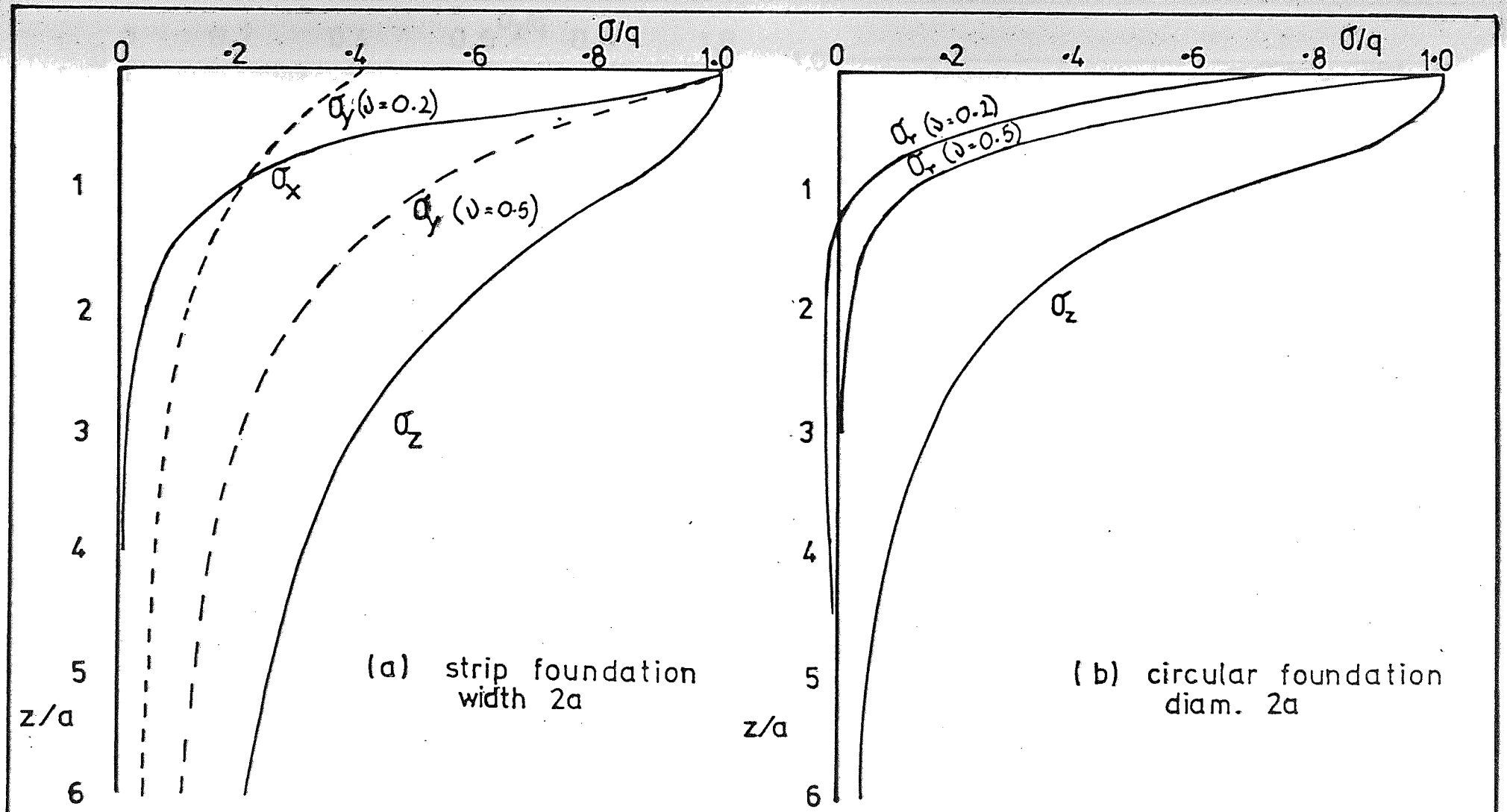

FIG. 3.2 Stresses beneath centre of foundations - (Boussinesq case)

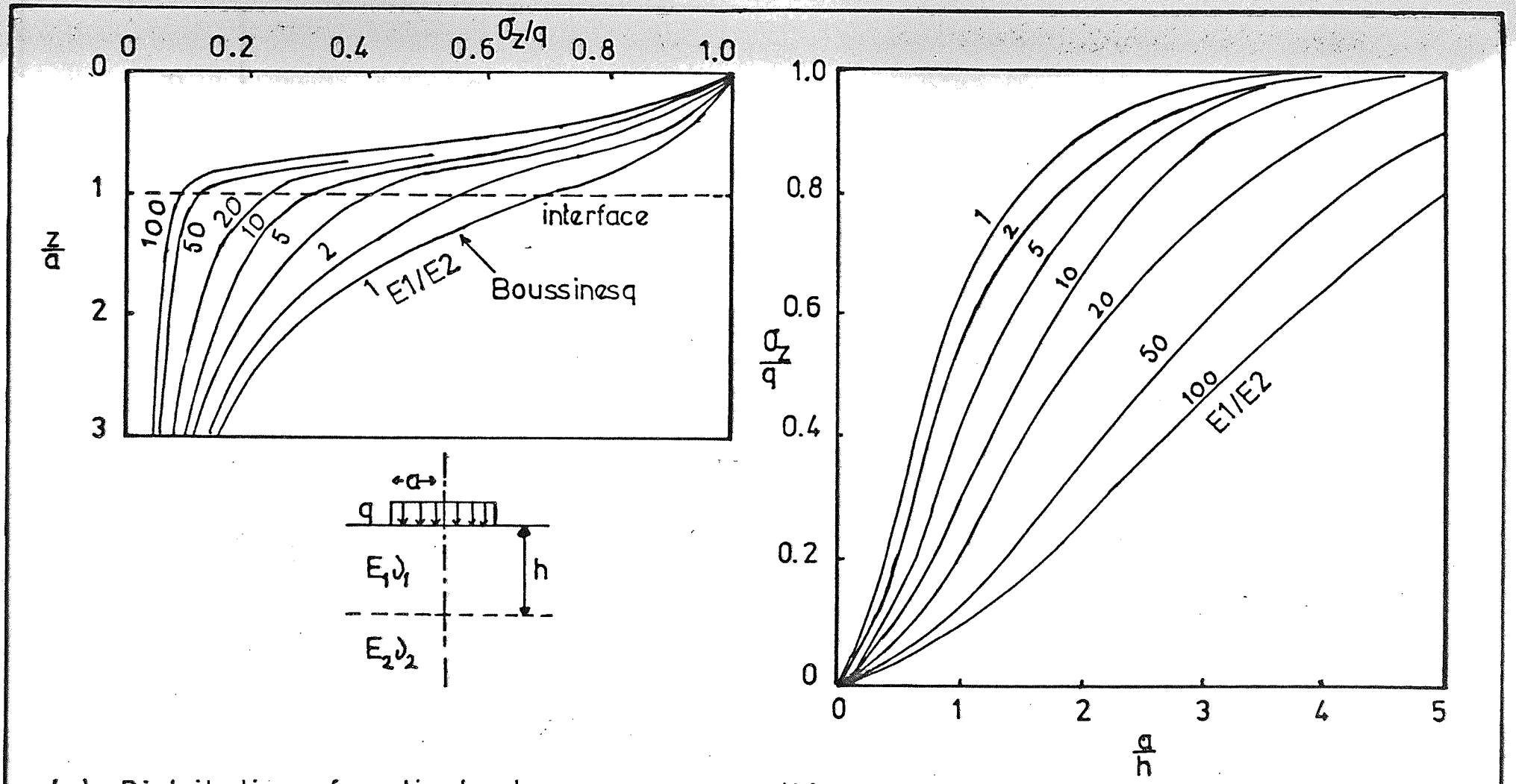

(a) Distribution of vertical stresses

(b) Vertial stress at the interface

FIG. 3.3 Two-layer elastic system: effect of rigidity and thickness of the upper layer on the vertical stress beneath the centre of a circular footing

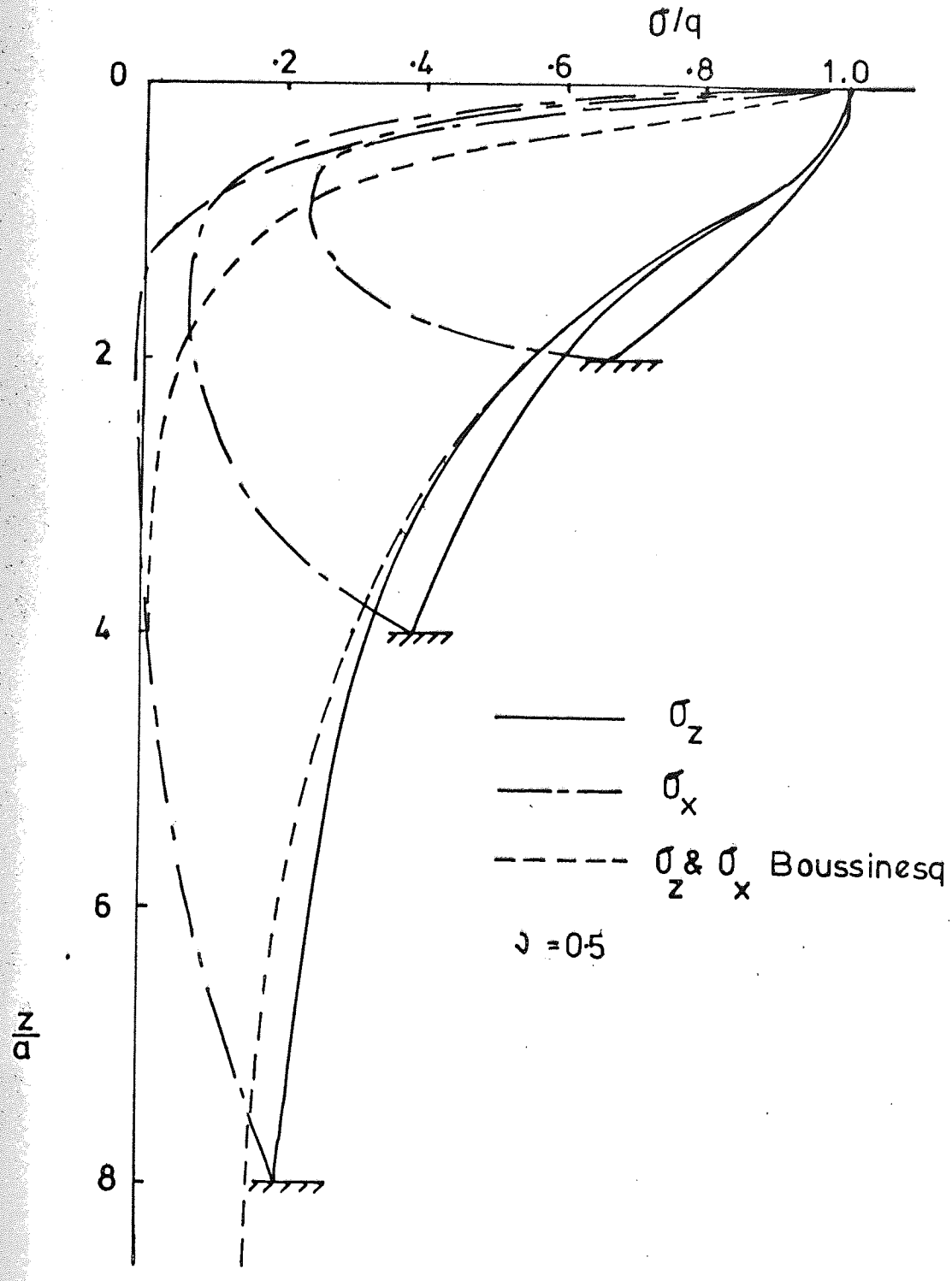

FIG. 3.4 Effect of rough rigid base on stresses below strip footing (Poulos 1967)

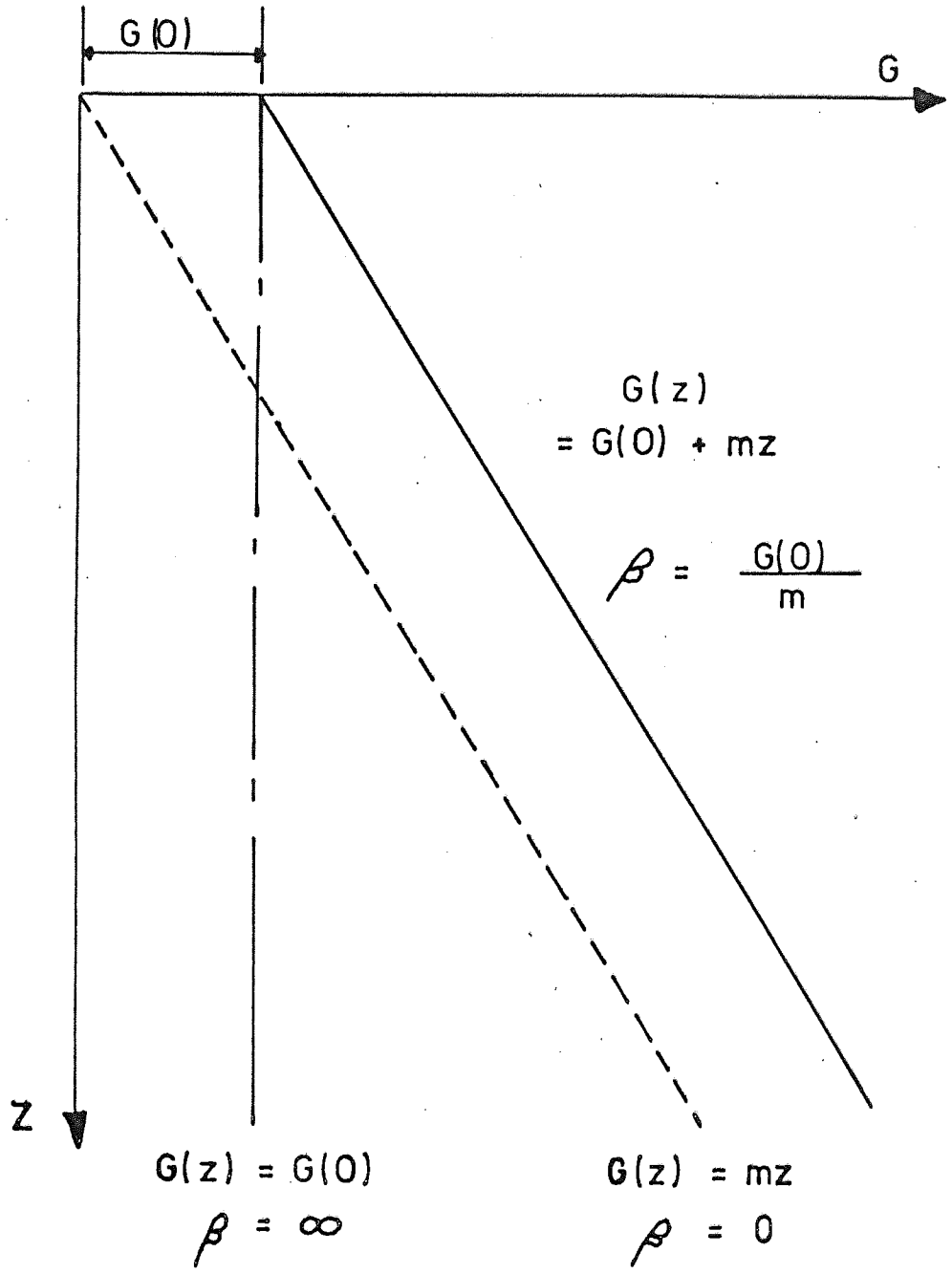

FIG. 3.5 Non-homogeneous elastic medium

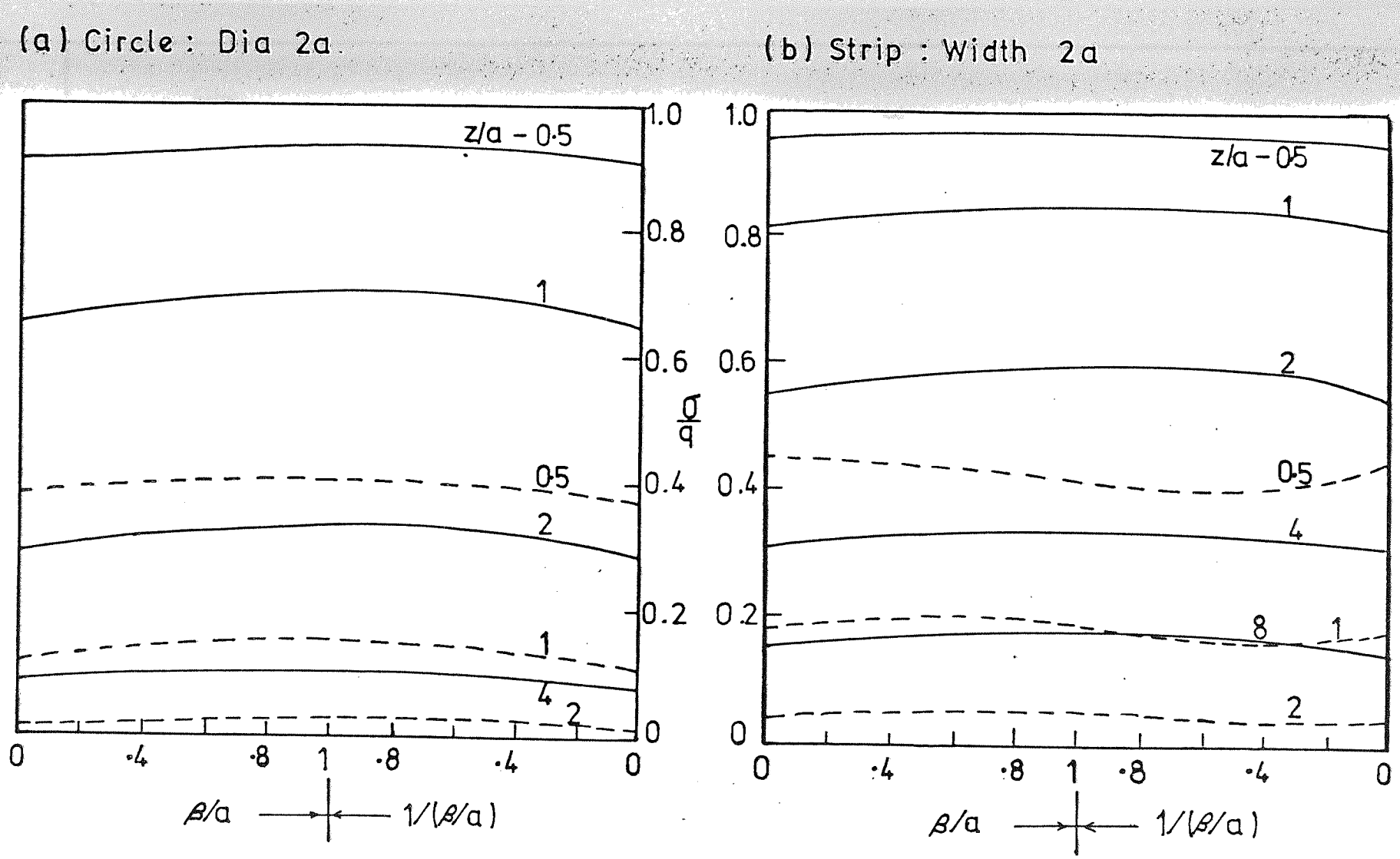

FIG. 3.6 Effect of non-homogeneity on the stresses beneath centre of foundations — (Som 1968)

—— σ_z

---- σ_x

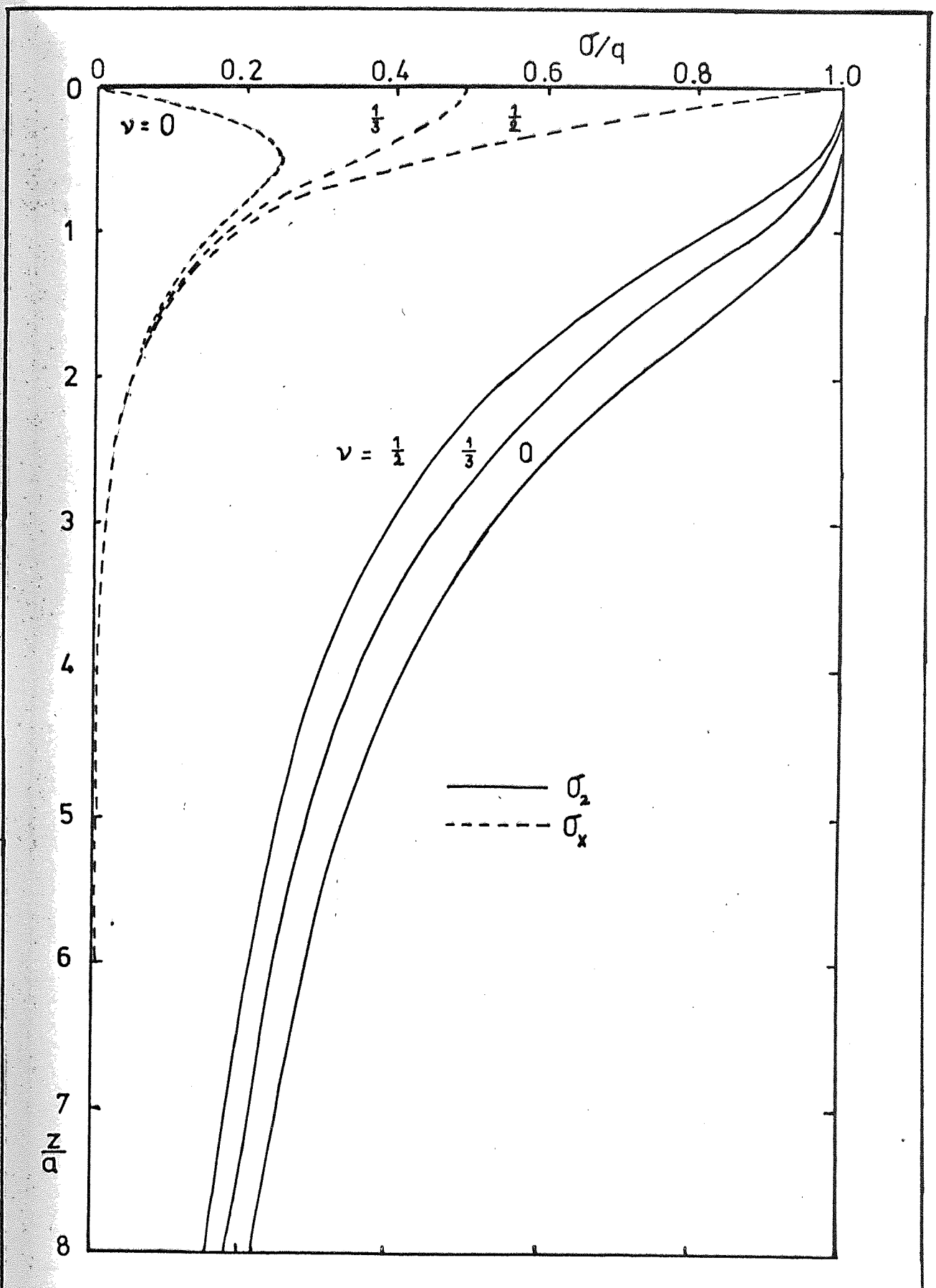

FIG. 3.7 Stresses beneath a strip footing (width 2a) on a non-homogeneous elastic half space - (Gibson and Sills 1971)

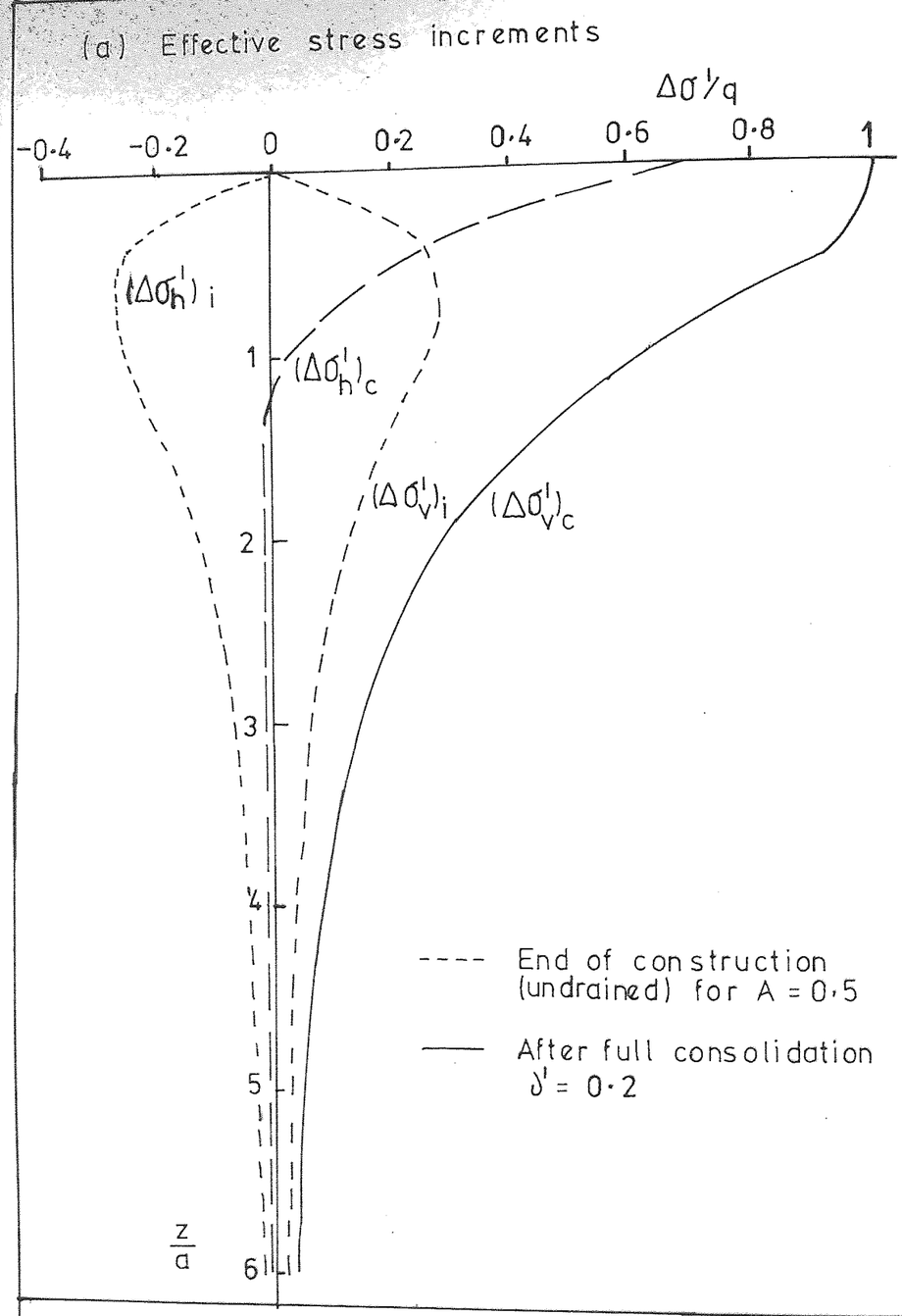

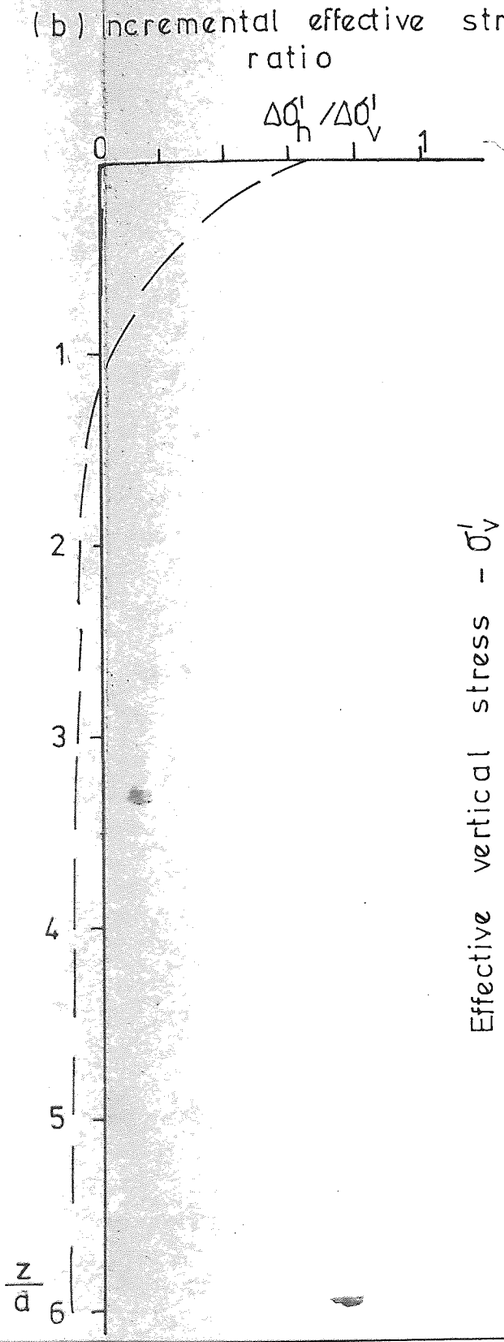

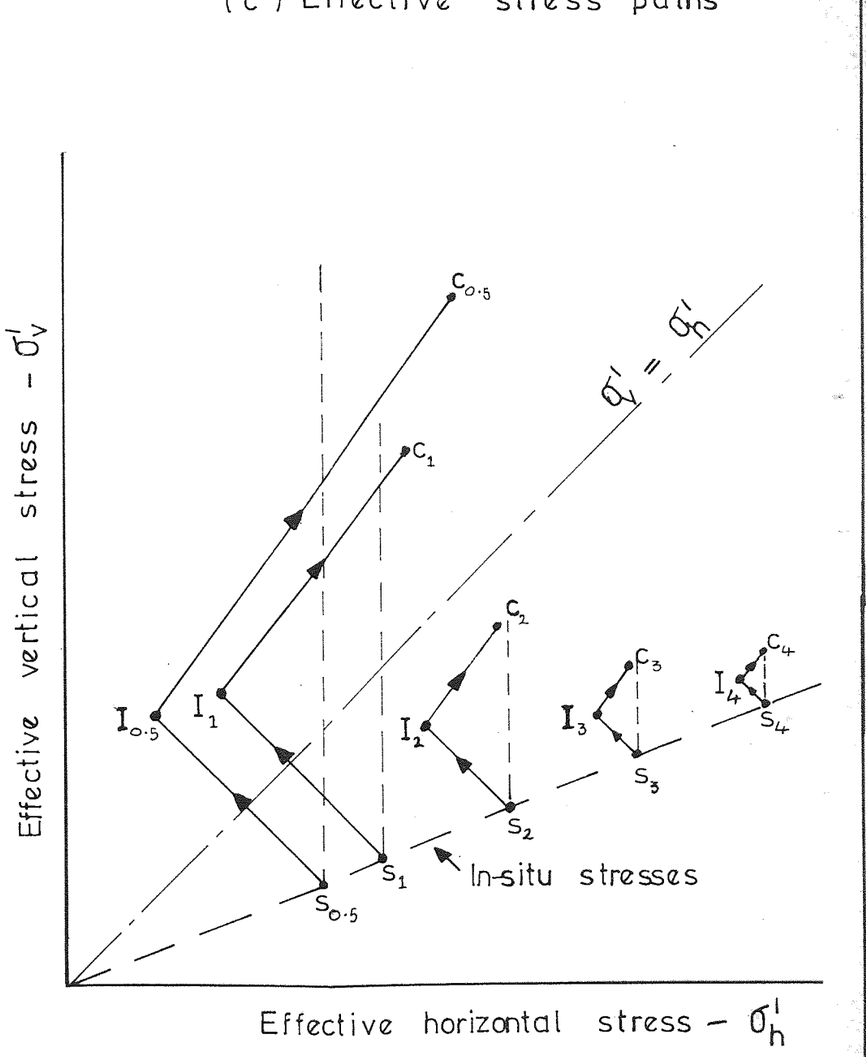

Fig. 3·8 Effective stress paths beneath centre of circular foundation

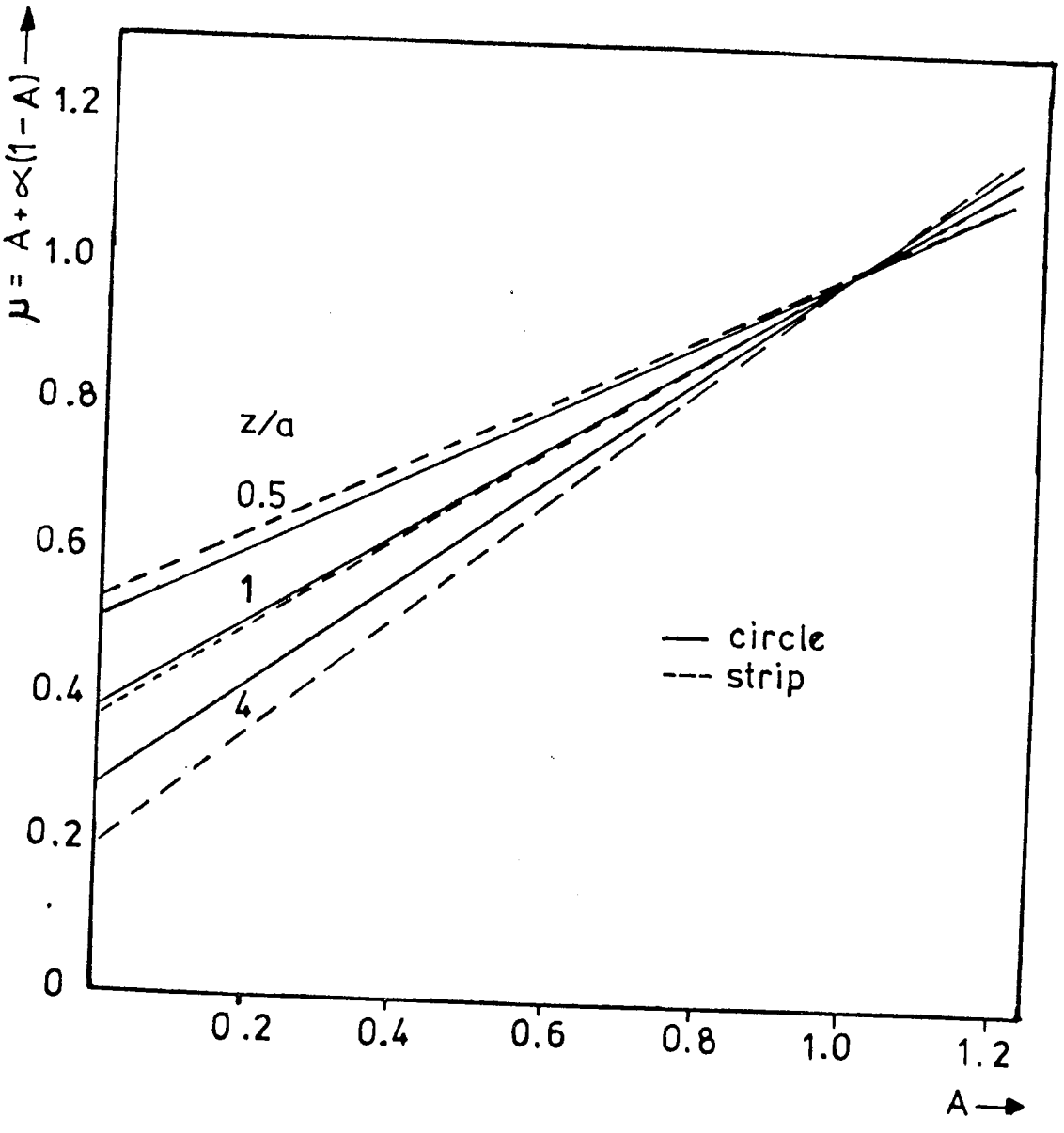

FIG. 3.9 μ factor against pore pressure parameter A - (Skempton and Bjerrum - 1957)

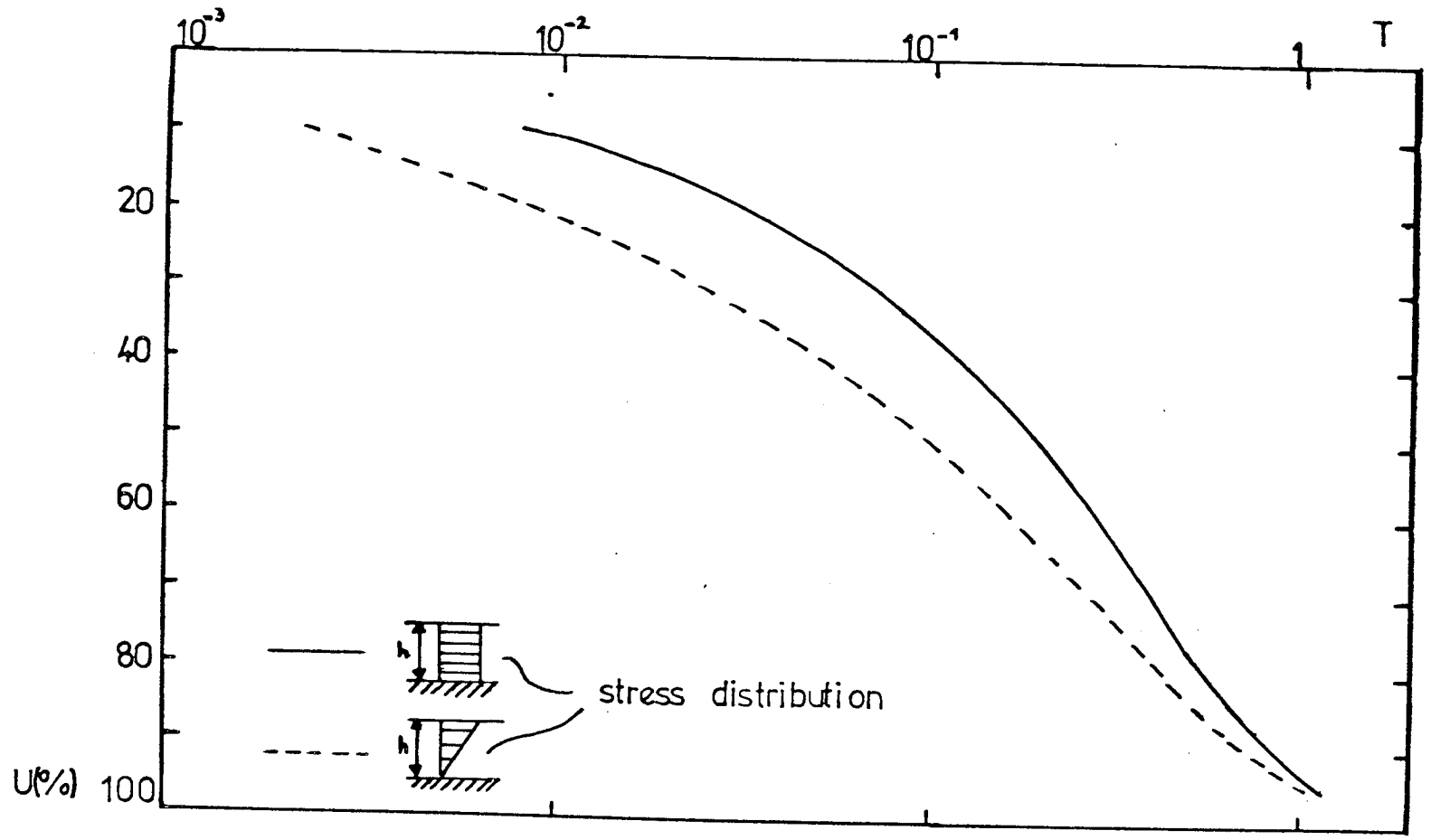

FIG. 3.10 U—T relationship for one-dimensional consolidation - (Terzaghi and Frohlich 1936)

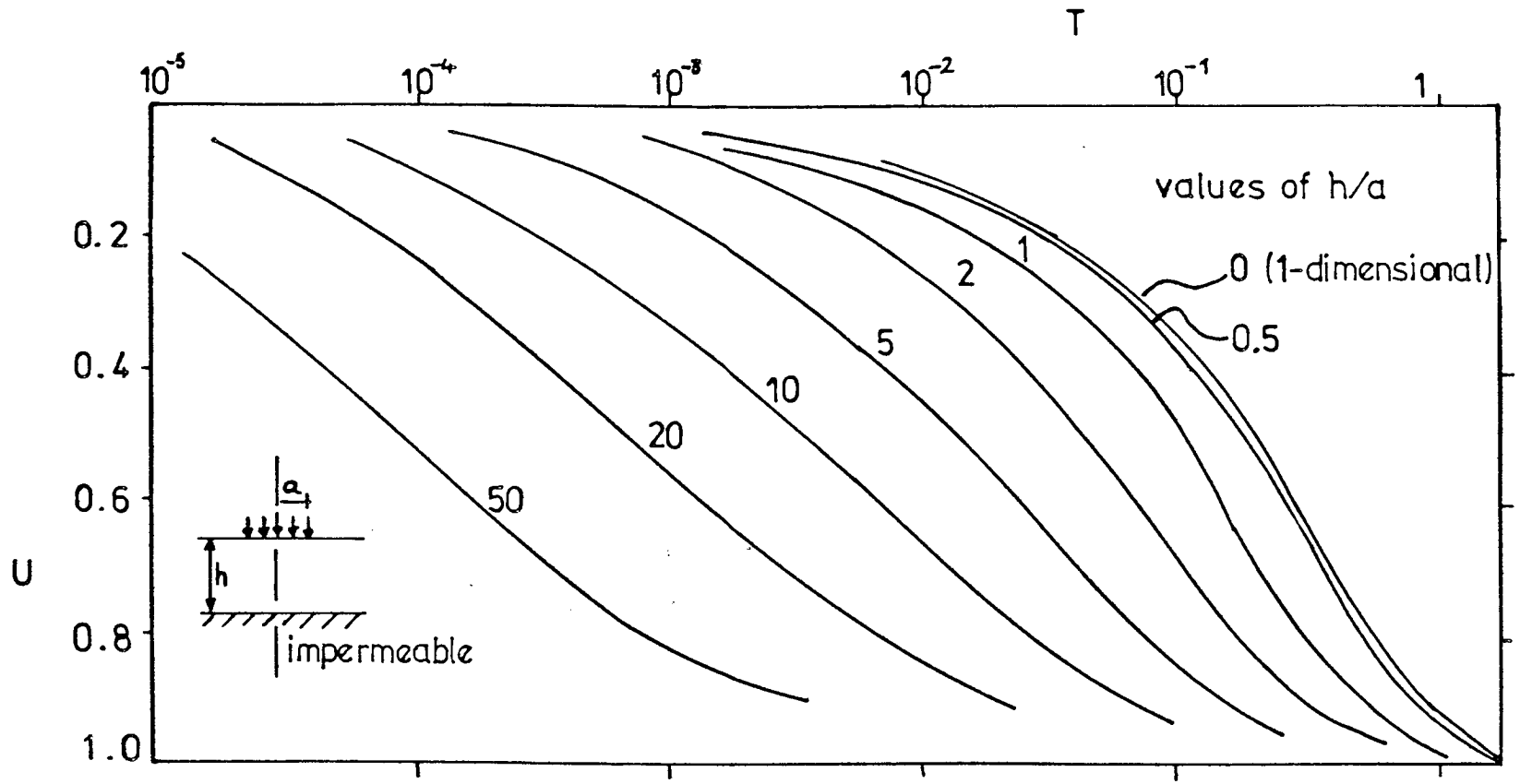

FIG. 3.11 (a) U - T relationship for three-dimensional consolidation circular loading - (Davis and Poulos 1972)

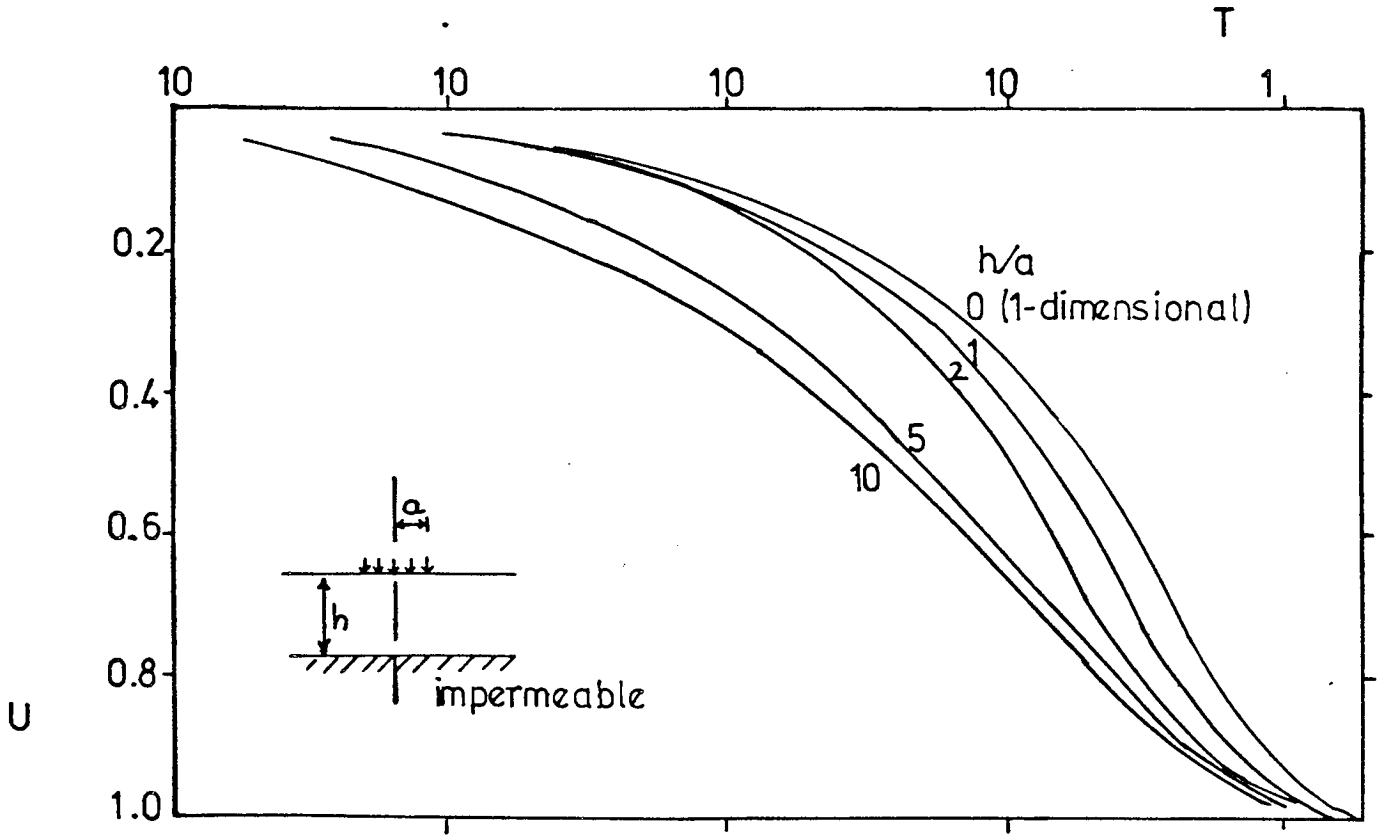

FIG. 3.11 (b) U - T relationship for three-dimensional consolidation strip loading (Davis and Poulos 1972)

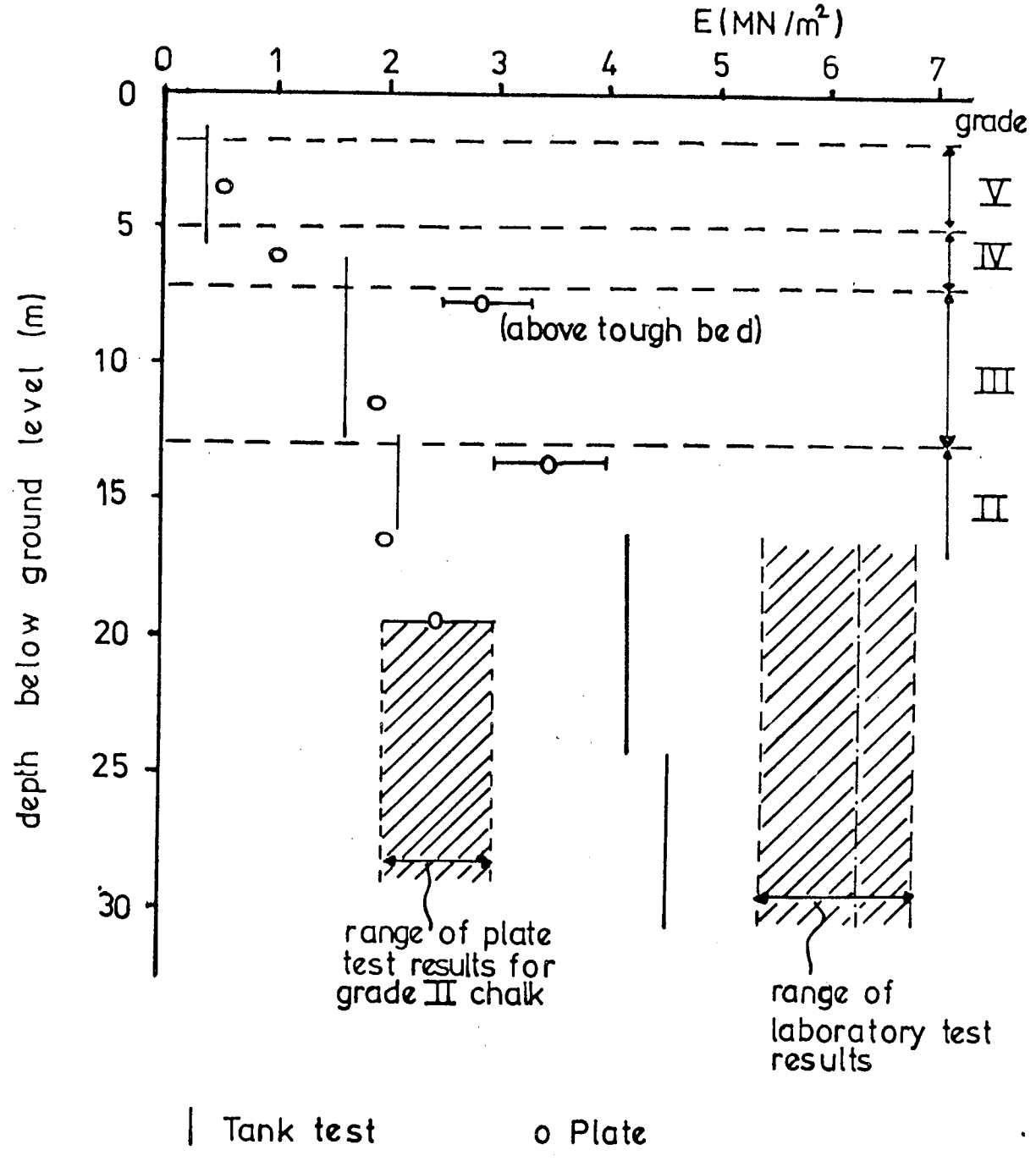

FIG. 3.12 Comparison of Young's modulus E from plate and laboratory tests with values from full-scale tank test - (Burland and Lord 1970)

CHAPTER 4

LOWER LIAS CLAY - GEOLOGY, SAMPLING AND PRELIMINARY MEASUREMENTS

4.1 LOWER LIAS CLAY

Lias is the name given to the lower Jurassic system of rocks, of the Mesozoic era (Table 4.1). The lower Jurassic, or Lias, is generally subdivided into the Upper, Middle and Lower Lias. The Lower Lias is further subdivided into the Lower Lias Clay, Blue Lias Limestone and White Lias at the base. The Lower Lias clay generally accounts for the greater portion of the Lower Lias deposits.

The Lias was deposited under marine conditions which covered much of England, Fig. 4.1(a), and Europe in the early Jurassic times. Fossils are thus generally abundant in the Lower Lias and include representatives of many animal groups. The most common fossil being the ammonite which underwent considerable development during the Jurassic age and hence is useful for the accurate correlation of horizons.

The Lias deposits were, in general, related to a series of 'basins' and 'swells'. The basins were sites of thick deposits, mainly clays, and, although the underlying Rhaetic is remarkably uniform in thickness, the basins began to subside differentially in the early lower Jurassic period. The areas of little subsidence which separated the basins have been called axes. There are three principle axes in Britain, the Mendip, Moreton-in-the-Marsh and Market Weighton axes, Fig. 4.1. The presence of these axes has had a considerable effect on the thickness of the Lias strata, Fig. 4.1(b).

The present day Lias outcrop has been reduced to a band, crossing England, from the Dorset coast through to the Yorkshire coast, Fig. 4.1(a), with the Lower Lias clay, in general, forming the

western fringe. To the north and west of this band most of the Lias has been eroded, only a few outliers remaining e.g. Prees, Carlisle, in Scotland and north east Ireland. To the south and east the Lias deposits remain buried under more recent deposits.

4.2 SAMPLING SITE

The main set of samples were obtained from the clay pit of the Northcot Brickworks, Blockley, North Gloucestershire, Fig. 4.2. This site was chosen because it offered an exposed face from which block samples could be obtained with minimum expense and without interrupting the running of the site.

The clay pit lies approximately 5 km west of the Moreton-in-the-Marsh axis (anticline) as shown on the geological map, Fig. 4.2, and is near the top of the Lower Lias deposits. This is evident from the figure as the site is only 1 km east of the Lower Lias - Middle Lias junction. The depth of the Lower Lias in this region is probably in excess of 180 m and could be as much as 260 m. Borehole records at Mickleton, 6 km north of the site, gives 293 m of Lower Lias while at Stow-on-the-Wold, 11 km south the depth is only 180 m.

The quarry has been worked for many years, and essentially consists of two clay pits, one old and the other, the present workings. The old pit now carries a lake, which during the times of sampling was approximately 2.2 m above the base of the present workings. Approximately 8 m of the deposits had been stripped for some considerable time, to remove material unsuitable for brick production. The sampling was carried out below this level at one end of the newer pit.

A geological section of the quarry (Coulthard 1972) including the material now removed is given in Fig. 4.3. It is seen that the weathered zone extends to just over two metres. Below this the material was described as blue grey clay, except for the section from 4.5 to 6 m. However below the sampling level the blue-grey Lower Lias clay was apparently uninterrupted to the depth of the pit although containing many fossils and occasional ironstone nodule.

4.3 GEOLOGICAL HISTORY OF THE BLOCKLEY AREA

As can be seen from the stratigraphical column, Table 4.1, there is the possibility of a substantial thickness of sediment above the Lower Lias clay, as it lies well below the Oxford, Weald, Gault and the much documented London clay. However, the extent of the various deposits and their depths was dependent on the Palaeogeography at the time of their depositions.

It is seen from texts on Stratigraphy (e.g. Bennison and Wright, 1969) that from the Eocene period onwards the areas of deposition have been confined to the south east of Britain, around the London Basin, therefore these deposits will have no effect on the overburden around the Blockley area. Thus to compute the overburden on the sampled horizon,the sediments from the Lower Lias to the end of the Cretaceous period only,need be considered.

As the samples were taken from near the top of the Lower Lias it was estimated that not more than 10 m of Lower Lias existed above this level. The Middle was up to 70 m thick, but since Blockley was on the edge of the Severn Basin, it is unlikely that the depth, here, was more than 30-35 m. The Upper Lias varies from about 80 m at Breden Hill 20 km west of Blockley, to 25 m at Stow-on-the-Wold, 11 km south of Blockley. It is estimated

that the depth at the sampling site was in the region of 30 to 45 m.

The Middle Jurassic was, in general, a shallow water deposit, producing the Oolite limestones. The estimated thickness of the Middle Jurassic in the Blockley area was 46 to 64 m.

The Upper Jurassic sediments were of much greater thickness than the Middle Jurassic. The Upper Jurassic being normally subdivided into:

Purbeck Beds

Portland Beds

Kimmeridge Clay

Corallian

Oxford clay with Kellaway Beds

The Oxford clay deposits were up to 183 m deep, but in the Blockley area were probably in the region of 122 to 153 m thick. This was followed by the thin Corallian, which was in the order of 4 m. The subsequent Kimmeridge clay was another deep deposit, up to 400 m in Dorset, but in the Blockley area it was only in the region of 245 to 305 m. Following the deposition of the Kimmeridge the central England area was uplifted to become land again, with the Portland and Purbeck Beds being confined to the South coast.

This meant that the overburden at the sampling site, at this time, was in the region of 487 to 616 m. However, during the Portland and Purbeck periods and in the early Cretaceous period, that followed, the central England landmass was eroded, (Allen 1959). It is very difficult to say how much erosion took place, but it could be in the region of 150 to 305 m.

During the latter part of the Lower Cretaceous, the Midlands and South of England became submerged again, and the Gault clay was deposited. The depth in the sampling area was approximately 95 m.

The Upper Cretaceous period saw most of England covered with a shallow sea, with no major landmass near, enabling Chalk to form. The depth of Chalk in central England is difficult to estimate because of the lack of deposits remaining in the central and western part of England. The probable limits of the thickness of the chalk deposits in this area are 245 to 305 m.

There is no evidence of further deposition in this area, so that the overburden at the end of deposition was in the range of 520 to 870 m, Table 4.2, but depends very much on the amount of erosion at the end of the Jurassic period.

Considering average values of depths of deposition and erosion, then the overburden would have been 550 m, at the end of the Jurassic, reducing to 320 m by erosion, and reloading to a maximum overburden of 690 m before unloading to the present overburden, as illustrated in Fig. 4.4.

4.4 SAMPLING AND STORAGE

The main set of samples was obtained from the site described in the previous section, at Blockley, Gloucestershire, but some samples from Gloucester were also tested during the early stages of the developments of apparatus and testing techniques. The types of samples obtained were tube, cored and block, as it was proposed to compare the quality of sample obtained from the three methods.

The tube and cored ('mechanical') samples were taken by

'Geotechnical Engineering Ltd.,' Gloucester. Three bore holes were sunk using water flush rotary drilling technique, with intermittent tube sampling. Each borehole was sunk to 6 to 7 m depth, positioned at approximately 1 m spacing in a triangular pattern and 1.5 m from the top edge of the quarry face. The first borehole was cored to its full depth, using a T-86 core barrel, (Fig. 4.5) which gives a core of nominal diameter of 72 mm. The first one metre was cored using the T-86 single tube core barrel, the remaining depth was cored using the T-86 double tube core barrel (Plate 4.1a). All cores were recovered and returned to the laboratory, selected lengths of core were wrapped on site, immediately after extrusion, and stored for subsequent testing. The second and third holes were cored in a similar manner, but in this case in addition to selected cores, U70 tube samples were taken and sealed on site. The U70 tubes (Plate 4.1b) are thin-walled, high tensile steel tubes of nominal inside diameter of 70 mm, with an area ratio of 20% and having an integral cutting edge of the same internal diameter as the tube i.e. zero inside clearance. The tubes were greased with unrefined petroleum jelly to help reduce friction between tube and sample. The depths of the samples retained for laboratory testing are shown in Fig. 4.6.

Before wrapping, the selected cores were dried of any excess surface water (due to the flushing water) with absorbant paper and a water content sample taken from the ends. The samples were tightly wrapped with a strip of tin foil, approximately 50 mm wide, (Plate 4.2) the ends were folded over tin foil end-discs and pressed down firmly. The ends of the wrapped sample were then repeatedly dipped into a molten micro-wax-petroleum jelly mixture (7 : 4 by weight) until a thickness of several millimetres

was obtained. The remainder of the sample was coated by painting the mixture on with a paint brush, again until a thickness of several millimetres was obtained. After labelling, the samples were placed in the core boxes and transported to the laboratory. On arrival at the laboratory the samples were checked for wrapping damage and if necessary rewrapped, and finally coated with pure microwax, which gave a much harder finish than the mixture, and stored until tested.

The tube samples were cleaned and dried of any excess water at either end, and water content samples taken. The tubes were sealed by placing a tin foil disc on either end of the sample under the molten wax mixture, this ensured that no air was trapped under the disc. The wax mixture plug, at each end, was at least 10 mm thick. The tubes were then labelled and transported to the laboratory and checked before storage, as the cored samples.

Block samples were obtained as close as possible to the 'mechanical' samples. An excavation was made in the face of the quarry, approximately 2.5 m wide and 1.5 to 2 m into the face at ground level, (Plate 4.3). Due to lack of finance excavation was not assisted by mechanical plant, but was all carried out by hand, using sharpened mattocks and spades. Initially a 610 mm Homelite petrol chain saw was used, but with very little success. Clogging and overheating of chain and guide, with excessive stretching of the chain being the main problems, progress and safety being better assisted by its absence.

The clay was carefully excavated so as to leave two blocks each about 400 mm square and at least 400 mm deep at each level (Plate 4.4). The blocks were then trimmed to 300 mm square using sharpened, cut-off spatulas or putty knives. This was essentially a slow process, otherwise smooth faces were not achieved,

therefore as soon as a face was finished it was coated with a thin layer of the wax mixture, to prevent, or reduce, drying. The top 50 to 100 mm of material was trimmed, a spot level taken and direction of orientation marked. A coat of wax mixture was applied and a sheet of tin foil pressed onto the top and over the sides, the wax mixture also helped to obtain a close fit of the foil as it was fairly tacky. In order to dislodge the block, it was undercut on all sides with a spatula, and finally severed from the ground with a spade. The bottom face was then trimmed, waxed and covered with the tin foil, all the joints were sealed with adhesive tape, Plate 4.5. The block was then carried to the top of the excavation on a board, and coated with the wax mixture ready for transportation back to the laboratory. As with the 'mechanical' samples, the blocks were examined, on arrival, for wrapping damage and then coated with the pure microwax to obtain a much harder and less tacky coating.

The block samples were obtained from three levels (Fig. 4.6) but as excavation and trimming was so slow only one level could be worked each day. To protect the excavated area from overnight rain, or drying, it was covered with polythene sheets and some of the excavated clay. However, although two blocks were recovered from each level, only one of each was returned to the 'soils' laboratory, the other being used by the Geology department, (Coulthard, 1972).

4.5 INSITU PORE PRESSURES

In order to be able to determine the insitu effective stresses it is essential to know the insitu pore pressure profile. Although the exact position of the ground water level was not evident from inspection of the site, it was obvious that it was below the level of the bulk of the samples. It was therefore

decided to try to establish the pore pressure profile by insitu measurements. As these measurements were to be made at the same time as the block samples were taken, it was necessary to use a readily portable apparatus with a pore pressure probe that could be installed manually.

A pore pressure probe was designed with a porous tip carried on the end of a length of galvanised tube (Plate 4.6). The tip carried an Aerox grade 6 ceramic stone (high air entry value stone), 13.5 mm diameter by 9.22 mm long, on a central core with ports connecting into a length of saran tubing. The tip was glued into a 380 mm length of 12.7 mm diameter galvanised tube, through which the saran tubing passed before connecting into a pressure measuring board. The pressure board comprised of a Bishop null indicator, a screw pump, mercury manometer and a container of deaired water; this enabled pressures (positive or negative) to be measured under zero volume change, providing the whole system was saturated. A diagramatic sketch of the pressure board and probe is shown in Fig. 4.7.

During the block sampling sessions pore pressure probes were inserted at the back of the excavation, to obtain the pore pressure profile over this range. To extend the profile over the depth range of the 'mechanical' samples it was necessary to insert probes at levels below the block sample excavations. At such levels small 'local' excavations were made to ensure that the probe was inserted at least 1 to 1.5 m into the quarry face. To install the probe a hole was drilled, in the back of the excavations, with a 12.7 mm diameter wood-workers brace and bit, (Plate 4.7a), to a depth of approximately 300 mm - this was the maximum length of a 12.7 mm bit. The first portion of the hole was drilled oversize, to enable easy insertion of the probe over this length, and the last 40 to 50 mm were drilled carefully

to ensure a tight fit for the porous tip at this depth. The probe was flushed with deaired water and the mercury level set in the null indicator. The probe was then pushed quickly into the drilled hole by hand and gently tapped with a hammer over the last 40 to 50 mm. The pressure board operator attempted to maintain a null position of the mercury thread during insertion and subsequently until equilibrium was obtained. The equalisation curves for several probes are shown in Fig. 4.8; it can be seen that equalisation was achieved in 2 to 3 hours. It was normally found that during insertion a fairly high suction (up to 50 kN/m^2) was required to maintain the null position of the mercury thread, but dropped considerably soon after insertion was complete. Water contents were taken at several of the probe sites to check that the probes had penetrated beyond the dessicated zone.

A plot of pore pressure readings against depth is shown in Fig. 4.9, a fairly wide scatter is evident. However, probes 'C' and '4' may be ignored; air bubbles were observed in a saran tubing on probe 'C', later found to be due to a poor connection, and at probe '4' the water content, of 15.7%, indicated that the probe was too near the quarry face. A straight line, of slope ($- 1/\gamma_\omega$) fits, reasonably, the remaining probes and the observed springs at the bottom of the quarry, and if taken to represent the insitu pore pressure distribution implies that all the samples were obtained from the capillary zone; this is somewhat varified by the fact that all the samples have degrees of saturation of approximately unity.

4.6 INSITU VERTICAL STRESSES

The insitu total vertical stress can be computed from the knowledge of the bulk densities of samples used in the triaxial and

oedometer tests. A plot of bulk density against depth, Fig. 4.10, shows that the density remains constant with depth at 2.19 gm/ml to an accuracy of ± 2%, thus giving a unit weight of 21.48 kN/m^3. The total insitu vertical stress therefore increases linearly with depth (σ_v = 21.48 Z), Fig. 4.11. The insitu effective vertical stress is obtained by subtracting the pore pressure-depth curve, (Fig. 4.9), from the total vertical stress-depth curve, producing the linear relationship A' - B' Fig. 4.11

4.7 PHYSICAL PROPERTIES

4.7.1 Water Content

During the sampling sessions water content samples were taken from the tubes, cores and blocks. The water contents determined from these samples are plotted, in Fig. 4.12, against depth. There is no apparent trend of change in water content with depth, nor is there any indication of the normal distribution of test results. The values are scattered between 16 and 21.8%, although the majority of points lie between 17 and 19.5%, with an overall average value of 18.4% This sort of variation in water content, for a fissured heavily overconsolidated clay, is not unusual - for example Skempton (1961), reports such variations for London Clay.

4.7.2 Atterberg Limits

Liquid and plastic limit tests were performed on samples from boreholes 2 and 3, at Blockley, according to the specifications set out in BS 1377 (1967). The values obtained for each borehole are plotted against depth, in Fig. 4.13. The liquid limit varies from 53 to 63%, with a mean of 59%. The plastic limit gives more consistent values varying from 25 to 29%, with

a mean of 27%. The mean value of the plasticity index for the clay then being 32%.

It was attempted to determine the shrinkage limit of the clay. The method used was based on the 'Linear Shrinkage' test, BS 1377, and is described in Appendix A. A typical plot of length of sample against water content is shown in Fig. 4.14. In the early stages the water content decreased without change in length, the volume change being due to initial dishing of the upper surface. On all the specimens longitudinal shrinkage commenced at a water content between 40 and 46% (i.e. consistency index of approximately 0.5). The length of the specimen then decreased linearly with decrease in water content, to approximately plastic limit, indicating specimen saturation. As the water content dropped below the plastic limit level the curve flattens to become horizontal. The shrinkage limit was taken as the intercept between the horizontal line, through the final dry length, and the saturated portion produced. The mean value of shrinkage limit obtained from this method, from ten tests, was 18%, with a maximum of 19.5% and a minimum of 17% (Fig. 4.13). This seems to be rather high for the shrinkage limit, particularly when many of the undisturbed samples had water contents below this with the degree of saturation still equal to unity. From a plot of the degree of saturation against water content, (Fig. 4.15) for the triaxial samples it would appear that the shrinkage limit was in the region of 15 to 15.5%.

The differences could be due to 'remoulded' as against 'undisturbed' state of the soil or due to the fact that the'Linear Shrinkage' technique is not reliable for the determination of the volumetric shrinkage. It is therefore considered that the value of shrinkage limit should be taken as 15-15.5%

4.7.3 Specific Gravity of the soil particles

Specific gravity tests were carried out in accordance to BS 1377 test 6(A), for fine grained soil. It was found necessary, for repeatability of results to allow the bottle plus soil and water to stand in a constant temperature bath overnight, rather than for 1 hour. A plot of specific gravity against depth is shown in Fig. 4.16(a) for boreholes 2 and 3 separately. It is found that the values of specific gravity varies from 2.67 to 2.75 with a mean of 2.72, which is the value used in all appropriate calculations.

4.7.4 Particle size distribution

A particle size analysis was carried out to the standard method for fine-grained soils (pipette method), B.S. 1377 (1967), test 7(c). Samples from various depths of boreholes 2 and 3 were analysed and the plot of percentage clay against depth is shown in Fig. 4.16(b). The mean grading curve for all the tests is shown in Fig. 4.17, which indicates a clay content of 43%.

Analysis of the same material by point counting from slides (Coulthard, 1972) gives a clay content of 80-90%, with 5% quartz, 2-6% Pyrite, up to 2% calcite and up to 2% organic matter. This would indicate that the treatment for preparation of the samples for the sedimentation analysis does not disperse all the clay particles and that some are still aggregated and are acting as silt sized particles. Similar observations have been made in the Keuper Marl research carried out at Birmingham University and reported by Birch (1966) among others.

Using the X-ray diffraction (X.R.D.) technique Coulthard showed

that of the clay particles, 60% were Illite, 38% Kaolin and the remaining 2% consisted of various other clay minerals.

TABLE 4.1 STRATIGRAPHICAL TABLE

ERA	SYSTEM		
QUATERNARY	Pleistocene		
TERTIARY	Pliocene		
	Oligocene		
	Eocene		London clay
MESOZOIC	Cretaceous		Gault clay Weald clay
	Jurassic	Upper	Oxford clay
		Middle	
		Lower (LIAS)	Lower Lias clay
	New red Sandstone	Triassic	Keuper Marl
		Permian	
PALAEOZOIC			

TABLE 4.2 PREDICTED OVERBURDEN AT SAMPLING SITE, BLOCKLEY

DEPOSIT	THICKNESS (m)	TOTAL OVERBURDEN ON SAMPLES (m)	OVERBURDEN USING AVERAGE THICKNESS (m)
Lower Lias clay	10	10	
Middle Lias	30-35	40-45	
Upper Lias	30-45	70-90	
Middle Jurassic	46-64	116-154	
Oxford clay	122-153	238-307	
Corallian	4	242-311	
Kimmeridge	245-305	487-616	520
EROSION	-(150-308)	182-446	320
Gault	95	277-541	
Chalk	245-305	522-846	690

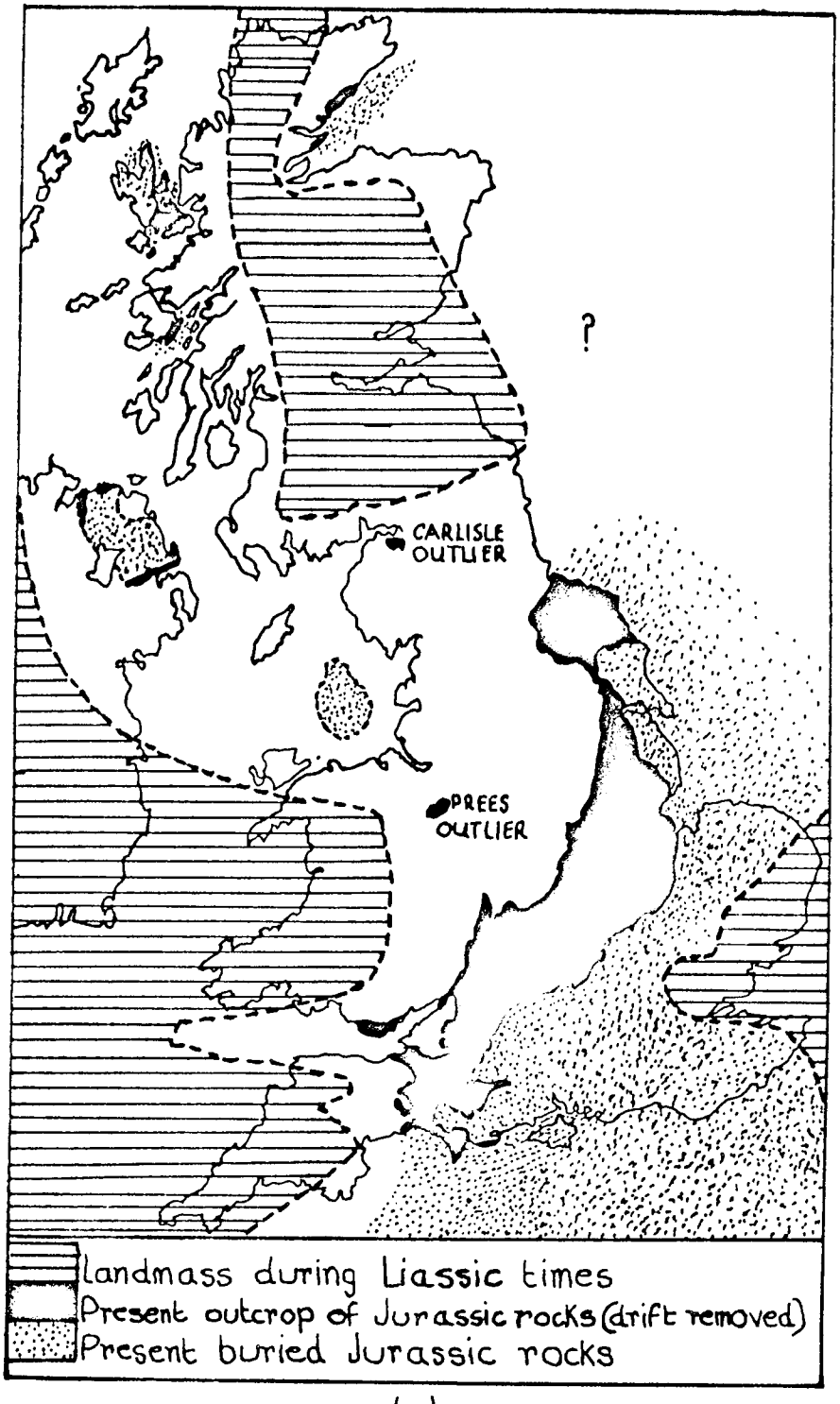

(a)

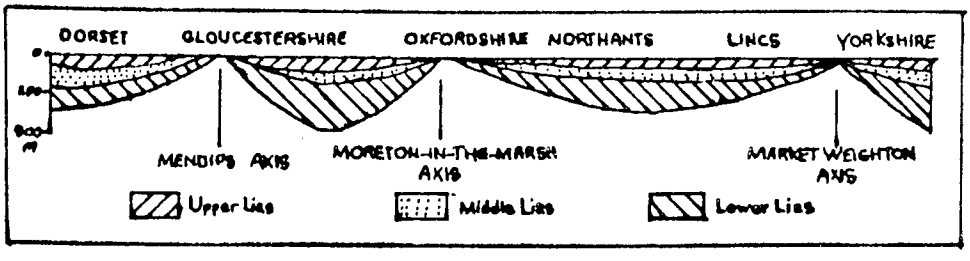

(b)

FIG 4.1 Extent of Liassic Deposits

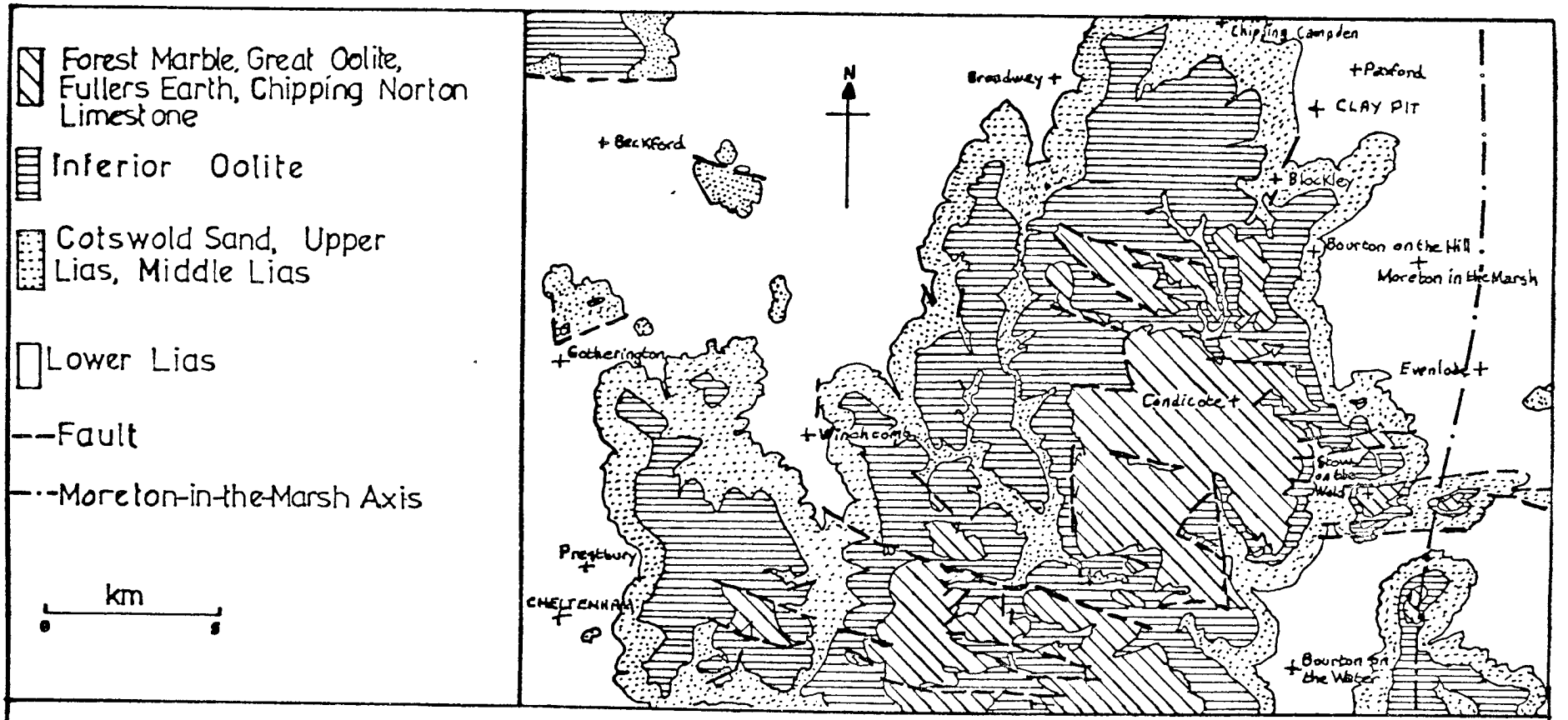

FIG. 4.2 Geological Map of the Sampling Area

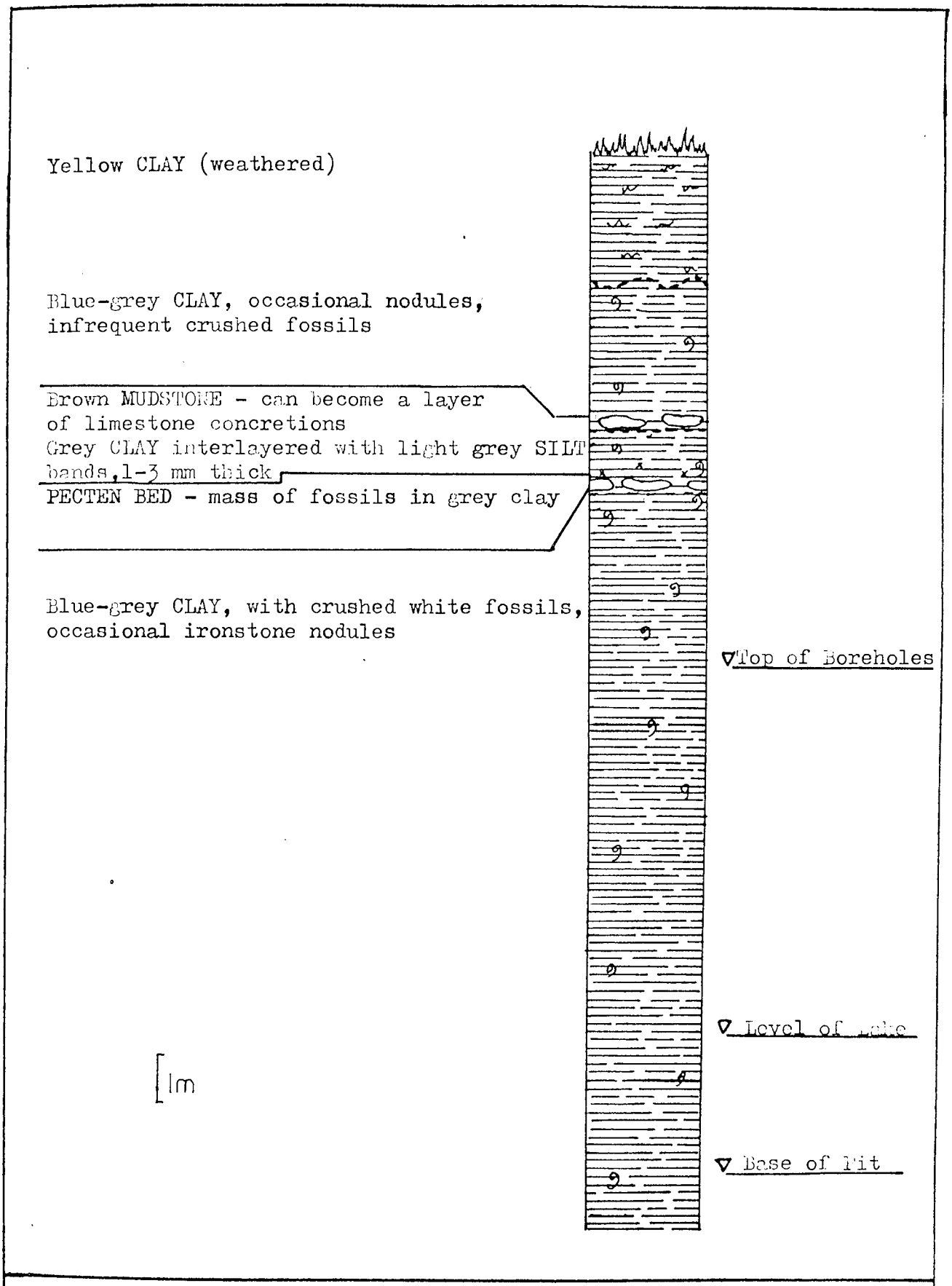

FIG. 4.3 Geological Section at Clay Pit, Blockley

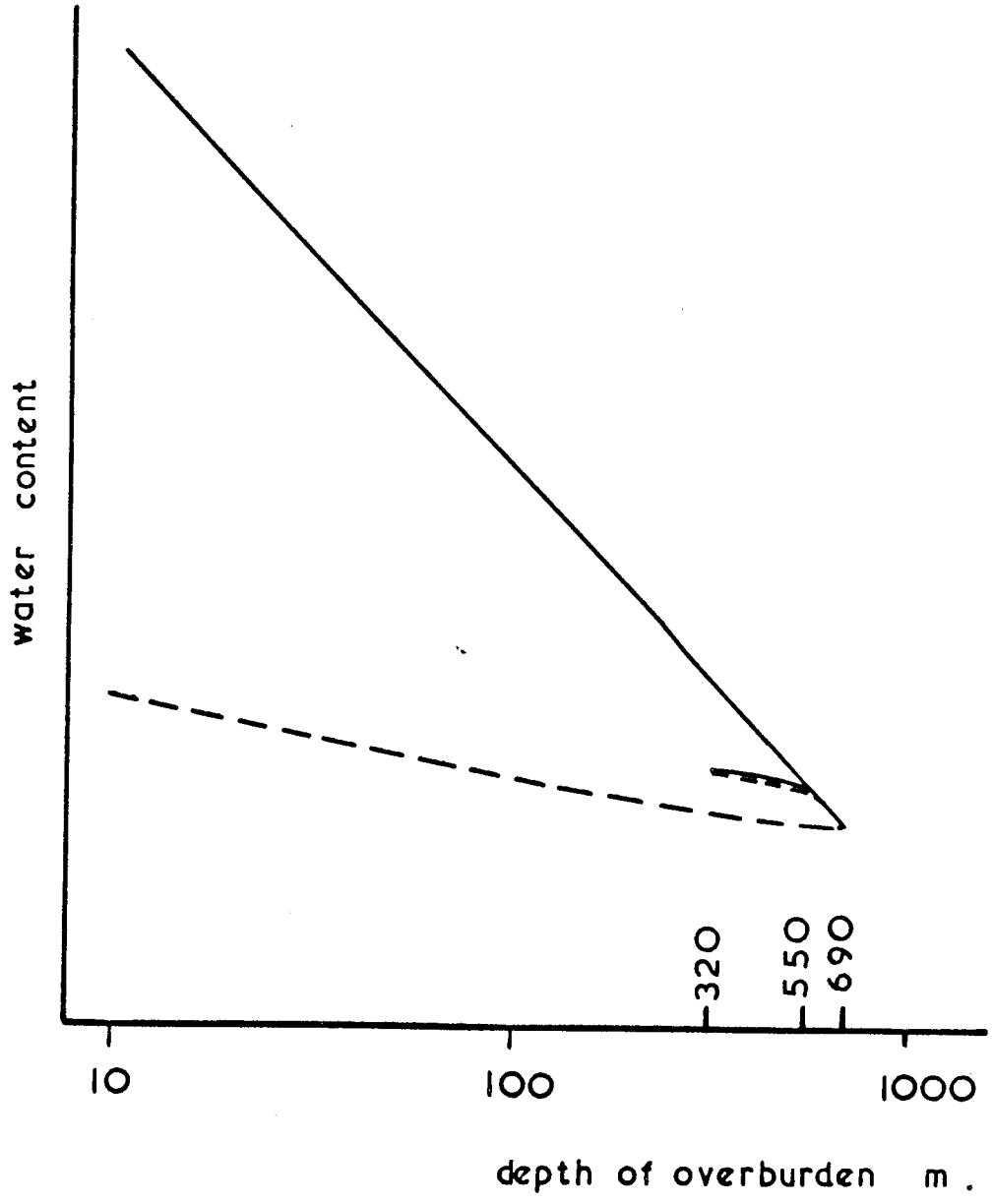

Fig. 4.4 Depositional history of sampling site

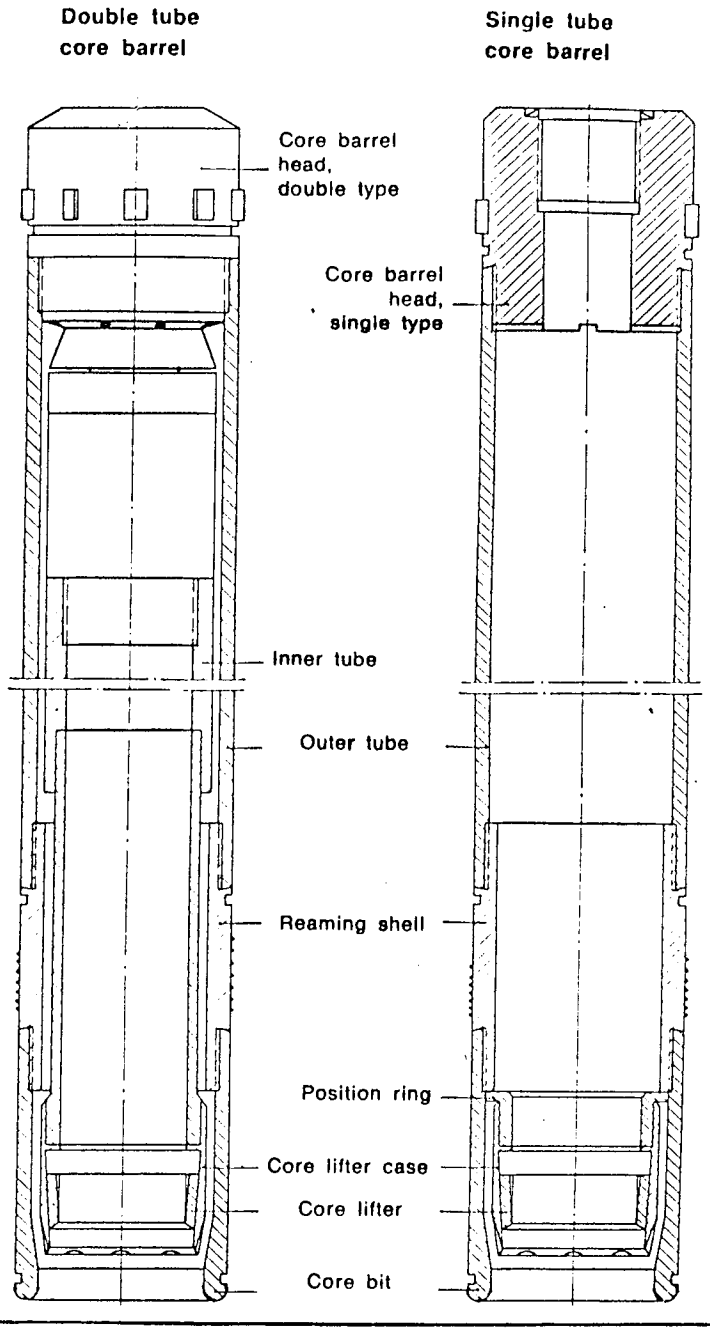

DIMENSIONS	METRIC HOLE SIZES						
Denomination	T-36	T-46	T-56	T-66	T-76	T-86	T-101
Outer tube outer diameter mm	35	45	55	65	75	85	99
Nominal hole diameter mm	36	46	56	66	76	86	101
Nominal core diameter mm	22	32	42	52	62	72	84
Core barrel head threaded for rod size as standard*	33	42	50	50	50	50	50
Core barrel lengths for all sizes as required	350 mm – 1500 mm – 3000 mm						

FIG. 4.5 T - Core Barrel

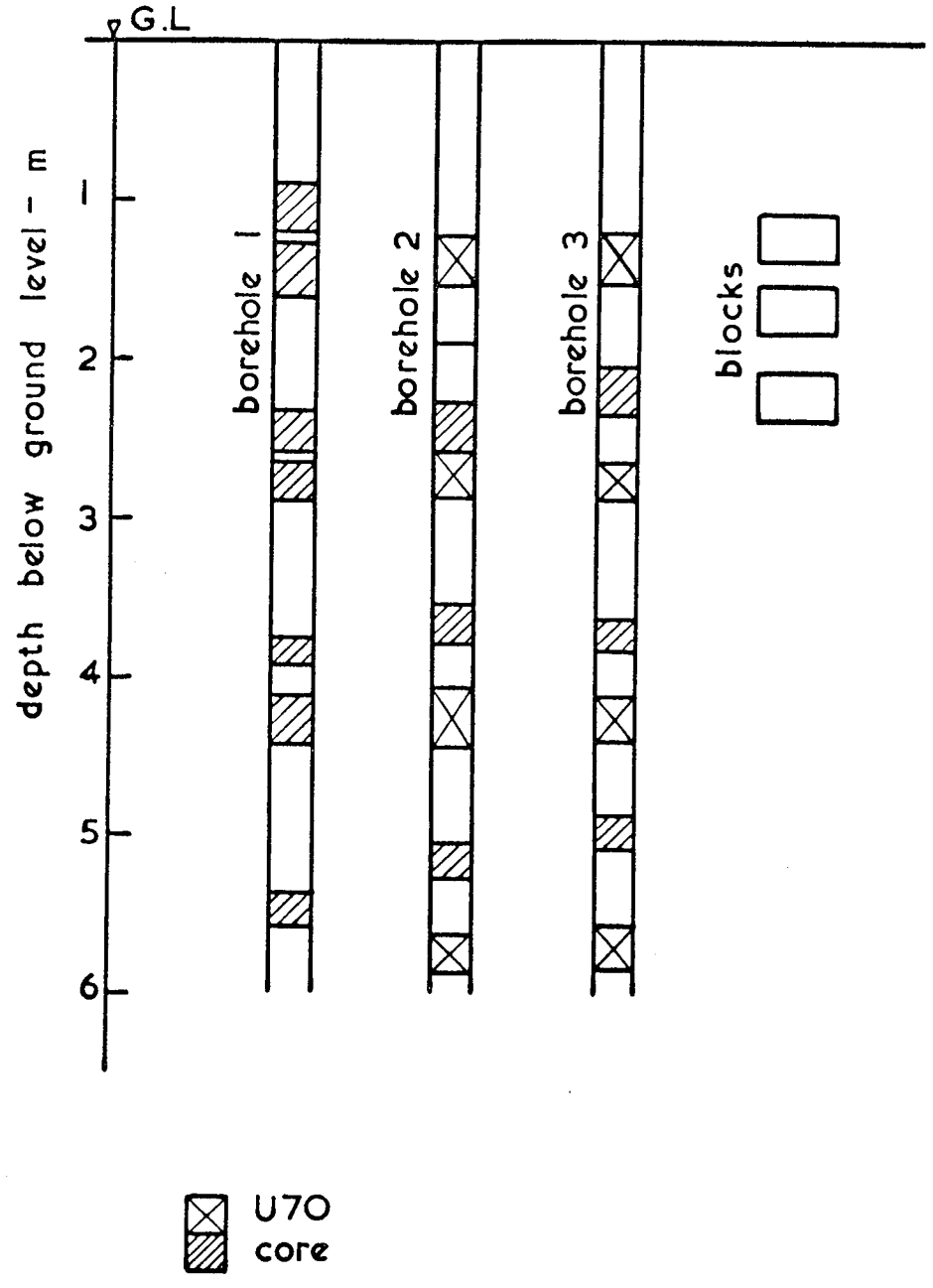

Fig .4.6 Depths of retained samples

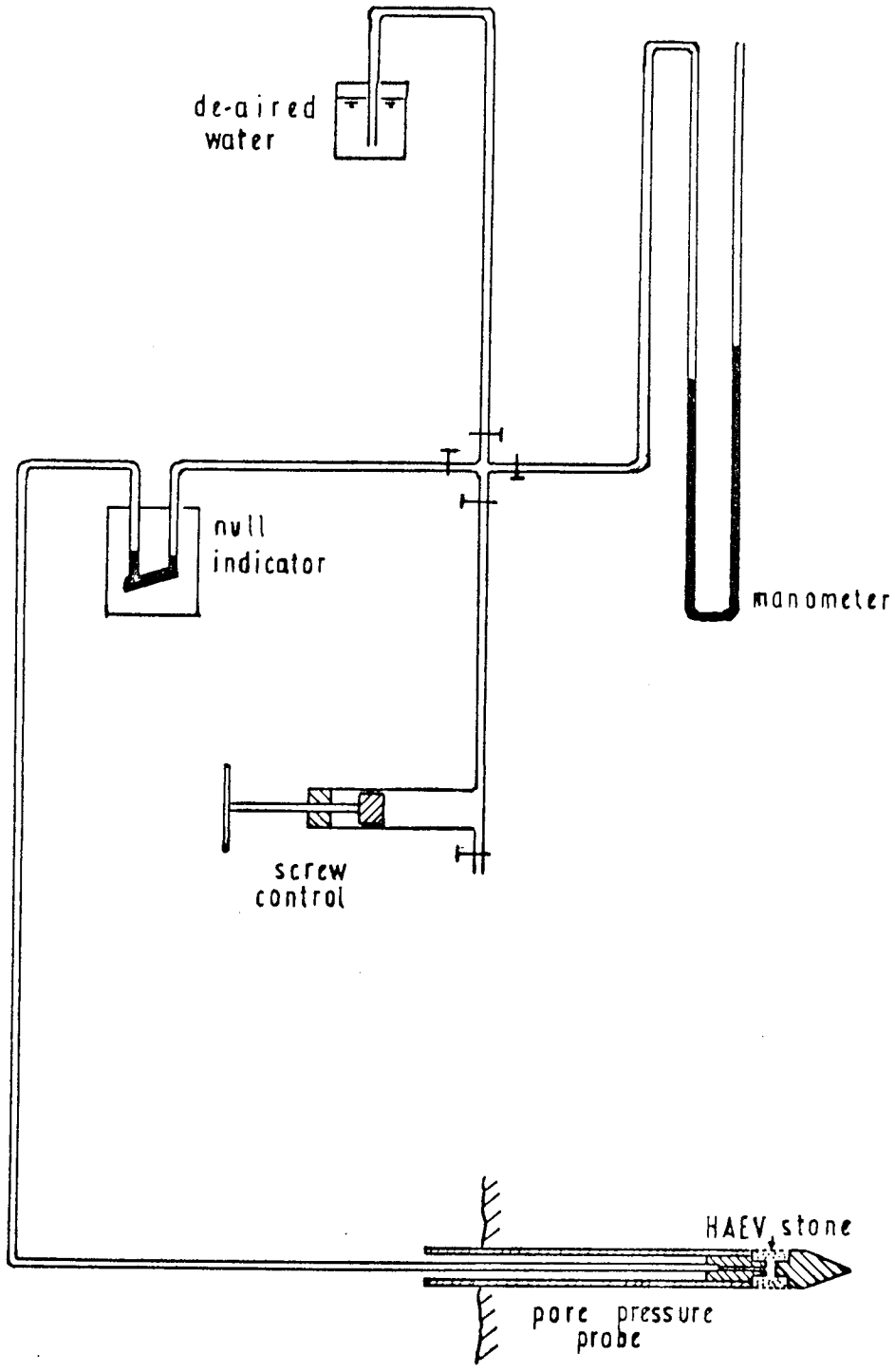

FIG. 4.7 Pore Pressure Probe and Board.
Schematic Diagram

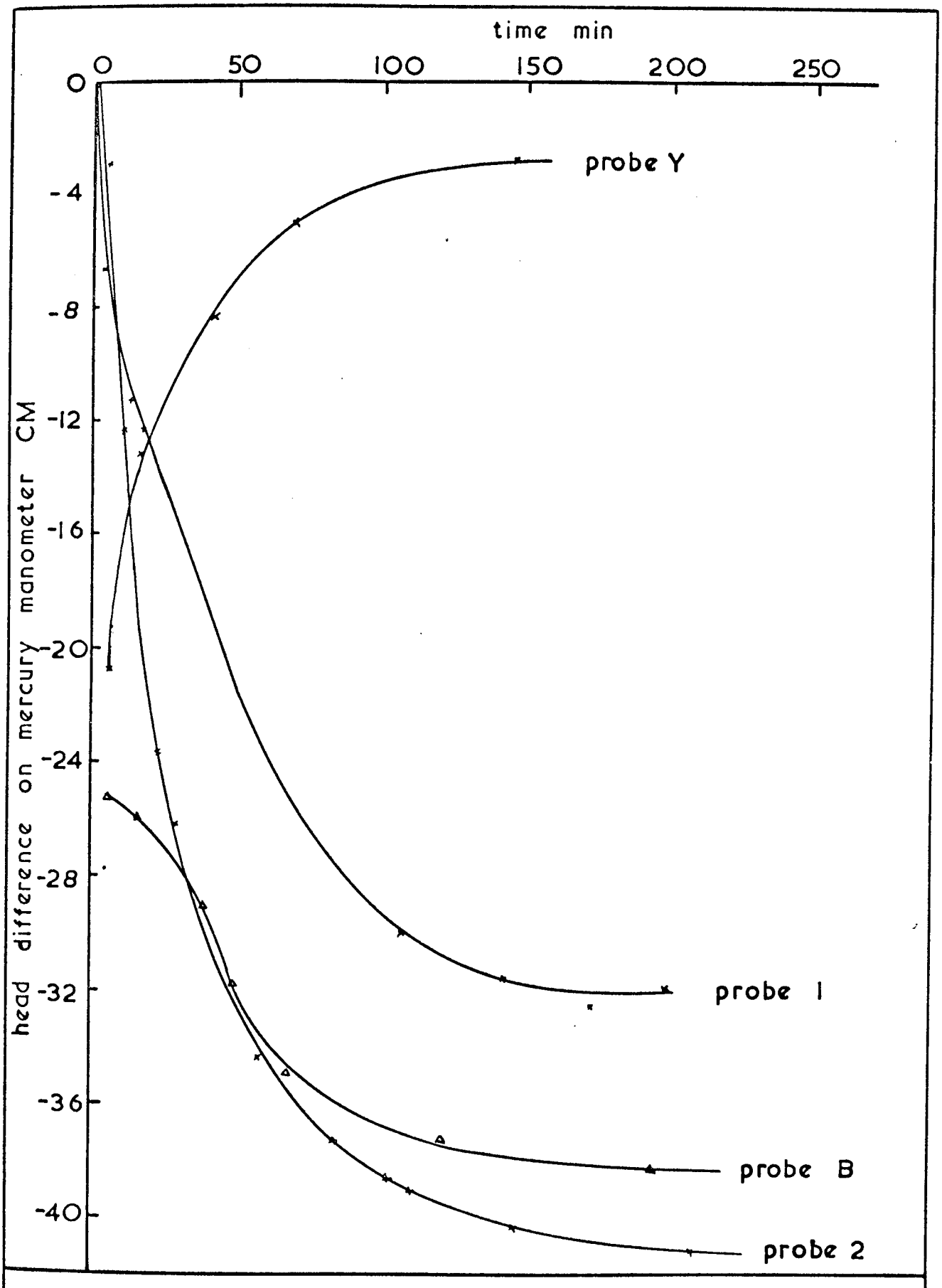

Fig. 4.8 Pore probe equalisation curves

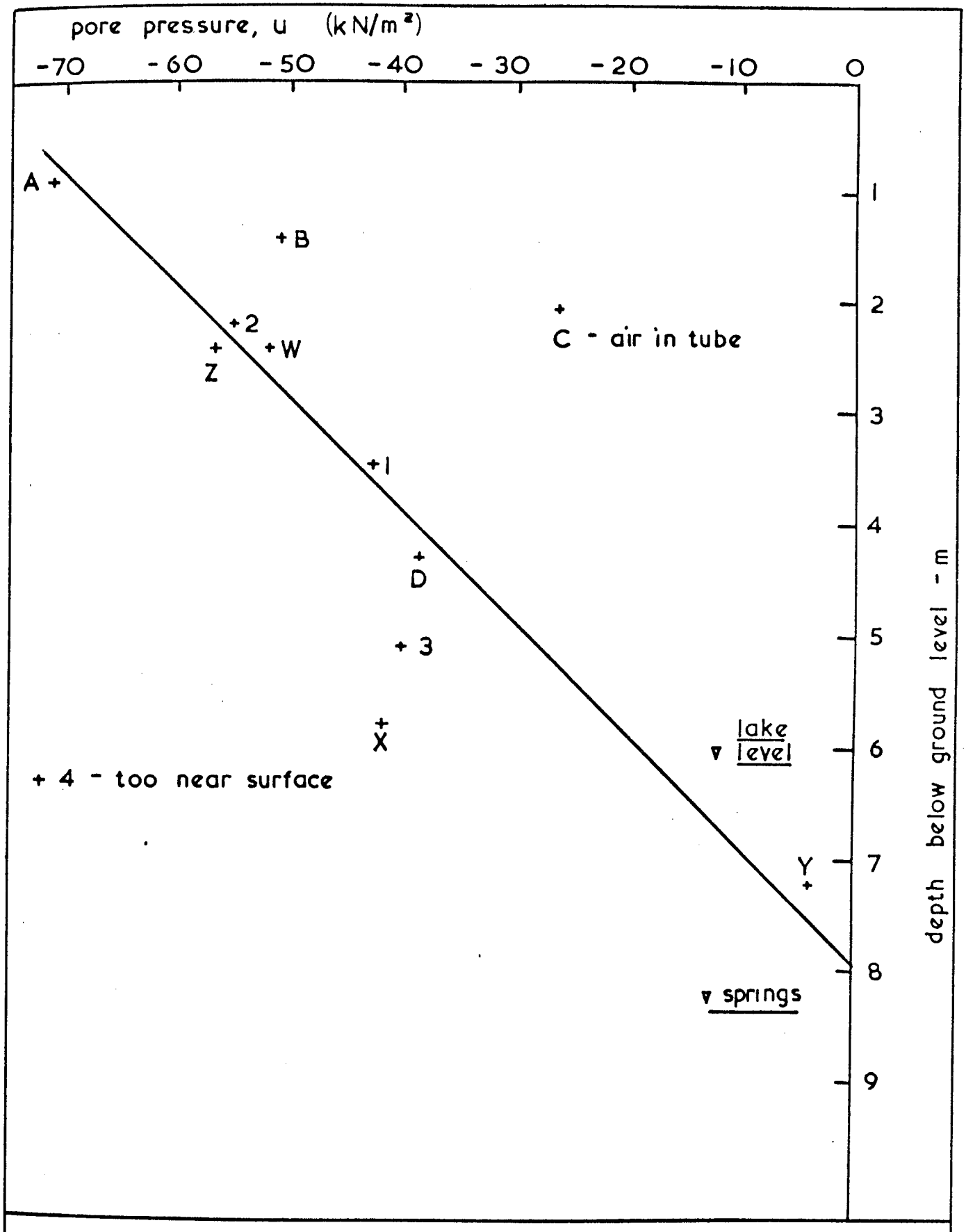

Fig. 4.9 Pore pressure measurements against depth

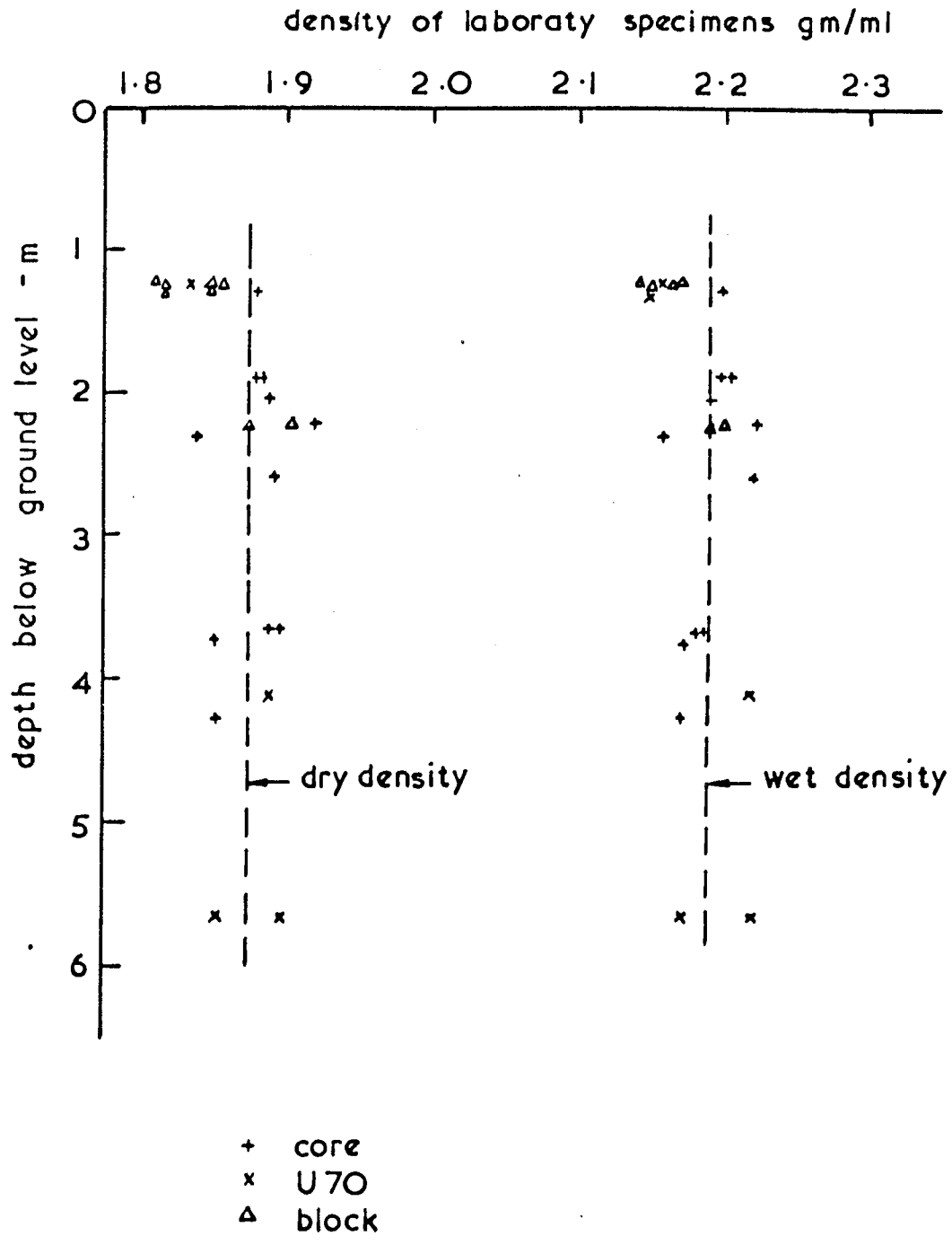

Fig 4.10 Wet and dry density against depth

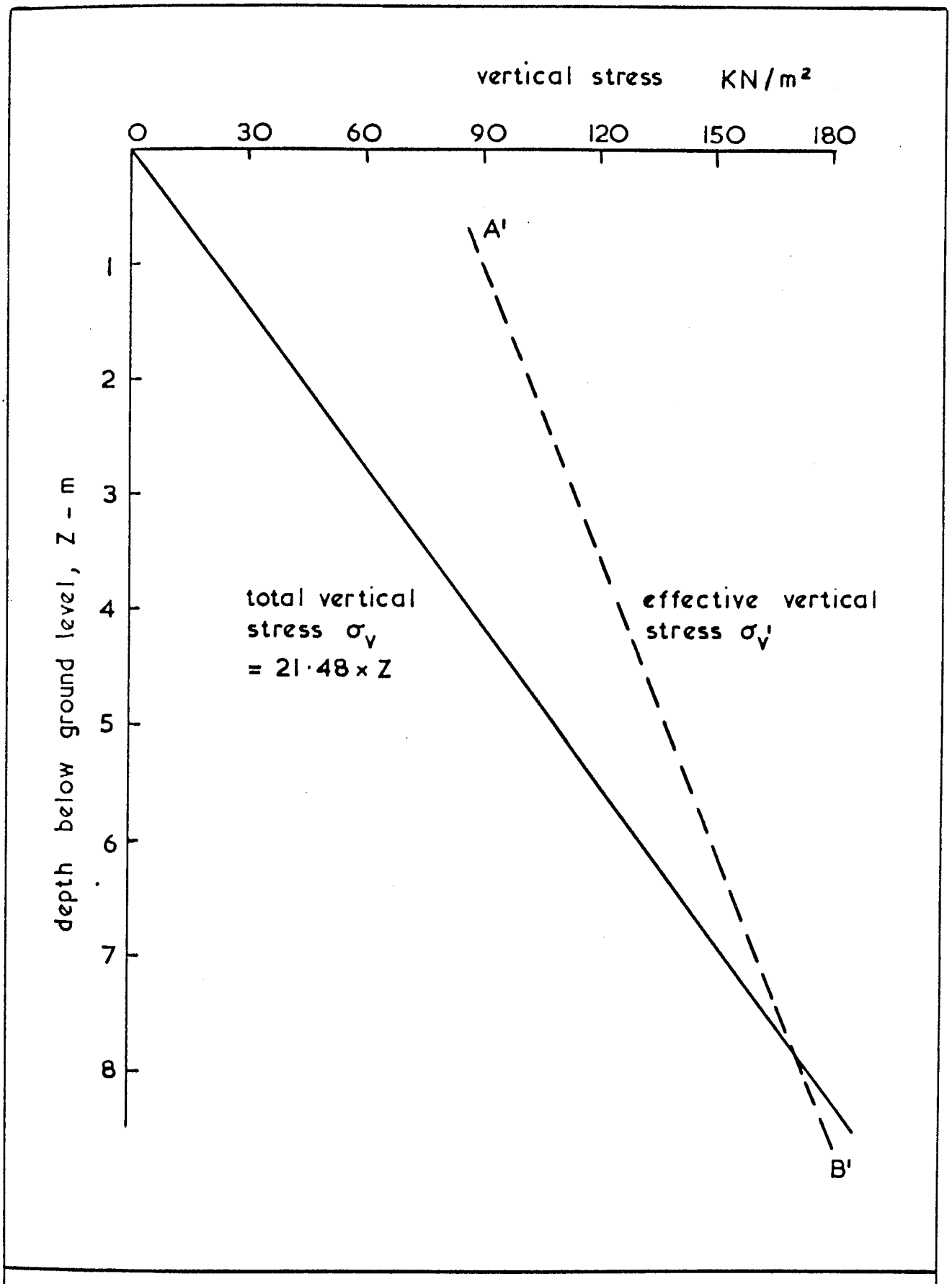

Fig. 4.11 Insitu vertical stress Blockley

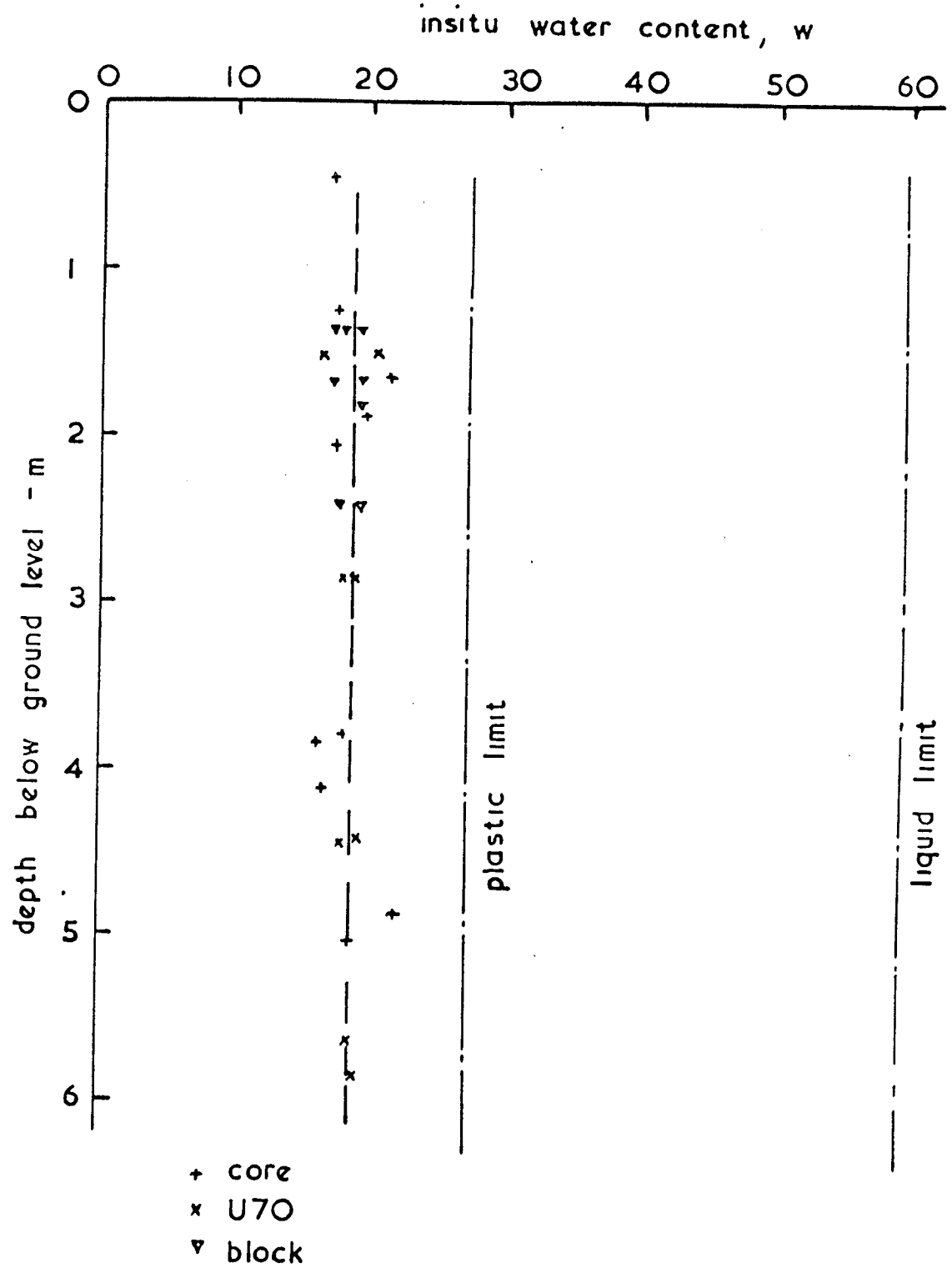

Fig 4.12 Insitu water content

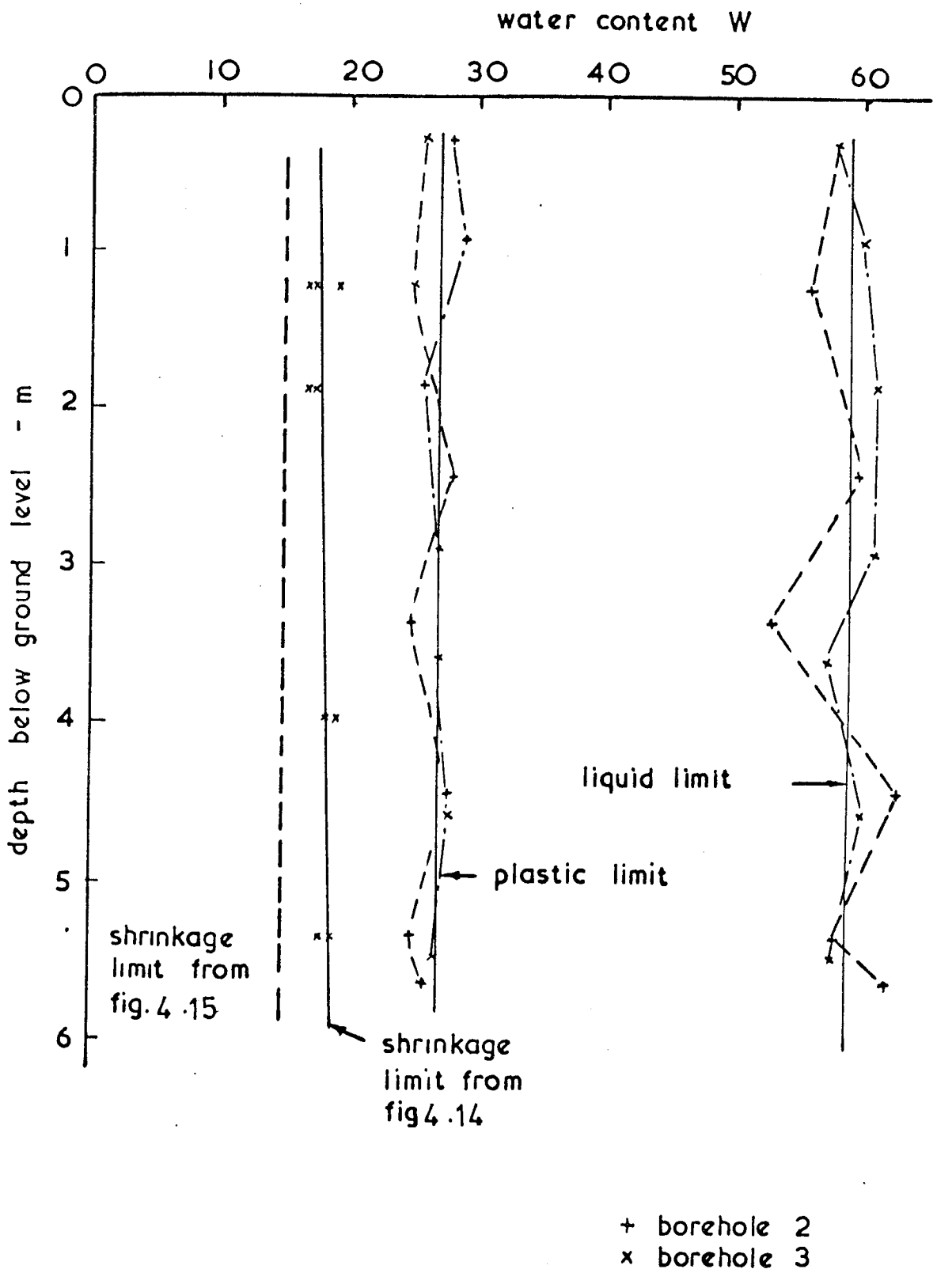

Fig . 4 .13 Atterberg limits

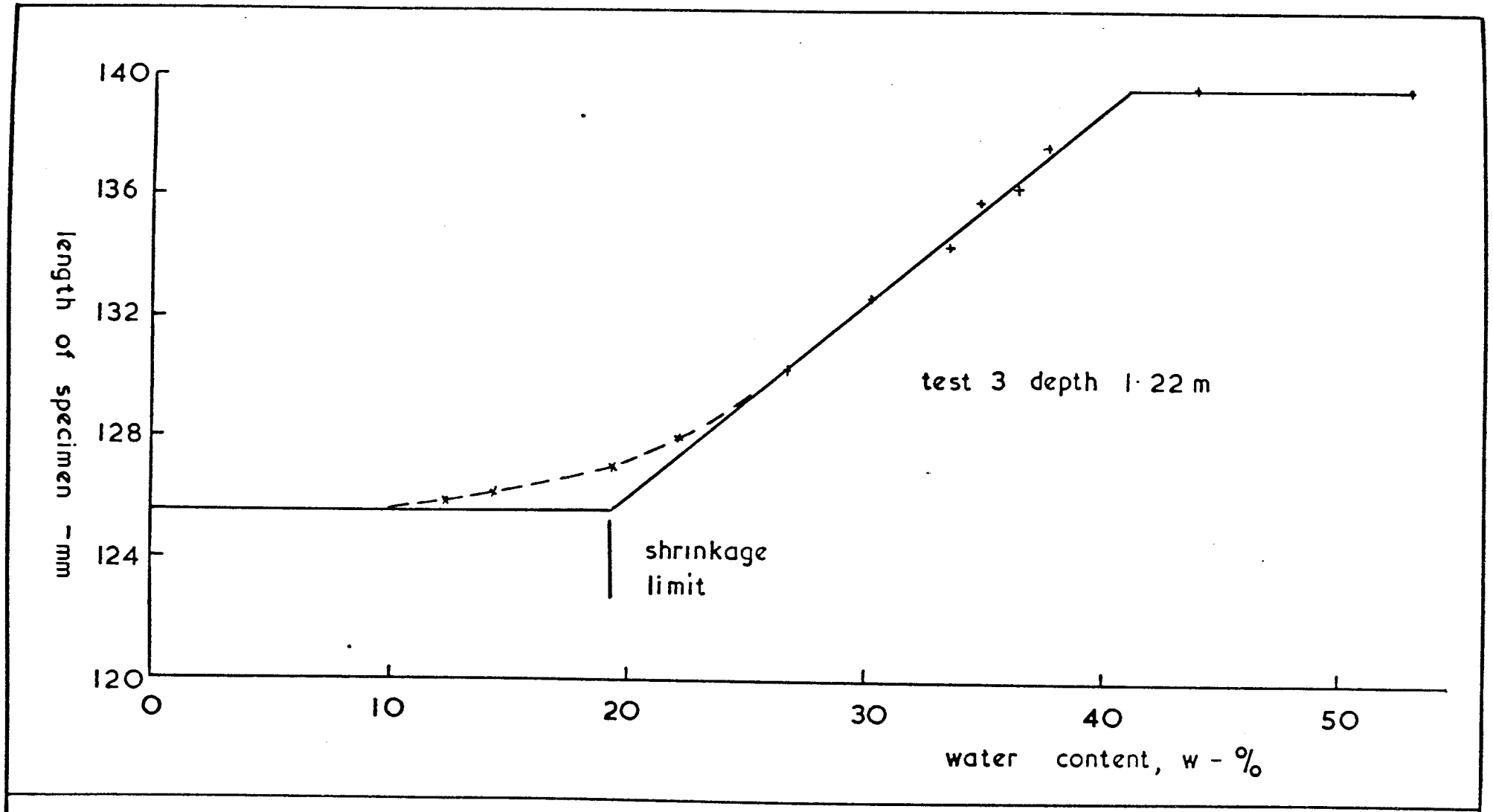

Fig 4.14 Shrinkage curve

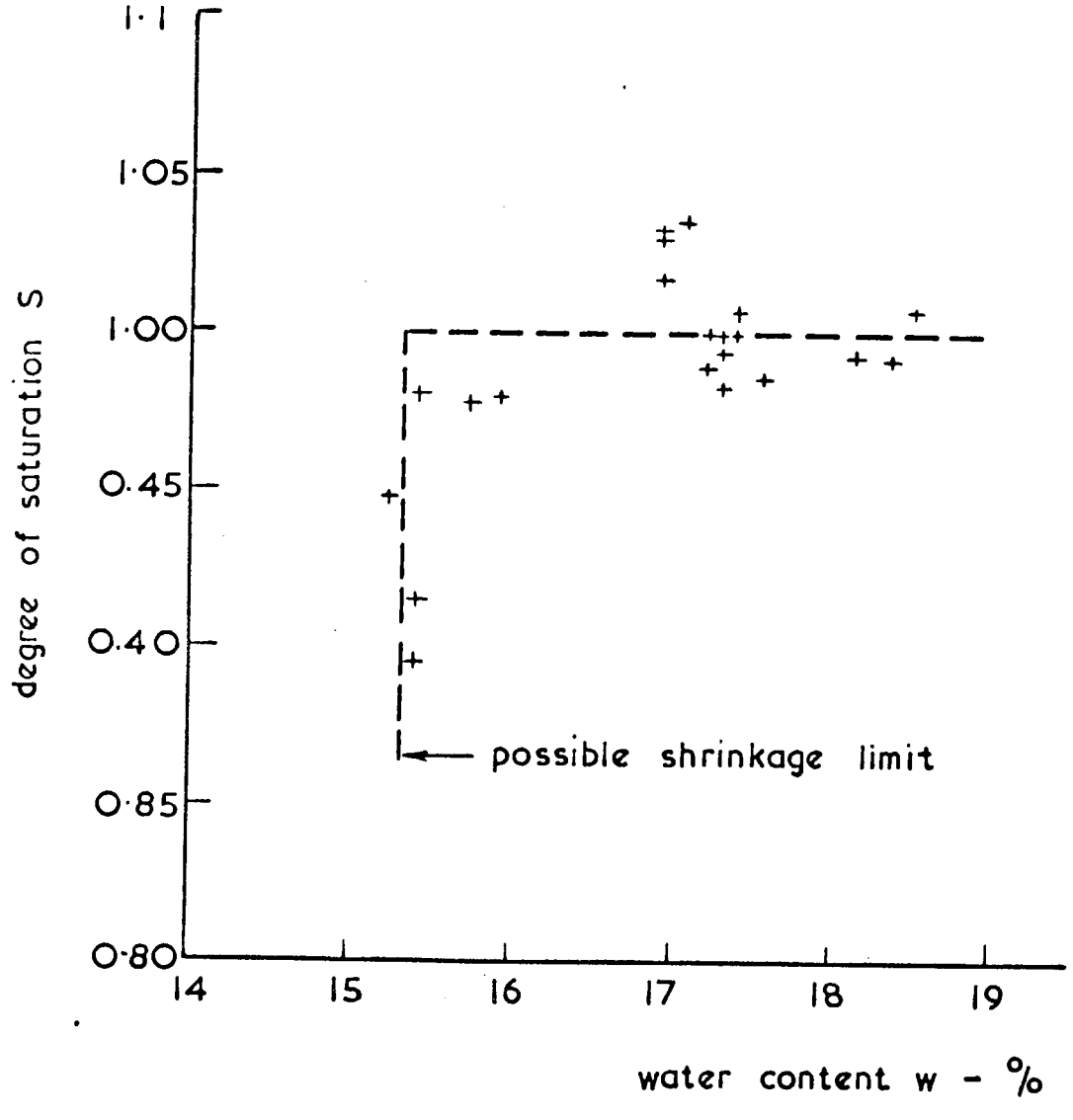

Fig. 4.15 Degree of saturation against water content

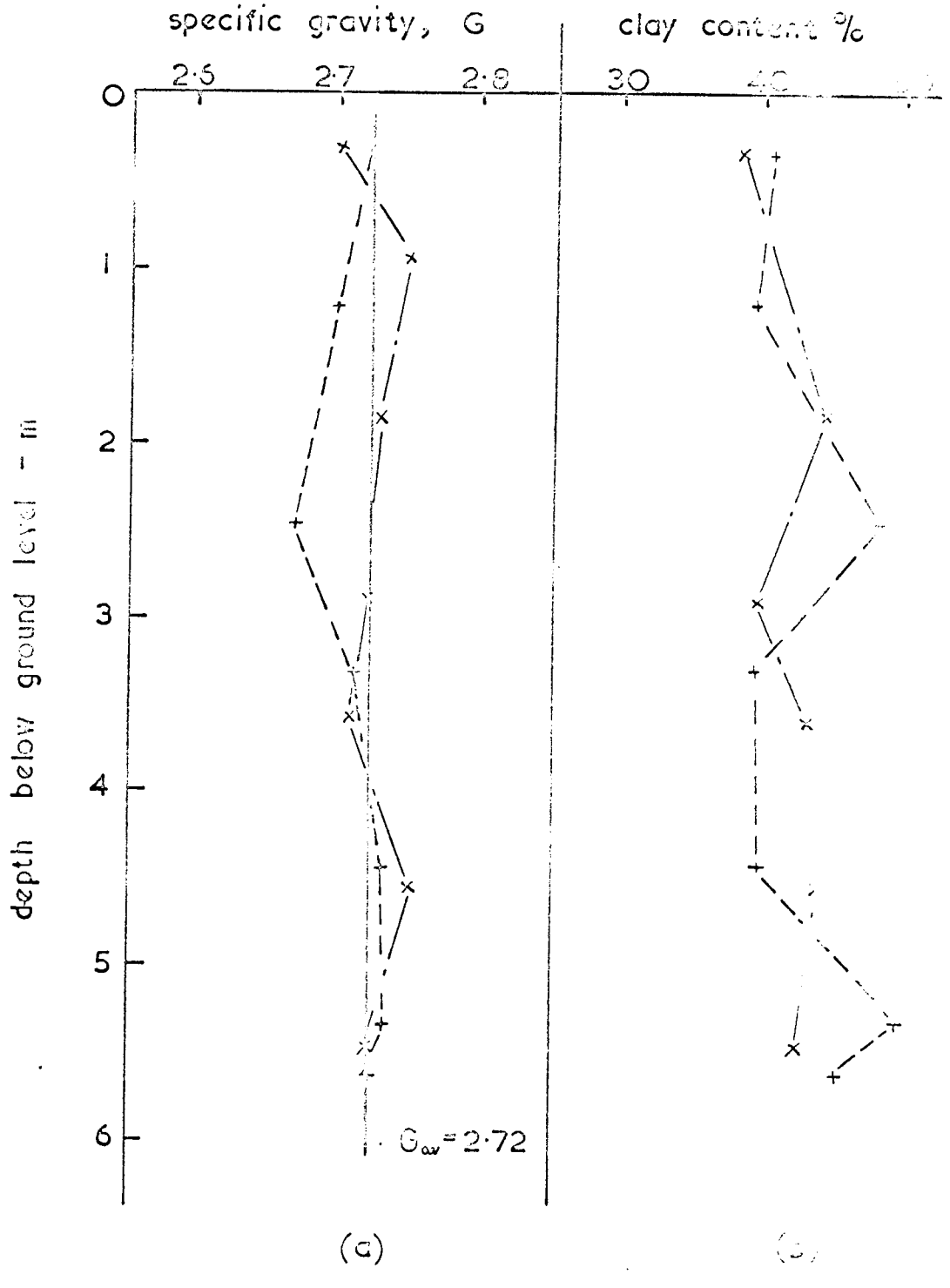

Fig. 4.16 Variation of (a) specific gravity and (b) clay content, against depth

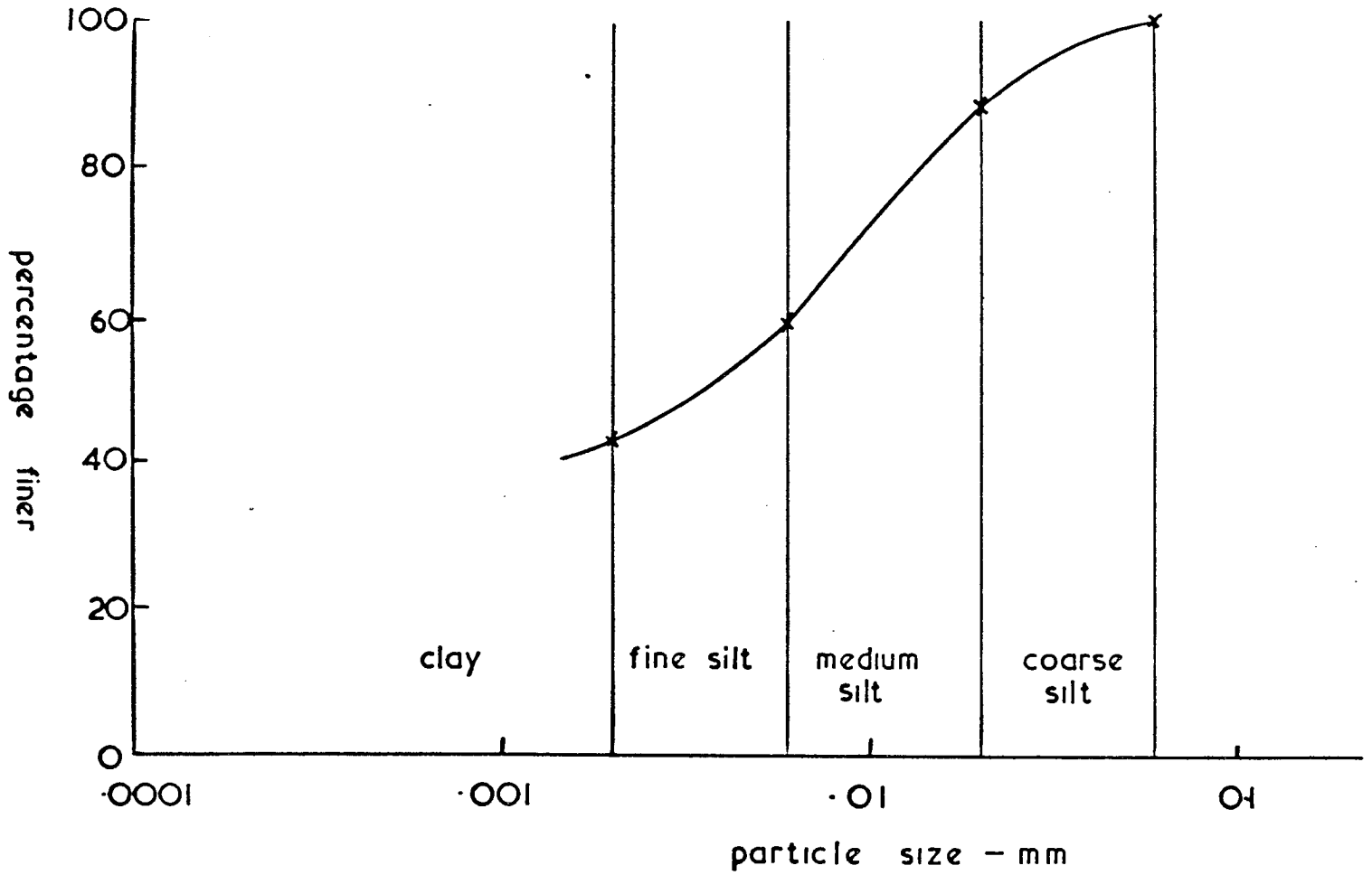

Fig. 4·17 Particle size distribution for Lower Lias clay at Blockley (sedimentation analysis)

(a) T-86 Double Core Barrel and Bit

(b) U70 Tube Sampler

PLATE 4.1 SAMPLING EQUIPMENT

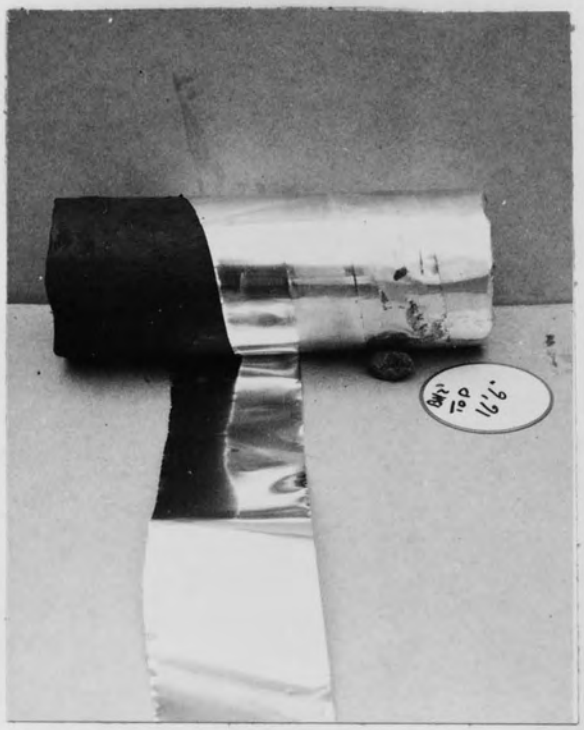

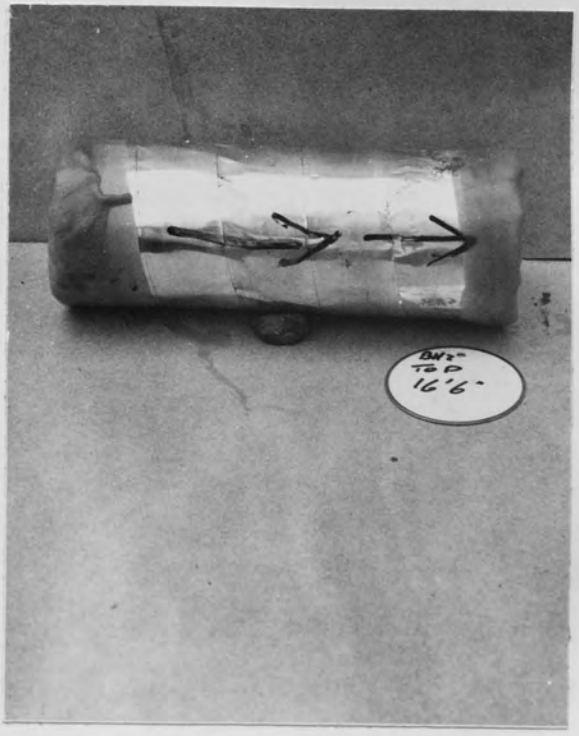

PLATE 4.2 STORAGE OF CORED SAMPLES

PLATE 4.3 SAMPLING SITE

PLATE 4.4 EXCAVATION OF BLOCK SAMPLES

PLATE 4.5 WRAPPED BLOCK SAMPLES

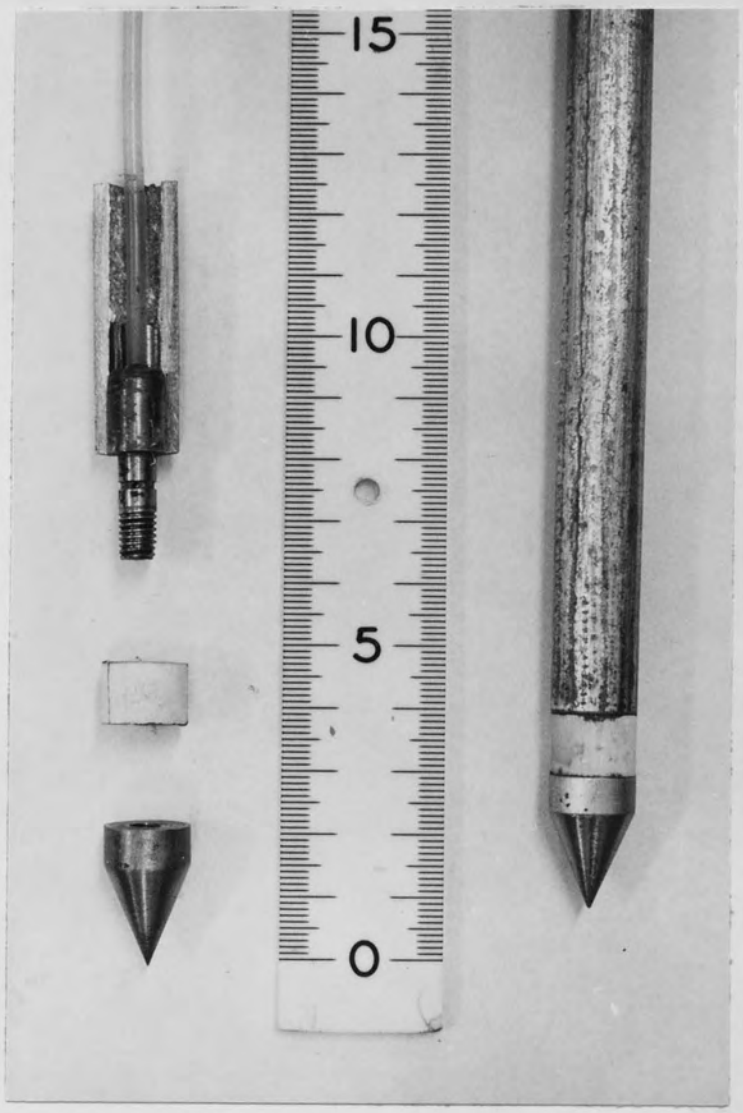

PLATE 4.6 PORE PRESSURE PROBE

(a)

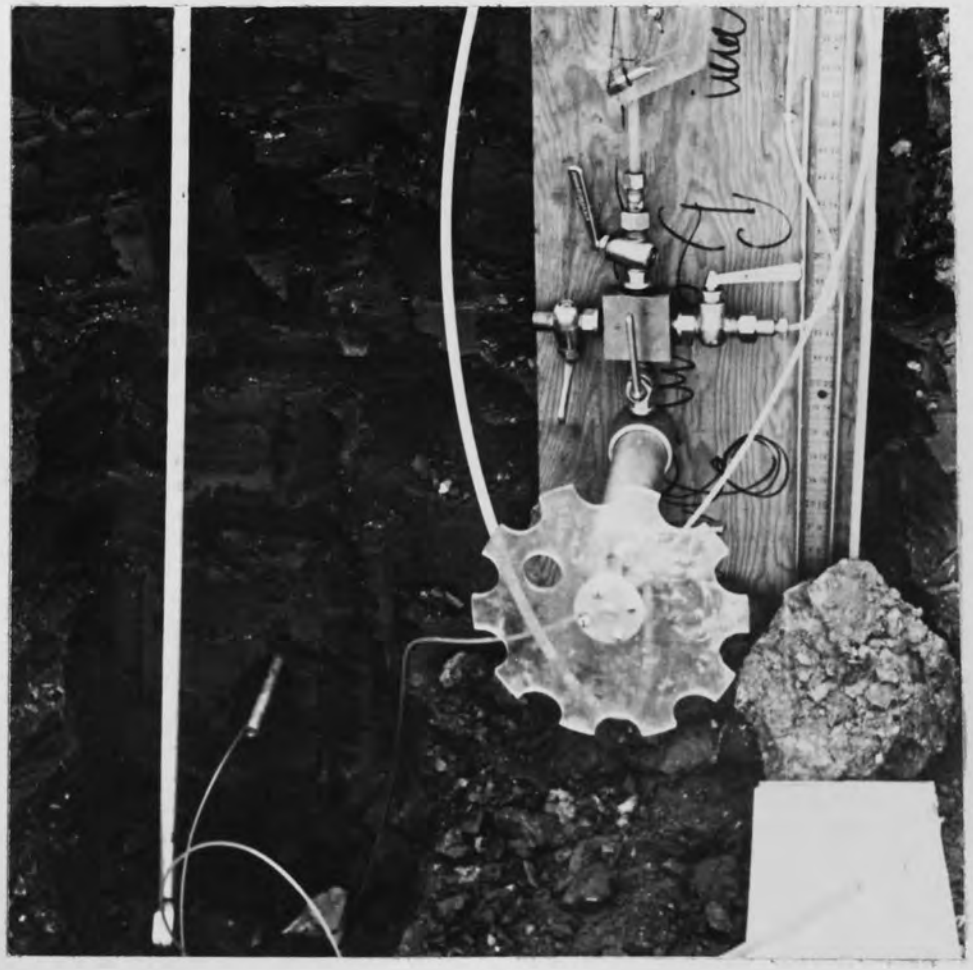

(b)

PLATE 4.7 INSTALLATION OF PORE PRESSURE PROBE

CHAPTER 5

LABORATORY TESTING PROGRAMME, APPARATUS AND TECHNIQUES

5.1 Introduction

5.2 Testing Programme

5.3 Oedometer Apparatus

5.4 Triaxial Apparatus

5.5 Specimen Preparation

5.6 Testing Techniques

5.1 INTRODUCTION

The aim of this project was to study the compressibility characteristics of the Lower Lias clay under differing stress paths in order to determine the general compressibility parameters for the soil. As this study consisted solely of laboratory testing the main testing programme was carried out in the triaxial and oedometer apparatuses.

The laboratory testing programme is described below together with the apparatus used and developed for this study. It has been discussed earlier that the in-situ value of K_o is probably greater than unity and that samples tested in the laboratory should initially be brought back to their in-situ effective stress state. Therefore a new Independent Stress cell was developed for part of the testing programme and is described in this chapter.

Finally the specimen preparations and testing procedure is described at the end of the chapter.

5.2 TESTING PROGRAMME

The testing programme is considered under the two main categories of testing apparatus, the oedometer and triaxial.

5.2.1 Oedometer Testing

The objectives of the oedometer series of tests were basically threefold:-

(i) to determine the equilibrium stress existing in the sampled soil,

(ii) to investigate the one dimensional compressibility and consolidation characteristics of the soil, and

(iii) to estimate the maximum overconsolidation stress, σ'_c, that the soil had experienced.

With these objectives in mind the following series of tests were planned:-

(a) O E series -

This series comprised the initial stage of all the oedometer tests on "undisturbed" samples (M O and C S series below). Initial swelling was just prevented when the sample was brought into contact with free water, so the the equilibrium stress (σ'_K) was determined as proposed by Skempton (1961) (section 2.3.1(a)).

(b) M O Series -

Starting from the equilibrium stress, σ'_K, the undisturbed samples were incrementally loaded according to one of the following methods:-

(i) the standard method of doubling each increment subsequent to the first increment, with σ'_K taken as the datum

i.e. $\Delta\sigma_i = (\sigma'_i - \sigma'_K)$

(ii) a series of incremental loads such that five equal increments of stress (each of 206 kN/m^2) were applied, followed by two further larger increments (each of 309 kN/m^2). For both methods all increments were applied for at least twenty four hours. An unload - reload cycle, following the same stress path, as the first loading were normally performed before subsequently unloading to zero stress.

(c) C S series -

Starting from the equilibrium stress the sample was loaded at a constant rate of strain, to a maximum stress of approximately 14,000 kN/m^2, and subsequently unloaded in the same manner.

(d) R M O series -

Remoulded samples were loaded and unloaded by the doubling increment method, to a maximum stress of 3,000 kN/m^2.

(e) R C S series -

A sample from a R M O test was reloaded under a constant rate of strain to a maximum stress of approximately 14,000 kN/m^2, and subsequently unloaded.

5.2.2 Triaxial Testing

A greater emphasis has been placed on the triaxial testing in this project because the apparatus is far more versatile than the oedometer. The basic aims of the triaxial testing programme were to determine:-

(i) the equilibrium stress existing in the undisturbed samples,

(ii) the basic parameters governing the axial and volumetric compressibility of the Lias under a variety of stress paths,

(iii) the radial consolidation characteristic, and

(iv) the effect of the sampling method (disturbance) on the measured compressibility parameters.

The order presented above does not represent the order of importance of the determinations. Item (ii) forms the major part of the triaxial investigation. All the specimens tested in the triaxial series were from "undisturbed" samples and, with the exception of the TDH series, were of vertical orientation. The types of tests carried out to fulfill the objectives indicated are given below.

(a) T E series -

This comprised the initial stage of all the triaxial tests.

A cell pressure was applied under undrained conditions and the pore pressure recorded, thus the equilibrium stress, σ'_K, was obtained as proposed by Skempton (1961) section 2.3.1(c). It was normal to apply at least a second increment of cell pressure, so as to determine the value of the pore pressure coefficient, B.

(b) T D V series -

Following the initial stage ((a) above) the specimens were isotropically consolidated under a cell pressure representing the in-situ mean stress. The specimen was then loaded along a vertical effective stress path, Figure 5.1(a). The axial stress being applied in a drained manner at a constant rate of strain, the radial stress remaining constant throughout the test. At an axial strain of approximately 2% an unload-reload cycle was carried out. On the second loading cycle the specimen was loaded to failure.

(c) T D H series -

An identical series to TDV, performed on "horizontal" samples rather than vertical samples

(d) T D 2 series -

Specimens were anisotropically consolidated to effective stresses representing the in-situ stress state, with $K_o > 1$. The specimen was then loaded along a vertical effective stress path in a manner identical to TDV series, Figure 5.1(b).

(e) T A 1 series -

Following the determination of the equilibrium stress the specimens were isotropically consolidated as in (b)(TDV). Increments of axial and radial stresses, at a ratio of 3 : 1, were applied simultaneously in an undrained manner.

For each stage after the equalisation of the pore pressure the drainage was opened and the sample allowed to consolidate. Four such increments were applied (Fig. 5.1(c)) and generally followed by drained compression to failure.

(f) T A 2 series -

Specimens were anisotropically consolidated as in (d) (TD2). The test then proceeded with incremental loading as in TA1 above. The stress path for this series is shown in Fig. 5.1(d).

(g) T A 3 series -

Specimens were isotropically consolidated as in (b) (TDV). The axial and radial stresses were then increased at a constant rate, and ratio of 3 : 1, in a drained manner to the same stress level as the TA1 series (Fig. 5.1(e)). The specimen was then sheared in the normal drained manner (i.e. increase in axial stress only).

(h) T C series -

Specimens were consolidated isotropically as in (b) (TDV series). Isotropic increments of stress were applied in an undrained manner, for each increment, the pore pressure was allowed to equalise before the drainage was opened to allow consolidation, Figure 5.1(e). Increments were applied up to the safe limit of the triaxial cell.

A further triaxial series was planned, TB series, where samples were consolidated anisotropically under zero lateral strain conditions using the Bishop mercury jacket system. However, the results of the TA3 series coupled with the inherent health danger, caused this series to be cancelled, despite much early work on perfecting this apparatus.

5.3 THE OEDOMETER APPARATUS

The oedometer series of tests was carried out with two types of apparatus; the MO and RMO tests were performed in a "Mechanical" oedometer, while the CS and RCS tests were performed in a "constant rate of strain" oedometer.

5.3.1 The "Mechanical" Oedometer

The mechanical oedometer was the standard Bishop type oedometer manufactured by Wykeham Farrance Engineering Ltd., Plate 5.1(a) with one simple, but significant, modification. An adjustable screw support was mounted at the back of the main frame, see above plate, this enabled the loading arm to be supported at any stage during a test, when additional load could be added to the hanger system, without increasing the load on the specimen until required.

The specimens were carried by a 3mm thick retaining ring with an inside diameter of 65mm. This size of ring was used because it was the maximum size sample which could be obtained from the nominal 70mm diameter "mechanical" samples, and still ensure that the samples could be trimmed to give a "good fit" and remove disturbed soil in the immediate viscinity of the sampler. For the undisturbed samples the retaining rings were a nominal 20mm high, while for the remoulded specimens the retaining rings were30mm high, in the latter case both 65 and the standard 76mm diameter rings were used. In all these cases "A 80 KV" bauxilite porous discs were used for top and bottom drainage. Deformation was measured with a standard Baty dial guage, graduated to 0.002mm.

5.3.2 The "Constant rate of Strain" Oedometer

In order to attempt the estimation of the overconsolidation stress

of the Lower Lias from the sampling site, it was necessary to have an oedometer in which specimens could be loaded to a stress level in excess of 7,000 kN/m^2 (this is the order of overconsolidation stress suggested by the study of the geological history of the site, section 4.3). It appeared that the best method by which this could be achieved was to design an oedometer which could be loaded in a standard compression test machine of sufficient capacity (e.g. Wykeham Farrance 5 tonne machine) and at a sufficiently slow rate of strain to enable adequate pore pressure dissipation during loading.

A fairly simple design evolved, which utilized the 70mm triaxial base used in part of the triaxial series (section 5.4.1). The specimen was contained in the 65mm internal diameter rigid brass ring (145mm outside diameter), which was bolted to the triaxial base and sealed onto the triaxial bottom platen by the O-ring seal "A" Fig. 5.2. A perspex cell was glued into a recess in the top of the brass ring, to enable the top cap and specimen to be flooded with water. The load was applied via a 19mm diameter stainless steel plunger screwed into the top cap to give a rigid connection. The top cap, similar to mechanical oedometer top cap, was constructed of a 6mm thick " A 80 KV" porous disc screwed into a 17mm thick brass disc. The apparatus was set up on a compression machine pedestal with a proving ring to record the applied loads. Compression of the specimen was recorded on a dial guage (graduated to 0.002mm) fixed to the plunger, Plate 5.1(b)). A stabiliser was provided near the top of the plunger to prevent tilting of the plunger and top cap. A pressure transducer was connected to the bottom porous stone so that the pore pressure could be recorded throughout the test, with drainage via the top cap only.

5.4 TRIAXIAL APPARATUS

As the Lias often contained a considerable number of fossils and tended to be fissured, 70mm diameter specimens were tested in preference to the normal 38mm specimens. Although, due to trimming problems, the TDH series was tested at 38mm diameter.

From the point of view of basic apparatus requirements the triaxial tests can be divided into two groups according to the initial consolidation stress conditions - isotropic ($K = 1$) or anisotropic with $K > 1$. In the case of the initially isotropically consolidated tests (TDV, TDH, TA1, TA3 and TC series) the standard type of triaxial cell could be suitably adapted to meet the test requirements. However for the 'anisotropically' consolidated, with $K > 1$, (TD2 and TA2 series) there was no suitable equipment available to test samples as large as 70mm diameter. A new triaxial cell was, therefore, developed as part of the research programme, where radial and axial stresses could be applied completely independently of each other, and will be referred to as the "Independent Stress Cell" (IS cell) subsequently in this thesis.

5.4.1 The standard Triaxial Apparatus

The apparatus used for the series TDV, TA1, TA3 and TC was basically a standard Wykeham Farrance triaxial cell for samples up to 102mm diameter which had been adapted for 70mm diameter specimens. The basic apparatus is described below and subsequently the modifications for particular tests are enumerated.

The standard cell base, sample and loading platen are shown in section in Figure 5.3, the bottom platen is of the form shown because it was originally designed to carry an "inner cell" for the Bishop type mercury jacket apparatus. Similarly the top platen was also designed for the mercury jacket type test

hence the comparatively large depth of the platen. The platens were fitted with a high air entry value (H.A.E.V.) ceramic discs (Aerox "Celloton" grade VI, air entry value approximately 200 kN/m^2). The bottom disc connected to two klinger valves, one of which connected to a pressure transducer block. The top disc connected via saran tubing and a Bishop "constant volume tap", to a volume change apparatus. The cell was fitted with a rotating bush, rotating at 2 revs/minute, to reduce ram friction, as the applied load is recorded on a proving ring outside the cell.

The modifications to this cell are basically in the loading system used for the various tests and are considered under the test type:-

(a) TDV series -

loading was applied in the standard manner for a drained compression test by straining the machine at a constant rate, with the load recorded on a proving ring mounted between the plunger and crosshead. The deflection of the sample was recorded by a dial gauge attached to the base of the proving ring, with its plunger resting on a stand fixed to the body of the cell. A constant cell pressure and back pressure was maintained throughout the test by use of the mercury pot system, (Bishop and Henkel, 1962).

(b) TA1 series -

this test was a stress controlled test, with stresses applied to the sample and maintained constant over a long period of time. The cell pressure was controlled by a mercury pot system in the normal manner. The deviatoric stress was applied through a 7 tonne Blackhawk hydraulic jack pressurised at low stresses by the mercury pot

system and at higher stresses by the Wykeham Farrance, 14,000 kN/m^2, Constant Pressure Apparatus. The applied load being recorded on a proving ring located between the jack and plunger.(Plate 5.2). The deflections were recorded the same as in (a).

(c) TA3 series -

in this series both axial and radial stress were increased continuously. The deviator stress was increased in the same manner as (a), while the cell pressure was increased by mechanising one of the mercury pot rails so that the pot was raised at a fixed speed. Applied load and deflection was recorded as in (a), while the cell and pore pressures were recorded on pressure transducers.

(d) TC series -

the TC series was performed on short (L : D = 1 : 1) samples with a dial gauge mounted inside the cell (Plate 5.3) and resting on the flat top platen to record the axial deflection. The cell pressure was applied with the mercury pots in the normal manner, and recorded on a pressure transducer.

(e) TDH series -

it was intended to test the TDH sample in the same apparatus as the TDV series. However due to trimming problems a sample was eventually tested in standard Wykeham Farrance 38mm ($1\frac{1}{2}$") cell. Ordinary "A150 KV" porous discs were used at either end, as no HAEV discs were available and time did not allow modification, as the use of this apparatus was not planned. A pressure transducer was connected to the bottom platen and volume change to the top platen as for the 70mm apparatus. Applied loads and deflections were recorded in a standard manner as for (a).

5.4.2 The Independent Stress Cell

It was required to develop a triaxial apparatus in which a specimen could be loaded under any stress conditions and in particular with $\sigma_r > \sigma_a$. Further, that this specimen could then be loaded under either "axial strain-rate controlled" or "axial stress controlled" conditions, with "radial stress control". It is considered pertinent, here, to mention other considerations which were in mind when designing this apparatus; it was proposed that this cell be the basis of an apparatus in which "laboratory overconsolidated" clays could be produced following a stress path comparable to that of the Lower Lias clays, so that the effects of sampling could be studied. This is the reason why such a heavy apparatus was developed with all structural parts made of cadmium plated mild steel to prevent corrosion.

The design requirements were satisfied by the cell shown in Figure 5.4 and Plate 5.4. The axial and radial stresses are applied from two separate chambers, the top cell and the main cell.

The main cell was sealed by the special specimen membrane (Appendix C) which was flanged at both ends, so that it sealed at the base between cell base plate and main cell and folded over the top of the main cell to be sealed by the top cell, Figure 5.4. The top orifice of the main cell was designed to give a diameter inside the membrane of 70mm, and hence allow the top platen to pass through it as a smooth sliding fit.

The top cell is basically a hydraulic jack with the top platen being the ram. The platen, Plate 5.5(a), was made of alloy, with a P.T.F.E. outer annulus to reduce frictional losses in the top chamber. Sealing of the top platen was achieved by fitting a silicon rubber membrane at the top of the platen with a retaining

ring. The O-ring on the retaining ring ensuring a good seal against the cell wall. As the platen always extended into the specimen membrane, to a depth of at least 10mm, and the radial stress would always be in excess of the pore pressure it was assumed that no pore water could migrate beyond the bottom of the top platen.

The axial load could be applied by means of a hydraulic pressure in the top cell (stress-controlled) or by the plunger in a standard compression machine (strain controlled). The plunger passes through a bronze bush in the cell top plate, and is sealed by a recessed O-ring, so that leakage around the plungrr, under high top cell pressures would not be a problem.

As some loss of axial load is inevitable with this type of loading system it was necessary to record the load at the bottom of the specimen. A Sangamo D90, electronic proving ring (25,000 lb capacity) was used in conjunction with a Sangamo direct reading transducer meter Type C52/5, which provided full scale readings on five load ranges (25,000, 10,000, 2,500, 1,000, 250 lb). For the present series of tests the 1,000 lb range was adequate, which gave a proving ring deflection of 0.0253mm (0.001 in.). Because of the size of the proving ring (248 x 109 x 155mm overall) it was necessary for it to be mounted externally, Plate 5.4, hence the bottom platen had to pass through the cell base plate (Figure 5,4) in a manner such that the load on the platen could be measured accurately. This could be achieved quite simply by leaving ample clearance around the sides of the platen stem and a gap of 0.05mm (.002 in.) between the cell base plate and the underside of bottom platen when screwed into the proving ring. The 0.05mm gap would not cause a leakage problem, because the specimen membrane was sealed onto the platen upstand,

Figure 5.4, with at least two rubber O-rings, to prevent leakage from the specimen, and continued with a flange to seal between the cell base plate and the main cell body, to prevent leakage from the main cell. Also, as the membrane thickness was 0.25-0.37mm (10 to 15 thou of inch), compared to the gap size of 0.05mm, the radial cell pressure would not force the membrane into the gap. However it was considered that this method would be susceptable to foreign matter entering the small gap and hence reducing the clearance. It was decided that it would be preferable to increase the gap to something like 5mm, and seal it with a soft rubber ring, Plate 5.6, (silcoset rubber was used), which would compress the required amount without carrying too much load.

The apparatus was calibrated (Appendix D) with the cell empty and at various cell pressures, as the radial stress on the rubber ring would produce an uplift effect on the bottom platen. It was found from calibration tests, both before and after long tests, that the calibration figures were repeatable, thus creep of the rubber ring did not appear to be an inherent problem.

Both platens were fitted with HAEV porous discs (as the ordinary triaxial apparatus), with connections to a pressure transducer block (bottom) Plate 5.4 and a volume change apparatus (top). Axial deformation was measured in the normal manner by recording the displacement of the plunger.

5.4.3 Subsidary Apparatus

(i) Volume Change Apparatus

In the triaxial tests a back pressure (of 200-300 kN/m^2) was always used, to ensure saturation. This meant that an open ended burette could not be used unless mounted on the atmosphere side of the mercury pot system (Davis and Poulos, 1963), this however

is not really suitable, as the apparatus records leaks and volume changes throughout the system. It was therefore decided to use the Bishop type paraffin volume change gauge (Bishop and Donald 1961, Bishop and Henkel 1962), which can be fitted between the specimen and the mercury pot system. A 15cc gauge, graduated to 0.05cc, was used for the 70mm diameter specimens, while a 5cc gauge, graduated to 0.02cc was used for the 38mm diameter specimens.

The 15cc gauge can be read to at least the nearest 0.02cc, for a good meniscus, and with a poor meniscus, normally to 0.05cc giving the volumetric strain to $\pm$ 0.002% to 0.005%, while for the 5cc gauge the corresponding reading can be made to the nearest 0.01cc and 0.02cc giving the volumetric strain to $\pm$0.005% to 0.01%. The inside of the measuring burette was treated with Repelcote (Webb 1966), to reduce the problem of drops of paraffin sticking to the walls and to give a more even meniscus.

Som (1968) reported a technique for measuring small volume changes, he used a length of saran tubing connected between the specimen and the back pressure and clamped horizontally on a bench against a scale. An air bubble was introduced into the otherwise waterfilled tubing, my menas of a hyperdermic syringe, and its movement gave a measure of the water expelled. A displacement of 0.5mm was equivalent to a volume change of $1mm^3$ (0.001 ml), therefore the accuracy of the readings is in the region of one order of magnitude better than the 5cc paraffin gauge. It is considered by the Author that if the applied back pressure was sufficient to ensure that the specimen be saturated then the air bubble in the volume gauge must also be dissolved. It is, perhaps, significant to note that with this apparatus a back pressure of 100 kN/m^2 (15 psi) was used compared to 200 kN/m^2 (30 psi) recommended by Bishop and Henkel, 1962, to ensure specimen saturation.

However the principle seemed a promising method of measuring small volume changes to a high degree of accuracy. A considerable amount of effort was invested in a similar apparatus, by the Author. A plate of perspex (525 x 340mm) had a series of parallel grooves machined to carry 5m of 3mm O.D. saran or nylon tubing: with a 'mercury injector resevoir' fitted at each end of the tubing. The whole system was saturated with water, with a supply of mercury, approximately half filling each resevoir, and pressurised to 200-300 kN/m^2 back pressure. A mercury thread could be introduced to either end of the tube by tilting the appropriate 'injector' so that a thread of mercury would be pushed into the tube with the general flow of water. With the mercury thread set the volume change could be recorded by the movement of the mercury. The injector system made the apparatus flexible, as a further thread could be introduced before the current thread went off the scale. The capacity ranged from 10cc for one full scale movement, up to (10 x N) where N is the number of threads available from the resevoir. However, despite apparent early success the apparatus was eventually discarded. The main problem was that with time the mercury developed some form of adhesion to the tubing (initially saran tubing was used, but this was replaced by several different nylon tubings) which caused the thread to break up or leave a smear of mercury on the tubing, this was particularly troublesome when the volume change was very slow. The inside of the tubing was 'wetted' with 'Repelcote' with the hope of preventing the problem, but, although it possibly improved it for a time, the problem was not solved. Another problem occuring was that simetimes water seemed to bypass the threads hence giving erroneous readings of volume changes. This could possibly be overcome by the use of smaller bore tubing if material could be found which did not suffer from the 'sticking' problem.

(ii) Pressure Measuring Apparatus

For measurement of cell pressures Budenberg Standard Test Gauges were used. These were checked at intervals, in the laboratory, by a Budenberg dead-weight pressure gauge tester.

Consolidated Electrodynamics (Bell and Howell) pressure transducers, type 4-326, were used for measurement of pore water pressures, (and cell pressures, as they became available). Each transducer was sealed into a rigid brass transducer block. One, or two water supply taps and a de-airing screw are interconnected with the transducer through small diameter holes in the block and the whole assembly is attached to a Klinger tap at the main cell (Plate 4.5, 4.6). Calibration of the transducers was made against the Budenberg dead-weight pressure gauge tester, at the same intervals as the Standard test gauge.

5.5 SPECIMEN PREPARATION

A brief description of preparation of specimens for laboratory testing is given, simply for completeness, as the methods used are fairly standard.

5.5.1 Oedometer Specimens

The specimens prepared from 'undisturbed' samples (undisturbed specimens) were cut by pushing the 'mechanical' oedometer ring, smeared with silicone grease, into the sample a little at a time, and trimming the surplus away with a sharp spatula. The ends of the specimen were trimmed with the spatula, aided by a 'surform' blade. The final surface, flush with the ring, was planed with a sharpened straight edge.

The remoulded samples were prepared from dried, ground clay which was mixed to the required water content. The material was mixed

thoroughly on a glass plate until a consistent mix was obtained. The mixture was then transfered into a galvanised dish and placed in an empty 'desicator'. A vacuum pump was attached and the vessel de-aired, and the specimen left under vacuum over night. The following day the clay was remixed again and replaced under vacuum for a further 24 hours.

The specimen retaining ring was placed, centrally on the saturated bottom oedometer porous stone, the clay was then pasted into the ring with a small spatula, a little at a time to minimise the amount of air bubbles entrapped. Using a straight edge the final surface was levelled, flush with the top of the ring.

5.5.2 Triaxial Specimens

Only undisturbed samples were used for the tests in the triaxial series. The U70 samples were extruded from their tubes, with a hydraulic extruder, these samples only needed cutting to length, as their diameter was normally slightly under 70mm. A three sectioned, split former was clamped around the specimens and the ends trimmed flush with those of the former. This was performed in an identical manner to the oedometer end trimming.

The core samples required some radial trimming as they were approximately 72mm diameter. As this only required 1mm all round, the trimmingwas performed with the surform blade. When trimmed to 70mm diameter the split former was fitted and the ends were trimmed in the same manner as the U70 samples.

The block samples were, unfortunately,not so easy to prepare. A prism of approximately 100mm square section by 300mm long was cut from the block with a Swedish logging saw. The outer 10mm was then trimmed off carefully with a sharp spatula and the ends squared. The sample was then mounted in a soil lathe, and further trimming

carried out, initially with the spatula and finally with the surform. A guide frame was fitted to ensure that a right cylinder of 70mm diameter was obtained. The sample was then placed in the split former and the ends trimmed as before.

The trimming of the block samples was not particularly successful, fossils, fissures and bedding planes, caused a great deal of trouble while trimming to the 70mm diameter, with pieces breaking out of the sides. This was the reason for the horizontal specimens being tested at 38mm diameter. In retrospect it is considered that better results may well have been obtained if the blocks were cut and trimmed immediately after sampling and then wrapped and stored in the same manner as the core samples, rather than storing the blocks for up to 18 months and then attempting to cut the specimens.

5.6 TESTING TECHNIQUES

It is not intended to describe the testing techniques in great detail, but to bring out those points that might be significant in the analysis of some of the results, and that could be of use to any future reader of this thesis.

5.6.1 Oedometer Tests

As the oedometer testing was fairly straight forward, the majority of the following detail is related to the setting up and initial stages of the tests.

(a) The measurement of the equilibrium stress (σ'_K)

As described in section (5.2.1) the initial stage of the oedometer tests on the undisturbed specimens was the determination of the equilibrium stress (OE series). It was indicated in section (2.3) that this method was

not favoured by researchers at Imperial College, although originally proposed by Skempton. However, the technique used in this series of tests varied from that used at I.C., therefore it will be described in some detail.

The specimen was prepared as described earlier (5.3), and placed in the oedometer cell, onto the saturated bottom porous stone. The rest of the apparatus was assembled quickly and the saturated top cap pressed firmly onto the specimen. The cell was set up in the oedometer loading frame ready for loading.

A 44.5N 'bedding' load was placed on the hanger, and with the screw support out of contact, a 'bedding-in' process was applied. The loading arm was pressed down by hand and quickly released, this produced a deflection on the dial gauge, with partial recovery on release. This process was repeated several times until the dial gauge returned to the same position twice in succession. This was then taken as the zero reading, and the screw support was raised to just make contact with the loading arm. The cell was filled with distilled water and further load was applied to the hanger when the dial gauge showed signs of swelling. The advantage of using the screw support is that when loads are added, the specimen does not carry it immediately but picks up the load as it tries to swell, hence preventing the otherwise inevitable proceedure of compression and swelling at each load increment, as the pore pressures equalise throughout the specimen.

When equilibrium was apparently achieved, thescrew support was lowered, the specimen was then left for at least 24 hours under this load before further testing was performed.

(b) MO and RMO Tests

The loading and unloading stages were carried out as outlined in section (5.2.2). For the loading stages the screw support was adjusted to carry the loading arm before the increment was placed on the hanger, the load was then applied to the specimen by quickly releasing the screw support.

At the end of the test the specimens were left for several days, and in some cases weeks, under zero load. The cell was drained one to two hours prior to dismantling, the specimen was removed and the surfaces dried of excess water with filter paper. The specimen was then measured and weighed before finally drying.

(c) CS and RCS Tests

The specimen was either cut and prepared in the ordinary mechanical oedometer ring (MO ring), or, in the case of the remoulded specimen, consolidated in the MO ring. In either case it was then necessary to transfer the specimen into the constant rate of strain oedometer ring (CRS ring). The MO ring was fitted into the recess on the top of the CRS ring (Figure 5.2) and the specimen pushed into the CRS ring with the top cap. The CRS ring was then bolted down, and the apparatus set up as in Plate 5.1(b). The specimen was 'bedded-in'; a load was quickly applied and released several times until the dial gauge gave repeatable readings for the initial contact. The cell was then filled with water, the load adjusted to prevent swelling, and the pore pressure recorded at the base. After equilibrium was obtained the specimen was loaded at a constant rate of strian, the slowest speed, 0.0008mm/min.,

was used in order to obtain the maximum pore pressure dissipation possible. Drainage was only permitted through the top stone, so that the pore pressure could be recorded at the base. Loading was continued until the capacity of the machine was reached (5 tonne load) then the specimen was unloaded at a similar rate. The specimen was dismantled in a similar manner to the MO and RMO tests.

5.6.2 Triaxial Tests

Before considering the techniques used during setting up and testing the triaxial specimens, the general drainage conditions should be discussed. It was found, when carrying out some provisional tests, that it was not uncommon for flat fossils (shells) to cover a considerable proportion ofthe cross-sectional area at some elevation which effected the vertical drainage conditions. Therefore it was considered that radial drainage would be preferable to vertical drainage in this material, if comparable drainage conditions were to prevail throughout the testing programme. Radial drainage was provided by a double thickness of Whatmans No. 4 filter paper. The filter paper was cut to give an integral top disc and side drains, such that the side drains were 10mm wide, with a 10mm gap between each, to the full length of the specimen. End drainage was prevented by use of latex membrane discs over each end of the specimen. Two membranes were used, at each end, with silicone grease between them, to help reduce the frictional end restraint on the specimen, even though long (2 : 1) specimens were tested. A hole was cut (approximately 5mm diameter) in the centre of the base membranes and replaced with filter paper so that the pore pressure could be recorded at the centre of the specimen base; this proved to be effective as will be shown in later chapters on the triaxial test results.

The techniques used in the triaxial testing tend to be mainly governed by the type of apparatus used, and it is therefore considered more pertinent to treat the subject under the "apparatus type" rather than "test type".

(a) Standard Triaxial Apparatus

The apparatus was thoroughly flushed with de-aired water, to ensure that the porous discs, associated connections, volume change device and pressure transducers were saturated. The bottom membranes were placed onto the flooded bottom platen, with the filter paper in the central hole. A little de-aired water was poured onto the centre of the membranes and the specimen placed on carefully to avoid trapping air beneath it. The top membranes were smoothed onto the specimen to avoid trapping air, the saturated filter papers were then placed on the top membrane and the strips smoothed down the sides of the specimen. A latex membrane, which had been soaked in water for at least one week, was checked for leaks, fitted over the specimen, and sealed onto the bottom platen with two or three rubber O-rings. The membrane was rolled back, at the top, to just below the top of the specimen. Water was slowly pumped through the bottom disc, this was then stroked up between the membrane and specimen to remove any entrapped air. A split ring carrying two or three rubber O-rings was threaded back over the de-aired top platen, and the platen placed on the specimen. The membrane was rolled up over the platen and a little water flushed through the top porous disc. As much air as possible was stroked out from between membrane and specimen before the O-ring was fixed over the top platen. A suction was then applied to the top platen to remove the flushing water, while the cell was filled with de-aired water. When the cell was full, a small cell pressure (50-100 kN/m^2) was

applied with the drainage tap open for a few minutes so that the free (flushing) water was removed from around the specimen. It was found from preliminary tests that the above "flushing" was necessary, if a saturated "set up" was to be achieved, although in many ways it is rather undesirable. Castor oil was introduced to the top of the cell to reduce leakage past the plunger, and also act as a lubricant for the plunger.

The TC series followed a slightly different course subsequent to the top rubber O-rings being fitted. The dial stand was screwed into the base of cell and the dial gauge fitted such that the plunger rested as near the centre of the top platen as possible. The cell was fitted and filled to the underside of the dial gauge face with de-aired water. The remainder of the cell was then filled with Shell Diala oil B (Plate 5.3) to prevent corrosion and sticking of the dial gauge.

A cell pressure of 200-250 kN/m^2 was applied under undrained conditions, and the pore pressure recorded, hence a value for the equilibrium stress, σ'_K was determined. After equalisation of the pore pressure, the cell pressure was increased to the test value (400-500 kN/m^2) under undrained conditions. The specimen was then consolidated into a back pressure of 250-300 kN/m^2, before loading under one of the stress paths described in section (5.1.2).

For all tests, except the TC series, a "bedding correction" was carried out. A small deviatoric load was quickly applied and released several times until the deflection dial gauge gave repeatable readings, at the point of contact between plunger and top cap. The subsequent loadings were obviously governed by the test type. The basic techniques are indicated below. The TDV and TDH series require no explanation as the axial load was applied at a constant rate of strain as is normal for a drained

compression test.

The TA1 series was loaded incrementally, with axial stress as well as the radial stresses being maintained constant for long periods of time by hydraulic means. The increments of load were initially applied with the drainage closed in an undrained manner. The pressure supplies were isolated from the cell and jack for a short time while the pressures were raised to the required level. The increased cell pressure was then applied to the sample slightly in advance of the application of the increased axial stress. This was purely as a precaution against the reverse happening, if attempting to apply both simultaneously, and causing undrained failure. The axial deformation, pore pressure and applied stresses were recorded against time. The drained stage was commenced simply by opening the constant volume tap between the sample and the volume change apparatus. The axial and volumetric deformations were recorded, together with the pore pressure and applied stress, against time until the pore pressure had dissipated to the value of the applied back pressure.

The TA3 series was required to be loaded in a drained manner such that the axial and radial stresses increased continuously and at a constant incremental stress ratio. The method used was rather crude but appeared to be reasonably effective, as will be seen in Chapter 7. The increase of radial stress was effected by raising the adjustable mercury pot at a constant rate using an electric motor. The rate of increase of cell pressure was 1.15 Kl/m^2/hour. The deviator stress was applied as in the ordinary drained tests by the constant rate of strain method. Axial and volumetric deformations were recorded together with the pore pressure and applied stresses at frequent intervals.

contact with the loading frame. A pressure of 50-100 kN/m^2 was applied to the main cell so that the flushing water and entrapped air was forced up around the top platen and through the porous disc. The top membrane was greased, with silicone grease, and sealed onto the top platen with the retaining ring. The drainage connection was made and a suction applied for 5 to 10 minutes to ensure that the flushing water was drained out. The drainage tap was closed, the cell pressure released and the apparatus wound down to allow the cell top plate to be fitted and the top cell filled. The dial gauge was fitted to the plunger to record axial deformations.

An axial and radial stress of 250 kN/m^2 was applied in an undrained manner, and the pore pressure recorded. It was necessary to apply a top cell pressure in excess of the required axial stress to overcome the frictional losses on the plunger and top cap, the load recording from the proving ring was used to compute the true axial stress. The stresses were then increased isotropically to the "test" radial stress, in an undrained manner. After equalisation of pore pressure the specimen was consolidated into a back pressure of 250 to 300 kN/m^2. The axial stress was then decreased under drained conditions to the required value to represent the in-situ stresses. After consolidating to the required K_o value the samples were subject to the TD2 or TA2 loading paths (Figure 5.1(b) and (d)).

The TD2 series requires strain controlled loading. Therefore it is necessary to change from the hydraulically controlled axial stress to strian controlled axial stress in order to carry out the TD2 tests. The apparatus is set up in a triaxial loading frame so that the plunger is in contact with the crosshead. The loading is then gradually taken up on the plunger while the top cell pressure is reduced. With the load fully transferred to the plunger

the applied cell pressure is switched off and the bleed valve opened to allow free volume change in the top cell. The sample is then loaded in the normal way by straining the frame at a constant rate.

The TA2 series is a stress controlled test and therefore the plunger is not in contact with the triaxial frame crosshead. The application of stress increments is very similar to the TA1 series. The pressure supplies to the top and radial cell are temporarily closed while the pressures are increased. However in this apparatus the two cells are opened to the increased cell pressures simultaneously. The procedure then follows the TA1 series during the undrained and drained deformation stages.

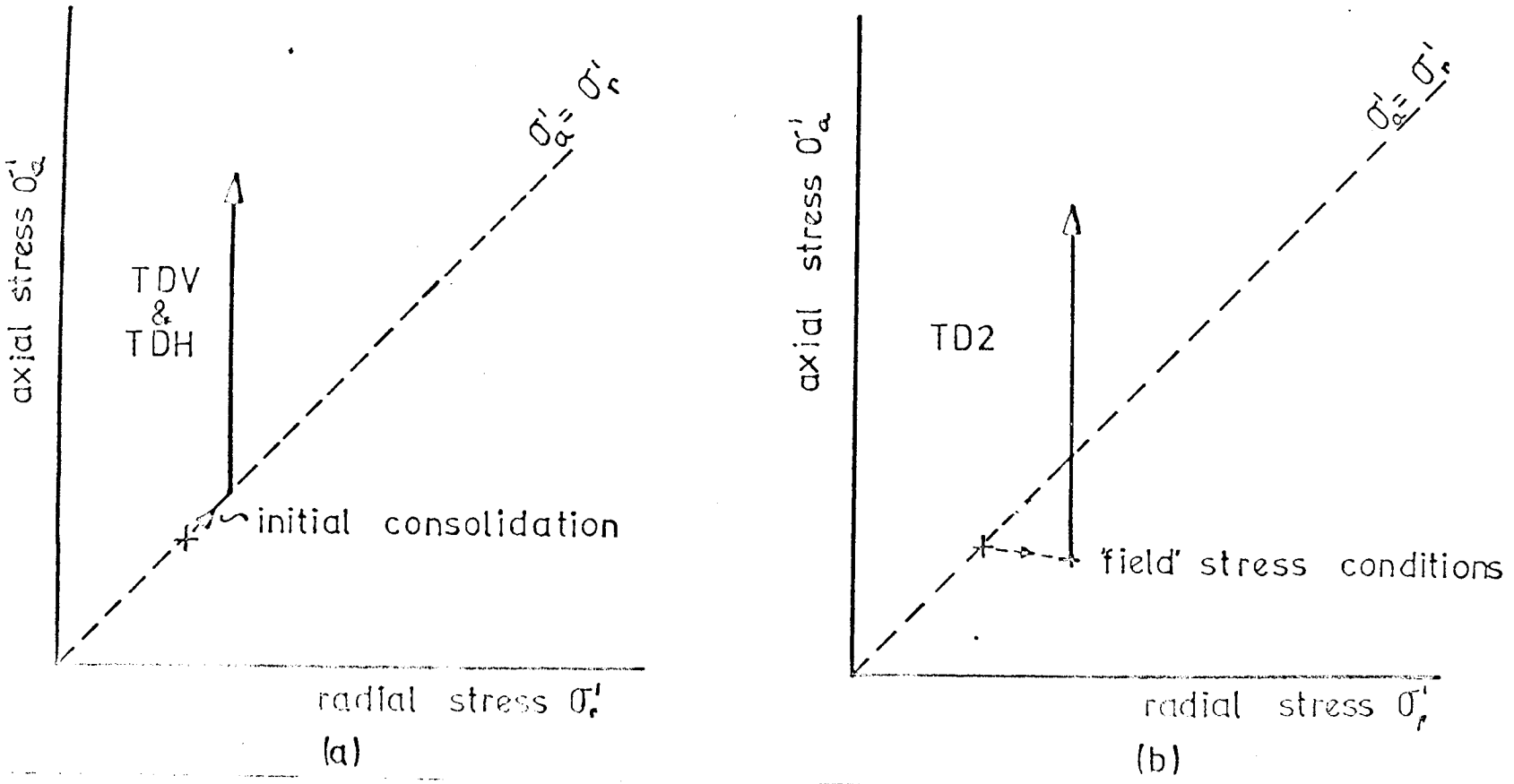

FIG. 5.1 Triaxial tests - Effective Stress Paths

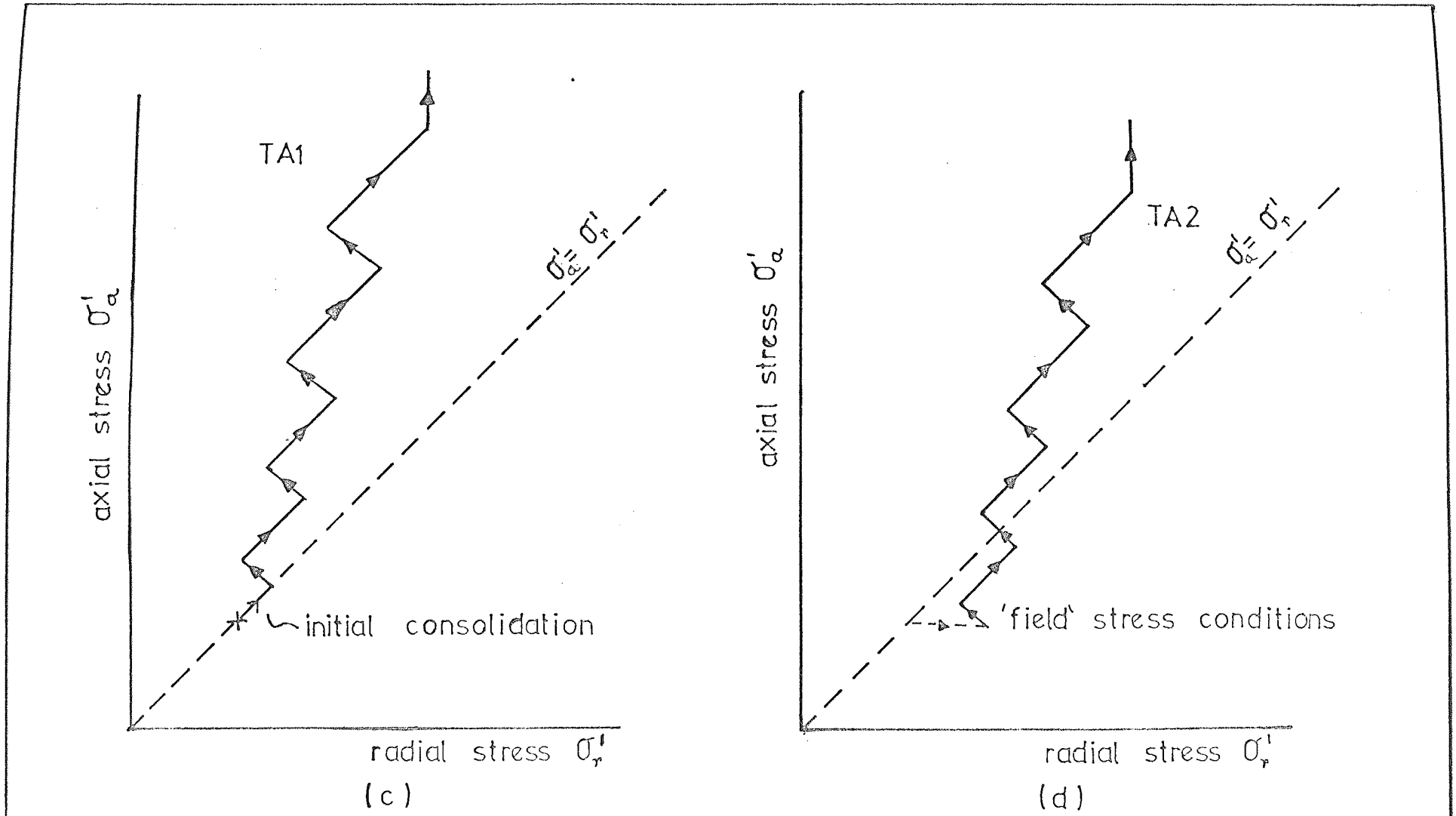

FIG. 5.1 Triaxial Tests - Effective Stress Paths

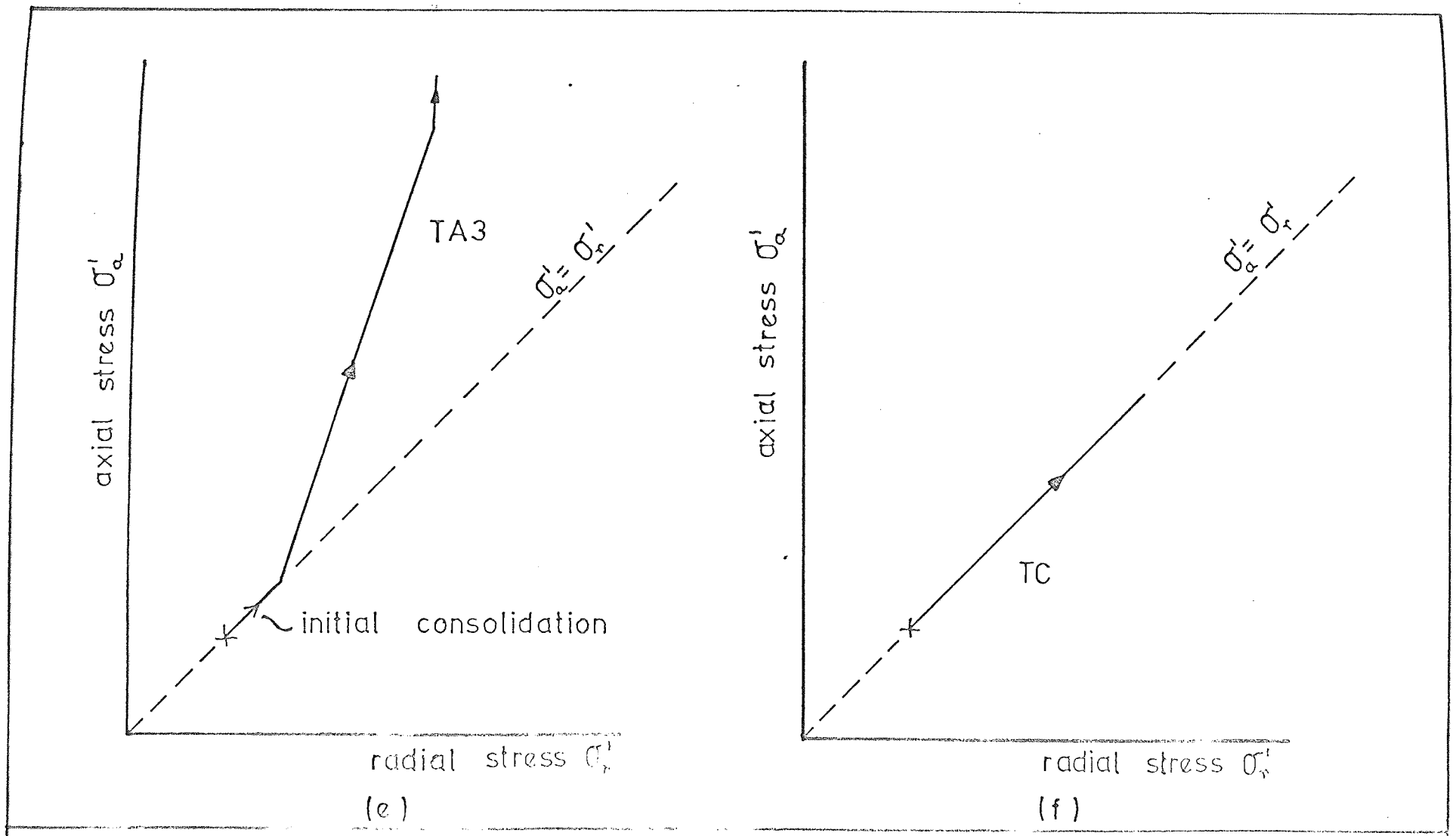

FIG. 5.1 Triaxial Tests - Effective Stress Paths

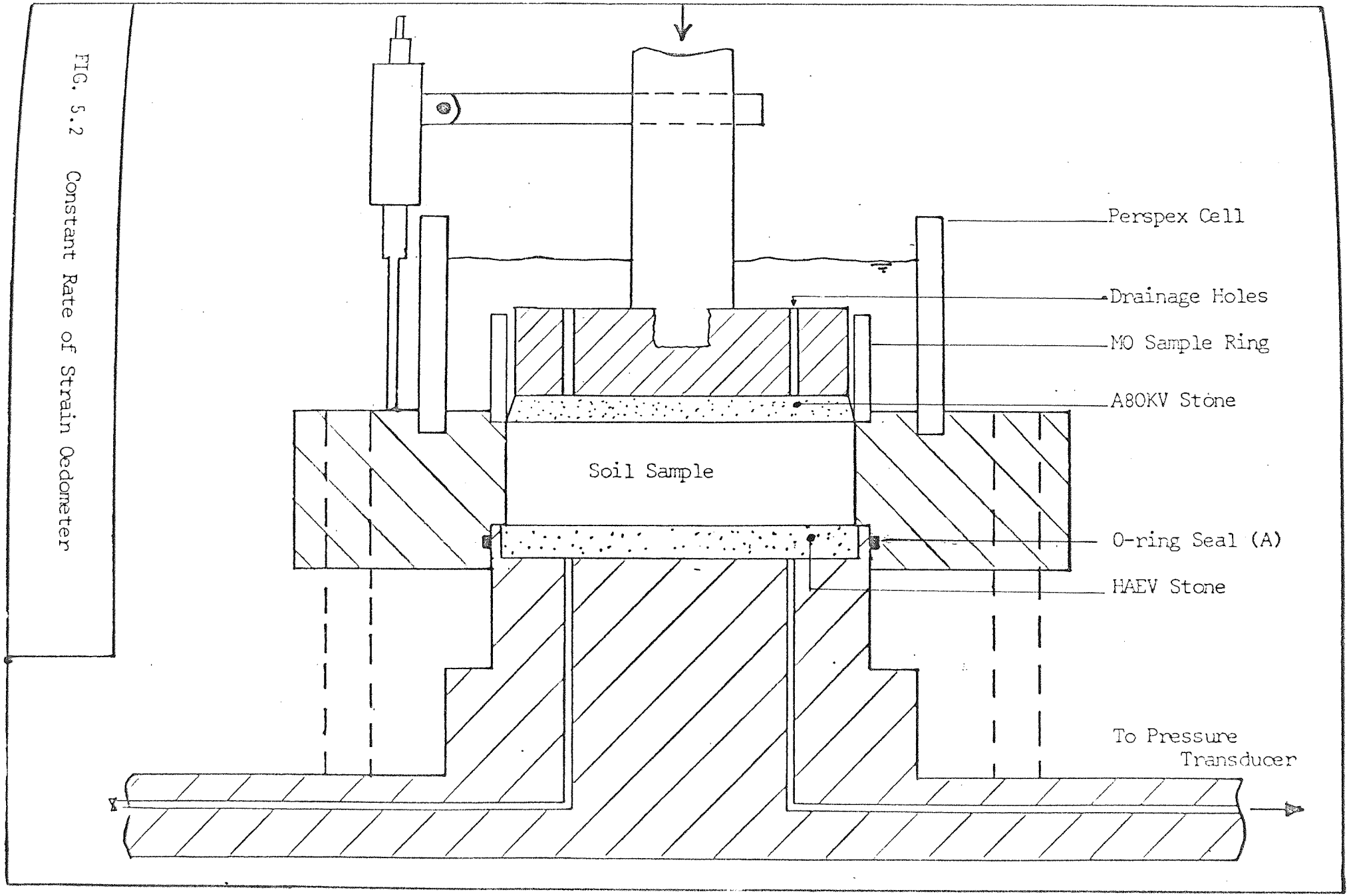

FIG. 5.2 Constant Rate of Strain Oedometer

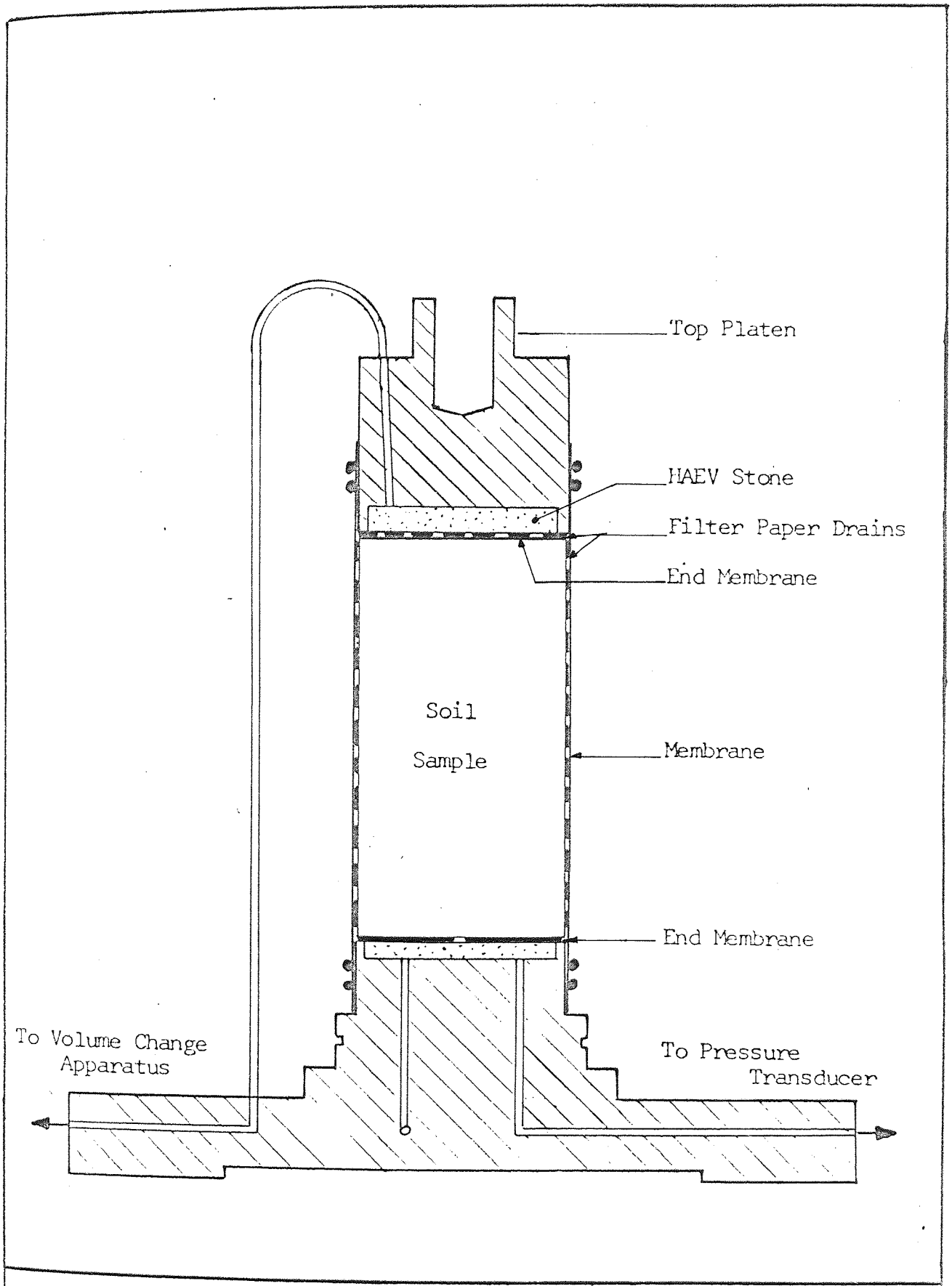

FIG. 5.3 Standard Triaxial Apparatus

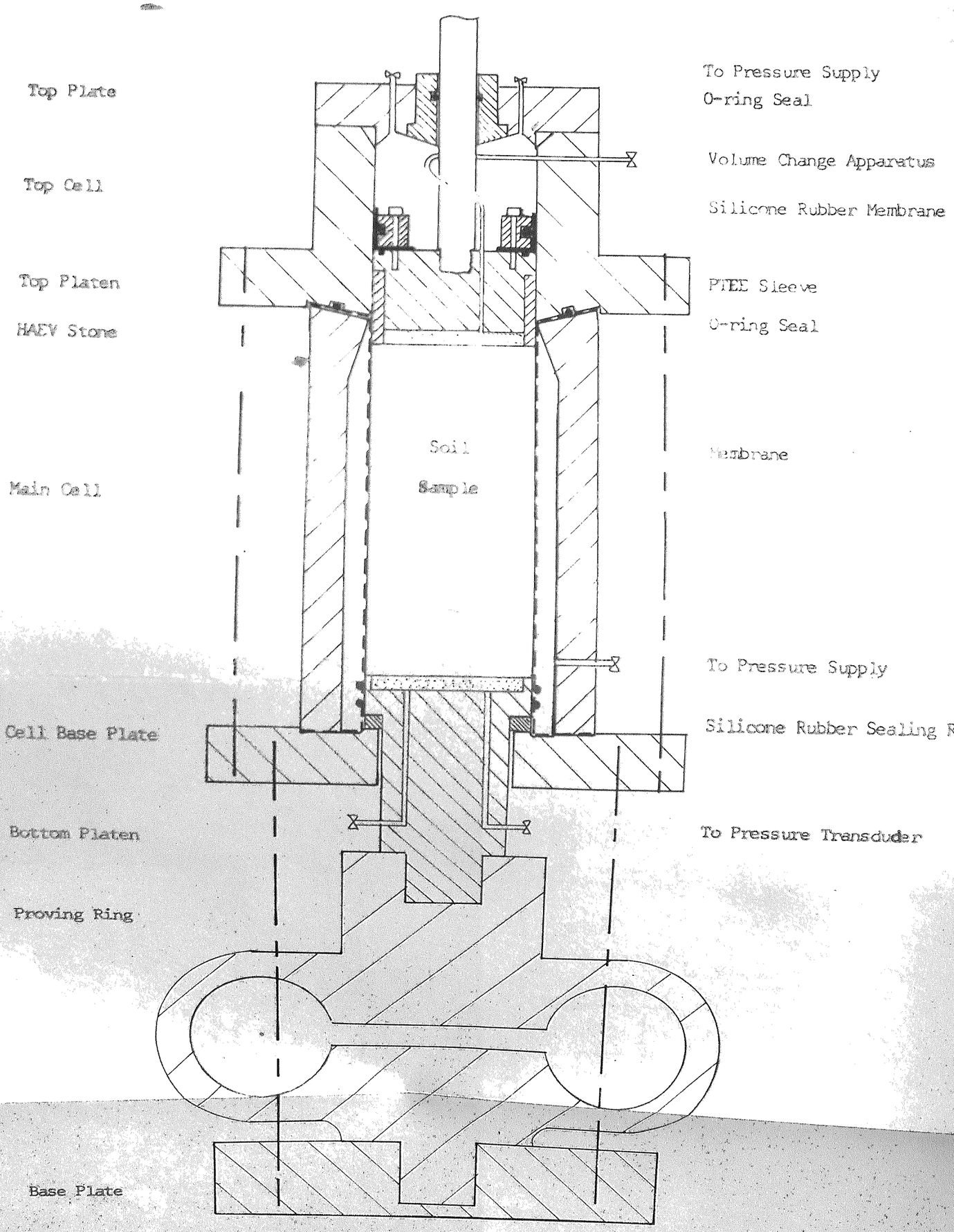

FIG. 5.4 Independent Stress Cell

(a) Mechanical Oedometer

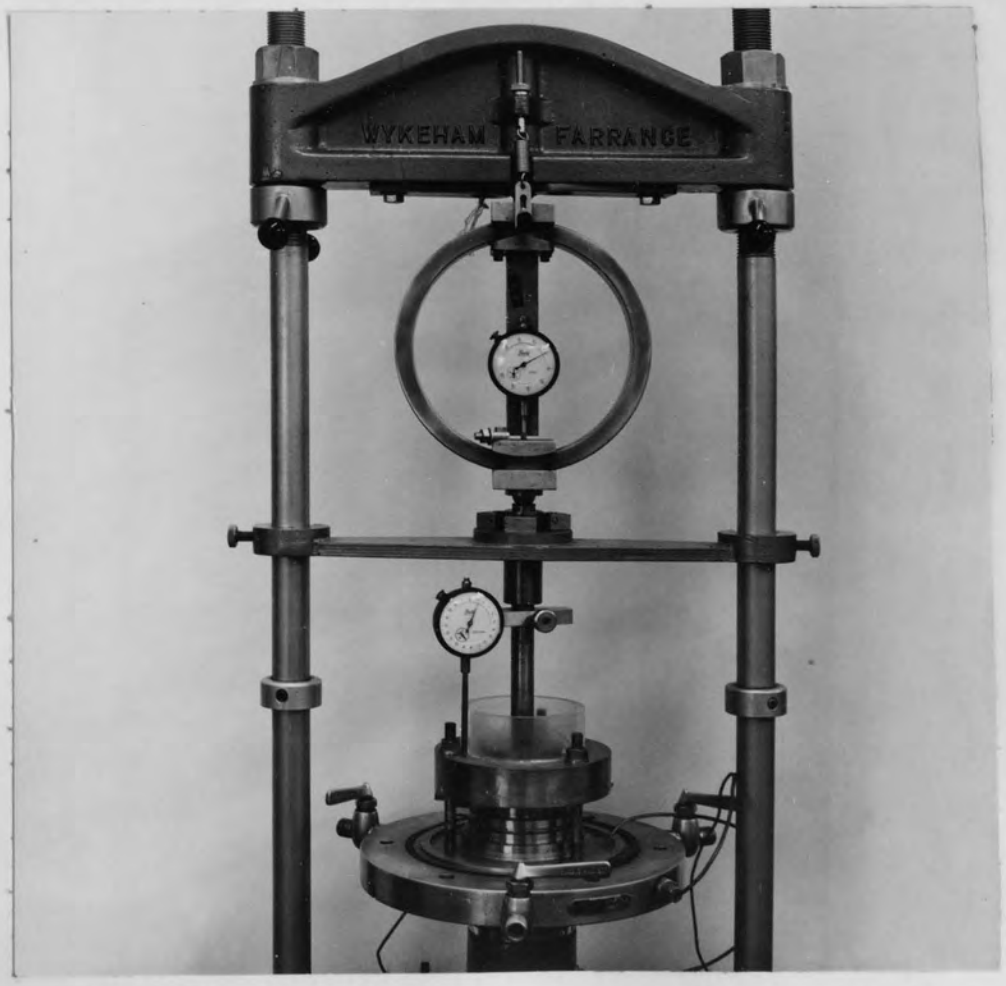

(b) Constant rate of strain Oedometer

PLATE 5.1 OEDOMETER APPARATUS

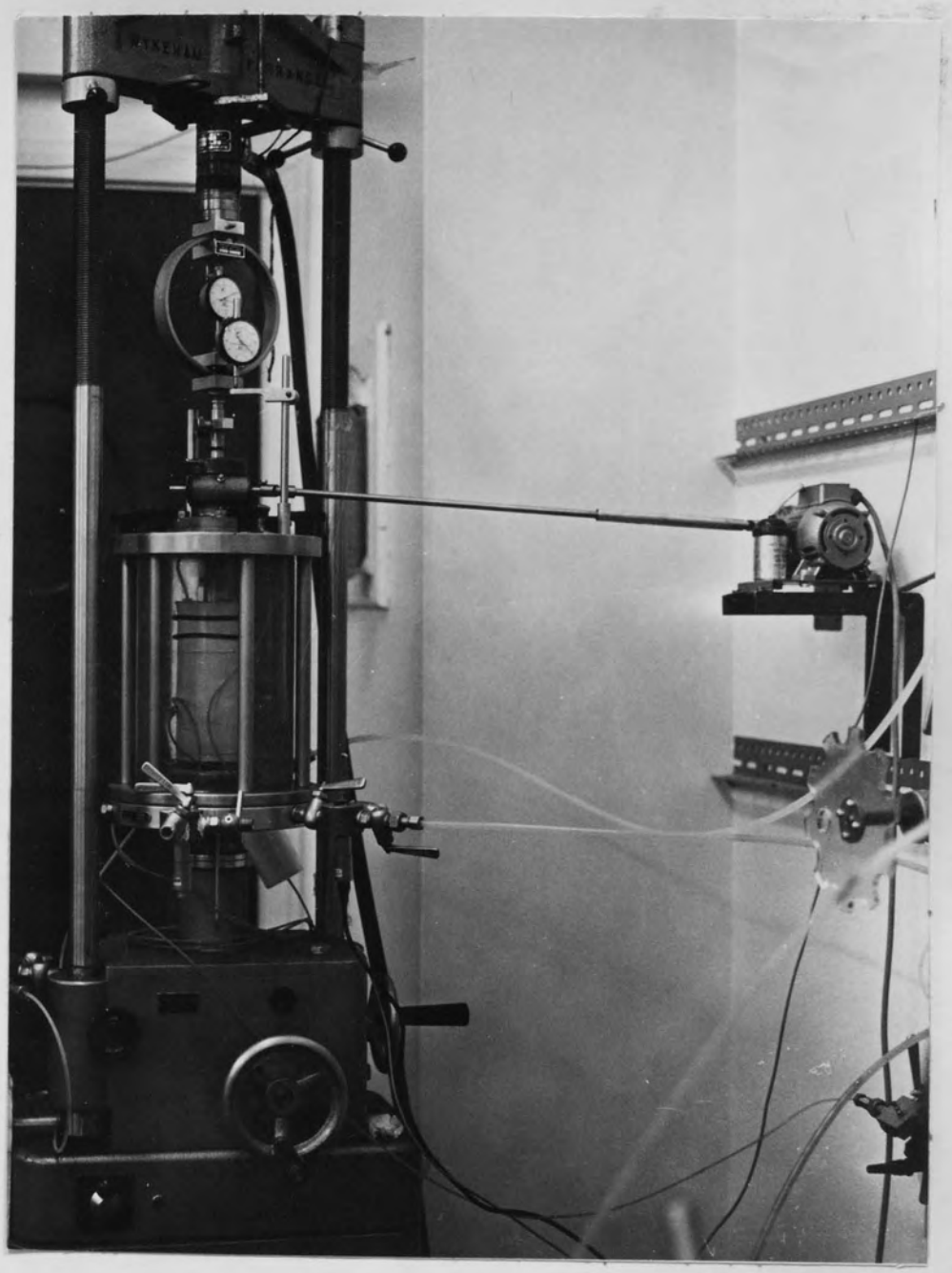

PLATE 5.2 TRIAXIAL APPARATUS - TA1 SERIES

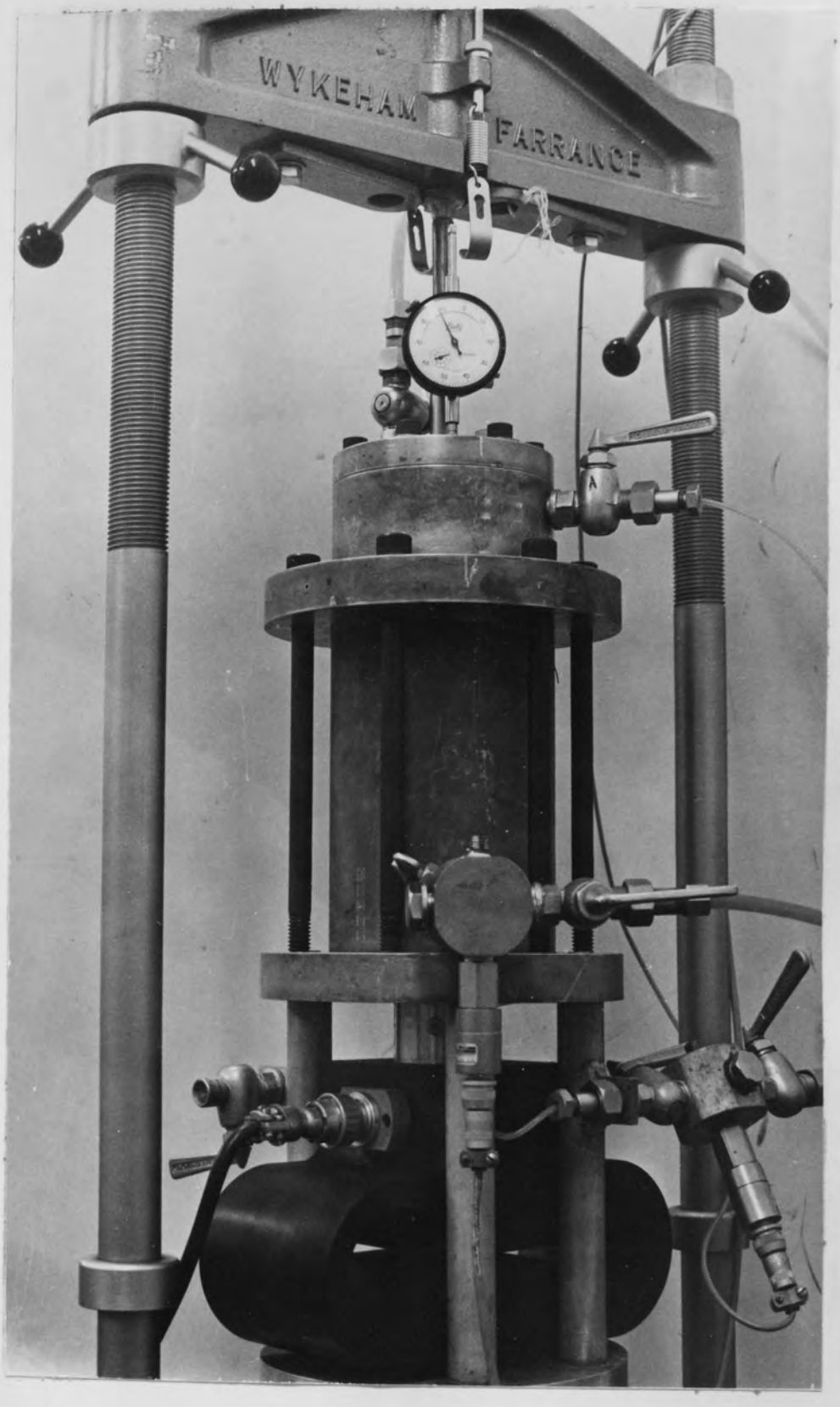

PLATE 5.4 INDEPENDENT STRESS CELL

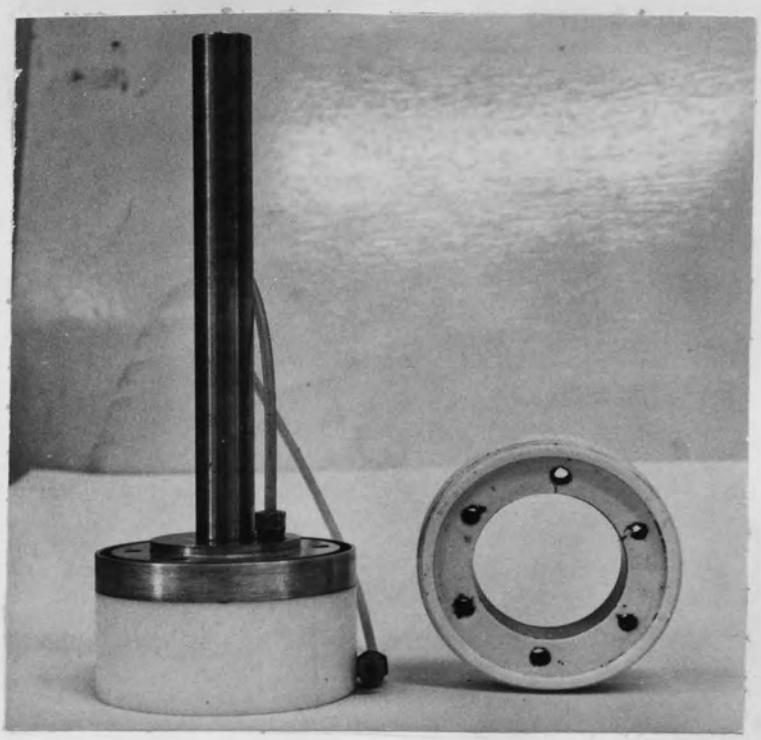

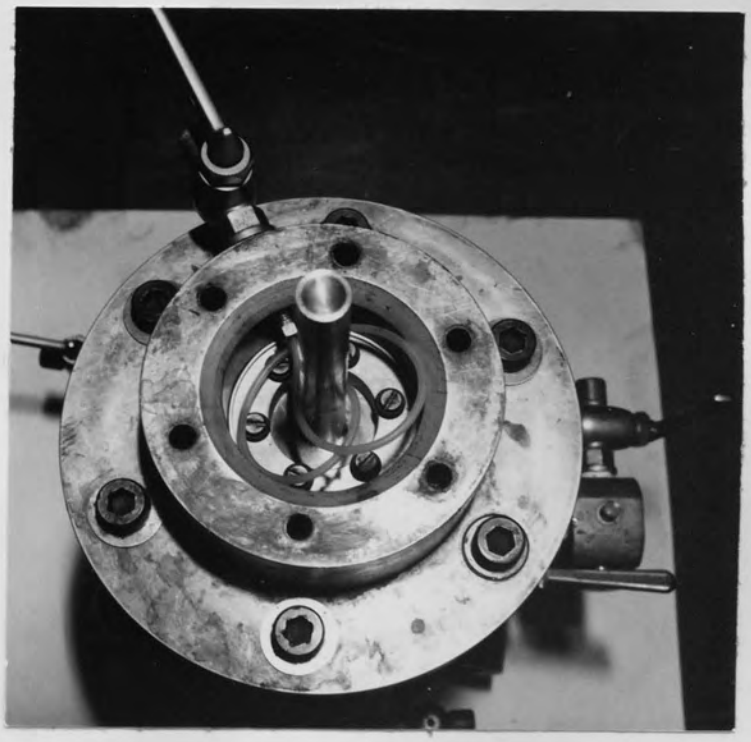

PLATE 5.5 IS CELL TOP PLATEN

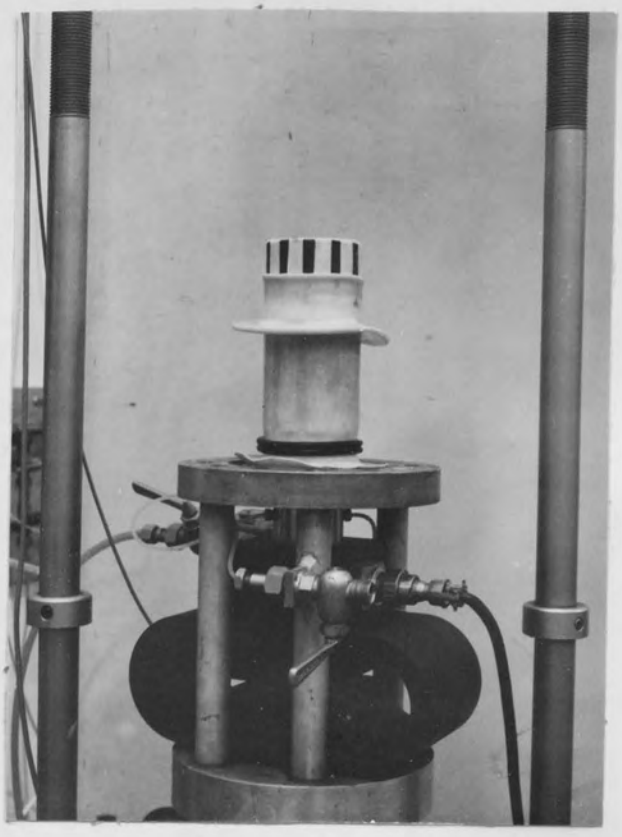

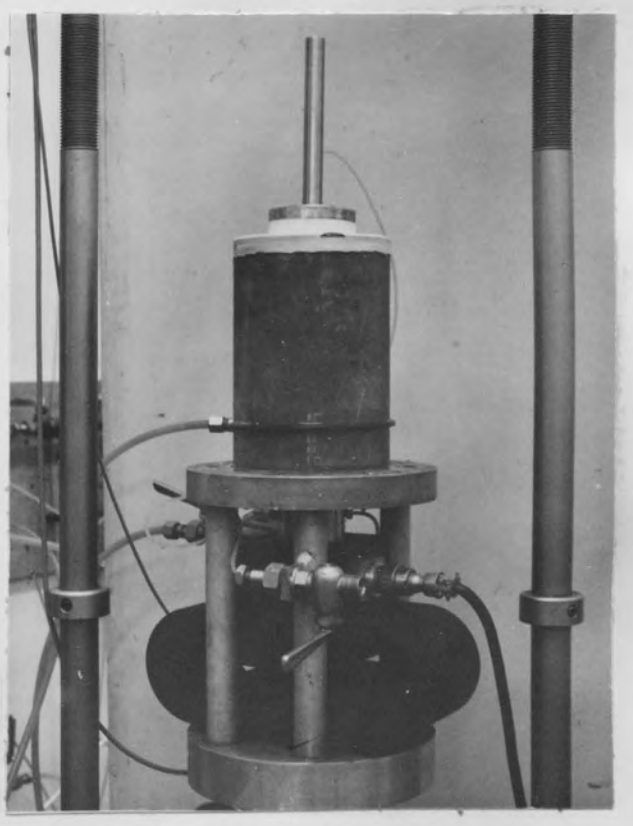

PLATE 5.7 SETTING UP INDEPENDENT STRESS CELL

CHAPTER 6

OEDOMETER TEST RESULTS

6.1 Introduction

6.2 Equilibrium Stress σ'_k

6.3 Compressibility

6.4 Rate of Consolidation

6.5 Preconsolidation Stress

6.1 INTRODUCTION

The results of the oedometer tests are described in this chapter. The order of presentation of the results is shown on the previous page. In general each topic will be subdivided to deal with different methods of testing seperately. A discussion of the results will be presented at the end of each section. Further discussion and comparison with the triaxial test results is presented in Chapter 8.

Where oedometer test results are used to determine the compressibility it is considered preferable to present them in the form of axial stress against axial strain, rather than the conventional void ratio against effective stress. It does not seem pertinent to transform the results to void ratios in this instance as it is likely to introduce unnecessary errors.

The compressibility of a soil determined in the oedometer is usually expressed by Terzaghi's coefficient of volume compressibility, m_v. However when the triaxial apparatus is used to study the compressibility of a soil, the quasi-elastic parameters, secant modulus (E) and Poissons ratio (ν) are used. As the results of these tests are frequently used side-by-side it would be preferable if this inconsistency was avoided. Janbu (1963) proposed that the compressibility for both types of test should be expressed as the tangent modulus (M) of the axial stress-strain plot, (i.e. $M = \partial\sigma'/\partial\varepsilon$). It is therefore proposed in this thesis that the compressibility be expressed by the axial deformation modulus (M_a) where

$$M_a = \partial\sigma'_a/\partial\varepsilon_a$$

and the volume deformation modulus (M_v) where

$$M_v = \partial\sigma'_a/\partial\varepsilon_v$$

In the case of the oedometer tests $M_a = M_v = (1/m_v)$ while for the triaxial test M_a and M_v will, in general, not be equal. The quasi-elastic parameters E and ν can be readily derived from M_a and M_v, and are used in Chapter 7 to examine the triaxial tests in greater detail.

6.2 EQUILIBRIUM STRESS (σ'_k)

The equilibrium stress, σ'_k, of the undisturbed samples was determined using the techniques described in section 5.2.1(a) and (e). The results of each test are tabulated in Table 6.1 together with the estimated in-situ vertical effective stress, σ'_v, determined in Chapter 4, (Figure 4.11). Also shown in the table are the water contents at the time of sampling, w_s, the water content at the time of testing, w_i, and the degree of saturation, S_i, at the time of testing.

The equilibrium stress is plotted as a function of the in-situ effective vertical stress (σ'_k/σ'_v) against depth (Figure 6.1). It is seen that σ'_k/σ'_v varies between 1.5 and 4.3, which suggests that the method is not very reliable. Three of the samples appear to have a degree of saturation less than 95% (Figure 6.1), two of these have relatively high values of σ'_k/σ'_v while the other is low. It seems unlikely that the graph can be corrected in any way due to lack of initial saturation. Treating the tests with Sr < 95% as suspect it would not appear unreasonable to consider a value of 2 to be a minimum value of σ'_k/σ'_v from the present data.

These values will be considered in Chapter 8 with the equilibrium stress obtained from the triaxial tests. The determination of the in-situ K_o will also be considered then, as a value of the pore pressure coefficient A is required.

6.3 COMPRESSIBILITY

The methods of preparation, setting up and loading of samples have been discussed in the previous chapter. Twelve undisturbed samples were tested in the oedometer, seven were loaded by the standard "doubling increment" method (5.2.1(b)(i)), four by the "constant increment" method (5.2.1(b)(ii)) and the other by a "constant rate of strain" method (5.2.1(c)).

6.3.1 Origin Correction

For mechanical oedometer tests (MO Series) the recorded compression was plotted against the square root and logarithim of elapsed time for each increment. The individual plots are not shown in the thesis, but are illustrated by the compression-root time plot for test MO7 (Figure 6.2). For each stress increment an origin shift (δh_c) was observed using the Terzaghi parabolic relationship between t and Δh in the early stages of the test, (Figure 6.2).

The accumulated origin correction, $\Sigma \delta h_c$ is plotted against the effective axial stress less the equilibrium stress ($\sigma'_a - \sigma'_k$) for the doubling increment and the constant increment methods in Figures (6.3(a) and (b) respectively. Superimposed on these graphs is the range of the machine error, as obtained from the oedometer calibration tests (Appendix E). It is seen that for the doubling increment method of loading the origin correction, for the first loading cycles, is up to 60% greater than the recorded machine error. However during reloading the origin corrections are reduced and lie within the range of the machine error (Figure 6.3(a)). For the constant increment tests the first loading cycle corrections all lay within the recorded machine error range (Figure 6.3(b)). However for this type of loading the recorded machine error covered a wider range, although it can be

seen from the calibration tests (Figure E1) that the majority of points lie within a band comparable to that of the doubling increment. Using this lower range of machine error the origin corrections appear to be up to 25% greater than the machine error. During reloading the origin corrections were found to lie within (or slightly less than) the lower range of the machine error, as for the doubling increment.

These results demonstrate that the "sample bedding" errors are eliminated during the first loading cycle and that the machine error can be a significant portion of this origin correction which is still present on relaoding. For the particular samples tested the origin corrections accounted for up to 25% of the recorded compression for each increment during both the loading and reloading cycles.

For the CS (constant rate of strain) test it is not possible to determine the origin correction from the test results. It was therefore decided that the apparatus should be calibrated for machine error (Appendix E), and the results used to correct the compression recorded during the CS test.

In all subsequent analyses of test results, the actual axial compression Δh_{cor} for any increment is taken as the recorded compression, Δh, less the origin correction, δh_c, as obtained from the $\Delta h - \sqrt{t}$ plot for the MO test or the machine error for the CS test

6.3.2 Stress-Strain Relationships

The results of the oedometer tests on the undisturbed samples are presented in the form of stress against axial strain. The strains are calculated from the corrected compressions as described above.

6.3.2.1 MO Series

The stress-strain plots for the MO Series of tests are shown in Figures 6.4, 6.5 and 6.6 for the block, core and tube samples respectively. Each test consists of two load-unload cycles with the exception of MO 13, which was not reloaded.

It is seen at the end of the first load-unload cycle that a significant proportion of the strain is not recovered (residual strain). Further that the average percentage residual strain varies for each sample type; 20% for the cored samples compared to 27% for the block and 35% for the tube samples.

During the second loading cycle the axial strain is, generally, more than 95% recoverable. The unloading curves for the two cycles are seen to be approximately parallel and often virtually coincident. The residual strains recorded in the first loading cycle are indicative of the amount of mechanical disturbance caused by the sampling process. Results from undrained triaxial tests on London Clay presented by Marsland (1971) show that the time between sampling and testing can have a significant effect on the origin corrections and the deformation modulus. However it was not possible to achieve any correlation between the residual strain and time before testing although as the first oedometer test was not carried out until 30 weeks after sampling the deteriation due to time may well have been substantially complete.

6.3.2.2 CS Test

The stress-strain curve of the single undisturbed CS test is shown in Figure 6.7. The initial portion of the curve (up to 2500 kN/m^2), Figure 6.7(b), is seen to compare favourably with the incrementally loaded core samples (e.g. 6.5(a)). During the test the pore pressure was recorded at the base of the sample to check its

dissipation. The recorded pore pressure is shown in Figure 6.7(a) as a percentage of the axial stress, it is seen that it does not rise above 4%. The pore pressure rises to approximately 35 kN/m^2 at σ'_a of 1500 kN/m^2 and remains effectively constant at that stress throughout the loading stage. The residual strain recorded after loading to 14000 kN/m^2 and unloading to the equilibrium stress was approximately 26%. This is still comparable with that recorded for the cored samples in the MO Series despite the loading being approximately six times greater.

6.3.3 Deformation Modulus

As described at the begining of this chapter the compressibility is expressed by the axial deformation modulus, M_a.

6.3.3.1 MO Series

The axial deformation modulus, M_a, is tabulated in Table 6.2 for each increment of stress and are shown plotted against the average axial effective stress, $(\sigma'_a)_{av}$ in Figures 6.8, 6.9 and 6.10 for the block, core and tube samples respectively. The results all indicate the same general trend with M_a increasing, approximately linearly, with the increase of axial stress after the initial load increment. The block and cored sample results were sensibly consistent, but the tube samples showed considerable scatter of results.

The results are replotted in the form $M_a/(\sigma'_a)_{av}$ (modulus number m - Janbu (1963)) against the increase of vertical effective stress $(\sigma'_a - \sigma'_k)$(Figures 6.11 to 6.13). As the equilibrium stress varied from 176 - 515 kN/m^2 it was decided to plot against the "increase of axial stress" rather than axial stress. It is seen that all the tests produce the same sort of relationship with an initially high value of $M_a/(\sigma'_a)_{av}$ reducing to an effectively constant value. This reflects the change in slope of the more familiar "void ratio - effective stress" plots (Figures 6.19 and 6.20).

The results of the two block samples (Figure 6.11) are seen to be consistent. For the first loading cycle the m value is constant at 41, except for the initial increment which is substantially higher. On reloading the same type of curve is obtained, with m becoming constant at a value of 52.5, which is an increase of 28% on the first cycle.

The core results (Figure 6.12) are of a similar nature, with little scatter. Here the constant m value obtained after the initial increment on the first loading cycle is approximately 40. Re-loading produces the same sort of curve with m becoming consistent at 50, an increase of 25%.

The results from the tube samples (Figure 6.13) show much more scatter than for the block or cores, but the same type of relationship is still evident. The first loading cycle showed that m reduced after the first, or second, increment to a constant of 32.5. Re-loading showed the same trend with the constant value at approximately 46 an increase of more than 40%. It is seen that the results of tests M02 and M03 gave high values of M_a, particularly on reloading. It is suspected that there was some variation in the samples as the rate of consolidation (see later) also yielded "individual" results, although no peculiarities were observed during preparations.

The type of sampling technique is seen to have a significant influence on the compressibility results obtained from the first loading curve. It is seen that the deformation moduli obtained from core and block samples are approximately equal, while that of the tube samples is lower by some 20%. In all cases the value of M_a was seen to increase during reloading with the most significant increase being obtained from the tube samples. The deformation modulus, on the reloading cycle, for the tube samples was only 10%

less than the block and core samples. It would thus appear that the first loading eliminates much of the influence of the mechanical disturbance.

6.3.3.2 CS Test

M_a is obtained from the stress-strain plot (Figure 6.7) for increments of stress comparable to those used in the MO series, (Table 6.3). The values obtained for the earlier part of the curve (σ'_a < 2500 kN/m^2) are shown in Figure 6.9 with the results of the MO series core samples. It is seen that the values from the CS test compares favourably with those from the MO series

The early values of $M_a/(\sigma'_a)_{av}$ are also plotted with the MO series core samples (Figure 6.12). Here, it is seen that the results are not as consistent as the MO tests. However the same shape curve is apparent with $M_a/(\sigma'_a)_{av}$ decreasing initially and then becoming approximately constant, at a value in the order of 10% greater than for the MO Series.

$M_a/(\sigma'_a)_{av}$ is plotted against the increase in axial stress over the full range in Figure 6.14. Plotted at this scale the approximately constant value suggested from the earlier tests is not evident. $M_a/(\sigma'_a)_{av}$ increase linearly with increase of stress to a stress of approximately 9500 kN/m^2, when a further increase in slope occurs. This is again reflected by the "void ratio - effective stress" plot Figure 6.20. The significance of these slope changes will be discussed after examination of similar results from remoulded tests.

6.3.3.3 RMO and RCS Tests

Three samples were consolidated from a slurry in the mechanical oedometer RMO1, 2 and 4 the latter was subsequently used for the RCS 1 test. The tests were primarily carried out to establish the virgin consolidation line. The axial deformation modulus was

determined in the same manner as for the undisturbed samples. The results of RMO 1, 2 and 4 are shown in Table 6.4 while the results of RCS 1 are shown in Table 6.5. $M_a/(\sigma'_a)_{av}$ is plotted against the increase of stress in Figure 6.15 for RMO 1, 2 and 4 tests and the early stage of RCS 1. It is seen that for the first loading cycle the modulus number reduces rapidly to a constant value of 15. The reloading curve for RMO 2 produces a result very similar to the undisturbed samples. The modulus number reduces to an approximate constant after the initial load at a value of 47.5. The preconsolidation pressure is not exceeded.

The sample tested at constant rate of strain (RCS 1) showed $M_a/(\sigma'_a)_{av}$ decreasing to a constant value of 15 and remaining at this level for the full range of stress (i.e. 14,000 kN/m^2), (Figure 6.14). The sharp change in slope at a stress of approximately 1000 kN/m^2 is coincident with the stress at which the reconsolidation curve returns to the virgin line (Figure 6.19). This is not true of RMO 2 when the change in slope occurs at 500 kN/m^2 which is well below the preconsolidation stress of 3,200 kN/m^2

6.3.4 Summary

It has been seen that for the initial loading cycle in the mechanical oedometer up to 25% of the recorded compression was a result of "machine" and "sample bedding" error, and that approximately 60% of this was due to machine error alone. During the reloading cycle the"sample bedding" error appears to be eliminated but there is still a significant error due to the machine. It is therefore apparent that origin corrections are essential for both loading and reloading cycles particularly with a material of such a high deformation modulus.

The methods of sampling appear to be reflected by the stress-strain

relationships obtained from the oedometer tests. The residual strains at the end of the first load cycle were of the order of 20, 27 and 35% for core, block and tube samples respectively. Similarly considering the modulus number ($M_a/(\sigma'_a)_{av}$) the tube samples gave the lowest value on the first and second loading cycles while the core and block were approximately equal. The value obtained from the first loading cycle for block, core and tube samples respectively were 20, 20 and 37% lower than the reloading value for the block and core samples. It would therefore appear that the degree of disturbance for the tube samples was considerably greater than that of the core and block samples.

For all tests a distinct change in slope of the $M_a/(\sigma'_a)_{av}$ against increase of stress curve was observed at a stress increase of 400 - 500 kN/m^2 for the MO series and approximately 1000 kN/m^2 for the CS and CRS test. Oedometer tests by Som (1968) with measurement of radial stress σ'_r, on undisturbed samples of London clay, indicated that the incremental stress ratio $\bar{K}_o$ was initially small, 0.28 and increased to 0.64 at a stress of approximately 700 kN/m^2. Webb (1966) reported similar results when testing London clay under zero lateral strain in the triaxial apparatus with the Bishop mercury jacket. It is therefore considered probable that the noted change in slope is attributed to such a change in incremental stress ratio. However, this will be considered later with the results of the triaxial tests.

6.4 RATE OF CONSOLIDATION

The coefficient of consolidation, C_v, was calculated for each load increment, during the MO series of tests, by the Taylor root time method and the Casagrande logarithmic method. The former fits the theoretical and experimental curves at 90% consolidation and this yields the time t_{90}. The latter fits the curves at 50%

consolidation and thus time t_{50} is obtained. The results are tabulated in Table 6.6 and plotted against the average axial stress in Figures 6.16, 6.17 and 6.18 for the block,core and tube samples respectively.

It is seen that the Taylor method invariably produces a higher value of C_v, than the Casagrande method, particularly on first loading. The latter method is also seen to be more consistent. During reloading the Taylor method gives high values for the initial loading followed by values approximately equal to the Casagrande method. As the Casagrande method appears to give less erratic results, the comparisons are made on the results obtained by this method. It is seen that for the block samples the values of C_v are approximately constant at a value of 1.2×10^{-4} cm^2/sec. Also it is seen that this value does not noticeably alter during the relaoding cycles. Similarly the core samples give approximately constant C_v values, at 1.0×10^{-4} cm^2/sec; again reloading has no noticable effect on C_v. The tube samples show a large scatter of results, particularly from the Taylor method where values from early loadings are up to one order of magnitude greater than subsequent values. Generally C_v varies between 1 and 2×10^{-4} cm^2/sec for both first and reloading cycles, however the reloading values show less scatter. Samples MO 2 and MO 3 are seen to give very scattered readings during the first loading, but are reasonably consistent on relaoding. A value of C_v approximately 3×10^{-4} cm^2/sec is obtained for these tests during the reloading cycles.

The following points were evident from the above results

(i) C_v obtained from the core and block samples are approximately equal, while those from the tube samples were greater by a factor of approximately 2.

(ii) C_v is effectively independent of applied stress

and

(iii) unaltered by reloading.

6.5 PRECONSOLIDATION STRESS

A study of the geological history of the site (Chapter 4) showed that this material could have experienced an overburden of 520-870m. Assuming that the sediments were submerged then the preconsolidation stress could lie in the stress range, 5·2 -8·7 MN/m^2.

The Casagrande construction for determination of the preconsolidation stress is not suitable for heavily preconsolidated clay. Schmertmann (1953) proposed a method based on the assumption that the geological rebound is parallel to the laboratory rebound curves, this method would appear to be the best method for such a heavily overconsolidated material.

A programme of tests consisting of three slurry samples consolidated in the mechanical oedometer, one of which was transferred to the constant rate of strain apparatus, plus a constant rate of strain test to a high stress on an undisturbed sample was carried out. Only one undisturbed sample could be tested due to delay in the manufacture of the apparatus. The remoulded specimens were prepared as described in 5.4.1. Samples RMO 1 and 4 were tested in a ring 65mm diameter by 30mm high, while 76mm diameter by 30mm high ring was used in RMO 2. The initial water contents were 63.2%, 54% and 55.8% for RMO 1, RMO 2 and RMO 4 respectively.

The voids ratio-effective axial stress relationship is shown in Figure 6.19. It is seen that the slope of the loading curves vary according to the initial moisture content, but converge as σ'_a increases. The unloading curves are approximately of equal slope although RMO 1 is slightly steeper than the others. The

sample from RMO 4 was used in RCS 1 test, the voids ratio - effective stress curve is plotted on the same diagram. It is seen that the reloading portion of the curve is virtually parallel to the reloading curve in RMO 2. On reaching the normally consolidation range the curve is found to agree very well with the virgin curves from the RMO tests. It is noted that the slope of the virgin curve is approximately equal to that reported by Som (1968) for undisturbed London clay loaded well above its preconsolidation stress.

The voids ratio - effective stress plot for the CS 1 test is presented in Figure 6.20. Superimposed on this diagram is the virgin curve and unloading curve obtained from the RCS 1. It is seen that the loading curves from CS1 and RCS 1 intersect at a stress of 10,000 kN/m^2. However the slope of CS 1 continues to decrease up to the maximum applied load of 14,000 kN/m^2. Hence it would appear that the preconsolidation is at least in the order of magnitude of 10,000 kN/m^2. Using the Schmertmann technique with the in-situ e value as 0.45 at a vertical effective stress of 100 kN/m^2 a curve with a slope similar to the unloading portion of CS 1 would pass through e = 0.45 at σ'_a = 0.1 MN/m^2 and the virgin line, from RCS 1, at σ'_a = 8 MN/m^2. However Schmertmann does require that the unloading curve should be obtained from a stress well in excess of the preconsolidation pressure, which was not the case in this instance. However it would appear that the preconsolidation stress σ'_c was at least 8000 kN/m^2 from the results obtained here. It is of interest to note that the loading and unloading curve obtained from CS 1 has a much shallower slope than obtained by Som (1968) on undisturbed London clay. This would suggest (Bjerrum 1967) that strong diagenetic bonds still exist in this material

Also shown in Figure 6.20 are the e - σ'_a relationships obtained from

MO 1 (tube), MO 9 (block) and MO 10 (core), it is seen that the slopes of the loading and unloading curves are similar to that obtained from CS 1. However these results are limited and rather inconclusive; obviously more high pressure consolidation tests are required and loading to even higher stresses may be valuable.

TABLE 6.1 -- EQUILIBRIUM STRESS (MO and CS Series)

Sample Type	Test No	Depth (m)	σ'_k (kN/m^2)	σ'_v (kN/m^2)	σ'_k/σ'_v	w_s	w_i	S_i
U70	MO1	1.45	257.6	95	2.71	0.205	0.1813	0.9336
U70	MO2	2.75	441.6	111	3.98	0.186	0.1542	0.8643
U70	MO3	4.11	316.5	126	2.51	0.191	0.1742	0.9808
U70	MO7	1.22	323.8	92	3.52	0.162	0.1756	0.9936
U70	MO8	5.64	515.0	147	3.50	0.184	0.1722	1.0005
U70	MO13	5.56	220.8	146	1.50	0.186	0.152	0.9217
CORE	MO4	2.21	206.0	104	2.02	0.173	0.1590	1.0227
CORE	MO10	1.88	206.0	100	2.06	0.196	0.1690	1.0308
CORE	MO11	3.66	176.6	121	1.45	0.191	0.1545	0.9595
CORE	CS1	1.88	170.0	100	1.70	0.196	0.1740	1.0514
BLOCK	MO9	2.14	206.0	103	2.00	0.177	0.1693	1.0188
BLOCK	MO12	2.4	442.0	103	4.29	0.177	0.1593	0.9708

TABLE 6.2 COMPRESSIBILITY (MO Series)

(a)

TEST No. MO9 BLOCK No. 3 2.135 m						
Stress Range (kN/m^2)	$(\sigma'_a)_{av}$ (kN/m^2)	$\Delta\sigma'_a$ (kN/m^2)	$\Delta\varepsilon_a$	M_a (kN/m^2)	$M_a/(\sigma'_a)_i$	$M_a/(\sigma'_a)_{av}$
FIRST LOADING						
206-353	279	147	0.660	22,400	108.8	80.4
353-646	500	293	1.415	20,850	59.2	41.7
646-1232	942	586	1.645	35,600	55.1	37.8
1232-2410	1823	1178	1.545	76,500	62.0	42.0
RELOADING						
206-353	279	147	0.385	38,200	185.4	137
353-646	500	293	1.055	27,700	78.5	55.5
646-1232	942	586	1.405	41,800	64.7	44.4
1232-2410	1823	1178	1.295	91,200	74	50.0

TABLE 6.2 COMPRESSIBILITY (MO Series)

(b)

TEST No. MO12 BLOCK No. 3 Depth 2.135 m						
Stress Range (kN/m^2)	$(\sigma'_a)_{av}$ (kN/m^2)	$\Delta\sigma'_a$ (kN/m^2)	$\Delta\varepsilon_a$	M_a (kN/m^2)	$M_a/(\sigma'_a)_i$	$M_a/(\sigma'_a)_{av}$
FIRST LOADING						
442-736	589	294	0.805	35,600	83.0	62.2
736-1324	1030	588	1.320	42,600	57.9	41.3
1324-2502	1913	1178	1.475	79,700	60.1	41.7
RELOADING						
442-736	589	294	0.455	65,000	147	110.5
736-1324	1030	588	0.955	61,500	83.5	59.6
1324-2502	1913	1178	1.120	105,000	79.3	54.9

TABLE 6.2 COMPRESSIBILITY (MO Series)

(c)

TEST No. MO4 CORE BH3 Depth 2.21 m						
Stress Range (kN/m^2)	$(\sigma'_a)_{av}$ (kN/m^2)	$\Delta\sigma'_a$ (kN/m^2)	$\Delta\varepsilon_a$	M_a (kN/m^2)	$M_a/(\sigma'_a)_i$	$M_a/(\sigma'_a)_{av}$
FIRST LOADING						
206-412	309	206	0.775	26,600	129.0	86.0
412-618	515	206	0.830	24,850	60.4	48.3
618-824	721	206	0.690	29,900	48.3	41.5
824-1030	927	206	0.620	33,200	40.4	35.8
1030-1236	1133	206	0.395	51,500	50.0	45.4
1236-1545	1391	309	0.550	56,200	45.4	40.3
1545-1854	1700	309	0.515	60,000	38.8	36.3
RELOADING						
206-412	309	206	0.665	31,000	150.3	100.3
412-618	515	206	0.685	30,100	73	58.5
618-824	721	206	0.460	44,800	72.5	62.0
824-1030	927	206	0.445	46,400	56.4	50.0
1030-1236	1133	206	0.370	55,700	54	49.1
1236-1545	1391	309	0.430	71,900	58.2	51.6
1545-1854	1700	309	0.340	91,000	58.9	55.1

TABLE 6.2 COMPRESSIBILITY (MO Series)

(d)

TEST No. MO10 CORE BH2 Depth 1.88 m						
Stress Range (kN/m^2)	$(\sigma'_a)_{av}$ (kN/m^2)	$\Delta\sigma'_a$ (kN/m^2)	$\Delta\varepsilon_a$	M_a (kN/m^2)	$M_a/(\sigma'_a)_i$	$M_a/(\sigma'_a)_{av}$
FIRST LOADING						
206-353	279	147	0.485	30,500	148	109.3
353-647	500	294	1.345	21,900	62.0	43.8
647-1235	942	588	1.635	36,200	56.0	38.4
1235-2411	1823	1176	1.405	83,700	67.7	45.8
RELOADING						
206-353	279	147	0.420	35,100	170.1	125.6
353-647	500	294	1.020	28,900	81.9	57.7
647-1235	942	588	1.330	41,100	63.6	43.7
1235-2411	1823	1176	1.355	87,000	70.4	47.7

TABLE 6.2 COMPRESSIBILITY (MO Series)

(e)

Test No. MO11 CORE BH3 Depth 3.66 m						
Stress Range (kN/m^2)	$(\sigma'_a)_{av}$ (kN/m^2)	$\Delta\sigma'_a$ (kN/m^2)	$\Delta\varepsilon_a$	M_a (kN/m^2)	$M_a/(\sigma'_a)_i$	$M_a/(\sigma'_a)_{av}$
FIRST LOADING						
176-324	250	146	0.810	18,150	103	72.5
324-618	471	294	1.680	17,580	54.3	37.3
618-1207	972	589	1.855	31,750	51.3	32.7
1207-2385	1796	1178	1.645	71,500	59.2	39.8
RELOADING						
176-324	250	146	0.545	26,800	152.3	107.3
324-618	471	294	1.125	26,200	81.0	55.6
618-1207	972	589	1.530	38,400	62.1	39.5
1207-2385	1796	1189	1.310	89,700	74.3	49.9

TABLE 6.2 COMPRESSIBILITY (MO Series)

(f)

TEST No. MO1 U70 BH3 Depth 1.45 m						
Stress Range (kN/m^2)	$(\sigma')_{a\,av}$ (kN/m^2)	$\Delta\sigma'_a$ (kN/m^2)	$\Delta\varepsilon_a$	M_a (kN/m^2)	$M_a/(\sigma')_{a\,i}$	$M_a/(\sigma')_{a\,av}$
FIRST LAODING						
257-463	360	206	0.855	24,100	93.9	67.0
463-669	566	206	0.910	22,650	49.0	40.1
669-875	772	206	0.730	28,200	42.2	36.5
875-1081	978	206	0.580	36,500	40.6	36.3
1081-1287	1184	206	0.535	38,500	35.6	32.5
1287-1596	1442	309	0.530	58,300	45.3	40.3
1596-1905	1750	309	0.510	60,600	38.0	34.7
RELOADING						
257-463	360	206	0.720	28,600	111.5	79.5
463-669	566	206	0.715	28,800	62.2	50.8
669-875	772	206	0.605	34,100	51.0	44.2
875-1081	978	206	0.465	44,400	50.7	45.3
1081-1287	1184	206	0.340	60,700	56.1	51.3
1287-1596	1442	309	0.480	64,500	50.2	44.7
1596-1905	1750	309	0.395	78,200	49.0	44.6

TABLE 6.2 COMPRESSIBILITY (MO Series)

(g)

TEST No. MO2 U70 BH3 Depth 2.74 m						
Stress Range (kN/m^2)	$(\sigma'_a)_{av}$ (kN/m^2)	$\Delta\sigma'_a$ (kN/m^2)	$\Delta\varepsilon_a$	M_a (kN/m^2)	$M_a/(\sigma'_a)_i$	$M_a/(\sigma'_a)_{av}$
FIRST LOADING						
442-648	545	206	0.300	78,800	178.5	144.3
648-854	751	206	0.445	46,300	71.5	61.6
854-1060	957	206	0.375	55,000	64.4	57.4
1060-1266	1163	206	0.420	49,000	46.1	42.0
1266-1472	1369	206	0.310	66,300	52.5	48.6
1472-1781	1627	309	0.480	64,400	43.5	39.6
1781-2090	1935	309	0.565	54,800	30.7	28.3
RELOADING						
442-648	545	206	0.250	82,500	186.5	151.3
648-854	751	206	0.310	66,500	102.5	88.5
854-1060	957	206	0.290	71,000	83.1	74.2
1060-1266	1163	206	0.260	79,300	74.7	68.1
1266-1472	1369	206	0.250	82,400	65.0	60.1
1472-1781	1627	309	0.245	125,200	85.1	77.0
1781-2090	1935	309	0.280	109,800	61.5	56.7

TABLE 6.2 COMPRESSIBILITY (MO Series)

(h)

TEST No. MO3 U70 BH3 Depth 4.12 m						
Stress Range (kN/m^2)	$(\sigma'_a)_{av}$ (kN/m^2)	$\Delta\sigma'_a$ (kN/m^2)	$\Delta\varepsilon_a$	M_a (kN/m^2)	$M_a/(\sigma'_a)_i$	$M_a/(\sigma'_a)_{av}$
FIRST LOADING						
316-522	419	206	0.485	42,500	134.3	101.5
522-736	629	206	0.705	30,400	58.7	48.8
736-942	839	206	0.695	29,700	40.3	35.4
942-1148	1045	206	0.485	42,500	45.2	40.6
1148-1354	1251	206	0.430	38,900	33.9	31.1
1354-1663	1509	309	0.680	45,500	33.6	30.2
1663-1972	1818	309	0.665	46,500	27.9	25.6
RELOADING						
294-500	397	206	0.350	59,000	200.2	148.5
500-706	603	206	0.390	52,900	105.5	87.7
706-912	809	206	0.330	62,500	88.5	77.4
912-1118	1016	206	0.365	56,500	62.0	55.6
1118-1428	1273	310	0.325	95,100	85	74.7
1428-1737	1582	309	0.280	110,000	77	69.5
1737-2046	1891	309	0.370	83,600	48.1	44.1

TABLE 6.2 COMPRESSIBILITY (MO Series)

(i)

TEST No. MO7 U7O BH2 Depth 1.22 m						
Stress Range (kN/m^2)	$(\sigma'_a)_{av}$ (kN/m^2)	$\Delta\sigma'_a$ (kN/m^2)	$\Delta\varepsilon_a$	M_a (kN/m^2)	$M_a/(\sigma'_a)_i$	$M_a/(\sigma'_a)_{av}$
FIRST LOADING						
324-617	471	293	1.070	27,600	85.2	58.5
617-911	765	294	1.040	28,400	46.0	37.2
911-1498	1201	587	1.510	38,950	42.7	32.4
1498-2670	2084	1172	1.93	61,000	40.7	29.2
RELOADING						
324-617	471	293	0.885	33,400	106	70.9
617-911	765	294	0.790	37,400	60.6	48.9
911-1498	1201	587	1.075	54,700	60.1	45.5
1498-2670	2084	1172	1.310	90,000	60.0	43.1

TABLE 6.2 COMPRESSIBILITY (MO Series)

(j)

TEST No. MO8 U70 BH2 Depth 5.65 m						
Stress Range (kN/m^2)	$(\sigma'_a)_{av}$ (kN/m^2)	$\Delta\sigma'_a$ (kN/m^2)	$\Delta\varepsilon_a$	M_a (kN/m^2)	$M_a/(\sigma'_a)_i$	$M_a/(\sigma'_a)_{av}$
FIRST LOADING						
515-809	662	294	0.505	58,200	113.0	88.0
809-1105	957	296	0.615	47,800	59.0	50.0
1105-1691	1398	586	1.015	48,000	43.4	34.3
1691-2865	2278	1174	1.385	84,900	50.1	37.3
RELOADING						
515-809	662	294	0.580	51,000	99	77
809-1105	957	296	0.565	52,300	64.5	54.6
1105-1691	1398	586	0.875	67,300	61.0	48.1
1691-2865	2278	1174	1.115	105,300	62.3	46.3

TABLE 6.2 COMPRESSIBILITY (MO Series)

(k)

TEST No. MO13 U70 BH3 Depth 5.63 m						
Stress Range (kN/m^2)	$(\sigma'_a)_{av}$ (kN/m^2)	$\Delta\sigma'_a$ (kN/m^2)	$\Delta\varepsilon_a$	M_a (kN/m^2)	$M_a/(\sigma'_a)_i$	$M_a/(\sigma'_a)_{av}$
220-441	331	221	0.57	41,400	187	125
441-838	622	442	1.075	41,100	93.2	62.2
838-1766	1352	883	2.210	40,000	45.3	30.2
1766-3533	2649	1767	2.085	84,700	48.0	31.9

TABLE 6.3 COMPRESSIBILITY (CS Series)

TEST No. CS1 CORE BH2 Depth 1.88 m						
Stress Range (kN/m^2)	$(\sigma'_a)_{av}$ (kN/m^2)	$\Delta\sigma'_a$ (kN/m^2)	$\Delta\varepsilon_a$	M_a (kN/m^2)	$M_a/(\sigma'_a)_i$	$M_a/(\sigma'_a)_{av}$
225-325	275	100	0.520	19,231	85.5	69.9
325-483	404	158	0.705	22,411	68.9	55.5
483-645	564	162	0.570	28,421	58.9	50.4
645-846	745	201	0.490	41,020	63.6	55.1
846-1015	930	169	0.415	40,723	48.1	43.8
1015-1286	1150	271	0.620	43,710	43.1	38.0
1286-1572	1929	286	0.485	58,969	45.9	41.26
1512-2026	1799	454	0.560	81,071	51.6	45.06
2026-2660	2343	643	0.590	107,458	53.0	45.9
2660-3360	3010	700	0.460	152,174	57.0	50.6
3360-4094	3727	734	0.350	209,714	62.4	56.3
4094-4927	4510	833	0.310	268,709	65.6	59.6
4927-5750	5338	823	0.250	329,200	66.8	61.7
5750-6735	6242	985	0.225	437,778	76.1	70.1
6735-7971	7353	1236	0.205	602,927	89.5	82.0
7971-9312	8641	1341	0.185	724,865	90.9	83.9
9312-11550	10431	2238	0.190	1177,895	126.5	112.9
11550-13607	12578	2057	0.110	1870,000	161.9	148.7

TABLE 6.4 COMPRESSIBILITY (RMO Series)

(a)

TEST No. RM01						
Stress Range (kN/m^2)	$(\sigma'_a)_{av}$ (kN/m^2)	$\Delta\sigma'_a$ (kN/m^2)	$\Delta\varepsilon_a$	M_a (kN/m^2)	$M_a/(\sigma'_a)_i$	$M_a/(\sigma'_a)_{av}$
7.4-15	11	11	2.898	380	51.4	34.6
15-29	22	14	4.642	302	20.1	13.7
29-59	44	30	5.24	593	19.7	13.0
59-118	88	59	5.47	1079	18.3	12.2
118-236	177	118	5.37	2197	18.6	12.4
236-471	353	235	4.88	4815	20.4	13.6
471-883	677	412	4.28	9626	20.4	14.2
883-1766	1325	883	4.04	21856	24.7	16.4
1766-2650	2208	889	2.26	39115	22.1	17.7

TABLE 6.4 COMPRESSIBILITY (RMO Series)

(b)

TEST No. RMO2						
Stress Range (kN/m^2)	$(\sigma'_a)_{av}$ (kN/m^2)	$\Delta\sigma'_a$ (kN/m^2)	$\Delta\varepsilon_a$	M_a (kN/m^2)	$M_a/(\sigma'_a)_i$	$M_a/(\sigma'_a)_{av}$
3.2-6.4	4.8	3.2	0.5755	557	173.8	115.8
6.4-13	9.7	6.6	2.7625	234.4	36.6	24.2
13-25	19	12	2.825	428	33.2	22.5
25-50	37.5	25	3.737	670	26.8	17.8
50-100	75	50	4.360	1,146	22.9	15.3
100-200	150	100	4.46	2,240	22.4	14.9
200-400	300	200	3.99	5,020	25.0	16.7
400-800	600	400	3.93	10,170	25.4	17.0
800-1600	1200	800	3.96	20,200	25.3	16.8
1600-3200	2400	1600	3.17	50,500	31.6	21.0
RELOAD						
100-200	150	100	0.27	37,040	370.4	24.7
200-400	300	200	0.82	24,400	122.0	81.3
400-800	600	400	1.29	31,000	77.5	51.7
800-1600	1200	800	1.24	64,500	80.7	53.7
1600-3200	2400	1600	1.50	106,750	66.7	44.5

TABLE 6.4 COMPRESSIBILITY (RMO Series)

(c)

TEST No. RM04						
Stress Range (kN/m^2)	$(\sigma'_a)_{av}$ (kN/m^2)	$\Delta\sigma'_a$ (kN/m^2)	$\Delta\varepsilon_a$	M_a (kN/m^2)	$M_a/(\sigma'_a)_i$	$M_a/(\sigma'_a)_{av}$
4.5-9	6.7	4.5	2.25	195.5	44.4	29.6
9-18	13.5	9	3.64	242.0	27.5	19.8
18-37	27	19	3.21	595.0	33.7	21.9
37-74	56	37	4.03	912.0	24.8	16.5
74-147	111	73	3.94	1870.0	25.4	16.95
147-294	221	147	3.98	3698.0	25.0	16.7
294-589	442	295	3.9	7550	25.6	17.13

TABLE 6.5 COMPRESSIBILITY (RCS)

TEST No. RCS1						
Stress Range (kN/m^2)	$(\sigma'_a)_{av}$ (kN/m^2)	$\Delta\sigma'_a$ (kN/m^2)	$\Delta\varepsilon_a$	M_a (kN/m^2)	$M_a/(\sigma'_a)_i$	$M_a/(\sigma'_a)_{av}$
11-26	18	15	0.234	6500	615	35.9
26-49	37	23	0.660	3550	134	95.0
49-100	75	51	1.18	4350	908.6	58.2
100-212	156	112	1.49	7460	74.1	47.8
212-330	271	118	1.04	11810	33.8	42.0
330-464	397	134	0.96	14000	42.4	35.2
464-575	520	111	0.74	15030	32.4	28.9
575-693	634	118	0.78	15120	26.3	23.8
693-844	769	151	0.97	15560	22.4	20.3
844-1068	956	224	1.42	15810	18.75	16.5
1068-1354	1211	286	1.63	17480	16.38	14.4
1354-1904	1629	550	2.34	23500	17.4	14.4
1904-2582	2243	678	2.04	33200	17.5	14.8
2582-3407	2994	825	1.21	68000	26.3	22.7
3407-4312	3860	905	2.07	43800	12.85	11.4
4312-5158	4735	846	1.10	76900	17.8	16.3
5158-5999	5579	841	0.96	87700	17.0	15.7
5999-6853	6426	854	0.79	108000	18.0	16.8
6853-7914	7383	1061	0.95	112000	16.3	15.2
7914-9506	8710	1592	1.18	135000	17.1	15.5
9506-11787	10698	2281	1.32	172500	18.2	16.2
11787-14196	12992	2409	1.30	185100	15.7	14.25

TABLE 6. 6 COEFFICIENT OF CONSOLIDATION (MO Series)

(a)

TEST No. MO9 BLOCK No. 3 Depth 2.135 m					
Stress Range (kN/m^2)	$(\sigma'_a)_{av}$ (kN/m^2)	$\sqrt{t_{90}}$ $(min)^{\frac{1}{2}}$	$C_{v_{90}}$ (cm^2/sec)	t_{50} (min)	$C_{v_{50}}$ (cm^2/sec)
FIRST LOADING					
206-353	280	8.2	2.1×10^{-4}	35	0.94×10^{-4}
353-646	550	11.4	1.07×10^{-4}	33.5	0.97×10^{-4}
646-1233	940	9.8	1.41×10^{-4}	31.5	1.00×10^{-4}
1233-2410	1821	7.4	2.39×10^{-4}	20.0	1.52×10^{-4}
RELOADING					
206-353	280	5.8	4.1×10^{-4}	26.0	1.23×10^{-4}
353-646	550	10.3	1.29×10^{-4}	42.5	0.75×10^{-4}
646-1233	940	10.5	1.22×10^{-4}	35.5	0.88×10^{-4}
1233-2410	1821	8.6	1.76×10^{-4}	21.0	1.43×10^{-4}

TABLE 6.6 COEFFICIENT OF CONSOLIDATION (MO Series)

(b)

TEST No. MO12 BLOCK No. 3 Depth 2.135 m					
Stress Range (kN/m^2)	(σ'_a) (kN/m^2)	$\sqrt{t_{90}}$ $(min)^{\frac{1}{2}}$	$C_{v_{90}}$ (cm^2/sec)	t_{50} (min)	$C_{v_{50}}$ (cm^2/sec)
FIRST LOADING					
442-736	589	4.5	6.97×10^{-4}	15.5	2.12×10^{-4}
736-1324	1030	7.6	2.4×10^{-4}	24.0	1.34×10^{-4}
1324-2502	1913	7.6	2.31×10^{-4}	19.5	1.61×10^{-4}
RELOADING					
442-736	589	7.3	2.64×10^{-4}	22.5	1.45×10^{-4}
736-1324	1030	10.0	1.36×10^{-4}	29.0	1.12×10^{-4}
1324-2502	1913	9.2	1.61×10^{-4}	22.0	1.44×10^{-4}

TABLE 6.6 COEFFICIENT OF CONSOLIDATION (MO Series)

(c)

TEST No. MO4 CORE BH3 Depth 2.21 m					
Stress Range (kN/m^2)	$(\sigma'_a)_{av}$ (kN/m^2)	$\sqrt{t_{90}}$ $(min)^{\frac{1}{2}}$	$C_{v_{90}}$ (cm^2/sec)	t_{50} (min)	$C_{v_{50}}$ (cm^2/sec)
FIRST LOADING					
206-412	309	8.4	2.0×10^{-4}	28.5	1.15×10^{-4}
412-618	515	9.8	1.42×10^{-4}	34.0	0.95×10^{-4}
618-824	721	9.3	1.58×10^{-4}	38.5	0.83×10^{-4}
824-1030	927	9.9	1.37×10^{-4}	34.0	0.92×10^{-4}
1030-1236	1133	9.1	1.60×10^{-4}	32.0	0.97×10^{-4}
1236-1545	1391	9.2	1.56×10^{-4}	26.5	1.16×10^{-4}
1545-1854	1700	8.4	1.85×10^{-4}	29.5	1.03×10^{-4}
RELOADING					
206-412	309	9.0	1.72×10^{-4}	32.5	0.99×10^{-4}
412-618	515	10.45	1.25×10^{-4}	38.5	0.83×10^{-4}
618-824	721	11.55	1.01×10^{-4}	39.0	0.80×10^{-4}
824-1030	927	11.5	1.01×10^{-4}	39.0	0.80×10^{-4}
1030-1236	1133	10.1	1.30×10^{-4}	34.0	0.90×10^{-4}
1236-1545	1391	9.0	1.62×10^{-4}	28.0	1.09×10^{-4}
1545-1854	1700	8.4	1.84×10^{-4}	24.0	1.26×10^{-4}

TABLE 6.6 COEFFICIENT OF CONSOLIDATION (MO Series)

(d)

TEST No. MO10 CORE BH2 Depth 1.88 m					
Stress Range (kN/m^2)	$(\sigma'_a)_{av}$ (kN/m^2)	$\sqrt{t_{90}}$ $(min)^{\frac{1}{2}}$	$C_{v_{90}}$ (Cm^2/sec)	t_{50} (min)	$C_{v_{50}}$ (cm^2/sec)
FIRST LOADING					
206- 353	279	8.0	2.2×10^{-4}	36.0	0.91×10^{-4}
353- 646	500	14.3	0.68×10^{-4}	57.0	0.57×10^{-4}
646-1233	940	11.1	1.10×10^{-4}	37.0	0.85×10^{-4}
1233-2410	1821	8.0	2.05×10^{-4}	27.0	1.13×10^{-4}
RELOADING					
206-353	279	8.0	2.17×10^{-4}	38.0	0.85×10^{-4}
353-646	500	12.9	0.83×10^{-4}	52.0	0.60×10^{-4}
646-1233	940	13.3	0.71×10^{-4}	47.0	0.66×10^{-4}
1233-2410	1821	8.0	2.05×10^{-4}	28.0	1.09×10^{-4}

TABLE 6.6 COEFFICIENT OF CONSOLIDATION (MO Series)

(e)

TEST No. MO11 CORE BH3 Depth 3.66 m					
Stress Range (kN/m^2)	$(\sigma'_a)_{av}$ (kN/m^2)	$\sqrt{t_{90}}$ $(min)^{\frac{1}{2}}$	$C_{v_{90}}$ (cm^2/sec)	t_{50} (min)	$C_{v_{50}}$ (cm^2/sec)
FIRST LOADING					
176-324	250	10.6	1.26×10^{-4}	39.0	0.84×10^{-4}
324-618	471	12.0	0.96×10^{-4}	42.0	0.77×10^{-4}
618-1207	912	9.7	1.43×10^{-4}	31.0	1.01×10^{-4}
1207-2385	1796	7.0	2.63×10^{-4}	20.0	1.50×10^{-4}
RELOADING					
176-324	250	5.6	4.35×10^{-4}	28.0	1.14×10^{-4}
324-618	471	8.4	1.92×10^{-4}	41.0	0.77×10^{-4}
618-1207	912	11.2	1.05×10^{-4}	32.0	0.96×10^{-4}
1207-2385	1796	8.5	1.71×10^{-4}	20.5	1.[illegible]

TABLE 6.6 COEFFICIENT OF CONSOLIDATION (MO Series)

(f)

TEST No. MO1 U70 BH3 Depth 1.45 m					
Stress Range (kN/m^2)	$(\sigma'_a)_{av}$ (kN/m^2)	$\sqrt{t_{90}}$ $(min)^{\frac{1}{2}}$	$C_{v_{90}}$ (cm^2/sec)	t_{50} (min)	$C_{v_{50}}$ (cm^2/sec)
FIRST LOADING					
257-463	360	7.1	2.8×10^{-4}	21.7	1.51×10^{-4}
463-669	566	9.0	1.71×10^{-4}	26.5	1.22×10^{-4}
669-875	772	9.2	1.62×10^{-4}	25.0	1.27×10^{-4}
875-1081	978	8.6	1.82×10^{-4}	21.0	1.49×10^{-4}
1081-1287	1184	8.2	1.97×10^{-4}	22.5	1.37×10^{-4}
1287-1596	1442	7.6	2.27×10^{-4}	16.0	1.90×10^{-4}
1596-1905	1750	7.4	2.37×10^{-4}	24.5	1.23×10^{-4}
RELAODING					
257-463	360	9.7	1.46×10^{-4}	26.0	1.23×10^{-4}
463-669	566	11.6	1.01×10^{-4}	26.0	1.21×10^{-4}
669-875	772	10.4	1.24×10^{-4}	28.5	1.13×10^{-4}
875-1081	978	8.7	1.75×10^{-4}	24.0	1.28×10^{-4}
1081-1287	1184	7.4	2.38×10^{-4}	19.0	1.59×10^{-4}
1287-1596	1442	8.1	1.98×10^{-4}	16.7	1.81×10^{-4}
1596-1905	1750	7.5	2.29×10^{-4}	12.5	2.40×10^{-4}

TABLE 6.6 COEFFICIENT OF CONSOLIDATION (MO Series)

(g)

TEST No. MO2 U70 BH3 Depth 2.74 m					
Stress Range (kN/m^2)	$(\sigma'_a)_{av}$ (kN/m^2)	$\sqrt{t_{90}}$ $(min)^{\frac{1}{2}}$	$C_{v_{90}}$ (cm^2/sec)	t_{50} (min)	$C_{v_{50}}$ (cm^2/sec)
FIRST LOADING					
442-648	545	3.2	13.75×10^{-4}	4.8	6.85×10^{-4}
648-854	751	4.2	7.92×10^{-4}	7.5	4.35×10^{-4}
854-1060	951	5.1	5.33×10^{-4}	9.0	3.60×10^{-4}
1060-1266	1163	4.8	5.99×10^{-4}	9.7	3.31×10^{-4}
1266-1472	1369	4.5	6.53×10^{-4}	8.0	3.96×10^{-4}
1472-1781	1627	4.4	7.01×10^{-4}	8.5	3.72×10^{-4}
1781-2090	1935	5.2	4.98×10^{-4}	13.0	2.40×10^{-4}
RELOADING					
442-648	545	5.3	4.90×10^{-4}	9.0	4.01×10^{-4}
648-854	751	5.6	4.38×10^{-4}	11.0	2.76×10^{-4}
854-1060	951	6.0	3.80×10^{-4}	11.5	2.76×10^{-4}
1060-1266	1163	6.0	3.77×10^{-4}	11.5	2.18×10^{-4}
1266-1472	1369	5.7	4.15×10^{-4}	10.0	3.14×10^{-4}
1472-1781	1627	5.3	4.77×10^{-4}	10.0	3.12×10^{-4}
1781-2090	1935	5.8	3.96×10^{-4}	12.5	2.47×10^{-4}

TABLE 6.6 COEFFICIENT OF CONSOLIDATION (MO Series)

(h)

TEST No. MO3 U70 BH3 Depth 4.12 m					
Stress Range (kN/m^2)	$(\sigma'_a)_{av}$ (kN/m^2)	$\sqrt{t_{90}}$ $(min)^{\frac{1}{2}}$	$C_{v_{90}}$ (cm^2/sec)	t_{50} (min)	$C_{v_{50}}$ (cm^2/sec)
FIRST LOADING					
316-522	419	3.6	10.9×10^{-4}	7.2	4.57×10^{-4}
521-736	629	4.8	6.05×10^{-4}	13.5	2.40×10^{-4}
736-942	839	5.6	4.40×10^{-4}	17.0	1.88×10^{-4}
942-1148	1045	5.2	5.02×10^{-4}	15.0	2.10×10^{-4}
1148-1354	1251	7.0	2.74×10^{-4}	15.0	2.08×10^{-4}
1354-1663	1509	5.0	5.33×10^{-4}	14.7	2.11×10^{-4}
1663-1972	1818	6.6	3.01×10^{-4}	26.0	1.17×10^{-4}
RELOADING					
294-500	397	5.2	5.0×10^{-4}	8.8	3.58×10^{-4}
500-706	603	5.8	4.0×10^{-4}	10.0	3.13×10^{-4}
706-912	809	6.0	3.7×10^{-4}	10.1	3.07×10^{-4}
912-1118	1015	5.2	4.88×10^{-4}	9.0	3.42×10^{-4}
1118-1427	1272	5.8	3.91×10^{-4}	8.0	3.84×10^{-4}
1427-1736	1581	6.2	3.39×10^{-4}	9.3	3.28×10^{-4}
1736-2036	1891	5.4	4.45×10^{-4}	10.2	2.96×10^{-4}

TABLE 6.6 COEFFICIENT OF CONSOLIDATION (MO Series)

(i)

TEST No. MO7 U70 BH2 Depth 1.22 m					
Stress Range (kN/m^2)	$(\sigma'_a)_{av}$ (kN/m^2)	$\sqrt{t_{90}}$ $(min)^{\frac{1}{2}}$	$C_{v_{90}}$ (cm^2/sec)	t_{50} (min)	$C_{v_{50}}$ (cm^2/sec)
FIRST LOADING					
324-617	471	3.6	10.86×10^{-4}	18.5	1.78×10^{-4}
617-911	765	7.7	2.32×10^{-4}	24.5	1.31×10^{-4}
911-1498	1204	8.1	2.06×10^{-4}	21.5	1.46×10^{-4}
1498-2670	2084	7.5	2.33×10^{-4}	16.0	1.90×10^{-4}
RELOADING					
324-617	471	9.4	1.54×10^{-4}	26.5	1.19×10^{-4}
617-911	765	9.0	1.64×10^{-4}	35.5	0.88×10^{-4}
911-1498	1204	9.1	1.59×10^{-4}	22.0	1.40×10^{-4}
1498-2670	2084	7.9	2.06×10^{-4}	14.0	2.14×10^{-4}

TABLE 6.6 COEFFICIENT OF CONSOLIDATION (MO Series)

(j)

TEST No. MO8 U70 BH2 Depth 5.65 m					
Stress Range (kN/m^2)	$(\sigma'_a)_{av}$ (kN/m^2)	$\sqrt{t_{90}}$ $(min)^{\frac{1}{2}}$	$C_{v_{90}}$ (cm^2/sec)	t_{50} (min)	$C_{v_{50}}$ (cm^2/sec)
FIRST. LOADING					
515- 809	662	3.4	12.2×10^{-4}	17.0	1.94×10^{-4}
809-1105	957	7.8	2.29×10^{-4}	28.0	1.16×10^{-4}
1105-1691	1398	6.1	3.70×10^{-4}	27.5	1.17×10^{-4}
1691-2865	2278	7.9	2.17×10^{-4}	25.0	1.12×10^{-4}
RELOADING					
515-809	662	9.6	1.51×10^{-4}	31.0	1.04×10^{-4}
809-1105	957	11.1	1.12×10^{-4}	38.0	0.84×10^{-4}
1105-1691	1398	10.9	1.15×10^{-4}	33.0	0.96×10^{-4}
1691-2865	2278	8.2	1.99×10^{-4}	20.0	1.56×10^{-4}

TABLE 6.6 COEFFICIENT OF CONSOLIDATION (MO Series)

(k)

TEST No. MO13 U70 BH3 Depth 5.63 m					
Stress Range (kN/m^2)	$(\sigma'_a)_{av}$ (kN/m^2)	$\sqrt{t_{90}}$ $(min)^{\frac{1}{2}}$	$C_{v_{90}}$ (cm^2/sec)	t_{50} (min)	$C_{v_{50}}$ (cm^2/sec)
FIRST LOADING					
221-442	331	2.9	16.81×10^{-4}	9	3.65×10^{-4}
442-883	662	4.6	6.61×10^{-4}	18	1.81×10^{-4}
883-1766	1325	8.5	1.90×10^{-4}	23.5	1.35×10^{-4}
1766-3582	2650	8.1	2.00×10^{-4}	16.0	1.90×10^{-4}

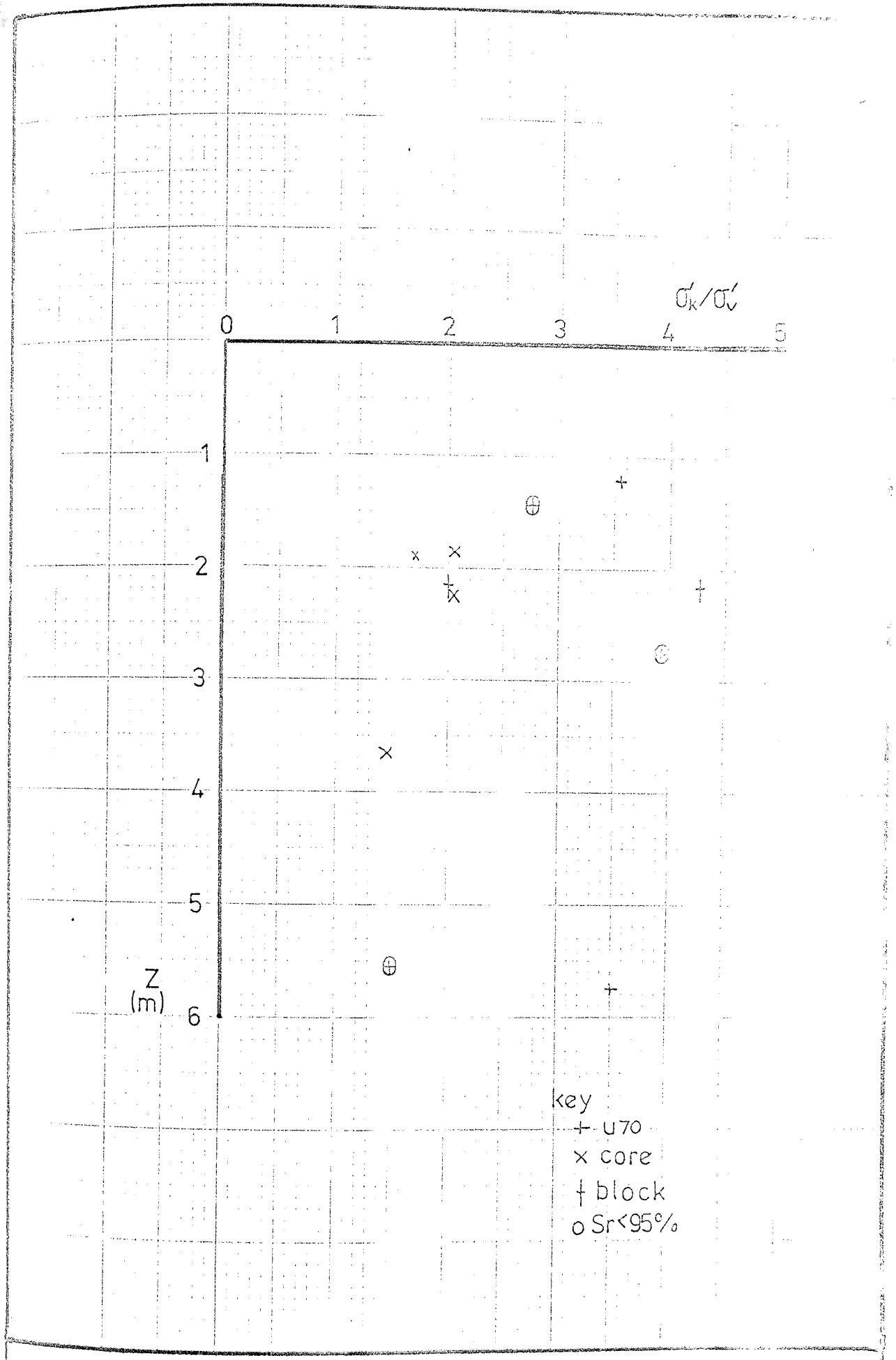

σ'_k/σ'_v against Depth (Z) from Oedometer Tests FIG. 6.1

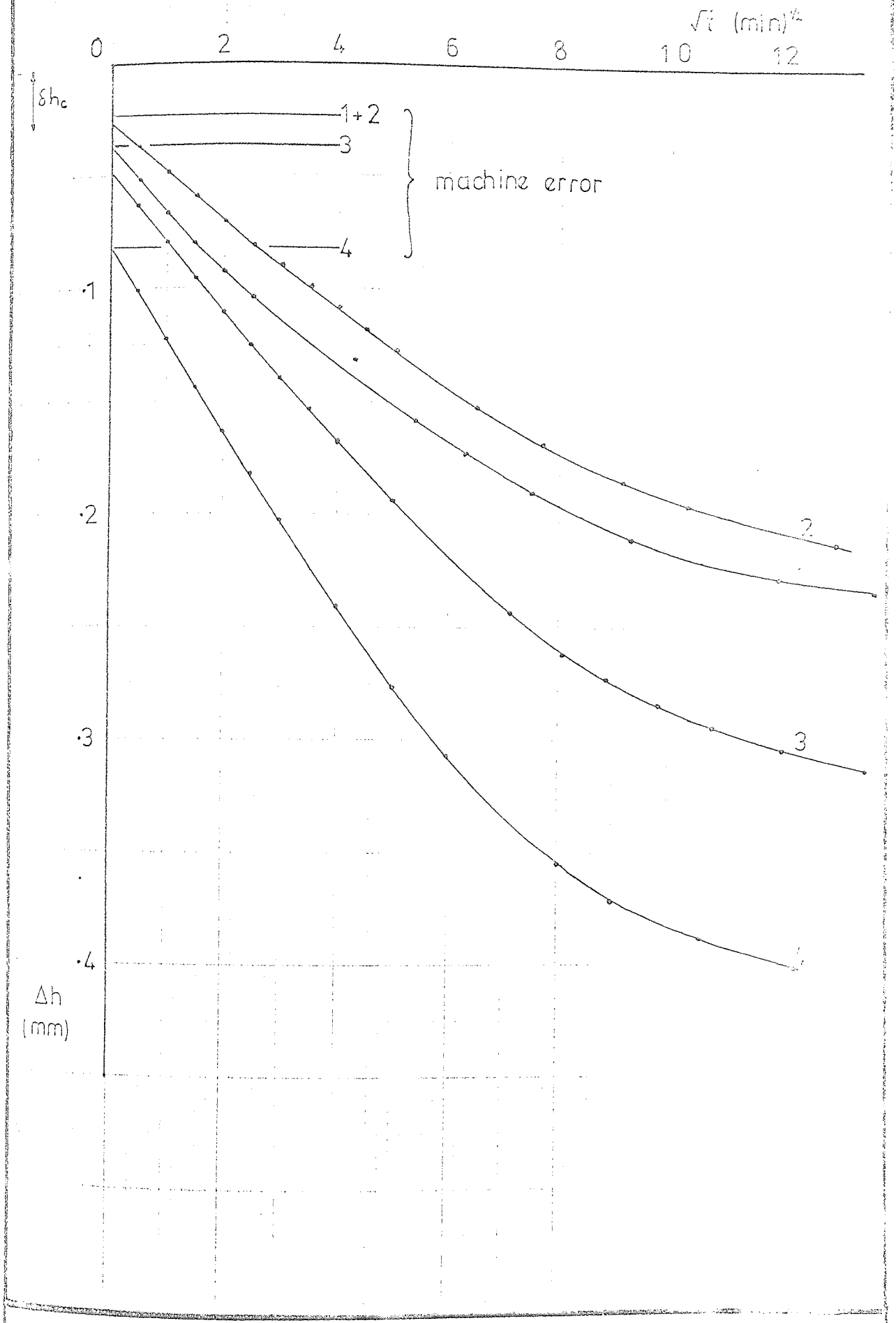

Compression vs Root Time - M07

FIG. ...

Origin Corrections vs Stress increase
- (a) Doubling Increment

FIG. C.3(a)

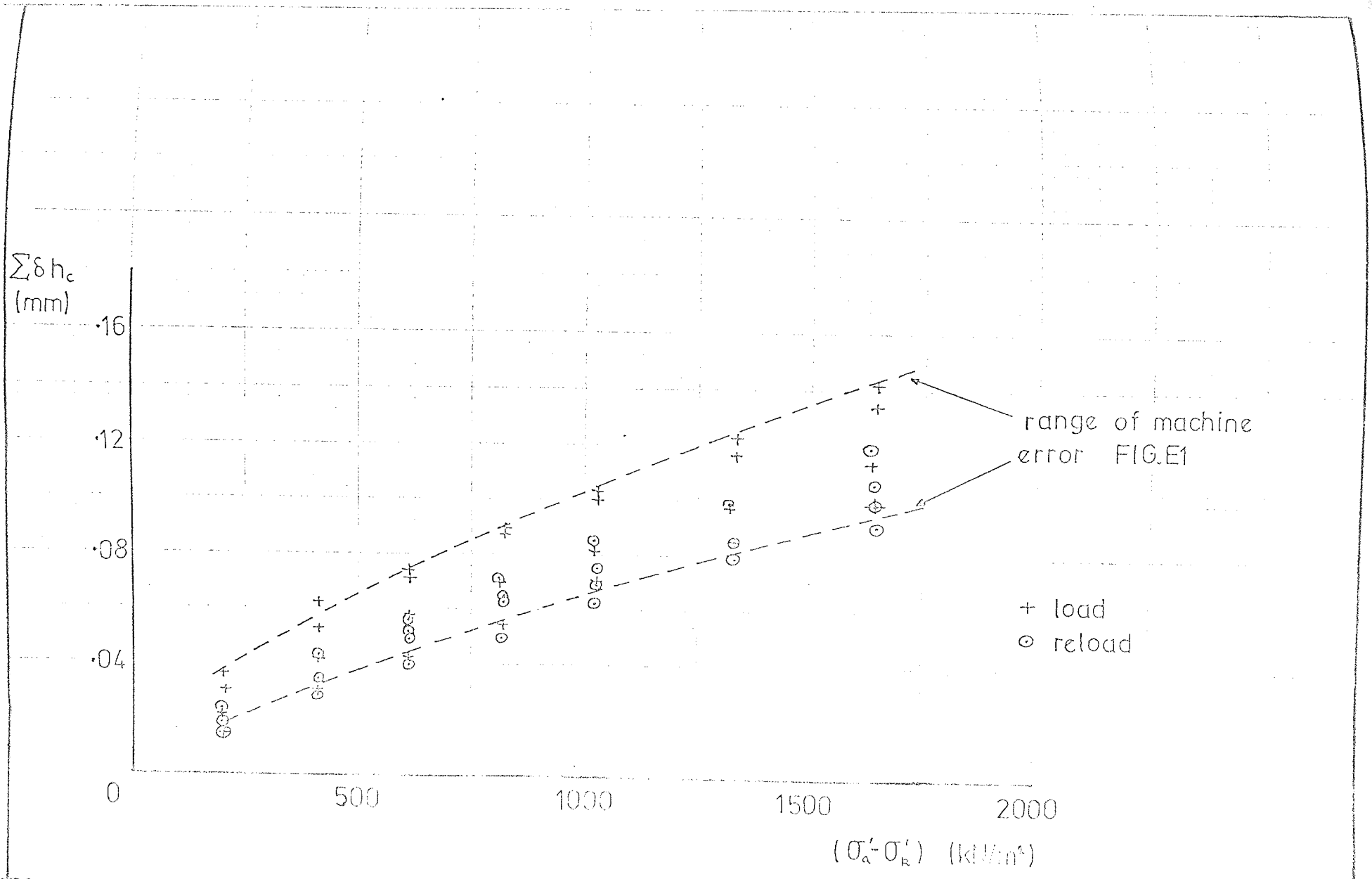
Origin Corrections vs Stress increase
- (b) Constant Increment
$\sum \delta h_c$ (mm)
·16
·12
·08
·04
0
500
1000
1500
2000
$(\sigma_a' - \sigma_r')$ (kN/m²)
range of machine error FIG.E1
+ load
⊙ reload

FIG. 3.3(b)

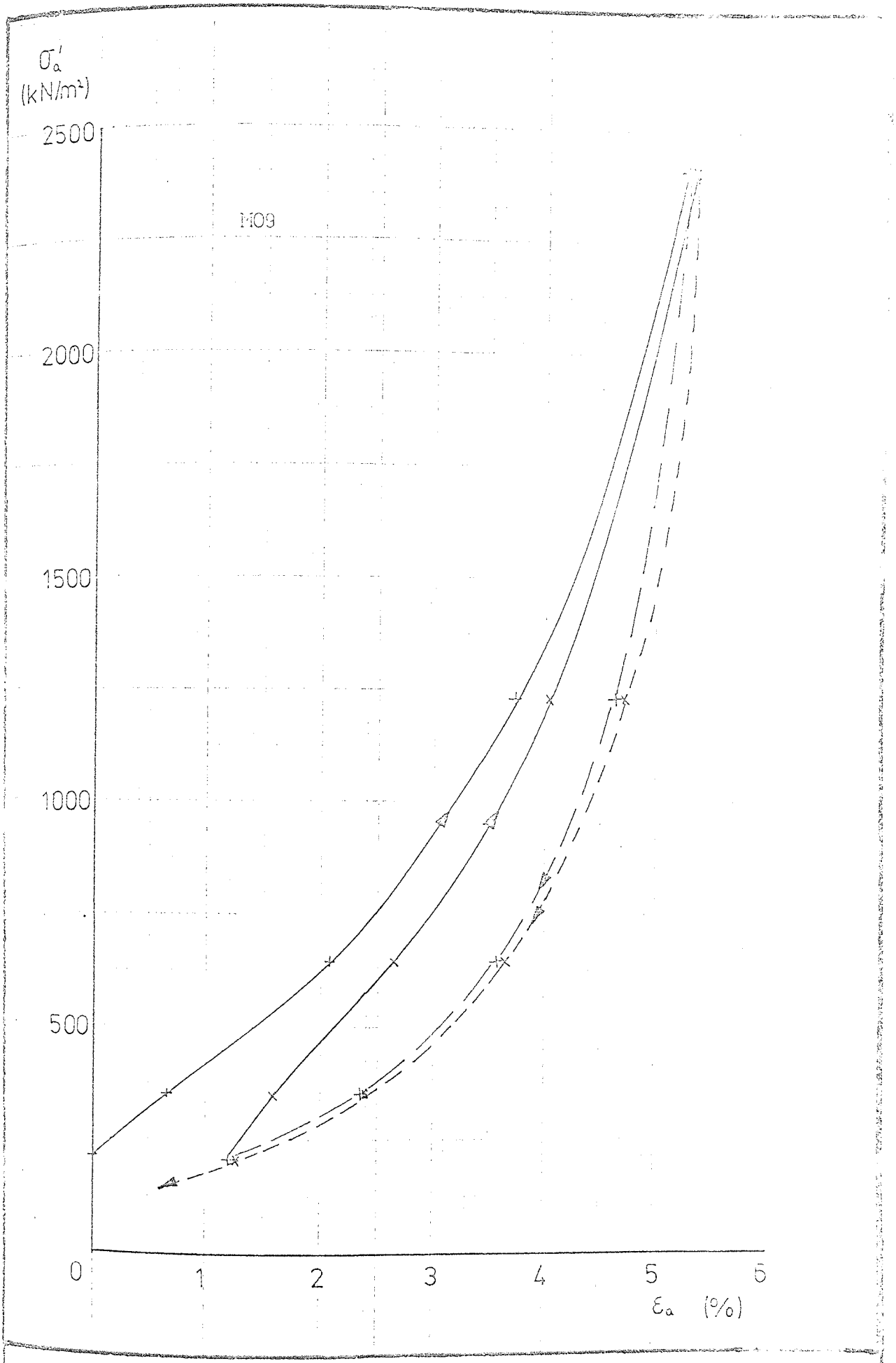

Axial Stress vs Axial Strain
- MO Series Block Samples

FIG. 6.4(a)

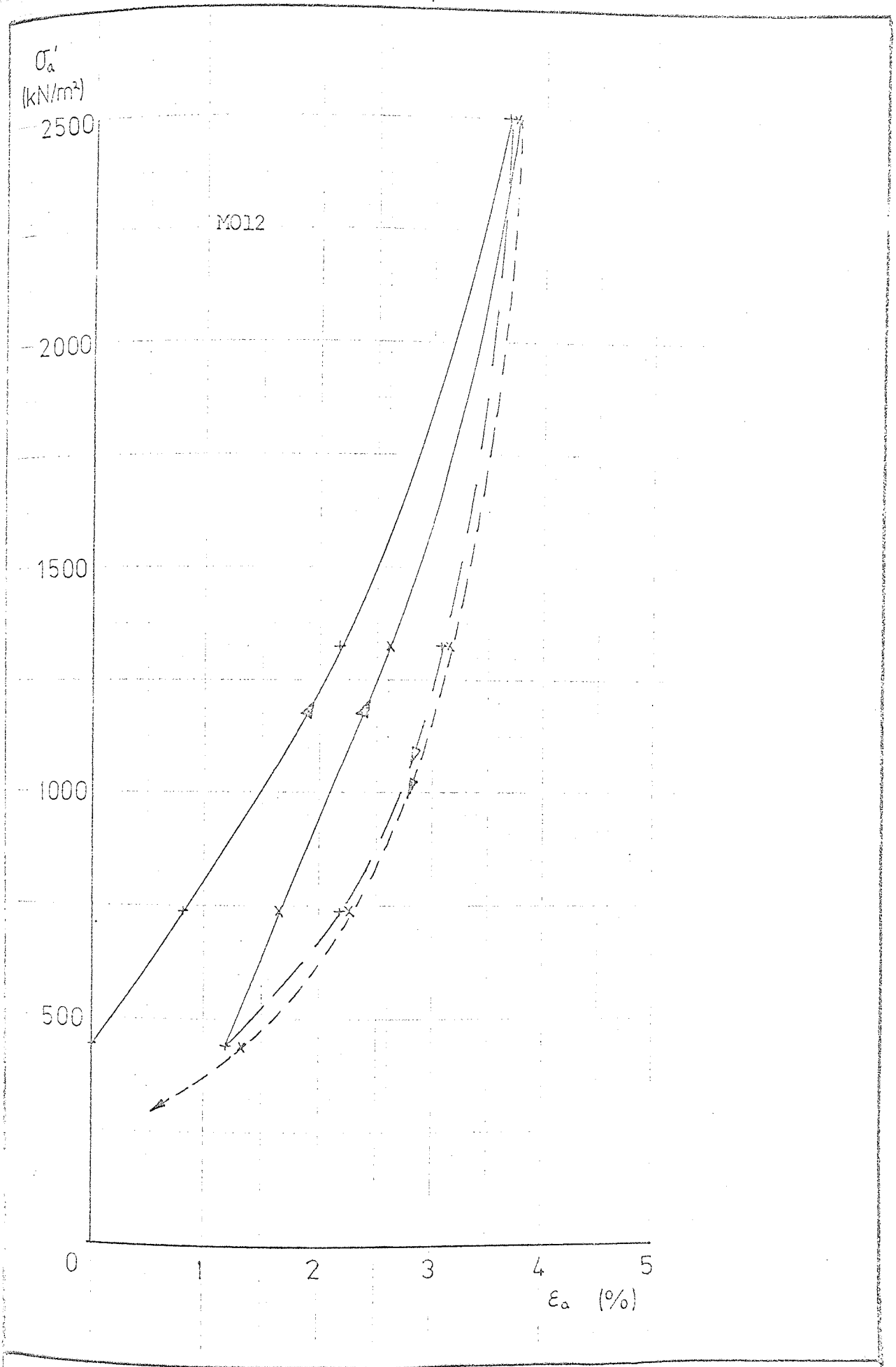

Axial Stress vs Axial Strain
- MO Series Block Samples

FIG. 6.4(b)

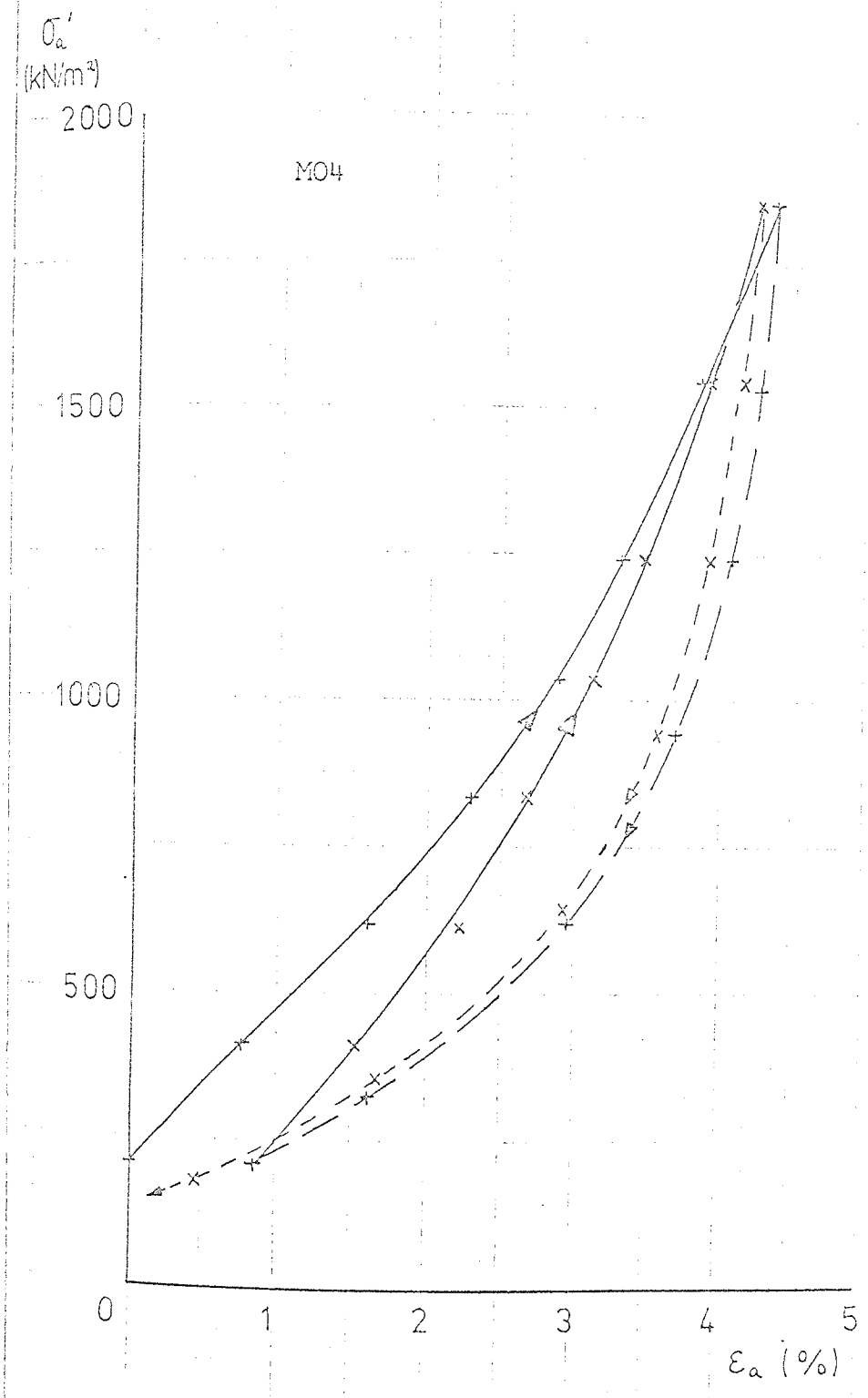

Axial Stress vs Axial Strain
- MO Series Core Samples

F.G. 8.5(a)

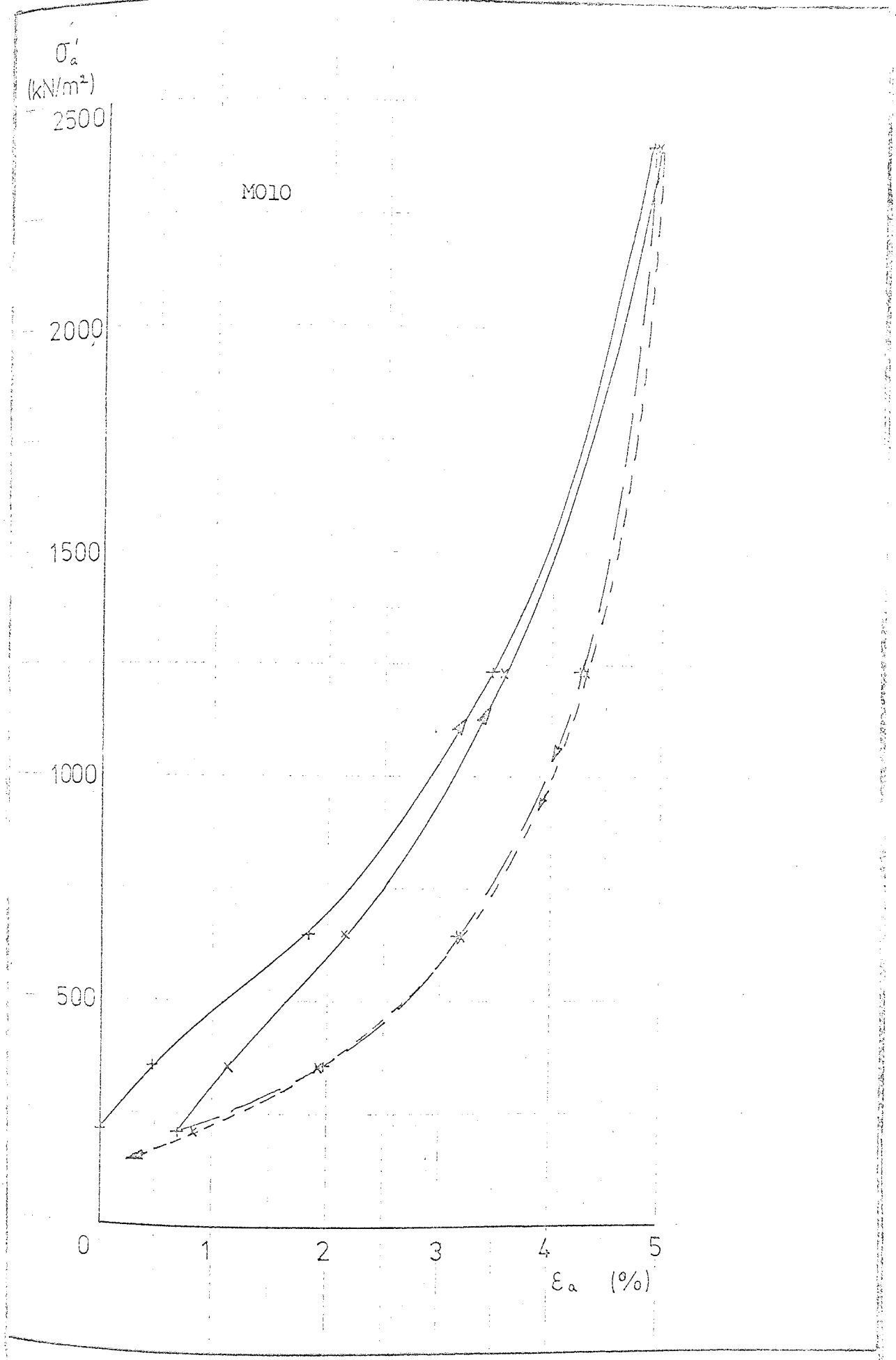

Axial Stress vs Axial Strain
- M0 Series Core Samples

FIG. 6.5(B)

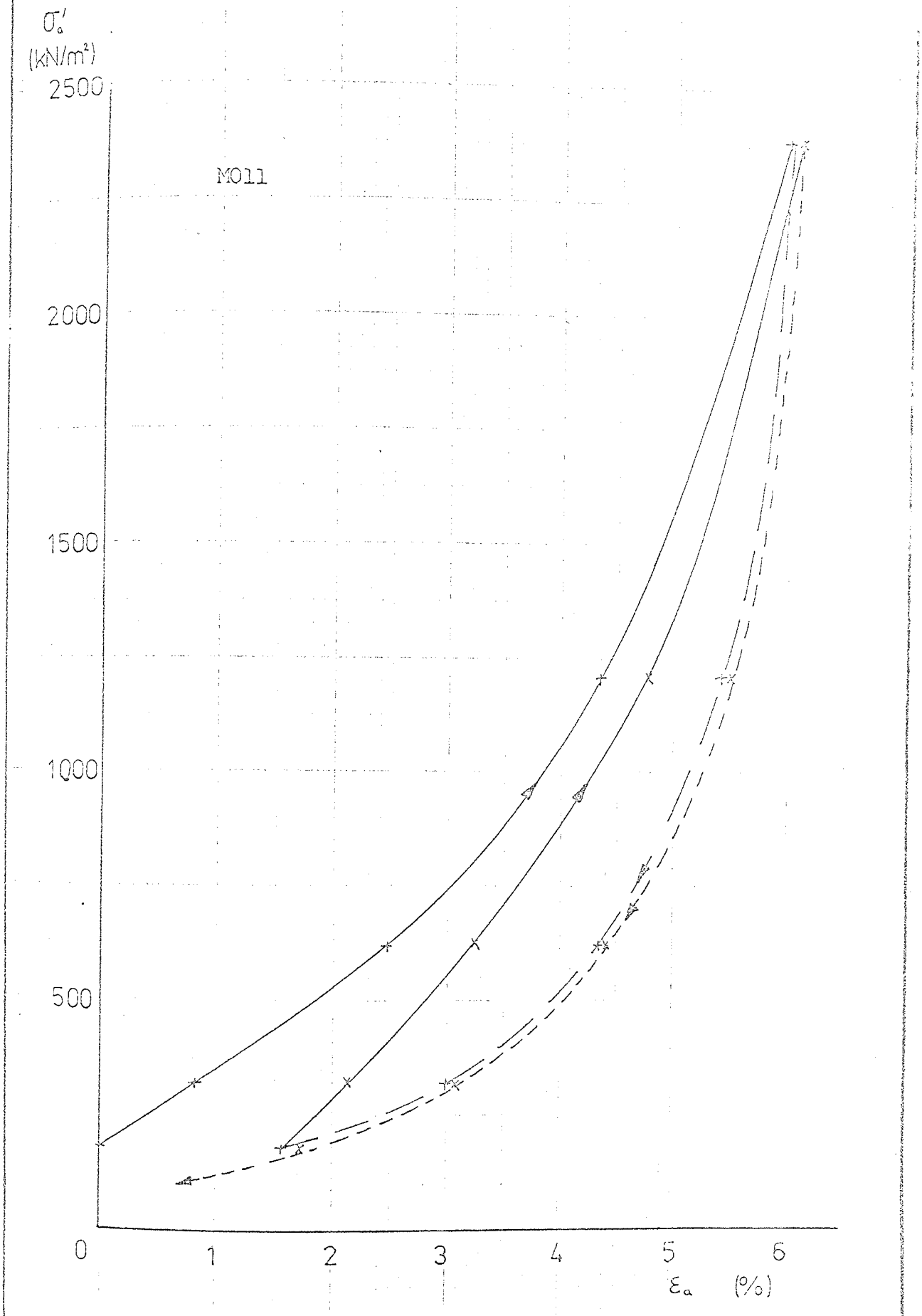

Axial Stress vs Axial Strain
- M0 Series Core Samples

FIG. 8.5(c)

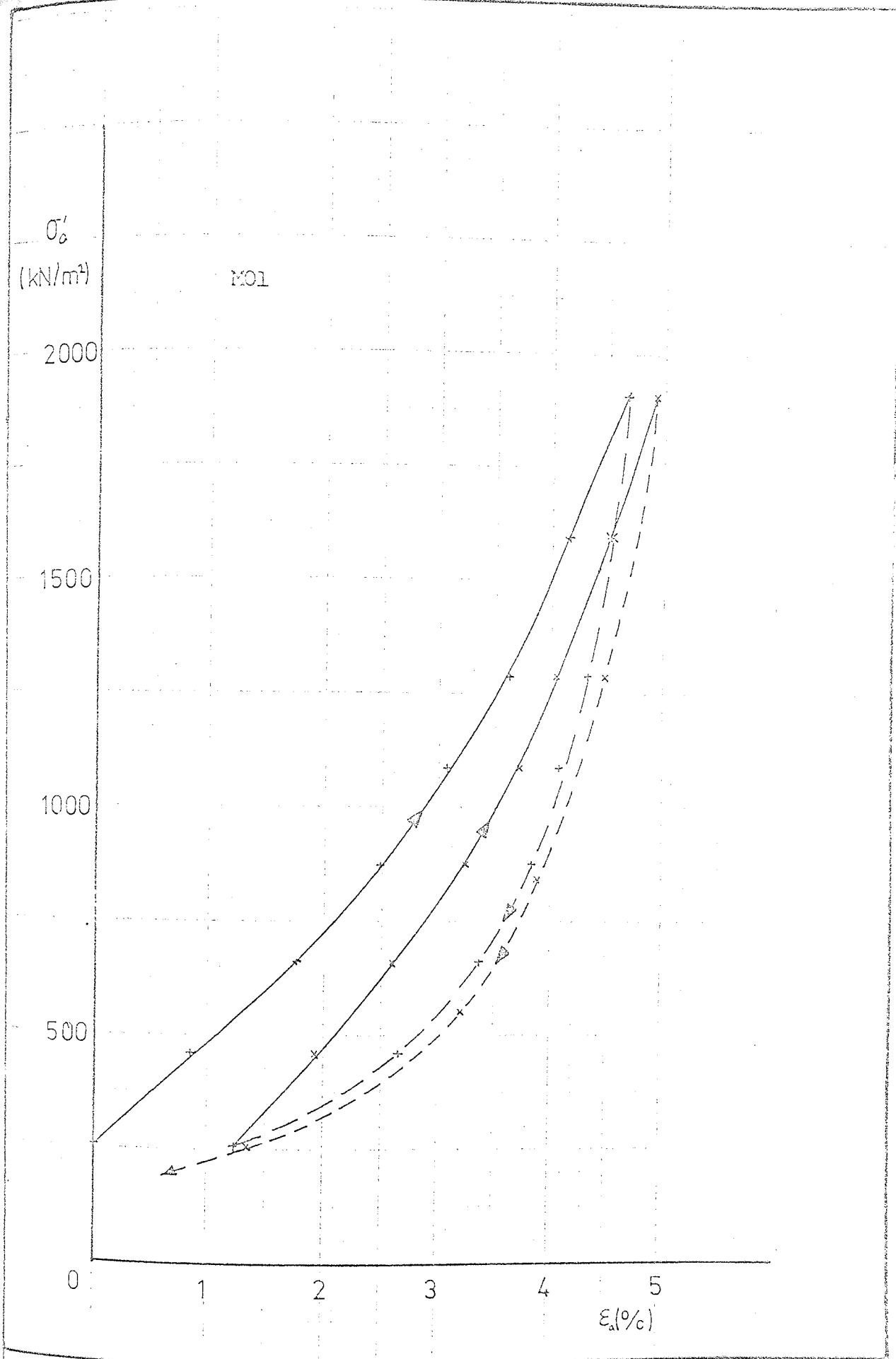

Axial Stress vs Axial Strain
- MO Series U70 Samples

FIG. 6.8(a)

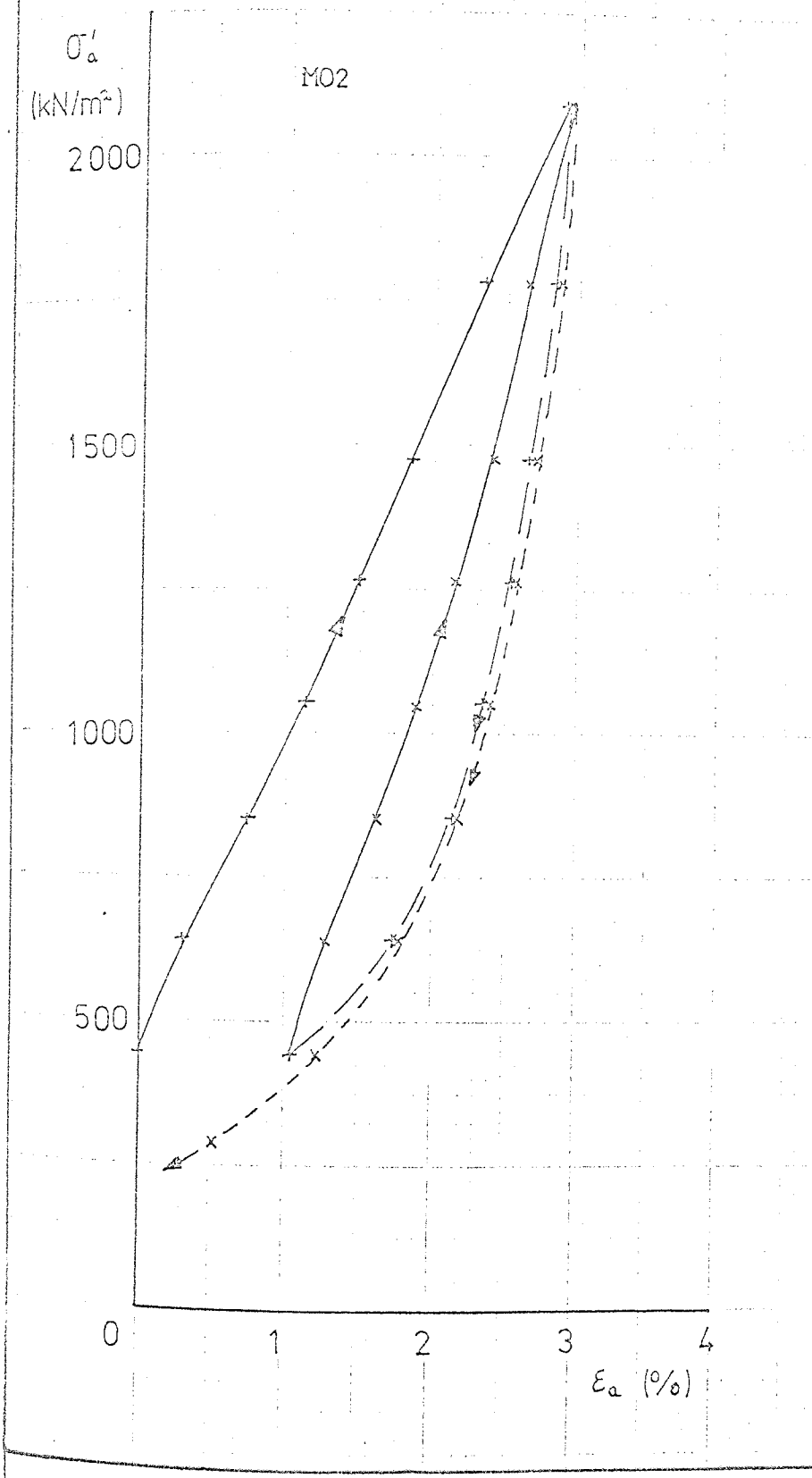

Axial Stress vs Axial Strain

- MO Series U70 Samples

FIG. 6.6(b)

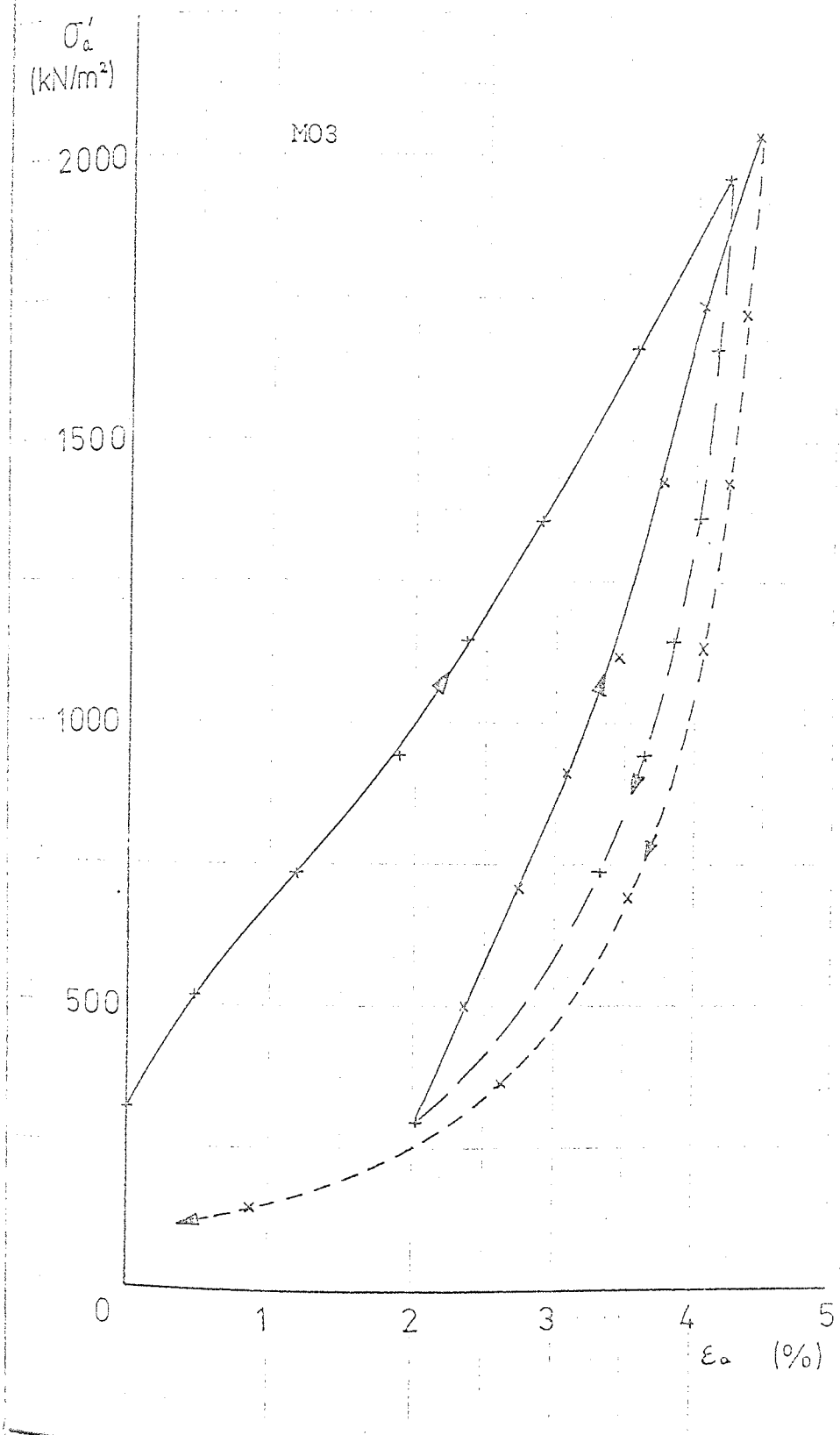

Axial Stress vs Axial Strain

- M0 Series U70 Samples

FIG. 6.6(c)

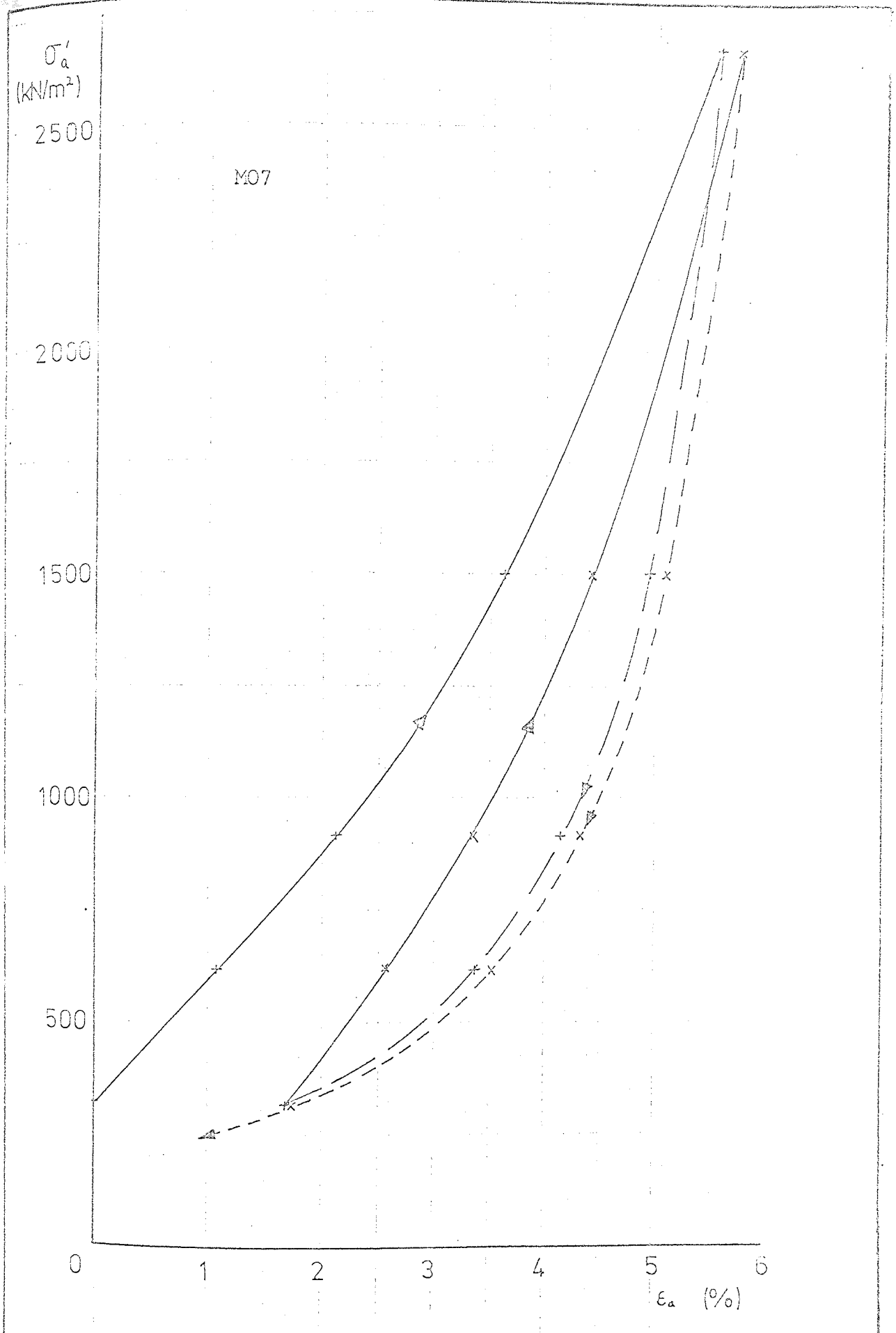

Axial Stress vs Axial Strain

- .0 Series U70 Samples

FIG. 5.6(d)

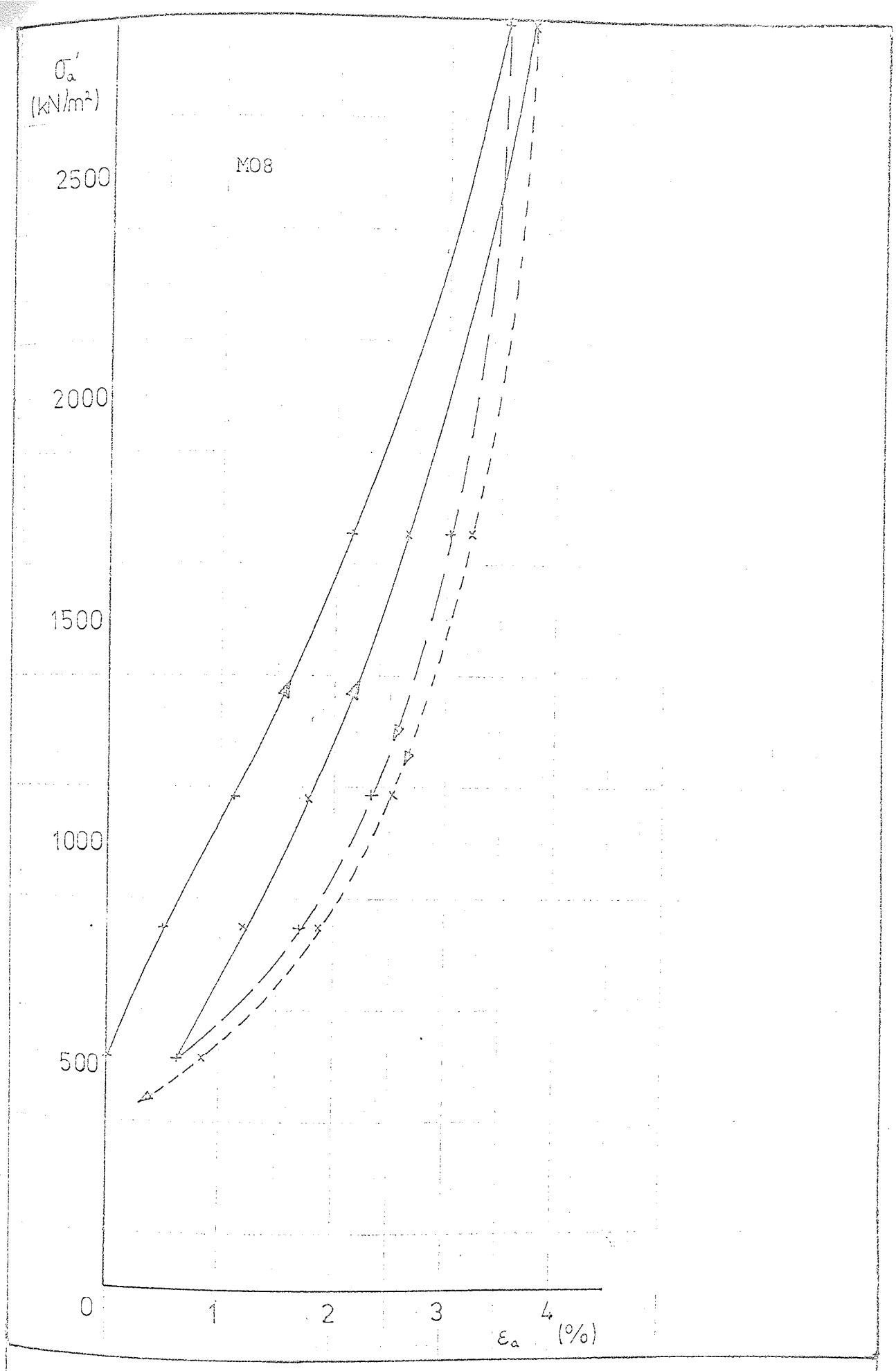

Axial Stress vs Axial Strain

- MO Series U70 Samples

FIG. 8.6(e)

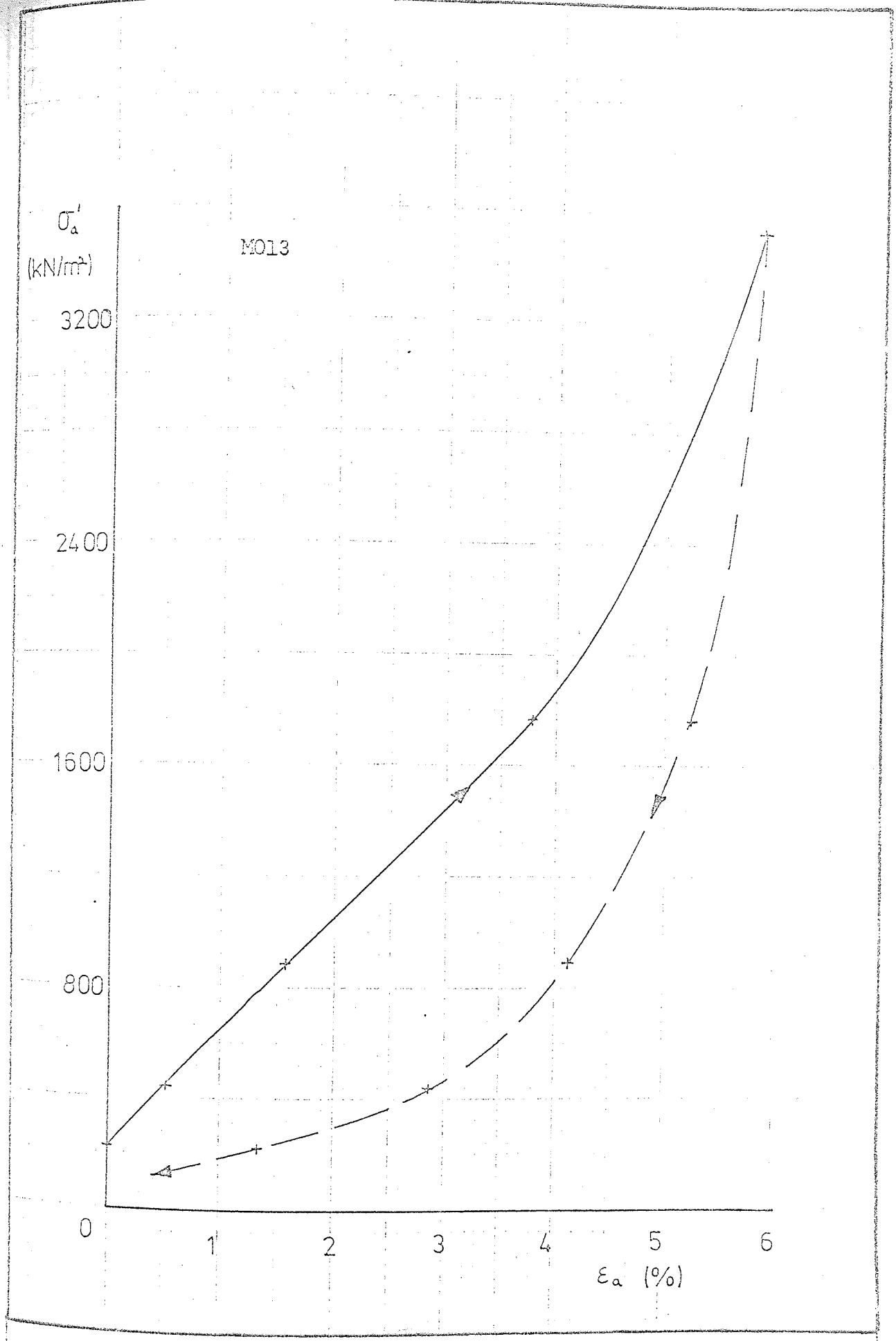

Axial Stress vs Axial Strain

- MO Series U70 Samples

FIG. 6.6(E)

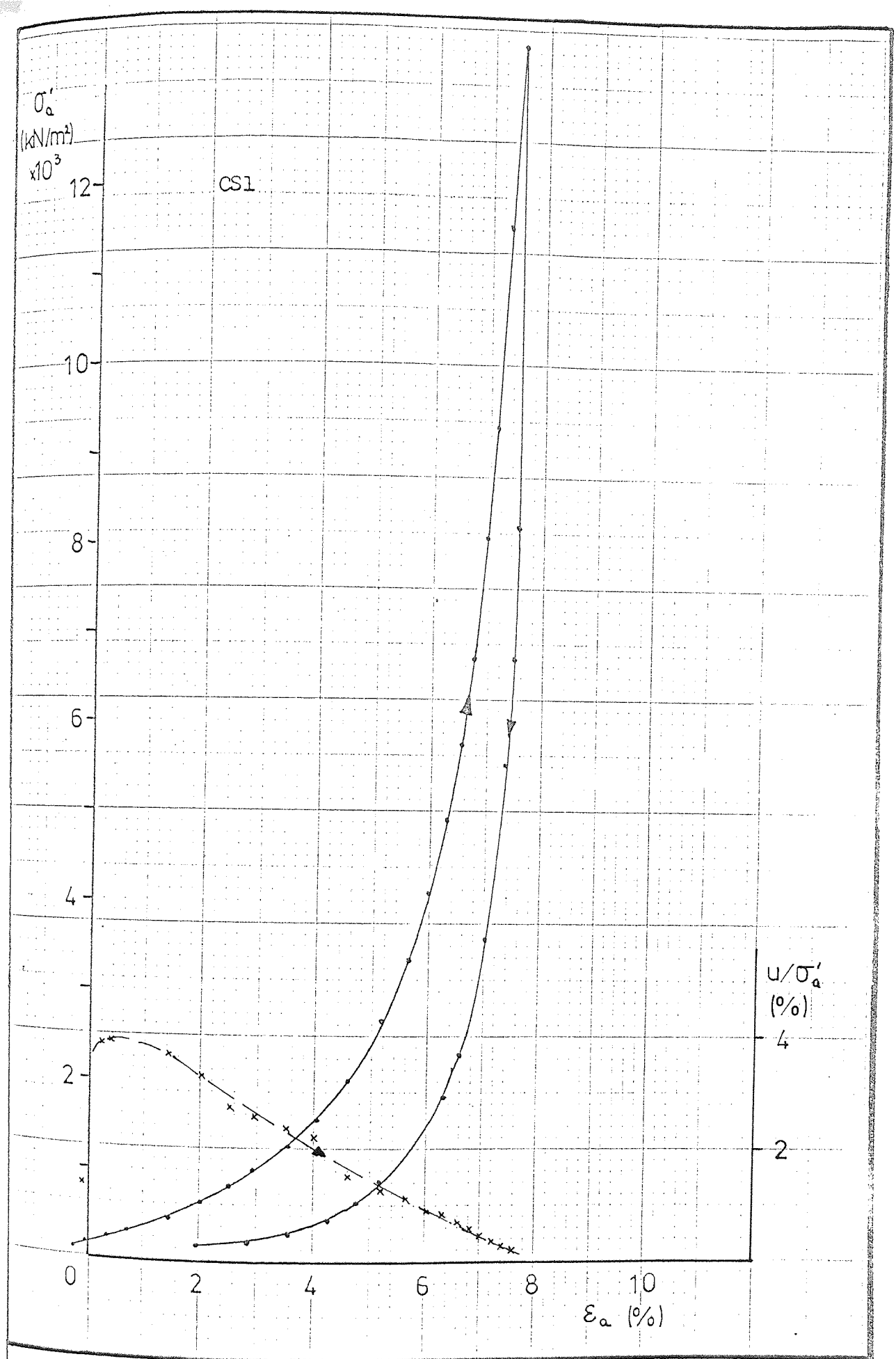

Axial Stress vs Axial Strain

- CS Series

FIG. 6.7(a)

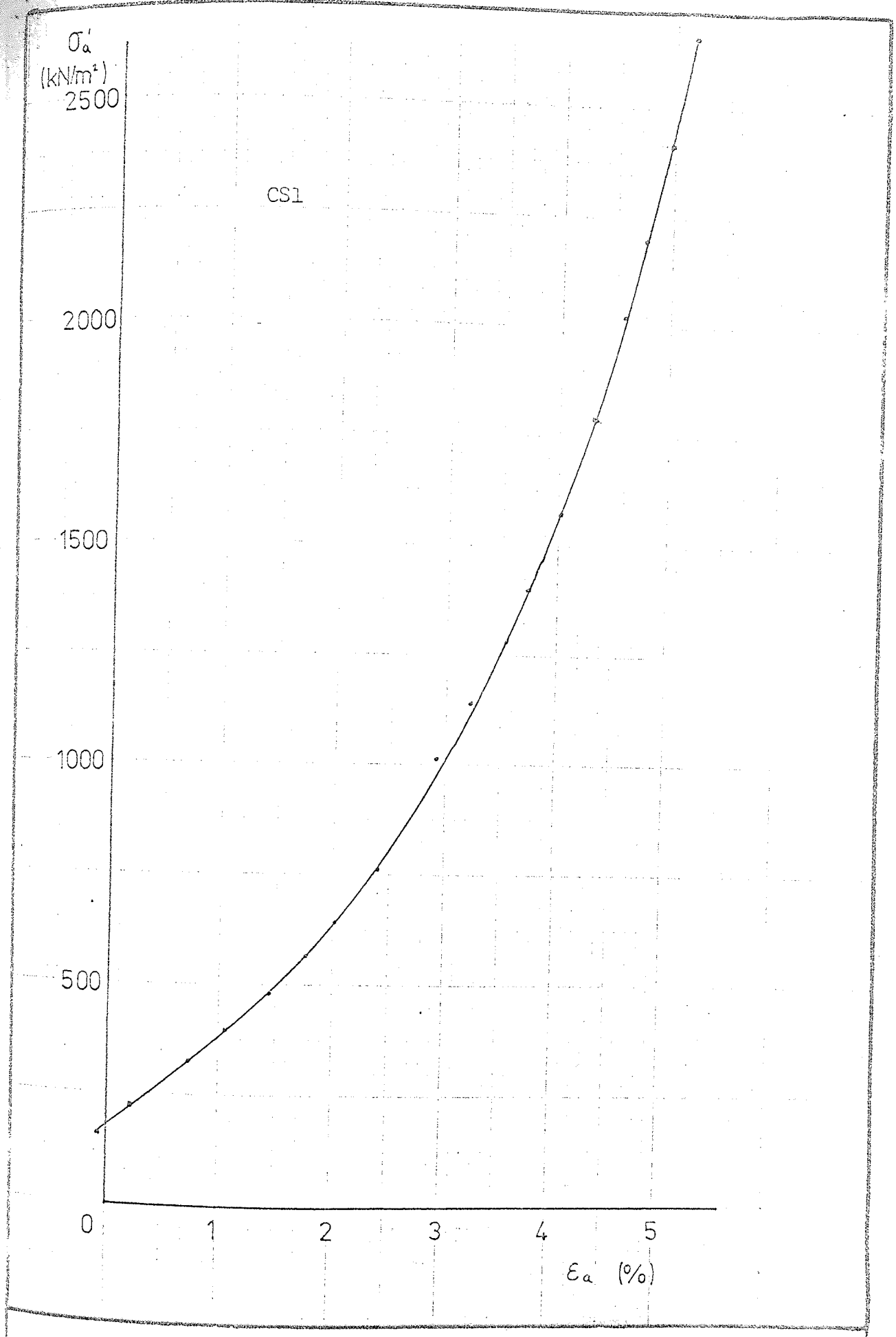

Axial Stress vs Axial Strain

- CS Series

FIG. 6.7(b)

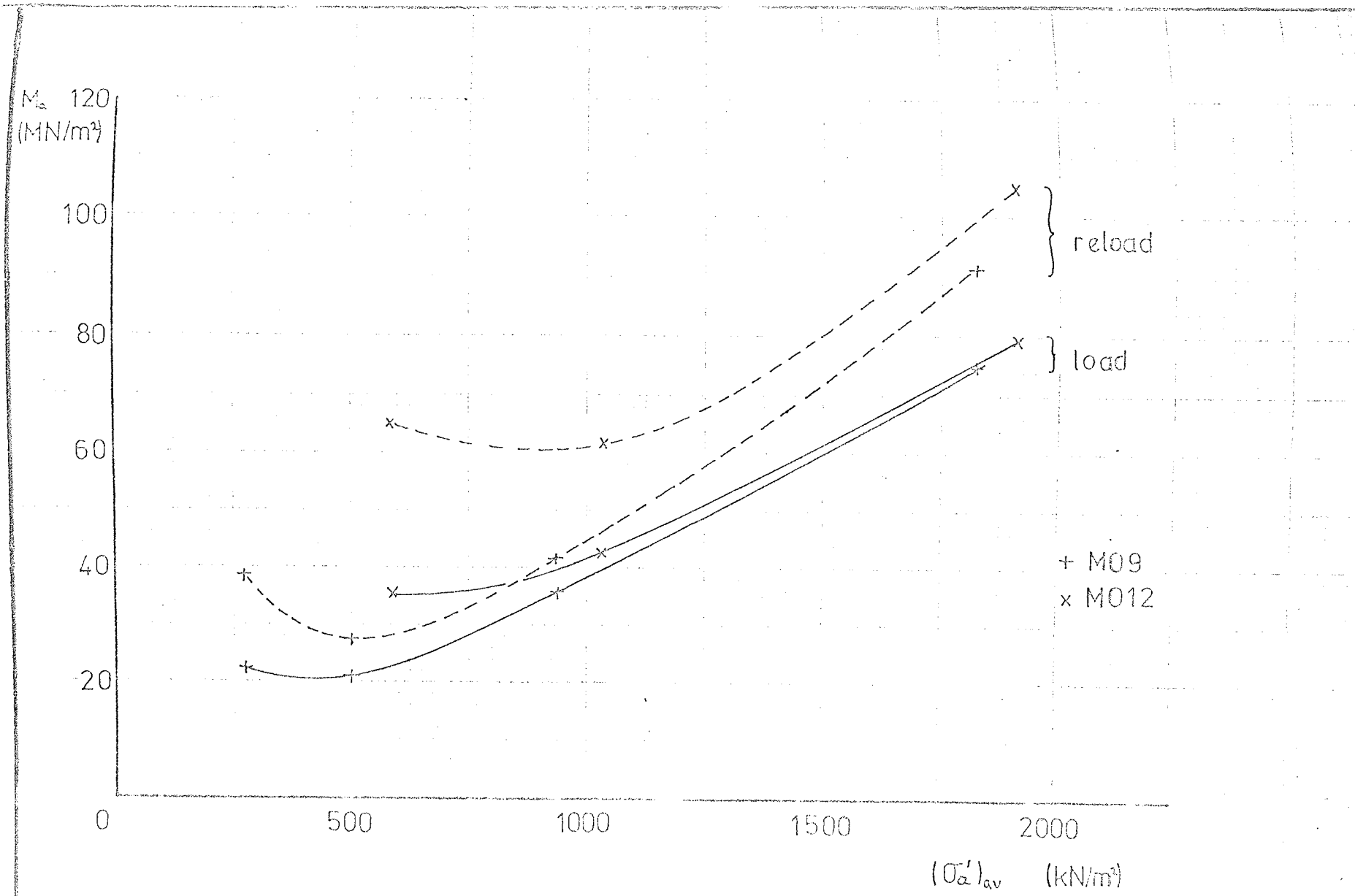

Axial Deformation Modulus v Axial Stress

- Block Samples

FIG. 6.3

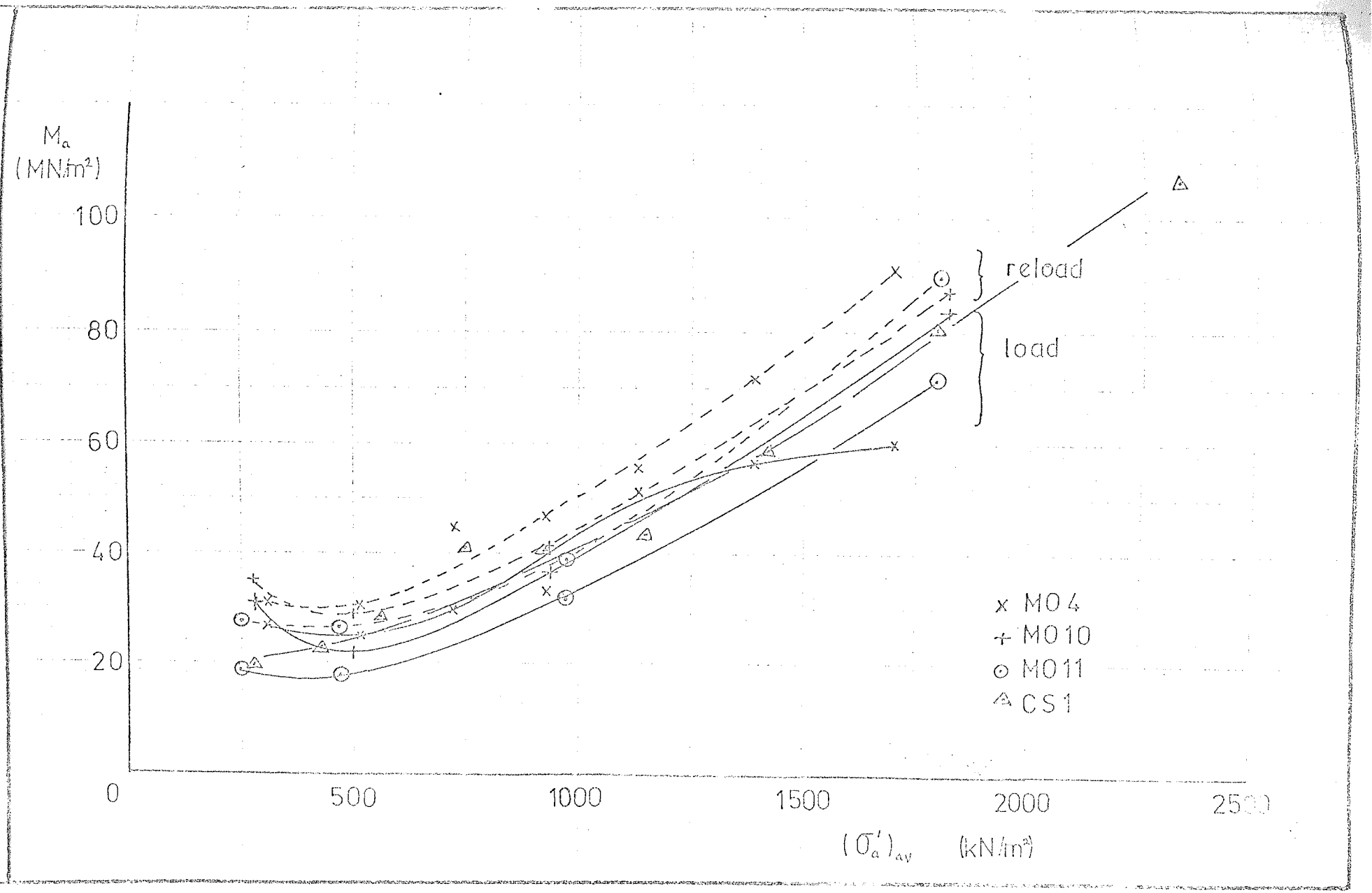

Axial Deformation Modulus v Axial Stress

- Core Samples

FIG. 6.9

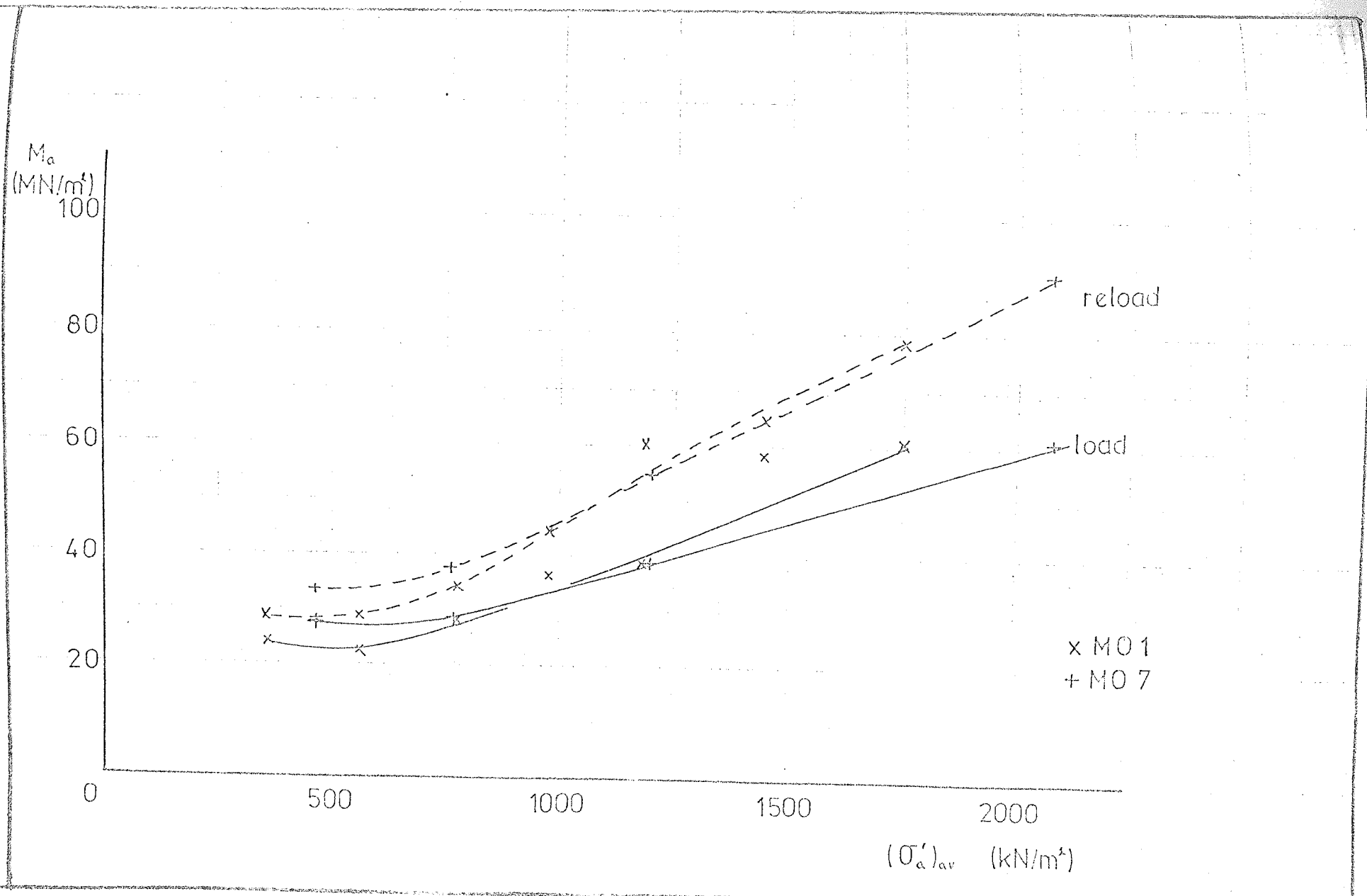

Axial Deformation Modulus v Axial Stress

- U70 Samples

FIG. 6.10(a)

Axial Deformation Modulus v Axial Stress

- U70 Samples

FIG. 8.10(b)

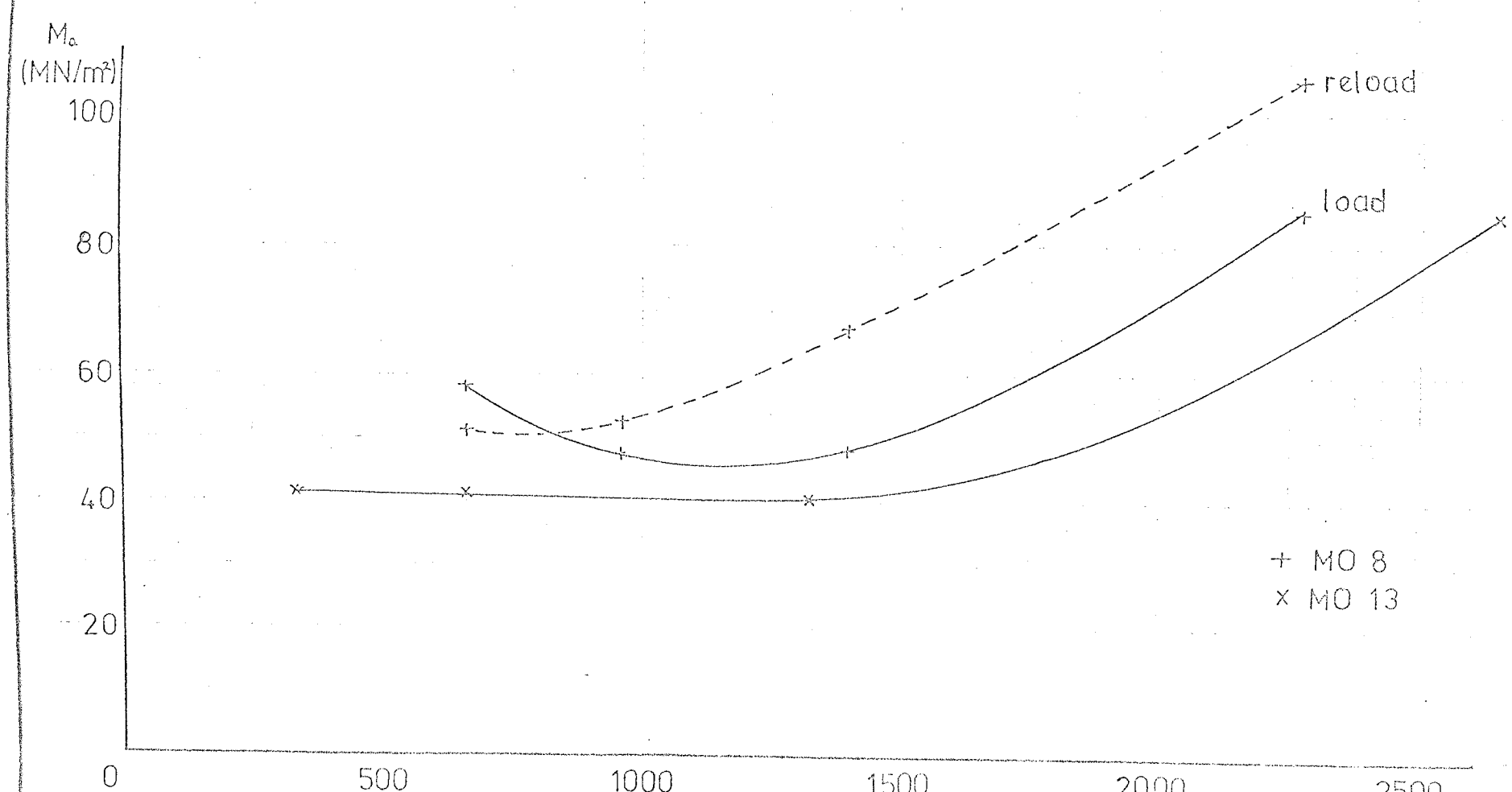

Axial Deformation Modulus v Axial Stress

- U70 Samples

FIG. 6.10(c)

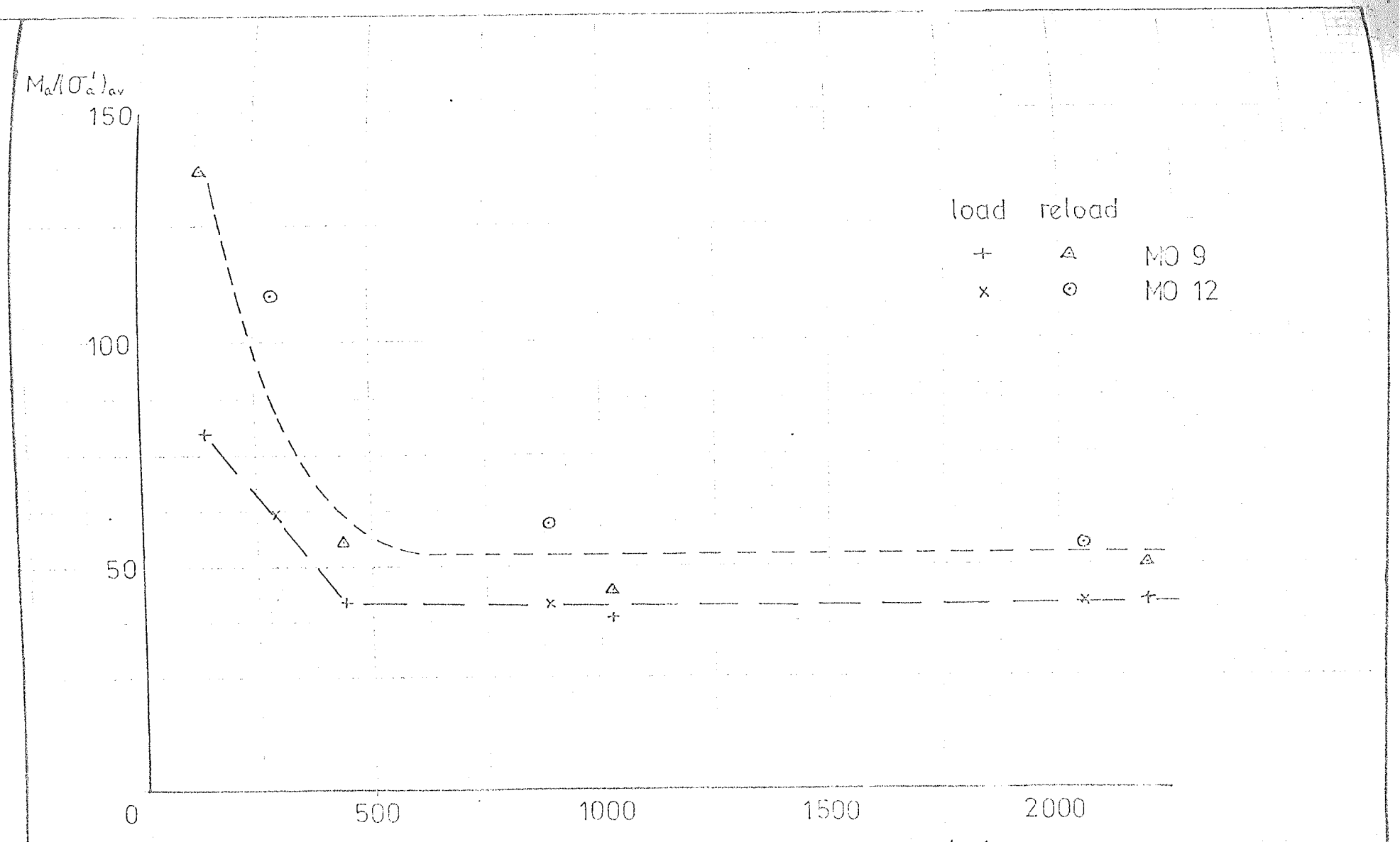

$M_a/(\sigma'_a)_{av}$ vs Axial Stress Increment

MO Series Block Samples

FIG. 6.11

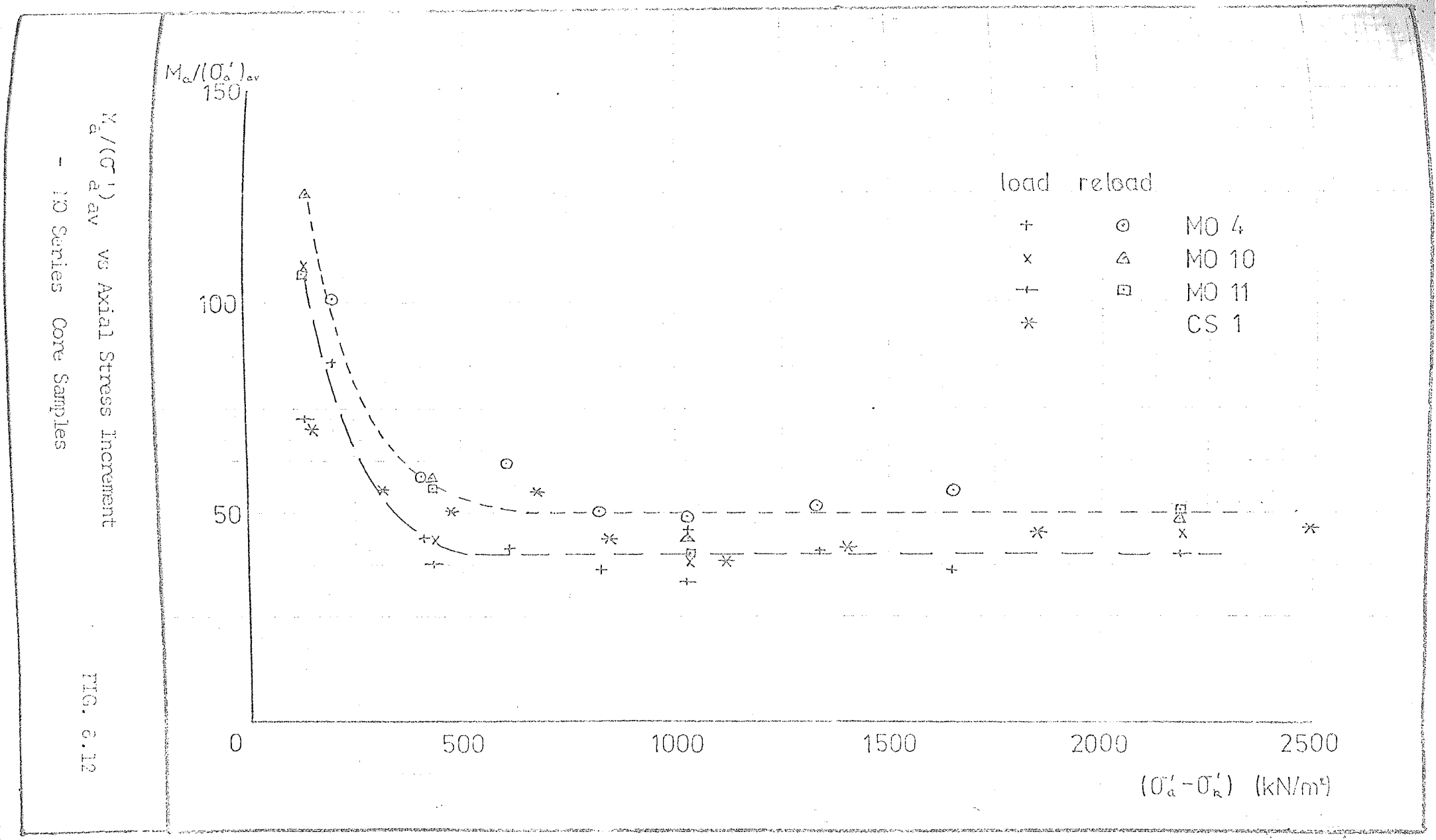

$M_a/(\sigma_a')_{av}$ vs Axial Stress Increment

- MO Series Core Samples

FIG. 6.12

$M_d/(\sigma'_d)_{av}$ vs Axial Stress Increment

- MO Series U70 Samples

FIG. 6.13

$M_d/(\sigma'_a)_{av}$ vs Axial Stress Increment

- CS Series

FIG. 8.14

$M_a/(\sigma'_a)_{av}$ vs Axial Stress Increment - RMO, RCS Series

FIG. 6.15

Coefficient of Consolidation vs Axial Stress

- Block Samples

FIG. 6.16(a)

Coefficient of Consolidation vs Axial Stress

- Block Samples Reloading

FIG. 6.16(b)

Coefficient of Consolidation vs Axial Stress

- Core Samples

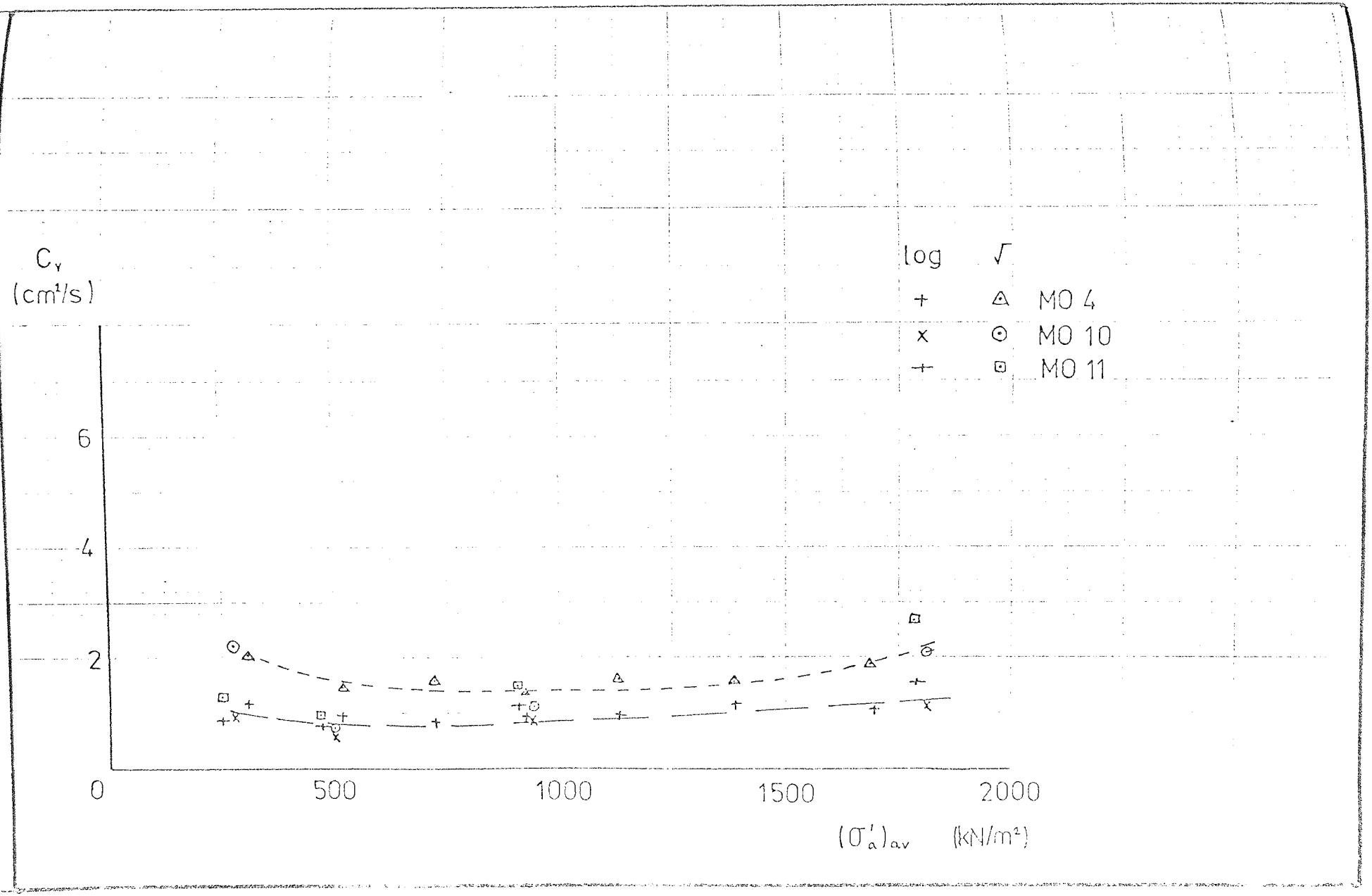

FIG. 6.11(a)

Coefficient of Consolidation vs Axial Stress

- Core Samples Reloading

FIG. 6.17(b)

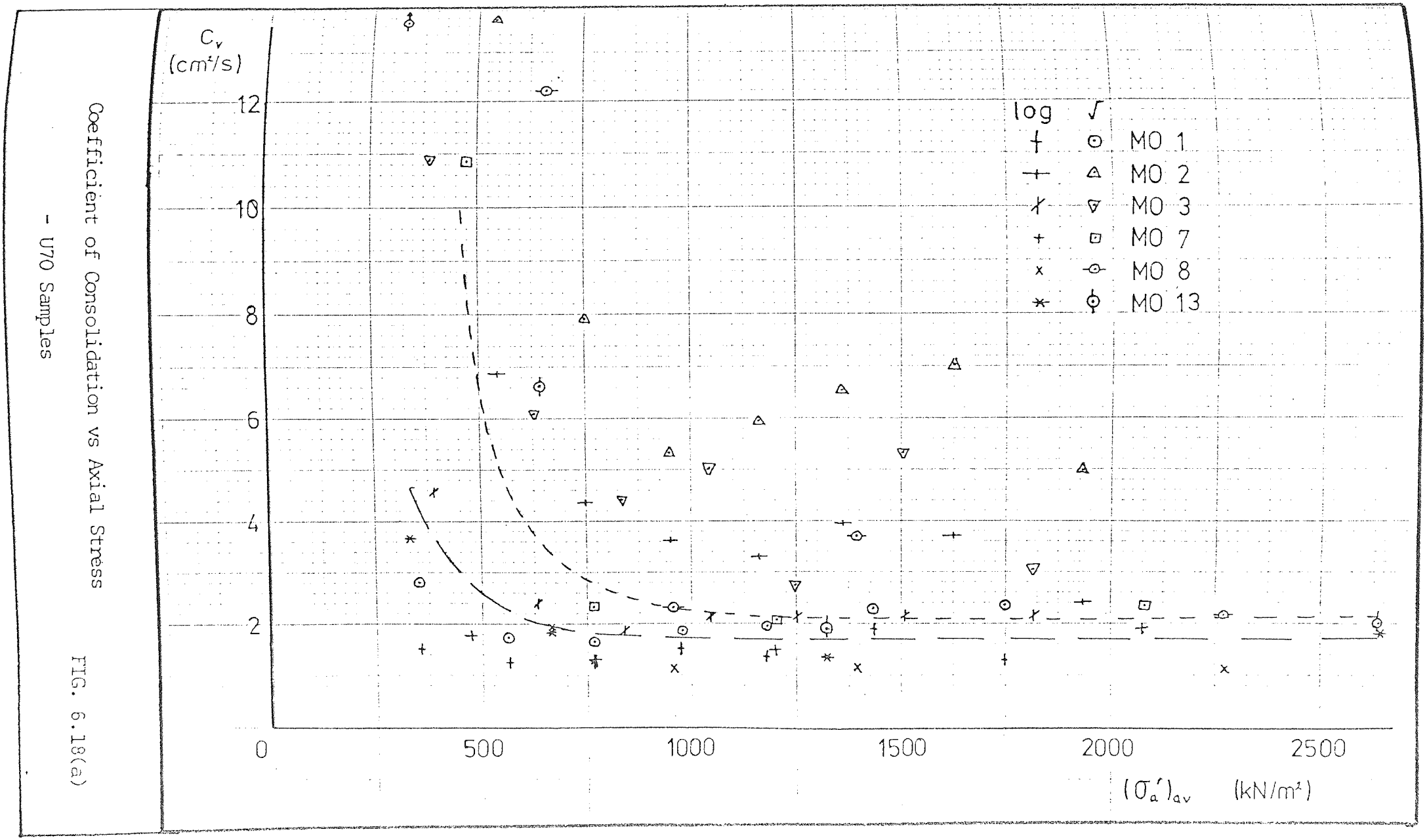

Coefficient of Consolidation vs Axial Stress

- U70 Samples

FIG. 6.18(a)

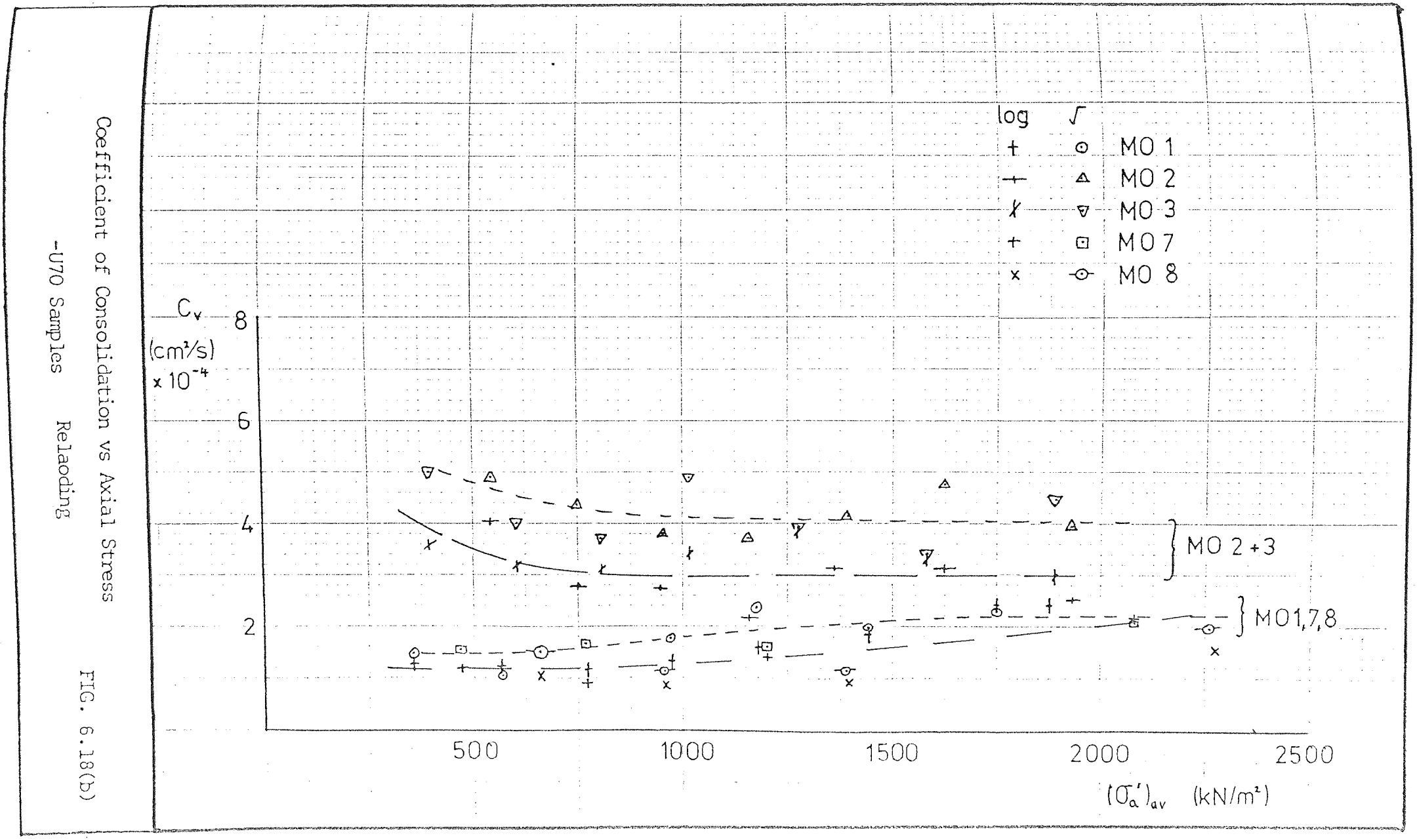

Coefficient of Consolidation vs Axial Stress

-U70 Samples Relaoding

FIG. 6.18(b)

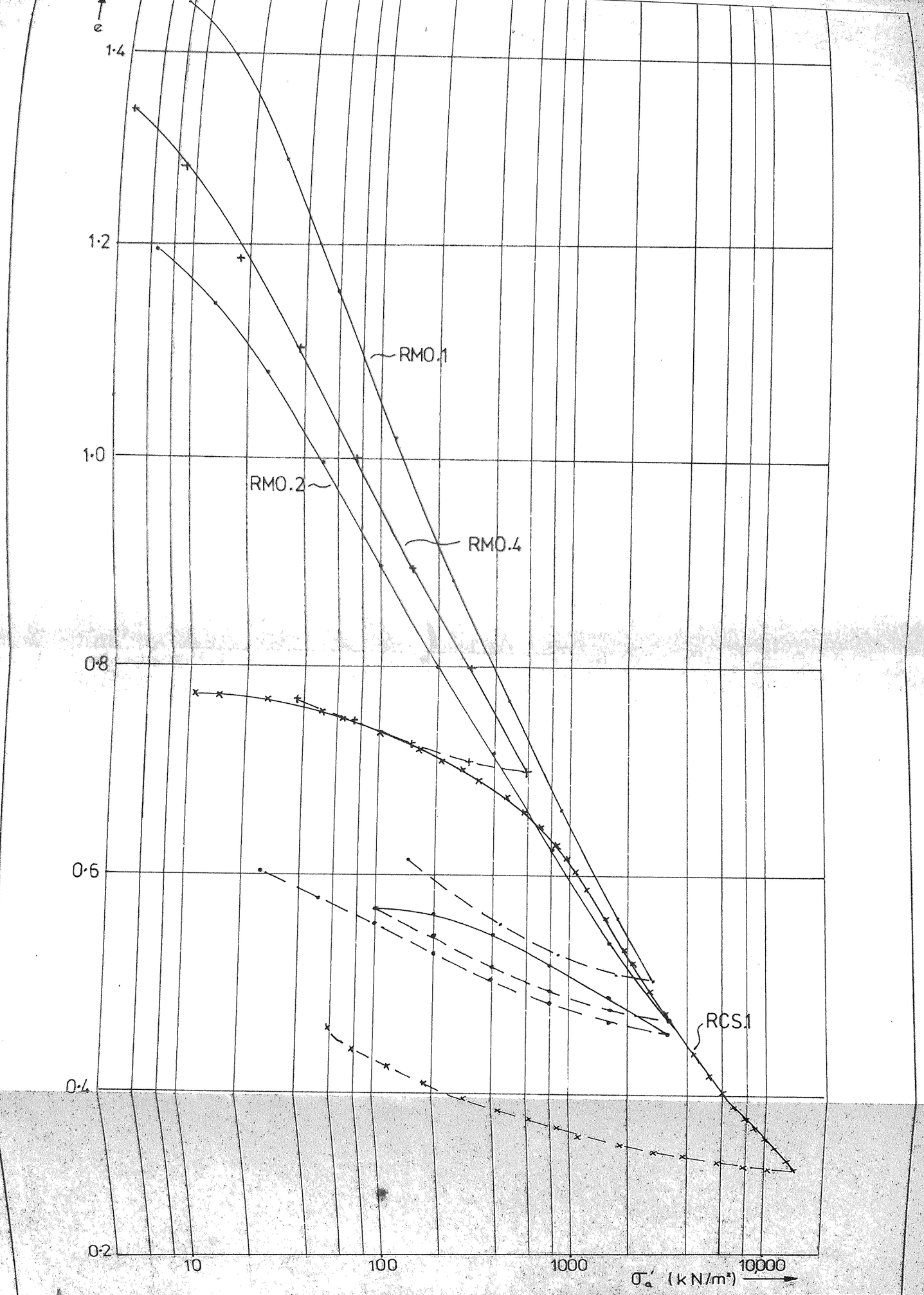

FIG. 6.19 Void ratio v. axial stress — Remoulded samples

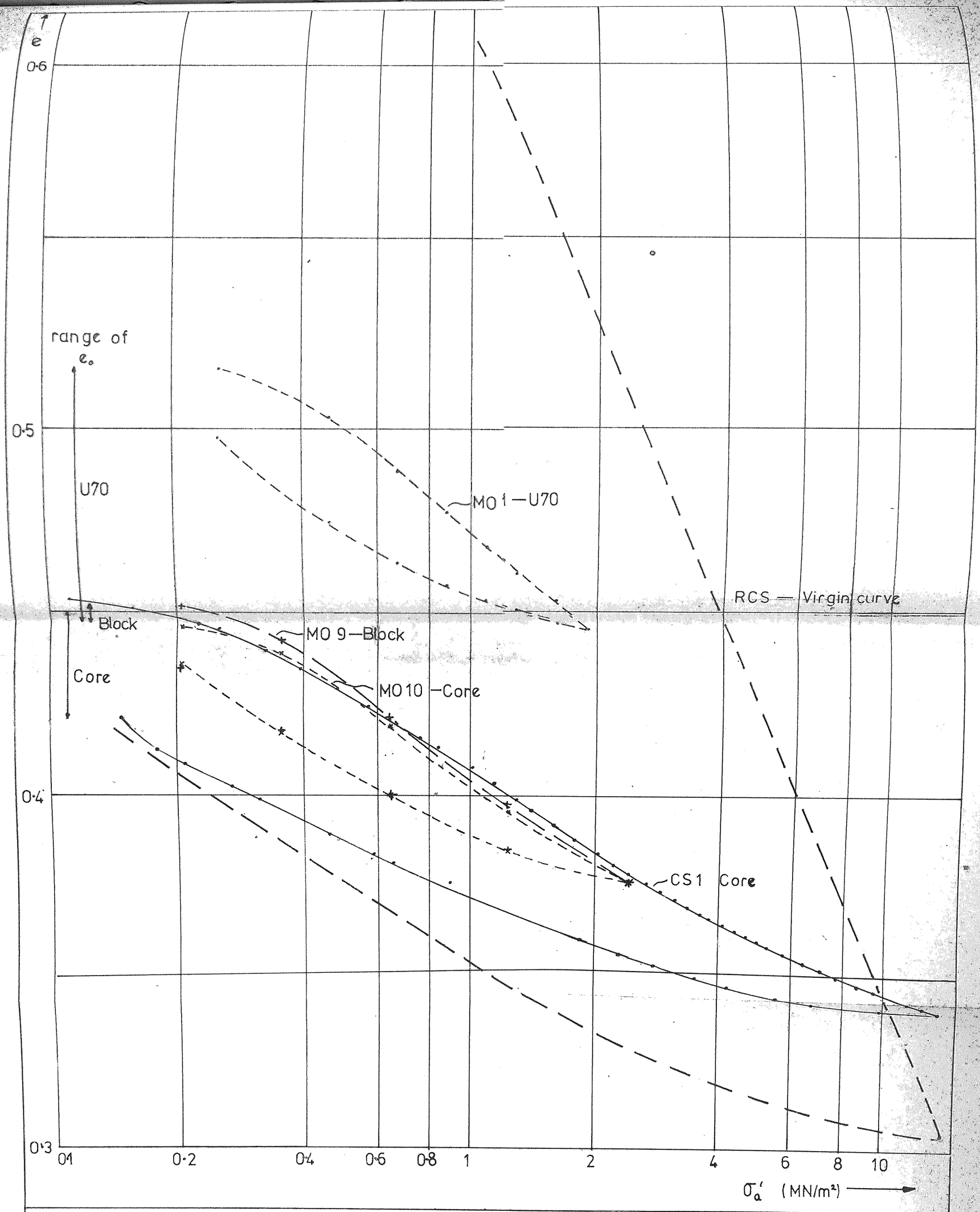

FIG 6.20 Void ratio v. axial stess — Undisturbed samples

CHAPTER 7

TRIAXIAL TEST RESULTS

7.1 INTRODUCTION

The triaxial testing programme, the testing apparatus and techniques were discussed in Chapter 5. The triaxial test results are presented and discussed in this chapter. The order of presentation does not follow the programme sequence described in Chapter 5. The results are presented in the order which best facilitates a progressive analysis of the results.

The results are initially presented and discussed for each test series ignoring the rate of consolidation. This subject is treated subsequently in section 7.8.

7.2 EQUILIBRIUM STRESS

As a preliminary stage of all the triaxial tests the equilibrium stress was determined. The specimens were subjected, under undrained conditions, to a hydrostatic stress, σ_c, greater than the expected equilibrium stress. The pore water pressure, u, was recorded and allowed to stabilise to a value, u_o. The equilibrium stress σ'_k, for a saturated clay is given by

$$\sigma'_k = \sigma_c - u_o \qquad (7.1)$$

The values obtained for σ'_k are tabulated in Table 7.1 together with the effective vertical overburden stress, σ'_v, as determined in Chapter 4 (Figure 4.11). It is clear from this table that the results, expressed as σ'_k/σ'_v, are widely scattered, varying from 0.38 to 3.32.

It was clear from preliminary tests (not reported) that the degree of saturation of the sample and system was unacceptably low unless the air was flushed out from around the sample during the setting up (Chapter 5). Obviously the flushing technique is likely

to cause a reduction in the pore water suction (equilibrium stress). However, as it is necessary to have a saturated "system" in order to measure the equilibrium stress therefore the flushing technique was adopted.

In the case of samples being tested in the ordinary triaxial cell the setting up time was generally short and therefore the effect of the flushing water may not be too serious. In the IS cell, however, the setting up process was far slower and flushing water could be in contact with the sample for up to 1 hour and sometimes more. On these grounds it is considered that the IS cell is unsuitable for the determination of the equilibrium stress. The results are presented in Table 7.1, but are not used any further than to illustrate the apparatus defficiency in this manner.

The values of σ'_k/σ'_v for all the samples tested in the ordinary cell are plotted against depth, Figure 7.1, and are seen to give considerable scatter. However, if samples are discarded where degree of saturation (S_i) less than 0.95 and/or the pore water pressure parameter, B, (Figure 7.2) obtained from the subsequent undrained loading is less than 0.80, the remaining results show that the ratio of σ'_k/σ'_v is approximately unity below 3m depth; above this level a wide variation is still apparent. The mean curve is shown in Figure 7.1 and is seen to increase to a maximum value of 1.6 just below two metre depth before reducing to approximately unity. It must be borne in mind, however, that these values may well have been reduced due to the initial flushing. A comparison with the oedometer ratios is made in Chapter 8 where the value of in-situ K_o will be considered.

7.3 STANDARD DRAINED TRIAXIAL COMPRESSION TESTS

A set of triaxial tests was performed such that, following the

initial consolidation to some predetermined values of axial and radial effective stresses, the specimen was loaded in a fully drained manner by increasing the axial stress while maintaining a constant radial stress. These tests are subdivided into three series TDV, TDH and TD2 as described in 5.2.2. The former two series were carried out in an ordinary triaxial cell starting from isotropic stress conditions on vertical and horizontal samples respectively. The latter series, TD2 was performed on vertical samples in the new cell starting from a stress condition where the radial stress was greater than the vertical (i.e. $K > 1$). The results of each series are presented and discussed below. An overall analysis of these results is made at the end of the section.

7.3.1 TDV Series

This series consisted of five tests on block (TDV 01), core (TDV 02, 06) and tube (TDV 03, 04) samples. In each case the specimen was loaded at a constant rate of strain (0.0004mm/min) to approximately 2% axial strain. At this stage an unload-reload cycle was performed, continuing the reloading cycle to failure. Throughout the test axial and volumetric deformations were recorded together with the applied stresses and pore pressure. The pore pressure was recorded to ensure that the rate of loading was sufficiently slow to allow adequate dissipation of water pressures. The variation of the recorded pore pressure from the applied back pressure was generally less than 2%. However, it was found necessary to reduce the unloading rate of strain to 0.0002mm/min to allow adequate equalisation of pore pressure.

The results of each test are presented in the form of axial stress against axial strain (Figures 7.3(a)-(e)). Also included on these

graphs are the plots of volumetric strain against axial strain. The results are also summarised in Tables 7.2(a)to (e) for increments of the loading and reloading cycles.

It is apparent from these curves (Figure 7.3) that very little bedding error is present. As horizontal fissures were frequently obvious during the sample preparation and that hydrostatic consolidation is believed to have little effect in reducing the bedding errors (Ward et al, 1959) then the technique described in Chapter 5 to eliminate such errors appears to be successful.

The axial stress-axial strain graphs are seen (Figures 7.3(a) to (e)) to be approximately linear over much of the first loading cycle giving a fairly constant axial deformation modulus (M_a). For comparison purposes these stress-strain curves are collected together (Figure 7.4(a)) and plotted on a larger scale. It is seen that axial deformation modulus over this range varies from approximately 10,600 kN/m^2 to 17,000 kN/m^2. In order to make some correction for the differing consolidation stress these results are replotted in the form $\Delta\sigma'_a/(\sigma'_a)_o$ (Figure 7.5(a)) where $(\sigma'_a)_o$ is the axial stress after consolidation (in this instance the same plot is obtained for axial, radial or mean effective stress after consolidation). This tends to bring the results into a slightly smaller band, and gives the range of the axial deformation modulus as $83(\sigma'_a)_o$ to $118(\sigma'_a)_o$.

It appears from these results that the drained axial deformation modulus is not significantly influenced by the method of sampling, as is generally reported for the undrained deformation modulus of heavily overconsolidated clays. However the strain paths (Volumetric strain-axial strain plot) Figure 7.3 (a) to (e) appear to be influenced by the sampling method. This is better illustrated by collecting all the strain paths together (Figure 7.6(a)). Here there is seen

to be excellent correlation between the block and core samples and also between the two tube samples, while these two sets of results are markedly different; in each case the strain paths are virtually linear.

The strain path for the core and block samples has a slope (strain ratio $\varepsilon_v/\varepsilon_a$) of 0.92 up to an axial strain of 1% (stress ratio $(1/_K)$ of approximately 2) indicating that the soil is deforming under axial load with very little radial strain. At axial strains greater than 1% the strain ratio reduces to approximately 0.75. The tube samples however appear to experience greater radial strains under axial loading, with a strain ratio of 0.60 up to an axial strain of 0.8% (stress ratio $(1/_K)$ of approximately 2) then reducing to 0.48. Thus under axial loading only it is seen that although sample disturbance has little effect on the axial deformation modulus, M_a, it has a significant effect on the volumetric deformation modulus, M_v. For the results obtained from this series the disturbance due to the tube sampling caused a reduction of 35% in the strain ratio $(\varepsilon_v/\varepsilon_a)$ and thus an increase of the volumetric deformation modulus, M_v.

During the unloading stage the strains are not fully recoverable. The unloading strain path for the block and core samples generally lie slightly below that for the loading curve, indicating a slightly greater percentage of volumetric strain recovery than axial strain recovery. The tube samples showed similar percentage axial strain recovery during unloading but the volumetric strain was virtually fully recovered.

On completing the reloading cycle (i.e. reloading to the effective stress at the end of the first loading stage) the recorded axial strain was no greater than 0.15% above that recorded on the first cycle (Figure 7.3). The axial deformation modulus during

the reloading stage is approximately 40% greater than for the first loading stage, ranging from 15,300 to 22,500 kN/m^2 (Figure 7.4(b)) or in Figure 7.5(b), from 116 $(\sigma'_a)_o$ to 158 $(\sigma'_a)_o$. As the stress increases above the initial loading level the stress-strain curve decreases in slope until failure.

The reloading strain paths coincide closely with the unloading strain paths. For comparison purposes the origin corrected strains occuring during the reloading are collected together in Figure 7.6(b). It is seen that the core sample strain ratio is the same as for the first loading, 0.92, up to approximately 1% corrected axial strain from where it gradually reduces to 0.65. However the initial strain ratio of the tube samples increases to 0.80, foraxial strains up to 1%. The block sample results on reloading coincide with the tube results.

It is seen that despite the substantial (approximately 40%) increase of the axial deformation modulus on reloading there is no observed effect on the strain ratio for the cored samples. However the tube samples which originally gave a low strain ratio showed an increase of approximately 25%, although the strain ratio was still less than for the core samples. It thus appears that for this type of loading mechanical disturbance has a greater effect on the volumetric deformation modulus than the axial deformation modulus.

7.3.2 TDH Series

This series was unfortunately reduced to a single test on a small (38mm diameter) block sample because of the difficulties in preparation of the test specimens. The sample was consolidated under a hydrostatic stress of 137 kN/m^2 and loaded at a constant rate of strain of 0.00067mm/min until failure. The results of the test are plotted in the form of axial stress, and volumetric strain

against axial strain (Figure 7.7). It is clear from this figure that substantial "bedding" error is present. However, beyond the corrected portion the stress-strain graph is approximately linear with an axial deformation modulus of 67,500 kN/m^2, which is seen to be considerably greater than for TDV series. The strain path is replotted in figure 7.8 to a larger scale. The central portion of this curve which is approximately linear, and is produced back to intersect the axial strain axis at a point which is presumed to be the corrected origin. The corrected strain path is thus linear (Figure 7.8) up to 1.1% uncorrected (0.8% corrected) axial strain (equivalent to effective stress ratio ($1/_K$) of greater than 4). The slope of this strain path is seen to be 1.19, i.e. the volumetric strain is greater than the axial strains under axial loading.

7.3.3 TD2 Series

This series consisted of three tests one on each type of sample - core (TD2.01), block (TD2.02) and tube TD2.03). Each sample was initially consolidated to an effective stress ratio (K) of approximately 1.7. The specimen was then loaded with a cyclic load as per the TDV series, at the same rates of strain. A summary of the test results is shown in Table 7.3(a) to (e) in the same manner as the TDV series.

The recorded results are plotted in the form of axial stress and volumetric strain against the axial strain (Figure 7.9(a) to (e)). The results indicate that bedding errors have again been eliminated as in the TDV series. The axial stress-strain curves each have an initially steep slope up to an effective stress ratio (K) of 1.1. Beyond this the slope reduces and becomes effectively linear. The increase of axial stress is plotted (Figure 7.10(a)) against axial strain for all tests. It is seen from this plot that the

initial axial deformation modulus varies from 30,000 to 48,500 kN/m^2, which reduces to 8,750 - 21,400 kN/m^2 for stress ratios (K) less than 1.1 To compensate for the effect of the higher consolidation stress the results are replotted in a non-dimensional form $\Delta\sigma'_a/(\sigma'_a)_o$ against axial strain as for TDV series (Figure 7.11(a)). This has the effect of reducing the divergence of results, and brings TD2.03 into line with the other two tests. The axial deformation modulus is then given as 160 $(\sigma'_a)_o$ for the initial part of the curve reducing to a range from 83 $(\sigma'_a)_o$ to 113 $(\sigma'_a)_o$. This gives remarkable agreement with the results of TDV within the same stress ratio range.

The strain paths for the first loading stage are shown in Figure 7.12(a). The strain path obtained for the block sample gives a strain ratio greater than unity, it is therefore considered that a slight leakage occured throughout the test. The other samples (core and tube) show that during loading to stress ratio (K) of 1,no lateral strain took place, as the volumetric strain is approximately equal to the axial strain. Beyond this, the slope reduces to 0.83 for the cored sample, while the tube tends to be less linear; the reduction in volumetric strain for the tube sample does not appear to be so accute as for the TDV series.

The samples were unloaded to an axial stress slightly in excess of the initial value, (Figure 7.9). The strain recovery for the block and core samples were approximately 50 to 75% whereas the tube sample showed virtually full axial and volumetric recovery. On completing the reloading cycle it is seen (Figure 7.9) that the recorded axial strain is within $\pm$ 0.1% of that recorded in the first loading stage.

The stress-strain relationship is seen to be approximately linear over a large portion of the reloading cycle. From the replotted results in figure 7.10(b) the axial deformation modulus, for reloading, is seen to range between 102 $(\sigma'_a)_o$ and 131 $(\sigma'_a)_o$, subsequent to the initial portion where $M_a = 240\ (\sigma'_a)_o$. These results are seen to be comparable with the TDV series. The strain paths during **reloading** virtually coincide with the first **loading** paths in the case of the core and tube, the block results being rejected on account of the suspected leakage. The strain ratio (Figure 7.12(b)) remains unchanged from the first loading at 0.83 up to an axial **strains** of approximately 1% (equivalent to a stress ratio $(1/_K)$ of approximately 2.5) beyond this the strain ratio reduces.

The results from this series are rather limited, however they indicate that the axial deformation modulus is high when **reloading** to K = 1 conditions beyond which the results are comparable with the TDV series. Reconsolidation to this higher K value appears to improve the volumetric strains for the tube samples. However more testing must be carried out from K > 1 before any conclusions can be made.

7.3.4 Elastic Analysis

It has been seen from these results that the stress-strain relationships are in general approximately linear, this is also true of the strain paths up to a stress ratio $(1/_K)$ of approximately 2. The unloading stages show that the strains are not fully recoverable and therefore the material is **not** behaving as a perfect elastic material. However, if it is considered that as the material behaves linearly, it may be treated as a linear pseudo-elastic material during loading. The results from the horizontal test show that the material has a greater stiffness in the horizontal

direction than in the vertical i.e. the material is anisotropic. It is reasonable to assume, however, that for this type of deposit the horizontal plane would be an isotropic plane (Barden 1963) (3.2.3) and thus the results are studied in the terms of "orthotropic" or "cross-anisotropic" elasticity.

7.3.4.1 Orthotropic Elastic Constants

The general stress-strain relationships for an orthotropic elastic material under principal stress increments are given in Appendix F together with the relevant nomenclature. Also shown in Appendix F are the stress strain relationships, in terms of isotropic and anisotropic elasticity for the relevant triaxial stress paths.

It is seen (Appendix F) that the deformation of vertical or horizontal samples in general is dependent on four elastic constants, E'_v, n, ν_{hv} and ν_{hh} (see Appendix F for explanation of symbols). In order to determine these four constants it is necessary to analyse the results of the vertical and horizontal samples together.

It is proposed to analyse the results of the core and block samples of the TDV series together with TDH (Block). In the case of standard drained tests where there is no change in the radial effective stress the vertical Young's modulus E'_v is numerically equal to the **axial** deformation modulus, M_a for a vertical sample whereas the horizontal Young's modulus E'_h is numerically equal to the axial deformation modulus of a horizontal sample. It is therefore seen Figure 7.4, that the vertical Young's modulus, E'_v varies from 10,600-17,000 kN/m^2 and that the horizontal Young's modulus, E'_h, is of the order of 67,500 kN/m^2 (Figure 7.7). From these results it is seen that the modulus ratio lies between 6.37

and 3.97. However, as E'_h was determined from a test on a small diameter sample, it is considered that this would be the upper limit for E'_h and therefore that the maximum value of E'_v should be used to compute the modulus ratio n, i.e. n = 3.97. The two Poisson's ratios ν_{hv} and ν_{hh} are determined from the strain ratios of the two vertical and horizontal samples respectively. It is seen from Appendix F that for a normal drained test on a vertical sample

$$\nu_{hv} = \tfrac{1}{2}(1 - \varepsilon_v/\varepsilon_a) \qquad (7.2)$$

and for a "horizontal"sample

$$\nu_{hh} = 1 - n\nu_{hv} - \varepsilon_v/\varepsilon_a \qquad (7.3)$$

Thus it is seen that with a strain ratio of 0.92 (Figure 7.6(a)) a surprisingly low value of ν_{hv} of 0.04 is obtained for a stress ratio $(1/K) < 2$. The Poisson's ratio ν_{hh} is obtained from equation 7.3, above, using a strain ratio of 1.19 (Figure 7.8), n of 3.97 and ν_{hv} of 0.04, gives a further surprising result that $\nu_{hh} = -0.3488$. The results satisfy the criterion for positive strain energy (Pickering 1970), which requires that

E'_v and E'_h are positive

$\nu_{hh} > -1$ and

$(n(1-\nu_{hh}) - 2n^2\nu_{hv}^2) > 0$

It was seen from the consideration of the tube samples (TDV.03 and 04) that the axial deformation modulus was of the same order as for the core/block samples, therefore E'_v appears not to be affected by mechanical disturbance. However the strain ratio recorded was much lower than for the cores, at 0.66, giving a value for the Poisson's ratio, ν_{hv} (during the first loading) of 0.17, which is considerably different from the 0.04 obtained for the core

samples. Unfortunately as it was not possible to test horizontal specimens from tube samples, it is not possible to access the effect of the mechanical disturbance on the remaining parameters. ν_{hh} and E'_h. However, it may be possible to make some assessment of this effect from the results of the TA series of tests later in this chapter.

7.3.4.2 Undrained Parameters

Undrained triaxial compression tests have not been carried out although undrained stages are included in the TA1 and TA2 series. However as the material behaves "elastically" the undrained behaviour can be predicted. If an increase of total axial stress ($\Delta\sigma_a$) is applied in an undrained manner, then the axial deformation is given by

$$\varepsilon_a = \frac{\Delta\sigma_a}{E_u}$$ where E_u is the undrained Young's modulus.

The axial deformation may also be expressed in terms of the effective stresses:

$$\varepsilon_a = \frac{\Delta\sigma'_a}{E'_v} - 2\nu'_{hv}\frac{\Delta\sigma'_r}{E'_v} \qquad (7.4a)$$

where $\Delta\sigma'_a = \Delta\sigma_a . (1 - A)$

and $\Delta\sigma'_r = \Delta\sigma_a . (-A)$

$$\therefore \varepsilon_a = \Delta\sigma_a \left[\frac{(1-A)}{E'_v} + \frac{2\nu'_{hv}}{E'_v} . A\right] \qquad (7.4b)$$

and $$E_u = E'_v/(1-A.(1-2\nu_{hv})) \qquad (7.5)$$

The pore pressure coefficient, A, is given in terms of the orthotropic elastic parameters (Pickering, 1970) by the following equation:

$$A = \frac{1 - 2\nu_{hv}}{1 - 4\nu_{hv} + \frac{2}{n}(1 - \nu_{hh})} \qquad (7.6)$$

Therefore, using the parameters determined earlier, the pore pressure coefficient A equals 0.60. Hence the undrained modulus for core or block samples is given by

$$E_u = 2.22\, E'_v \qquad (7.7a)$$

and for a tube sample, assuming A is **not** affected by disturbance,

$$E_u = 1.65\, E'_v \qquad (7.7b)$$

a reduction of 25%. If in fact A is affected by disturbance it would be expected that its value would be reduced and hence E_u reduced further.

It is seen that the affects of sampling disturbance observed for E'_v and ν_{hv} do not contradict the widely reported effect on the undrained deformation modulus according to the "elastic" theory.

7.4 INCREMENTAL SPHERICAL LOADING (TC SERIES)

The TC series was carried out on three short (height to diameter ratio of 1) cored samples as described in Chapter 5. Throughout the tests the axial and volumetric strains were recorded together with the cell and pore water pressures. The results, summarised in Table 7.4, are presented and discussed below. The rate of deformation and **pore** pressure dissipation are discussed later in section 7.8.

Each increment of cell pressure was applied under undrained conditions and the pore pressure allowed to equalise before the drainage tap was opened. During the undrained stage there was no deflection of the axial dial gauge. The increase of pore pressure (δu) for each undrained loading increment ($\delta\sigma_r$) is

shown in Figure 7.13. The results of TC 02 and 03 are seen to correlate well, with a pore pressure parameter, B, greater than 0.90. TC 01 on the other hand gives much lower response to the change in cell pressure with the parameter B only in the order of 0.5.

7.4.1 Stress-Strain Relationship

The axial stress-axial strain curves (Figure 7.14) show no obvious bedding errors; as the loading is hydrostatic it is probably that any "bedding-in" or closing up of fissures would not be evident (Ward et al 1959). In each case the slope of the curve, i.e. the axial deformation modulus M_a, increases with increase of stress level. Plotting the increment of axial stress ($\Delta\sigma'_a$) against axial strain Figure 7.15) for all the tests it is seen that TC 02 and TC 03 correlate closely whereas the results of TC 01 fall well below them. The stress-strain relationship obtained from TC 02 and 03, Figure 7.15, is approximately linear up to 2% axial strain, beyond this level the curve becomes progressively steeper.

It was seen in the TD series that the stress-strain curve remained approximately linear until failure was approached when the slope decreased. It would therefore appear that the axial deformation modulus (M_a) is a function of the radial stress. However it is considered that this should be treated later, in the light of further information obtained from the TA set of tests.

7.4.2 Strain-Strain Relationship (Strain Paths)

The strain paths for the individual tests are shown in Figures 7.14 (a) to (c). It is seen that the slope of the strain paths are approximately linear over the test range studied. The results of all three tests are plotted collectively to a larger scale in Figure 7.16. A close correlation of the results is achieved for

the tests, including TC 01. The results prove to be remarkably linear over the full range giving a strian ratio of 1.55. This result suggests that the material is behaving "elastically" but exhibits marked anisotropy as the strain ratio deviates significantly from the isotropic value of 3.

7.4.3 Elastic Predictions and Analysis

The deformation of the sample under the applied stresses is considered below in terms of the orthotropic elastic constants derived from the TD series. These values will then be considered in the light of the results obtained from this series of tests.

As all the samples tested in the TC series are cored samples then the deformation predictions will be made using the elastic constants obtained from the core/block samples of the TD series -
i.e. $E'_v = 17{,}000\ kN/m^2$, $\nu_{hv} = 0.04$, $\nu_{hh} = -0.3488$ and $n = 3.97$.

The axial deformation for $\bar{K} = 1$, is given by the equation

$$\varepsilon_a = \frac{\Delta\sigma'_a}{E'_v}\left[1 - 2\nu_{hv}\right] \qquad (7.8)$$

It is seen that the predicted curve, Figure 7.15 shows a reasonable fit to the observed deformations of samples TC 02 and TC 03 up to a stress increment of approximately 350 kN/m^2. Beyond this point the recorded deformations are less than the predicted.

The strain ratio, for the hydrostatic loading case, is represented by the equation

$$\frac{\varepsilon_v}{\varepsilon_a} = \frac{1 - 4\nu_{hv} + 2(1-\nu_{hh})/n}{1 - 2\nu_{hv}} \qquad (7.9)$$

This indicates (Figure 7.16) the slope of the strain path to be slightly steaper than recorded at 1.65. The agreement is good

and demonstrates that the values obtained from the TD series where $\bar{K} = 0$, are equally applicable to this series where $\bar{K} =$ ... This confirms that within the stress range considered the material behaves as linearly "elastic" material and may be expected to do so for any stress paths between $\bar{K} = 0$ and $\bar{K} = 1$.

It was seen from the TD series that the Young's modulus, E'_v ... considerably, and thus a range of values of the modulus ratio, n, was obtained 6.37 to 3.97. It is now possible to evaluate ν_{hv}, ν_{hh} and n from the far more consistent strain ratios. Considering the experimental strain ratios for the TDV, TDH and TC tests, respectively, we have

$$0.92 = 1 - 2\nu_{hv} \qquad (7.10a)$$

$$1.19 = 1 - \nu_{hh} - n\nu_{hv} \qquad (7.10b)$$

$$1.55 = \left[1 - 4\nu_{hv} + 2(1 - \nu_{hh})/n\right]/1-2\nu_{hv} \qquad (7.10c)$$

On solution of these three equations from ν_{hv}, ν_{hh} and n we obtain $\nu_{hv} = 0.04$, $\nu_{hh} = -0.38$ and $n = 4.70$.

Thus n is found to be higher than the initially assumed value of 3.97 but is within the range suggested by the recorded vertical and horizontal Young's moduli in the TD series. The Poisson's ratio ν_{hv} remains unaltered and ν_{hh} is only slightly higher. These values thus satisfy the strain ratios for the stress increment ratios, $\bar{K}$ at 0 and 1, in the range of axial to radial effective stress ratio ($1/_K$) of 1 to 2.

7.5 CONSTANT STRESS INCREMENT RATIO TESTS (TA3 SERIES)

A series of three triaxial tests was performed on one ... e ... 3) and two block (TA3 01 and 02) samples where the axial ... l ... stresses were both increased continuously at a constant str... s

increment ratio as described in Chapter 5. The rate of loading was governed to allow the sample to follow a fully drained stress path (Figure 5.1(e)).

7.5.1 Stress Paths

It was found to be difficult to maintain a constant effective stress increment ratio ($\overline{K}$) and in practice the ratio varied between 0.25 and 0.36 over the three tests (Figure 7.17(a) to (c)). The stress paths for TA3 02 and 03 are very similar although they start from different consolidation stresses; at the start incremental stress ratio $\overline{K}$ is in the region of 0.34 up to a stress increment approximately equal to the consolidation stress but beyond this level it reduces to 0.26. The other test, TA3 01 starts with an incremental stress ratio of 0.25 up to a stress increment of twice the consolidation stress but beyond this level it increases to 0.37; this sample failed during loading, at an effective stress ratio ($1/_K$) of 2.15, along a failure plane inclined at 20° to horizontal plane.

7.5.2 Stress-Strain Relationships

The stress-strain relationships for the individual tests are shown in the form of axial stress against axial strain and summarised in Table 7.6,(Figures 7.18(a) to (c)). These results indicate that bedding error has been eliminated prior to the commencement of the loading cycle as described in Chapter 5. The slope of the stress-strain curves are similar to those recorded in the TC series with the axial deformation modulus increasing with increase of stress level.

The stress-strain results are replotted collectively in the form $\Delta\sigma'_a$ against ε_a and it is seen that the results correlate reasonably well. In the early stage the relationship is approximately

linear although the slope can be seen to be increasing with increase of stress, again indicating that the axial deformation modulus is a function of the effective radial stress. This is considered later in section 7.7.

7.5.3 Strain path

The volumetric strain-axial strain relationships are shown individually in figure 7.18 (a) to (c). The results from the two block samples (TA3 01 and 03) clearly show that the strain ratio ($\varepsilon_v/\varepsilon_a$) is greater than unity. The strain path of the third sample lies below the line of equal strains. However it is seen that the slope of the strain path is greater than unity due to an apparent bedding error. The strain path for TA3 02 (Figure 7.18(b)) is seen to deviate slightly from a linear relationship, this may be partly caused by the non linear stress path. Replotting the strain paths, figure 7.20, it is clear that the relationships can be approximated to a linear one although the slope changes at approximately 3% axial strain. The block samples indicate a strain ratio of 1.1, while the core sample (TA3 03) has a strain ratio slightly less than the block samples at 1.05. Beyond 3% axial strain (approximate stress ratio ($1/K$) of 2) both sets of results indicate a strain ratio of 0.90 before the rate decreases further as failure is approached. A similar phenomenon was observed in the TDV series at approximately the same stress ratio.

7.5.4 Elastic Predictions and Analysis

The axial stress-strain relationship and the strain ratio are considered below using the parameters determined from the TD and TC series and compared with the observed results. The relevant parameters are therefore $\nu_{hv} = 0.04$, $\nu_{hh} = -0.38$ and $n = 4.70$, the

value of the vertical Young's modulus may vary, although a value of 17,000 kN/m^2 is preferred from these two series.

A general case is considered with the incremental stress ratio $\bar{K} = 0.30$, as this is an average value of $\bar{K}$ for this series of tests. The axial strain (ε_a) is expressed by the equation

$$\varepsilon_a = \frac{\Delta\sigma_a}{E'_v} (1 - 2 \bar{K} \nu_{hv}) \qquad (7.11)$$

the resulting stress-strain curve is shown in Figure 7.19. It is seen that the predicted strain is initially less than the observed. However up to approximately 2% axial strain the observed strains are sensibly predicted using Young's modulus value of 14,000 kN/m^2, which is within the range determined from the TD series. The strain ratio can be predicted from the equation

$$\frac{\varepsilon_v}{\varepsilon_a} = \frac{1 - 2\nu_{hv} + 2 \bar{K} \left\{\frac{1}{n} (1 - \nu_{hh}) - \nu_{hv}\right\}}{1 - 2\nu_{hv} \bar{K}} \qquad (7.12)$$

Substituting the appropriate elastic constants and a $\bar{K}$ value of 0·3 a strain ratio of 1.098 is obtained, and is shown in Figure 7.20. It is seen that this coincides with the observed results of TA3 02 and closely fits the results of the other two tests up to an effective stress ratio of approximately 2. It is therefore seen that the numerical values of ν_{hv}, ν_{hh} and n predicted from the TD and TC series are also applicable to the TA3 series.

7.6 INCREMENTAL LOADING TESTS (TA1 and TA2 SERIES)

Two series of tests were carried out where the samples were incrementally loaded. In the first series (TA1) the specimens were initially consolidated under hydrostatic stress, whereas in the second series (TA2) the samples were initially consolidated to a stress condition where the radial stress was greater than the

axial stress (i.e. K > 1). The results of these tests are presented below.

7.6.1 TA1 Series

This series consisted of eight tests on block (TA1 05 and 06), core (TA1 04, 07 and 08) and tube (TA1 01, 02 and 03) samples.
The apparatus and method of testing have been described in Chapter 5. Each sample was subjected to a series of increments of axial and radial stresses at a ratio of 3 : 1. The increments were initially applied under undrained conditions, and the magnitude of the increments was selected to avoid failure during the undrained stage. Following the undrained loading the samples were then allowed to consolidate into a back pressure in the order of 250 kN/m^2. Throughout the test the stresses, pore pressure and deformations were recorded as described in Chapter 5. The results of these tests are presented and discussed below and the recorded stress and strains at the end of each stage are shown in Table 7.6. The subject of rate of consolidation will be considered later in section 7.8.

7.6.1.1 Stress Paths

The effective stress paths for each test are shown in Figure 7.21 (a) to (c). Also shown in these figures is the compression failure envelope for this material as determined by Lal (1971) for 38mm diameter damples cut from the block samples.

The undrained stages take the samples close to the failure line. This was especially true of tests TA1 04, 05 and 06, where the effective stresses due to the undrained loading often fell on the failure envelope. Samples TA1 03 and TA1 08 failed under the final undrained increment. During the consolidation stage the effective

stress paths moved away from the failure envelope and the factor of safety against failure increased. The "end of consolidation stresses" lie on a stress path approximately equivalent to that of the TA3 series.

7.6.1.2 Pore Pressure Parameter "A"

During the undrained loading an excess pore pressure is induced. For a saturated clay (B = 1.0) the increase of pore water pressure, due to the increment of total load, is dependent on the pore pressure parameter "A" (Skempton 1954). The magnitude of "A" is reflected by the slope of the undrained portion of the effective stress paths (Figure 7.21). The slope of the undrained effective stress paths for the block samples (Figure 7.21(a)) are generally similar and the determined "A" values are of the order of 0.55 to 0.67 (Table 7.6(a)) with the exception of the first increment of TA1.06. The core samples indicate similar "A" values, 0.55 to 0.77 (Table 7.6(b)), to the block, with the exception of TA1.04 where the values are generally lower, 0.39 - 0.57. The tube samples (Figure 7.21(c)) however give values of "A" much lower than the core and block samples despite the fact that the factor of safety against failure is much greater. It was found that "A" for the tube samples varied in the range 0.27 to 0.55, Table 7.6(c). In figure 7.22 the pore pressure parameter "A" is plotted against the effective stress ratio ($1/_K$) for all tests. A wide scatter of results is evident but it is seen that the general trend is for "A" to decrease as $1/_K$ increases, with the values of "A" in the region of 0.5 to 0.7 for the cores and blocks, while varying from 0.3 to 0.6 for the tube samples. Similar results have been reported by Lal (1971) for Lias clay and by Som (1968) for London Clay from an extensive series of laboratory tests on block samples.

7.6.1.3 Stress-Strain Curves

The axial stress and volumetric strain are plotted against the axial strain in Figure 7.23(a) to (h) indicating the effective axial stress and the strains at the end of each undrained and drained stage of loading.

If a plot is considered passing through the end of the consolidation stages then a stress-strain curve is obtained which is basically similar to the TA3 series with the slope of the curve increasing with increase of the stress level. The points indicating the end of the undrained stage generally fall below the above curve. Test TA1 06 is an exception where the first undrained point falls on the drained graph.

The increase in axial stress is plotted against the axial strain for all tests at the end of the consolidation stages (Figure 7.24). The results show a considerable amount of scatter. However it is observed that the individual sets of results fall on smooth lines of approximately similar slope, and follow the same general trend of increase of slope with increase of stress level. There is no obvious differences between the tube, core and block results as determined in this series.

7.6.1.4 Strain paths

The strain paths are shown in figures 7.23(a) to (h) together with the stress-strain results. It is seen that the strain paths fall below the one dimensional strain path line (i.e. $\varepsilon_v/\varepsilon_a = 1$) with the exception of TA1 06 which lies on this line. The ratio of immediate axial strain (strain at the end of the undrained stage) to the total axial strain (strain at the end

of consolidation) is plotted against the increase of axial stress in Figure 7.25. In the first two increments the undrained deformation accounts for 40 to 50% of the total axial strain for the core and block samples, (Figure 7.25) whereas it accounts for 60-70% for the tube samples. On the third increment, where the magnitude of the increment was increased, the undrained axial strain accounts for 60-70% of the total strain for all types of sample. The slope of the consolidation strain path is observed to be in the region of 1.5 to 1.6 for the core and block samples, with the exception of TA1 04 where the slope is in the region of 1.9. For tube samples the slope is in the region of 1.8 - 1.9 with one exception, TA1 02, where the slope is approximately 1.5.

During the consolidation stage the change of stress is hydrostatic as it is solely due to the dissipation of pore pressure. It is therefore interesting to note that despite considerable undrained deformation the core and block samples yield the same results as the TC series where $\varepsilon_v/\varepsilon_a = 1.55$. However the tube samples give a steeper strain path, which is a rather surprising result as the overall strain ratio from this series and the stress ratio from the TD series is less than for the core samples. This is probably due to the greater undrained deformation of these samples reducing the degree of anisotropy.

The "end of consolidation" strain paths are summarised in Figure 7.26. This emphasises that the overall strain ratio from the tube samples is less than for the core and block samples. It is seen here that the overall strain ratios for the block, core and tube samples are 0.99, 0.86 and 0.61 respectively.

7.6.2 TA2 Series

Four triaxial tests consisting of one block (TA2 01), one tube

(TA2 03) and two core (TA2 02 and 04) samples, were carried out in this series. Samples were initially reconsolidated to a K_o greater than unity, in the order of 1.5 to 1.7. A further core sample was to have been tested at a K_o = 2.5, however the sample sheared in extension during the reconsolidation stage. The samples were then loaded with incremental loadings similar to the TA1 Series. Throughout the tests the stresses, pore pressures and deformations were recorded as described in Chapter 5.

7.6.2.1 Stress Paths

The effective stress paths applied during the tests are shown in figure 7.27(a) to (b) together with the compressions and extension failure envelopes as determined by Lal (1971). It is clear that the undrained stages do not take the samples so close to the failure envelope as in the TA1 series. It may therefore be expected that the immediate deformations will be less than was the case for the TA1 series, this will be discussed later in this section.

7.6.2.2 Pore Pressure Parameter, A

It is seen from the slope of the undrained stress paths that the "A" values are fairly constant. The values generally vary between 0.5 and 0.7, Table 7.7, and are plotted against the effective stress ratio ($1/_K$), together with the results of the TA1 series in Figure 7.22. There is a considerable scatter of results but they generally follow the trend indicated by TA1 series, that "A" decreases with increase of the stress ratio ($1/_K$). The tube sample tends to give lower values of "A" than the other types, as found with the TA1 series.

7.6.2.3 Stress-Strain Relationship

The axial stress-strain relationships are shown in Figure 7.28(a) to (d) and tabulated for the end of each stage condition in Table 7.7. The results show the same general pattern as for the TA1 series with the slope of the 'drained' curve increasing with increase of the stress level. However the undrained deformations are significantly less than in the TA1 series. This trend was expected for the stress paths of this series because the stress ratio ($1/_K$) under the undrained increment was significantly lower than in the TA1 series and hence much less undrained creep would be expected. The results are replotted in the form of axial stress increase ($\Delta\sigma_a$) against axial strain in Figure 7.29. The results show some scatter, although TA2 01 and TA2 04 correlate reasonably well together as do TA2 02 and TA2 03. The general trend for both sets is for the axial deformation modulus M_a to increase with increase of the stress level.

7.6.2.4 Strain Paths

The strain paths in Figures 7.28(a) to (d) are steeper than for the TA1 series, with a strain ratio of approximately unity at the end of the first two drained stages. The ratio of immediate axial deformation to total axial deformation for each stage is shown in Figure 7.30 and increases with increase of applied stress. For the core and block samples the undrained deformation accounts for 30-40% of the axial strain for the first two increments and up to 65% for the final two increments. The tube sample shows a higher proportion of undrained deformation which increases from 44% (for the first increment) to 70% for the two final increments. The ratio of the undrained deformation to total deformation is seen to be less for this type of test, particularly in the early loading stages, the difference between the tube and core samples was

also smaller however as only one tube sample was tested in this series it would be unwise to attach too much significance to this result. The strains at the end of consolidation are replotted in Figure 7.31. There is some scatter of results, however a strain ratio of 0.99 is obtained from TA3 01 and 04 up to an axial strain of 3% which decreases to 0.67 at greater strains. It is seen that the core sample TA2 02 lies above this line with a strain ratio of 1.13, while the tube sample, subsequent to the first increment, lies below. These results indicate that due to the smaller undrained deformation the strain ratio from this series is generally greater than for the TA1 series. The slopes of the strain paths during the consolidation stage, where the stress path is isotropic, is seen to be in the region of 1.5 to 1.6 for the first two stages of TA2 01 (block) and TA2 04 (core) and increasing to approximately 1.75 during the later loading. However the slope of the strains for TA2 02 (core) and TA2 03 (tube) is seen to be greater at 1.70 - 1.90 over the full range of increments. These strain ratios during consolidation are thus seen to be of the same order as for TA1 series with the cores and block samples behaving in the same manner as the cores in the TC series despite the shear deformation during the undrained loading.

7.6.3 Elastic Predictions

The results of the TD and TC series are used to predict the behaviour of the TA1 and TA2 series, and are compared with the observed results.

The results of previous tests have shown that the Lias clay is behaving as an orthotropic linearly "elastic" material during initial loading. For such a material it may be expected that the pore pressure parameter, "A", varies considerably from the isotropic elastic value of one third. Pickering (1970) expressed A in

terms of the orthotropic elastic parameters (7.3.4.2)

$$A = \frac{1-2\,\nu_{hv}}{1-4\nu_{hv}+\frac{2}{n}(1-\nu_{hh})} \qquad (7.6)$$

Thus using the values of n, ν_{hv} and ν_{hh} obtained from TD and TC series on core and block samples the value of A is found to be 0.645 for an effective stress ratio ($1/_K$) less than 2. From the TD series it was seen that the value of ν_{hv} increases to 0.125 at stress ratios greater than 2, while the term ($1-\nu_{hh} - n\nu_{hv}$) remains constant to a stress ratio of up to approximately 4. It would therefore appear that the value of A should reduce to approximately 0.60 for a stress ratio ($1/_K$) of 2 to 4. It is seen in figure 7.22 that the core and block results, with some scatter tend to agree with these values, showing that during undrained loading the material "constants" do not depart seriously from the values obtained from drained tests.

The predicted stress-strain relationship for the end of consolidation condition for each stage is shown in figures 7.24 and 7.29 using E'_v = 17,000, n = 4.7, ν_{hv} = 0.04 and ν_{hh} = -0.38. For the TA1 series this is seen to give a reasonable upper bound fit for the first two increments beyond which the predicted strains are greater than the observed. Similar results are also shown for the TA2 series. A better fit may be obtained if E'_v was expressed as some function of theeffective radial stress; this will be considered later. The undrained axial strain is estimated from the "elastic" constants appropriate to($1/_K$)less than 2 and greater than 2 respectively to be 29% and 40% of the total axial strain.

The effective stress ratios ($1/_K$) is generally greater than 2 for the TA1 series, with the exception, in some cases of the first increments whereas for the TA2 series it is less than two on the

first two increments and then increases to more than 2 in the final stages. It is seen in Figures 7.25 and 30 that for both series this ratio is generally greater than predicted, indicating that the undrained modulus E_u is less than predicted from the drained 'elastic' parameters (Equation 7.5). The error is likely to be less when the undrained loading is not so close to the failure condition.

The slope of the strain paths during consolidation were seen to be equivalent to that of the TC series for the cored and block samples indicating that during consolidation the samples behaved "elastically". The slopes of the strain paths of the tube samples are not predicted well by elastic theory. Using ν_{hv} of 0.17, from the TD series, and assuming that $\frac{1}{n}(1 - \nu_{hh})$ has the same value as determined from the core samples, i.e. 0.293, the predicted strain ratio from equation (7.9) is 1.37. Hence it would appear that $\frac{1}{n}(1-\nu_{hh})$ is also affected by tube sampling.

The predicted strain paths through the "end of consolidation" points are shown in Figures 7.26 and 7.31 for TA1 and TA2 series respectively. The strain ratio is predicted as 1.117 for the core and block samples. It is seen that for the TA1 series all the strain paths fall below the predicted. In the TA2 series the predicted strain path coincides with the TA2 02 while the other tests have a lower strain ratio. It is then seen that the strain ratios are in general not predicted well by the elastic theory. This would appear to be due to the undrained loading stage where samples, particularly in the TA1 series were close to failure, therefore taking the sample beyond its limit of linearity.

7.7 DISCUSSION OF RESULTS

The stress-strain behaviour of block, core and tube samples of Lias clay have been presented for several different loading paths.

An overall analysis of these results is presented below. It was clear from the results presented that the sample disturbance in the tube samples significantly affected the strain paths, although the affect on the axial stress strain-curves appeared to be less serious. The general discussion of results will thus be focused on the core and block samples.

7.7.1 Strain Paths

It has been shown in the previous sections that the volumetric-axial strain relationships are approximately linear and that a change in slope occurs in the region of an effective stress ratio ($1/_K$) of 2. It must be appreciated that the straight line relationships are somewhat idealised interpretation of the test results. However it has been shown, Som (1968), that the strains path for heavily overconsolidated clays can be approximately linear.

Analysis of the individual series of tests has shown that the soil exhibits a high degree of anisotropy. It has further been shown that the "elastic" parameters governing the strain ratios are sensibly constant from one series of tests to another. The values of these constants, for a stress ratio ($1/_K$) less than 2, were determined from the TD and TC series as

$$\nu_{hv} = 0.04, \; \nu_{hh} = -0.3782, \; n = 4.70$$

The relationship between the strain ratio and the incremental stress ratio, $\bar{K}$, for an othotropic elastic material is given by the equation (7.12)

$$\frac{\dot{\varepsilon}_v}{\dot{\varepsilon}_a} = \frac{1 - 2\,\nu_{hv} + 2\bar{K}\left[\frac{1}{n}(1 - \nu_{hh}) - \nu_{hv}\right]}{1 - 2\,\nu_{hv} \cdot \bar{K}}$$

Substituting the above values for the "elastic" constants we attain

$$\frac{\varepsilon_v}{\varepsilon_a} = \frac{0.92 + 2\,\bar{K}\,(0.2532)}{1 - 0.08\,\bar{K}}$$

This relationship has been plotted in Figure 7.32, on which also the strain ratios of individual tests on core and block sample are indicated. It is seen that the strain ratio for two of the three TA3 tests are predicted accurately. The recorded strain ratio for the third test, TA3 01, is higher than the predicted however it was generally found (section 7.5) that this sample deviated somewhat from the other two. Also indicated is the range of the individual strain ratios recorded in the consolidation stages of TA1 and TA2 series, where the final effective stress ratio ($1/_K$) was less than 2. It is seen that they agree reasonably well with the predicted value despite the fact that the samples had experienced considerable undrained deformation prior to consolidation.

It was seen in sections 7.3 and 7.5 that the slope of the strain paths changes in the region of the effective stress ratio ($1/_K$) of 2, for the TDV, TD2 and TA3 series. From the TDV series it is seen that the Poisson's ratio ν_{hv} increases to 0.125. However it appears, from the TDH test that the value of ($1 - \nu_{hh} - n\nu_{hv}$) and the deformation modulus ratio, n, remains reasonably constant up to an effective stress ratio of 4. Thus the strain ratio can be predicted for $1/_K > 2$ using the modified values of the elastic constants, giving

$$\frac{\varepsilon_v}{\varepsilon_a} = \frac{0.75 + 2\bar{K}\,(0.2532)}{1 - 0.25\,\bar{K}}$$

The predicted strain ratio is shown in Figure 7.33, for the range of incremental effective stress ratio between zero and unity. Indicated on this graph are the recorded strain ratios from TDV, TD2, TA3 and the range of strain ratios during the consolidation

stages of TA1 and TA2 series when $(1/K)$ at the end of the consolidation was greater than 2. It is seen that the recorded values generally agree well with the predicted curve, although a large scatter of results was observed for the TA1 and TA2 series. Considering the incremental effective stress ratios ($\bar{K}$) for the strain ratio of unity, i.e. $\bar{K}_o$, it is seen that $\bar{K}_o$ varies from 0.15, for $1/K < 2$, to 0.33 for $1/K > 2$. Som (1968) recorded the effective stress ratio $\bar{K}_o$ in the oedometer apparatus on undisturbed samples of London clay. He demonstrated a similar phenomenon (Figure 7.34), where $\bar{K}_o$ increased from 0.28 to 0.64 at an effective stress ratio $K = \left(\frac{\sigma'_r}{\sigma'_a}\right)$ of 0.64, which remained constant during the remainder of the one dimensional loading. The values predicted from results presented above are lower than recorded for the London clay probably because of the higher degree of anisotropy of the material, requiring less radial restraint to maintain one dimensional deformation.

7.7.2 Stress-Strain Relationship

It has been seen earlier in this chapter that the axial stress-strain relationships for all the test series are approximately linear up to an increment of axial stress of the order of 400 kN/m^2. The mean value of M_a obtained from the plots of $\Delta\sigma'_a$ against ε_a (Figures 7.4(a), 7.15, 7.19, 7.24 and 7.29) are plotted against the incremental stress ratio $\bar{K}$ in Figure 7.35. It is seen that M_a increases from 14.5 MN/m^2 for $\bar{K} = 0$ to 20.0 MN/m^2 for $\bar{K} = 1$ an increase of 38%.

The volumetric deformation modulus M_v was determined from M_a and the observed strain ratios $\varepsilon_v/\varepsilon_a$, as

$$M_v = M_a/(\varepsilon_v/\varepsilon_a) \qquad (7.13)$$

and plotted against $\bar{K}$ in Figure 7.35. In this case it is seen that M_v decreases from 15.7 MN/m^2 for $\bar{K}$ = 0 to 12.9 MN/m^2 for $\bar{K}$ = 1 a reduction of approximately 18%. Hence it is seen that the volumetric deformation modulus is less effected by the radial stress increase than the axial deformation modulus. A similar result was observed by Som (1968) for London clay, where it was observed that the volumetric modulus was independent of the incremental stress ratio $\bar{K}$ in the range 0.7 to 1.0, but the ordinary drained test ($\bar{K}$ = 0) the volumetric deformation modulus was 20 to 40% greater than for $\bar{K}$ = 1. Som's results also indicated that the axial deformation modulus was significantly influenced by the incremental stress ratio.

The theoretical relationships between the deformation moduli, M_a and M_v and the incremental stress ratio $\bar{K}$ are shown in Figure 7.35 using the "elastic" parameters obtained from the observed strain ratios (ν_{hv} = 0.04, ν_{hh} = -0.38 and n = 4.70) and values of E'_v of 14 MN/m^2 and 17 MN/m^2.

It can be seen from figure 7.35 that the observed axial deformation modulus increases far more than predicted by the elastic theory and that M_v decreases less than predicted with increase of $\bar{K}$. As it was observed from the strain ratios that the Poisson ratios ν_{hv}, ν_{hh} and the modulus ratio n were not sensitive to the value of $\bar{K}$ then it appears that E'_v increases with increase of $\bar{K}$ over this range of stresses. The apparent relationship between E'_v and $\bar{K}_o$ is shown in Figure 7.36 and with the limited results available it appears that the increase of E'_v is approximately linear with $\bar{K}$, however it would be necessary to obtain results for other stress ratios before any conclusions can be drawn with regard to this relationship. In order to study the influence of the radial stress increment on the deformation moduli over the full range of stresses

observed the deformation moduli, obtained from increments of stress (Tables 7.2 to 7.7) are plotted as a function of the average axial stress for the increment ($M/(\sigma'_a)av$) against increase of axial stress ($\Delta\sigma'_a$)

The values of $M_a/(\sigma'_a)_{av}$ (equal to m', apparent modulus number) are plotted against the increase of axial stress $\Delta\sigma'_a$ in Figure 7.37 (a) to (e). It is seen that m' decreases with increase of axial stress up to 300 - 400 kN/m^2. Beyond this level, for all tests except for the TD series which ended at an increment of approximately 300 kN/m^2, m' reduces to a very flat slope or becomes constant (Figure 7.36(b) to (e)). The TC series ($\overline{K}$ = 1) shows that m' becomes constant at 50. However the TA1, TA2 and TA3 series does not reduce to a constant value but reduces to a very flat slope with m' decreasing from approximately 30 to 20 over the stress range 400 to 1000 kN/m^2.

The plots of $M_v(\sigma'_a)_{av}$ (m", apparent modulus number) against $\Delta\sigma'_a$ shown in Figures 7.38(a) to (e) indicated a similar relationship to the axial modulus. Again it is seen that m" decreases with increase of axial stress up to a stress increment of approximately 300-400 kN/m^2. Beyond this level, for all tests, again with the exception of TD series, m" is seen to reduce to a constant value despite some scatter of results in the TA1 and TA2 tests particularly. The constant value obtained is seen to be approximately equal for all tests at a value of 32. The TA1 series tends to be a little higher than this even with the core and block samples.

These results indicate that the axial deformation modulus, M_a, is significantly affected by the incremental stress ratio ($\overline{K}$) over the whole range of stress studied, but that the volumetric deformation modulus is not significantly affected by $\overline{K}$ over the range of stress

of 400 to 1000 kN/m^2, although it was slightly affected in the lower stress range. It is also observed that the volumetric deformation modulus M_v is directly proportional to the effective axial stress (σ'_a) above the stress increment of 400 kN/m^2. The axial deformation modulus, M_a, is seen to be a function of the effective axial stress (σ'_a) and the incremental stress ratio $\overline{K}$, in the stress increment range of 400 to 1000 kN/m^2.

The results suggest that within the normal stress increments below a foundation on a heavily overconsolidated clay (i.e. less than 400 kN/m^2) that the soil deforms during loading as a linear orthotropic pseudo elastic material. Although deformation moduli appear to depend on the value of the incremental stress ratio.

7.8 RATE OF CONSOLIDATION

In the triaxial tests where incremental loading was applied initially in the undrained manner - TC, TA1 and TA2 - the rate of consolidation was observed during the consolidation stage. It is not the intention to study the rate of deformation in depth but merely report on observations made.

It will be recalled, Chapter 5, that drainage was prevented in the axial direction by rubber end membranes and drainage was facilitated by vertical filter paper drains on the curved surface. Therefore drainage is in the radial direction only, thus the coefficient of consolidation is that appropriate to the horizontal plane and is designated as C_r. Provision was made for monitoring the pore water pressure at the base of the sample through a hole cut centrally in the end membrane (Chapter 5). Assuming this system worked

efficiently the pore pressure recorded represented the pore pressure in the axis of the sample.

The deformation time relationships are not presented for all the tests, but are illustrated by the results of a core sample from each of the approproate series, (TC 03, TA1 04 and TA2 02) in Figure 7.39(a) to (c) (note that the TA1 and TA2 deformations have been plotted to include the undrained deformation, therefore the axial strain is displaced downward). It is seen from these curves that the undrained deformation experienced by the TA1 and TA2 tests does not significantly affect the slope of the deformation time curves.

The radial coefficient of consolidation, C_r, has been determined for each test from the axial and volumetric strain curves. In each case the final reading of the particular stage was considered to represent 100% consolidation, thus no account is made for secondary consolidation.

The experimental curve was fitted to the theoretical U - T curve for radial consolidation (Carshaw and Jaegar, 1947 , presented by Gibson and Lumb, 1953) at 50% degree of consolidation, using $T_{50} = 0.0650$.

The values of elapsed time at 50% consolidation, t_{50} are tabulated in Table 7.8 for both axial and volumetric curves. It is seen that the value t_{50} obtained from the two curves are generally in close agreement. The coefficient of consolidation C_r is obtained from the mean value of t_{50} from the axial and volumetric strain curves, Table 7.8 and is plotted (Figure 7.40) against the average effective axial stress $(\sigma'_a)_{av}$. The graph shows a considerable scatter of results, although C_r appears to decrease with increase of stress

level, with a mean value decreasing from 0.75×10^{-4} to 0.50×10^{-4} cm^2/sec over the loading range.

The value of the radial coefficient of consolidation obtained from the triaxial series will becompared with the vertical coefficient obtained from the oedometer series in the following chapter.

The pore pressure was recorded as described previously throughout the consolidation stages. In all tests it was observed that the recorded pore pressure registered a significant increase in the early stages after the opening of the drainage valve before dissipating to the level of the applied back pressure. This phenomenon is illustrated with the results from TA1 04, Figure 7.41. It is seen from this graph that the pore pressure peak is reached after 40 to 60 minutes before dissipating to the back pressure. The curves obtained from the first two increments virtually coincide throughout the consolidation stage. The third and fourth stages are again of similar shape although the excess pore pressure is greater due to the greater applied increments of load.

The phonomenon illustrated by these results is known as the Mandel-Cryer effect (Mandel 1950, 1953; Cryer 1963). It was illustrated by these two authors that, according to the Biot theory of three-dimensional consolidation during the early stages of the consolidation process the pore water pressure at the centre of a surface draining soil may experience an increase, prior to subsequent dissipation. The existence of the Mandel-Cryer effect has been verified experimentally on remoulded clays for a consolidating sphere by Gibson et al (1963) and De Jong and Verruijt (1965).

The physical explanation of this phenomenon is that as the pore

water pressure starts to dissipate in the outer layers,which then consolidates,part of the total load tends to be transferred to the inner core of the sample and hence causes a temporary increase of pore pressure. Eventually the pore water starts to drain from the centre of the sample and pore pressure starts to dissipate.

The fact that this increase of pore pressure on the axis was recorded demonstrates that the end membranes were efficient and the pore pressure was recorded over the limit contact area between specimen and pore pressure measuring system.

TABLE 7.1 - EQUILIBRIUM STRESS, σ'_k

Sample Type	Test No	Depth (m)	σ'_k (kN/m^2)	σ'_v (kN/m^2)	σ'_k/σ'_v	w_s	w_i	S_i	B
U 70	TDV.03	1.22	192.01	92.0	2.09	0.162	0.1756	0.9852	0.9277
U 70	TDV.04	5.64	270.48	143.5	1.88	0.184	0.1700	1.0636	0.4836
U 70	TA1.01	1.22	237.68	92.0	2.58	0.205	0.1813	0.9929	0.512
U 70	TA1.02	2.59	358.24	107.9	3.32	0.183	0.1542	0.9157	0.457
U 70	TA1.03	4.11	159.15	125.7	1.27	0.191	0.1742	1.0794	0.988
CORE	TDV.02	1.27	93.84	92.5	1.01	0.175	0.1705	1.0348	0.9587
CORE	TDV.06	4.27	80.06	127.5	0.63	0.164	0.1730	0.9999	0.9837
CORE	TC.01	2.31	124.18	104.7	1.19	0.186	0.1790	1.002	0.838
CORE	TC.03	2.59	127.58	107.9	1.18	0.186	0.1572	0.9725	0.81
CORE	TC.02	2.21	181.74	103.5	1.76	0.186	0.1535	0.9996	0.917
CORE	TA1.04	2.03	95.73	101.4	0.94	0.173	0.1590	0.9791	0.986
CORE	TA1.07	3.66	111.92	120.38	0.93	0.159	0.1525	0.9472	0.92
CORE	TA1.08	5.03	123.2	136.4	0.90	0.184	0.1760	1.0009	0.946
CORE	TA3.03	5.36	116.87	140.2	0.83	0.185	0.1850	0.9685	0.939

TABLE 7.1 (Continued)

Sample Type	Test No	Depth (m)	σ'_k (kN/m^2)	σ'_v (kN/m^2)	σ'_k/σ'_v	w_s	w_i	S_i	B
BLOCK	TDV.01	1.22	91.99	92.0	1.00	0.182	0.1834	0.9915	0.9344
BLOCK	TDH.01	2.13	217.59	102.6	2.12	0.177	0.1720	1.0588	0.9481
BLOCK	TA1.05	1.22	102.2	92.0	1.11	0.182	0.1720	0.9892	0.965
BLOCK	TA1.06	2.13	230.08	102.6	2.24	0.177	0.1543	0.9801	1.055
BLOCK	TA3.01	1.22	94.35	92.0	1.06	0.182	0.1730	0.9933	0.942
BLOCK	TA3.02	1.22	93.94	92.0	1.02	0.182	0.1540	0.8960	0.928
U70	TD2.03	5.56	54.58	142.6	0.38	0.186	0.1420	0.8693	0.632
U70	TA2.03	4.06	147.24	125.12	1.18	0.177	0.1677	0.8337	0.132
CORE	TD2.01	2.31	74.46	104.7	0.71	0.186	0.1734	0.9819	0.976
CORE	TA2.02	1.88	125.04	99.6	1.26	0.196	0.1690	1.0319	1.104
CORE	TA2.04	3.73	75.13	121.27	0.62	0.164	0.1740	1.0071	0.688
BLOCK	TD2.02	1.22	56.77	92.0	0.62	0.182	0.1737	1.0008	1.007
BLOCK	TA2.01	1.72	65 85	92.0	0.72	0.182	0.1850	1.0081	1.051

TABLE 7.2 COMPRESSIBILITY TDV SERIES

(a)

Test No TDV 01 BLOCK

σ'_a kN/m^2	σ'_r kN/m^2	$\Delta\sigma'_a$ kN/m^2	ε_a	ε_v	M_a kN/m^2	M_v kN/m^2
130	130					
175	130	45	0.0038	0.0036	11842	12500
250	130	120	0.0112	0.0101	10135	11538
325	130	195	0.0197	0.0158	8941	13333
RELOAD						
144	130	ZERO	0.0082	0.0070		
175	130	31	0.0102	0.0082	15500	24800
250	130	106	0.0148	0.0122	16304	18987
325	130	181	0.0200	0.0159	14423	20270
400	130	256	0.0279	0.0201	9494	17857
450	130	306	0.0339	0.0222	8333	23810

TABLE 7.2 COMPRESSIBILITY TDV SERIES

(b)

Test No. TDV 02 CORE

σ'_a kN/m^2	σ'_r kN/m^2	$\Delta\sigma'_a$ kN/m^2	ε_a	ε_v	M_a kN/m^2	M_v kN/m^2
140	140					
200	140	60	0.0048	0.0043	12500	13953
275	140	135	0 0098	0.0089	15000	16304
350	140	210	0.0149	0.0132	14706	17442
455	140	315	0.0225	0.0185	13815	19811
RELOAD						
148	140	ZERO	0.0086	0.0055		
200	140	52	0.0103	0.0073	30588	28889
275	140	127	0.0140	0.0107	20270	22059
350	140	202	0.0176	0.0137	20833	25000
450	140	302	0.0223	0.0177	21277	25000
550	140	402	0.0279	0.0213	17858	27778
650	140	502	0.0338	0.0247	16949	29412
750	140	602	0.0397	0.0270	16949	43478
850	140	702	0.0459	0.0284	16129	71428

TABLE 7.2 COMPRESSIBILITY TDV SERIES

(c)

Test No. TDV 03 U70						
σ'_a kN/m^2	σ'_r kN/m^2	$\Delta\sigma'_a$ kN/m^2	ε_a	ε_v	M_a kN/m^2	M_v kN/m^2
132	132					
200	132	68	0.0059	0.0034	11525	20000
275	132	143	0.0123	0.0068	11719	22388
350	132	218	0.0199	0.0087	9868	38461
RELOAD						
157	132	ZERO	0.0086	0.0005		
200	132	43	0.0113	0.0024	11781	22632
275	132	118	0.0158	0.0058	16483	22059
350	132	193	0.0214	0.0088	13393	25000
420	132	263	0.0134	0.0107	10000	36842

TABLE 7.2 COMPRESSIBILITY TDV SERIES

(d)

Test No TDV 04 U70						
σ'_a kN/m^2	σ'_r kN/m^2	$\Delta\sigma'_a$ kN/m^2	ε_a	ε_v	M_a kN/m^2	M_v kN/m^2
145	145					
200	145	55	0.0032	0.0018	17187	30555
300	145	155	0.0090	0.0052	17241	29411
400	145	255	0.0149	0.0083	16949	32258
460	145	315	0.0193	0.0100	13636	35294
RELOAD						
158	145	ZERO	0.0058	-0.0012		
200	145	42	0.0077	0.0002	22105	30000
300	145	142	0.0126	0.0039	20408	27027
400	145	242	0.0172	0.0074	21739	28571
500	145	342	0.0220	0.0102	20833	35714
600	145	442	0.0278	0.0125	17241	43478
700	145	542	0.0334	0.0135	17857	100000

TABLE 7.2 COMPRESSIBILITY TDV SERIES

(e)

Test No. TDV 06 CORE						
σ'_a kN/m^2	σ'_r kN/m^2	$\Delta\sigma'_a$ kN/m^2	ε_a	ε_v	M_a kN/m^2	M_v kN/m^2
200	200					
250	200	50	0.0028	0.0025	17857	20000
350	200	150	0.0093	0.0085	15385	16666
457	200	257	0.0195	0.0143	13049	18448
RELOAD						
208	200	ZERO	0.0096	0.0075		
250	200	42	0.0105	0.0085	46666	2038
350	200	142	0.0135	0.0109	33333	1111
450	200	242	0.0178	0.0143	23256	581
544	200	336	0.0299	0.0192	7768	156

TABLE 7.3 COMPRESSIBILITY TD2 SERIES

(a)

Test No. TD2 01 CORE						
σ'_a kN/m^2	σ'_r kN/m^2	$\Delta\sigma'_a$ kN/m^2	ε_a	ε_v	M_a kN/m^2	M_v kN/m^2
98	171					
L35	171	37	0.0012	0.0014	30833	26429
170	171	72	0.0040	0.0042	12500	12500
225	171	127	0.0108	0.0101	8088	9322
303	171	205	0.0206	0.0187	7959	9070
RELOAD						
135	171	ZERO	0.0096	0.0086		
170	171	35	0.0108	0.0108	15909	15909
225	171	90	0.0151	0.0143	15714	15714
300	171	165	0.0208	0.0188	16667	16667
400	171	265	0.0288	0.0246	17241	17241
500	171	365	0.0378	0.0298	19231	19231
600	171	465	0.0460	0.0338	25000	25000

TABLE 7.3 COMPRESSIBILITY TD2 SERIES

(b)

Test No. TD2 02 BLOCK						
σ'_a kN/m^2	σ'_r kN/m^2	$\Delta\sigma'_a$ kN/m^2	ε_a	ε_v	M_a kN/m^2	M_v kN/m^2
103	174					
135	174	32	0.0012	0.0018	26666	17778
175	174	72	0.0034	0.0051	18182	12121
250	174	147	0.0097	0.0123	11905	10416
325	174	222	0.0166	0.0194	10870	10563
RELOAD						
125	174					
175	174	50	0.0063	0.0102	27778	21739
250	174	125	0.0110	0.0153	15957	14706
325	174	200	0.0163	0.0202	14151	15306
400	174	275	0.0220	0.0249	13158	15957
500	174	375	0.0297	0.0292	12987	23256

TABLE 7.3 COMPRESSIBILITY TD2 SERIES

(c)

Test No. TD2 03 U70						
σ'_a kN/m^2	σ'_r kN/m^2	$\Delta\sigma'_a$ kN/m^2	ε_a	ε_v	M_a kN/m^2	M_v kN/m^2
200	335					
270	335	70	0.0014	0.0014	50000	50000
340	335	140	0.0041	0.0040	25926	26923
400	335	200	0.0068	0.0062	22222	27273
475	335	275	0.0103	0.0090	21428	26786
550	335	350	0.0142	0.0115	19231	30000
640	335	440	0.0192	0.0142	18000	33333
RELOAD						
208	335	ZERO	0.0008	0.0016		
270	335	62	0.0022	0.0030	44286	14286
340	335	132	0.0048	0.0050	17500	35000
400	335	192	0.0077	0.0074	20690	25000
475	335	267	0.0112	0.0010	21429	28846
550	335	342	0.0150	0.0121	19737	35714
650	335	442	0.0197	0.0145	21277	41667
750	335	542	0.0247	0.0164	20000	52631
850	335	642	0.0306	0.0179	16949	66666
950	335	742	0.0398	0.0178	10869	-

TABLE 7.4 COMPRESSIBILITY TC SERIES

(a)

Stage	σ_r kN/m²	σ'_r kN/m²	u kN/m²	$\Delta\delta'_r$ kN/m²	ε_a	ε_v	M_a kN/m	M_v kN/m
Test No TC 01 CORE								
Consol	310.3	130.2	180.1					
Undr.	413.7	151.4	262.3					
Drain	413.7	222.0	191.7	92	0.01110	0.01376	8288	6686
Undr.	517.1	279.5	237.6					
Drain	517.1	292.9	224.2	162	0.01800	0.02582	10145	5804
Undr.	758.5	406.9	351.6					
Drain	758.5	552.3	206.2	422	0.02996	0.04591	21739	12942
Test No.TC 02 CORE								
Consol	398.1	177.3	220.8					
Undr.	564.6	193.4	371.2					
Drain	564.6	339.6	225.0	162	0.00760	0.01200	21316	13500
Undr.	895.3	361.6	533.7					
Drain	895.3	670.5	224.8	493	0.02089	0.03201	24906	16542
Undr.	1124.8	684.4	440.4					
Drain	1124.8	890.4	234.4	713	0.02669	0.04099	36066	24499

TABLE 7.4 COMPRESSIBILITY TC SERIES

(b)

Test No. TC 03 CORE								
Stage	σ_r kN/m^2	σ'_r kN/m^2	u kN/m^2	$\Delta\delta'_r$ kN/m^2	ε_a	ε_v	M_a kN/m^2	M_v kN/m^2
Consol	201.3	127.6	73.7					
Undr.	401.2	144.1	257.1					
Drain	401.2	172.8	228.4	45	0.00185	0.00318	24324	14151
Undr.	546.6	178.0	386.6					
Drain	564.6	342.6	222.0	215	0.01165	0.01905	17347	10712
Undr.	728.5	341.9	386.6					
Drain	728.5	502.9	225.6	375	0.01926	0.03057	21025	13889
Undr.	928.5	507.3	421.2					
Drain	928.5	695.6	232.9	568	0.02558	0.04081	30979	18848

TABLE 7.5 COMPRESSIBILITY TA3 SERIES

(a)

Test No. TA3 01 BLOCK							
σ'_a kN/m^2	σ'_r kN/m^2	$\Delta\sigma'_a$ kN/m^2	$\Delta\sigma'_r$ kN/m^2	ε_a	ε_v	M_a kN/m^2	M_v kN/m^2
136.5	136.5						
250	164	113.5	27.5	0.0088	0.0110	12878	10318
350	189	213.5	52.5	0.0145	0.0160	17544	20000
450	220	313.5	83.5	0.0190	0.0175	22222	66666
550	257	413.5	120.5	0.0250	0.0177	16667	-
600	287	463.5	150.5	0.0300	0.0177	10000	-

TABLE 7.5 COMPRESSIBILITY TA3 SERIES

(b)

Test No. TA3 BLOCK							
σ'_a kN/m^2	σ'_r kN/m^2	$\Delta\sigma'_a$ kN/m^2	$\Delta\sigma'_r$ kN/m^2	ε_a	ε_v	M_a kN/m^2	M_v kN/m^2
136.0	136.0						
250	176	114	40	0.0089	0.0103	12809	11068
350	209	214	73	0.0160	0.0174	14084	13158
450	237	314	101	0.0224	0.0252	15151	13699
550	263	414	127	0.0285	0.0312	10949	16667
650	288	514	152	0.0340	0.0365	18182	18868
750	313	614	177	0.0388	0.0409	20033	22727
850	338	714	202	0.0430	0.0449	23810	25000
950	366	814	230	0.0466	0.0480	30303	32258
1050	398	914	262	0.0497	0.0509	32258	34483
1150	427	1014	291	0.0530	0.0537	30303	35714

TABLE 7.5 COMPRESSIBILITY TA3 SERIES

(c)

Test No. TA3 03 CORE							
σ'_a kN/m^2	σ'_r kN/m^2	$\Delta\sigma'_a$ kN/m^2	$\Delta\sigma'_r$ kN/m^2	ε_a	ε_v	M_a kN/m^2	M_v kN/m^2
231.4	231.4						
350	270	118.6	38.6	0.0082	0.0075	14463	15813
450	306	218.6	74.6	0.0150	0.0145	16129	14286
550	337	318.6	105.6	0.0210	0.0205	16669	16667
650	364	418.6	132.6	0.0264	0.0260	18518	18182
750	389	518.6	157.6	0.0309	0.0302	22222	23809
850	415	618.6	183.6	0.0350	0.0341	21390	25641
950	444	718.6	212.6	0.0390	0.0376	25000	28571
1050	472	818.6	240.6	0.0428	0.0411	26316	28571
1150	496	918.6	264.6	0.0467	0.0439	25641	35714
1250	518	1018.6	286.6	0.0511	0.0462	22727	45478

TABLE 7.6 COMPRESSIBILITY - TA1 SERIES

(a)

Test No. TA1 01 U70										
Stage	σ'_a kN/m^2	σ'_r kN/m^2	u kN/m^2	$\delta\sigma_a$ kN/m^2	$\delta\sigma_r$ kN/m^2	A	ε_a	ε_v	M_a kN/m^2	M_v kN/m^2
Consol	247.4	247.4	314.3							
Undr.	356.2	207.4	420.5	108.8	-40.0	0.2688	0.00995			
Drain	459.3	310.5	317.4	211.9	63.1		0.01403	0.00766	15099	27670
Undr.	524.3	241.2	459.4	65.0	-69.3	0.5116	0.01899			
Drain	662.4	379.3	321.3	203.1	68.8		0.02443	0.01688	19531	22014
Undr.	806.4	309.4	497.0	144.0	-69.9	0.3268	0.03579			
Drain	989.4	492.4	314.0	327.0	113.1		0.04079	0.02611	19996	35442
Undr.	1115.0	404.8	502.7	125.6	-87.6	0.4109	0.05118			
Drain	1307.1	594.9	312.6	317.7	102.5		0.05539	0.03379	21759	41359

TABLE 7.6 COMPRESSIBILITY - TA1 SERIES

(b)

Test No. TA1 02 U70										
Stage	σ'_a kN/m^2	σ'_r kN/m^2	u kN/m^2	$\delta\sigma_a$ kN/m^2	$\delta\sigma_r$ kN/m^2	A	ε_a	ε_v	M_a kN/m^2	M_v kN/m^2
Consol	332.3	332.3	277.1							
Undr.	409.5	265.5	399.6	75.2	-66.8	0.4704	0.00609			
Drain	524.2	385.5	278.6	191.9	53.2		0.00964	0.00526	19900	36469
Undr.	589.1	306.0	426.6	64.9	-79.5	0.5506	0.01500			
Drain	732.5	451.7	280.9	208.3	66.2		0.01933	0.01159	21510	32904
Undr.	853.3	356.2	481.3	120.8	-95.5	0.4415	0.02714			
Drain	1050.2	560.1	277.4	317.7	108.4		0.03157	0.01886	25946	43725
Undr.	1160.4	455.9	458.4	110.2	-104.2	0.4860	0.03734			
Drain	1328.8	632.6	281.7	278.6	72.5		0.04017	0.02361	52403	58646

TABLE 7.6 COMPRESSIBILITY - TA1 SERIES

(c)

Test No. TA1 03 U70

Stage	σ'_a kN/m^2	σ'_r kN/m^2	u kN/m^2	$\delta\sigma_a$ kN/m^2	$\delta\sigma_r$ kN/m^2	A	ε_a	ε_v	M_a kN/m^2	M_v kN/m^2
Consol	161.9	161.9	305.4							
Undr.	249.8	110.3	423.6	87.9	-51.6	0.3699	0.00957			
Drain	369.7	229.8	304.0	208.8	67.9		0.01601	0.01171	13042	17831
Undr.	457.3	172.2	430.5	87.6	-57.6	0.3967	0.02362			
Drain	595.3	312.7	290.0	225.6	82.9		0.02856	0.02125	17976	23648
Undr.	736.7	242.5	459.0	141.4	-70.2	0.3318	0.04500			
Drain	890.6	398.0	301.5	295.3	86.3		0.04866	0.03070	14692	31249
Undr.	1021.8	324.8	483.1				0.05965	Sheared		

TABLE 7.6 COMPRESSIBILITY - TA1 SERIES

(d)

Test No. TA1 04 CORE										
Stage	σ'_a kN/m^2	σ'_r kN/m^2	u kN/m^2	$\delta\sigma_a$ kN/m^2	$\delta\sigma_r$ kN/m^2	A	ε_a	ε_v	M_a kN/m^2	M_v kN/m^2
Consol	97.8	97.8	302.8							
Undr.	180.4	45.2	422.6	82.6	-52.6	0.3891	0.00969			
Drain	299.9	165.1	302.7	202.1	67.3		0.01709	0.01413	11825	14303
Undr.	376.0	110.1	424.1	76	-55	0.4198	0.02310			
Drain	509.7	242.8	291.3	209.8	77.7		0.02894	0.02470	17407	19566
Undr.	612.1	143.3	491.2	102.4	-99.5	0.4928	0.03854			
Drain	812.8	343.3	291.2	303.1	100.5		0.04458	0.03604	18816	26064
Undr.	886.9	264.0	492.8	74.1	-100.7	0.5761	0.04813			
Drain	1083.3	438.0	298.8	270.5	94.7		0.05287	0.04448	31162	30878

TABLE 7.6 COMPRESSIBILITY - TA1 SERIES

(e)

Test No. TA1 05 BLOCK										
Stage	σ'_a kN/m^2	σ'_r kN/m^2	u kN/m^2	$\delta\sigma_a$ kN/m^2	$\delta\sigma_r$ kN/m^2	A	ε_a	ε_v	M_a kN/m^2	M_v kN/m^2
Consol	136.5	136.5	298.9							
Undr.	187.8	53.0	445.7	51.3	-83.5	0.6194	0.00924			
Drain	334.2	200.1	298.7	197.7	63.6		0.02174	0.01969	9092	10039
Undr.	386.2	115.4	452.8	54.0	-84.7	0.6107	0.02767			
Drain	536.6	267.0	301.2	202.4	66.9		0.03632	0.03324	13556	14659
Undr.	629.6	151.1	514.7	93.0	-115.9	0.5548	0.04623			
Drain	849.3	368.0	279.8	312.7	101		0.05358	0.004602	17448	23633
Undr.	934.4	252.6	512.1	85.1	-115.4	0.5756	0.05839			
Drain	1137.1	454.0	310.8	287.8	86.0		0.06317	0.05469	28382	316953

TABLE 7.6 COMPRESSIBILITY - TA1 SERIES

(f)

Test No. TA1 06 BLOCK

Stage	σ'_a kN/m²	σ'_r kN/m²	u kN/m²	$\delta\sigma_a$ kN/m²	$\delta\sigma_r$ kN/m²	A	ε_a	ε_v	M_a kN/m²	M_v kN/m²
Consol	144.6	144.6	290.3							
Undr.	224.3	93.0	403.6	79.7	-50.4	0.3874	0.00487			
Drain	337.6	211.7	284.9	193.0	67.1		0.01130	0.01067	16921	17920
Undr.	387.1	117.0	447.5	49.5	-94.7	0.6567	0.01469			
Drain	537.2	269.7	294.9	199.6	58.0		0.02264	0.02219	17397	17143
Undr.	624.2	151.2	511.8	87.0	-118.5	0.5766	0.02673			
Drain	852.4	380.8	282.2	315.2	111.1		0.03423	0.03346	26575	27359
Undr.	920.2	242.4	521.8	67.8	-138.4	0.6712	0.03688			
Drain	1147.2	474.2	290.0	294.8	93.4		0.04246	0.04161	36443	34973

TABLE 7.6 COMPRESSIBILITY - TA1 SERIES

(g)

Test No. TA1 07 CORE										
Stage	σ'_a kN/m^2	σ'_r kN/m^2	u kN/m^2	$\delta\sigma_a$ kN/m^2	$\delta\sigma_r$ kN/m^2	A	ε_a	ε_v	M_a kN/m^2	M_v kN/m^2
Consol	212.0	212.0	222.1							
Undr.	251.6	125.1	372.1	39.6	-86.9	0.6870	0.00782			
Drain	397.9	272.8	224.4	185.9	60.8		0.01728	0.01397	10778	13332
Undr.	440.7	184.5	379.5	42.8	-88.3	0.6735	0.02343			
Drain	604.5	348.6	215.4	206.6	75.8		0.03083	0.02529	14991	17995
Undr.	671.1	212.1	415.0	66.6	-136.5	0.6721	0.04035			
Drain	833.9	373.3	253.8	229.4	24.7		0.04568	0.03409	14964	25404
Undr.	935.8	286.6	443.4	101.9	-86.7	0.4597	0.0r187			
Drain	1155.1	508.7	221.2	321.2	135.4		0.05949	0.04198	22186	39321

TABLE 7.6 COMPRESSIBILITY - TA1 SERIES

(h)

Test No. TA1 08 CORE

Stage	σ'_a kN/m^2	σ'_r kN/m^2	u kN/m^2	$\delta\sigma_a$ kN/m^2	$\delta\sigma_r$ kN/m^2	A	ε_a	ε_v	M_a kN/m^2	M_v kN/m^2
Consol	228.0	228.0	228.0							
Undr.	283.3	152.0	379.7	55.3	-76	0.5788	0.00814			
Drain	437.9	307.3	224.4	209.9	79.3		0.01817	0.01593	11552	13176
Undr.	468.4	201.5	394.0	30.5	-105.8	0.7762	0.02454			
Drain	639.8	374.6	220.9	201.9	67.3		0.03189	0.02789	14723	16889
Undr.	710.4	246.0	453.2	70.6	-128.6	0.6456	0.04754			
Drain	937.2	471.1	228.1	298.4	96.5		0.05422	0.03991	13363	24825
Undr.	1005.0	352.3	448.2	Sheared			0.06530			

TABLE 7.7 COMPRESSIBILITY - TA2 SERIES

(a)

Test No. TA2 01 BLOCK										
Stage	σ'_a kN/m²	σ'_r kN/m²	u kN/m²	$\delta\sigma_a$ kN/m²	$\delta\sigma_r$ kN/m²	A	ε_a	ε_v	M_a kN/m²	M_v kN/m²
Consol	107.7	179.3	269.0							
Undr.	162.9	99.5	4.7.8	55.2	-79.8	0.5911	0.00539			
Drain	307.3	238.8	278.5	199.6	59.5		0.01607	0.01686	12420	11839
Undr.	353.2	154.0	435.8	45.9	-84.8	0.6488	0.02179			
Drain	507.2	312.9	276.8	199.9	74.1		0.03071	0.03049	13654	14666
Undr.	587.4	194.8	494.9	80.20	-118.1	0.5956	0.04266			
Drain	813.4	410.9	278.9	306.2	98.0		0.04923	0.04192	16533	26789
Undr	886.0	305.2	492.9	72.6	-105.7	0.5928	0.05770			
Drain	1099.4	515.4	282.7	286.0	104.5		0.06257	0.05066	21439	32723

TABLE 7.7 COMPRESSIBILITY - TA2 SERIES

(b)

Test No. TA2 02 CORE										
Stage	σ'_a kN/m^2	σ'_r kN/m^2	u kN/m^2	$\delta\sigma_a$ kN/m^2	$\delta\sigma_r$ kN/m^2	A	ε_a	ε_v	M_a kN/m^2	M_v kN/m^2
Consol	123.0	189.1	249.8							
Undr.	186.5	106.1	399.1	63.5	-83.0	0.5666	0.00417			
Drain	341.6	275.1	230.1	218.6	86.0		0.01342	0.01583	15808	13401
Undr.	387.6	184.5	385.9	46.0	-90.6	0.6633	0.07739			
Drain	552.6	328.7	241.7	211.0	53.6		0.02426	0.02750	19166	17793
Undr.	643.2	239.5	431.3	90.6	-89.2	0.4961	0.03089			
Drain	846.8	433.3	237.5	294.2	104.6		0.03762	0.03952	21519	23800
Undr.	936.1	331.1	347.4	89.3	-102.2	0.5337	0.04150			
Drain	117.1	518.4	250.1	270.9	85.1		0.04605	0.04741	30927	32999

TABLE 7.7 COMPRESSIBILITY - TA2 SERIES

(c)

Test No. TA2 03 U70										
Stage	σ'_a kN/m^2	σ'_r kN/m^2	u kN/m^2	$\delta\sigma_a$ kN/m^2	$\delta\sigma_r$ kN/m^2	A	ε_a	ε_v	M_a kN/m^2	M_v kN/m^2
Consol	189.5	272.7	238.8							
Undr.	241.5	199.7	371.4	52.0	-73.0	0.5840	0.00416			
Drain	357.6	331.8	239.3	168.1	59.1		0.00948	0.00986	17722	17049
Undr.	409.0	253.4	384.3	51.4	-78.4	0.6040	0.01567			
Drain	563.9	396.0	241.7	206.3	64.2		0.02118	0.07878	18636	23128
Undr.	670.1	312.5	425.0	106.2	-93.5	0.4402	0.03323			
Drain	862.8	502.0	235.5	298.9	106.0		0.03791	0.02766	17866	33660
Undr.	949.5	417.4	418.8	86.7	-84.6	0.4939	0.04638			
Drain	1154.6	597.1	239.1	291.8	95.1		0.04034	0.03503	23475	39593

TABLE 7.7 COMPRESSIBILITY - TA2 SERIES

(d)

Test No TA2 04 CORE										
Stage	σ'_a kN/m^2	σ'_r kN/m^2	u kN/m^2	$\delta\sigma_a$ kN/m^2	$\delta\sigma_r$ kN/m^2	A	ε_a	ε_v	M_a kN/m^2	M_v kN/m^2
Consol	235.1	339.4	167.0							
Undr.	282.8	240.0	331.2	47.5	-99.4	0.6757	0.00663			
Drain	442.2	400.2	171.0	206.9	60.8		0.01803	0.01765	11481	11728
Undr.	480.6	315.1	320.9	38.4	-85.1	0.6891	0.02282			
Drain	632.9	471.5	164.5	190.7	71.3		0.03037	0.02925	15454	16440
Undr.	716.4	354.0	374.6	83.5	-112.5	0.5740	0.04111			
Drain	904.5	549.4	184.2	271.9	77.9		0.04735	0.04042	15013	24342
Undr.	938.6	404.6	430.2	33.8	-144.8	0.8108	0.05521			
Drain	1170.5	641.4	193.4	265.7	92.0		0.06076	0.04952	19814	28266

TABLE 7.8 - COEFFICIENT OF CONSOLIDATION

Test No (Sample)	Stress Range kN/m^2	$(t_{50})_a$ min	$(t_{50})_v$ min	$(t_{50})_m$ min	C_r cm^2/sec
TC.01	130-222	195	220	207	0.64×10^{-4}
(Core)	222-293	300	325	312	0.43×10^{-4}
	293-552	430	435	432	0.32×10^{-4}
TC.02	177-340	255	190	222	0.61×10^{-4}
(Core)	340-670	165	145	155	0.86×10^{-4}
	670-894	230	170	200	0.66×10^{-4}
TC.03	172-342	115	90	102	1.31×10^{-4}
(Core)	342-503	145	145	145	0.92×10^{-4}
	503-696	170	170	170	0.70×10^{-4}
TA1.01	247-459	170	152	161	0.83×10^{-4}
(U70)	459-662	150	152	151	0.88×10^{-4}
	662-989	170	165	167	0.79×10^{-4}
	989-1307	230	200	215	0.62×10^{-4}
TA1.02	332-524	170	165	167	0.79×10^{-4}
(U70)	524-732	185	175	170	0.78×10^{-4}
	732-1050	190	185	187	0.71×10^{-4}
	1050-1328	215	205	210	0.63×10^{-4}
TA1.03	162-370	170	160	165	0.80×10^{-4}
(U70)	370-595	210	200	205	0.64×10^{-4}
	595-890	285	370	327	0.45×10^{-4}

TABLE 7.8 (Continued)

Test No (Sample)	Stress Range kN/m²	$(t_{50})_a$ min	$(t_{50})_v$ min	$(t_{50})_m$ min	C_r cm²/sec
TA1.04	98-300	230	215	222	0.60×10^{-4}
(Core)	300-510	260	240	250	0.53×10^{-4}
	510-813	325	295	310	0.43×10^{-4}
	813-1083	420	420	420	0.32×10^{-4}
TA1.05	137-334	160	143	151	0.88×10^{-4}
(Block)	334-537	200	177	188	0.71×10^{-4}
	537-849	200	183	191	0.69×10^{-4}
	849-1137	230	127	178	0.75×10^{-4}
TA1.06	145- 338	132	83	107	1.24×10^{-4}
(Block)	338- 537	160	150	155	0.86×10^{-4}
	537- 852	170	140	155	0.86×10^{-4}
	852-1147	194	180	187	0.71×10^{-4}
TA1.07	212- 398	350	320	335	0.40×10^{-4}
(Core)	398- 604	440	430	435	0.31×10^{-4}
	604- 844	550	500	525	0.25×10^{-4}
	844-1155	500	640	570	0.23×10^{-4}
TA1.08	228- 438	270	263	266	0.50×10^{-4}
(Core)	438- 640	275	300	288	0.46×10^{-4}
	640- 937	335	340	337	0.39×10^{-4}

TABLE 7.8 (Continued)

Test No (Sample)	Stress Range kN/m^2	$(t_{50})_a$ min	$(t_{50})_v$ min	$(t_{50})_m$ min	C_r cm^2/sec
TA2.01	108-307	225	210	217	0.61×10^{-4}
(Block)	307-507	345	330	337	0.39×10^{-4}
	507-813	440	440	440	0.30×10^{-4}
	815-1099	600	580	590	0.22×10^{-4}
TA2.02	123-342	170	170	170	0.78×10^{-4}
(core)	342-553	220	230	225	0.59×10^{-4}
	553-847	260	270	265	0.50×10^{-4}
	847-1118	320	300	310	0.43×10^{-4}
TA2.03	190-358	90	95	92	1.44×10^{-4}
(U70)	358-564	112	106	109	1.22×10^{-4}
	564-863	130	122	126	1.05×10^{-4}
	863-1155	240	235	237	0.56×10^{-4}
TA2.04	235-442	250	365	357	0.37×10^{-4}
(Core)	442-633	600	835	717	0.19×10^{-4}
	635-905	680	900	790	0.17×10^{-4}
	905-1170	1080	1150	1115	0.12×10^{-4}

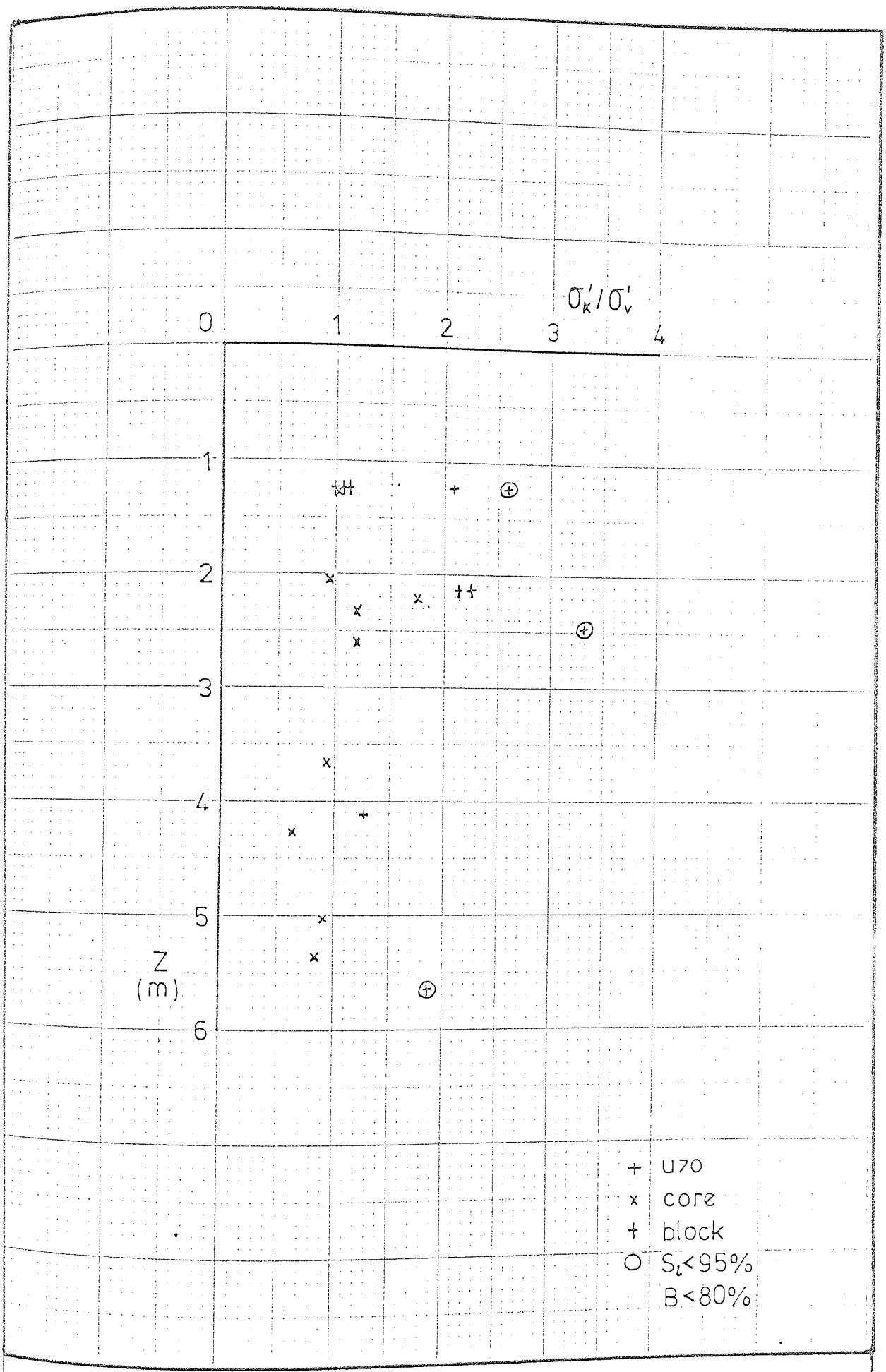

σ'_k/σ'_v vs Depth

FIG. 7.1

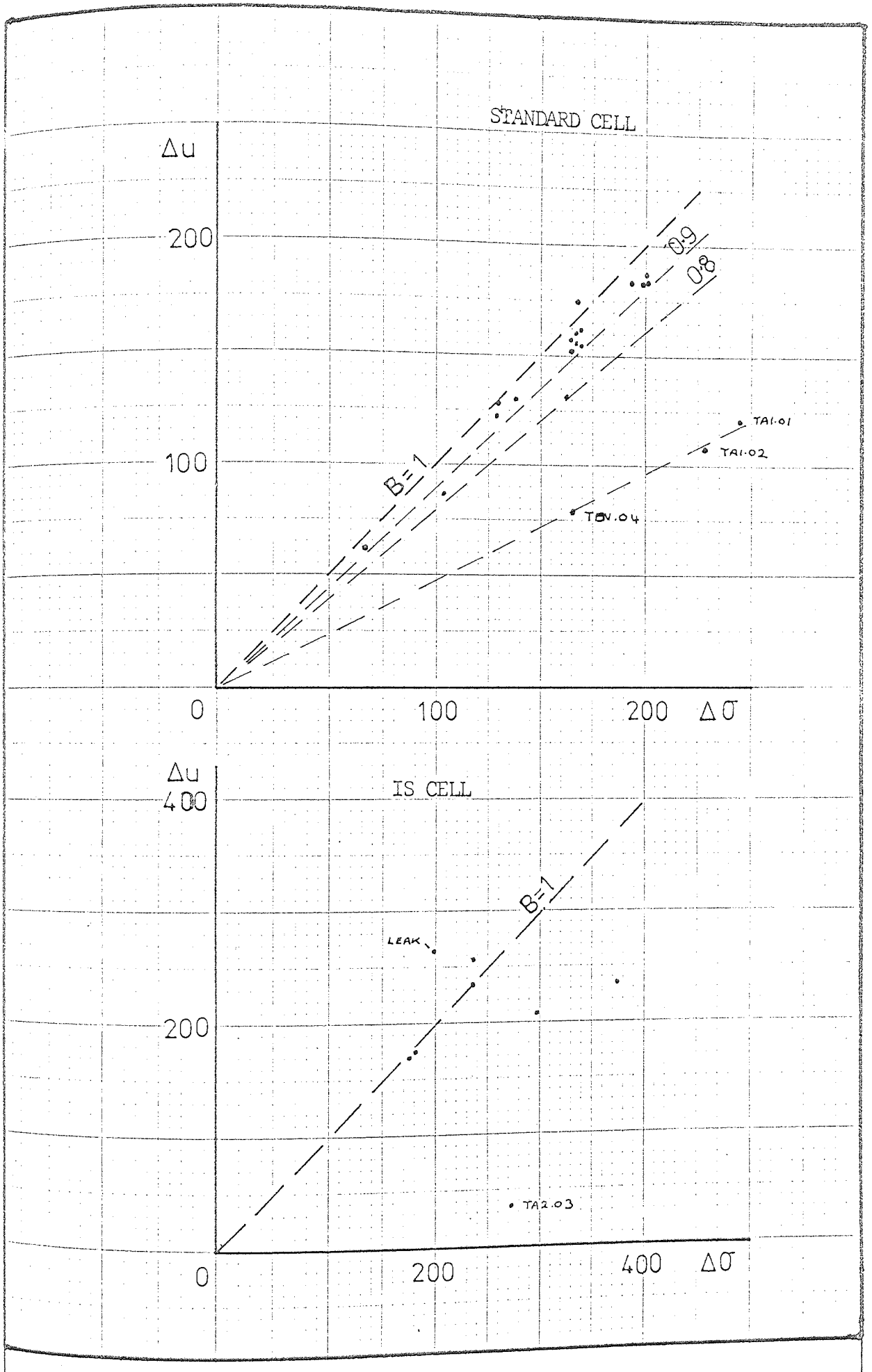

Change in Pore Pressure due to Change in Cell Pressure FIG. 7.2

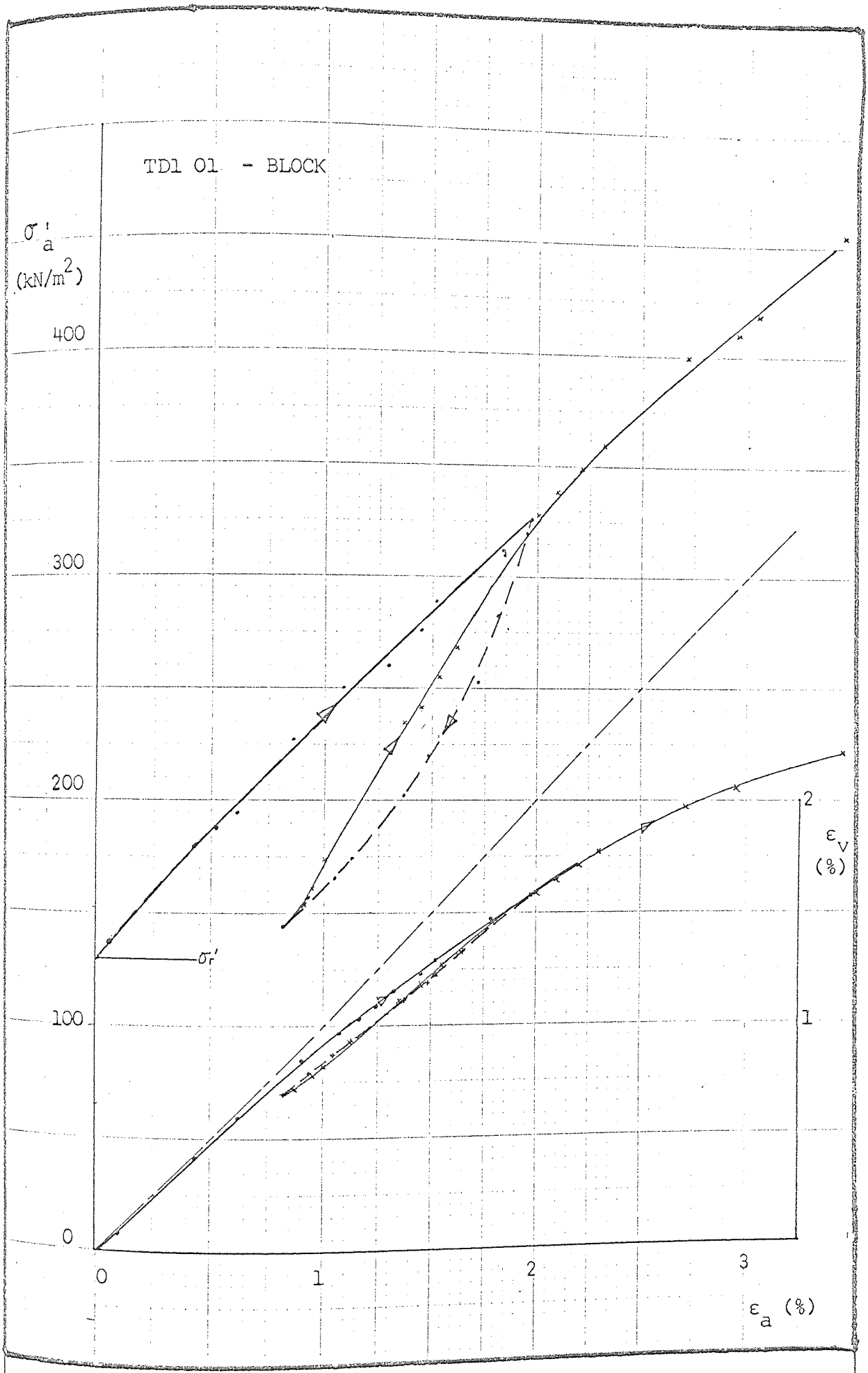

Axial Stress and Volumetric Strain vs Axial Strain - TDV Series

FIG. 7.3(a)

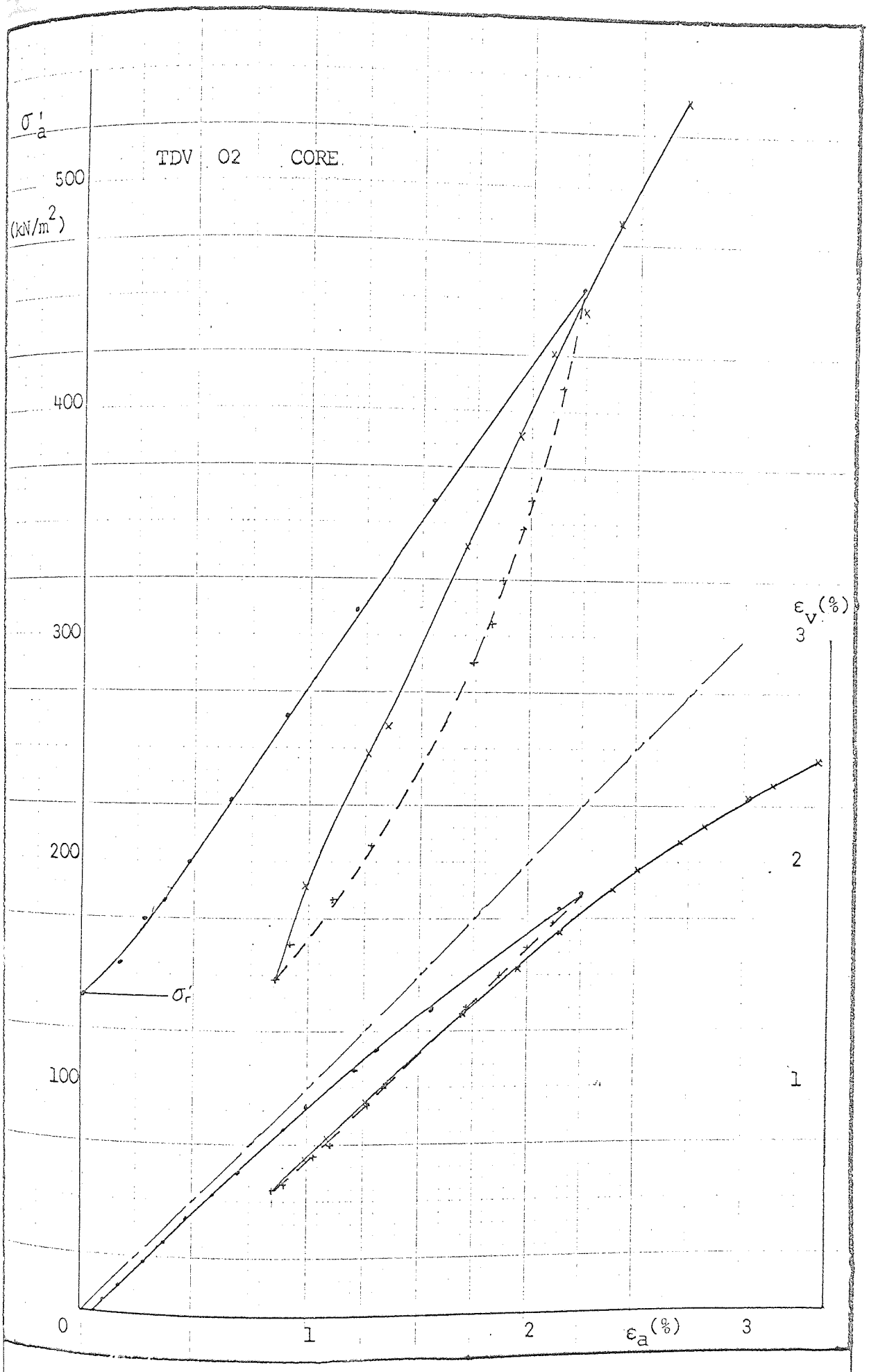

Axial Stress and Volumetric Strain vs Axial Strain - TDV Series

FIG. 7.3(b)

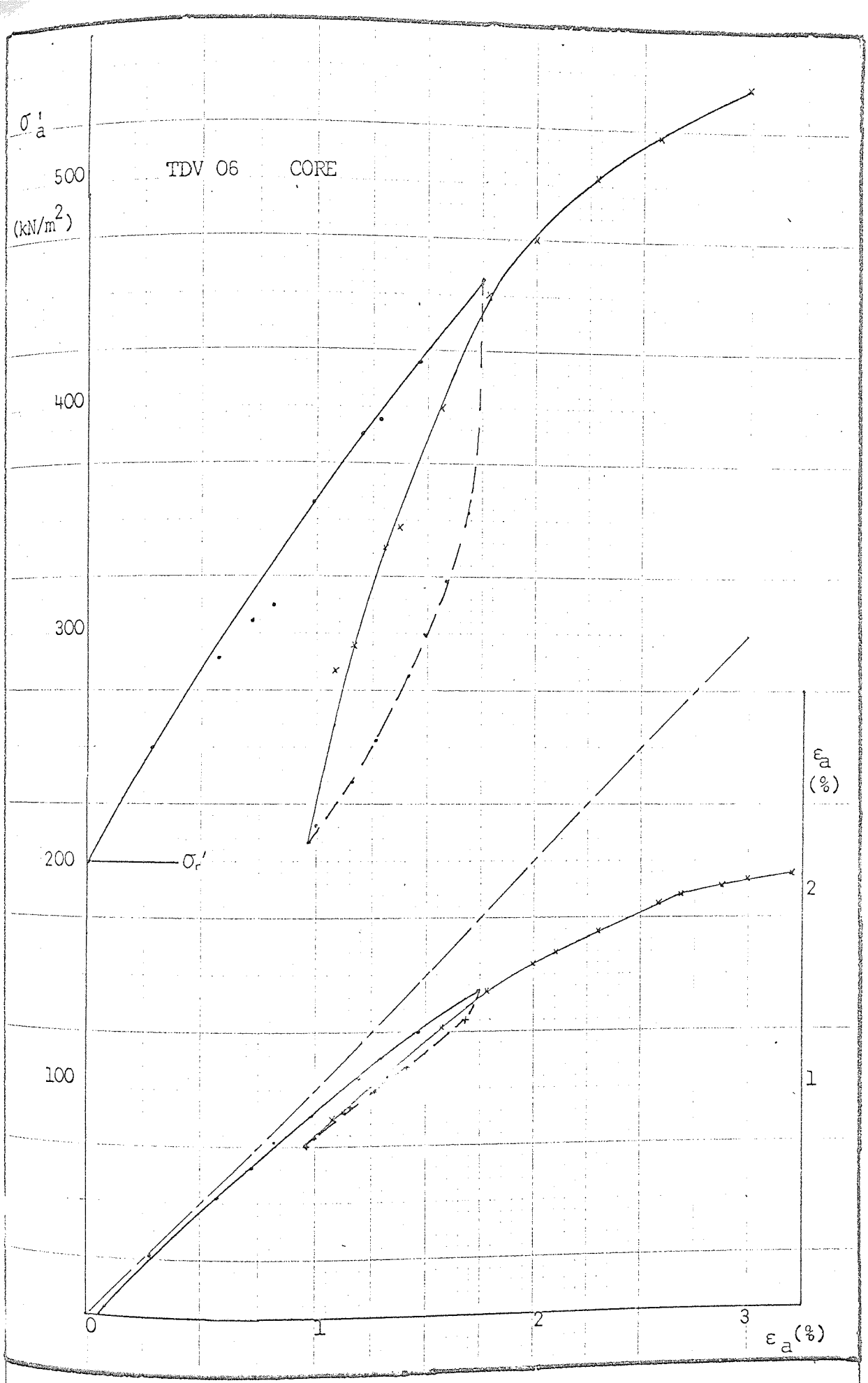

Axial Stress and Volumetric Strain vs Axial Strain - TDV Series

FIG. 7.3(c)

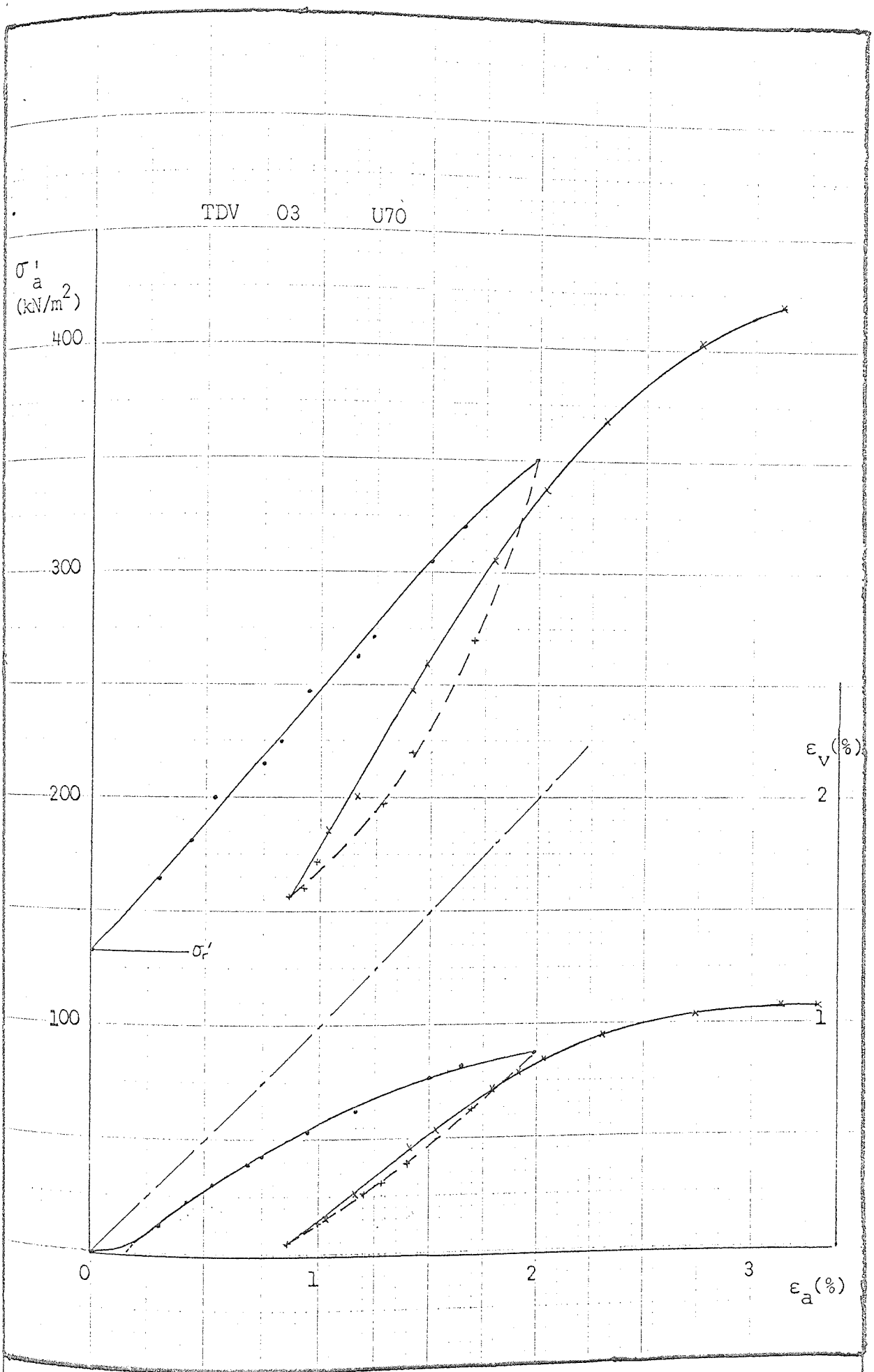

Axial Stress and Volumetric Strain vs Axial Strain - TDV Series

FIG. 7.3(d)

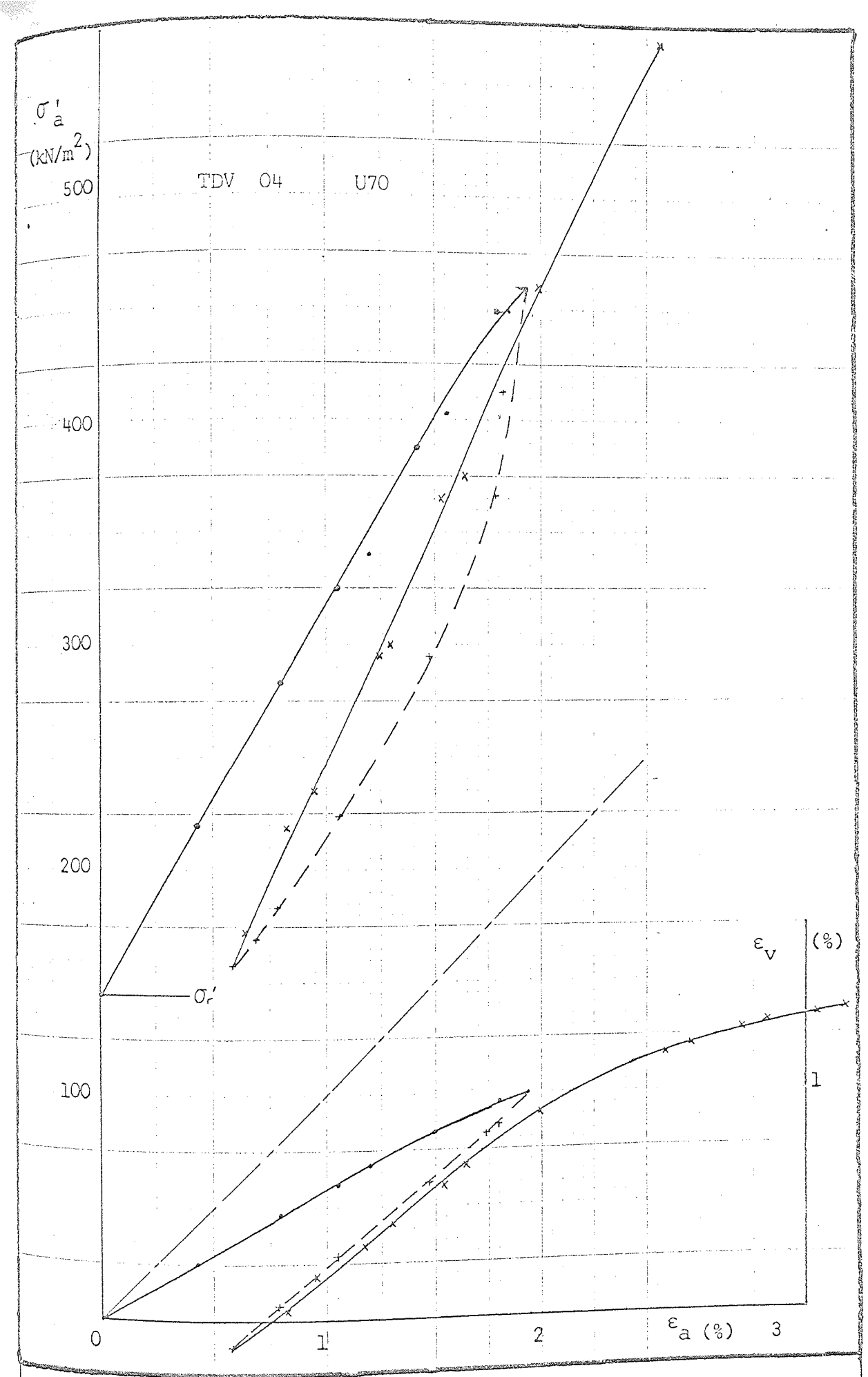

Axial Stress and Volumetric Strain vs Axial Strain - TDV Series

FIG. 7.3(e)

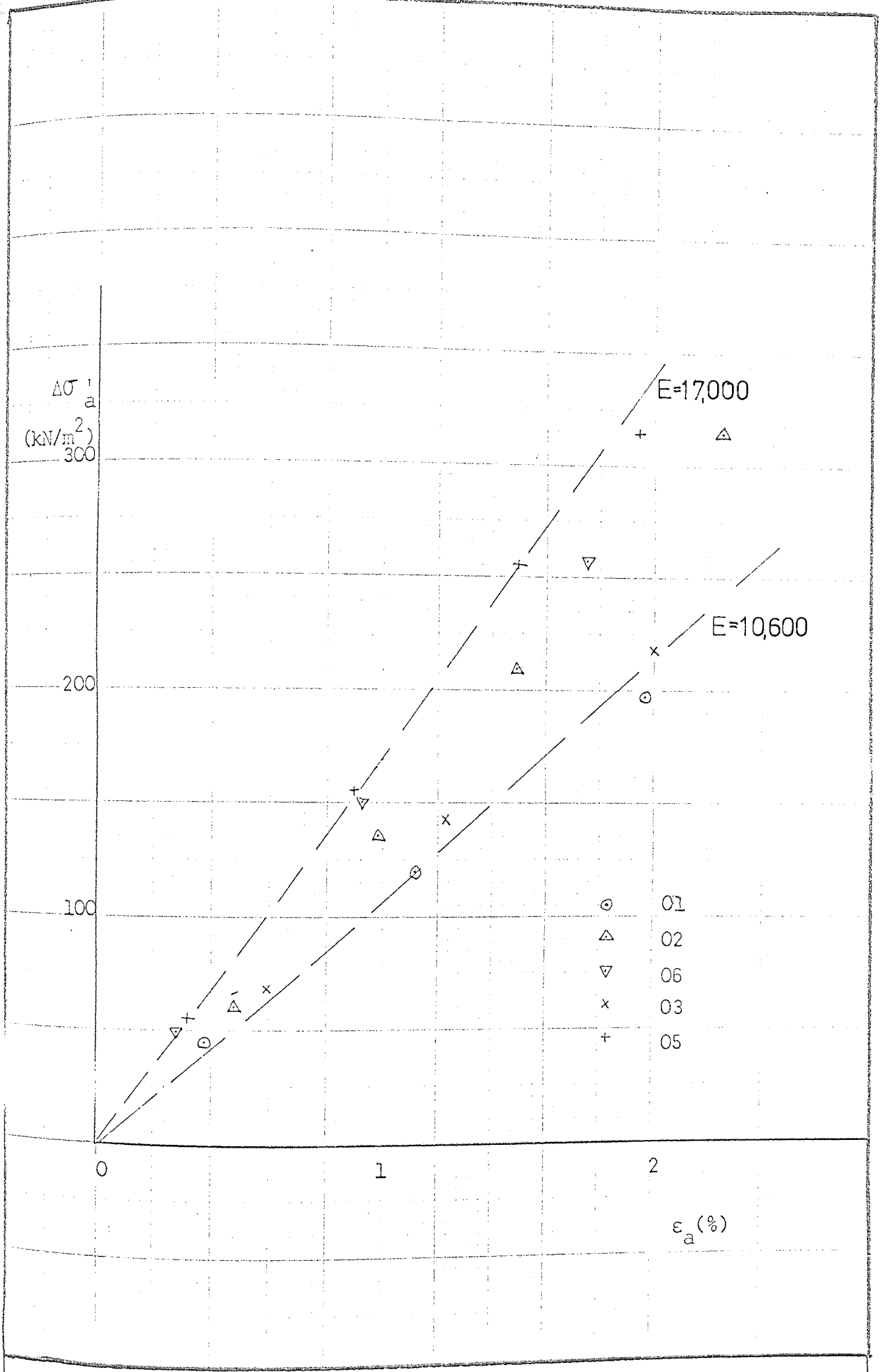

Increment of Axial Stress vs Axial Strain - TDV Series 1st Loading

FIG. 7.4(a)

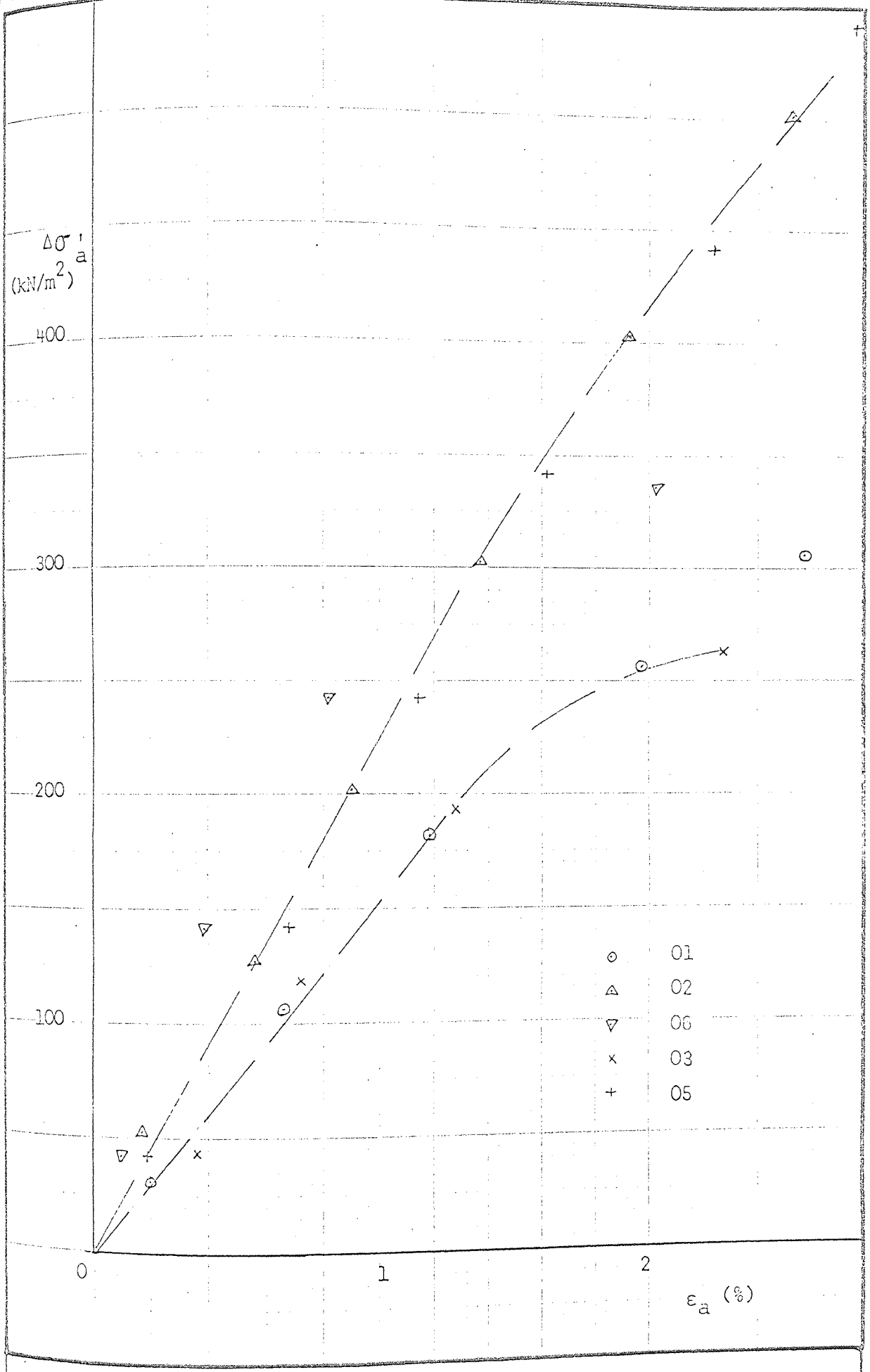

Increment of Axial Stress vs Axial Strain

- TDV Series 2nd Loading

FIG. 7.4(1)

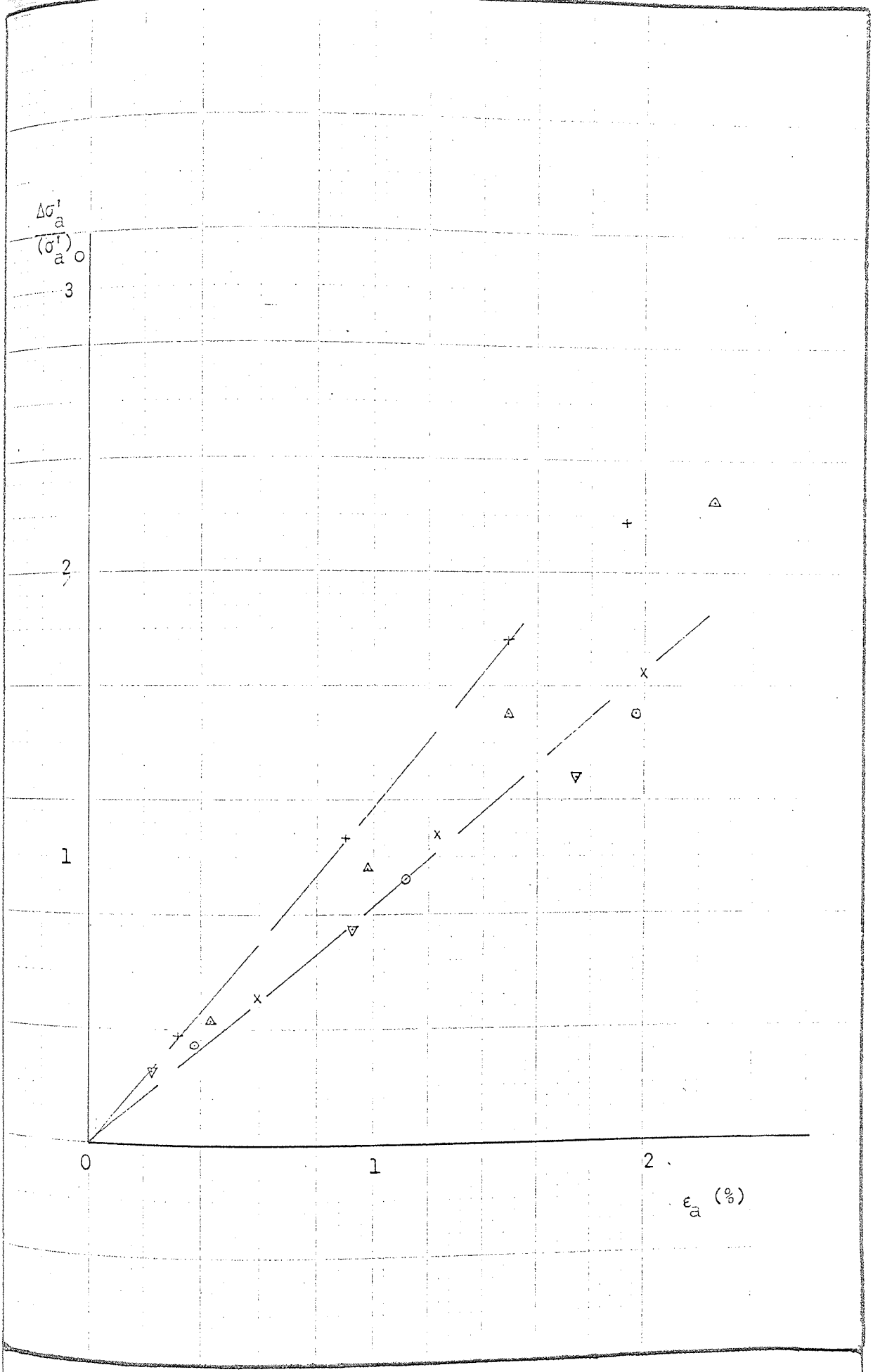

$\Delta\sigma'_a/(\sigma'_a)_o$ vs Axial Strain

- TDV SERIES 1st Loading

FIG. 7.5(a)

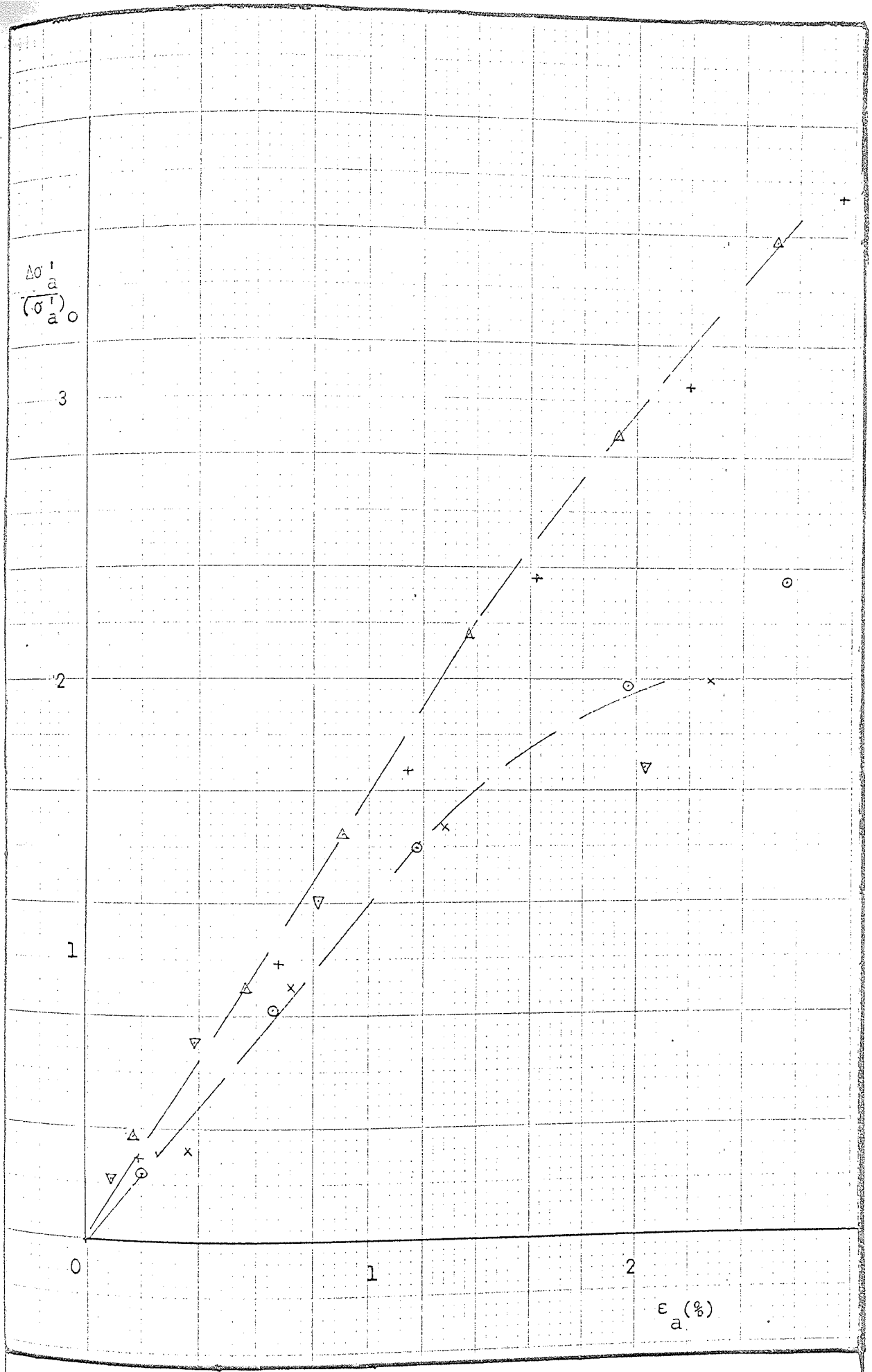

$\sigma'_a/(\sigma'_a)_o$ vs Axial Strain

FIG. 7.5(b)

TDV Series 2nd Loading

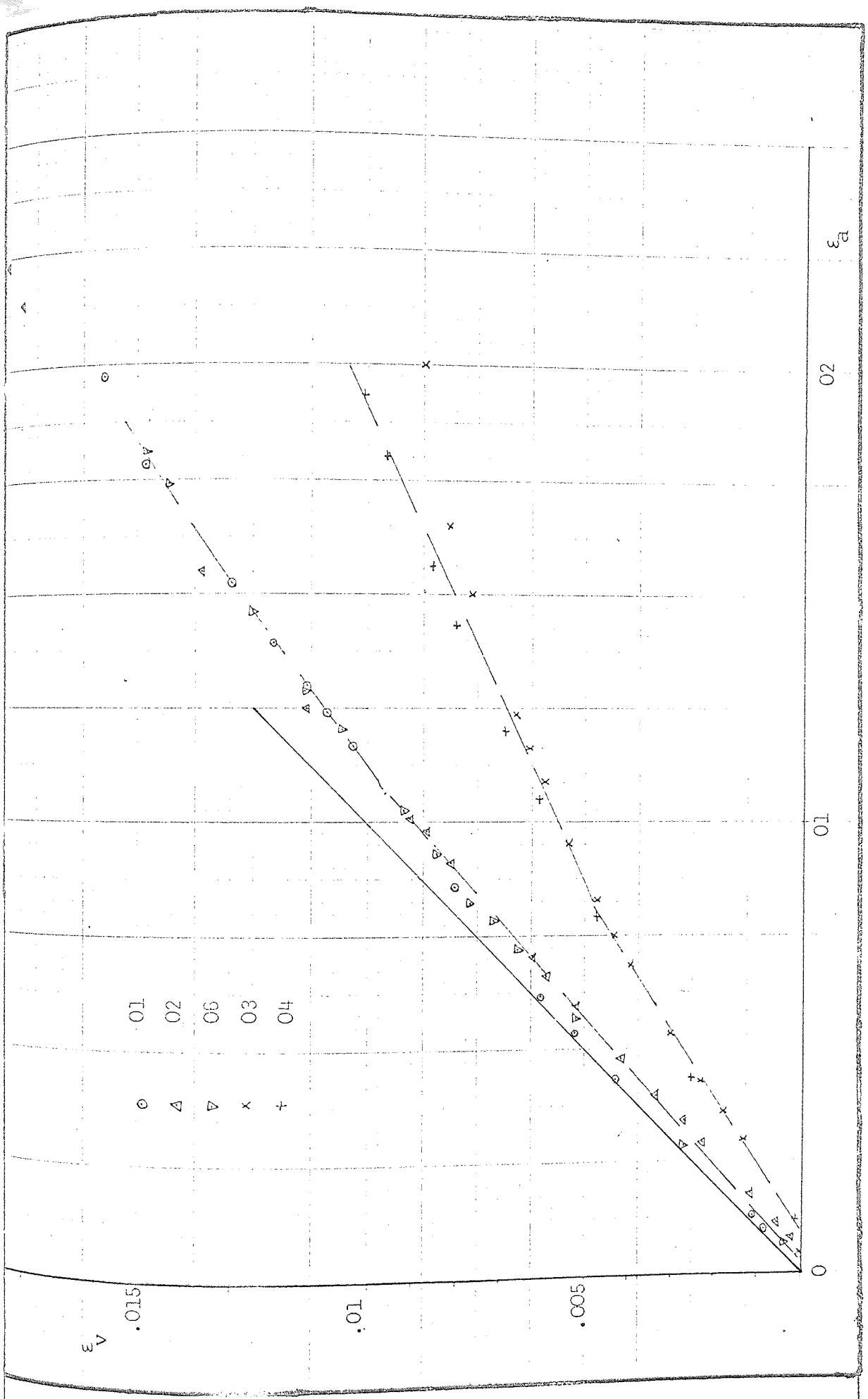

Volumetric Strain vs Axial Strian (Strain Path)

- TDV Series 1st Loading

FIG. 7.6(a)

Volumetric Strain vs Axial Strain (Strain Path)

-TDV Series 2nd Loading

FIG. 7.6(b)

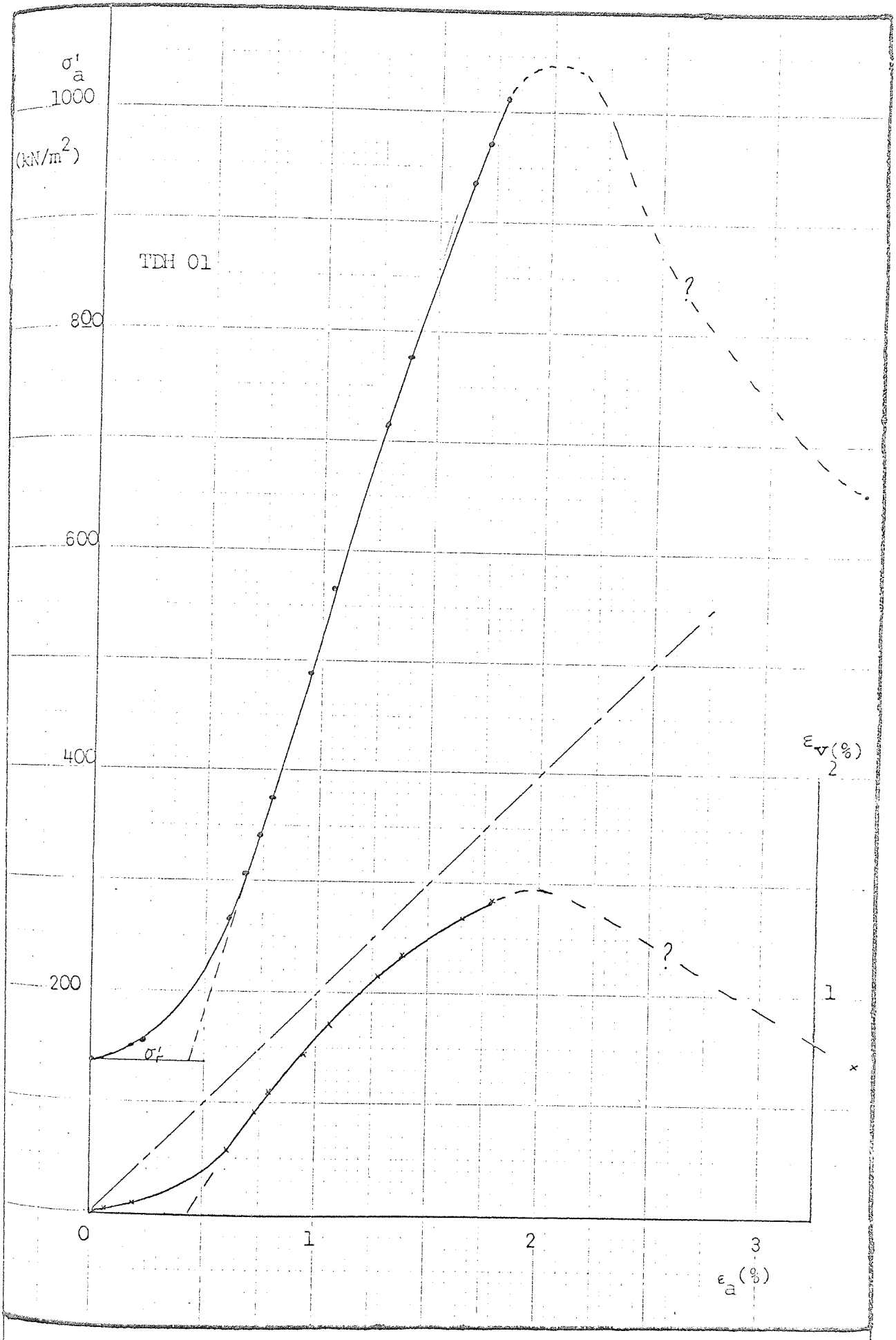

Axial Stress and Volumetric Strain vs Axial Strain - TDH Series

FIG. 7.7

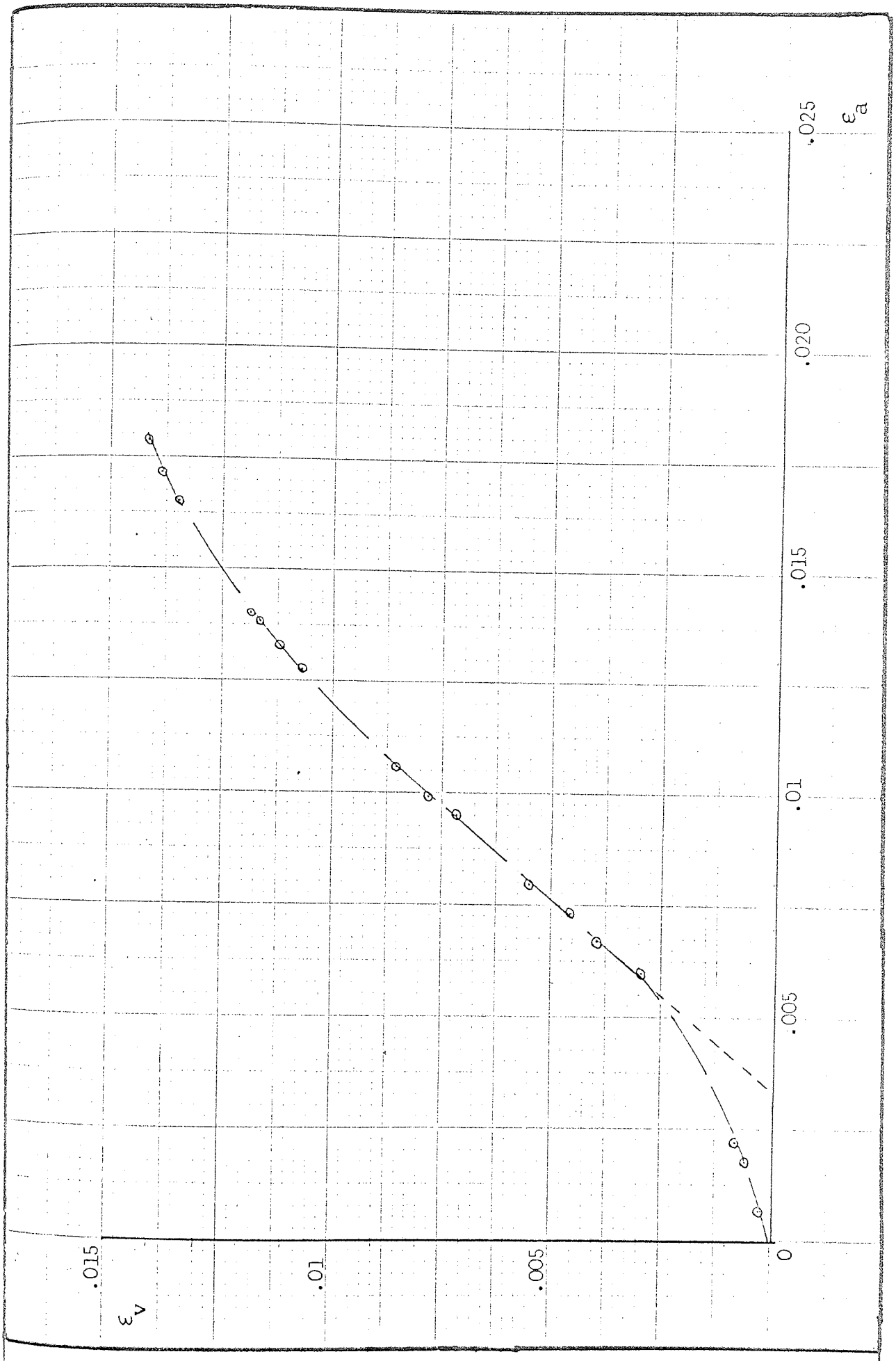

Strain Path - TDH Series

FIG. 7.8

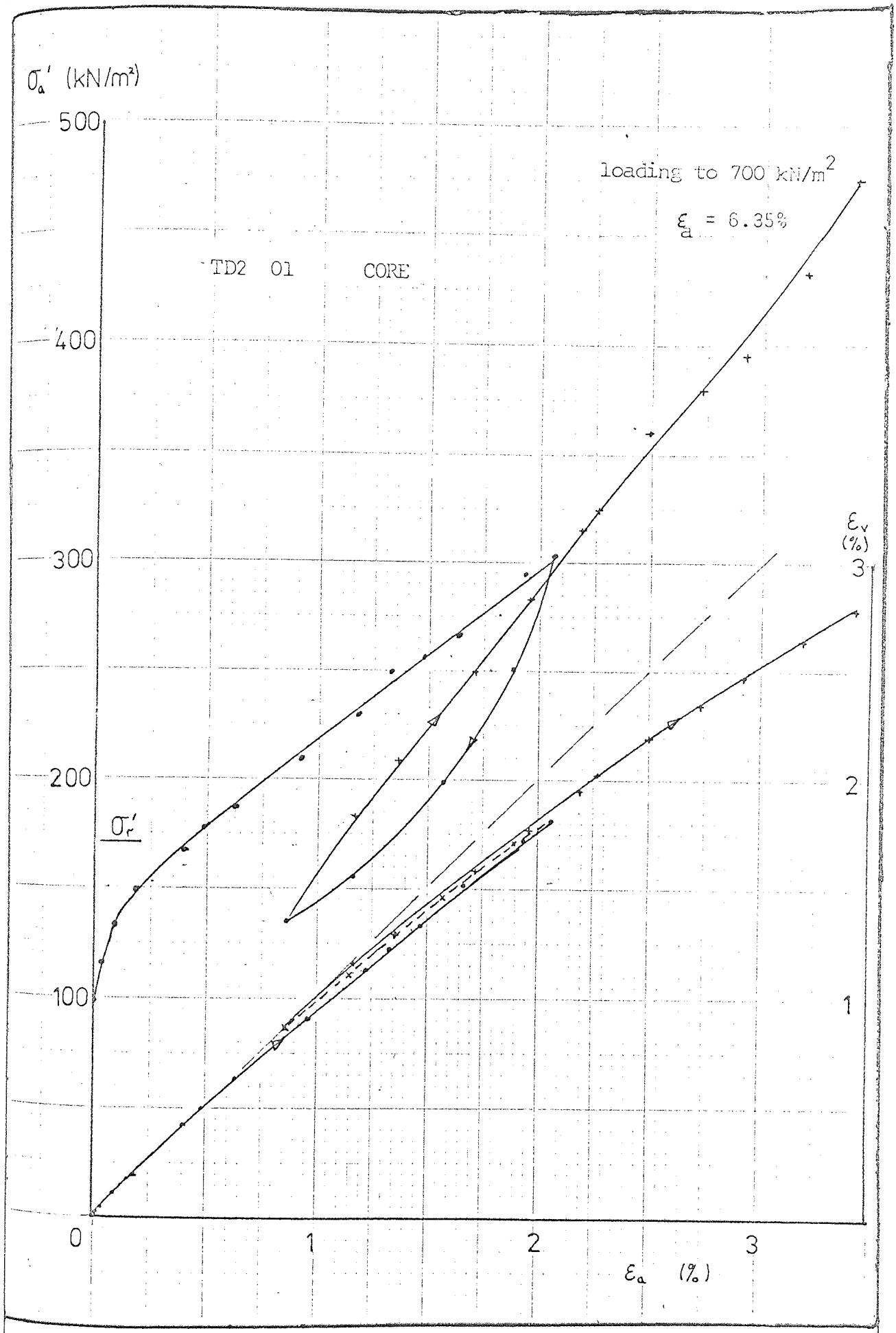

Axial Stress and Volumetric Strain vs Axial Strain - TD2 Series

FIG. 7.9(a)

Axial Stress and Volumetric Strain vs Axial Strain

- TD2 Series

FIG 7.9(b)

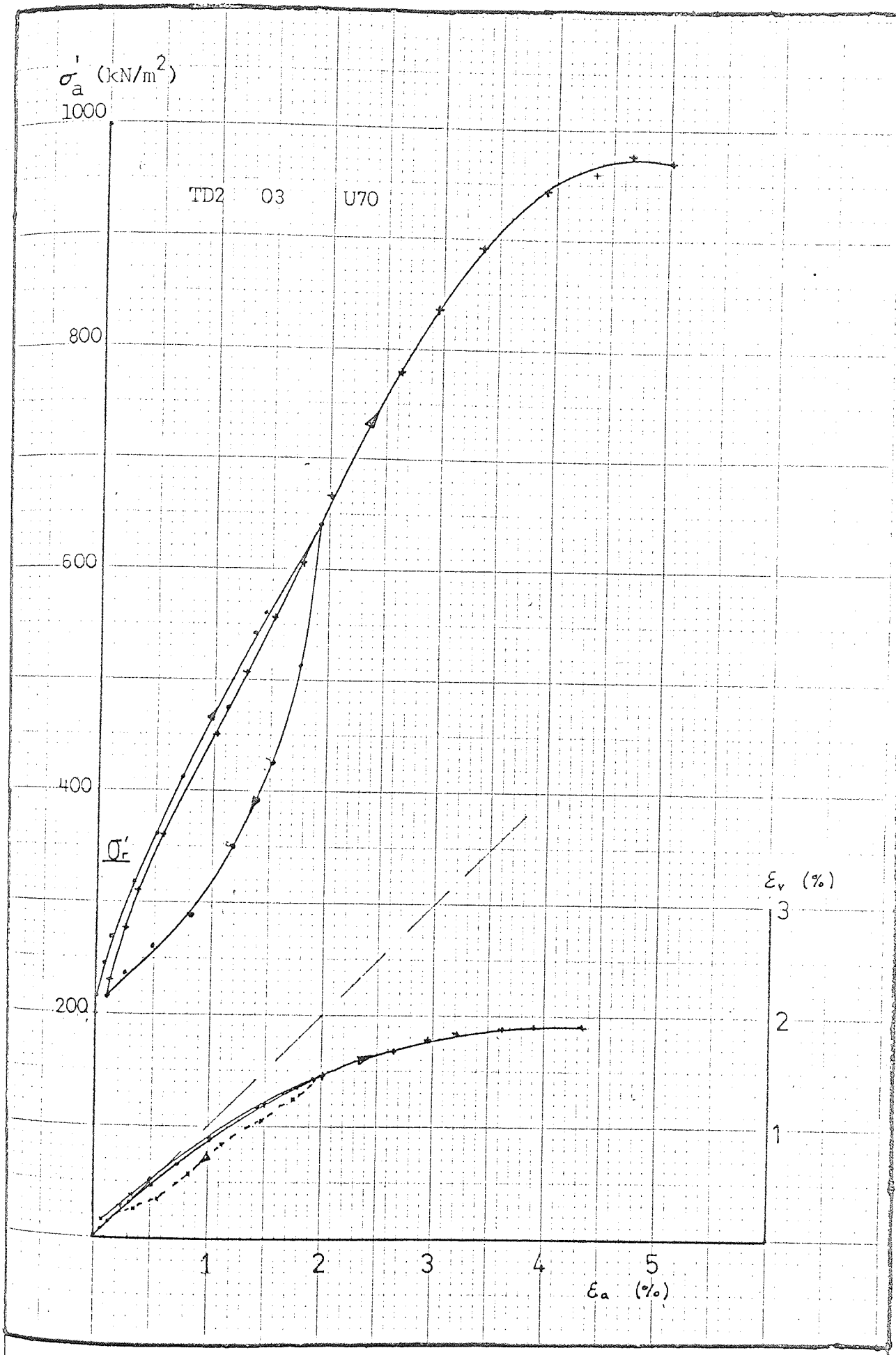

Axial Stress and Volumetric Strain vs Axial Strain

- TD2 Series

FIG. 7.9(c)

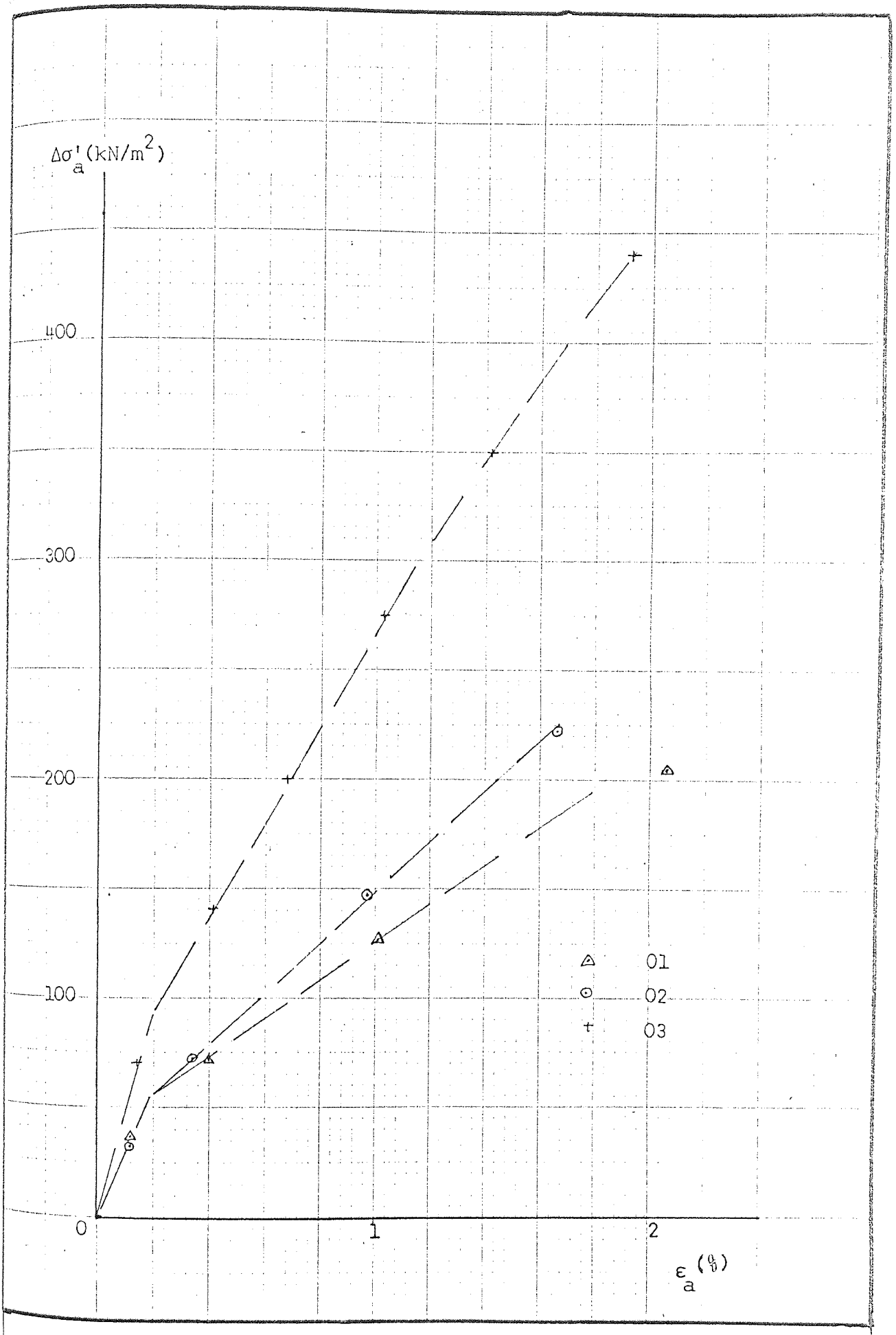

Increment of Axial Stress vs Axial Strain

TD2 Series 1st Loading

FIG. 7.10(a)

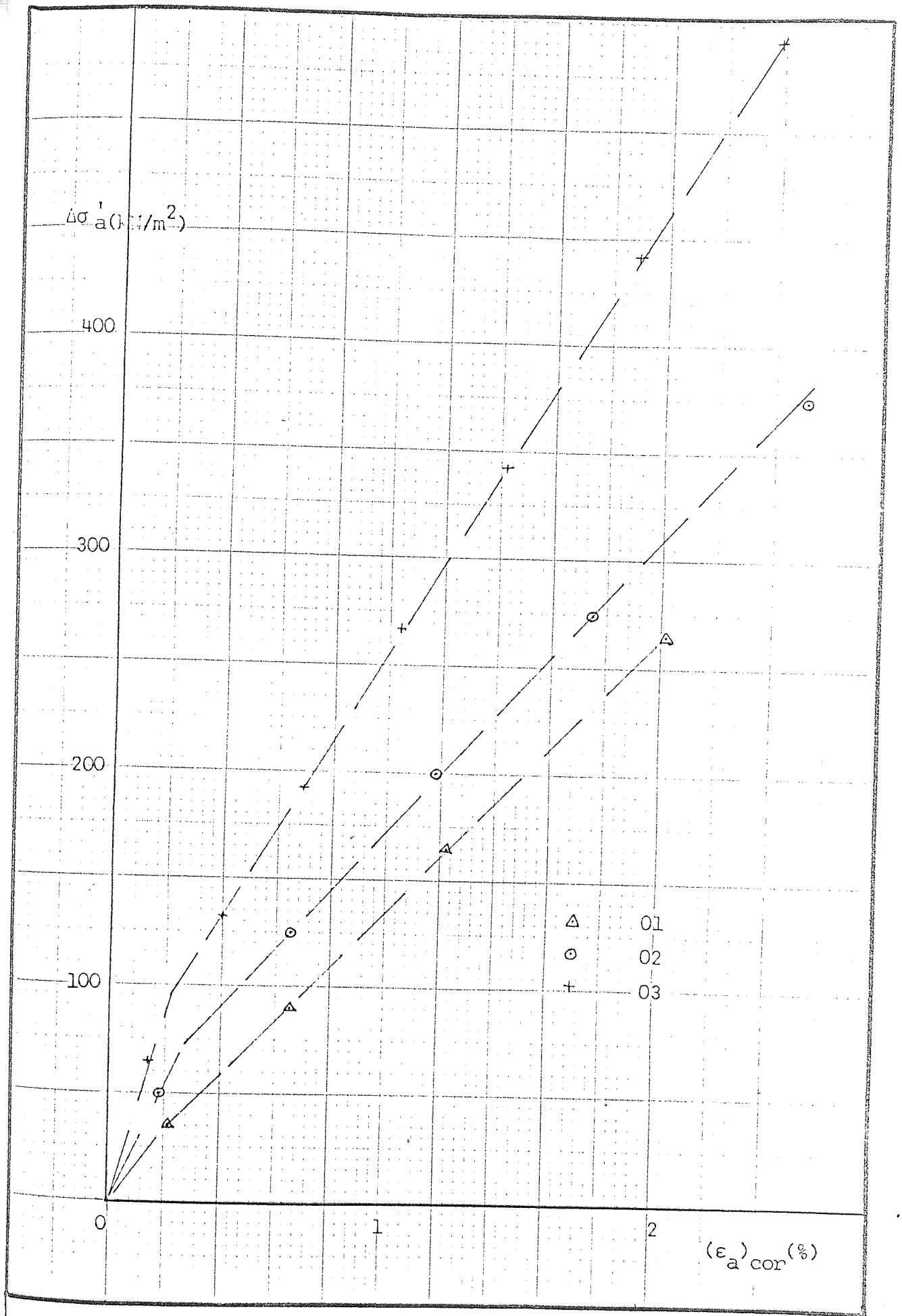

Increment of Axial Stress vs Axial Strain

TD2 Series 2nd Loading

FIG. 7.10(b)

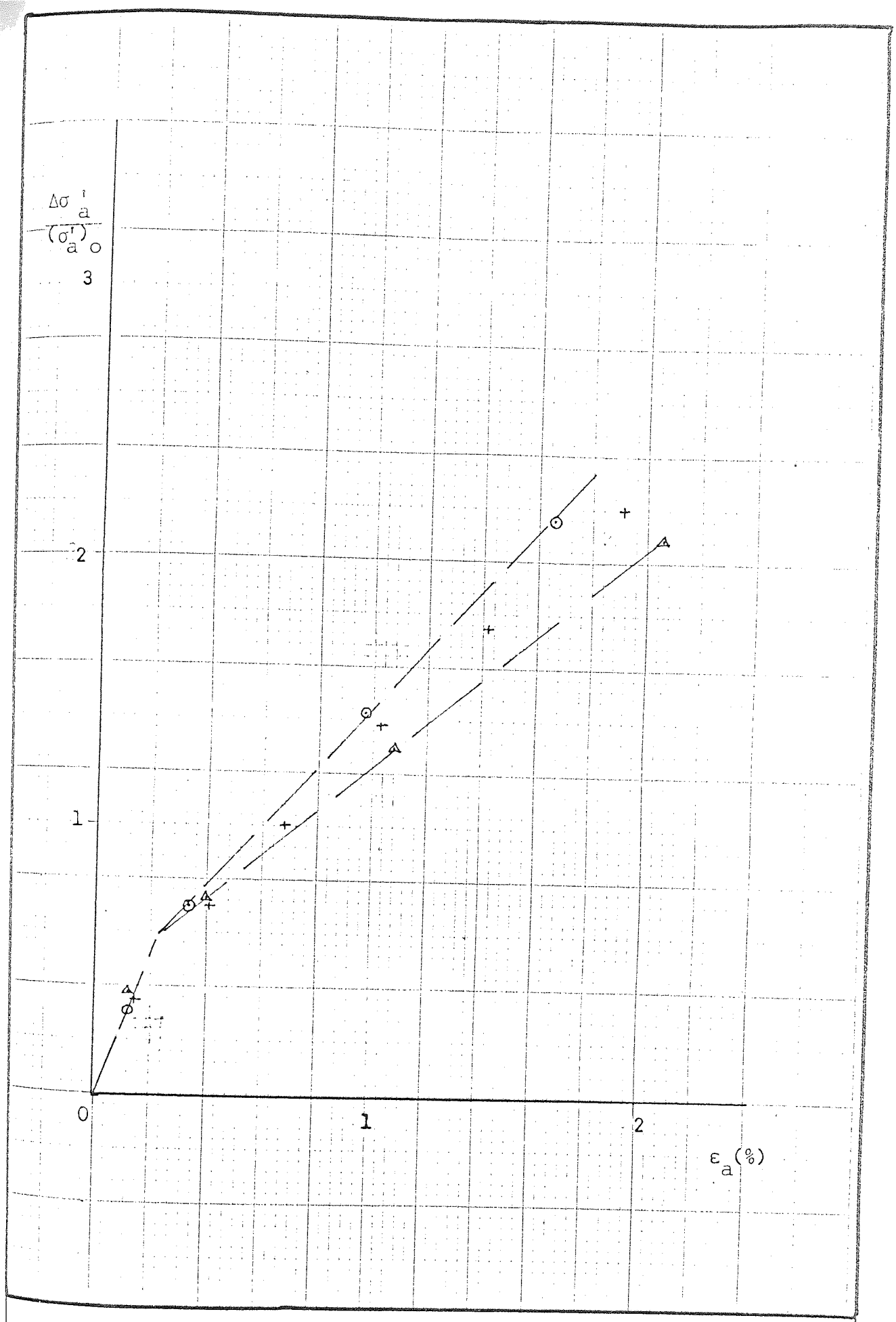

$\Delta\sigma'_a/(\sigma'_a)_o$ vs Axial Strain - TD2 Series 1st Loading

FIG. 7.11(a)

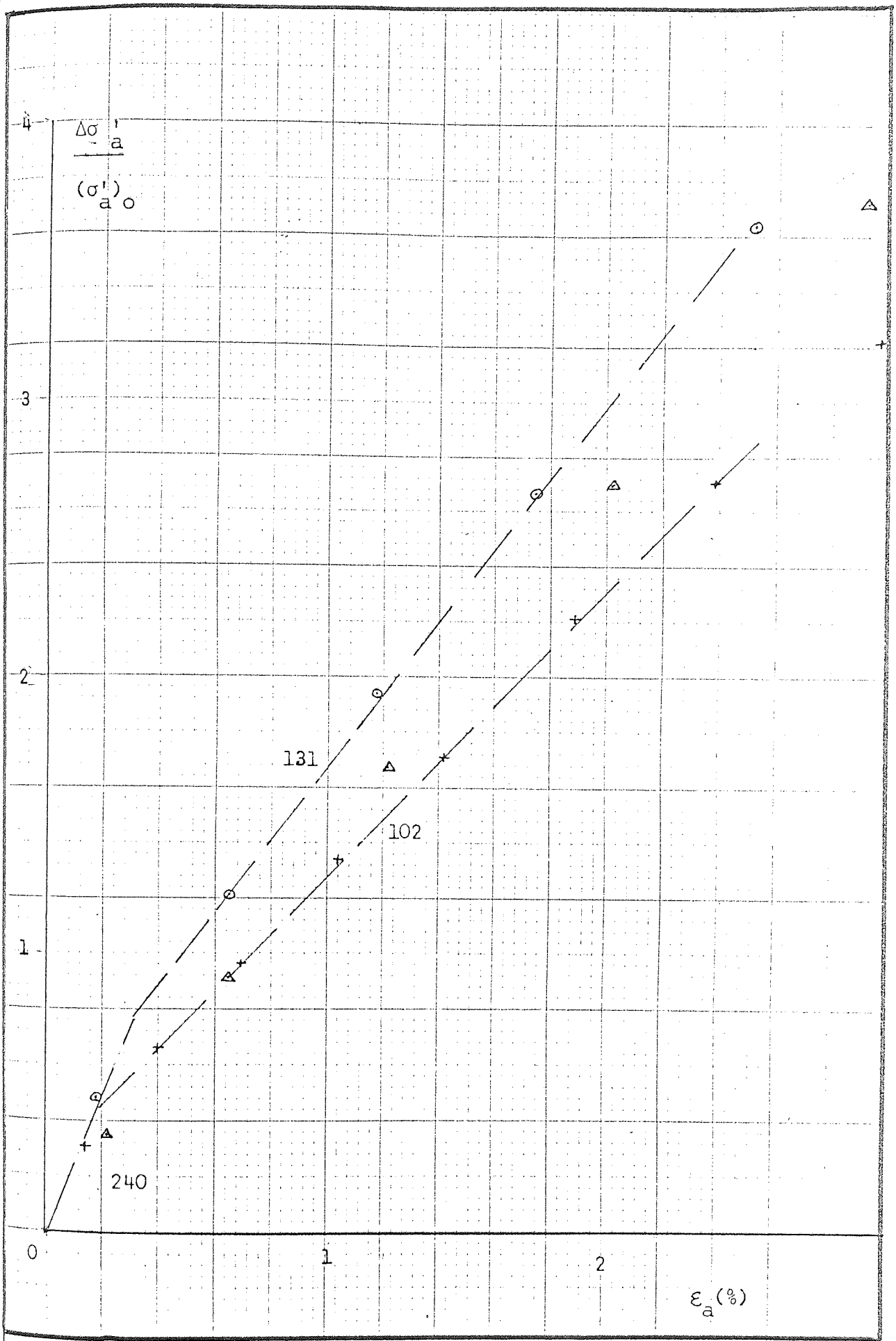

$\Delta\sigma'_a/(\sigma'_a)_o$ vs Axial Strain - TD2 Series 2nd Loading

FIG. 7.11(b)

Strain Paths - TD2 Series 1st Loading

FIG. 7.12(a)

Strain Paths - TD2 Series 2nd Loading

FIG 7.12(b)

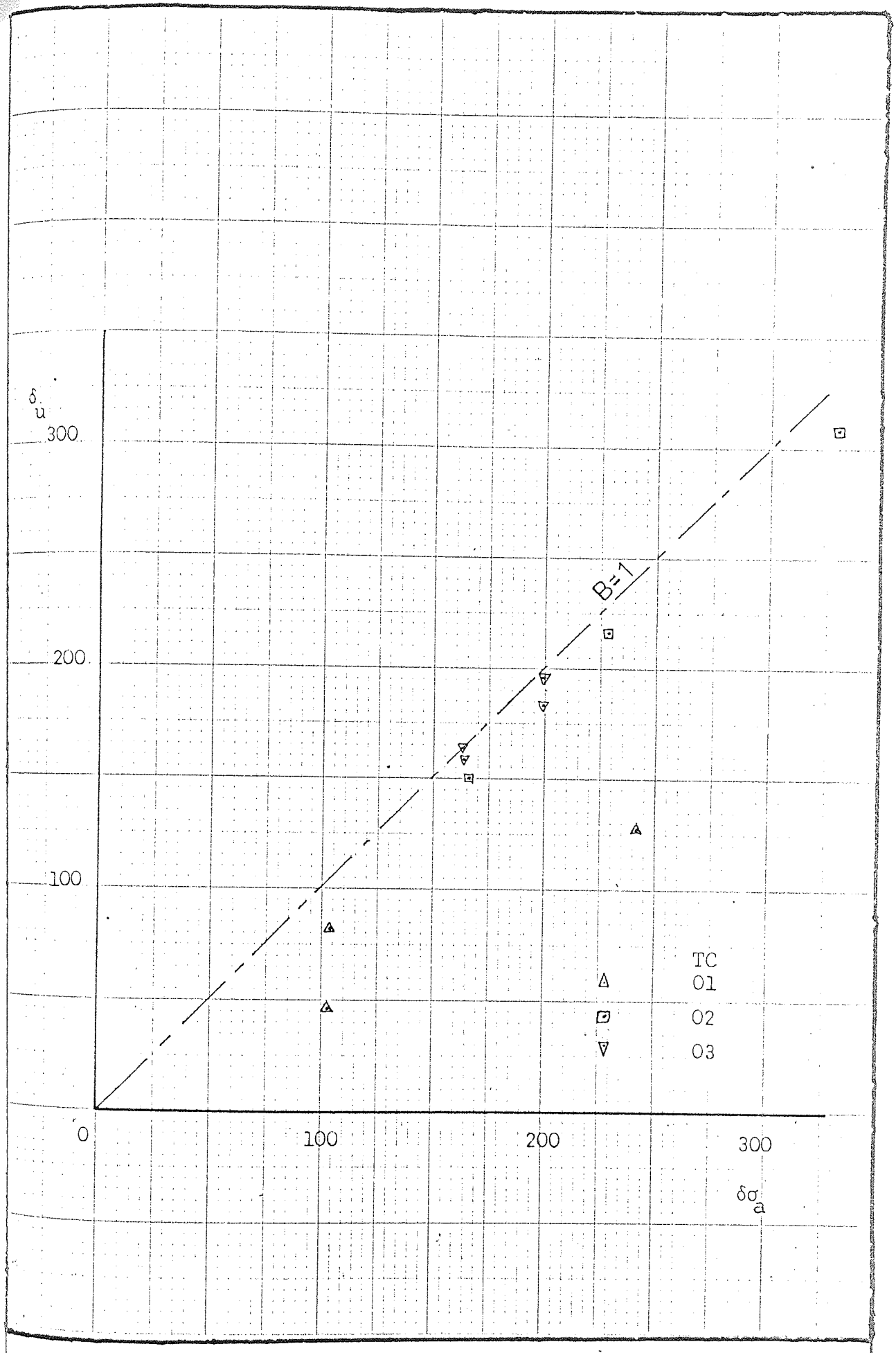

Change in Pore Pressure due to Change in Cell Pressure in TC Series

FIG. 7.13

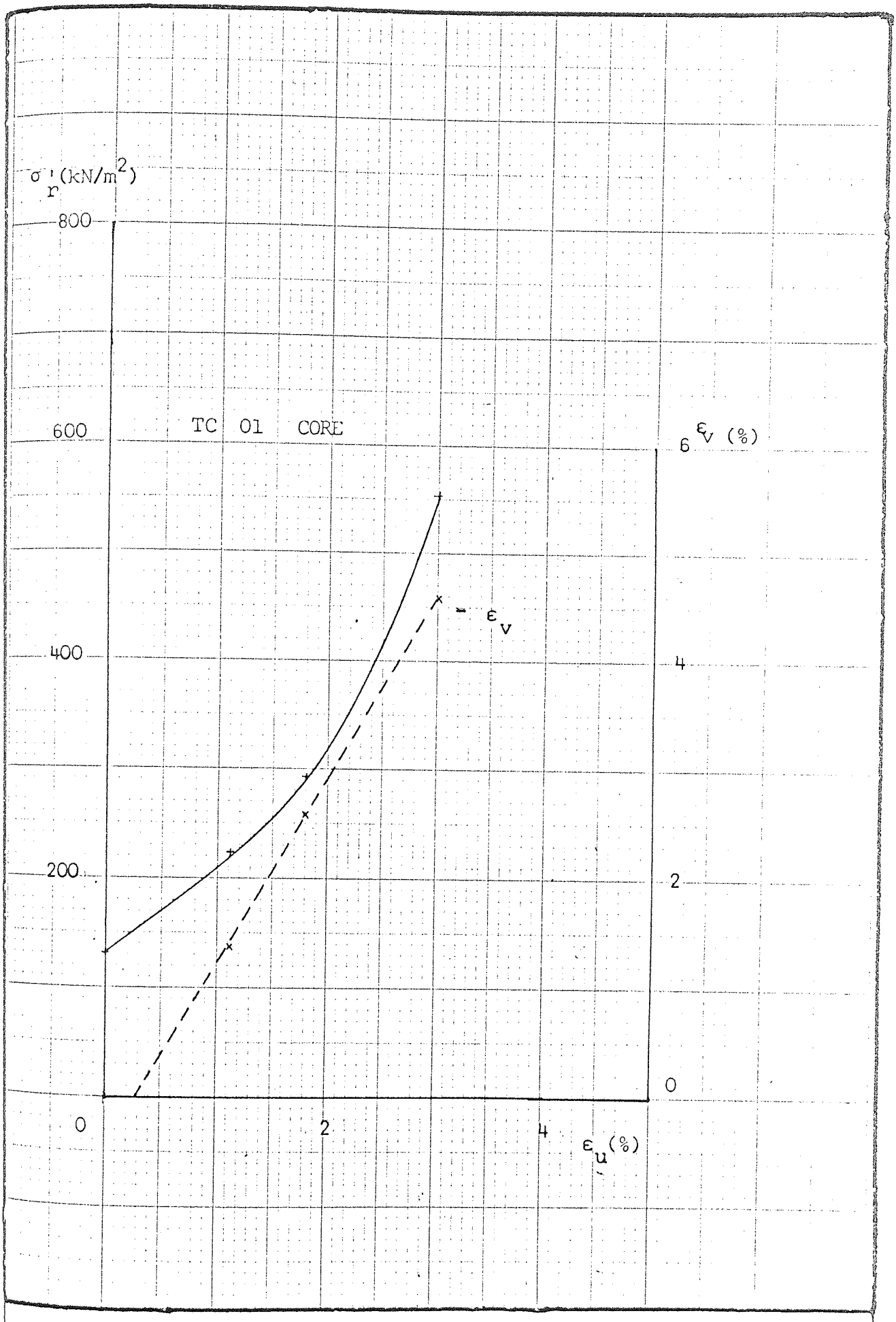

Cell Pressure and Volumetric Strain vs Axial Strain - TC Series

FIG. 7.14(a)

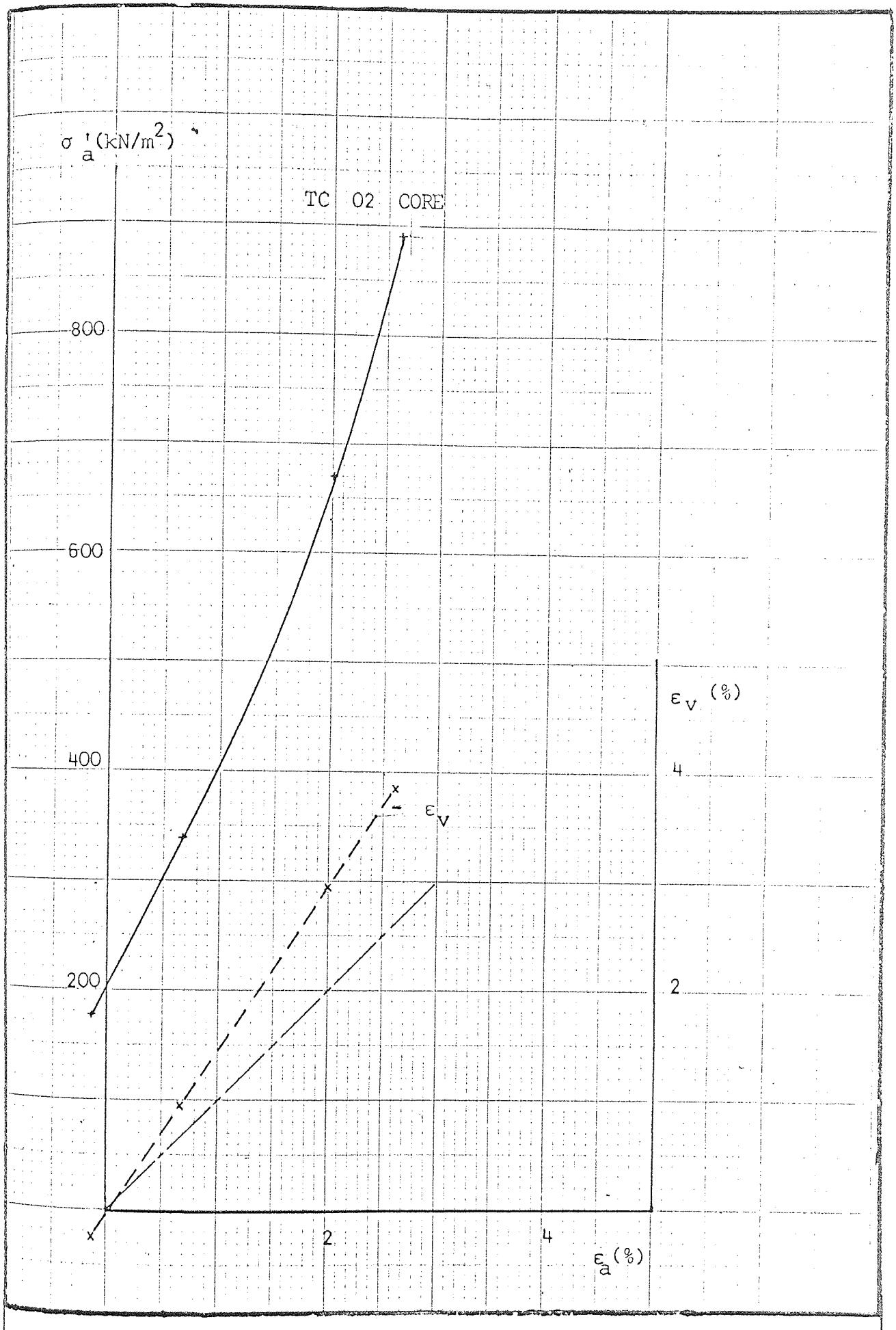

Cell Pressure and Volumetric Strain vs Axial Strain

- TC Series

FIG. 7.14(b)

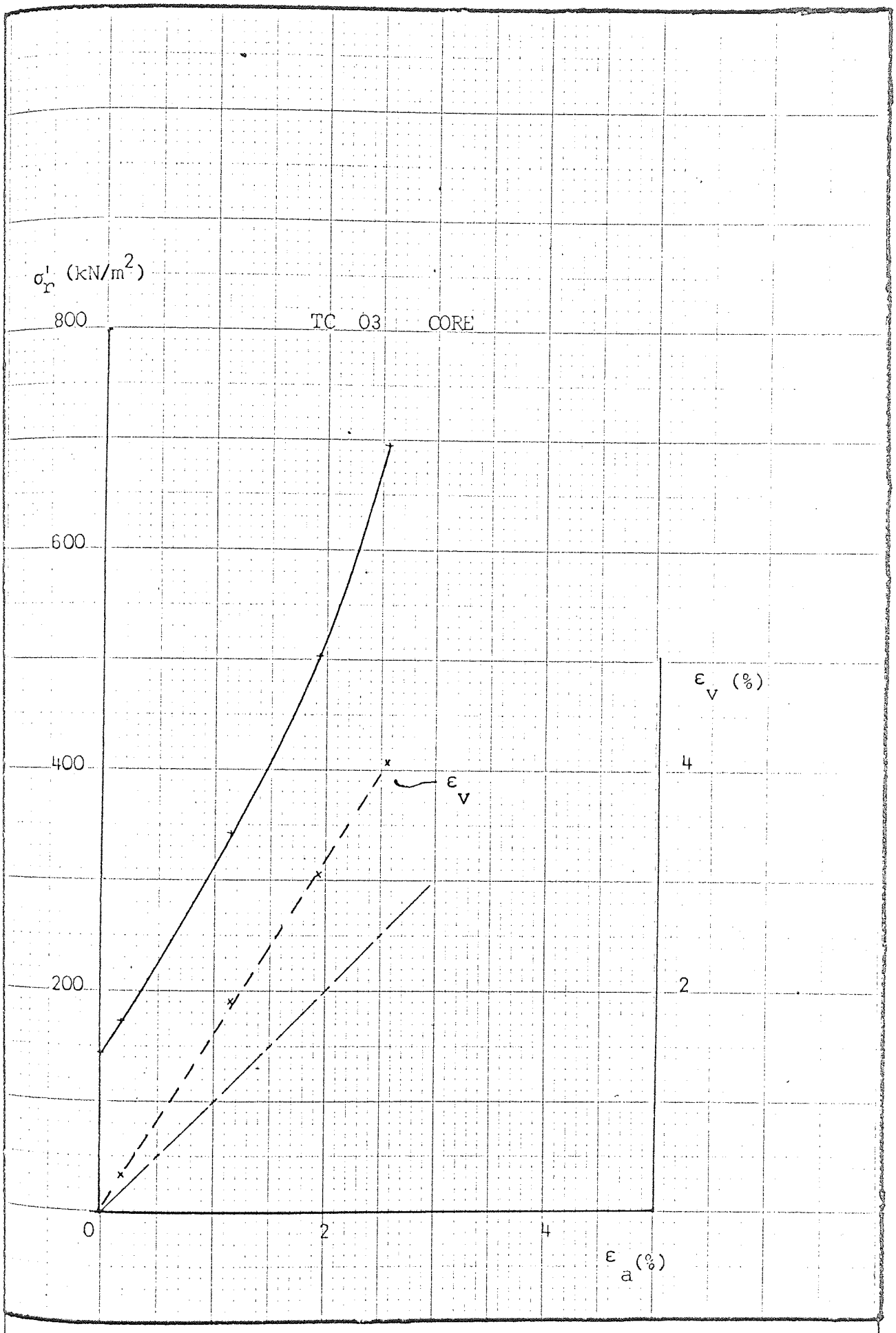

Cell Pressure and Volumetric Strain vs Axial Strain

- TC Series

FIG. 7.14(c)

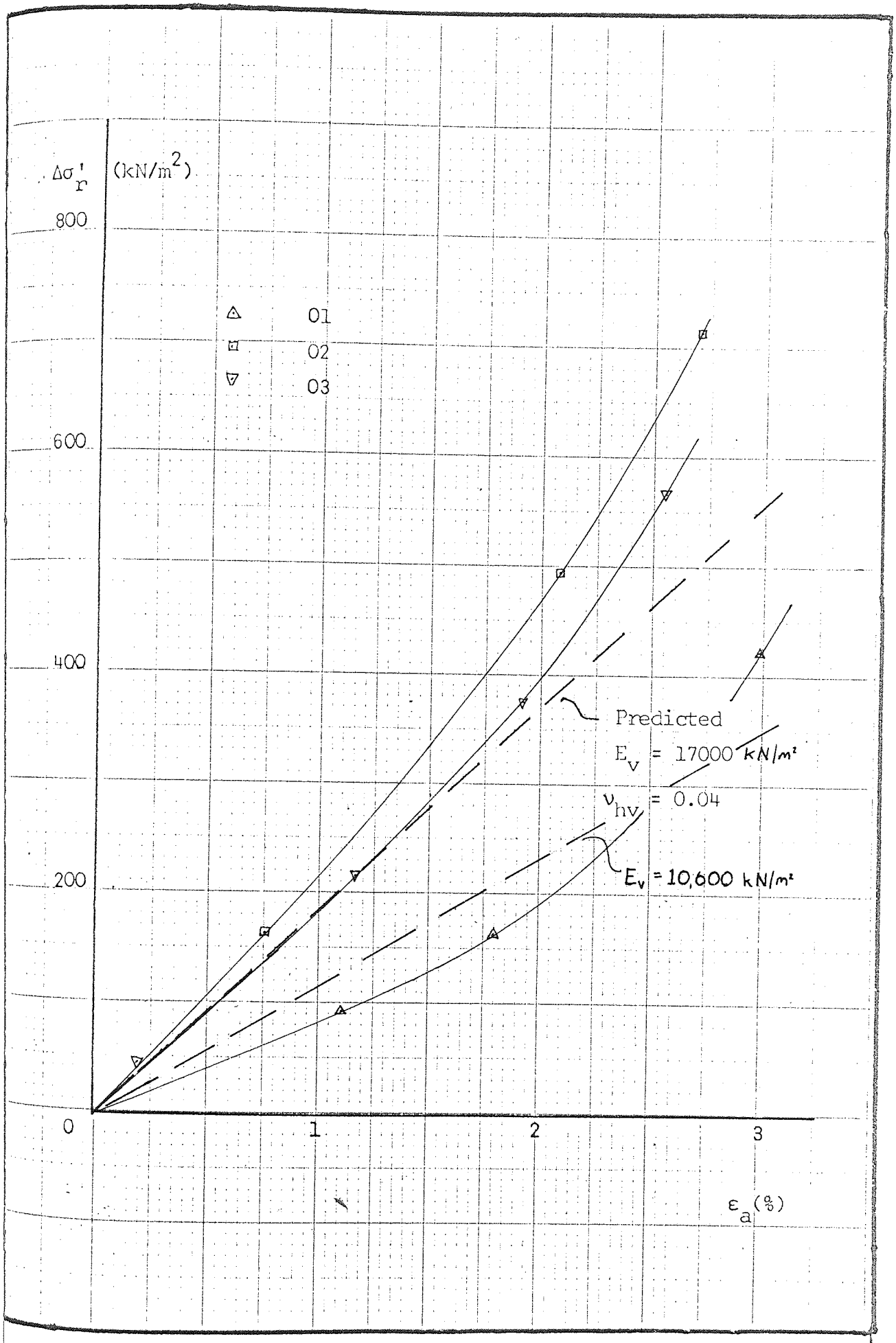

Increment of Cell Pressure vs Axial Strain

- TC Series

FIG. 7.15

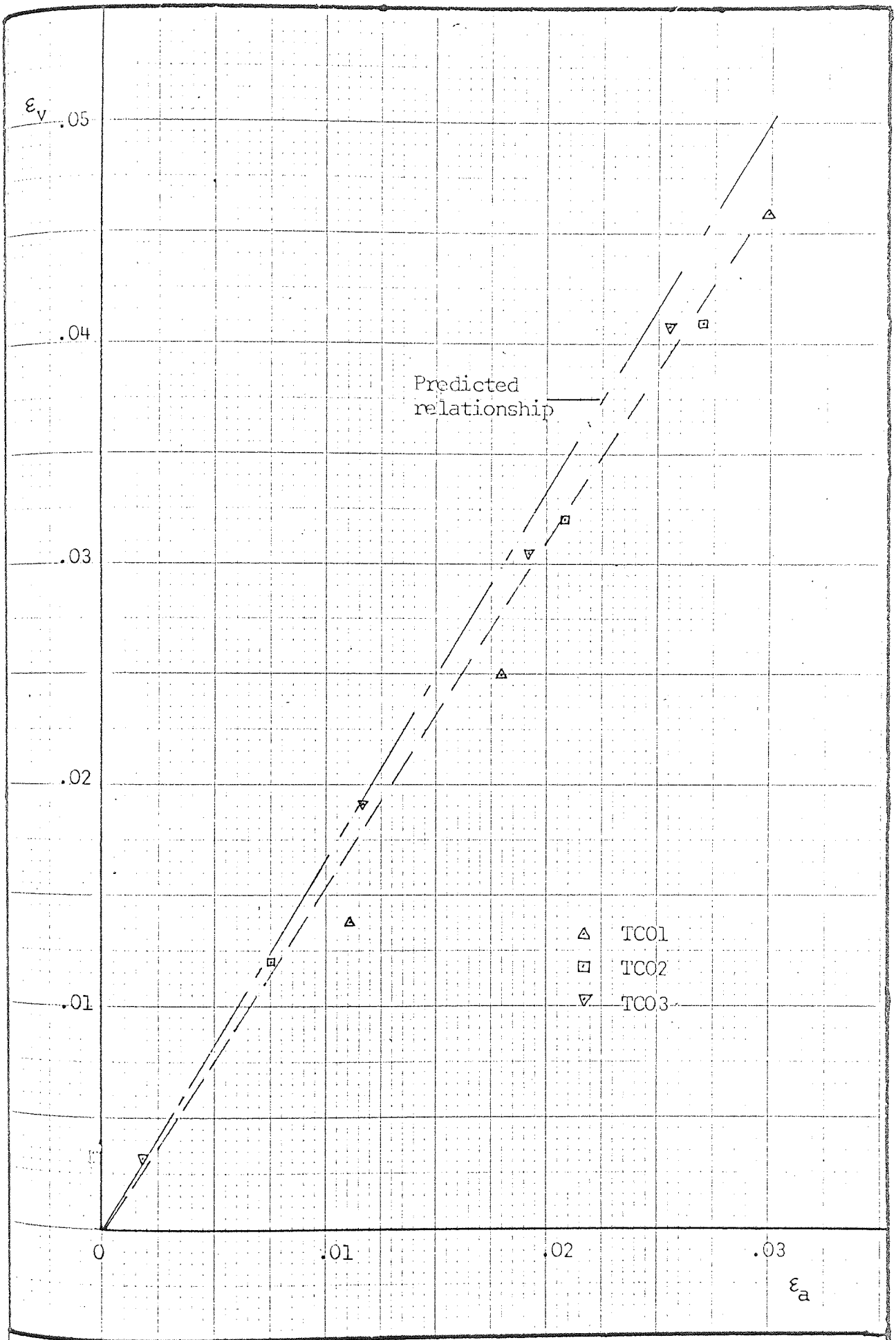

Strain Paths - TC Series

FIG. 7.16

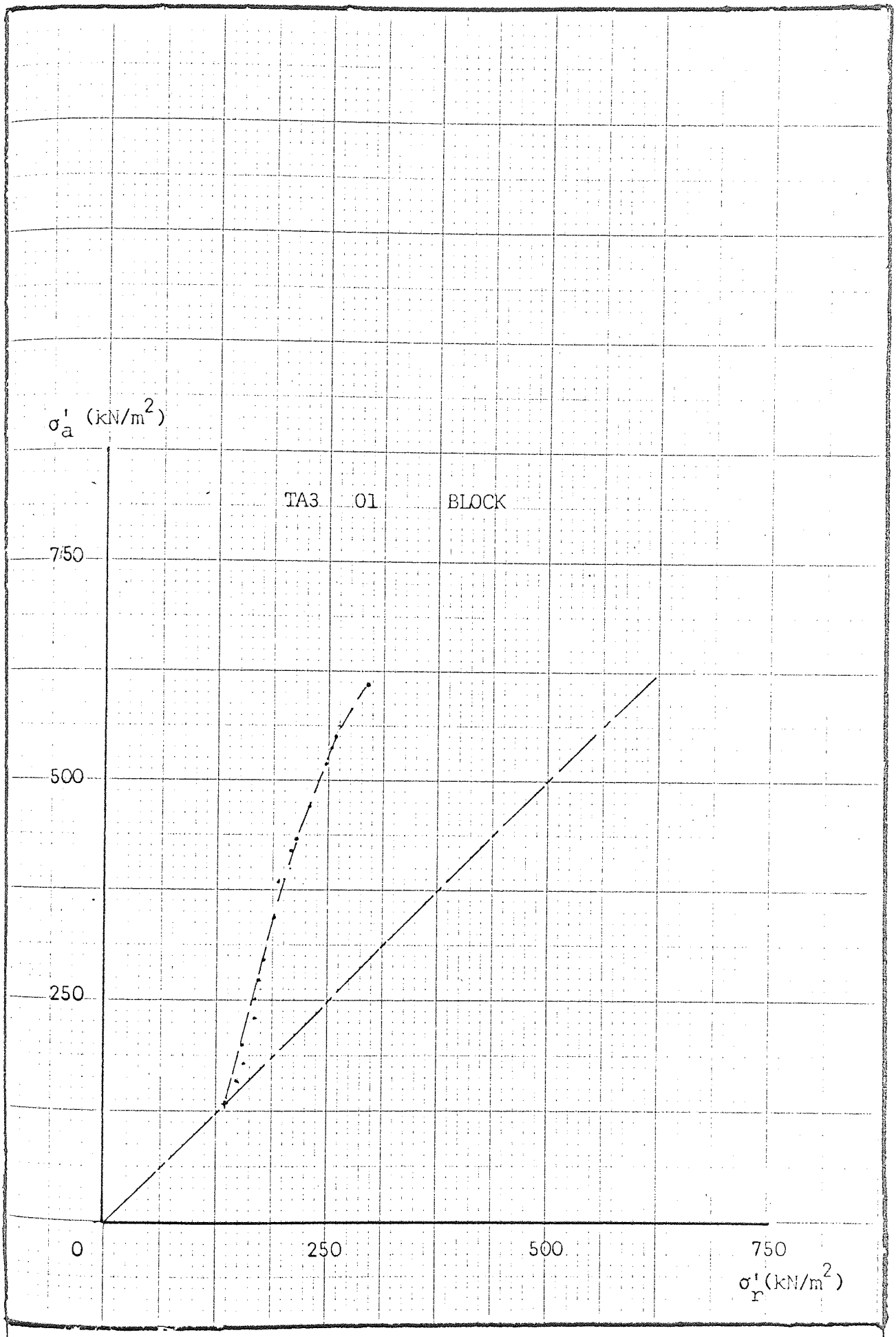

Stress Paths - TA3 Series

FIG. 7.17(a)

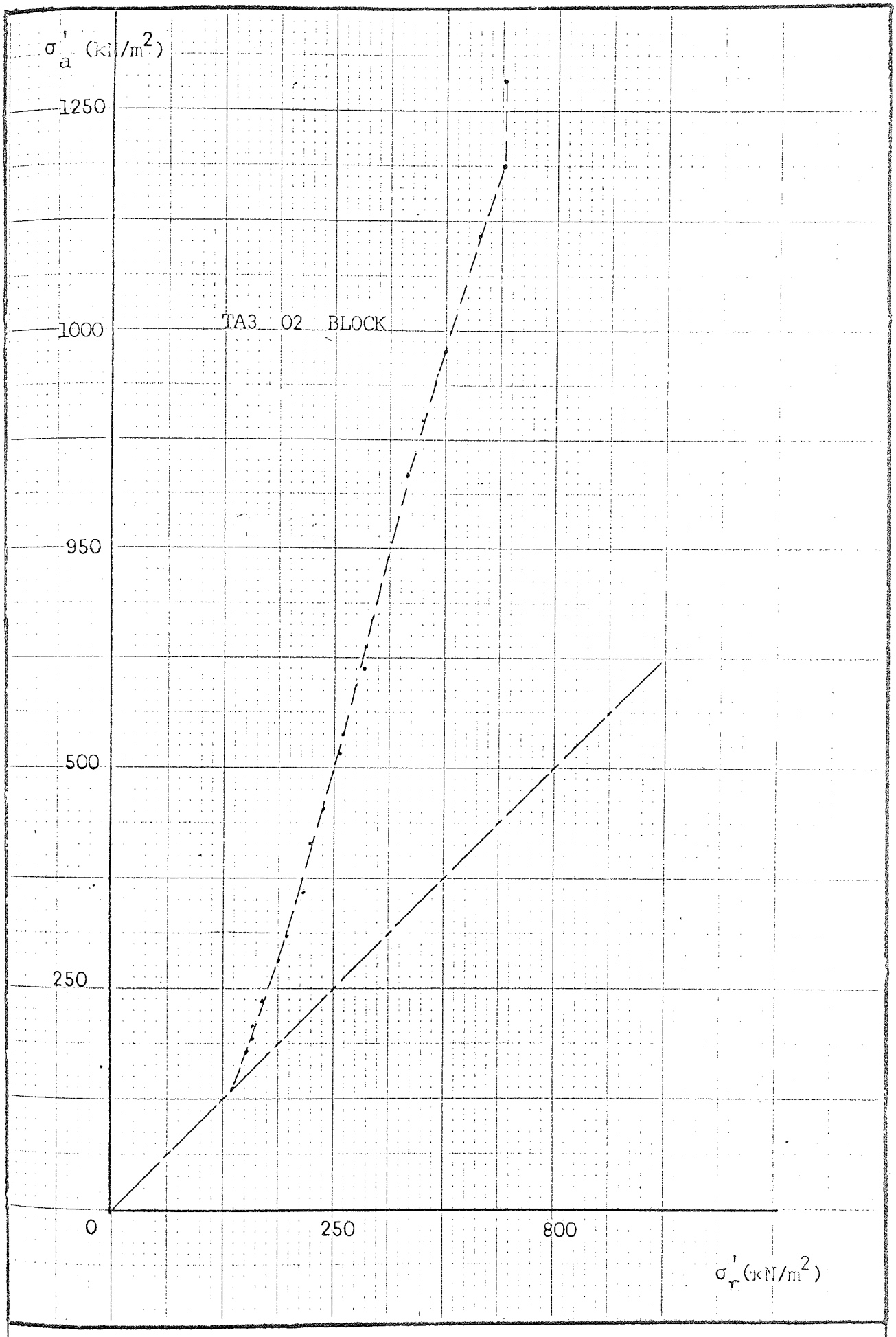

Stress Paths - TA3 Series

FIG. 7.17(b)

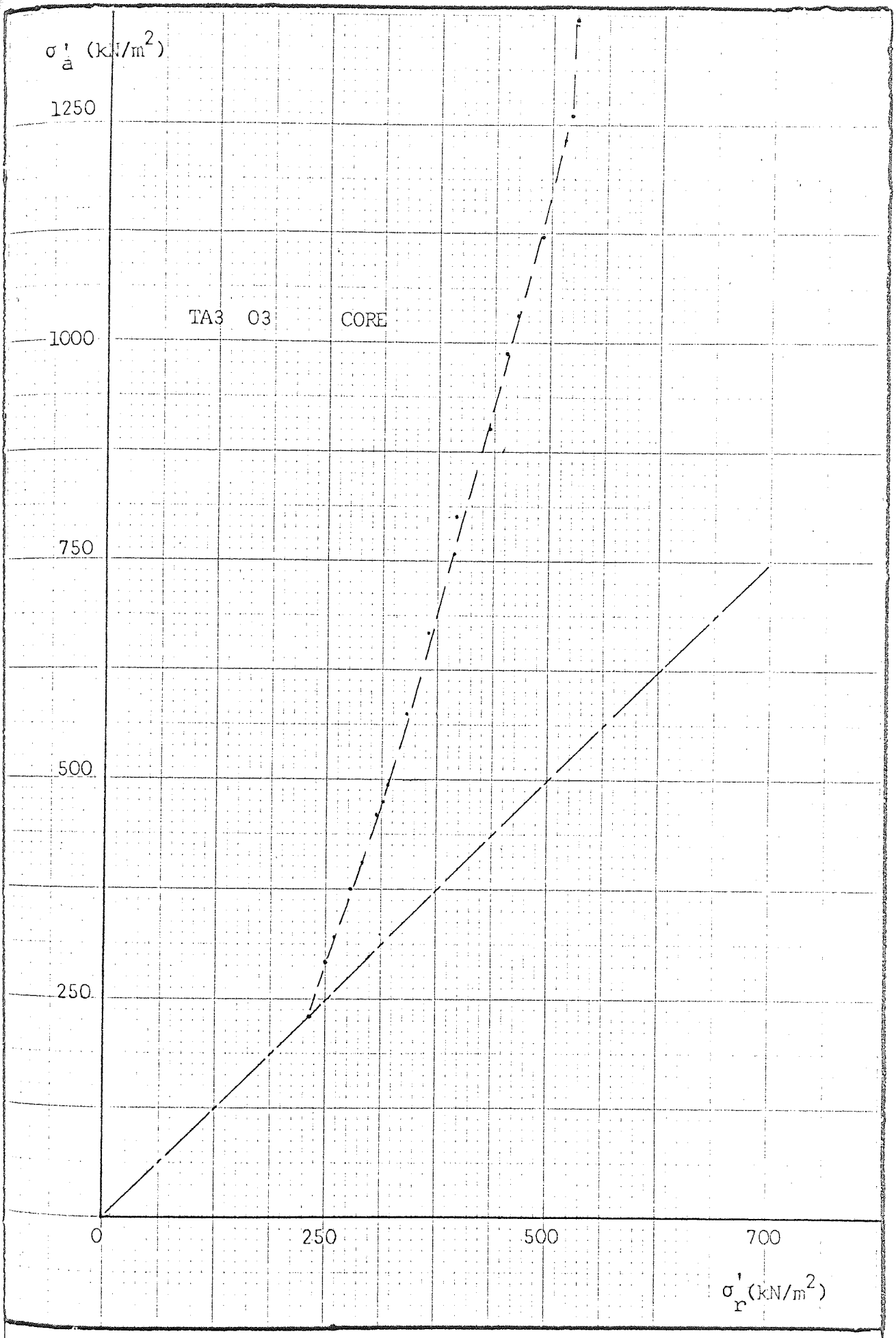

Stress Paths - TA3 Series

FIG. 7.17(c)

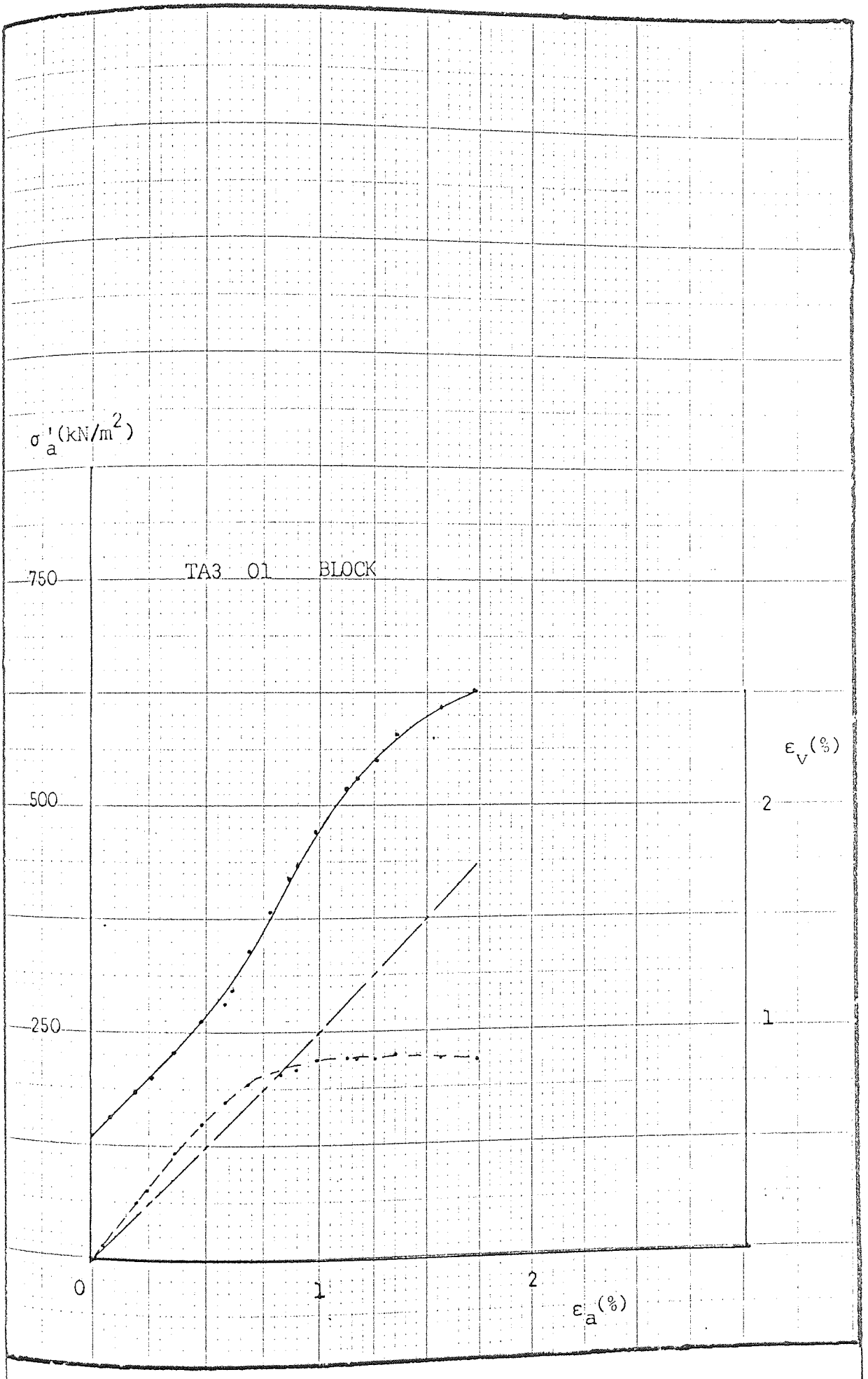

Axial Stress and Volumetric Strain vs Axial Strain - TA3 Series

FIG. 7.18(a)

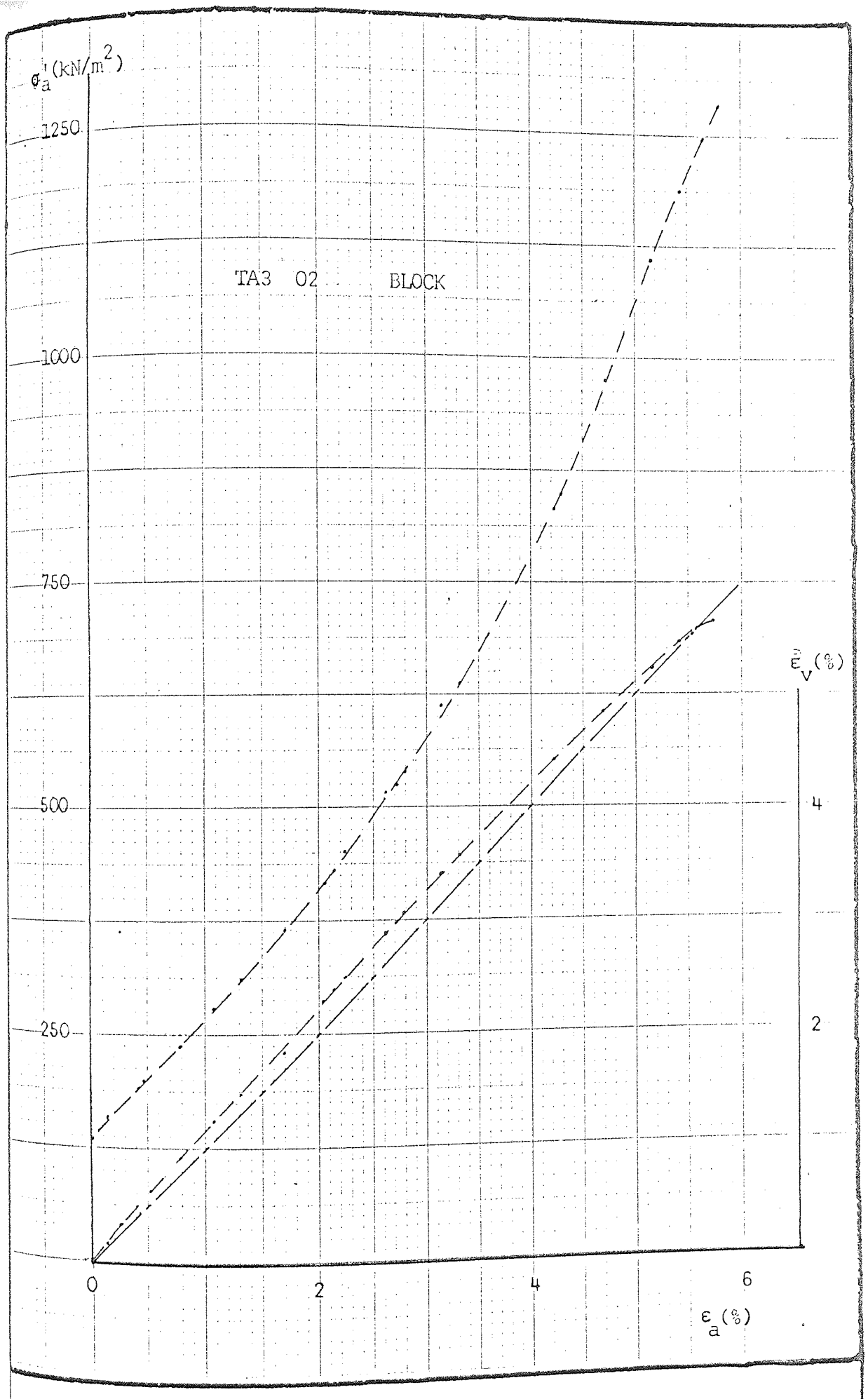

Axial Stress and Volumetric Strain vs Axial Strain - TA3 Series

FIG. 7.18(b)

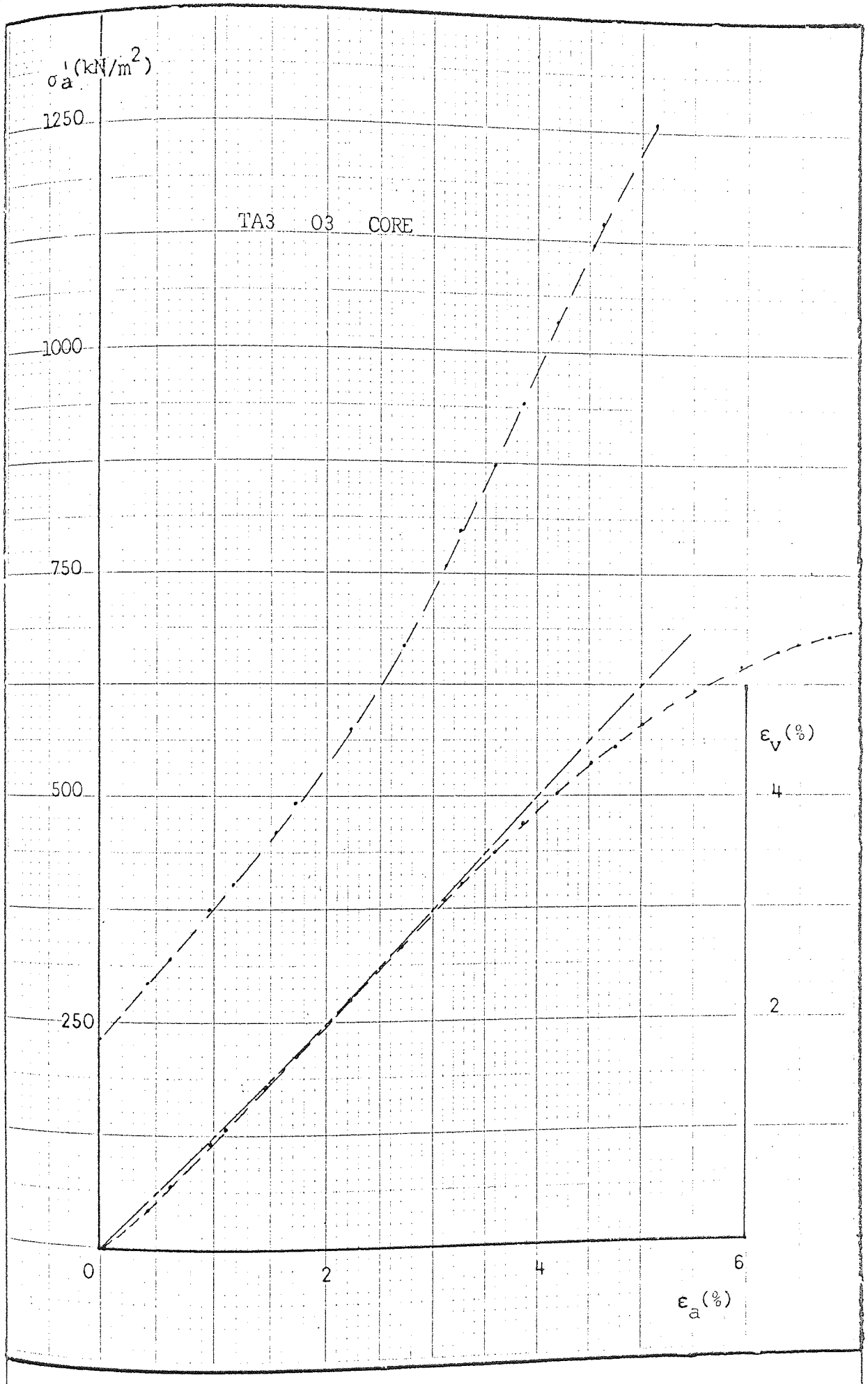

Axial Stress and Volumetric Strain vs Axial Strain - TA3 Series

FIG. 7.18(c)

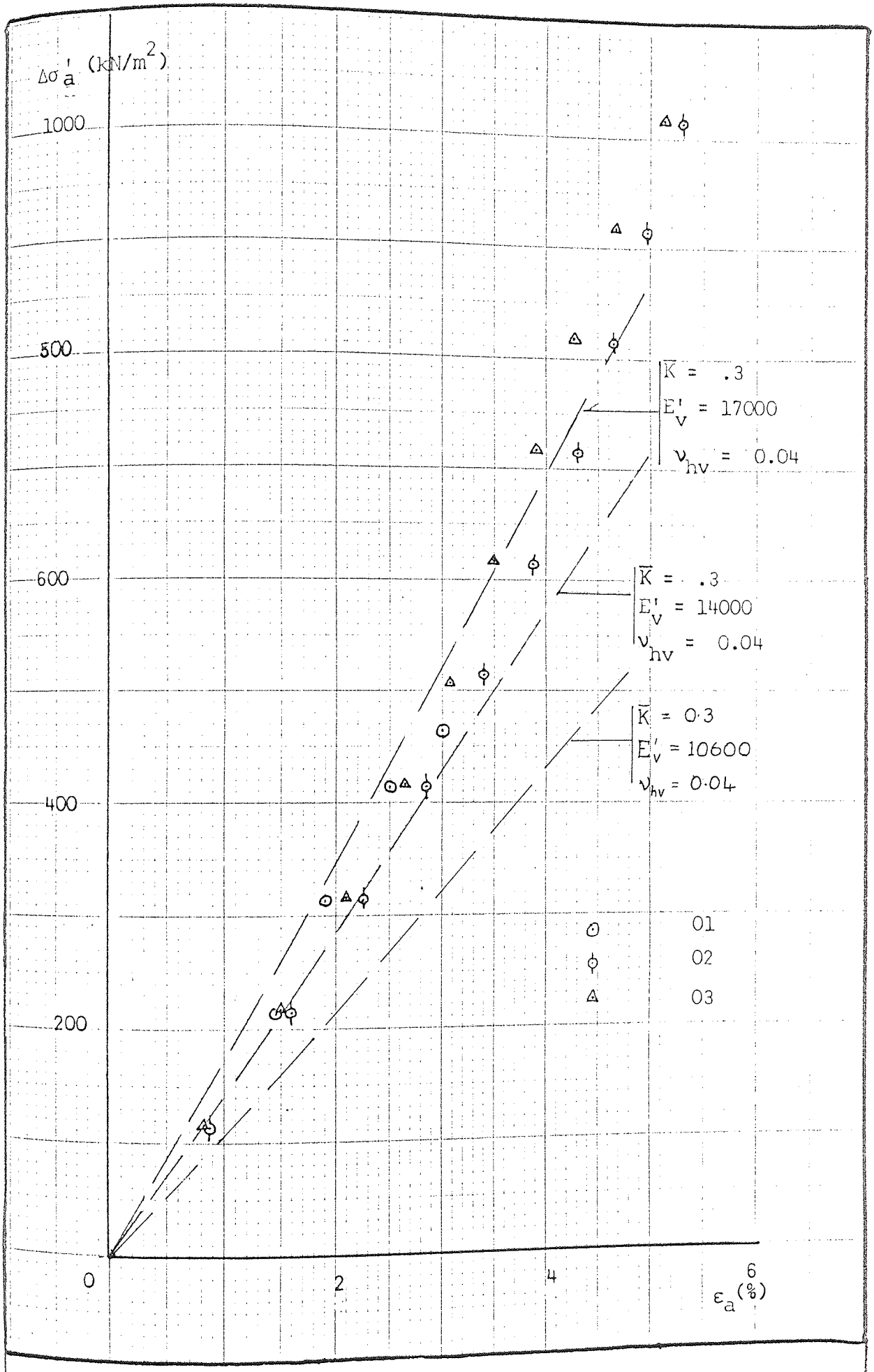

Increment of Axial Stress vs Axial Strain

FIG. 7.19

- TA3 Series

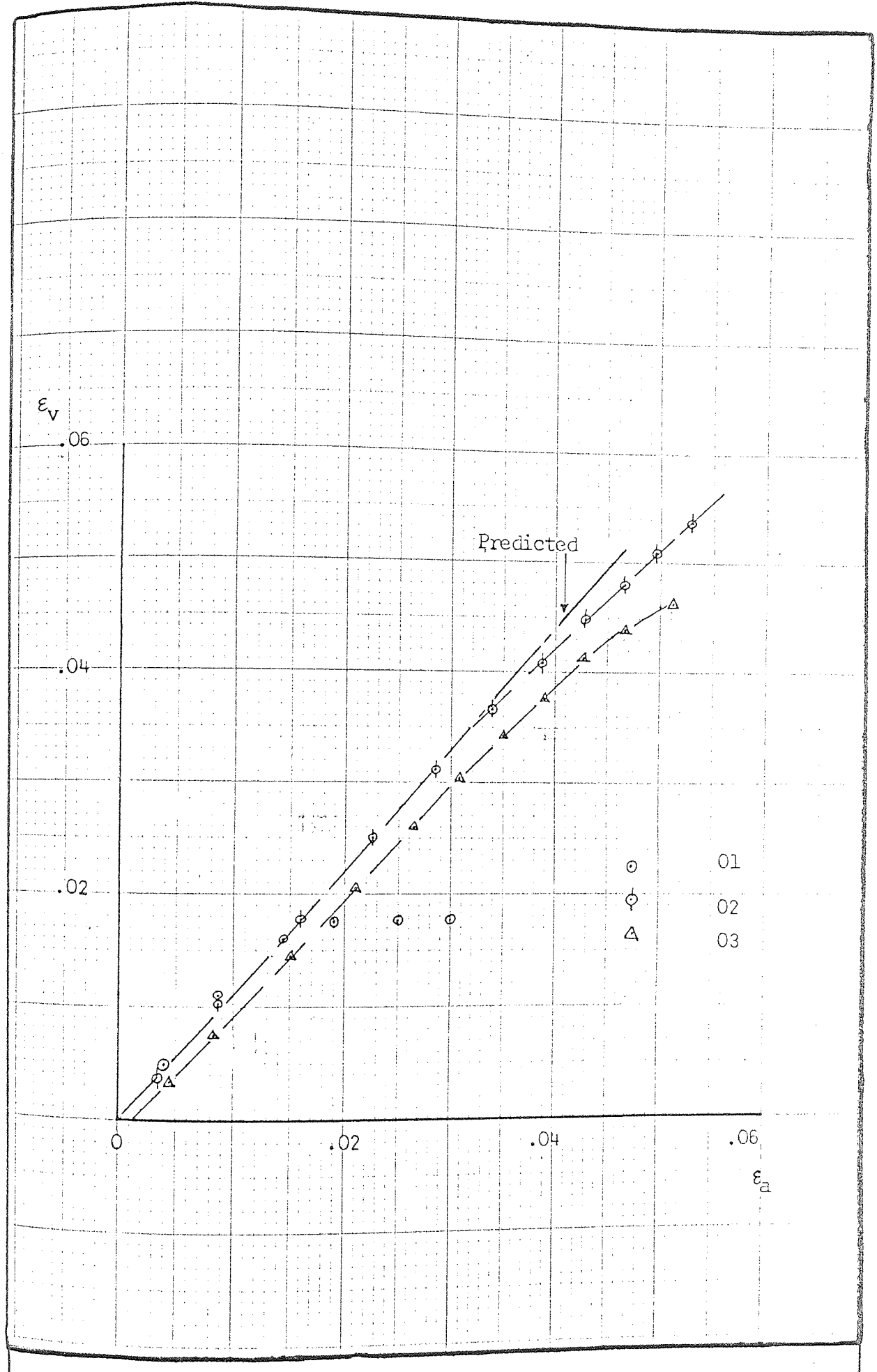

Strain Paths - TA3 Series FIG. 7.20

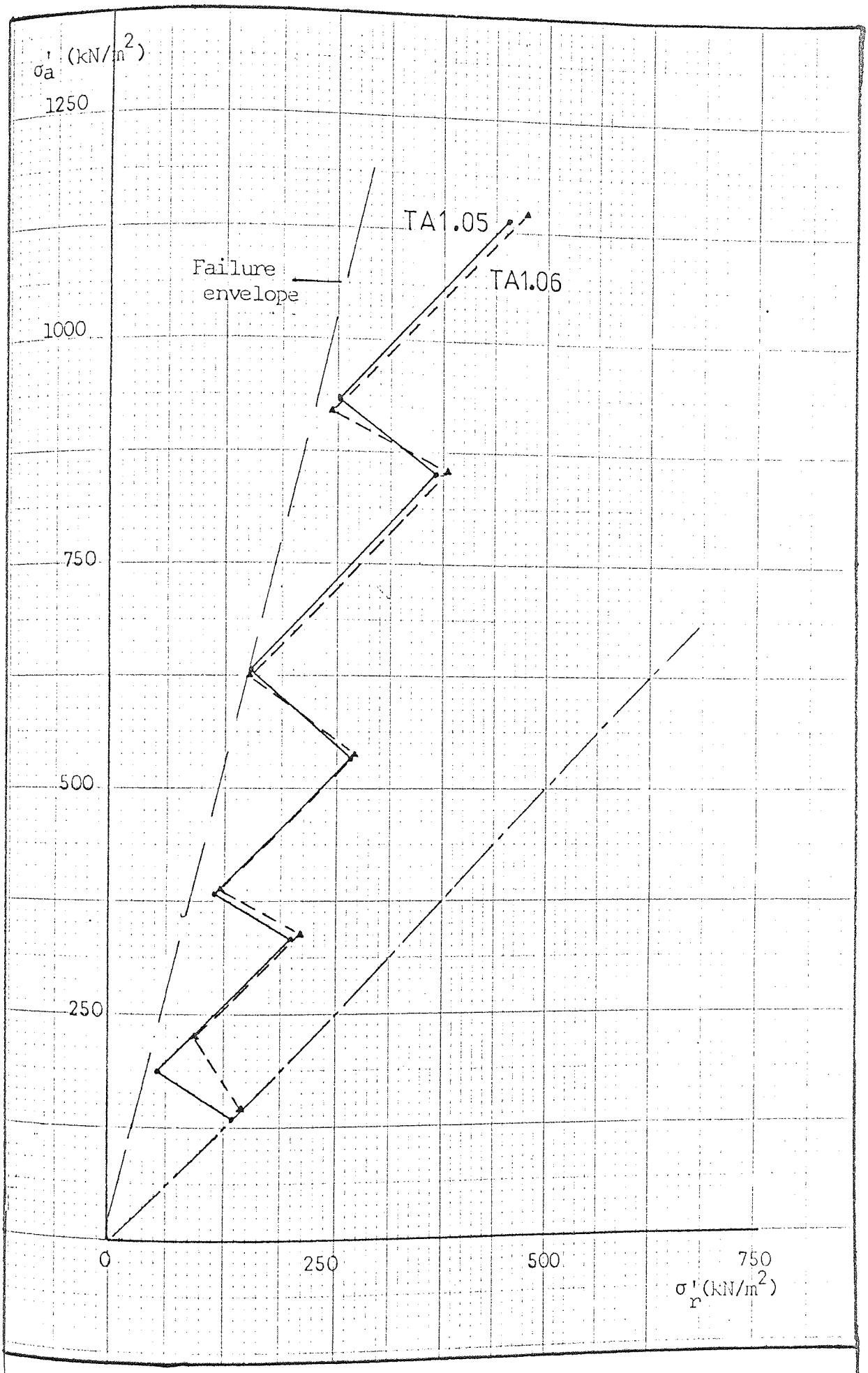

Stress Paths - TA1 Series - Block

FIG. 7.21(a)

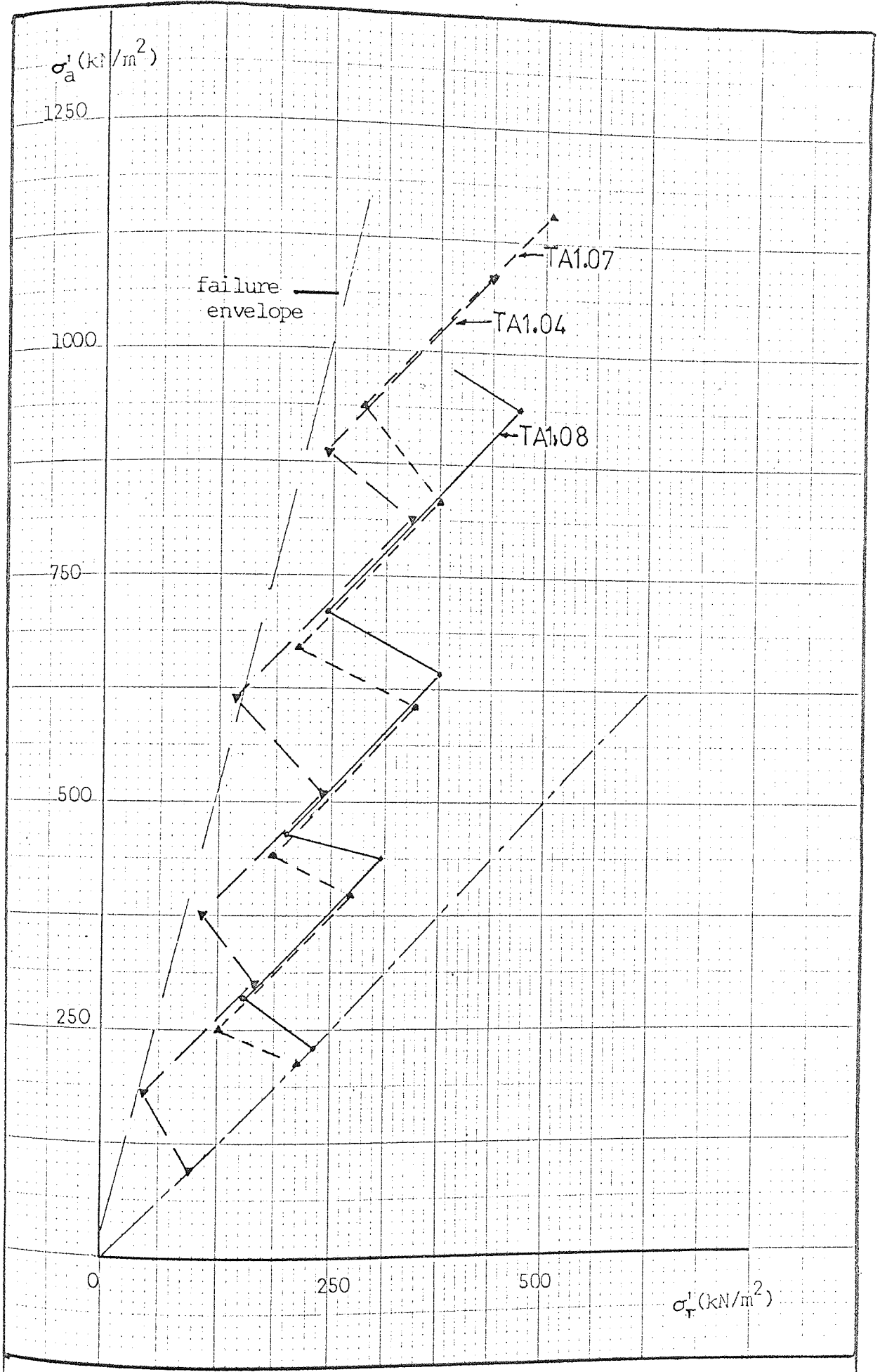

Stress Paths - TA1 Series - Core

FIG. 7.21(b)

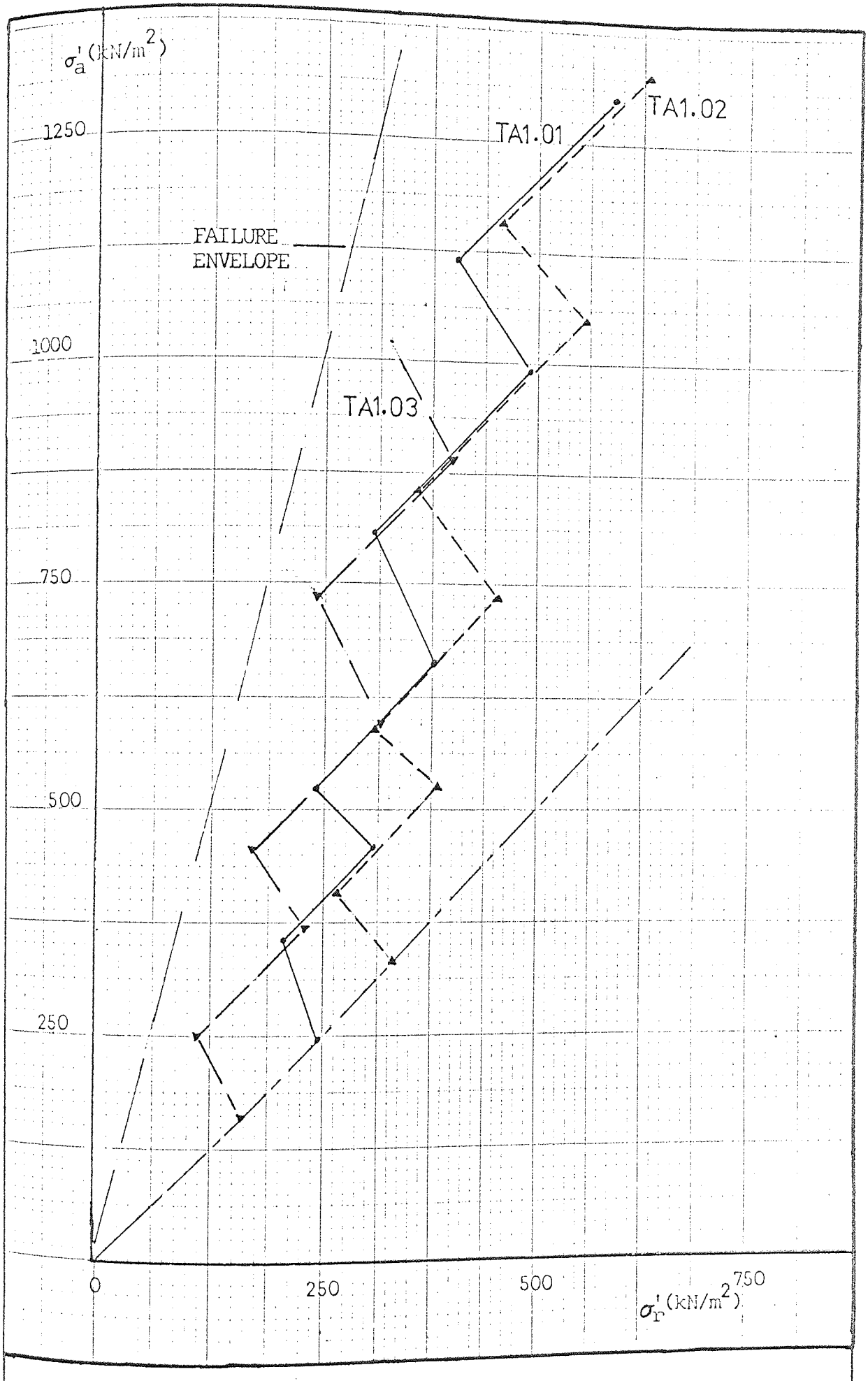

Stress Paths - TA1 Series U70

FIG. 7.21(c)

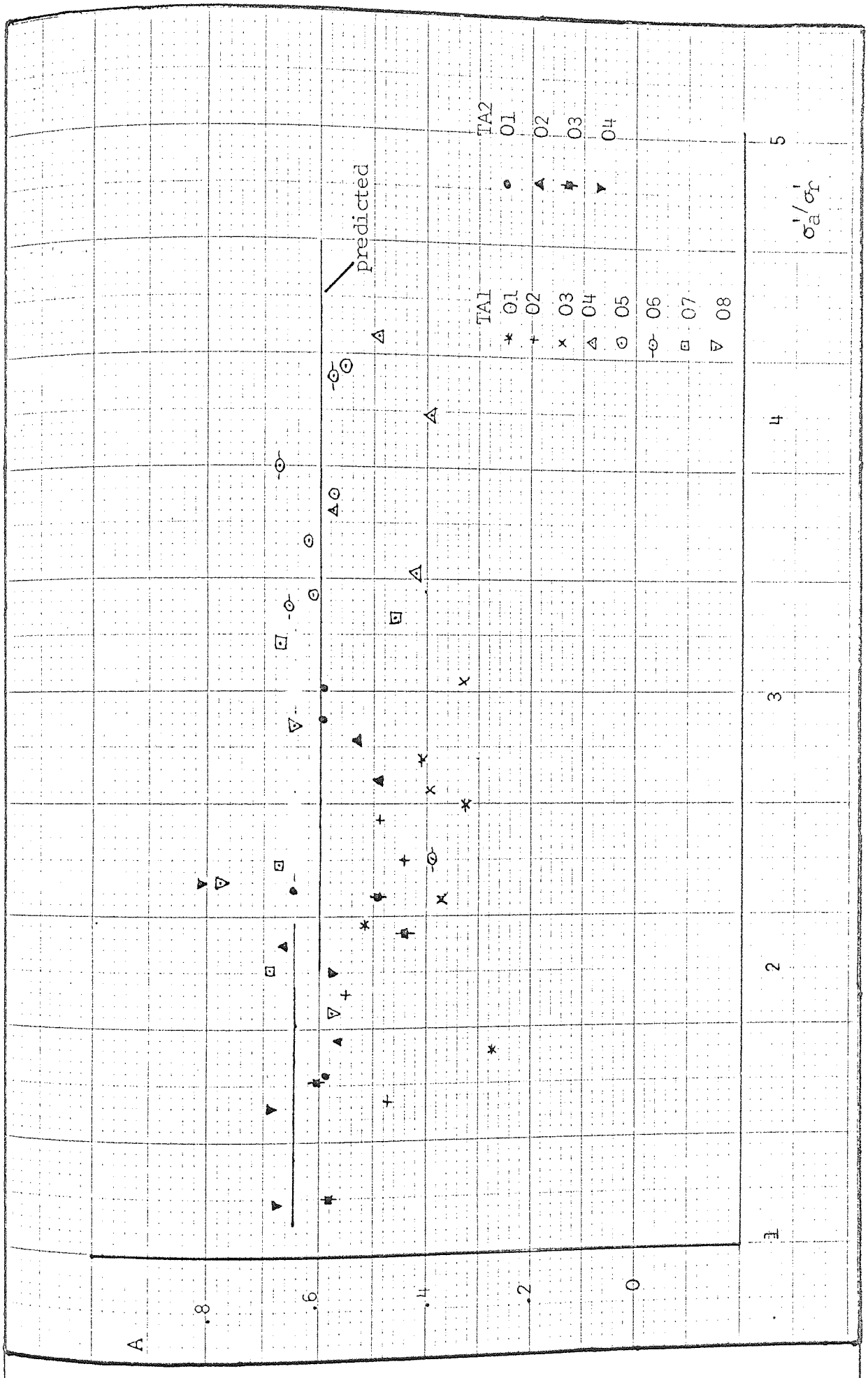

Pore Pressure Parameter, A, vs Stress Ratio($1/K$)

- TA1 and TA2 Series

FIG. 7.22

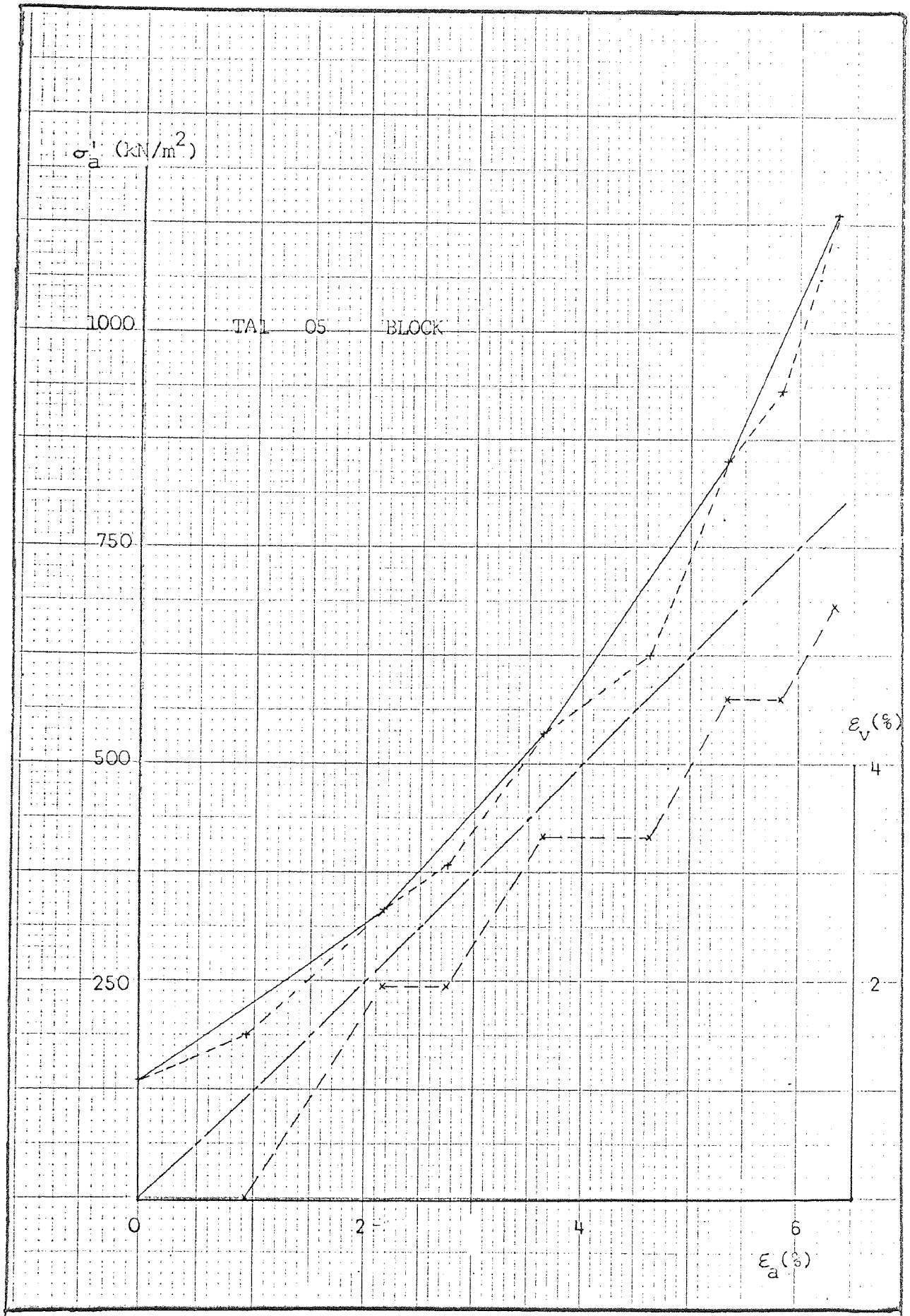

Axial Stress and Volumetric Strain vs Axial Strain - TA1 Series

FIG. 7.23(a)

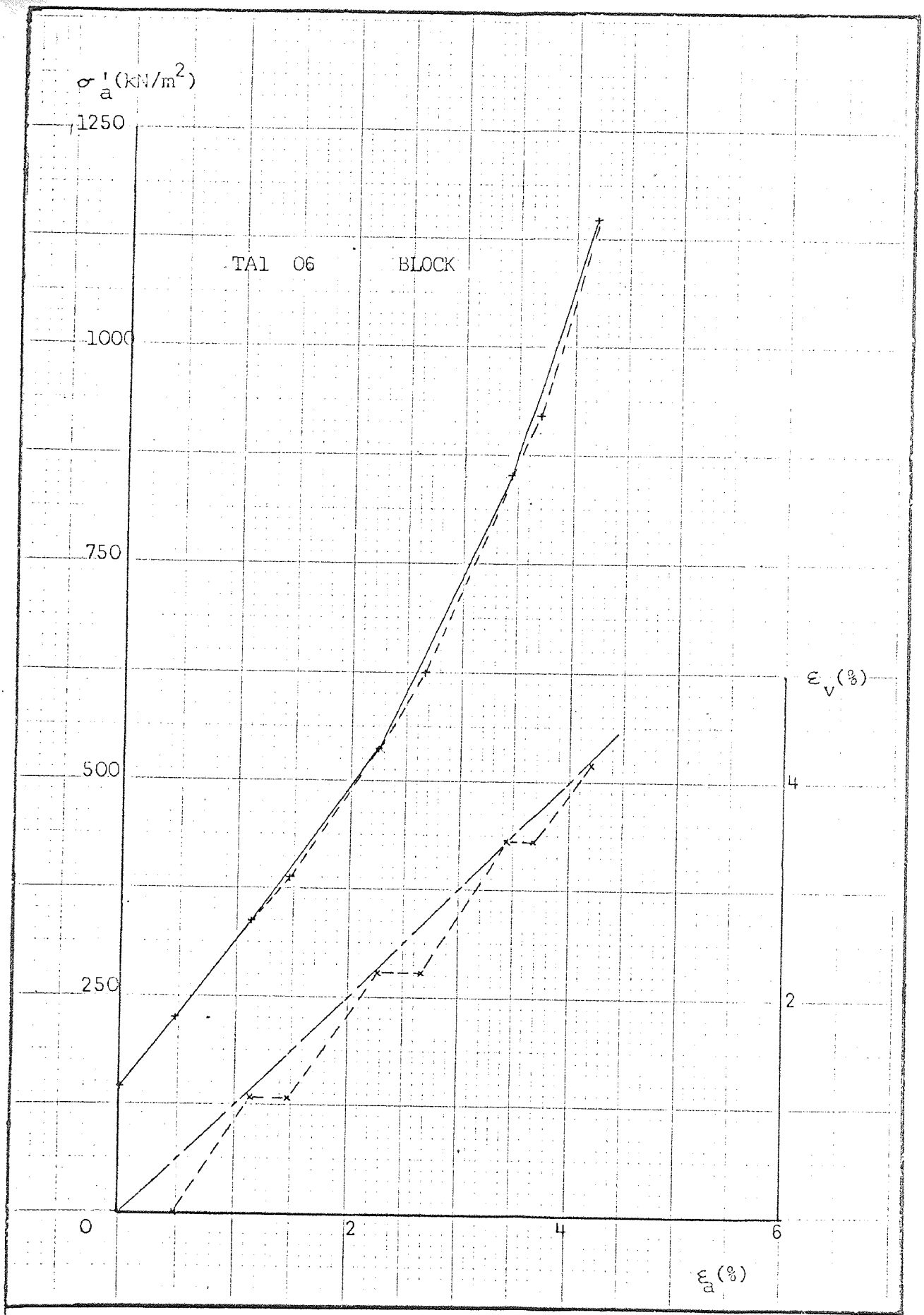

Axial Stress and Volumetric Strain vs Axial Strain - TA1 Series

FIG. 7.23(b)

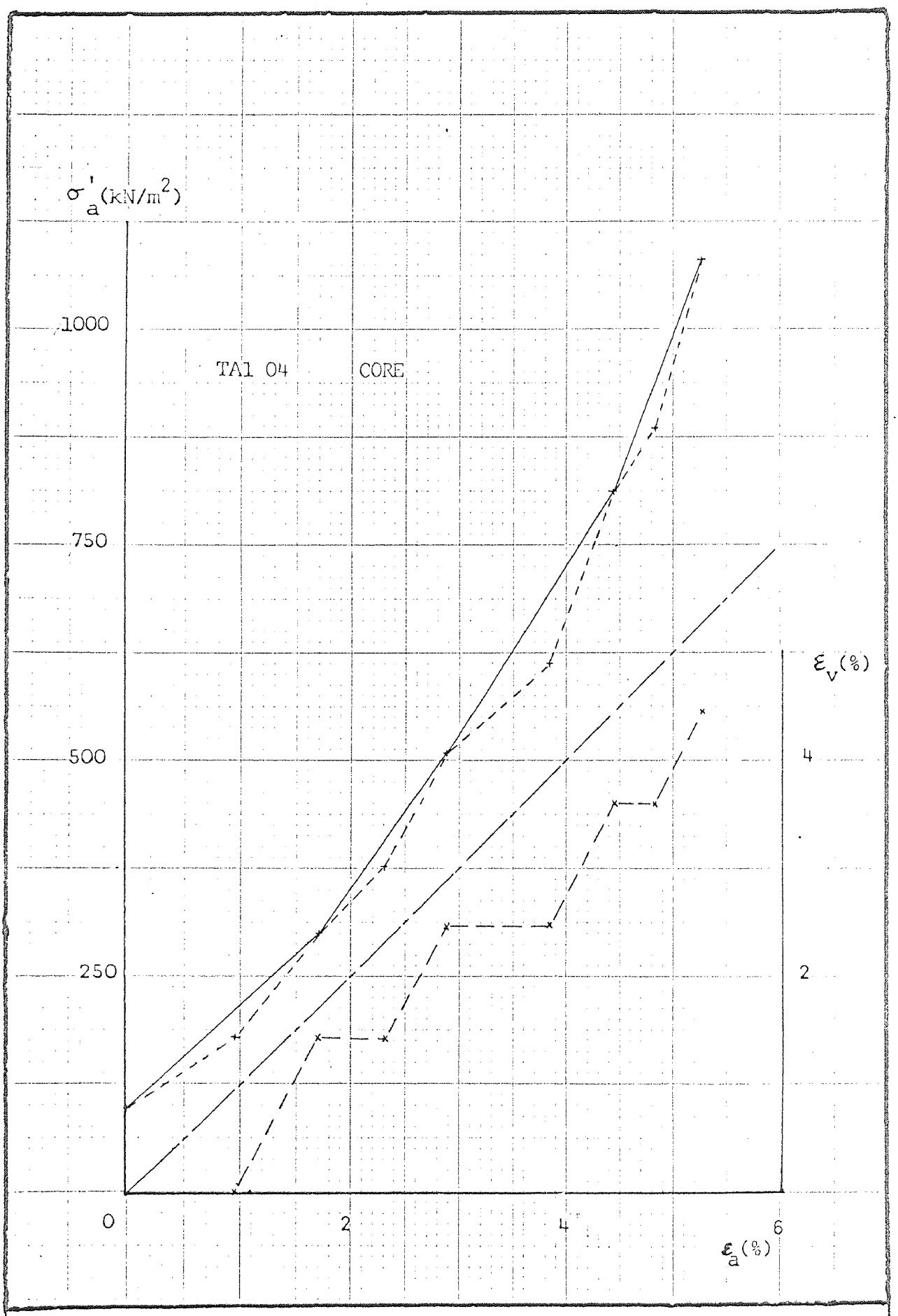

Axial Stress and Volumetric Strain vs Axial Strain - TA1 Series

FIG. 7.23(c)

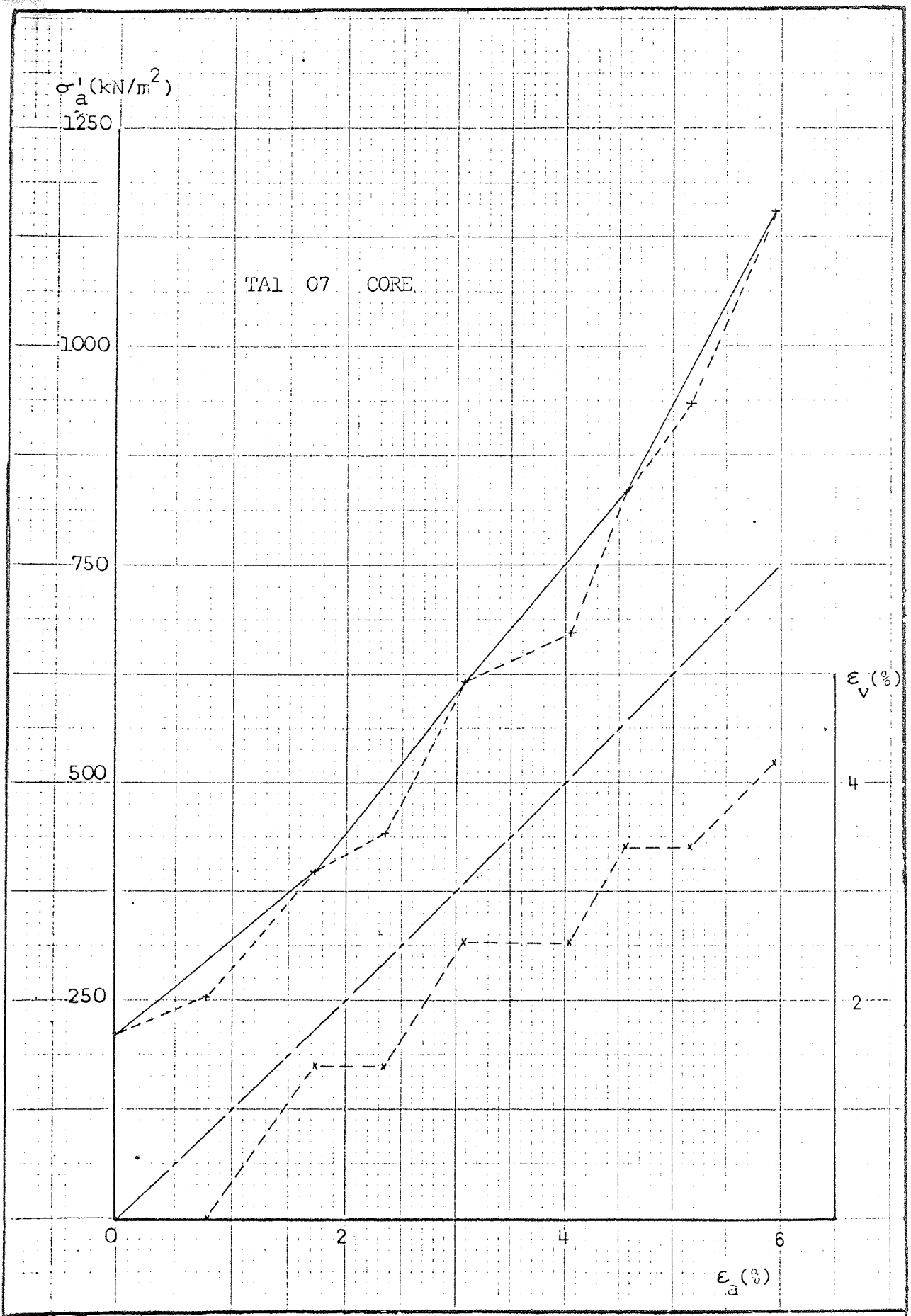

Axial Stress and Volumetric Strain vs Axial Strain - TA1 Series

FIG. 7.23(d)

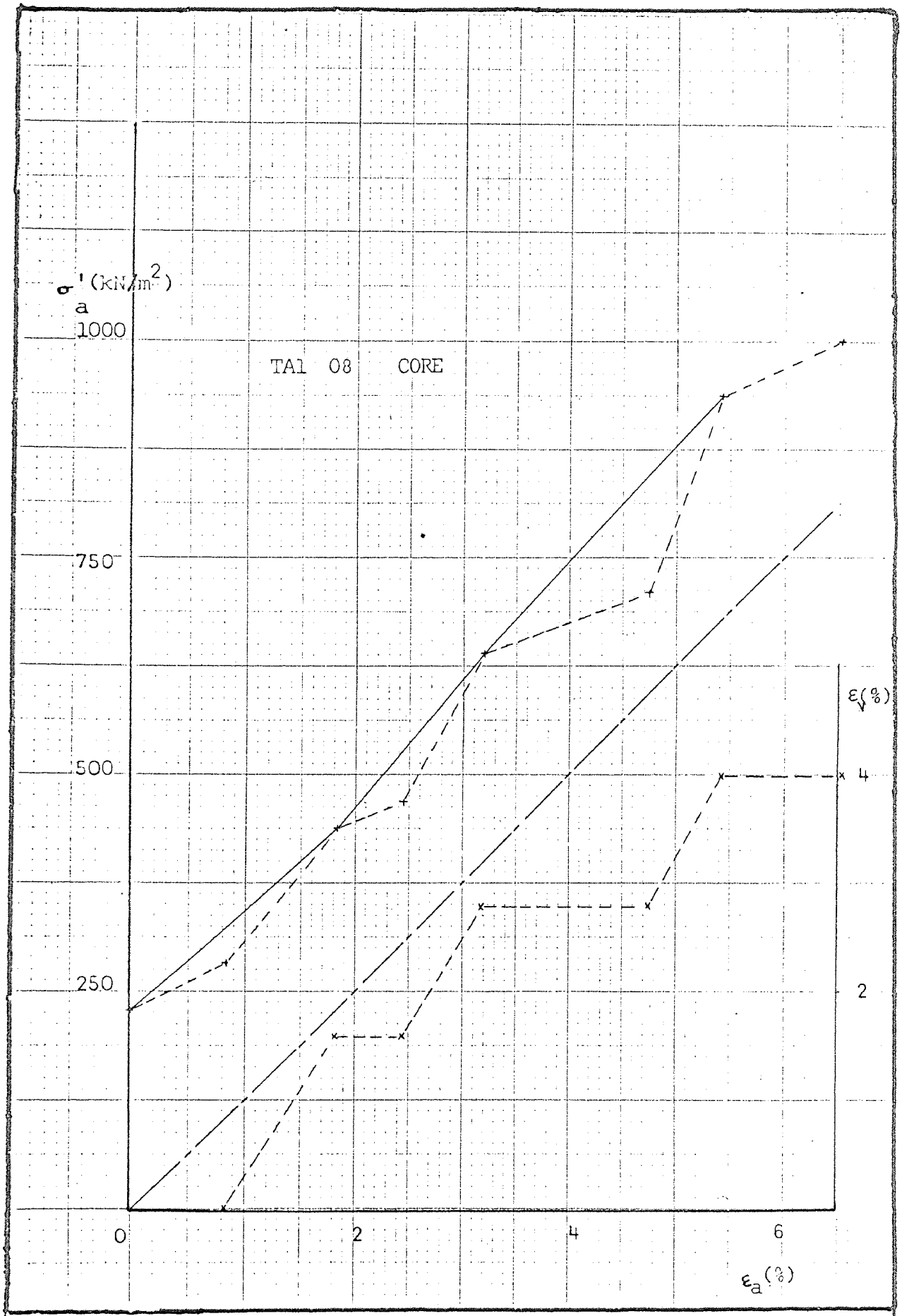

Axial Stress and Volumetric Strain vs Axial Strain - TA1 Series

FIG. 7.23(e)

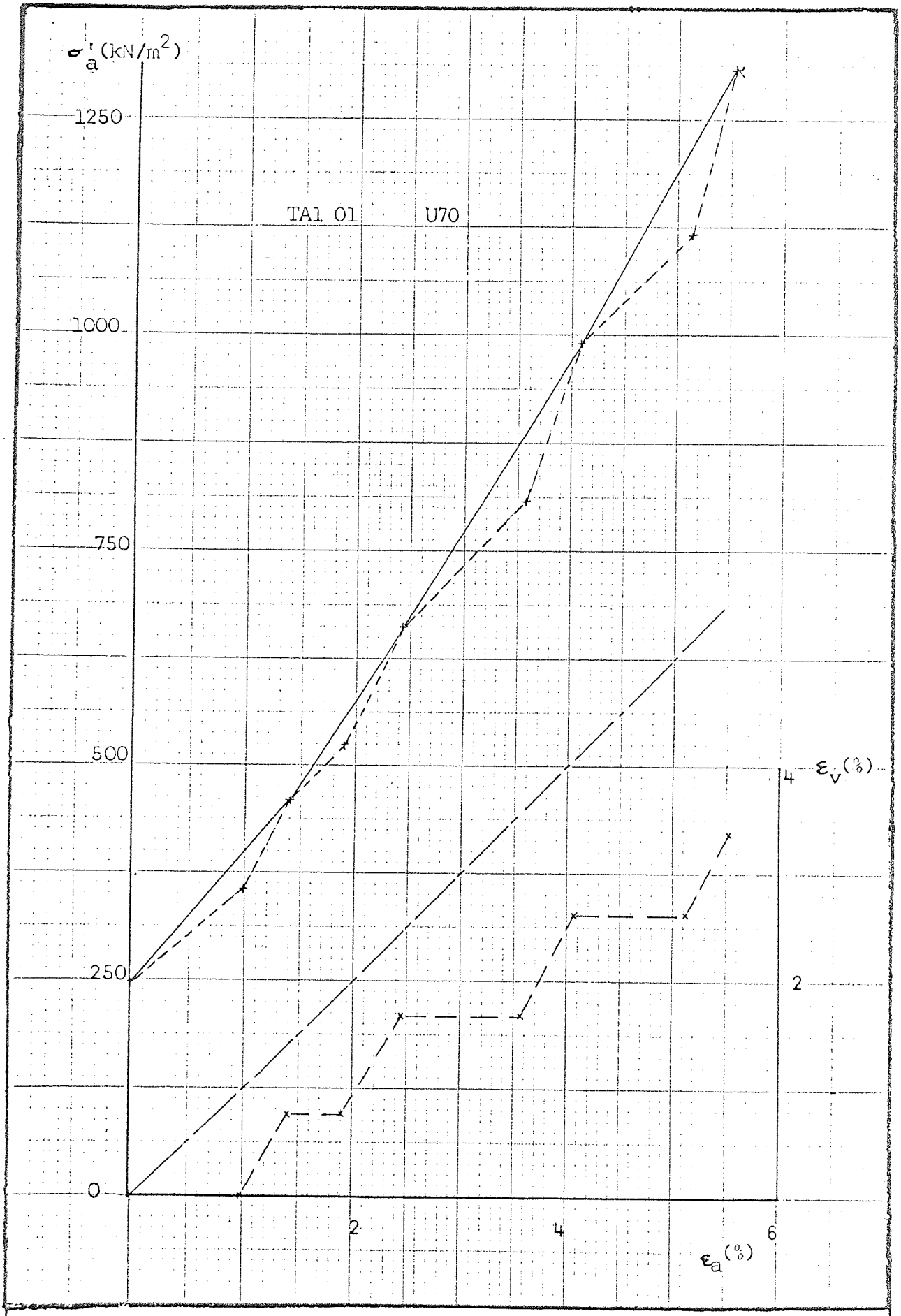

Axial Stress and Volumetric Strain vs Axial Strain - TA1 Series

FIG. 7.23(f)

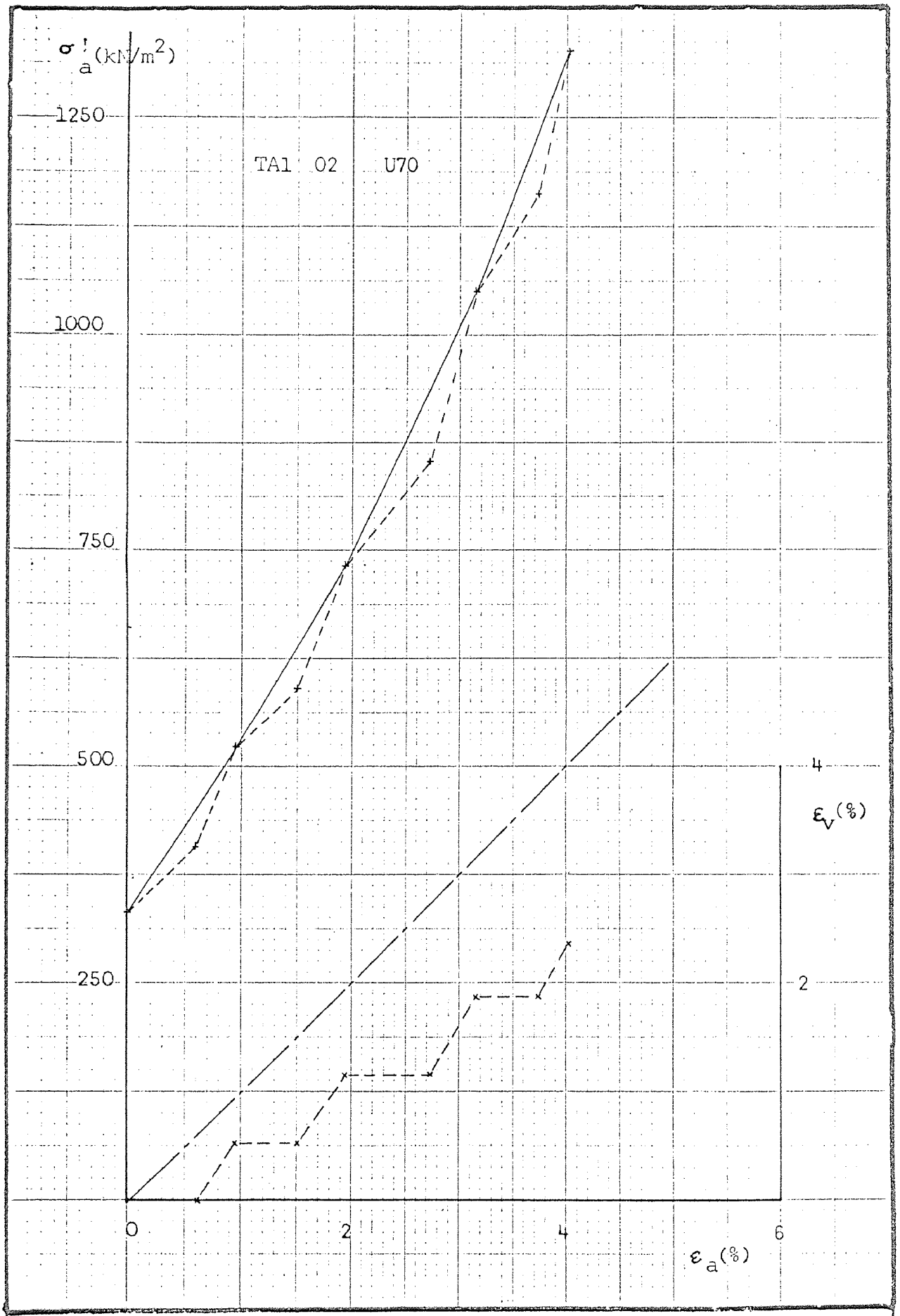

Axial Stress and Volumetric Strain vs Axial Strain - TA1 Series

FIG. 7.23(g)

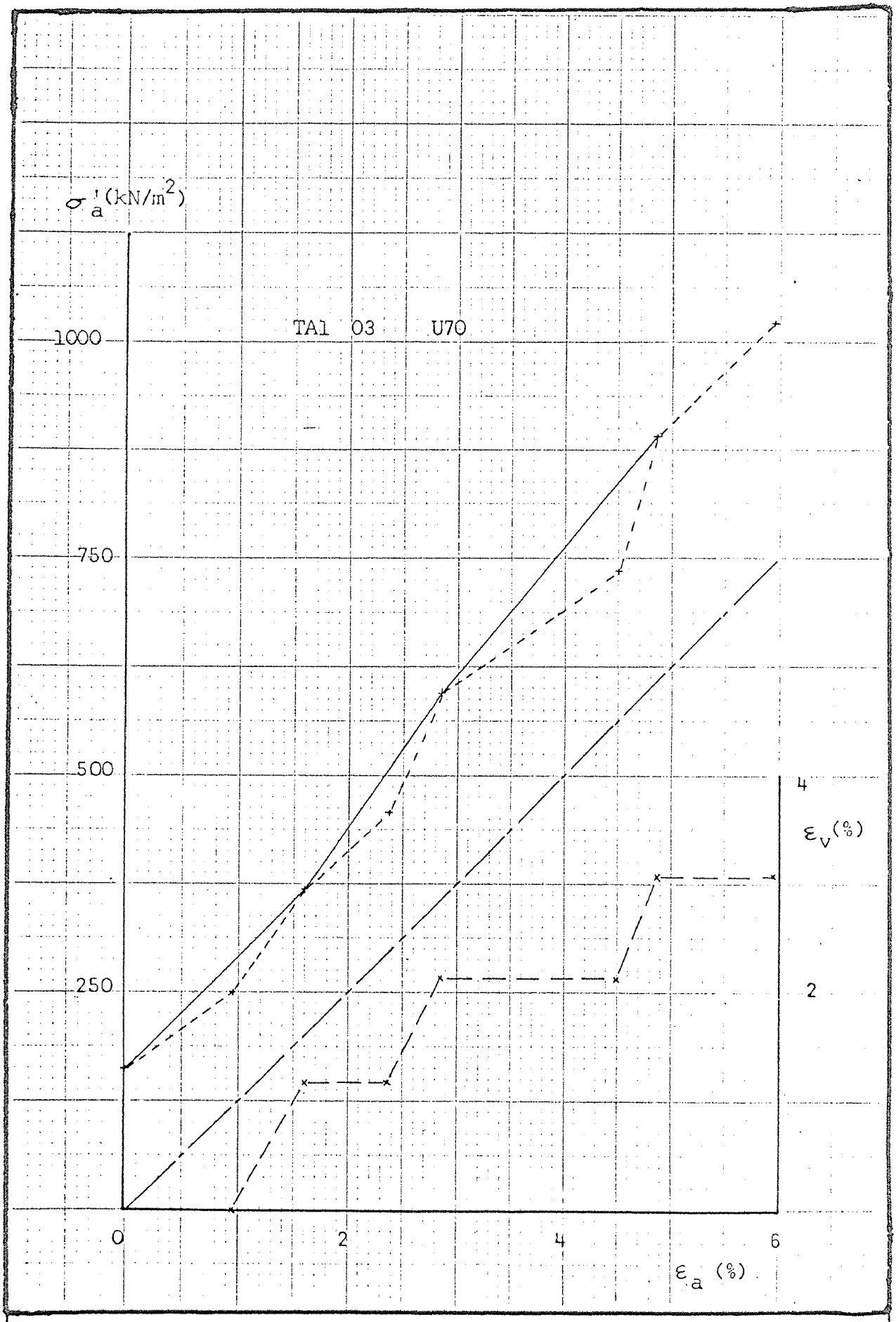

Axial Stress and Volumetric Strain vs Axial Strain - TA1 Series

FIG. 7.2 3(h)

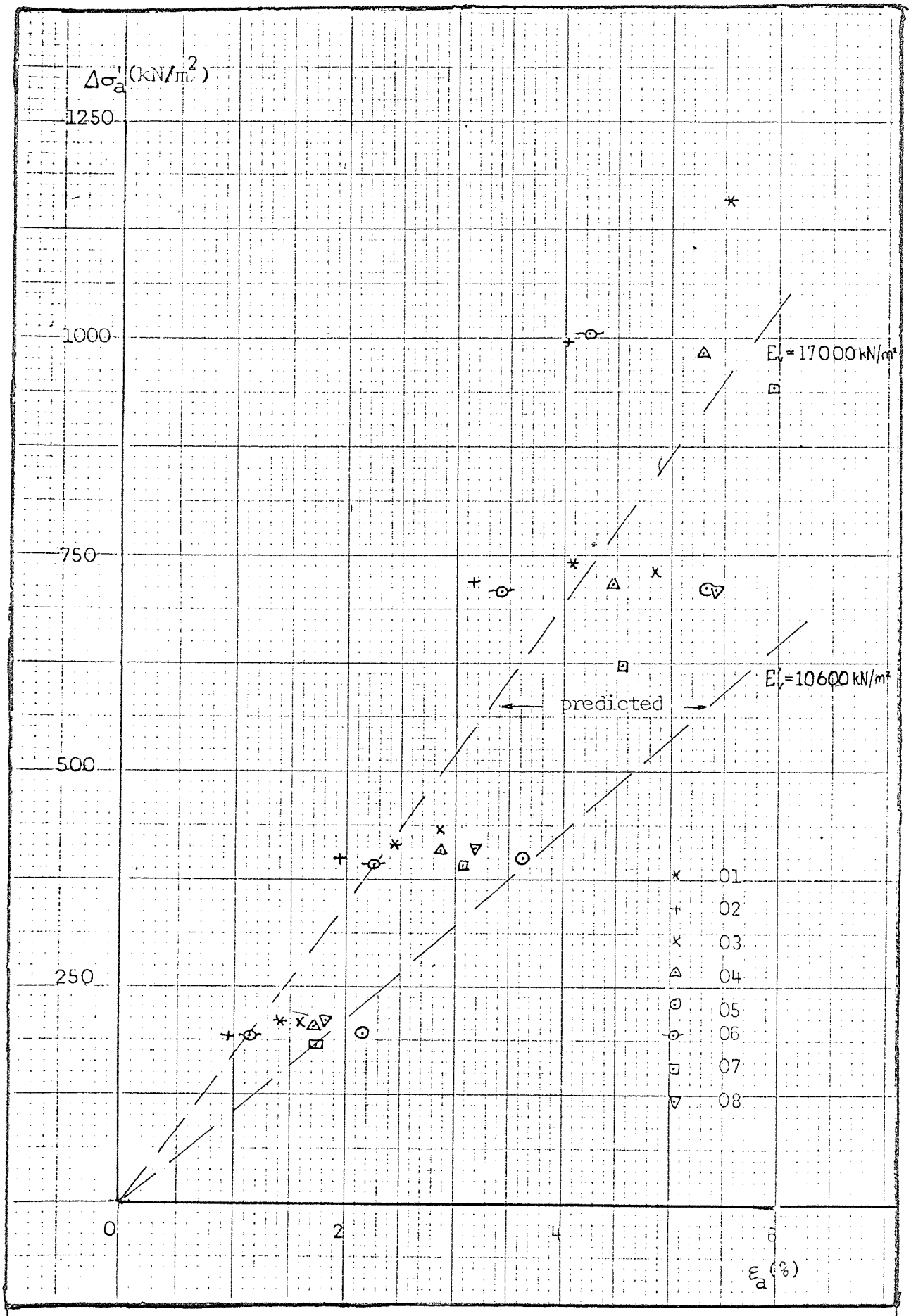

Increment of Axial Stress vs Axial Strain

FIG. 7.24

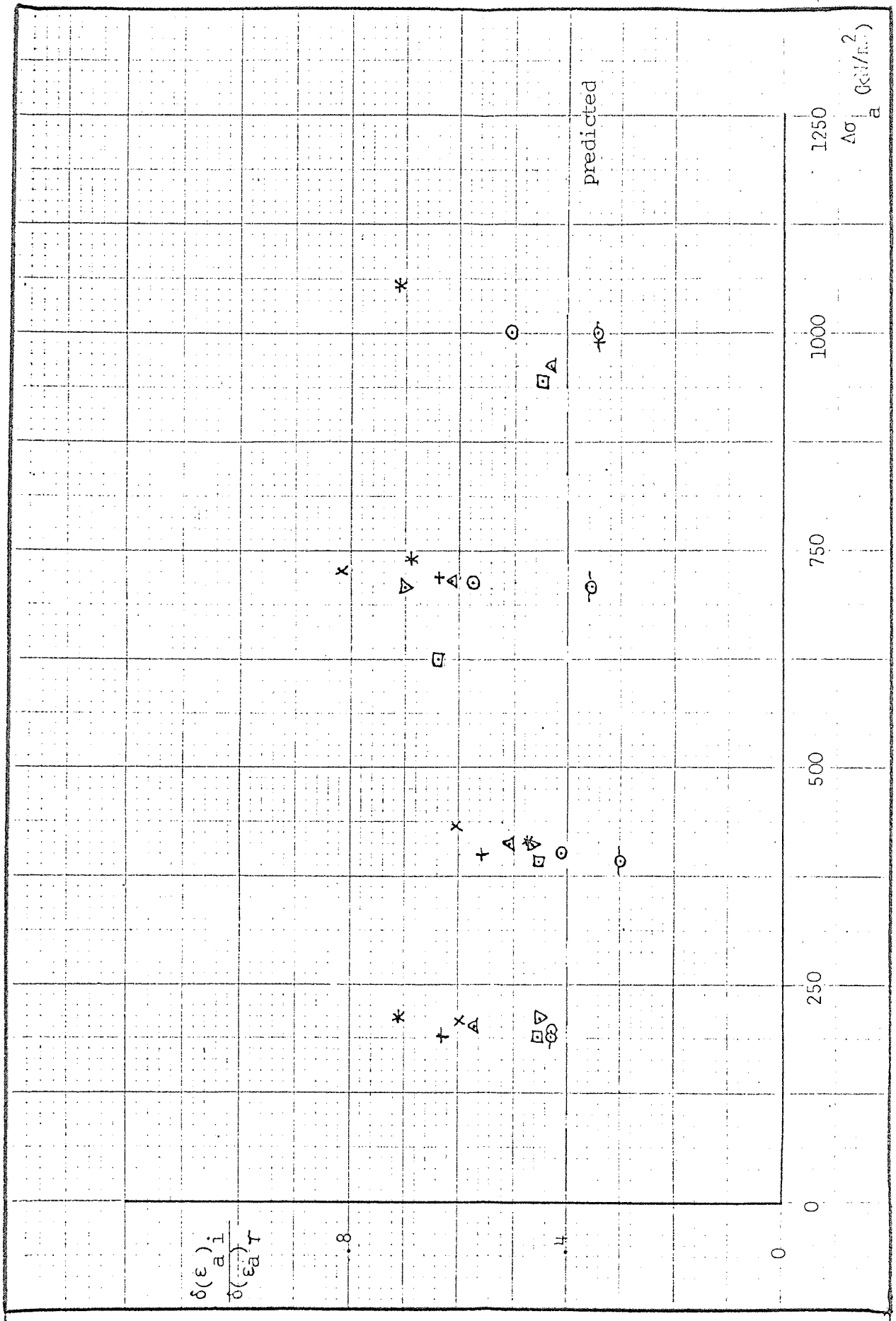

Ratio of Initial total Axial Strain vs Axial Stress Increment - TA1 Series

FIG. 7.25

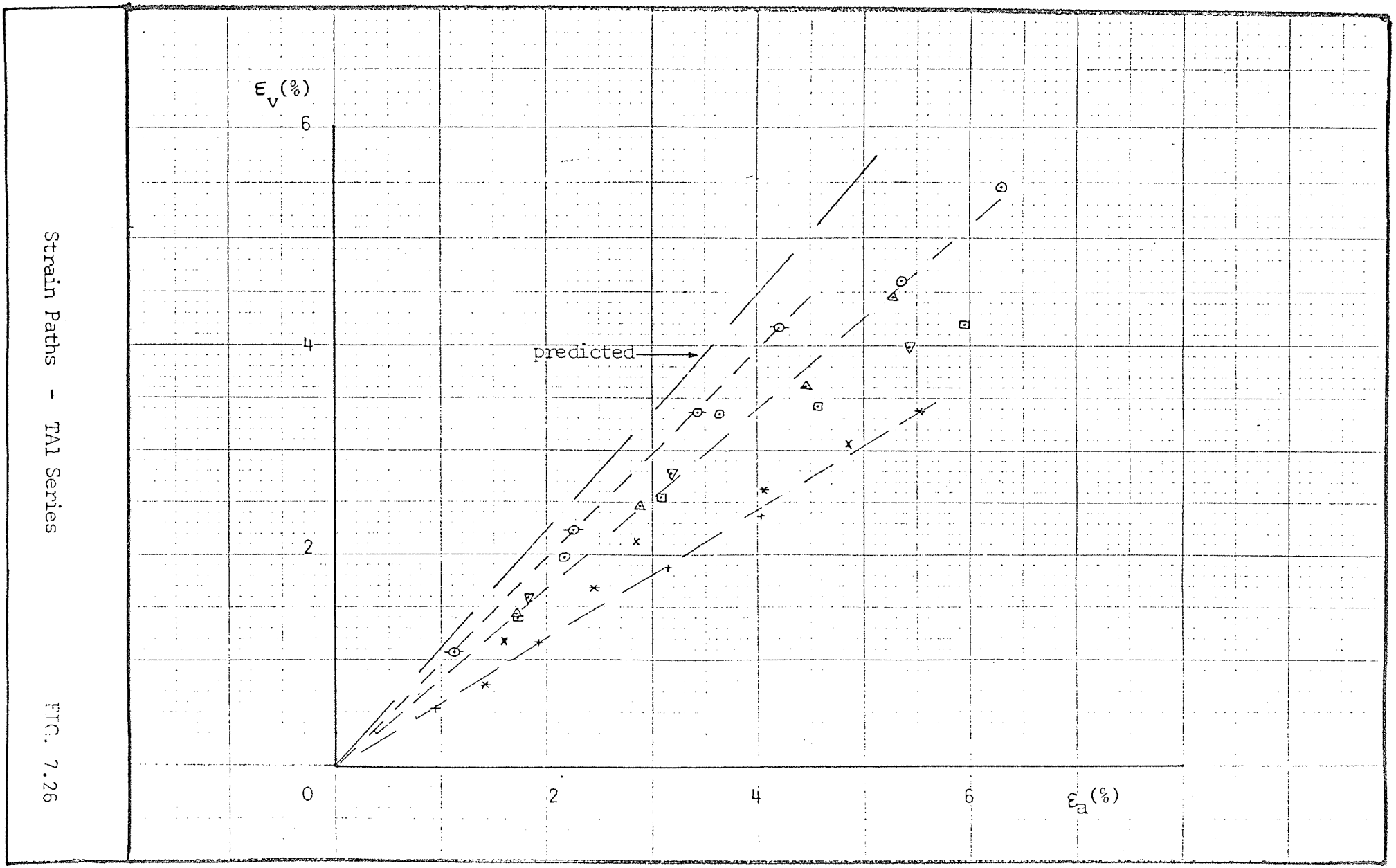

Strain Paths - TA1 Series

FIG. 7.26

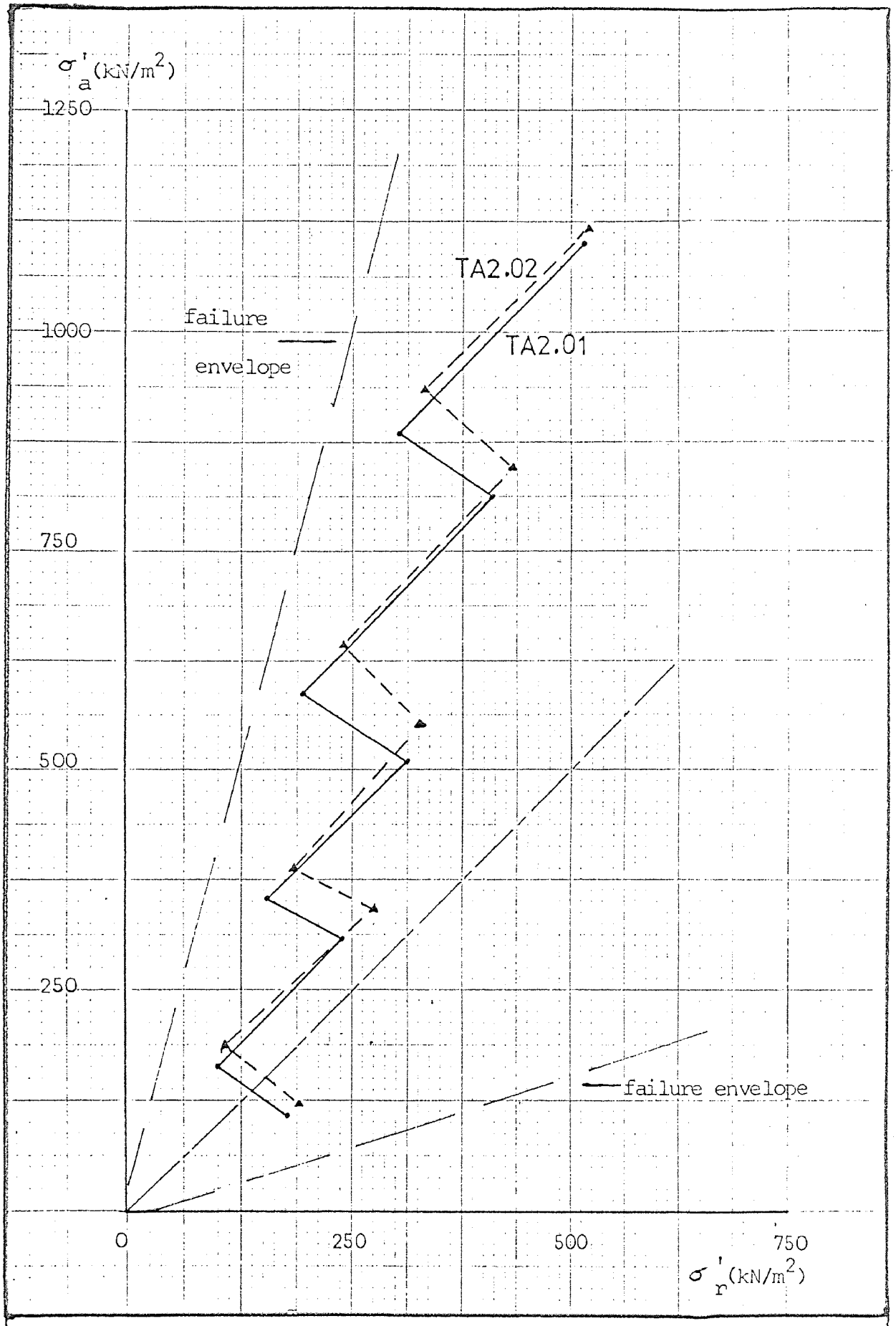

Stress Paths - TA2 Series FIG. 7.27(a)

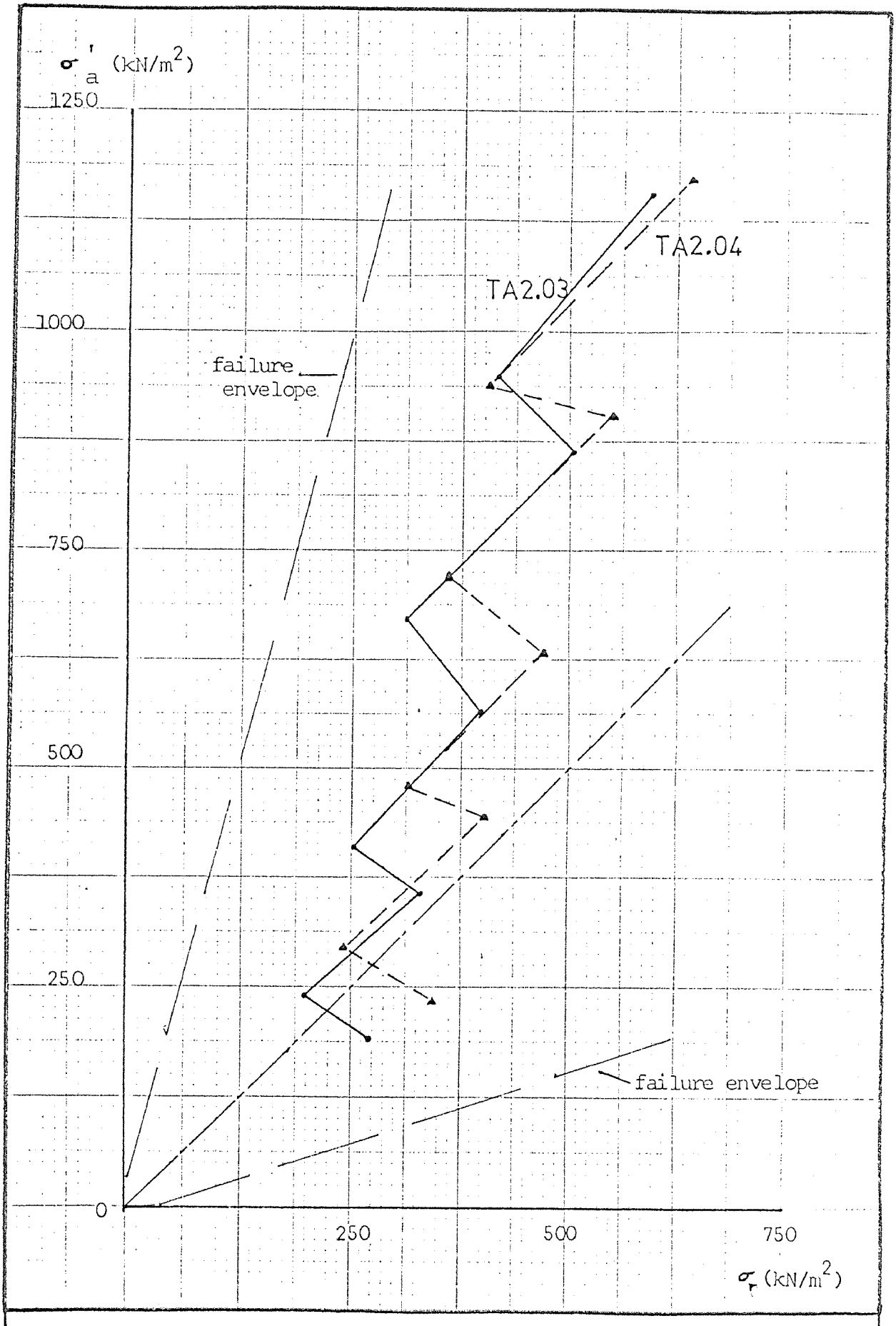

Stress Paths - TA2 Series

FIG. 7.27(b)

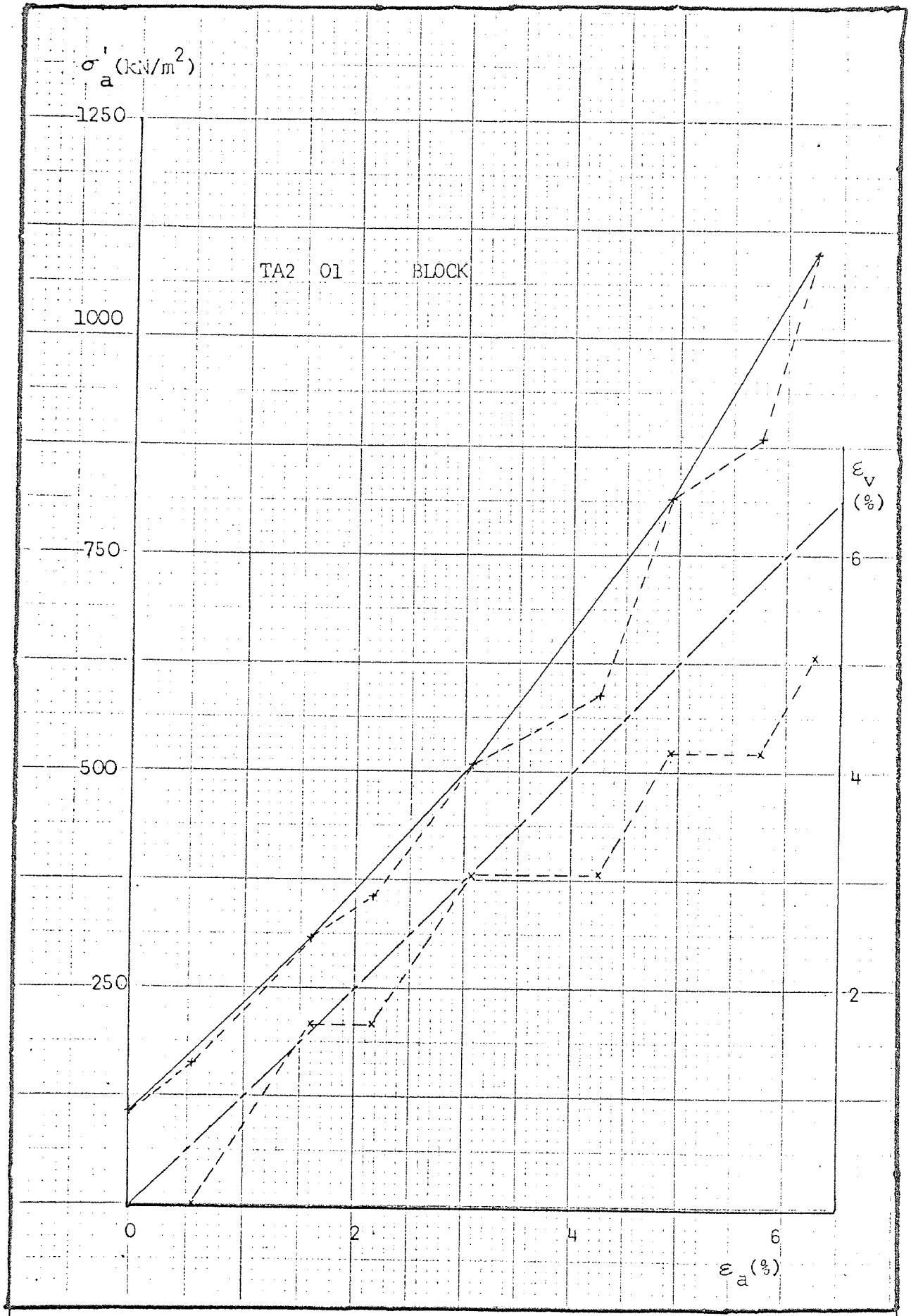

Axial Stress and Volumetric Strain vs Axial Strain - TA2 Series

FIG. 7.28(a)

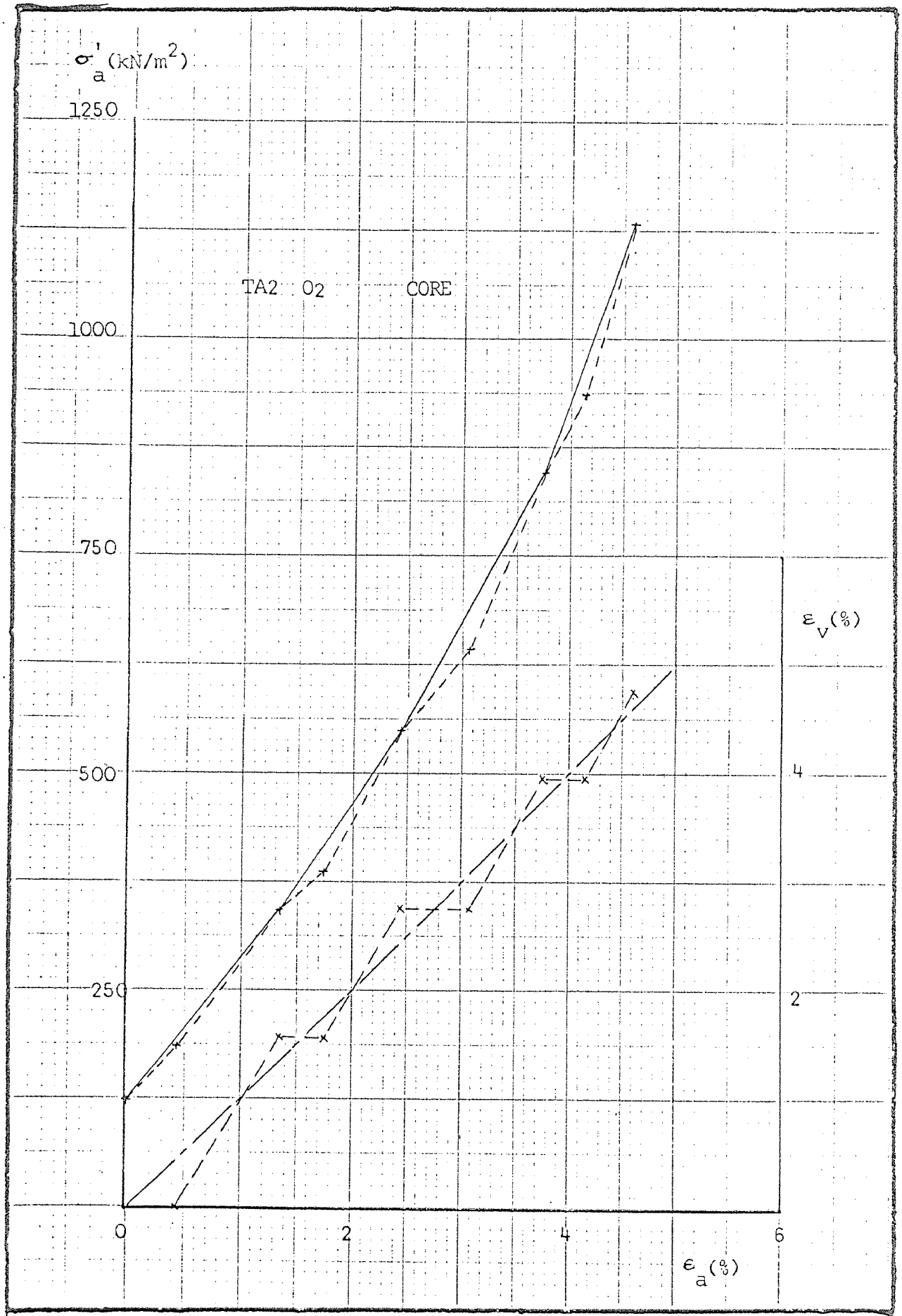

Axial Stress and Volumetric Strain vs Axial Strain - TA2 Series

FIG. 7.28(b)

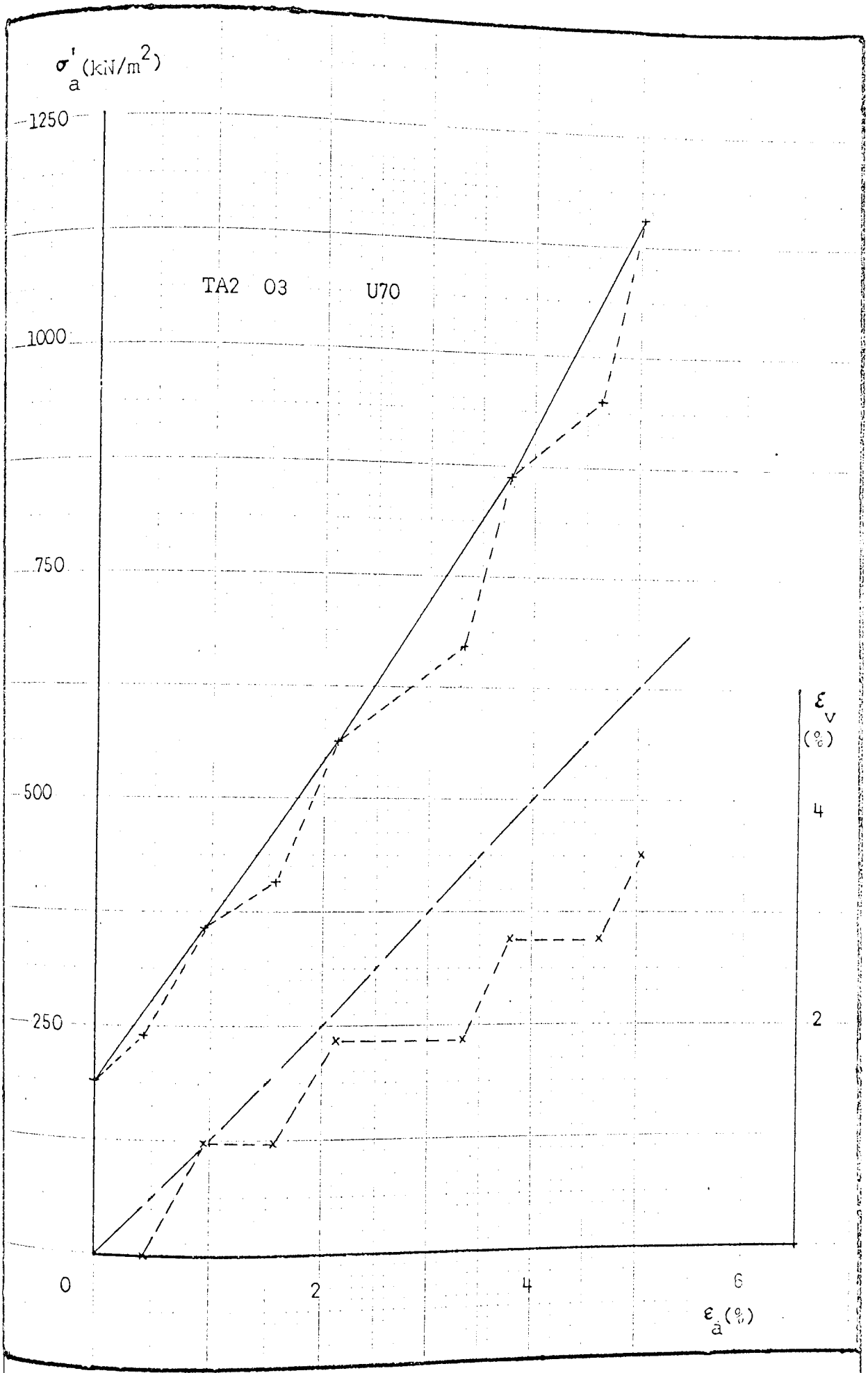

Axial Stress and Volumetric Strain vs Axial Strain - TA2 Series

FIG. 7.28(c)

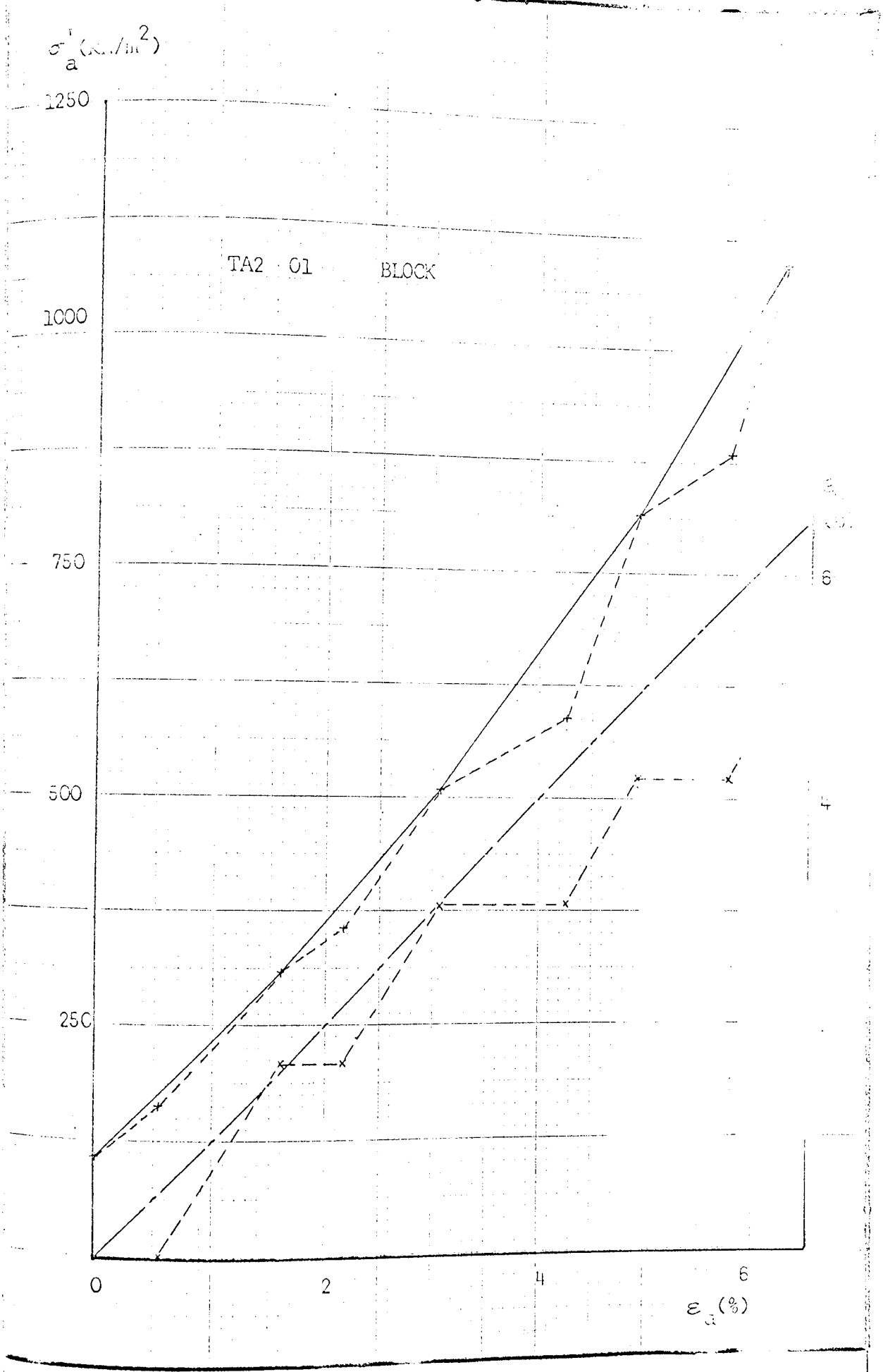

Axial Stress and Volumetric Strain vs Axial Strain - TA2 Series

(G.)

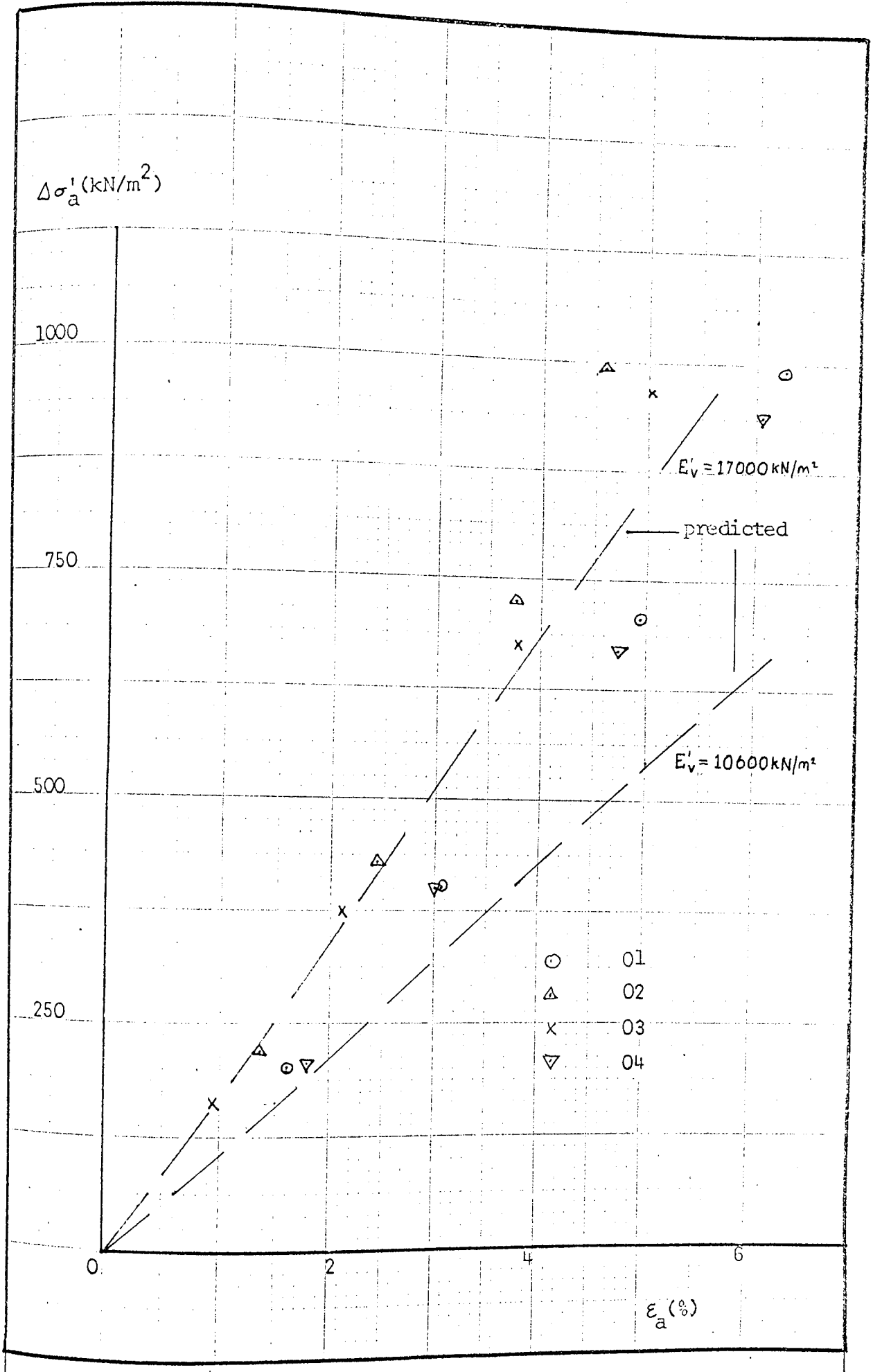

Increment of Axial Stress vs Axial Strain

- TA2 Series

FIG. 7.20

Ratio of Initial total Axial Strain vs Axial Stress Increment - TA2. Series

FIG. 7.30

Strain Paths - TA2 Series

FIG. 7.31

Strain Ratio v incremental Stress Ratio

$-(1/K) < 2$

FIG. 7.32

Strain Ratio v Incremental Stress Ratio

$-(1/K) > 2$

FIG. 7.33

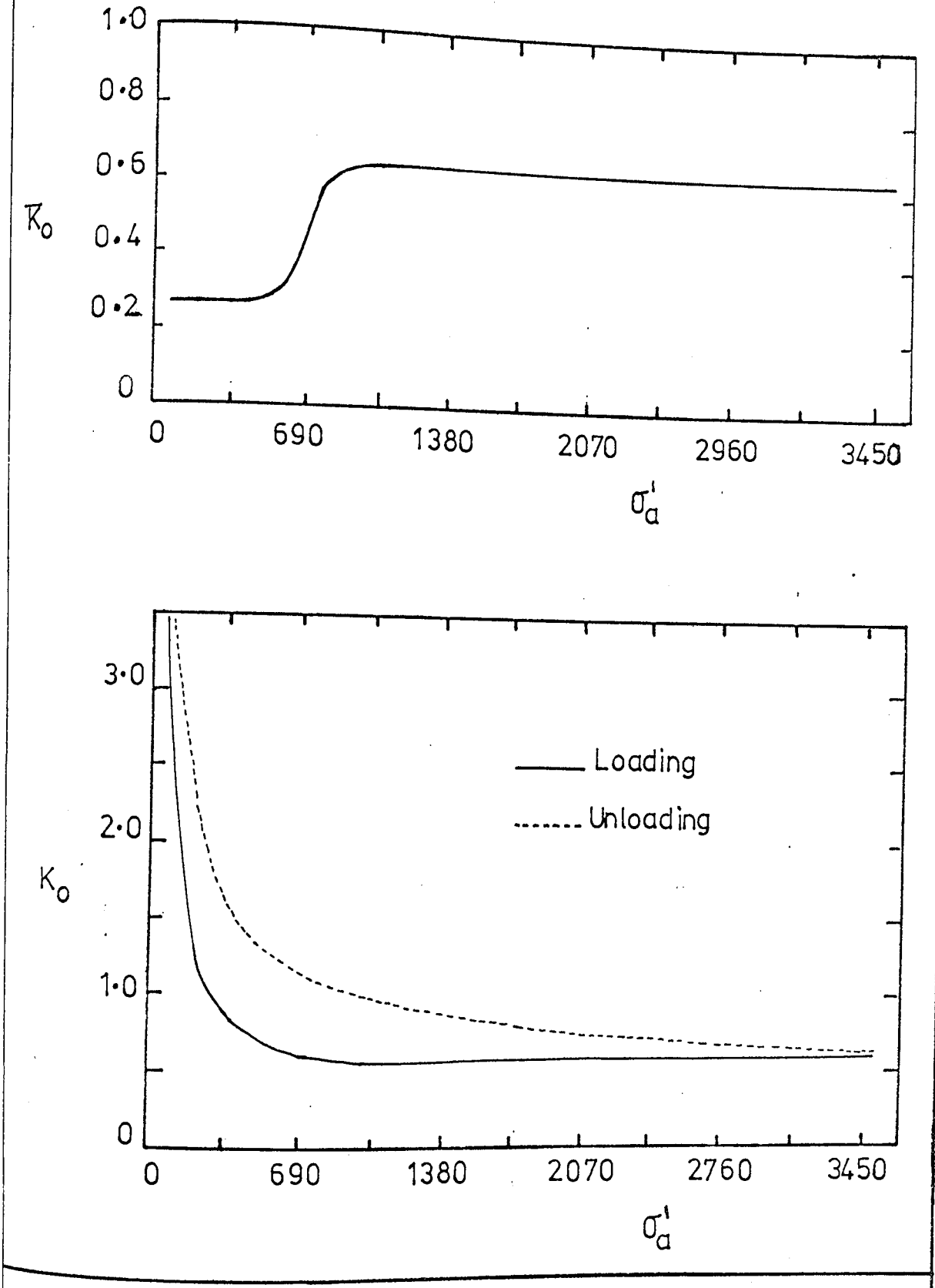

FIG. 7.34 Recorded stress ratios from oedometer tests - after Som (1968)

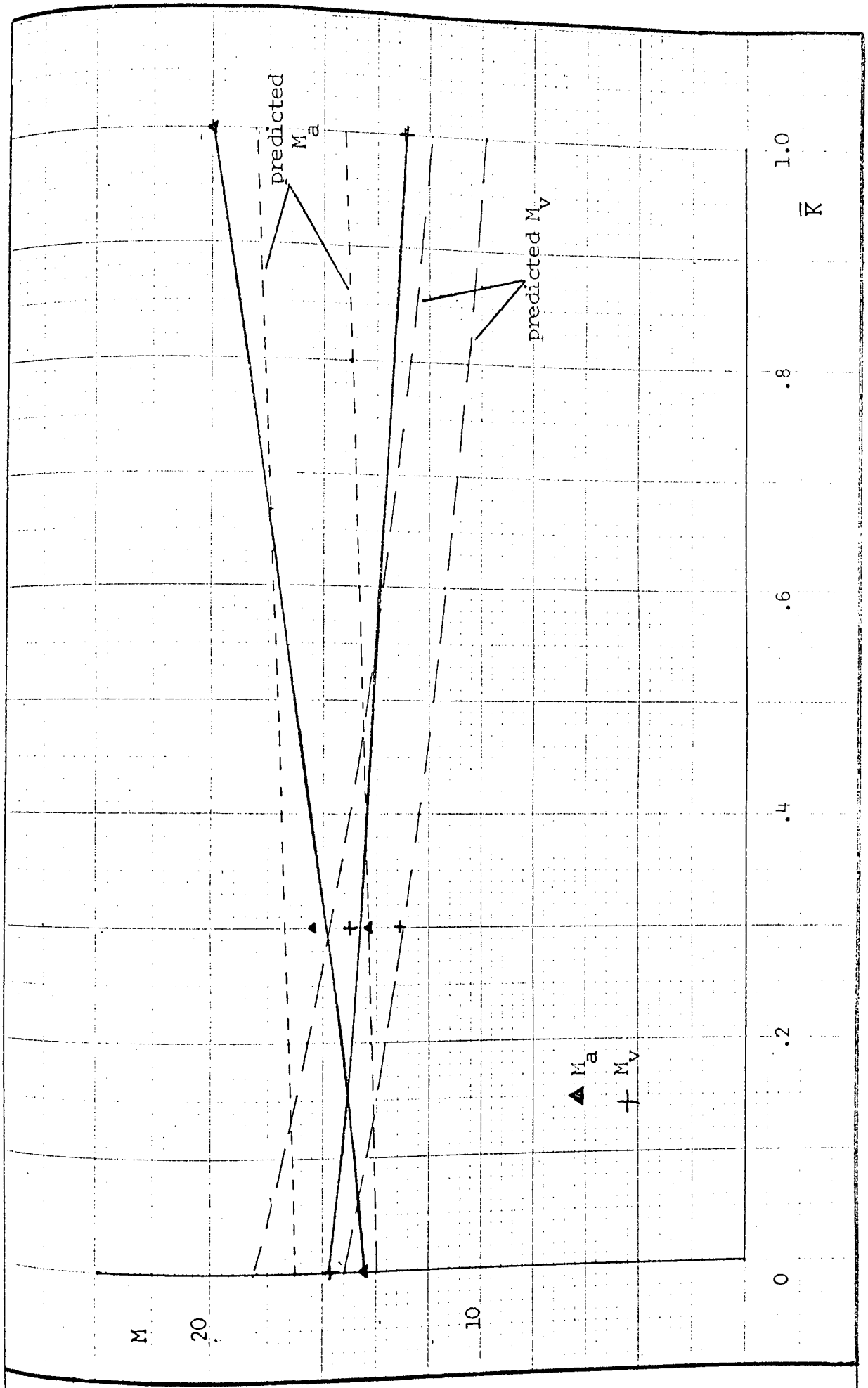

Axial and Volumetric Deformation Modulus vs Incremental Stress Ratio

FIG. 7.35

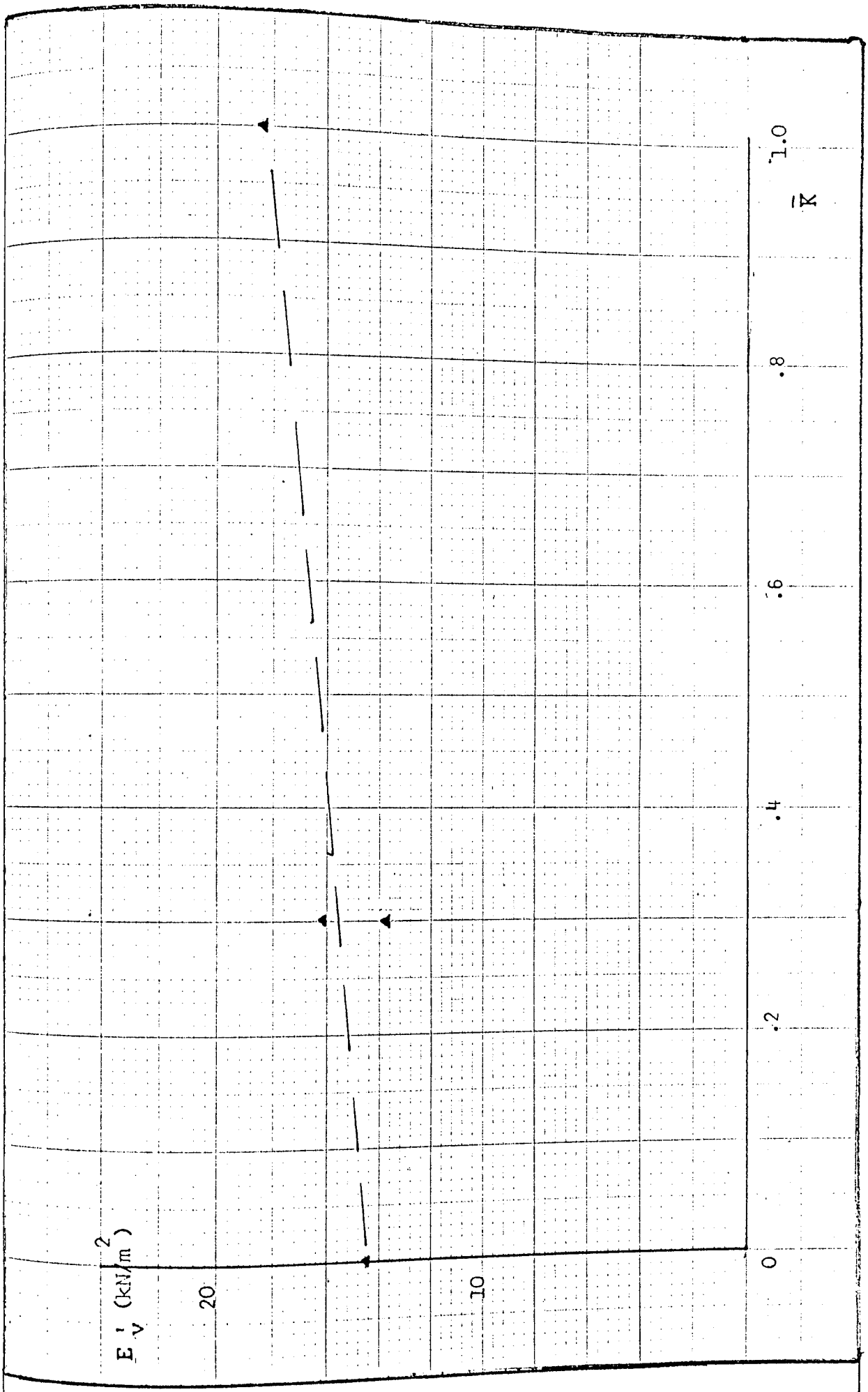

Vertical "Young's" Modulus vs Incremental Stress Ratio

FIG. 7.36

$M_a/(\sigma'_a)_{av}$ vs Increase of Axial Stress

- TDV, TD2 Series

FIG. 7.37(a)

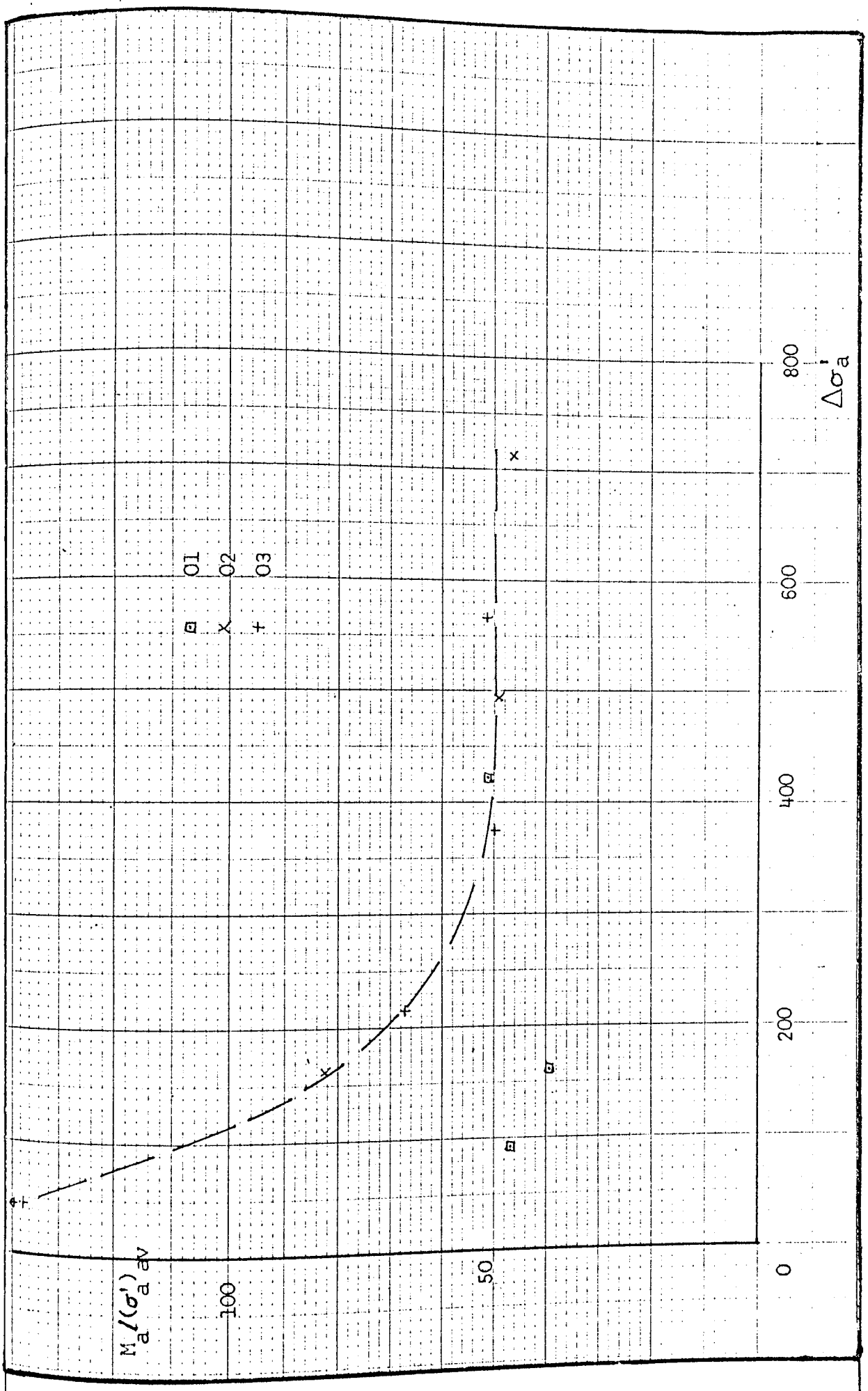

$M_a/(\sigma'_a)_{av}$ vs Increase of Axial Stress

- TC Series

FIG. 7.37(b)

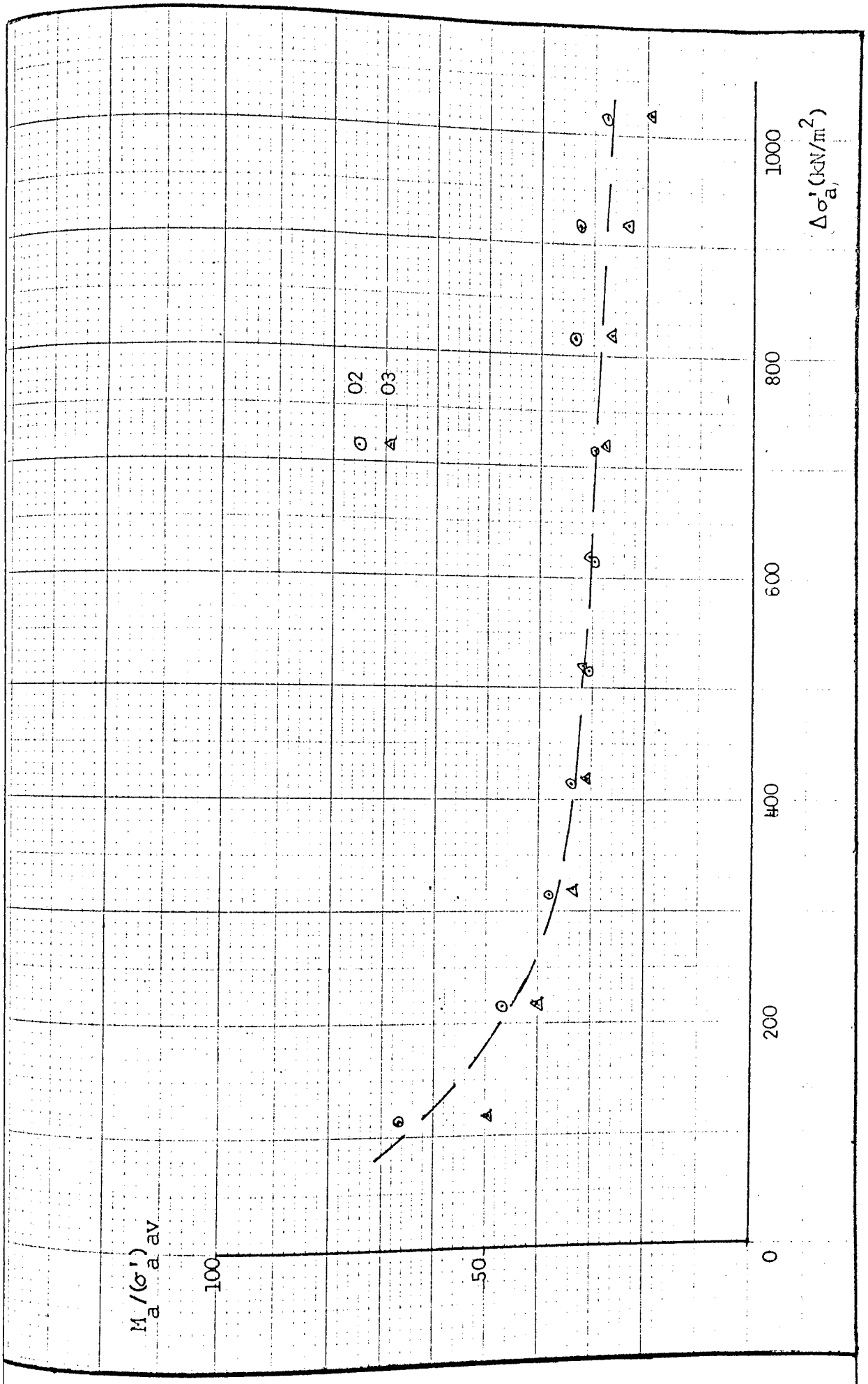

$M_a/(\sigma'_a)_{av}$ vs Increase of Axial Stress - TA3 Series

FIG. 7.37(c)

$M_a/(\sigma'_a)_{av}$ vs Increase of Axial Stress

-TA1 Series

FIG. 7.37(d)

$M_a/(\sigma'_a)_{av}$ vs Increase of Axial Stress

- TA2 Series

FIG. 7.37(e)

$M_v/(\sigma'_a)_{av}$ vs Increase of Axial Stress

- TDV and TD2 Series

FIG. 7.38(a)

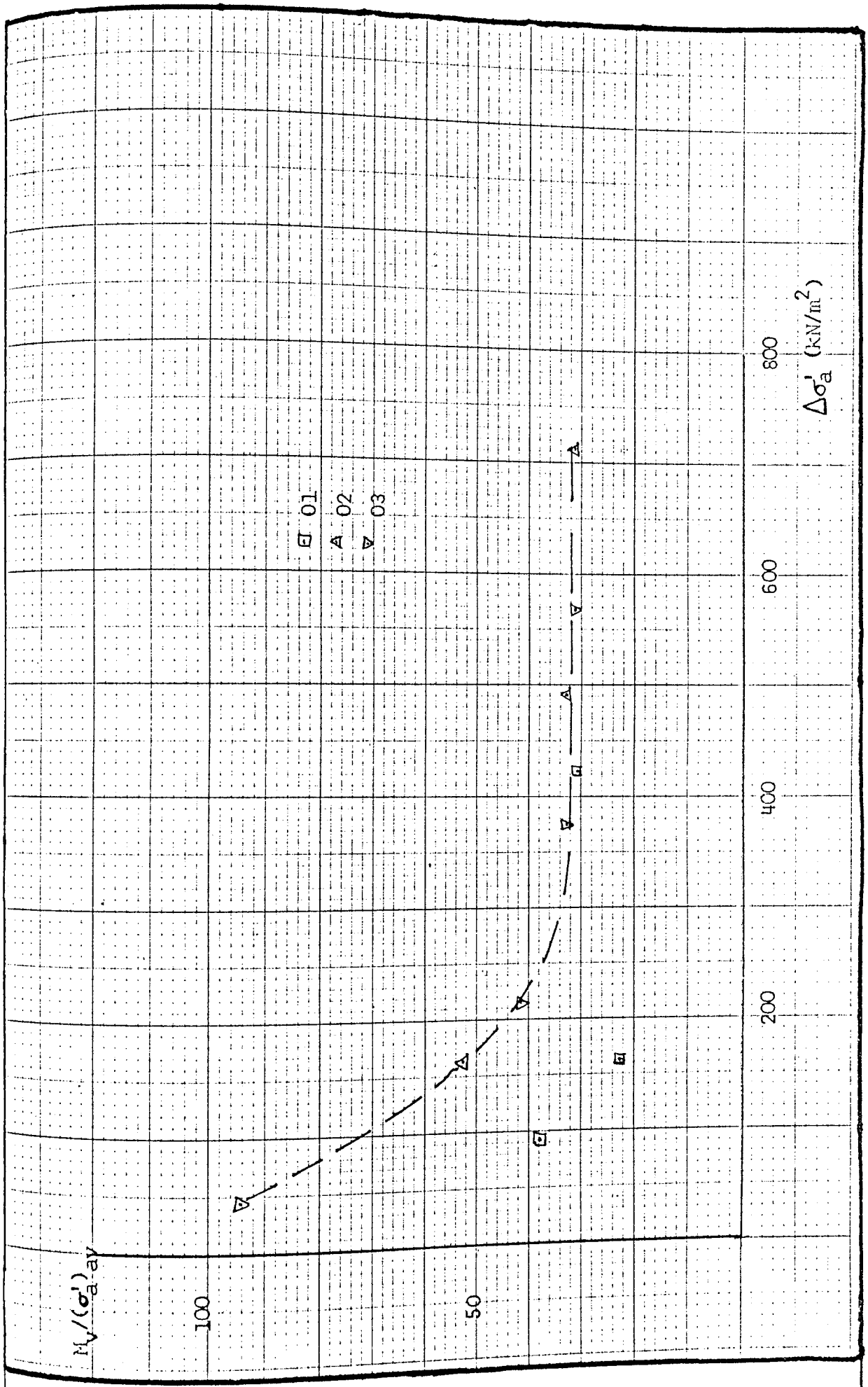

$M_v/(\sigma'_a)_{av}$ vs Increase of Axial Stress - TC Series

FIG. 7.38(b)

$M_v/(\sigma'_a)_{av}$ vs Increase of Axial Stress

- TA3 Series

FIG. 7.38(c)

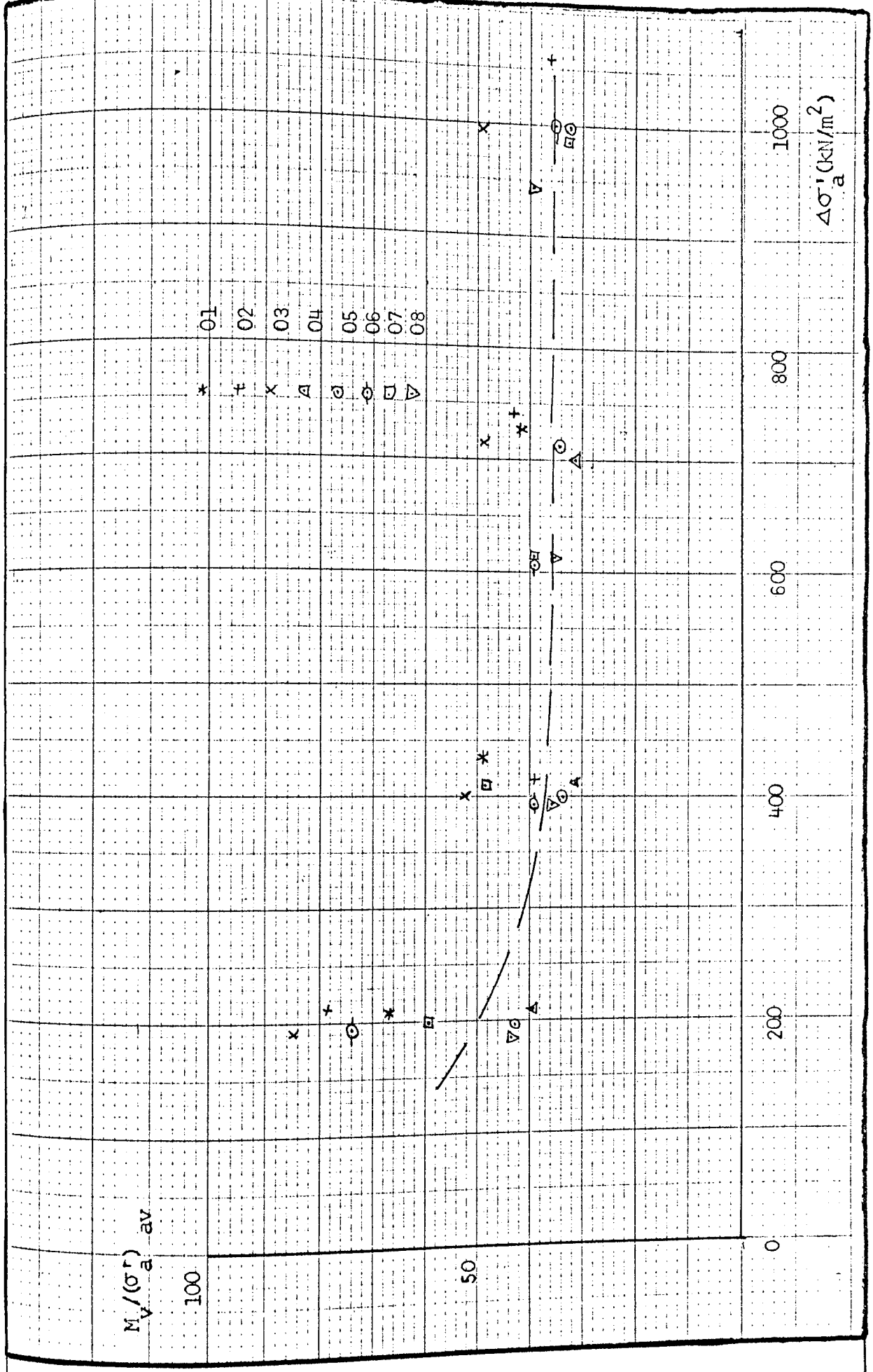

$M_v/(\sigma'_a)_{av}$ vs Increase of Axial Stress

- TA1 Series

FIG. 7.38(d)

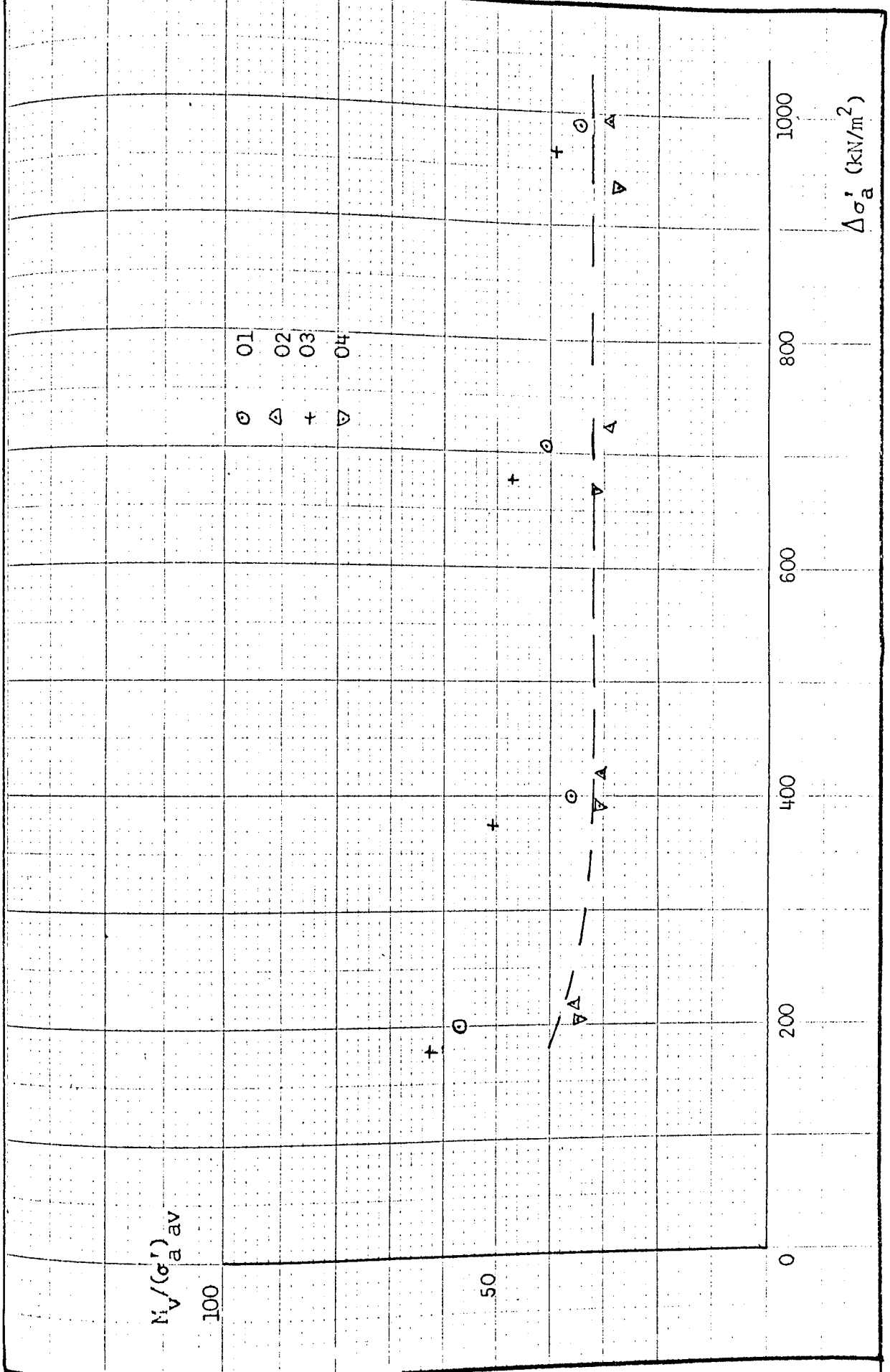

$M_v/(\sigma'_a)_{av}$ vs Increase of Axial Stress - TA2 Series

FIG. 7.38(e)

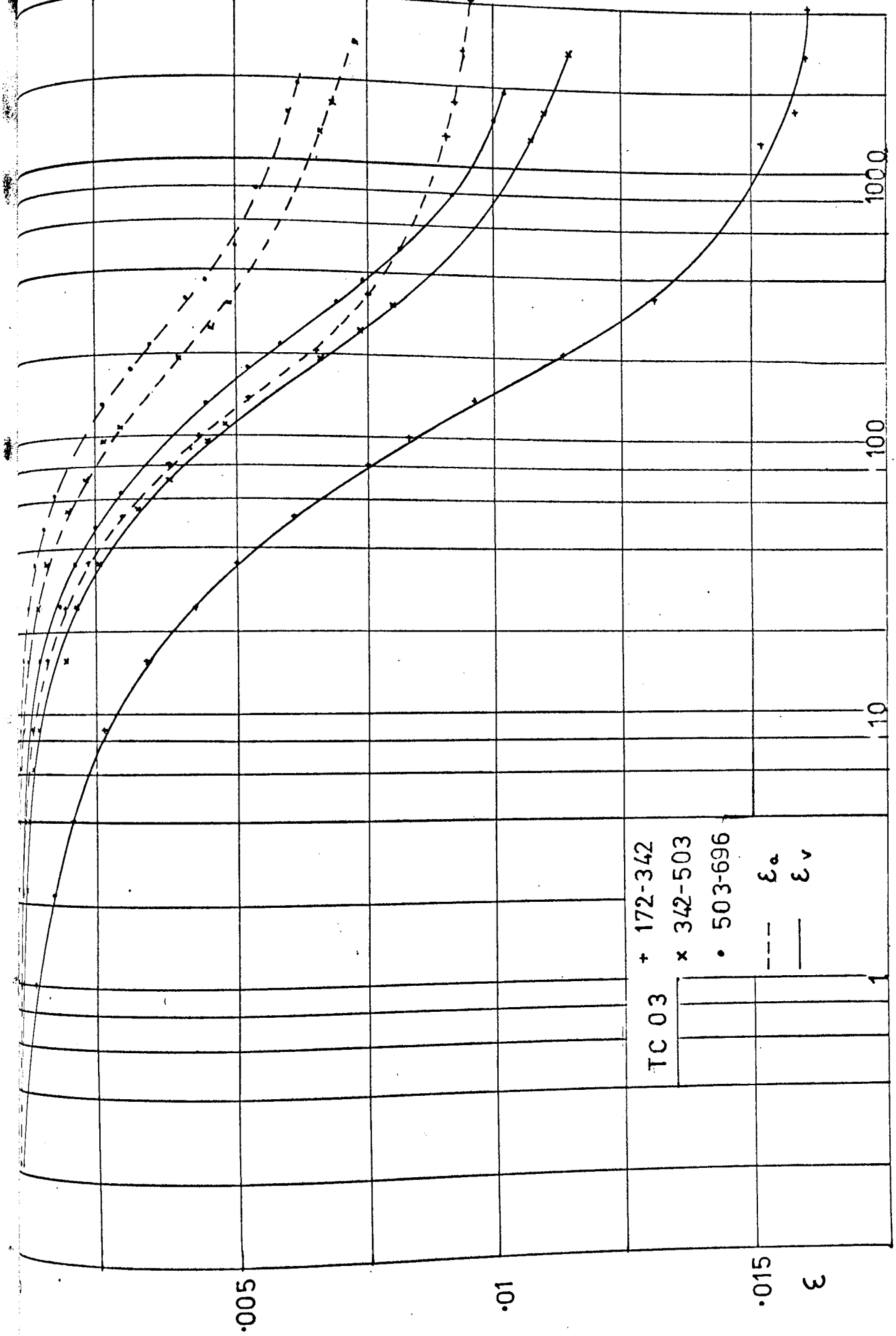

Axial and Volumetric Strain vs Log time - TC Series

FIG. 7.39(a)

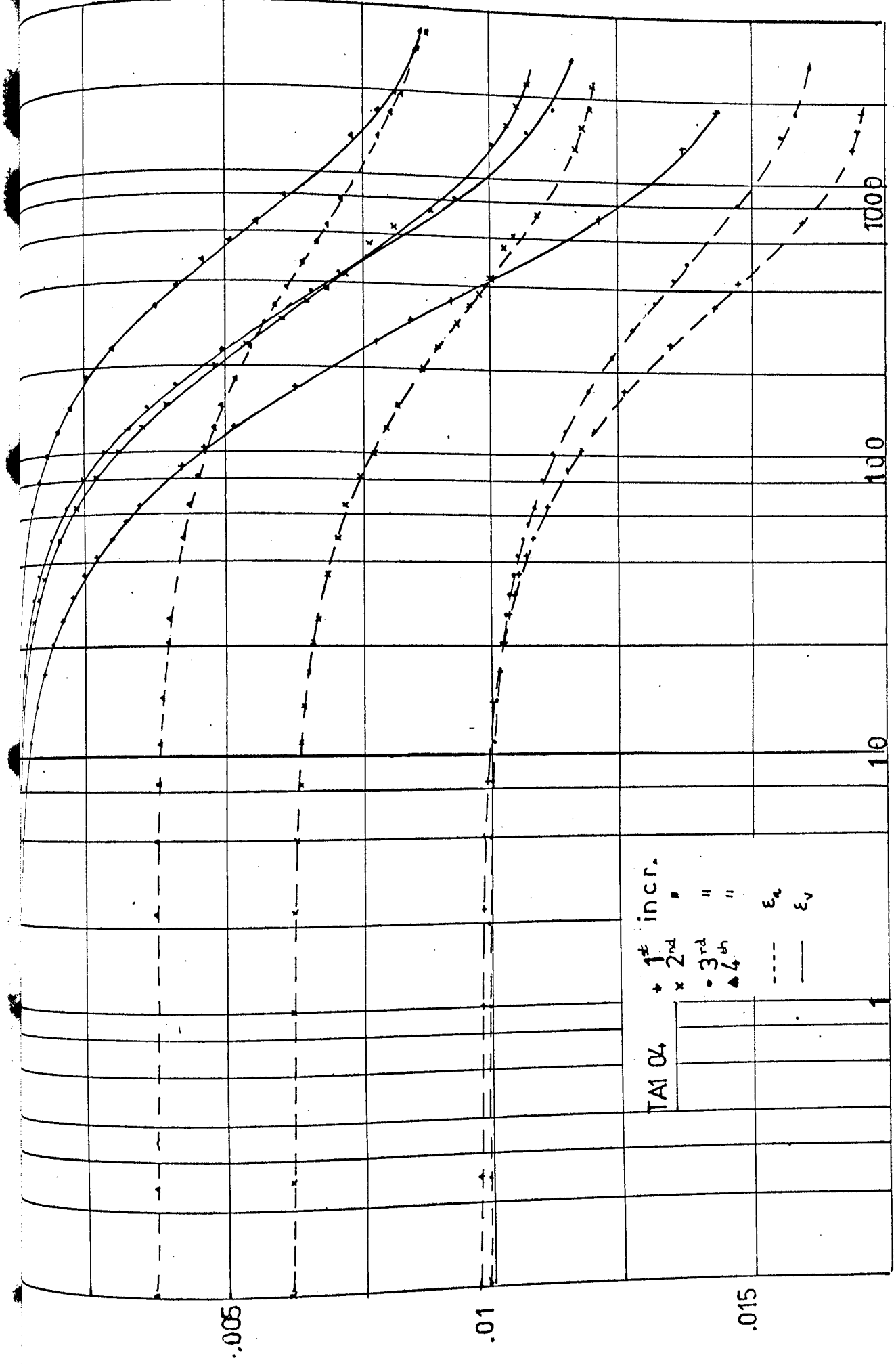

Axial and Volumetric Strain vs Log time
- TA1 Series

FIG. 7.39(b)

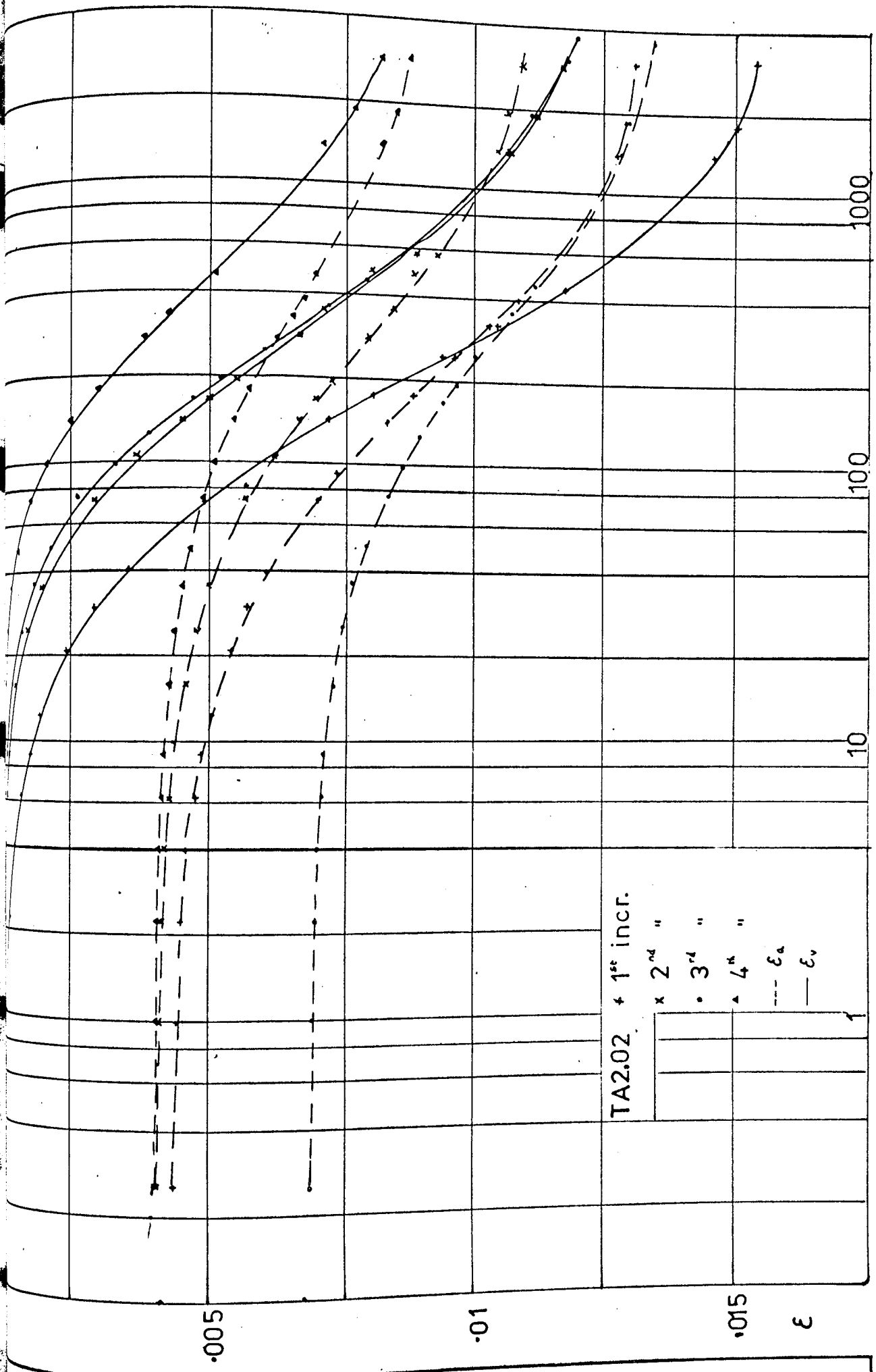

Axial and Volumetric Strain vs Log time
- TA2 Series

FIG. 7.39(c)

Radial Coefficient of Consolidation vs Axial Stress

FIG. 7.40

Dissipation of Pore Pressure vs time - TA1 04

FIG. 7.41

CHAPTER 8

COMPARISON OF OEDOMETER AND TRIAXIAL RESULTS

8.1 Equilibrium Stress σ'_k

8.2 Deformation Moduli

8.3 Rate of Consolidation

8.1 EQUILIBRIUM STRESS σ'_K

The results of the equilibrium stress determined from the initial stages of the oedometer and triaxial tests have been presented in the previous chapters. It was seen that both gave a scatter of results, however the general trend showed that the values obtained from the triaxial tests were on the whole lower than from the oedometer. It has already been indicated that the 'setting up' technique used in the triaxial tests would probably reduce the pore suction in the sample, and it would appear from these results that this was the case.

The results from both sets of tests are plotted in Figure 8.1 for samples with computed degree of saturation greater than 95%. It is seen that the majority of the results are obtained from the samples extracted from 1 to 2.5m below existing ground level, where σ'_K/σ'_V varies from 1 to 2.3 with the exception of two much higher values. Below 2.5m the results are predominantly from the triaxial tests with a ratio of σ'_K/σ'_V in the vicinity of unity.

It is considered that the results below a level of 2.5m are not representative and therefore they will be disregarded in further discussion of the results. It would appear, due to the scatter of results, that in order to obtain a representative value of σ'_K/σ'_V, for evaluation of the in-situ K_O, the mean value of all the results presented in Figure 8.1 between 1m and 2.5m depth should be used, the value obtained for σ'_K/σ'_V is thus 1.8.

It was seen (Equation 2.8(b)) that the value of the in-situ K_O can be obtained from the relationship $\sigma'_K/\sigma'_V = K_O - A_s(K_O - 1)$ for the case of $K_O > 1$.

It is considered appropriate to use the value of A obtained from the first undrained loading increment in the TA2 series. The mean value of A obtained from this test (Table 7.7(a) to (d)) was 0.6. Therefore on substitution of this value into the above equation, K_o is found to be of the order of 3.0. This is approaching the passive failure condition value of 3.4 obtained by Lal (1971),(Fig. 7.27). It is surprising that K_o is so high at this site as the samples were obtained from near the quarry face (Page 54) where much of the horizontal stress must have been relieved. The relationship between K_o, σ'_k / σ'_v and A is shown graphically in Figure 8.2. It can be observed that with increase of A the estimated value of K_o becomes increasingly sensitive to the value of σ'_k/σ'_v. The shaded area on the graph indicates the range of estimated K_o for values of σ'_k/σ'_v equal to $1.8 \pm 10\%$ and a value of A between 0.55 and 0.65 during sampling. It is seen that this gives a range of K_o between 2.4 and 3.8, thus showing that the determination of K_o is very sensitive to the laboratory measured parameters.

8.2 DEFORMATION MODULI

Comparison of the oedometer and triaxial test results can only be made in terms of the axial and volumetric deformation moduli because the analysis of these results in terms of the 'elastic' constants requires the knowledge of radial stresses which could not be measured in the oedometer apparatus used in this series of tests.

8.2.1 Volumetric Deformation Modulus, M_v

It was seen from the triaxial results in Chapter 7 that the volumetric deformation modulus, M_v, could be considered, in general, to be independent of the increment of radial stress, although in

the stress range up to approximately 350 kN/m^2 it was found that $\bar{K}$ did have a slight influence on M_v. However in this low stress range the modulus obtained under any particular stress path was reasonably constant, and for the core and block samples was of the order of 15.7 MN/m^2 for $\bar{K}$ = 0 and 12.9 MN/m^2 for $\bar{K}$ = 1 (Figure 7.35). Similarly it was found (Chapter 6) that for, the core and block samples, in the first two increments in the oedometer tests, M_v ($=M_a$) was approximately constant at a value of 20 to 22 MN/m^2, (Figure 6.8 and 6.9). However this is significantly greater than the one dimensional value of M_v predicted from the triaxial series which the intersect of the M_a and M_v lines (Figure 7.35) would be of the order of 15.1.

It was observed in the triaxial series that the volumetric strain was significantly less for tube samples than for the core or block samples, thus yielding a higher value of M_v (Figures 7.38 (a), (d) and (e)) which compares favourably with the oedometer results on the core samples. It has also been observed in the oedometer tests that the tube samples (Figures 6.10 (a) to (c)) give a higher value of M_v than the core and block samples (Figures 6.8 and 6.9)). These results suggest that disturbance during in-situ tube sampling causes a change in the sample structure resulting in an increase of the volumetric modulus. Further, as the volumetric deformation modulus from the oedometer core and block samples was comparable to that of the triaxial tube samples it is suggested that the sub-sampling and trimming of the oedometer samples caused significant mechanical disturbance (Van Zeist, 1948) and that this disturbance is of a similar nature and magnitude to that caused by the U70 sampling tube.

To consider the volumetric deformation modulus from the oedometer and triaxial tests over the full range of stresses observed, the results from the core and block samples are plotted in the form of $M_v/(\sigma'_a)_{av}$ against the increase of effective axial stress in Figure 8.3. It can be seen that the resultant graphs are of the same form, but not coincident, with an initially high value of $M_v/(\sigma'_a)_{av}$ reducing at approximately the same slope to constant values of 39.5 and 32 at stress increments of 400-500 kN/m^2 and 300-400 kN/m^2 for the oedometer and triaxial tests respectively.

It should be noted that in the higher stress range ($\Delta\sigma'_a$ > 400 kN/m^2) that for the tube samples the value of $M_v/(\sigma'_a)_{av}$ measured in the oedometer becomes less than for the core and block samples (Figures 6.11, 6.12 and 6.13)), while in the triaxial tests it generally remains greater than for the other samples (Figures 7.38(a), (d) and (e)).

In Chapter 6 it was attempted to explain the change of the slope of the deformation modulus curve for the oedometer specimens with the change of $\bar{K}_o$ during loading as demonstrated by Som (1968). However, as an identical form of this curve is obtained from the triaxial tests, including the hydrostatic loading ($\bar{K}$ = 1), this can obviously not be the cause of this phenomenon. Also as this was reflected in the hydrostatic loading case, it can not be associated with any particular effective stress ratio, as this ratio remains constant at unity throughout the test.

Janbu's (1963) results suggest that such a change in slope, with $M_v/(\sigma'_a)_{av}$ becoming constant is indicative of the preconsolidation stress. However a preconsolidation stress of only 300-400 kN/m^2

for this material is not realistic.

It was seen in the previous section that the in-situ value of K_o for material tested appears to be of the order of 3, thus as the effective vertical stress varies from 100 - 150 kN/m^2 over the sampling depth, the in-situ horizontal stress of the order of 300 to 450 kN/m^2. It is therefore possible that this change in slope of M_v curve coincides with the axial stress exceeding the in-situ effective horizontal stress. In the light of the data available it is not possible to go beyond making this tentative suggestion.

8.2.2 Axial Deformation Modulus, M_a

It was seen in Chapter 7 that the strain ratios were reasonably linear over much of the stress range observed, although the strain ratio was dependent on the incremental stress ratio $\bar{K}$ (Figure 7.32 and 7.33).

The relationship between $M_a/(\sigma'_a)_{av}$ against increases of effective axial stress, for core and block samples, is shown in Figure 8.4 where it is clear that M_a is dependent on the incremental stress ratio. The oedometer results (from Figure 8.3) are superimposed on this plot, and it is seen that the curve falls between the two triaxial curves. However, as discussed in the previous section, it appears that these samples were significantly disturbed during preparation and therefore as the deformation is restricted (one dimensional) it may be expected that the value of M_a from the oedometer would be in excess of the corresponding result from the triaxial apparatus.

Again, within the stress range up to 300 - 400 KN/m^2, the axial deformation modulus is reasonably constant for any particular

stress path (e.g. Figures 7.4(a) and 7.15). It is seen that the value of the axial deformation modulus, M_a, obtained from the oedometer is comparable to M_a from the hydrostatic loading (i.e. $\bar{K} = 1$).

8.2.3 Summary

It is thus seen that the deformation moduli obtained from the oedometer tests are significantly different to those obtained from the triaxial tests. It appears from the available information that this variance is in part if not wholly due to structural disturbance of the oedometer sample during laboratory sub-sampling and trimming.

In the case of the volumetric deformation modulus the oedometer results are some 30% greater than the triaxial results in the low stress range, this subsequently reduces to approximately 25% above a stress increment of 400 kN/m^2.

8.3 RATE OF CONSOLIDATION

The rate of consolidation has been determined in both oedometer and triaxial apparatus. However because of the type of drainage provisions provided the coefficient of consolidation obtained was the vertical (C_v) and radial (C_r) for the oedometer and triaxial respectively. The results from the oedometer tests were fitted by the 'root time' and 'log time' methods (see Chapter 6). However it was found that the 'log' method gave more consistent results and it is therefore these results which are considered here.

The general range of C_r and C_v are shown in Figure 8.5, it is seen that both sets of results show considerable scatter, but it is clearly indicated that the radial coefficient is less than the

vertical. For the range from 200 - 1200 kN/m^2 it is seen that the average value of C_r (.75 - 0.5 x 10^{-4} cm^2/s) is approximately half that of C_v (1.4 - 1.2 cm^2/s).

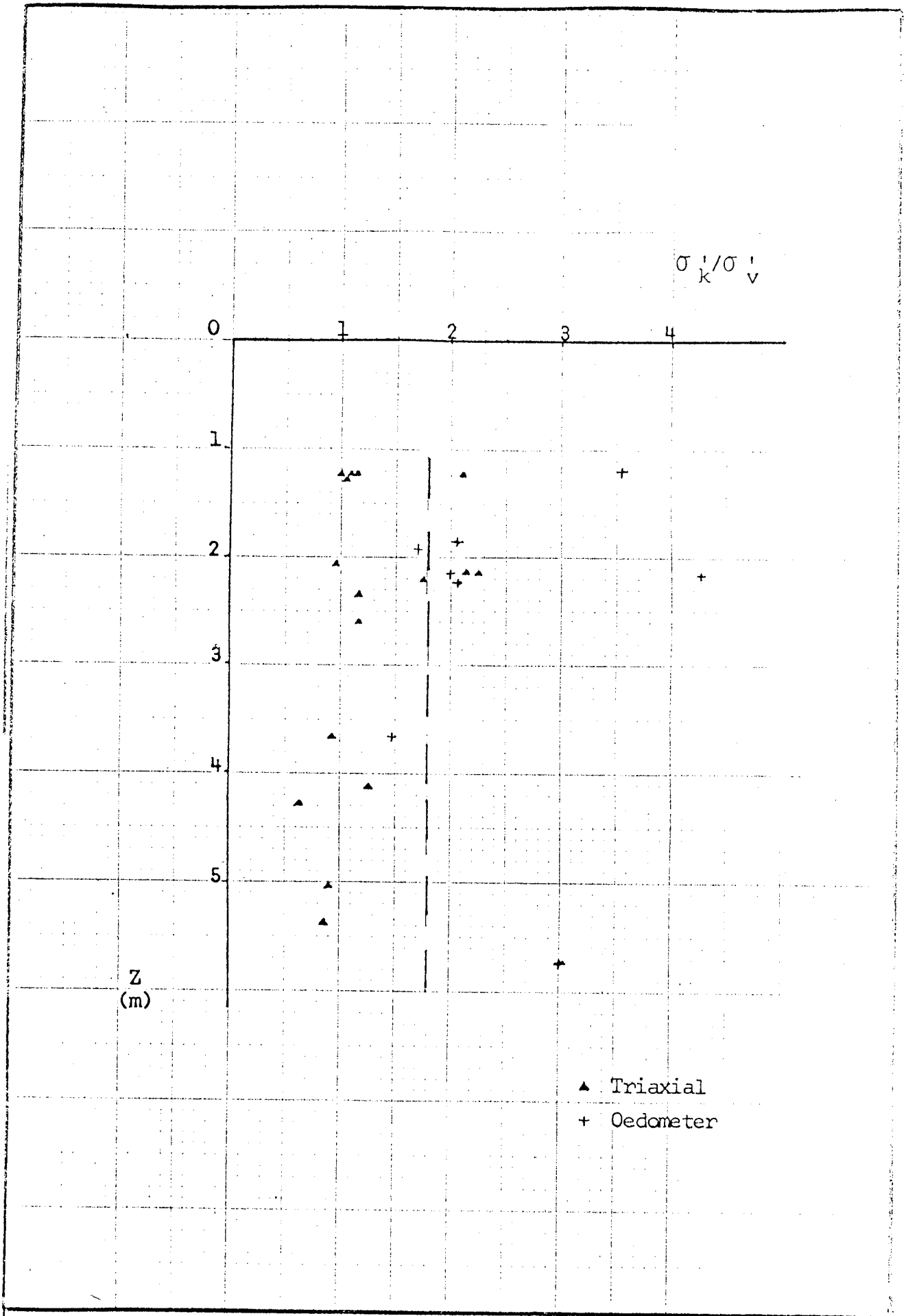

σ'_k/σ'_v vs Depth from Triaxial and Oedometer Tests FIG. 8.1

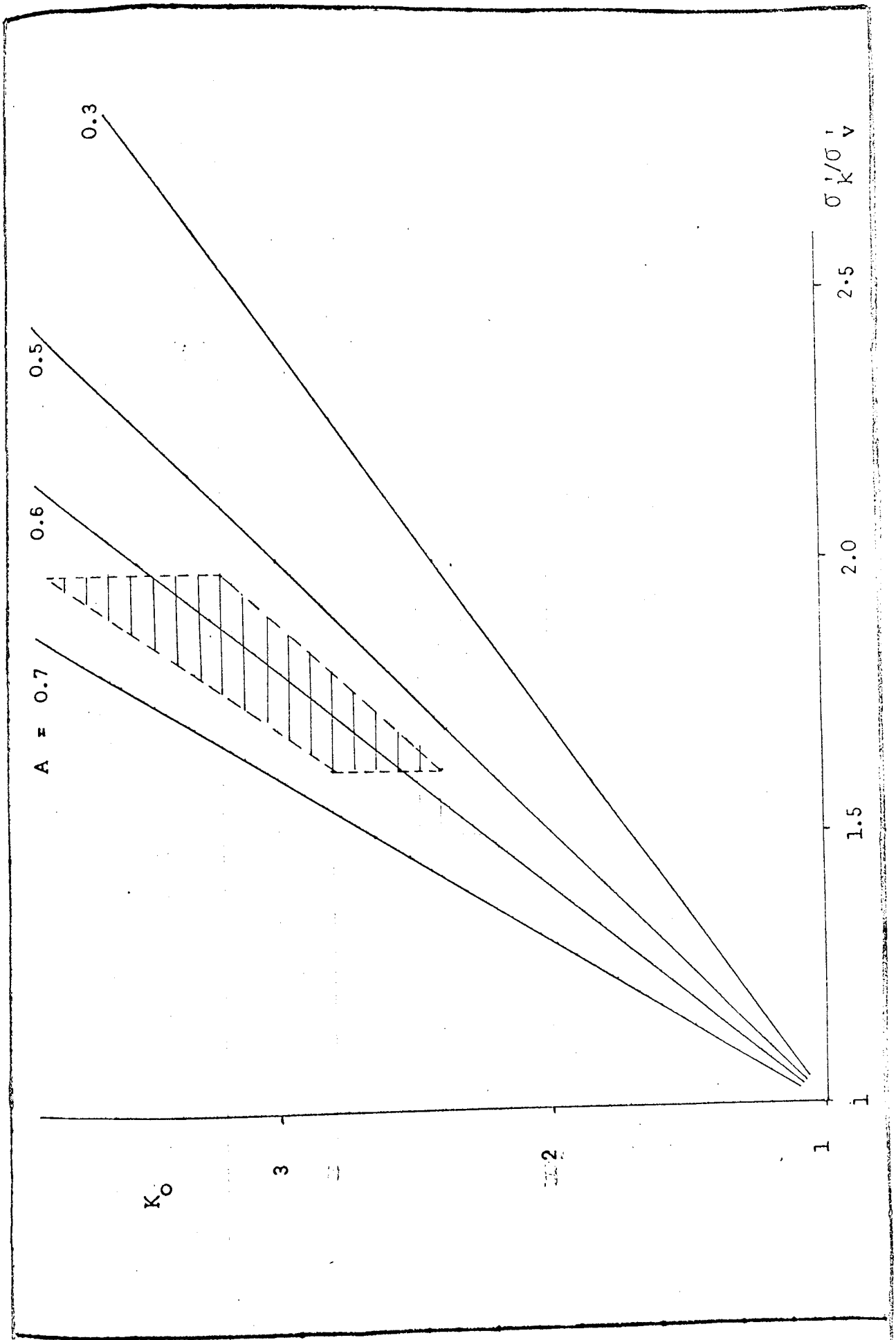

Determination of K_o from Equilibrium Stress

FIG. 8.2

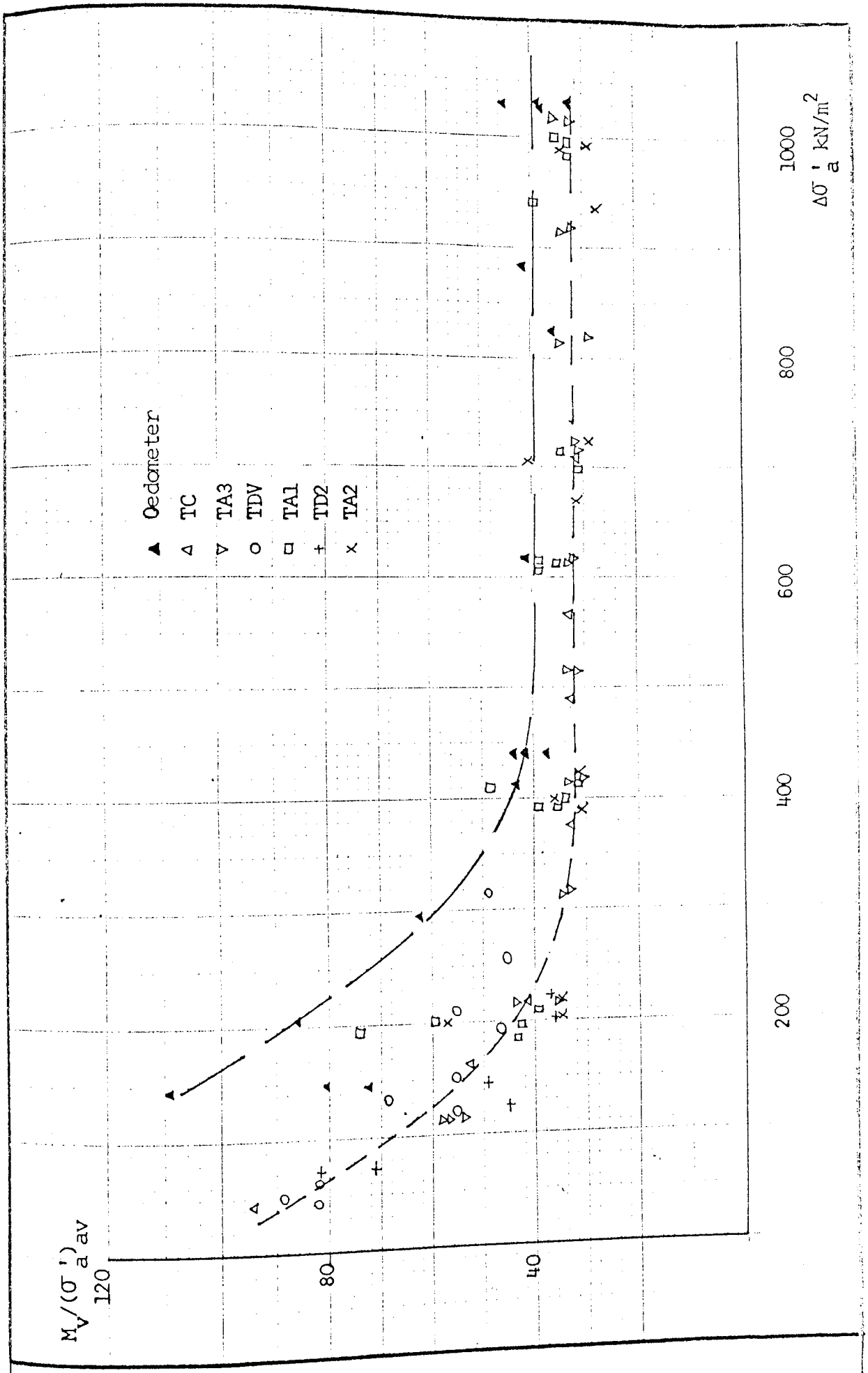

Volumetric Deformation Modulus vs Axial Stress Increment - Core and Block Samples

FIG. 8.3

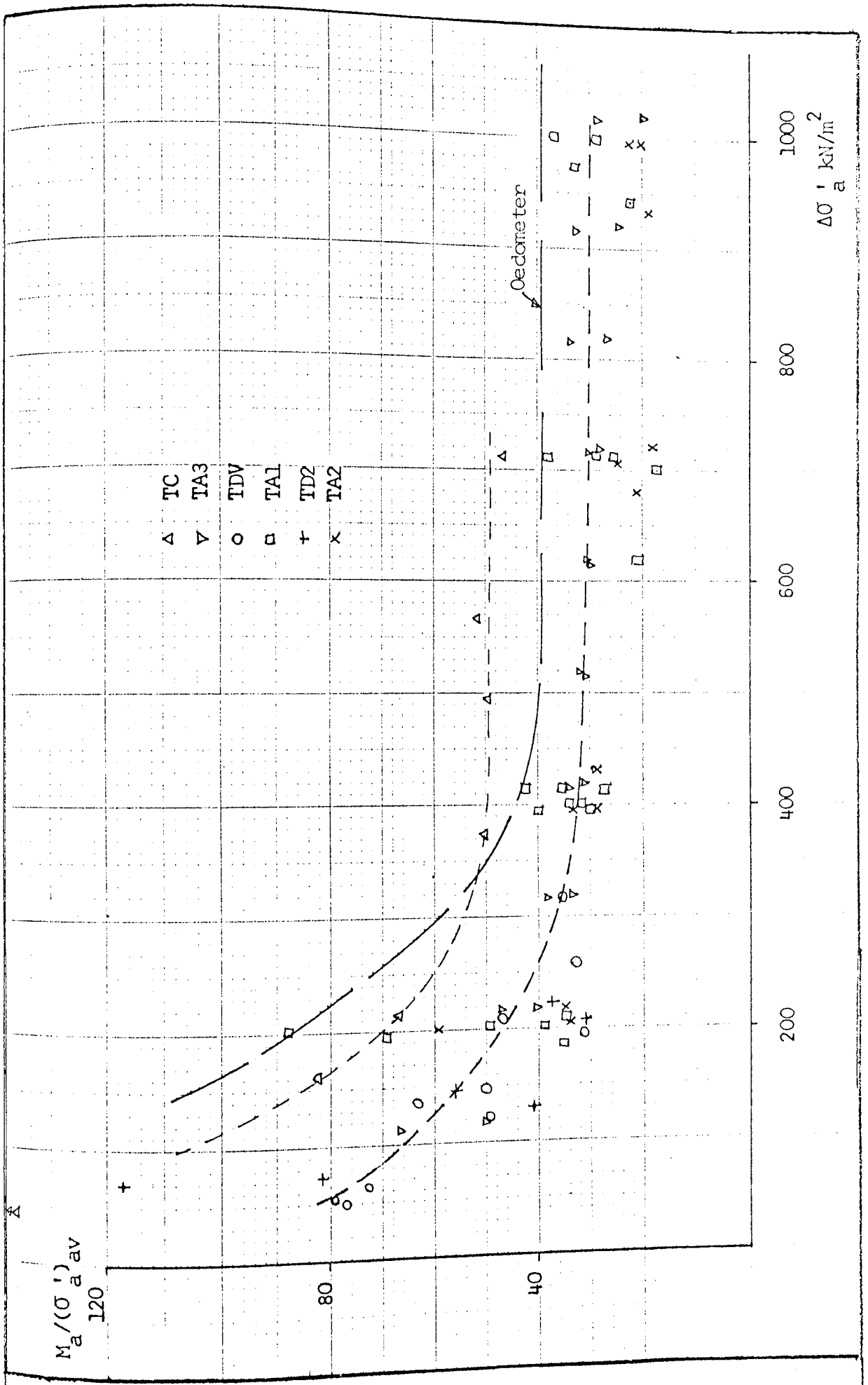

Axial Deformation Modulus vs Axial Stress Increment
- Core and Block Samples

FIG. 8.4

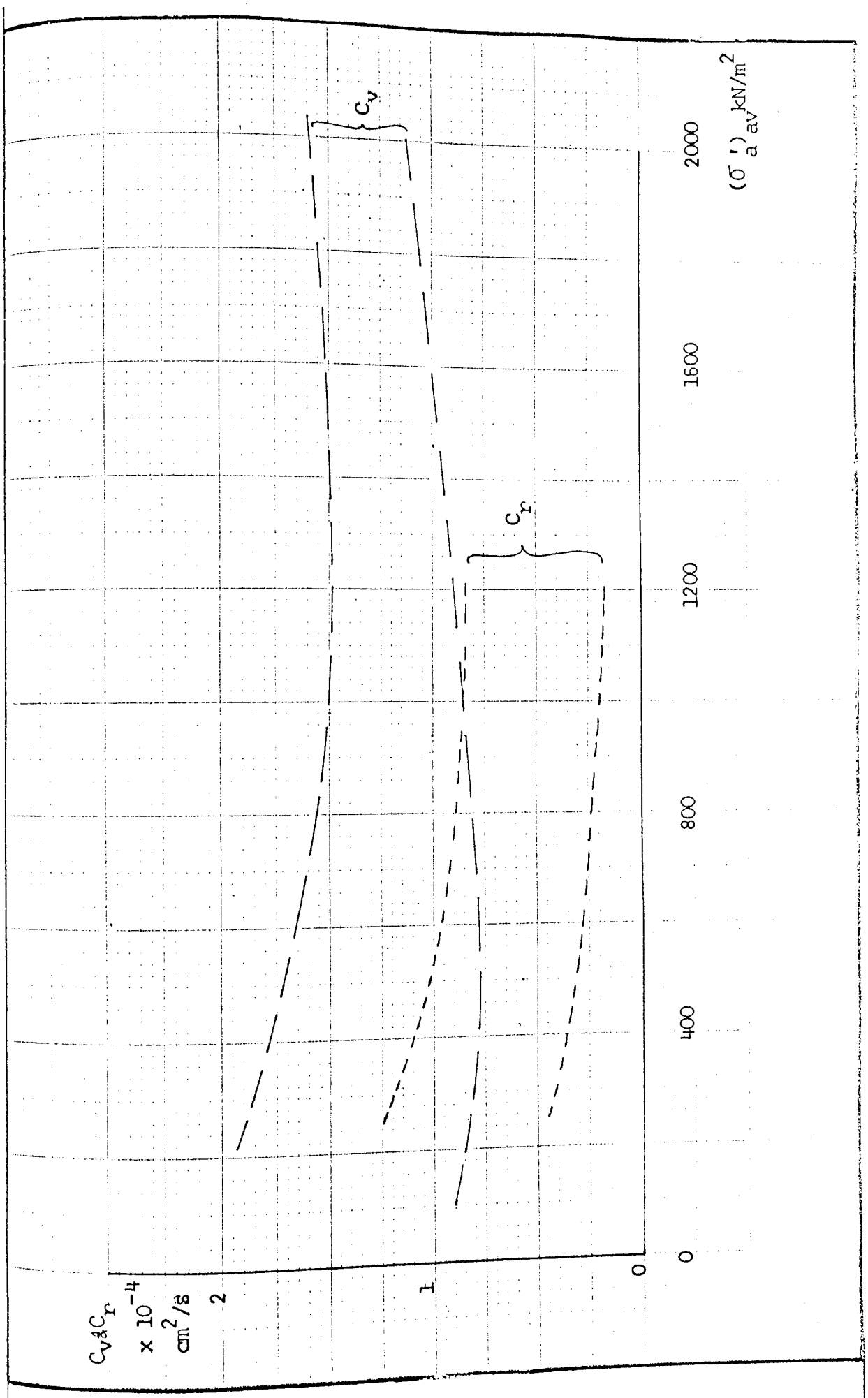

Coefficient of Consolidation vs Axial Stress

FIG 8.5

CHAPTER 9

SUMMARY AND CONCLUSIONS

9.1 Summary and Conclusions

9.2 Suggestions for Further Research

9.1 SUMMARY AND CONCLUSIONS

The majority of this research programme has been concerned with the investigation of the deformation properties of the Lower Lias Clay under a variety of stress paths in the triaxial apparatus. These tests have been supplemented by a study of the one-dimensional deformation in the oedometer apparatus and a general study of some physical properties of the clay.

The Lower Lias Clay tested in this programme was from near the top of the Lower Lias sequence (Section 4.3) and from a study of the Stratigraphy of the area was predicted to have been subjected to an overburden of 520m to 870m by the end of the Cretaceous period.

In-situ pore pressure measurements (Section 4.5) and the determined degree of saturation indicated that the samples came from the capillary zone above the water table. The in-situ average wet unit weight of the material was determined in the laboratory from the samples as 21.8 kN/m^3 with a natural moisture content of approximately 18.4% which was seen to be well below the plastic limit, 27%, of the material.

The preconsolidation stress cannot be readily determined for such a heavily overconsolidated clay. The study in the oedometer apparatus suggests that the preconsolidation stress of these samples was of the order 8000 - 10000 kN/m^2. However results are by no means conclusive, although they appear to correlate reasonably well with the predicted overburden depth of 520 - 870m.

Under the prevailing site conditions (Section 4.4 & 8.1) a surprisingly high value of the in-situ K_o was obtained in the order of 3.0 from laboratory measurements of the sample equilibrium stress,

σ'_K and the pore pressure parameter, A. The measurement of the equilibrium stress in the triaxial apparatus appeared to give low results due to the method of setting up. It would appear that for this type of material it is necessary to determine σ'_K from tests without filter paper drains where it should be possible to obtain a saturated 'set up' without the need for flushing water between the sample and membrane. The results indicate that the oedometer can be used to determine the equilibrium stress providing suitable precautions are taken to ensure initial 'bedding in' of the sample. Whatever method is used to determine σ'_K, a sufficient number of results must be available to reduce the error as K_o is seen to be very sensitive to the value of σ'_K/σ'_v for high values of the pore pressure parameter A_s.

The most significant results from this research programme were those obtained for the study of the deformations in the triaxial apparatus under a variety of stress paths.

The results from the ordinary drained triaxial tests on a single 'horizontal' and five 'vertical' samples clearly indicated (Sect.7.3.4) that the soil was exhibiting a high degree of anisotropy. It was seen that the strain paths for core and block samples showed far better correlation than the axial deformation modulus. These strain paths showed that very little radial strain occurs during ordinary triaxial loading up to a stress ratio (σ'_a/σ'_r) of 2; the strain ratio ($\varepsilon_v/\varepsilon_a$) recorded in this range of stress increment was 0.92. For the ordinary triaxial test on the 'horizontal' sample the strain ratio of 1.19 indicates that the application of a compressive stress in one horizontal direction causes a compressive strain in the orthagonal horizontal direction, i.e. negative Poisson's ratio in that plane. The hydrostatic consolidation tests gave a strain ratio of 1.55 which is

significantly less than for an isotropic soil (i.e. 3). Analysis of the strain paths for these three series enables the Poisson ratios ν_{hv} and ν_{hh} and the modulus ratio n ($=E'_h/E'_v$) to be determined independently of the stress-strain curve; the values obtained for ν_{hv}, ν_{hh} and n (Section 7.4.3) were 0.04, -0.38 and 4.7 respectively.

The theoretical strain ratio ($\varepsilon_v/\varepsilon_a$) incremental stress ratio ($\bar{K}$) for an orthotropic elastic material (Equation 7.12) is evaluated (Fig. 7.32) using the above constants. It was seen that a good correlation was obtained for the TA3 series where $\bar{K}$ = 0.3. The overall strain ratios for the TA1 Series incremental loading was not predicted well, this appeared to be due to the undrained yielding of the soil under the 'near failure' conditions. This is somewhat verified by the TA2 Series, where the samples were not on the verge of undrained failure, and the overall strain ratio predictions were generally good. In both cases the strain ratio during the consolidation stage was predicted well and appeared to be unaffected by the severe undrained deformation in the TA1 series.

The pore pressure parameter A determined in the TA1 and TA2 Series for the core and block samples was generally in the region of 0.6, this is close to the predicted value of 0.645 from the orthotropic elastic constants.

The axial stress-strain curves were generally reasonably linear up to 300-400 kN/m^2 thus indicating a constant value of the vertical effective Young's Modulus, E'_v. However it appears that E'_v is dependent on the incremental stress ratio $\bar{K}$ (Figure 7.36)

The resultant effect on the axial and volumetric strains due to

change of incremental stress ratio, $\bar{K}$, is best illustrated by considering the axial and volumetric deformation moduli, Ma and M_v, Fig.7.35. It is seen that the axial and volumetric strains would vary by less than 40 and 20%, respectively over a $\bar{K}$ range of zero to unity. Thus compared with London clay, Som (1968), changes in radial stress, during drained deformation, is less significant for the Lias Clay tested.

It was seen from the triaxial results, particularly the ordinary drained tests, that the sample disturbance of the tube samples had little effect on the vertical effective Young's Modulus, but significantly influenced the volumetric strain recorded during the ordinary triaxial loading, giving a greater value of Poisson's ratio ν_{hv}. It was also deduced from the strain paths in the consolidation stages of the incremental loading tests that the value of $\frac{1}{n}(1 - \nu_{hh})$ was also significantly influenced by disturbance. It was also suggested by the oedometer tests, that laboratory sub-sampling, with the oedometer ring, similarly disturbed the sample. This resulted in significant variation in the determined volumetric deformation modulus.

It is concluded from these results that the Lower Lias Clay exhibits a high degree of anisotropy and that the strain ratio $(\varepsilon_v/\varepsilon_a)$ can be predicted by the orthotropic elastic theory presented in this thesis. However the vertical effective elastic modulus, E'_v appears to be dependent on the incremental stress ratio, $\bar{K}$.

It was intended to attempt to quantify the effect of the determined 'elastic' values on the settlement of a foundation by a finite difference analysis, however the computer program was not fully developed when the author left the university, and changes in the computing services at the university, coupled with the submission time limit, has resulted in this work not

being included.

9.2 Suggestions for Further Research

It would appear from the results obtained from this research programme that further studies should be continued along similar lines, however it is suggested that testing should be restricted to core and/or block samples so that the additional variable of sample disturbance is eliminated.

It is suggested that future work should concentrate on the stress-strain behaviour over the lower stress range with particular emphasis on the effect of the incremental stress ratio, $\bar{K}$, on the vertical effective elastic modulus E'_v. It should be endeavoured to carry out the majority of tests from the in-situ stress state and particular emphasis placed on the study of the behaviour up to the effective stress ratio (σ'_a/σ'_r) of unity. It would be desirable to obtain samples from a greater depth range, than used in this thesis, to establish the effect of depth on the elastic parameters.

The effect of anisotropy on the induced stresses and deformations, both below foundations and in the problem of deep excavations, should be considered. This work would be particularly useful if field measurements are available for comparison and also back-analysis.

APPENDIX A - DETERMINATION OF SHRINKAGE LIMIT

An attempt to determine the shrinkage limit of a sample of remoulded Lias Clay was made using a method based on the Linear Shrinkage Test, Test 5 BS 1377 (1967), with the mould recommended for that test.

A sample of dry ground clay was thoroughly mixed at a water content approximating to the liquid limit, the mixture was then placed in an airtight container for 24 hours and remixed on removal. The inner surface of the mould was smeared with a silicone grease. The mould was then filled with the mixed soil, and tapped regularly to avoid trapping air,and finally leveled off with a pallette knife.

The mould was then placed in a draught free position and the sample allowed to air dry. The sample was weighed at 2 hourly intervals and the dimensions checked with vernier calipers. Once the length had ceased to decrease the sample was oven dried. The change of length was then plotted against water content as shown in Figure 4.14, and the shrinkage limit was determined as described in Section 4.7.2

APPENDIX C - SPECIAL MEMBRANE FOR IS CELL

A special specimen membrane was required with top and bottom flanges for use in the IS Cell. The flanges being used to form a seal at top and bottom of the main cell.

The membranes were manufactured in the laboratory from vulcanised, ammonia-stabilized latex. The process is described by Dyson(1970) in some detail. In brief, a perspex former, of the desired membrane shape, is immersed initially in a coagulent (20% solution of calcium nitrate in industrial methylated spirit) and then into a tank of the latex at a slow, uniform rate. The membrane is cured on the former, in an oven at 70-80^{o}C for 2 to 3 hours. After curing it is immersed in water for 24 hours, then stripped and checked against leakage. The membrane is then stored immersed in water until required for use. It was found that if the soaking process was not carried out then the membranes were significantly permeable. The average thickness of the membranes was 0.3 - 0.35mm.

APPENDIX D - 'CALIBRATION OF IS CELL ELECTRONIC PROVING RING'

The Independent Stress (IS) cell was described in Chapter 5, it is seen that a soft rubber ring was used to form a seal between the bottom platen and the cell base plate. It was therefore necessary to calibrate the proving ring in the apparatus to allow for any loss of axial load due to load transfer to the cell base plate via the rubber ring. Also as the ring was subjected to the radial cell pressure, it was necessary to carry out a series of calibration tests at various cell pressures in order to calibrate the amount of uplift on the bottom platen produced by the deformation of the sealing ring under the applied radial stress.

The bottom part of the apparatus was assembled with the sealing ring fitted. This assembly was initially loaded with the top platen bearing directly onto the bottom platen thus ensuring no loss of the applied load above the level of the bottom platen. The loading was applied in the triaxial frame with the applied load recorded on a standard proving ring mounted between top platen and triaxial frame crosshead. During loading the output of the electronic proving ring was recorded on a digital voltmeter.

A steel 'sample' was set up on the bottom platen with the main cell filled with water and top cell fitted as normal. The top platen was located onto the steel sample but the rubber seal and the top cell plate were not fitted to ensure minimum frictional loss in the top cell. Load was again applied via a standard proving ring to the plunger. It was found that the calibration under zero cell pressure was identical to the earlier loading method and is shown on Figure D.1. Thus it was indicated that without the rubber seal

on the top platen and top cell plate there was no measurable frictional loss. The loading sequence was then repeated for cell pressures of 138, 276, 414, 552, 690 and 1034, the electronic proving ring output is plotted against applied load in Figure D1.

The calibration was checked on several subsequent occasions but there appeared to be no ageing effect on the rubber ring that affected its behaviour.

It is seen that the output is affected but that the effect appears to be linear. Provision was made in the computation of stresses to allow for the effect of the cell pressure.

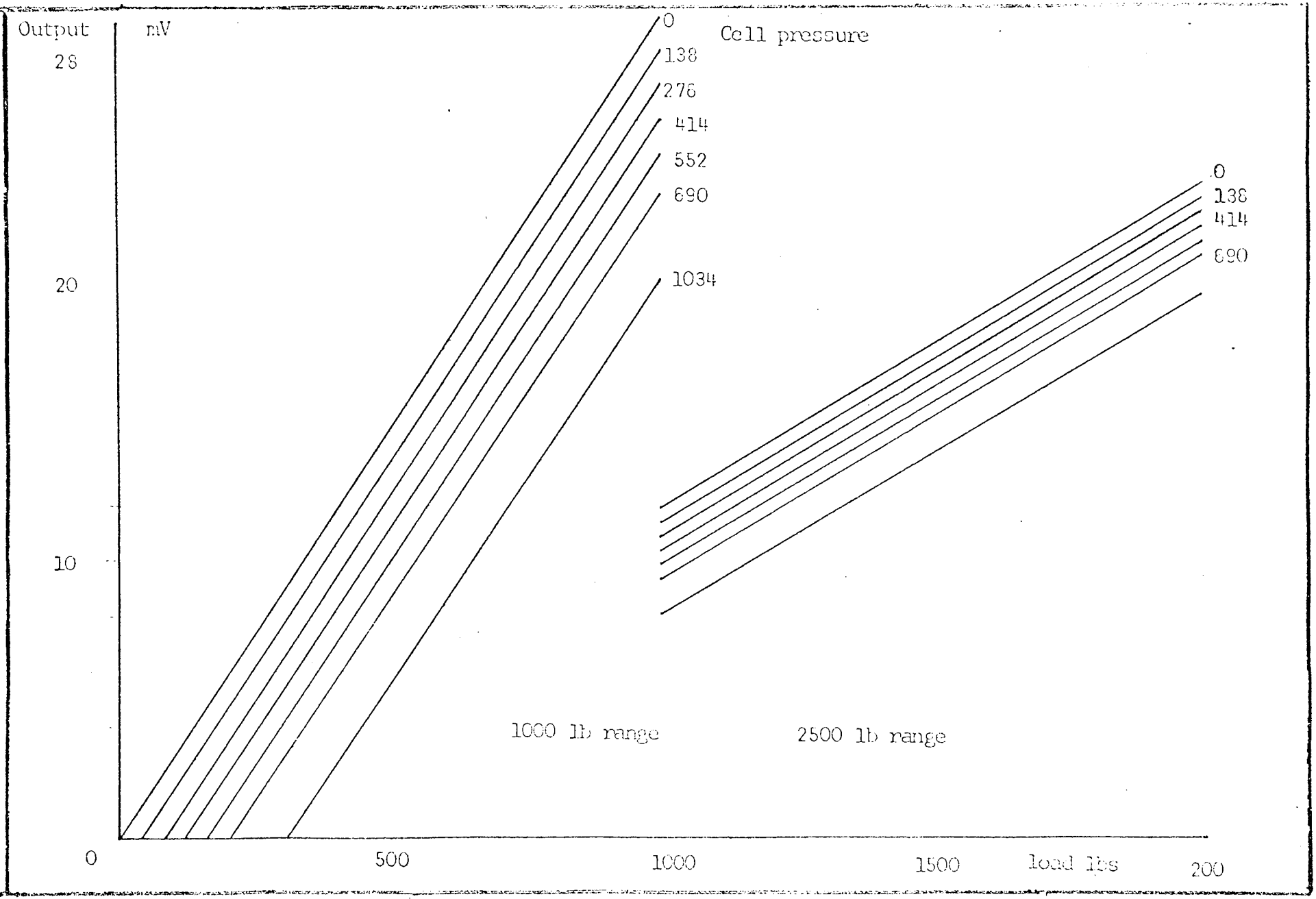

Calibration of IS Cell Electronic Proving Ring FIG. D1.

APPENDIX E - "OEDOMETER CALIBRATION TESTS"

E.1 MECHANICAL OEDOMETER

It was observed during the relaoding cycles of the mechanical oedometer tests that a substantial amount of origin correction was obtained from the compression time curves. The machines were therefore calibrated for machine deformations. The calibrations were carried out by loading steel 'samples' (Toms 1966) using the same method and increments of loading as in the MO Series (Chapter 5). Each oedometer was loaded and unloaded four times with both 'doubling increment' loading and 'constant increment' loading, subsequent to a 'bedding in' load and process as described in Section 5.6.1.

The recorded deformations are presented on Figures E1 and E2 for the 'constant increment' and the 'doubling increment' respectively.

E.2 CONSTANT RATE OF STRAIN OEDOMETER

In the'constant rate of strain'oedometer test it is not possible to obtain origin corrections from compression-time curves as in the mechanical oedometer test. The apparatus was therefore calibrated for machine error by loading a steel 'sample' at a constant rate and recording the deformations, the recorded deformation is taken as the machine error. The recorded error is plotted against the proving ring reading in Figure E3, these results were then used to estimate the true axial deformation of the samples tested in the CS and RCS Series

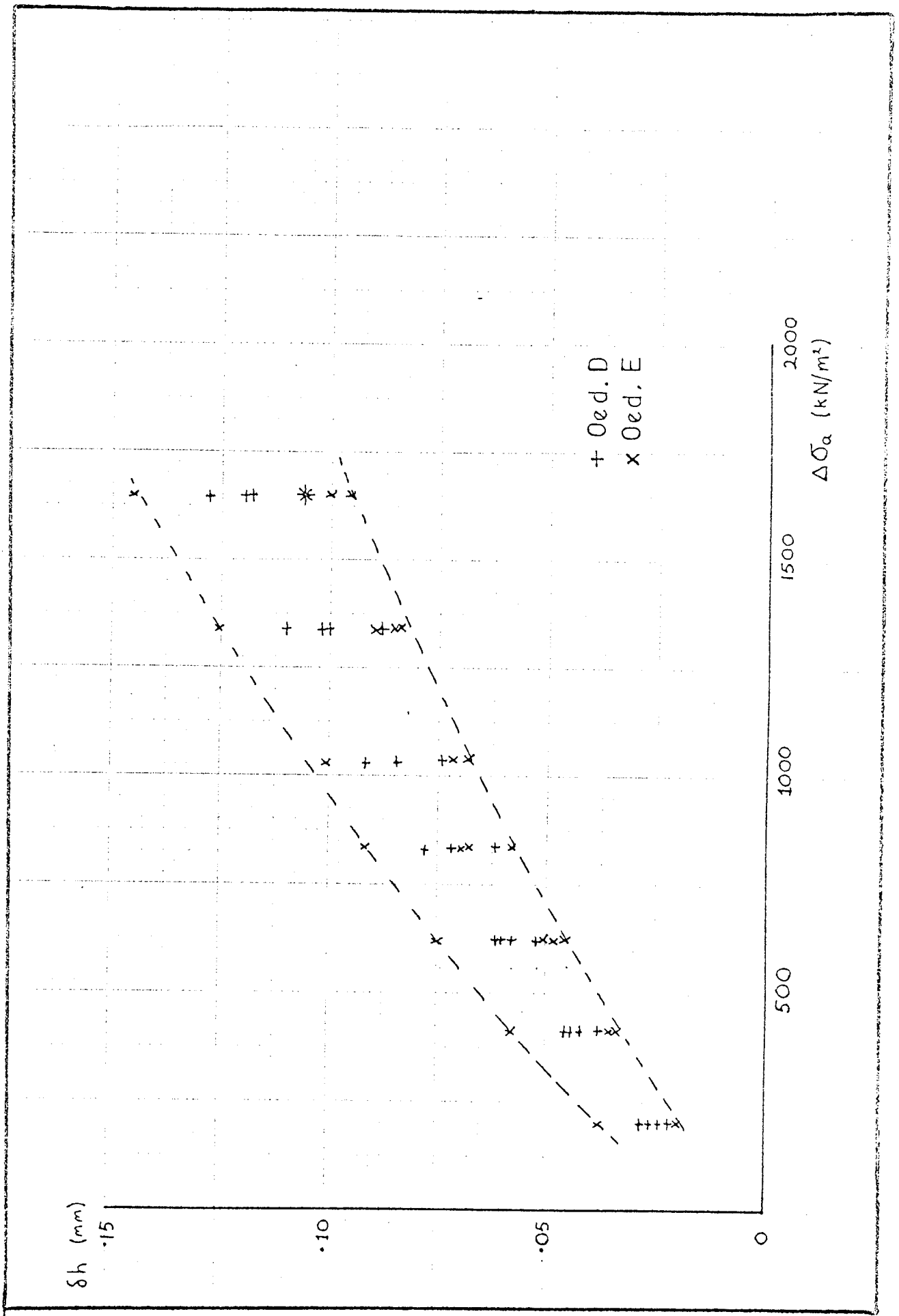

Machine Deformation vs Axial Stress

-'Constant Increment'

FIG. 11

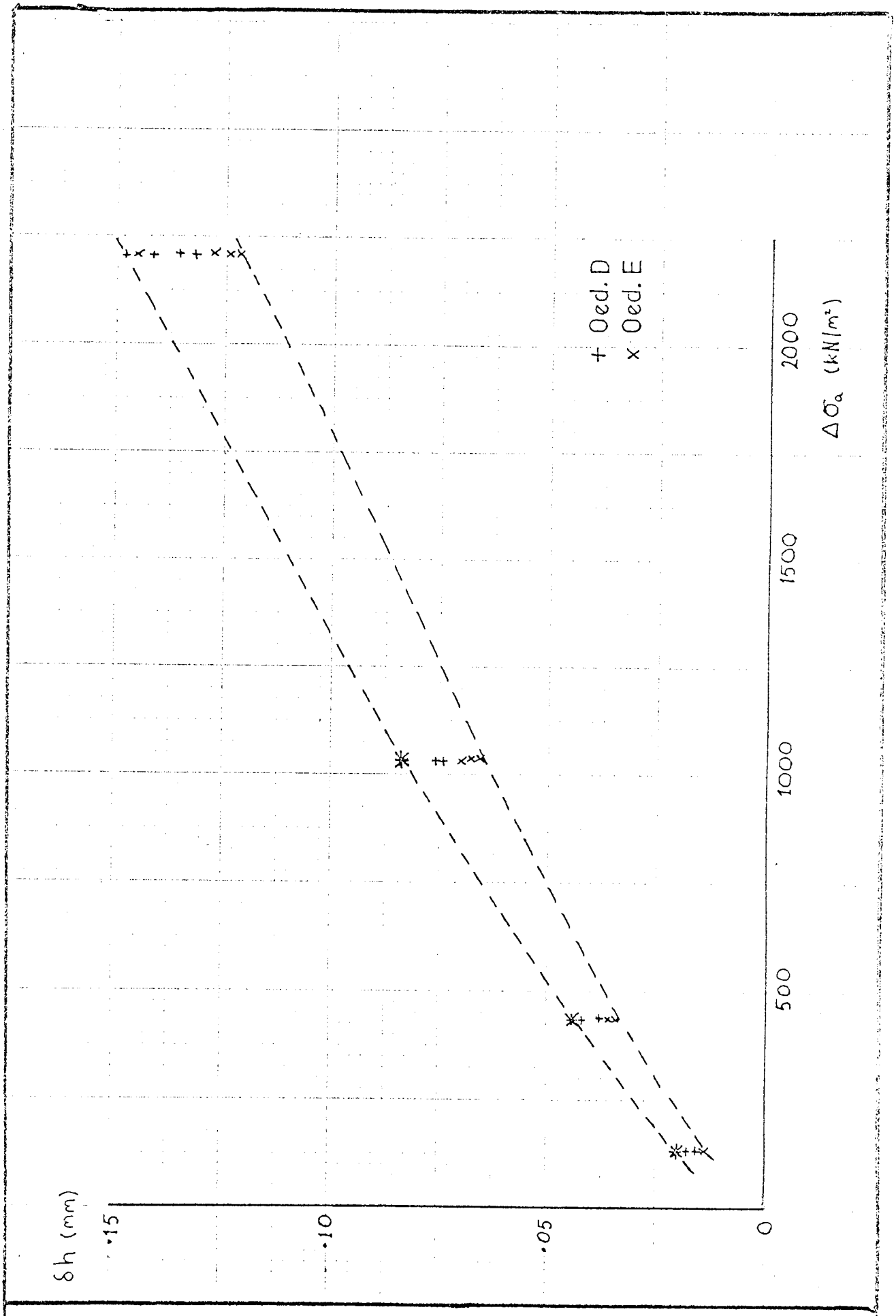

Machine Deformation vs Axial Stress
- 'Doubling Increment'

FIG. E2

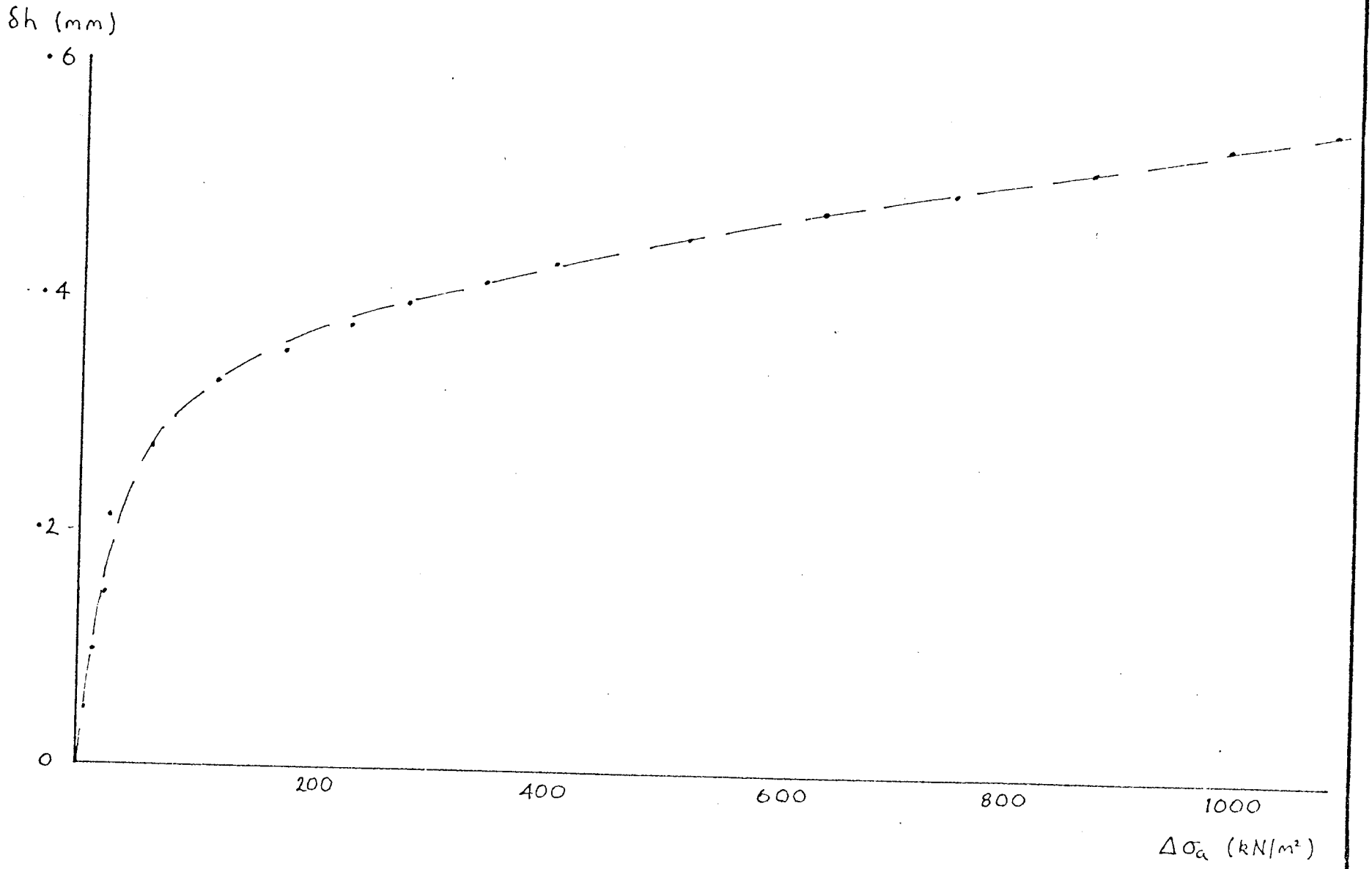

Machine Deformation vs Axial Stress
- 'Constant Rate of Strain Oedometer

FIG. [illegible]

APPENDIX F - "ANALYSIS OF TEST RESULTS AS AN ORTHOTROPIC ELASTIC MATERIAL"

The triaxial stress-strain results are analysed in terms of orthotropic elasticity. The appropriate stress-strain relationships for an orthotropic elastic material are given below.

Elastic constants:-

E'_v - effective stress Young's modulus in the vertical direction

E'_h - effective stress Young's modulus in the horizontal direction

ν_{hv} - Poisson's ratio for the effect of vertical strains on horizontal strains

ν_{vh} - Poisson's ratio for the effect of horizontal strains on vertical strains

ν_{hh} - Poisson's ratio for the effect of horizontal strain on horizontal strain in the orthoganal direction.

From considerations of energy it can be shown that

$$\frac{\nu_{hv}}{E'_v} = \frac{\nu_{vh}}{E'_h}$$

If $\frac{E'_h}{E'_v} = n$ - the modulus ratio

then $\nu_{vh} = n\nu_{hv}$

The strains in the axial and radial directions for increments of axial and radial stress $\Delta\sigma'_a$ and $\Delta\sigma'_r$ on a vertical sample may be written

$$\varepsilon_a = \frac{\Delta\sigma'_a}{E'_v} - \frac{2\nu_{vh}}{E'_h} \cdot \Delta\sigma'_r$$

$$= \frac{\Delta\sigma'_a}{E'_v} \left[1 - 2\nu_{hv}\right] \bar{K} \qquad (F.1)$$

where $\bar{K} = \dfrac{\Delta\sigma'_r}{\Delta\sigma'_a}$

$$\varepsilon_r = -\nu_{hv}\frac{\Delta\sigma'_a}{E'_v} + \frac{\Delta\sigma'_r}{E'_h} - \nu_{hh}\frac{\Delta\sigma'_r}{E'_h}$$

$$= \frac{\Delta\sigma'_a}{E'_v}\left[-\nu_{hv} + \frac{\bar{K}}{n}(1 - \nu_{hh})\right] \qquad (F.2)$$

and therefore the volumetric strain is given by

$$\varepsilon_v = \frac{\Delta\sigma'_a}{E'_v}\left[1 - 2\nu_{hv}\bar{K} - 2\nu_{hv} + \frac{\bar{K}}{n}(1 - \nu_{hh})\right]$$

$$= \frac{\Delta\sigma'_a}{E'_v}\left[1 - 2\nu_{hv} + 2\bar{K}\left(\frac{1}{n} - \frac{\nu_{hh}}{n} - \nu_{hv}\right)\right] \qquad (F.3)$$

therefore the strain ratio is given by

$$\frac{\varepsilon_v}{\varepsilon_a} = \frac{1 - 2\nu_{hv} + 2\bar{K}\left(\frac{1}{n} - \frac{\nu_{hh}}{n} - \nu_{hv}\right)}{1 - 2\nu_{hv}\bar{K}} \qquad (F.4)$$

The equation of axial and volumetric strains are given in Table F1 for particular loading conditions in terms of isotropic and orthotropic elasticity. Also shown in this table are the relationships between the axial and volumetric deformation moduli and the elastic constants.

TABLE F1

Test	Isotropic Elasticity	Orthotropic Elasticity
Standard Drained Test $\bar{K} = 0$	$\varepsilon_a = \frac{\Delta\sigma'_a}{E'_v}$ $\varepsilon_v = \frac{\Delta\sigma'_a}{E'_v}(1 - 2\nu')$ $M_a = E'_v$ $M_v = E'_v/(1 - 2\nu')$	$\varepsilon_a = \frac{\Delta\sigma'_a}{E'_v}$ $\varepsilon_v = \frac{\Delta\sigma'_a}{E'_v}(1 - 2\nu_{hv})$ $M_a = E'_v$ $M_v = E'_v/(1 - 2\nu_{hv})$
Hydrostatic Stress $\bar{K} = 1$	$\varepsilon_a = \frac{\Delta\sigma'_a}{E'_v}(1 - 2\nu')$ $\varepsilon_v = \frac{\Delta\sigma'_a}{E'_v}(3 - 6\nu')$ $M_a = E'_v/(1 - 2\nu')$ $M_v = E'_v/(3 - 6\nu')$	$\varepsilon_a = \frac{\Delta\sigma'_a}{E'_v}(1 - 2\nu_{hv})$ $\varepsilon_v = \frac{\Delta\sigma'_a}{E'_v}(1 - 4\nu_{hv} + \frac{2}{n} - 2\frac{\nu_{hh}}{n})$ $M_a = E'_v/(1 - 2\nu_{hv})$ $M_v = E'_v/(1 - 4\nu_{hv} + \frac{2}{n} - 2\frac{\nu_{hh}}{n})$

TABLE F1 (continued)

Test	Isotropic Elasticity	Orthotropic Elasticity
Incremental Loading $\bar{K}$	$\varepsilon_a = \frac{\Delta\sigma'_a}{E'_v}(1 - 2\nu'\bar{K})$ $\varepsilon_a = \frac{\Delta\sigma'_a}{E'_v}(1 - 2\nu')(1 + 2\bar{K})$ $M_a = E'_v/(1 - 2\nu'\bar{K})$ $M_v = E'_v/(1 - 2\nu')(1 + 2\bar{K})$	$\varepsilon_a = \frac{\Delta\sigma'_a}{E'_v}(1 - 2\nu_{hv}\cdot\bar{K})$ $\varepsilon_a = \frac{\Delta\sigma'_a}{E'_v}(1 - 2\nu_{hv} + 2\bar{K}((1-\nu_{hh})/n - \nu_{hv}))$ $M_a = E'_v/(1 - 2\nu_{hv}\cdot\bar{K})$ $M_v = E'_v/(1 - 2\nu_{hv} + 2\bar{K}((1-\nu_{hh})/n - \nu_{hv}))$
Standard test on horizontal sample	As for vertical sample	$\varepsilon_a = \frac{\Delta\sigma'_a}{nE'_v}$ $\varepsilon_v = \frac{\Delta\sigma'_a}{E'_v}(\frac{1}{n} - \frac{\nu_{hh}}{n} - \nu_{hh})$ $M_a = nE'_v = E'_h$ $M_v = E'_v/((1 - \nu_{hh})/n - \nu_{hv})$

REFERENCES

AGARWAL K.B., (1967). The Influence of Size and Orientation of Sample on the Undrained Strength of London Clay. Ph.D. Thesis University of London.

AHLVIN R.G. and H.H. ULERY (1962). Tabulated Values for Determining the Complete Pattern of Stresses, Strains and Deflections Beneath a Uniform Circular Load on a Homogeneous Half Space. H.R.B. Bulletin No. 342 p.1.

ALLEN P., (1959). The Wealden Environment Anglo-Povis Basin. Phil. Trans. R.Soc.B., Vol.242, p285.

ARKELL J.W., (1933). Jurassic System in Britain. Oxford University Press, London.

BS1377 (1967). Methods of testing Soils for Civil Engineering purposes.

BARDEN L., (1963). Stresses and Displacements in Cross-Anisotropic Soil. Geotechnique, Vol. 13, No. 3.

BARDEN L., and J.W. McDERMOTT, (1965). Use of Free Ends in Triaxial Testing of Clays. Journal of SM & FE Div., Proc. ASCE 1965, SM6.

BENNISON G.M., and A.E. WRIGHT, (1969). Geological History of the British Isles. Edward Arnold (Publishers) Ltd., London.

BIOT M.A., (1941). General Theory of Three-Dimensional Consolidation. J. of Applied Physics, Vol. 12, p155-164.

BIRCH N., (1966). Proceedings of the Midland Soil Mechanics and Foundation Engineering Society. Paper No. 31, Vol. 6, 1966.

BISHOP A.W., (1954). The Use of Pore Pressure Coefficients in Practice. Geotechnique - Vol. 4, p148-152.

BISHOP A.W., (1958). Test Requirement for Measuring the Coefficient of Earth Pressure at Rest. Brussels Conf. 1958 on Earth Pressure Problems, Vol. 1, p2-15.

BISHOP A.W. (1958). Contribution to Discussions, Brussels Conf. on Earth Pressure Problems, Vol. 3, p38.

BISHOP A.W., (1966). Strength of Soils as Engineering Materials. Geotechnique, Vol. 16, June 1966.

BISHOP A.W. and R.E. GIBSON (1963). The Influence of the Provisions for Boundary Drainage on Strength and Consolidation Characteristics of Soils measured in the Triaxial Apparatus. Laboratory Shear Testing of Soils, A.S.T.M., SPEC. TECH. Publn. No.361, p435-451.

BISHOP A.W. and D.J. HENKEL (1962). The Measurement of Soil Properties in the Triaxial Test. Arnold 1962.

BISHOP A.W. and A.L. LITTLE, (1967). The Influence of Size and Orientation of the Sample on the Apparent Strength of London Clay at Maldon, Essex. Proc. Geotechnical Conf. (Oslo) 1967, Vol. 1 p89-96.

BISHOP A.W., D.L. WEBB and P.I. LEWIN, (1965). Undisturbed Samples of London Clay from the Ashford Common Shaft : Strength Effective Stress Relationships. Geotechnique Vol. 15, No. 1, p1-31.

BISHOP A.W., D.L. WEBB and A.E. SKINNER, (1965). Triaxial Tests on Soil at Elevated Cell Pressures. 6th Int. Conf. SM & FE, Montreal 1965, Vol. 1, p170-174.

BJERRUM L., (1965). Mechanism of Progressive Failure in Slopes of Overconsolidated Plastic Clay and Clay Shales. 3rd Terzaghi Lecture, J. ASCHE SMFT, Vol. 93, SM5.

BJERRUM L., (1967). Engineering Geology of Normally Consolidated Marine Clays as Related to Settlement of Buildings. Geotechnique, Vol. 17, June 1966.

BOZOZUK M., (1963). The Modulus of Elasticity of Leda Clay from Field Measurement. Canadian Geot. Journal 1963, Vol. 1, No. 1, p43.

BROOKER E.W. and H.O. IRELAND,(1965). Earth Pressures at Rest Related to Stress History. Canadian Geotechnical Journal, Feb. 1965, Vol. II, No. 1.

BURLAND J.B. and J.A. LORD, (1969). The Load-deformation behaviour of the Middle Chalk at Mundford, Norfolk; a comparison between full scale performance and in-situ and laboratory measurements. Proc. Conf. In-situ Investigations in Soils and Rocks, BGS.

BURMISTER D.M., (1943). Theory of Stresses and Displacements in Layered Systems. Proc. HRB Vol. 22, p127-148.

BURMISTER D.M., (1952). The Application of Controlled Test Methods in Consolidation Testing. ASTM Spl. Tech. Pub. No. 126.

BURMISTER D.M., (1956). Stress and Displacement Characteristics of a Two-layer Rigid Base Soil System Influence Diagrams and Practical Applications. Proc. Highway Res. Board, Vol. 35.

BURMISTER D.M., (1958). Evaluation of Payment Systems of the WASHO Road Testing Layered System Methods. Highway Res. Board, Bull 177.

BUTLER F.G. and J.A. HOOPER, (1966). Some Numerical Results Concerning the Shear Strength of London Clay. Geotechnique, Dec. 1966.

CALHOUN, M.L., (1954). Effect of Sample Disturbance on Strength of a Clay. ASCE Proc. Dec. 1954, Vol.80, No. 570.

CAROTHERS S.D., (1920). Direct Determination of Stresses. Proc. Royal Society (London) Ser. A. Vol. 97.

CASAGRANDE, A., (1936). The Determination of Preconsolidation

Load and its Practical Significance. Proc. 1st ICSMFE, Cam. Mass. Vol. 3.

CHANDLER R.J., (1967). The Strength of a Stiff Silty Clay. Proc. Geo. Conf. Oslo Vol. 1, p103.

CHANDLER R.J., (1968). A note on the Measurement of Strength in the Undrained Triaxial Compression Test. Geotechnique Vol. 18, p261-268.

COOLING L.F.,(1948). Settlement Analysis of Waterloo Bridge. Proc. 2nd Int. Conf. SM, 2,p130.

COOLING L.F., (1948). Settlement Observations on Four Grain Soils. Proc. 2nd Int. Conf. SM2,p135.

COOLING L.F. and R.E. GIBSON, (1955). Settlement Studies of Structures in England. Conf. Corr. Calc. and OBS. Stresses and Displacements of Structures, Vol. 1, p.295.

COOLING L.F. and SKEMPTON A.W., (1942). A Laboratory Study of London Clay. J. ICE., Vol. 17, No. 3, p251.

COULTHARD M., (1972). Unpublished work for Ph.D. Thesis : The University of Aston in Birmingham.

CRYER C.W., (1963). A Comparison of the Three-dimensional theories of Biot and Terzaghi. J. Mech. Appl. Math. 16.

DAVIS E.H. and H.G. POULOS, (1963). Triaxial Testing and Three-dimensional Settlement Analysis. Proc. Fourth Aust. N.Z. Conf. Soil Mech. p.233.

DAVIS E.H. and H.G. POULOS, (1967). Laboratory Investigations of the Effects of Sampling. Proc. Inst. of Engineers, Australia, April 1967. p.86-94.

DAVIS E.H. and H.G. POULOS,(1972). Rate of Settlement under two and three-dimensional conditions. Geotechnique Vol. 22 No. 1.

DOOLEY J.C., (1964). Correspondence to Geotechnique. Geotechnique Vol. 14, No. 2.

DONARTH A.D., (1891). Untersuchungen Veber Den Erddruck Auf Stuetzwaende. Zeitschrift Fuer Bauwesen (Berlin, 1891).

DYSON S., (1970). The Strength and Deformation Behaviour of a Cohesionless Soil Under Generalised Stress Conditions. Ph.D. Thesis Department of Civil Engineering, The University of Aston in Birmingham.

FLAMANT A, (1892). Compt. Rend. Vol. 114.

FOX E.N., (1948). The Mean Elastic Settlement of a Uniformly Loaded Area at a Depth Below the Ground Surface. Proc. Second Int. Conf. Soil Mech. 1, 129.

GEOLOGICAL SURVEY PUBLICATION (1929). The Country around Moreton-in-the-Marsh.

GERRARD C., (1968). Stresses and Displacements in Layered, Cross-

Anisotropic, Elastic Systems. Proc. 5th Aust.-N.Z. Conf. on SM & FE 1968.

GIBSON R.E, (1967). Some Results concerning Displacement and Stresses in Non-Homogeneous Elastic Half Space. Geot. Vol. 17. No. 1, p58-67.

GIBSON R.E., (1968). Letter to Geotechnique. Vol. 18 No. 2.

GIBSON R.E., G.L. HUSSEY and M.J.L.ENGLAND, (1967). The Theory of One-dimensional Consolidation of Saturated Clays. Geotechnique, Vol. 17, No. 3.

GIBSON R.E., K. KNIGHT and P.W. TAYLOR, (1963). A critical experiment to examine theories of three-dimensional consolidation. Proc. Eur. Conf. Soil Mech. Weisbaden 1.

GIBSON R.E. and B.P. LUMB (1953). Numerical Sol^{n} of some problems in the Consolidation of Clay. Proc. Instn. Civ. Engrs. 2, Part 1, p182-198.

GIBSON R.E. and G. SILLS, (1971). Some results concerning the plane deformation of a non-homogeneous elastic half space. Roscoe Memorial Symposium, 1971.

HANSEN B., (1957). Discussion. Proc. 4th Int. Conf., Vol. 3.

HARR M.E., (1966). Foundations of Theoretical Soil Mechanics. McGraw-Hill, New York.

HENKEL D.J., (1960). The Relationships between the Effective Stresses and Water Content in Saturated Clays. Geotechnique 10, p41-5 (1960).

HENKEL D.J. and N.H. WADE, (1966). Plane Strain Tests on Saturated Remoulded Clay. 3 ASCE SMED, Vol. 92 SM6 p67.

HOOPER J.A. and F.G. BUTLER, (1966). Some Numerical Results Concerning the Shear Strength of London Clay. Geotechnique, Dec. 1966.

HUANG, Y.H., (1968). Stresses and Displacements in Non-linear soil Medium. J. ASCE,SMFD, Vol. 94, SM. 1.

HVORSLEV M.J., (1949). Subsurface exploration and sampling of Soil for Civil Engineering purposes. Waterways Experiment Station, Corps of Engineers, U.S. Army.

JAKY, (1944). A nyugalmi nyomas tenyezeje. Maryar Mernok - es Epitexa Eyglet Kozlonye, p35.

JANBU N., (1963). Soil compressibility as determined by oedometer and triaxial tests. Proc. Eur. Conf. Soil Mech. Weisbaden 1.

JANBU N. and E.I. HJELDNES, (1965). Principal stress ratios and their influence on the compressibility of soils. Proc. 6th Int. Conf. SM and FE 2.

JONES A., (1962). Table of stresses in three-layer elastic system. HRB Bulletin, No. 342.

HENKEL D.J. (1972). The relevance of laboratory-measured parameters in field studies. Proc. Roscoe Memorial Symposium

JONG G.J.De and A. VERRUIJT, (1965). Primary and secondary consolidation of a spherical clay sample. Proc. 6th Int. Conf. Soil Mech., Montreal 1.

JURGENSON L., (1934). Application of Theories of Elasticity and Plasticity to Foundation Problems. J. Boston Soc. of Civil Eng., Vol. 21, No. 3.

KELLAWAY G.A. and F.B.A. WELCH,(1968). British Regional Geology - Bristol and Gloucester District.

KERISEL J. and M. QUATRE, (1968). Settlement under foundations - Calculation using the Triaxial Apparatus. Civil Eng. and Public Works Review, May 1968 and June 1968.

KJELLMANN W., (1936). Report on an Apparatus for the Consummate Investigation of the Mechanical Properties of Soils. Proc. 1st Int. Conf. Soil Mech and Found. Eng. 2, p16-20.

KNIGHT K and G.E. BLIGHT, (1965). Studies of some effects resulting from the unloading of soils. 6th Int. Conf. SMFE Vol. 2. 1965.

LADD C.C., (1964). Stress-strain modulus of Clay in Undrained Shear. J. ASCE SMFD Vol 90 SM5 p103-132, 1964.

LADD C.C., (1965). Stress-Strain behaviour of Anisotropically consolidated clays during undrained shear. Proc. Sixth Int. Conf. Soil Mech. 1, p282.

LADD C.C. and J. VARALLYAY, (1965). The Influence of stress system on the behaviour of saturated leays during undrianed shear. Waterways Experiment Station, Corps of Engineers, U.S. Army.

LAL R., (1971). Shear Strength of Lower Lias Clay from Blockley clay pit, Gloucestershire. M.Sc. Thesis, The University of Aston in Birmingham.

LAMBE T.W., (1964). Methods of Estimating Settlement. J. Mech. FDNS. DIV. AM. SOC. CIV. ENGRS. 90, No. SM5 p43.

LAMBE T.W., (1967). The Stress Path Method. J. ASCE SMFD, Vol. 93, SM6, p309-331.

LANG J.G.,(1967). Longitudinal Variations of Soil Disturbance within Tube Samples. Proc. 5th Australia-New Zealand Conference on Soil Mechanics and F.E., 1967.

LANGER, (1936). The Influence of the speed of loading on the pressure-void ratio diagram of undisturbed samples. Proc. 1st Lat. Conf. SMFE Vol. 2.

LEKHNITSHII S.G., (1963). The Theory of Elasticity of an Anisotropic Elastic Body.

LOVE A.E.H., (1928). The Stress Produced in a Semi-Infinite Solid by Pressure on part of the Boundary. Phil. Trans. of the Royal Society Series A. Vol 228. p.377.

MANDEL J., (1953). Consolidation des Soils (etude mathematique). Geotechnique 3, No. 7.

MARSLAND A., (1971)(a). The Shear Strength of Stiff Fissured Clays. Proc. Roscoe Memorial Symp. 1971.

MARSLAND A., (1971)(b). Laboratory and in-situ measurements of the deformation moduli of London Clay. Proc. Midland Soil Mech. Symp. 1971.

MARSLAND A. and M.E. BUTLER, (1967). Strength Measurements on Stiff Fissured Barton Clay from Cawley, Hampshire. Proc. Geotechnical Conf. (Oslo) 1967. Vol. 1 p 136-146.

MICHELL J.H., (1900). The Stress Distribution in an Aelotropic Solid with Infinite Boundary Plane. Proc. London Math. Soc. Vol. 32.

MILLER R.J. and P.F. LOWE, (1963). Threshold Gradient for Water Flow in Clay Systems. Proc Soil Science Soc of America Madison, Wis., Vol. 27, No. 6, p605.

NEWMARK N.M., (1942). Influence Charts for Computation of Stresses in Elastic Foundations. Univ. Illinois, Eng. Expt. Sta. Bull. 12.

NOORANY I. and H.B.SEED, (1965). In-situ strength characteristics of soft clays. J. SM and Foundation Div. ASCE. March 1965, SM2.

PETERSON R., (1958). Rebound in Bearpaw Shale in Western Canada. Bull. Geol. Soc. of America Vol. 69, p1113.

PHUKAN A.L.T., (1968). Non-linear deformation of rocks. Ph.D. Thesis, University of London.

POULOS H.G., (1967). Stresses and Displacements in an Elastic Layer underlain by a rough rigid base. Geotechnique 17, No.4, p378-410.

PARRY R.H.G., (1963). Testing small undisturbed samples. 4th Aust. N.Z. Conf. SM and FE 1, 61.

PARRY R.H.G., (1968). Field and Laboratory behaviour of a lightly overconsolidated clay. Geotechnique, 18, p151-171.

ROWE P.W., (1958). General Report on papers in Section 1. Brussels Conf. 1958 on Earth Pressure problems. Vol. 3, p25-30.

RUTLEDGE P.C. (1944). Relation of Undisturbed sampling to laboratory testing. Trans. ASCE Vol 109, 1944, p 1155 (Paper No. 2229.)

SCHMERTMANN J.H., (1953). Estimating the time-consolidation behaviour of clay from laboratory test results. Proc. ASCE, Vol. 79 Separate No 311.

SCHMERTMANN J.H., (1955). The undisturbed consolidation behaviour of clay. Trans. ASCE, Vol. 120, 1955, p1201 (Paper No. 2775.)

SEED H.B., (1965). Settlement Analysis - A Review of Theory and Testing Procedures. J.ASCE. SMFD, Vol. 91 SM7, p5946.

SKEMPTON A.W., (1954). The Pore Pressure Coefficients A and B. Geotechnique, Vol. 4. p.143.

SKEMPTON A.W., (1960). Letter to Geotechnique. Vol. 10, No. 4.

SKEMPTON A.W., (1961). Horizontal Stresses in an over-consolidated eocene clay. Proc. 5th Int. Conf. SM and FE Vol. 1., 1961, p251-357.

SKEMPTON A.W. and L. BJERRUM, (1957). A contribution to the Settlement Analysis of Foundations on Clay. Geotechnique, Vol 7, No. 4.

SKEMPTON A.W. and D.J. HENKEL, (1957). Tests on London Clay Deep Borings at Paddington, Victoria and South Bank. Proc. 4th ICSMFE, London, Vol. 1, p.100.

SKEMPTON A.W., R.B. PECK and J. MacDONALD, (1955). Settlement Analysis of six structures in Chicago and London. Proc. Instn. Civ. Engrs. 4, Part 1, p 525.

SKEMPTON A.W. and V.A. SOWA, (1963). The Behaviour of Saturated clays during sampling and testing. Geotechnique, Vol. 13, No. 4, Dec. 1963, p269-290.

SHIBATA T, and D.KARUBE, (1965). Influence of the intermediate principal stress on the mechanical properties of normally consolidated clay. Proc. 6th Int. Conf. Soil Mech. and Found. Eng., 1965, Vol. 1, p.259.

SIMONS N.E., (1957). Settlement Studies on two structures in Norway. Proc. 4th Int. Conf. SM 1, p431.

SIMONS N.E., (1958). Contribution to Discussion. Brussels Conf. on Earch Pressure Problems, Vol. 3, p50.

SIMONS N.E., (1963). Settlement studies of a nine storey apartment building at Okernbraten, Oslo. Proc. Eur. Conf. SM FE, Wiesbaden.

SIMONS N.E. and N.N. SOM, (1970). Settlement of structures on clay, with particular emphasis on London clay. CIRIA Report 22.

SMITH and REDLINGER, (1953). Soil Properties of Fort Union Clay shale. Proc. 3rd ICSMFE Vol. 1. p62.

SOM N.N., (1968). The Effect of Stress path on the Deformation and Consolidation of London Clay. Ph.D. Thesis, University of London.

SOWA V., (1963). A comparison of Isotropic and Anisotropic consolidation on the Shear behaviour of a clay. Ph.D. Thesis, Univeristy of London.

STEINBRENNER W., (1936). A rational method for the determination of the vertical normal stresses under foundations. Proc. Int. Conf. SM FE Vol. 2.

SYMPOSIUM ON SAMPLING, (1969). Arranged by the Swedish Geot. Soc. 28th October 1969.